

# New Functional Molecules in Molecular Junctions

## Inauguraldissertation

zur  
Erlangung der Würde eines Doktors der Philosophie

vorgelegt der

**Philosophisch-Naturwissenschaftlichen Fakultät  
der Universität Basel**



Von

**Sergio Grunder**

Aus

**Vechigen (BE), Schweiz**

Basel 2010

Originaldokument gespeichert auf dem Dokumentenserver der Universität Basel  
[edoc.unibas.ch](http://edoc.unibas.ch)



Dieses Werk ist unter dem Vertrag „Creative Commons Namensnennung-Keine kommerzielle Nutzung-Keine Bearbeitung 2.5 Schweiz“ lizenziert. Die vollständige Lizenz kann unter [creativecommons.org/licences/by-nc-nd/2.5/ch](http://creativecommons.org/licences/by-nc-nd/2.5/ch) eingesehen werden.



## Namensnennung-Keine kommerzielle Nutzung-Keine Bearbeitung 2.5 Schweiz

---

### Sie dürfen:



das Werk vervielfältigen, verbreiten und öffentlich zugänglich machen

### Zu den folgenden Bedingungen:



**Namensnennung.** Sie müssen den Namen des Autors/Rechteinhabers in der von ihm festgelegten Weise nennen (wodurch aber nicht der Eindruck entstehen darf, Sie oder die Nutzung des Werkes durch Sie würden entlohnt).



**Keine kommerzielle Nutzung.** Dieses Werk darf nicht für kommerzielle Zwecke verwendet werden.



**Keine Bearbeitung.** Dieses Werk darf nicht bearbeitet oder in anderer Weise verändert werden.

- Im Falle einer Verbreitung müssen Sie anderen die Lizenzbedingungen, unter welche dieses Werk fällt, mitteilen. Am Einfachsten ist es, einen Link auf diese Seite einzubinden.
- Jede der vorgenannten Bedingungen kann aufgehoben werden, sofern Sie die Einwilligung des Rechteinhabers dazu erhalten.
- Diese Lizenz lässt die Urheberpersönlichkeitsrechte unberührt.

#### Die gesetzlichen Schranken des Urheberrechts bleiben hiervon unberührt.

Die Commons Deed ist eine Zusammenfassung des Lizenzvertrags in allgemeinverständlicher Sprache: <http://creativecommons.org/licenses/by-nc-nd/2.5/ch/legalcode.de>

#### Haftungsausschluss:

Die Commons Deed ist kein Lizenzvertrag. Sie ist lediglich ein Referenztext, der den zugrundeliegenden Lizenzvertrag übersichtlich und in allgemeinverständlicher Sprache wiedergibt. Die Deed selbst entfaltet keine juristische Wirkung und erscheint im eigentlichen Lizenzvertrag nicht. Creative Commons ist keine Rechtsanwalts-gesellschaft und leistet keine Rechtsberatung. Die Weitergabe und Verlinkung des Commons Deeds führt zu keinem Mandatsverhältnis.

Genehmigt von der Philosophisch-Naturwissenschaftlichen Fakultät der Universität Basel  
auf Antrag von:

Prof. Dr. Marcel Mayor

Prof. Dr. Andreas Pfaltz

Dr. Heike Riel

Basel, den 08.12.2009

Prof. Dr. Eberhard Parlow





*Dedicated to:*

Richard Grunder



Es gäbt no vell z verzelle  
das hemmer gar ned welle  
doch was mer ned chönd senge  
esch tüüf i jedem enne.

*Willi Baumgartner*



Einfach machen.



## **Acknowledgments**

First of all I would like to thank Prof. Dr. Marcel Mayor. Marcel, it was a great pleasure and honour to work in your group. I learned a lot during this time, which was of great importance to my chemical career but also for my life.

I would like to thank Prof. Dr. Andreas Pfaltz and Dr. Heike Riel for being co-referee.

I would like to thank the whole Mayor group. From all the members I would like to say a special thank you to Marcel Müri for being a great lab mate.

A great thank goes to my collaborators which enabled the experimental investigations on molecular electronics. Namely, Dr. Michel Calame, Prof. Dr. Christian Schönenberger, Dr. Songmei Wu, Dr. Roman Huber and Dr. Jianhui Liao from the Department of Physics, University of Basel, and Christoph Marquardt and Dr. Ralph Krupke from the Karlsruhe Institute of Technology.

I would like to thank Dr. Daniel Häusinger, Dr. Torsten Peterle and Fabian Sander for undertaking NMR-experiments, Dr. Heinz Nadig for FAB and EI mass spectrometry measurements and Werner Kirsch for elemental analysis.

Then I would like to thank the technical staff: Markus Hauri, the Werkstatt team, Roy Lipps, Andi Pfiffner and Franz Stehlin. Also the secretaries Beatrice Erismann and Brigitte Howald are acknowledged.

I acknowledge Tom Eaton, Nicolas Weibel, Yann Leroux and Jens Tüxen for proof reading this thesis.

ben may studio is acknowledged for cover artwork.

Big thanks go to my family. To know that you support me in any situation is very encouraging and enabled the work of this thesis.

Denise you are you, and without you, I am not me.

Thank you so much for your love, support and loyalty.

And I thank all my friends for being my friends.





## Table of Contents

---

1 Introduction.....	1
1.1 Molecular Electronics .....	1
1.1.1 Integration of Molecules into Electronic Circuits .....	4
1.1.2 Correlating Molecular Structure with Electronic Properties.....	19
1.1.3 Basic Electronic Functions Transferred to a Molecular Level .....	23
2 Molecular Rods as Model Compounds for Electron Transport Investigations.....	51
2.1 Design of Molecular Rods .....	51
2.2 Synthesis of Molecular Rods.....	53
2.2.1 Synthetic Strategy .....	53
2.2.2 Synthesis and Characterization .....	54
2.3 Transport Investigations through Molecular Rods.....	62
2.3.1 Connecting Single Molecules to Two Electrodes.....	62
2.3.2 Exploring Different Contacts.....	64
2.3.3 Molecular Junctions Based on Aromatic Coupling.....	68
2.3.4 From Single Junctions to Two-Dimensional Gold Nanoparticle Arrays.....	75
2.4 Conclusion .....	80
3 Molecular Switches.....	81
3.1 Coordination Induced Switches.....	82
3.1.1 Principle.....	82
3.1.2 1 <sup>st</sup> Generation Cruciform Structures .....	84
3.1.3 Investigations on Rod Substructures .....	98
3.1.4 2 <sup>nd</sup> Generation Cruciform Structures .....	100
3.2 Redox Switches .....	113
3.2.1 A 1,1'-Dithioalkyl Functionalized Ferrocene as Model Compound for Redox Switches .....	114
3.2.2 A 1,1'-Distyrene-Ferrocene Based Redox Switch .....	124
4 Rectifiers.....	141
4.1 Cross-Conjugated Molecular Rectifiers.....	141
4.1.1 Molecular Design and Synthetic Strategy.....	141
4.1.2 Synthesis.....	143
4.1.3 Conclusion.....	148

---

5 Molecules “Waving” Inside the Gap: Electroluminescence in a Single-Walled Carbon Nanotube Junction.....	151
5.1. Introduction .....	151
5.1.1 Single-Walled Carbon Nanotubes as Potential Electrodes for Molecular Electronic Devices .....	152
5.2 Project Description .....	157
5.3 Molecular Design and Synthetic Strategy .....	158
5.4 Synthesis and Characterization .....	163
5.5 Photophysical Characterization.....	182
5.6 Investigations in a SWNT Junction .....	188
5.6.1 Setup .....	188
5.6.2 Fiat Lux.....	189
5.6.3 Changing the Core-Substituent .....	191
5.7 Conclusion .....	192
6 Summary and Conclusions.....	193
7 Experimental Section.....	201
7.1 Materials and Methods.....	201
7.2 Synthetic Procedures .....	204
7.2.1 Molecular Conductors.....	204
7.2.2 Molecular Switches.....	216
7.2.3. Cross-Conjugated Molecular Rectifier .....	265
7.2.4 A Characteristic Emission Signal from a Single Molecule Contacted With Two Electrodes.....	277
8 Abbreviations.....	297
9 Literature .....	301
10 Appendix.....	313
10.1 Contributions .....	313

# 1 Introduction

## 1.1 Molecular Electronics

Molecular electronics has become a very active research area and the number of people from different disciplines of science contributing to it is steadily increasing. The basic idea of molecular electronics is to embed molecules between electrodes and let them perform electronic functions.<sup>[1-6]</sup>

The semiconductor industry has seen a remarkable miniaturization trend of the active components in the last four decades. Gordon E. Moore predicted in 1965 that the number of transistors which can be inexpensively placed on a chip doubles every two years, referred to as Moore's law.<sup>[7, 8]</sup> Indeed, Moore's law has held true until today and the numbers of transistor on a chip has increased exponentially. However, also Moore's second law, which states that the capital cost of a semiconductor production plant increases exponentially over time strikes as predicted.<sup>[8, 9]</sup> Figure 1 depicts the reduction in size of amplification devices used in electronic circuits over the last century, and the further size reduction potential when implementing molecules.

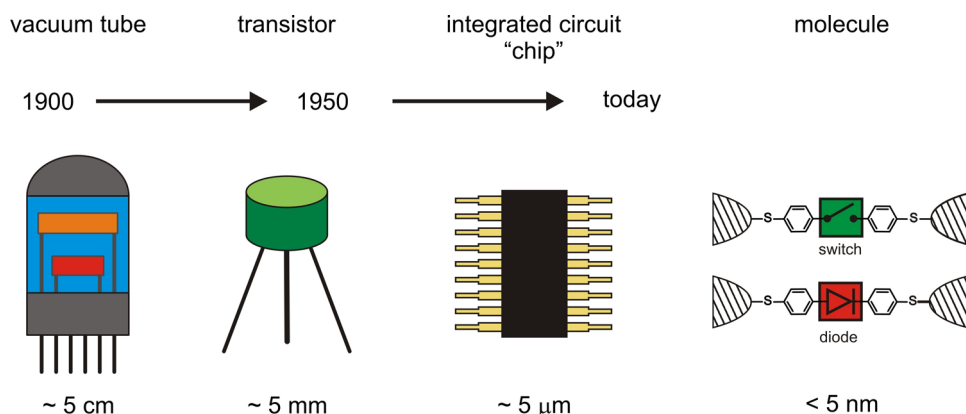


**Figure 1:** Miniaturization of amplification devices used in electronic circuits over the last century. From left to right starting with the vacuum tube to the transistor to current integrated circuits. In the future this miniaturization might be taken up with molecules undertaking functions.

While reducing the size of objects down to a nanometer scale, bulk properties yield to quantum phenomena and intrinsic problems arise.<sup>[10]</sup> The chip fabrication became steadily more laborious and expensive, however the size of the market also increased which balances the higher costs of a production plant. Both, the decrease

in size of top down fabricated silicon based circuits, and the increase in expenses will reach a limit where it is no longer possible to smaller fabricate devices. Therefore there is a vast search for new concepts which help to overcome these limits, on one side to overcome physical barriers and on the other to find concepts which allow cheaper chip fabrication. Hence, molecular electronics can be a solution, using molecules as the smallest feature units. The concept to profit from molecules as functional units has numerous very appealing aspects. The ability of chemists to correlate function with structure, to design and to provide tailor-made functional molecules is central to molecular electronics. Further, molecules are probably the smallest units still capable of providing a rich structural variety. An outstanding functional density was predicted as a consequence of the minute size of molecules.<sup>[11-13]</sup> But, the minute size of molecules still restricts the number of contacts of a molecular structure to two.<sup>[5]</sup> The limited number of massive parallel contacting concepts, poor reliability prospects, and the anticipated heat management challenges are issues drawing back the potential of high integration density.<sup>[14-16]</sup> Thus, the size of molecules is rather a disadvantage, and leads to a scientific challenge. However, from the two described limits mentioned before, the physical limit and the economic limit, the later will be reached sooner, and therefore the main driving force of molecular electronics is the money.

The restriction of two contacts of a molecule, prevents amplification of an electronic signal which requires subunits that are connected to at least three electrodes such as tubes or transistors.<sup>[2, 11]</sup> As amplification is required in almost every logic circuit, it is rather unlikely that molecules will substitute such kinds of electronic circuits. However, there are particular applications for which molecular devices might supplement CMOS circuits in the future, resulting in hybrid CMOS-molecular electronic circuits. For example the production of memory cells using CMOS technology is laborious and expensive, since numerous production steps are required to arrange several transistors to store one bit of information. A molecular device which displays hysteretic switching between two metastable states could also act as a memory cell.<sup>[17, 18]</sup> Silicon based electronic circuits demonstrated that only a very limited number of electronic functions were required in order to assemble highly functional devices. Probably the most important functions which have to be undertaken by molecules to achieve molecular electronic devices are switching and

rectification. If switching and rectification will be achieved by molecules, molecular electronic devices are very promising to find applications in electronic circuitry.

The visionary concept of integrating designed molecular structures in electronic circuits as minute functional units roots in Kuhn's ideas of "molecular engineering" proposed in the 1960's.<sup>[19]</sup> Soon after, Aviram and Ratner discussed potential rectification emerging from a molecular structure based on a theoretical model.<sup>[20]</sup> While this pioneering suggestion moved molecules, as the smallest unit providing the required structural variation, further into the focus of interest, the concept remained on a theoretical level due to the missing tools required to realize single molecule transport experiments. Only within the last two decades the tremendous improvement of physical set-ups enabled the integration of monomolecular films,<sup>[21-26]</sup> small assemblies<sup>[27]</sup> and even single molecules providing the experimental base for "molecular electronics".<sup>[1, 3-5, 28]</sup>

In the following sections methods to contact molecules with electrodes are reported. Further correlation of molecular structure with electronic properties and investigations on basic functions such as rectification and switching transferred to a molecular level will be discussed.

### 1.1.1 Integration of Molecules into Electronic Circuits

To achieve molecular electronic devices, molecules have to be integrated between electrodes. The development of this interface between macroscopic electronic circuits and nano-scale molecular objects is one of the biggest challenges in modern nanotechnology. Several methods and techniques have been reported to contact molecules. We divide these integration techniques into two parts, first methods which are well suited to contact monomolecular films by sandwiching the molecules between two electrodes (A in Figure 2), and second methods which allow contacting single molecules (B in Figure 2) are discussed.

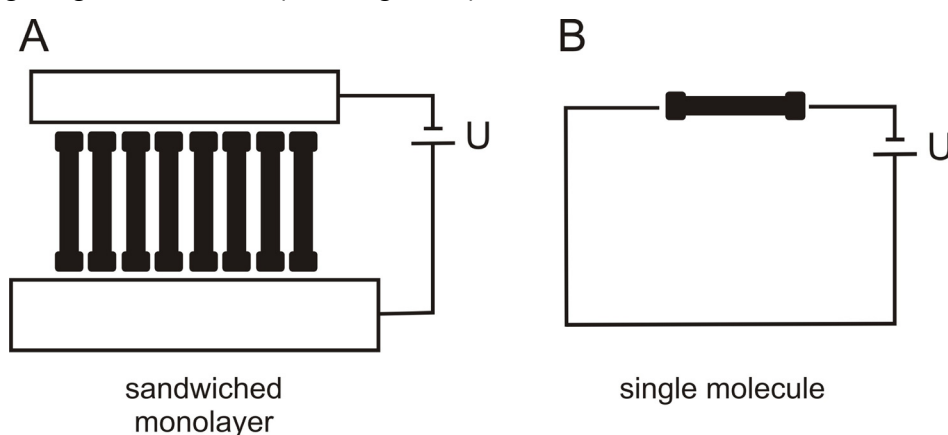


**Figure 2:** Two different approaches to address molecules with electrodes. A) A monolayer of molecules (either SAM or LB film) is sandwiched between two electrodes. B) Single molecules are connected with two electrodes.

Figure 3 displays an overview of the techniques and integration strategies which will be discussed in the following in more detail. Crossed-wire junctions (A), mercury droplet junction (B), electromigration (C) are techniques to address ensembles of molecules. 2D-Nanoparticle arrays (D) provide extended junctions. The STM-carpet approach (E), Nanoparticle coupled conducting AFM (F), mechanically controllable break junction (G) and STM break junction (H) allow contacting of single molecules.

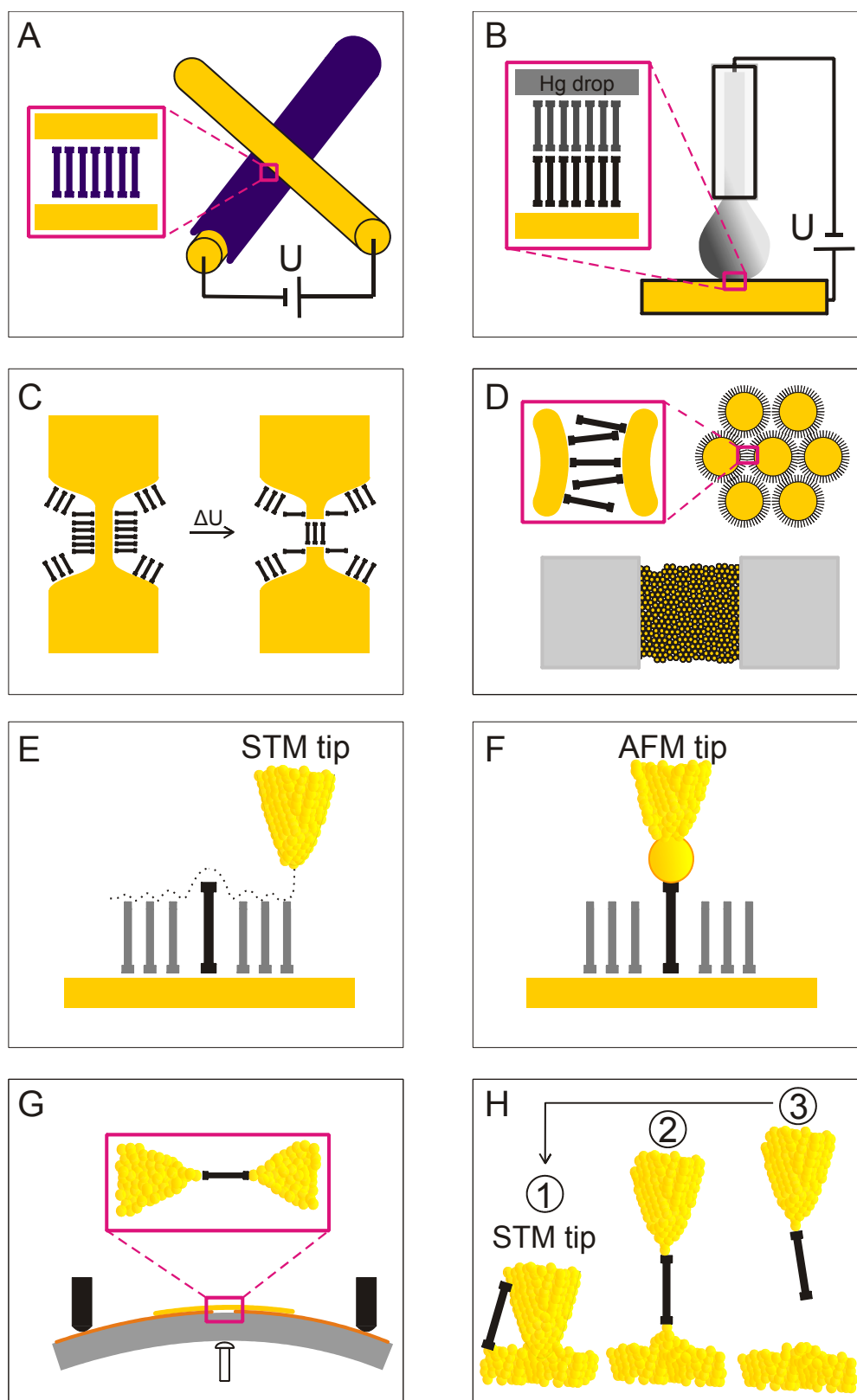


**Figure 3:** Various techniques used to address monolayers of molecules (A, B, C) or single molecules (E, F, G, H). A) crossed-wire junction, B) Hg droplet junction, C) electromigration techniques, D) 2D-gold nanoparticle arrays, E) STM-carpet approach, F) Nanoparticle coupled conducting probe AFM, G) Mechanically controllable break junction, H) STM break junction.

### 1.1.1.1 Contacting Ensembles of Molecules with Electrodes

Probing individual molecules electronically is a challenge because issues arise of how to attach the probe electrodes to either side of a molecule. The difference in size of electrodes and molecules is enormous and makes it very difficult to contact molecules with electrodes. The organization of the molecules within the junction is usually based on some sort of self assembly using chemisorption or physisorption methods to form monolayers.<sup>[29]</sup> In the case of molecular films, either self assembled monolayers (SAMs)<sup>[30, 31]</sup> or Langmuir-Blodgett (LB)<sup>[32, 33]</sup> films provide the order at the molecular level. Chemisorption includes the formation of SAMs where heteroatoms such as sulfur bind to gold or similar metals.<sup>[30, 31]</sup> Strong bonds are formed which are hard to remove and which displace previously adsorbed adsorbents. Disadvantages of chemisorption are that the degree of coverage is hard to determine and chemical reactions might take place. Further, surface-dipoles are formed and are referred to as Schottky barriers.<sup>[34]</sup> On the other side, no Schottky-barriers are formed and the coverage ratio is detectable when films are prepared from physisorption methods such as LB-films. Disadvantages of physisorption methods are that the structure might change over time as the physisorbed films are less stable, and that during the film formation other adsorbents are not displaced.

#### A. Crossed-wire junction

Starting with A in Figure 3 we take a closer look at crossed-wire junctions.<sup>[10, 17, 23, 35-38]</sup>

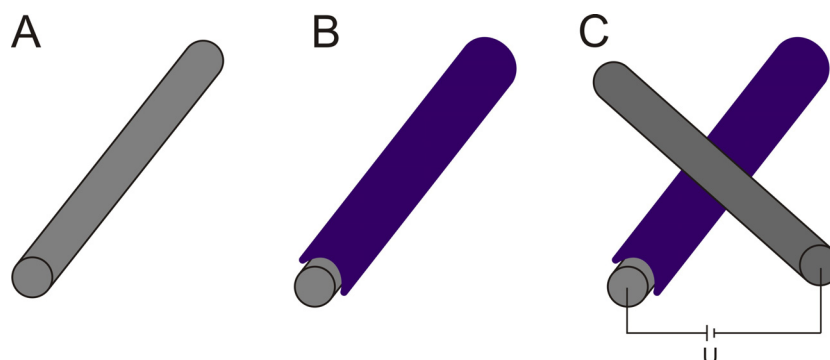


**Figure 4:** Schematic representation of a crossed-wire junction formation. A metal wire (A) is covered with a SAM (blue) of the molecule of interest (B). The covered layer is then topped perpendicular with a second metal wire. The touching area of the two wires with the sandwiched molecules form the active device when connecting the two wires (C).



The principle is that a metal wire is covered with a SAM (B in Figure 4) which is subsequently topped with a perpendicular second metal wire (C in Figure 4). The crossing area of the two metal bars, with the molecular film in between forms the junction. With a feedback loop comparable to a scanning tunneling microscopy (STM) configuration the contact intensity between both wires can be adjusted. An advantage of the crossed-wire junction is that the two wires can be individually functionalized with molecules. This enables contacting the molecules in a certain order or covering the two wires with different SAMs. Further, the electrodes are mobile and do not need to be evaporated onto the SAM.

### *B. Mercury droplet junction*

Similar to the crossed-wire junctions, mercury droplet junctions do not require a laborious fabrication of the electrodes (B in Figure 3). Nevertheless, the mercury droplet junction has been reported as a reliable tool to address molecular films.<sup>[39-42]</sup> Similar to gold, mercury can form thiol-based SAMs.<sup>[43]</sup> The junction is created by forming a mechanical contact of a SAM supported on a solid substrate and a SAM supported on a mercury drop. The resulting metal-SAM-SAM-metal junction allows for the measurement of pure and mixed monolayers. Using transparent metal substrates further allows addressing the molecular films with a light source while measuring transport properties.<sup>[39]</sup>

### *C. Electromigration*

Electromigration was exploited to form molecular junctions (C in Figure 3).<sup>[44-48]</sup> Continuous metallic wires on insulating films are prepared by electron-beam lithography. The wires are cleaned and placed in a diluted solution of the molecule of interest to facilitate SAM formation. The SAM coated wires are then broken by electromigration, by ramping the potential between their two ends to large voltages. This produces gaps of about 1-2 nm wide, across which molecules can bridge. Without laborious and expensive setups small gaps can be produced, however not very precisely.

#### D. 2D-Gold nanoparticle arrays

Calame and coworkers reported on a method to extend single metal-molecule-metal junctions to two-dimensional gold nanoparticle arrays (D in Figure 3).<sup>[49, 50]</sup> Gold colloidal particles with a 10 nm diameter were synthesized by reduction of hydrotetrachloroaurate with trisodium citrate and tannic acid.<sup>[51]</sup> After transferring the nanoparticles to ethanol by centrifugation, the particles were stabilized with octanethiol ligands. The nanoparticles were dispersed in chloroform and spread on a convex water surface. In this way, alkanethiol-capped 10 nm gold nanoparticles were self-assembled into two-dimensional close-packed arrays at the air/water interface. A polydimethylsiloxane (PDMS) stamp with the desired imprinted structures was then used to transfer the nanoparticles from the air/water interface onto a solid substrate (Shown in Figure 5 C). This combination of self-assembly and microfabricated printing leads to the formation of patterned two-dimensional nanoparticle arrays.<sup>[50-53]</sup> Lines of nanoparticles with a typical width of 25  $\mu\text{m}$  and a spacing of 30  $\mu\text{m}$  were herewith prepared. Metallic contact pads (5 nm Ti and 45 nm Au) were evaporated on top of these lines using a transmission electron microscope (TEM) grid as a shadow mask. Figure 5 A shows a scanning electron microscope (SEM) image of a typical sample.

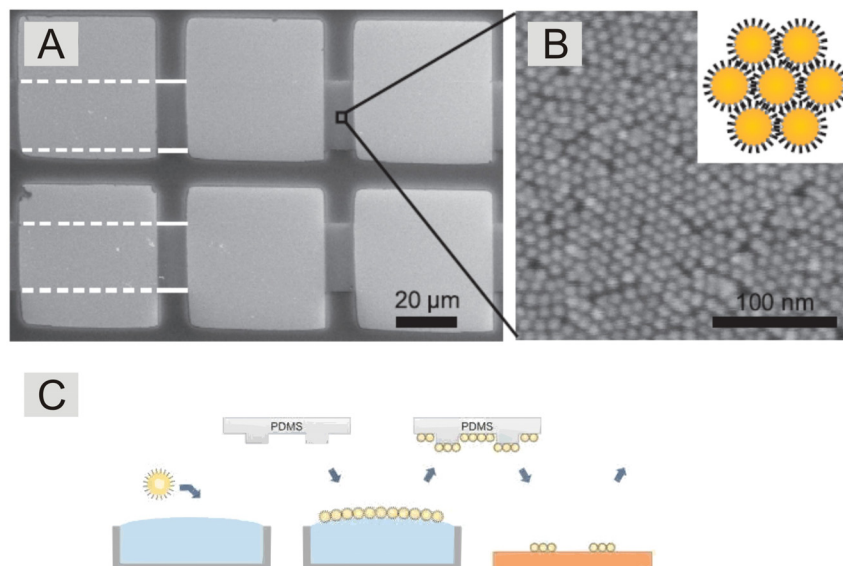


**Figure 5:** A SEM image of devices prepared by evaporation of metallic contact pads on top of printed nanoparticle monolayer lines is shown in inlet A. Inlet B shows a high magnification SEM image. The hexagonal arrangement of nanoparticles is visible. The inset in B is a schematic picture of alkanethiol-capped gold nanoparticles before exchange. The microimprinting technique is described by picture C.

---

The edges of the printed lines are emphasized with a white line (dashed when underneath gold contact pads). Between every pair of neighboring contact pads, typically  $10^6$  molecular junctions are present. Conjugated molecules are introduced into the arrays using place-exchange while immersing a sample in a solution of the incoming molecule. The conductance can be measured before and after exchange of the alkyl thiols with conjugated molecules. Exchange of alkylthiols with a dithiolated oligo(phenylene ethynylene) (OPE) leads to a drastic increase in conductance.<sup>[49, 50]</sup>

### 1.1.1.2 Contacting Single Molecules with Electrodes

All of the previously discussed techniques have been elaborated to contact ensembles of molecules. Contacting individual molecules is very challenging due to the minute size of molecules, and the large size of electrodes. First attempts to address individual molecules relied on isolated molecules in mixed SAMs, which were addressed with bulk contacts (E and F in Figure 3). To directly contact single molecules atomic sized contacts are required, and will be discussed secondly (G and H in Figure 3).

#### 1.1.1.2.1 Addressing Isolated Molecules

##### *E. Scanning tunneling microscopy*

Scanning tunneling microscopy (STM) was used to analyze few or even individual molecules.<sup>[54]</sup> STM measures the topography by monitoring a feedback loop that maintains a constant tunneling current. This technique has the advantage of being able to image and to measure the transport properties of individual molecules, however, the interpretation of the I/V-characteristics is complicated. Using directed self-assembly, individual molecules can be isolated either as individual molecules or in small bundles in an insulating SAM matrix and addressed by STM for characterization (Figure 6).

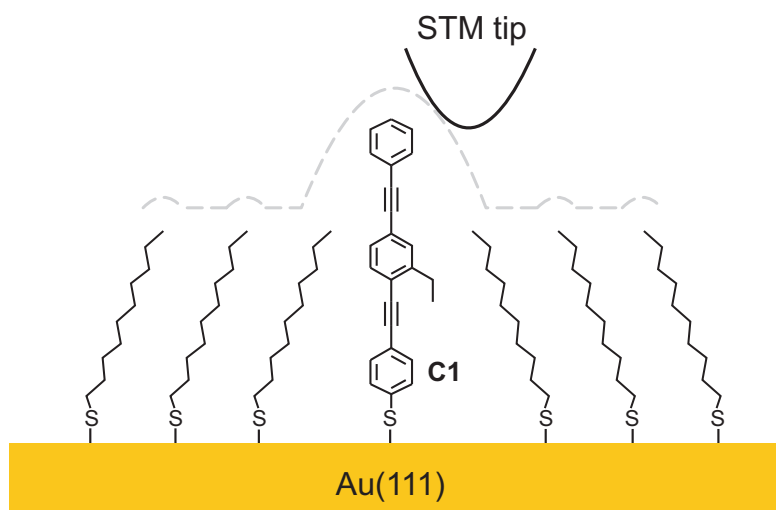


**Figure 6:** Schematic representation of the STM-carpet approach. The conjugated OPE **C1** is inserted into an insulating SAM of decanethiol and then probed with an STM tip.

Bumm and coworkers investigated the conjugated molecule **C1** in a SAM of insulating decanethiol. The molecule **C1** was identified by imaging and by measuring

the apparent tunneling barrier height (ATBH). The ATBH over the wire **C1** was at least twice the height of the surrounding decanethiol SAM matrix. This higher relative ATBH, when concurrent with greater tip substrate separation, indicates that the junction contains regions of higher conductivity when over a wire. This STM-carpet approach allowed addressing individual molecules and deducing the relative conductivity, even though only qualitatively but not quantitatively. The molecules are not connected to both ends because metal-molecule-gap-tip junctions are formed.

#### *F. Gold nanoparticle coupled conducting probe atomic force microscopy*

Conducting probe atomic force microscopy (cp AFM) was used to address single molecules. To overcome the limiting problem of large cp AFM tips ( $\approx 15 \text{ nm}^2$ ), gold nanoparticles were placed on 1,8-dithioloctane isolated in an 1-octanethiol SAM (Figure 7).<sup>[55]</sup>

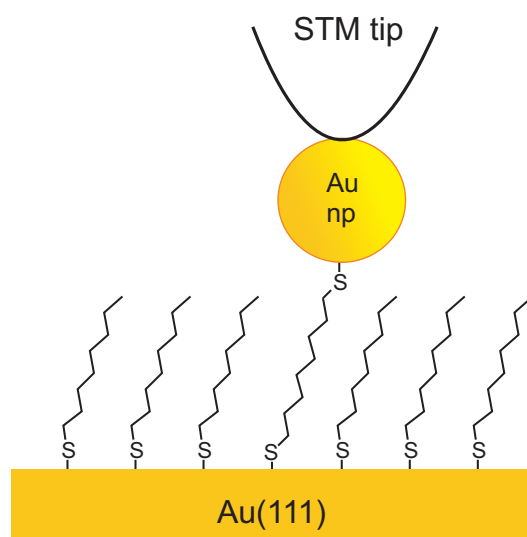


**Figure 7:** Gold nanoparticles are placed on isolated dithiolalkanes to form metal-molecule-metal junctions which are probed with cp AFM.

The gold nanoparticles are covalently bound to the molecules leading to a metal-molecule-metal junction that can be probed by cp AFM. A significant advantage of this technique is the ability to measure single molecules without a tunneling junction. However, it can not be excluded that the nanoparticle is bound to only one molecule.

### 1.1.1.2.2 Atomic Sized Contacts to Connect Single Molecules with Electrodes

To directly address single molecules, atomic sized contacts are required. This was realized by mechanically controllable break junction (MCBJ) or STM break junction techniques. However, reducing the size of an electrode down to single atoms leads into the quantum regime which drastically changes electron transport behavior.

In a macroscopic regime, the conductance  $G$  of a conductor is defined as the ratio between the current  $I$  passing through it and the applied bias voltage  $V$ .

$$G = \frac{I}{V}$$

The linear increase of  $I$  with applied voltage  $V$  and the constant conductance  $G$  is known as Ohm's law. Ohm's law typically holds true in macroscopic devices, however drastically changes when the size of conductor decreases. In a macroscopic conductor, electrons travel in a diffusive manner. Macroscopic conductors consist of a pool of electrons and the electrons passing through the conductor have an average elastic mean free path  $l$  (classical Ohm's law). The conductance  $G$  is directly proportional to the transverse Area  $A$ , inversely proportional to the sample length  $L$  and depends on the materials conductivity constant  $\sigma$ .

$$G = \frac{\sigma A}{L}$$

However, when the size of the conductor decreases and the elastic mean free path  $l$  becomes larger than  $L$ , the electrons travel in a ballistic way (Figure 2) and the Ohm's law is no longer valid.

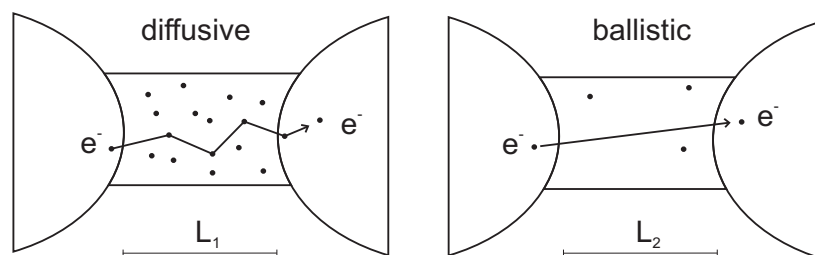


**Figure 8:** Diffusive vs. ballistic electron transport. Note that  $L_1 \gg L_2$ .

In an atomic sized contact, the contact width is in the range of the de Broglie Wavelength  $\lambda_F$  and we enter into a quantum regime. In this quantum regime the current flows as a transmission process described by the Landauer formula. With the assumption of a one-dimensional conductor with one conductance channel, the Landauer formula can be solved to give

$$G_0 = \frac{2e^2}{h} = 77.5 \mu S$$

(where  $e$  is the electron charge and  $h$  is Plank's constant)

The conductance of a single atom is therefore limited, and characterized as  $G_0$ . The conductance of a small molecule can not overcome  $G_0$ .

### *G. Mechanically controllable break junction*

Mechanically controllable break junction (MCBJ) is an approach to form symmetrical atomic sized electrodes.<sup>[18, 56-62]</sup> The principle of an MCBJ is depicted in Figure 9 A. A metal lead with a free-standing constriction in its middle (80-150 nm wide) is fabricated on an electrically isolated, flexible spring-steel substrate. A scanning electron microscope (SEM) image of a microfabricated gold structure is shown in Figure 9 B. By mounting the substrate in a three point bending mechanism, the constriction can be stretched and eventually broken. This results in two atomic gold tips which can be brought back into contact by relaxing the substrate. The gap distance  $d$  between the electrodes can be adjusted in the range of 0.1 nm by controlling the pushrod position, therefore the two tips of the broken wire form ideal electrodes to contact single molecules.

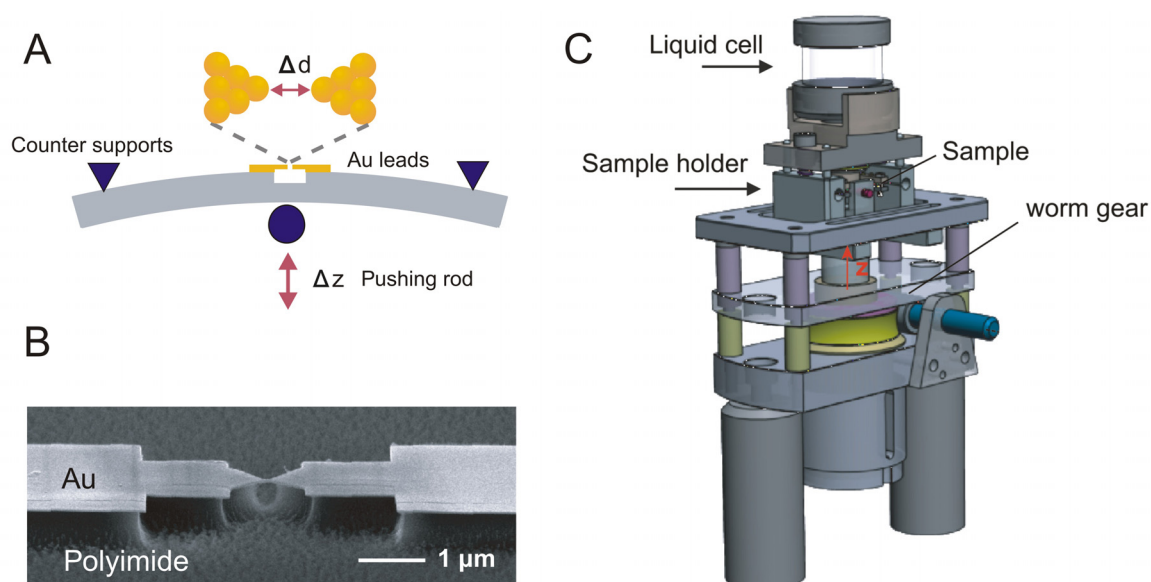


**Figure 9:** **A)** Schematic representation of the three-point bending mechanism. While the counter supports fix the sample, the  $\Delta z$  position can be varied by changing the position of the pushing rod, resulting in a tip to tip distance change ( $\Delta d$ ) in a picometer regime. **B)** An SEM image showing a microfabricated gold structure. **C)** MCBJ setup comprising a liquid cell, sample holder and pushing rod motor (worm gear).

Calame and coworkers developed an MCBJ setup within a liquid environment.<sup>[60]</sup> The setup of the MCBJ (Figure 9 C) comprises a liquid cell placed on the sample. This enables conductance measurements within a liquid environment and investigations of molecules in solution. With the worm gear, the position of the pushing rod can be varied. The conductance  $G(z)$  of the suspended gold bridge can be measured during the breaking process controlled by a vertical pushrod movement  $z$ . In a first instance the breaking process of the gold fabricate is investigated in pure solvent. While the substrate is bended the Au bridge is stretched (C in Figure 4) and the conductance  $G(z)$  decreases. In Figure 4 A and B three typical conductance traces are shown. When the bridge enters in the range of several strands of Au atom chains, the decrease evolves in conductance plateaus (1 in Figure 10). By further bending, a so called “last plateau” is obtained, where  $G = G_0$ .

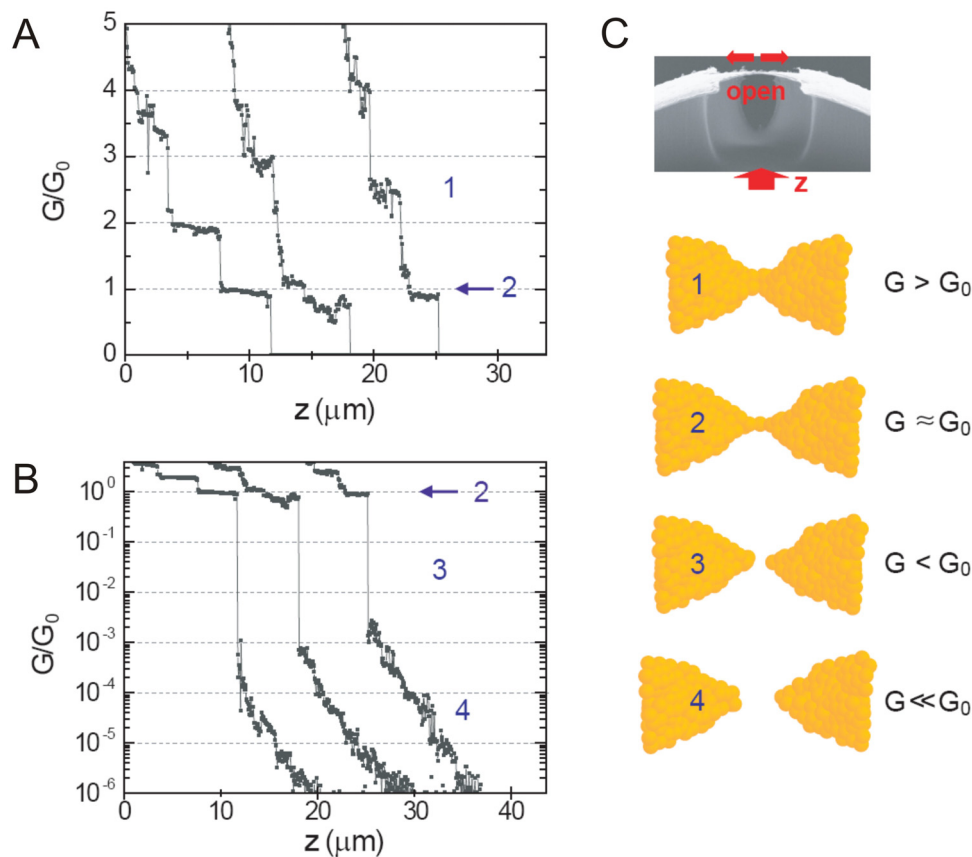


**Figure 10:** Three typical conductance traces are shown in A and B. The conductance is recorded as a function of  $z$ .  $G(z)$  decreases when stretching the gold structure and conductance plateaus are obtained when the gold bridge consists of few gold-strands (1). The “last plateau” is obtained when one single atom is contacted (2) and has the value of  $G_0$ . Upon further breaking the bridge breaks, resulting in a abrupt current down jump (3) followed by an exponential decay curve characteristic for the tunneling regime (4).



This last plateau corresponds to a single Au atom (2 in Figure 10). When the bridge is further elongated, the contact breaks resulting in an abrupt decay of conductance (3 in Figure 10) caused by a sudden contraction and rearrangement of the Au atoms. The down jump of conductance typically stops at a value of  $G \approx 10^{-3} G_0$ , when electron tunneling sets in. The tunneling current exponentially decays with the gap distance  $d$ .

To form metal-molecule-metal junctions 1,8-dithiioctane was investigated as model compound.<sup>[63]</sup> While the current exponentially decayed after breaking the last gold-gold bridge in absence of molecules, plateaus in the conductance traces with conductance values below  $G_0$  were obtained when 1,8-dithiioctane was exposed to the setup (Figure 11). In about 50% of the recorded current traces distinct plateau features appeared. Some of the plateaus were clean (blue in Figure 11), others were noisier (red in Figure 11). The other 50% of the conductance traces showed irregular decay curves, attributed to poor junction formation (green in Figure 11).

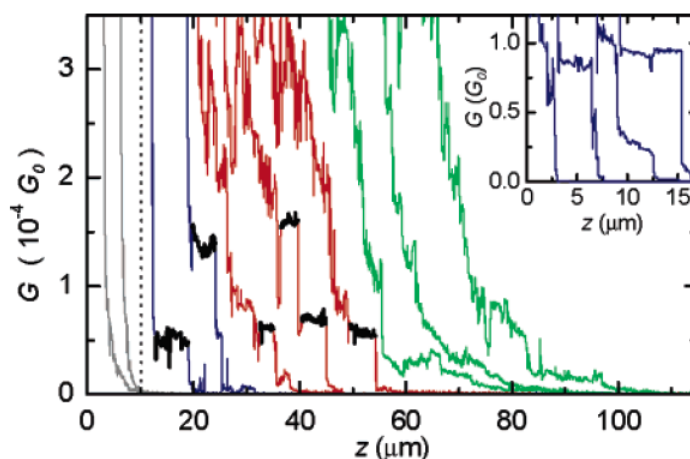


**Figure 11:** Conductance traces recorded during the breaking process.<sup>[64]</sup> When only solvent molecules were present, exponential decay curves were obtained (gray). When 1,8-dithiioctane was exposed to the junction, plateaus were obtained in about 50% of the conductance traces. Some plateaus are clean (blue) and others are noisier (red). The other 50% of the conductance traces show irregular decay (green).<sup>[63]</sup>

These plateaus are the signature of single (or few) molecules. The plateaus are understood to be a stable metal-molecule-metal junction. The sulfur-gold bond is stable, however the gold atoms are mobile and the two electrode tips can rearrange. By increasing  $z$ , the gold atoms of the electrode tips rearrange, however the effective metal-molecule-metal junction remains the same leading to the same conductance value for a distinct  $z$  integral, observed as a plateau in the current trace. Similar to

atomic junctions, this-metal-molecule-metal bridge holds the two sides together via its chemical bonds and postpones the breaking.

Due to fluctuations in the conductance curves of the single molecule junctions, a statistical analysis is necessary. Therefore, hundreds of current traces were recorded, and the current traces were projected to the conductance axis. Doing so, histograms are obtained with peaks where plateaus were present. The forthcoming histograms were calculated for all the current traces, not just those showing plateaus. All data were factored into the histogram formation and no selection was made, except for subtracting the background. No peaks appeared in the histogram of the measurement of pure solvent, however, distinct peaks were obtained in the measurement of 1,8-dithioloctane, indicated by the arrows in Figure 11 (a). This suggested that particular molecular configurations were formed with a high probability.

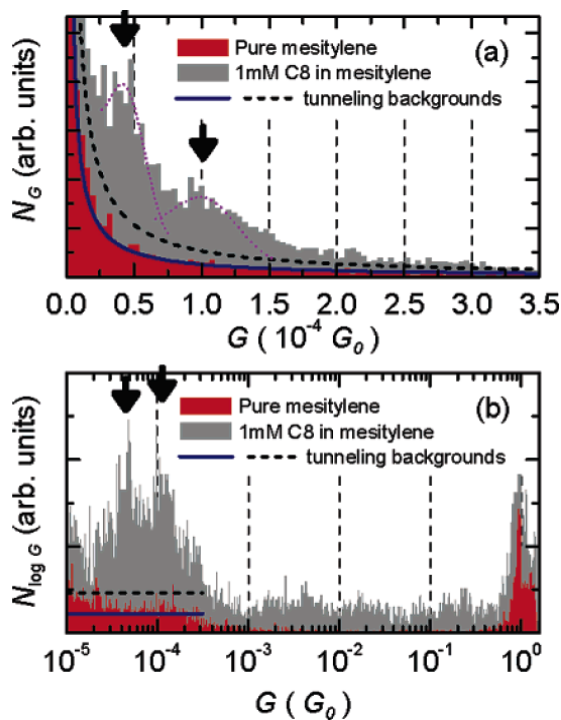


**Figure 12:** Conductance histograms built from approximately 100  $G(z)$  curves in pure solvent (red) and in a solution of 1,8-dithioloctane (gray). The arrows indicate the conductance peaks that appear when octanedithiol is added in solution. (b) Histograms of  $\log G$  built from the same data as in (a).<sup>[64]</sup>

However, the peaks in Figure 11 (a) were masked by a strong background, therefore a data processing method was performed.<sup>[64]</sup> The data is most convincingly represented in a  $\log G$  histogram rather than in a  $G$  histogram. A  $\log G$  histogram of 1,8-dithioloctane is shown in Figure 11 (b). Without any data selection, distinct peaks

were obtained. Besides the peak at  $G_0$  (corresponding to the last gold-gold contact) two peaks were observed, indicated with the arrows, from which the last peak was attributed to a single metal-molecule-metal contact.

How do we know that only one molecule is connected to the electrodes? Reichert and coworkers performed MCBJ measurements at low temperature under high vacuum. Current-voltage ( $I/V$ ) characteristics of spatially symmetric and asymmetric but otherwise similar molecules (**C2** and **C3**, Figure 13) were investigated.<sup>[57]</sup> The  $I/V$ -curves of the symmetric molecule **C2** were symmetric (A in Figure 13). While exploring the  $I/V$ -characteristics of **C3**, interesting asymmetric features were obtained (B in Figure 13).

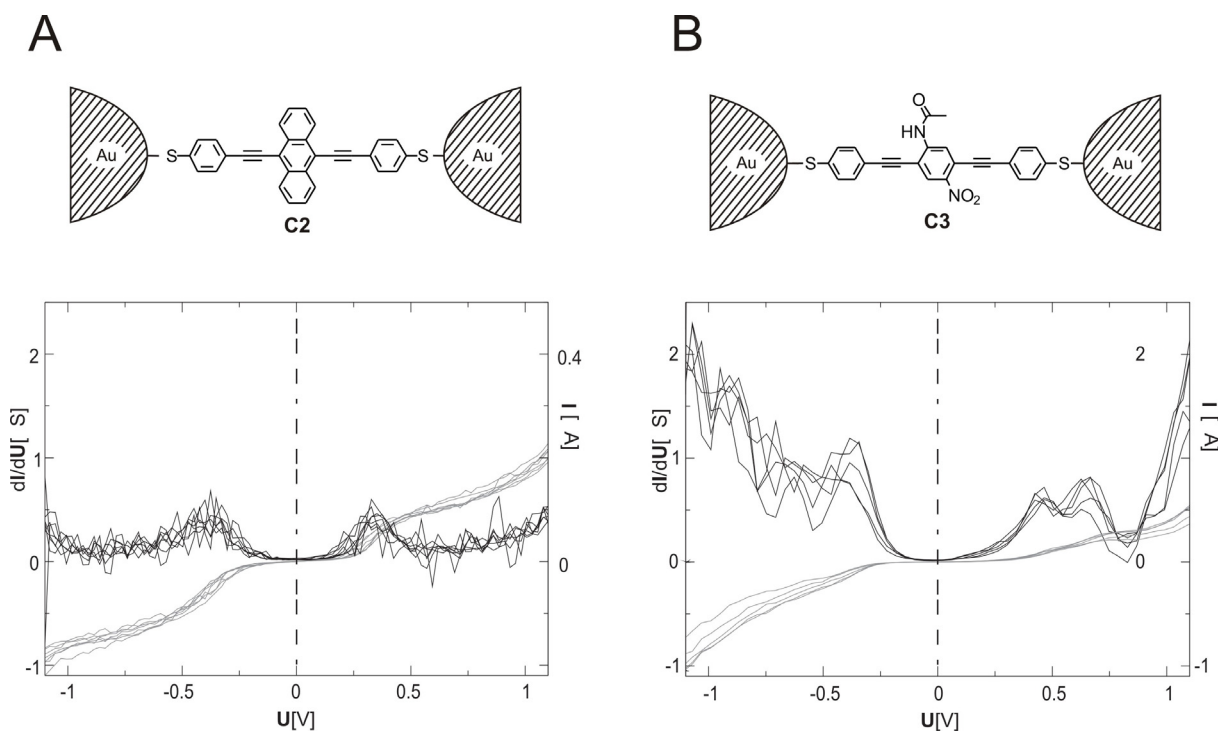


**Figure 13:** The molecules **C2** (symmetric) and **C3** (asymmetric) were investigated in an MCBJ.<sup>[57]</sup> The  $I/V$ -characteristics of **C3** showed asymmetric features revealing that single molecules are connected to the gold electrodes.

If several molecules were forming the junction, the asymmetric features would be canceled due to a random alignment between the electrodes. The fact the measured  $I/V$ -characteristics were asymmetric unambiguously demonstrated that the electron transport through a single molecule and not a large ensemble of molecules was measured.

### H. STM break junction

An STM break junction approach was also reported to form junctions suitable for single molecule investigations.<sup>[54, 55, 65]</sup> Tao and coworkers improved the technique such, that due to repeated formation and breaking of the STM break junction a statistical analysis of single metal-molecule-metal contacts was made. In their setup an STM tip is placed above a gold substrate (A in Figure 14) and then piled into it (B in Figure 14). While keeping a constant x-y-position, the STM tip is then gently lifted. Due to the mobility of gold, the atoms migrate towards the tip such that single gold atoms bridge the STM tip with the substrate (C in Figure 14). Further lifting of the tip causes the gold structure to break and two atomically sharp electrodes are formed, suitable to contact single molecules (D in Figure 14). When the tip moves to its initial position (E in Figure 14) the metal-molecule-metal junction breaks and the process is repeated several times to get statistical analysis. Doing so, the conductance of a single bipyridine molecule was deduced.<sup>[65]</sup>

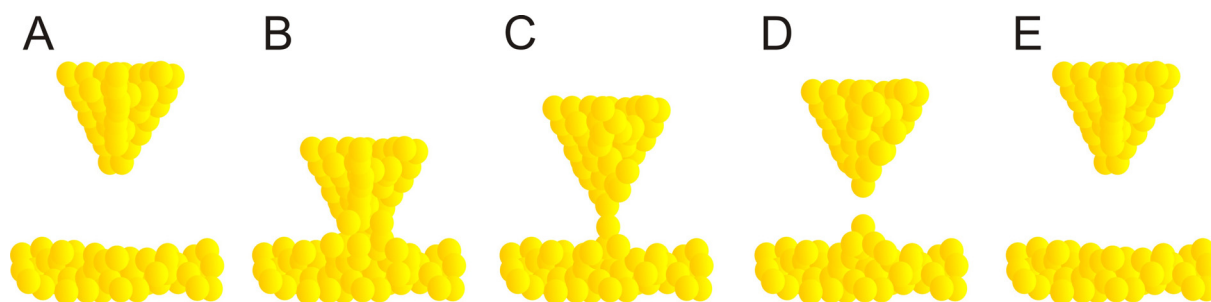


**Figure 14:** STM break junction approach. The STM tip is placed over the gold substrate (A) and then piled into the substrate (B). While keeping a constant x-y-position the tip is lifted. Due to the mobility of gold the atoms migrate toward the tip (C). At one point the gold structure breaks and two ideal electrodes to form metal-molecule-metal junctions are formed (D). After further pulling apart, the tip is again in its initial position.

### 1.1.2 Correlating Molecular Structure with Electronic Properties

The achievement to contact small assemblies of molecules or even single molecules enables investigating correlations on electronic properties with molecular structure. Factors that influence the current-voltage characteristics of molecules include intrinsic properties such as molecular length and conformation. In addition, the type of molecule-electrode contact affects the electronic properties.

The transport through individual molecules connected between electrodes is expected to be different from bulk transport because of the inherently small size of molecules. The conductance  $G$  through a molecule with a distance  $d$  is described in the tunneling physics theory by the Landauer formula as:

$$G = A \cdot e^{-\beta d}$$

The decay constant  $\beta$  is determined by electronic parameters of the molecule backbone.  $A$  is the prefactor and depends on the electron density-of-states at the point where the molecule contacts the electrodes.

Increasing the length of a molecule and therefore the electronic pathway electrons have to tunnel through, the conductance decreases exponentially.<sup>[66-68]</sup> Alkanethiols served as ideal model compounds to investigate the dependence of current on molecule length. The length can be systematically varied without affecting the molecule's backbone and therefore keeping the decay constant  $\beta$  constant. Independent of the metal contacts (gold, mercury), the integration setups (cp-AFM, mercury droplet junction, STM, crossed-wire junction) and the number of contacted molecules, the conductance decreases exponentially with increasing molecular length  $d$ .<sup>[68]</sup>

Considering the Landauer formula, it is obvious that the anchor groups of a molecule are not only for fixing the molecule to the electrodes, they also provide electronic coupling between the molecule and electrodes.<sup>[69]</sup> It is important to design proper molecule-electrode contacts because the contacts play a critical role in the electron-transport properties of molecules.<sup>[70-75]</sup> To date, the most widely used anchoring groups to adsorb on gold surfaces are thiols,<sup>[76, 77]</sup> although pyridine,<sup>[78]</sup> isocyanides,<sup>[71, 79]</sup> selenium<sup>[80-82]</sup> and amines<sup>[83]</sup> have also been studied. Anchoring group effects on single-molecule conductance were systematically investigated in an STM break junction.<sup>[76]</sup> *n*-Alkanes were chosen as model compounds, because by varying the number of CH<sub>2</sub> groups it was possible to isolate the molecule-electrode

contact effects from other factors. Three anchor groups, thiols, amines and carboxylic acids were compared.

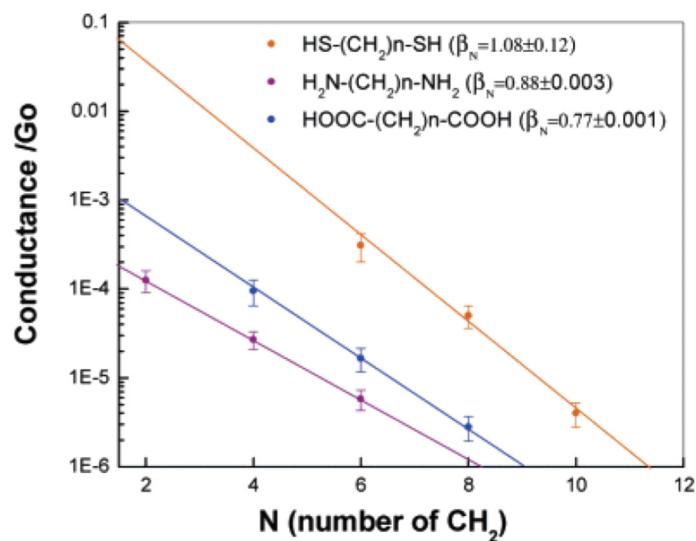
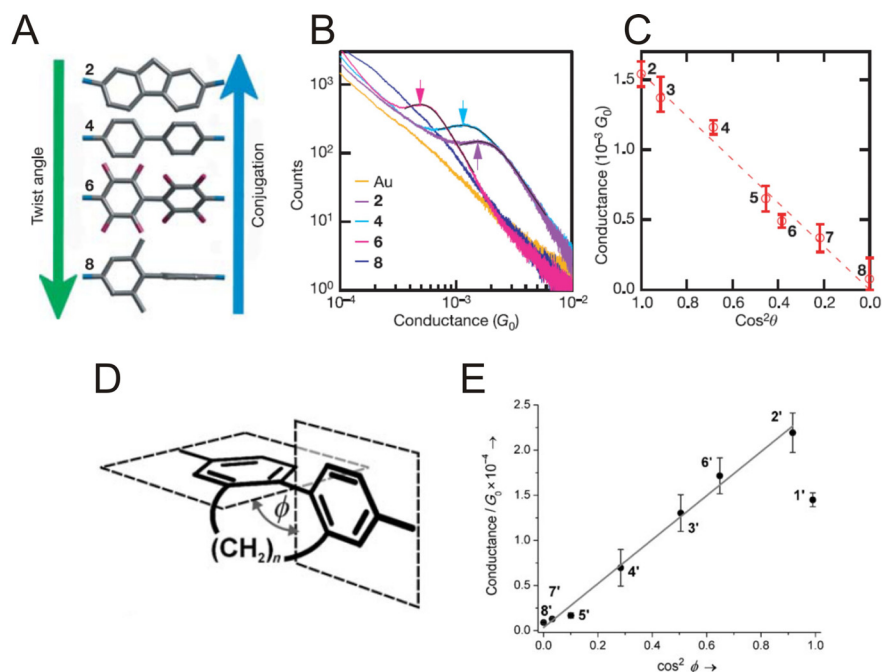


Figure 15: Logarithmic plots of single-molecule conductance vs. molecular length for dithiol- (orange), diamine- (blue), and dicarboxylic-acid-terminated (purple) alkanes. The conductance decreases exponentially with increasing length.<sup>[70]</sup>

For each anchor group the conductance decays exponentially with molecular length. The prefactor  $A$  is highly sensitive to the type of anchoring group, and varies in the order of  $\text{Au-S} > \text{Au-NH}_2 > \text{Au-COOH}$ . This large dependence is attributed to different electronic coupling efficiencies provided by the different anchor groups. Binding strength information was obtained by measuring the average length over which one can stretch each molecular junction until it breaks. The binding strength varies in the order of  $\text{Au-S} > \text{Au-NH}_2 > \text{Au-COOH}$ .

Considering compounds comprising more than one aromatic ring in the electron pathway, the effect of the angle between the rings was investigated.<sup>[84-86]</sup> Venkataraman and co-workers reported on the interdependence between the calculated molecular conformation and the single-molecule conductance of a series of various substituted biphenyls bearing terminal amino groups.<sup>[84]</sup> Despite several varying parameters such as electron density on the phenyl rings and steric repulsion of the substituents, a linear correlation was found between the conductance and the square of the cosine of the calculated torsion angle  $\Phi$  between the planes of the two rings (Figure 16 C). Vonlanthen *et al.* systematically investigated the effect of torsion angle on thiol anchor groups comprising biphenyl systems.<sup>[86]</sup> The torsion angle was

chemically controlled while bridging the two phenyl units with different length alkyl chains and was experimentally obtained from the X-ray structures (D in Figure 16). The conductivities of the thiol terminated biphenyls were deduced from single-molecule junctions by STM break junction measurements and linearly correlated with  $\cos^2(\phi)$  (E in Figure 16).



**Figure 16:** The effect of the torsion angle of a biphenyl system on the conductance was investigated in amine terminated biphenyl systems<sup>[84]</sup> (A, B, C) and in thiol terminated biphenyl structures with a fixed torsion angle in STM break junctions.<sup>[86]</sup> While increasing the torsion angle, the conjugation is reduced (A) which leads to a decrease in conductance (B). The conductance linearly correlates with the cosine of the square of the torsion angle.

The electric current through a molecular rod was investigated in relation to the position of the anchor group. Two rods consisting of a conjugated  $\pi$ -system comprising two thiol anchor groups either in *meta*- or *para*-position were investigated in an MCBJ setup (Figure 17).<sup>[87]</sup>

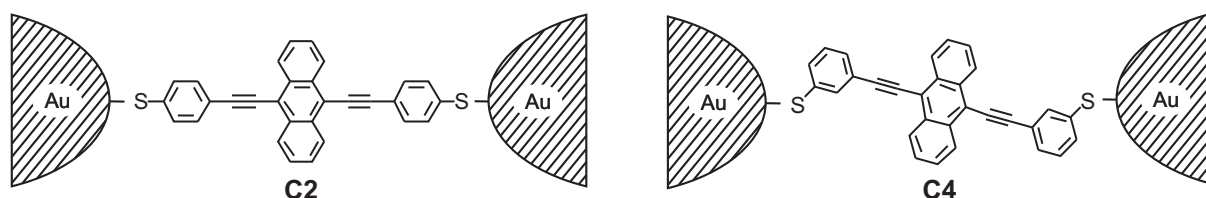


**Figure 17:** The conductance through a molecule was investigated in relation to the position of the anchor groups. **C2** bears the thiol anchor groups the in *para*-positions and is better conducting than **C4** with the thiol anchor groups the in *meta*-positions.

The *para*-substituted compound **C2** was found to be better conducting than the meta-functionalized compound **C4**, which is attributed to decoupling the molecule from the electrodes while breaking its conjugation.

These selected examples indicate that electronic properties can be tuned by carefully designing molecular structures. The very rich palette of functional groups provides an infinite variety of molecular structures which are accessible by synthetic organic chemistry. Molecules are very promising objects for future applications in nanotechnology because not only their structure, but also their properties can be tailored.



### 1.1.3 Basic Electronic Functions Transferred to a Molecular Level

The most fundamental electronic function is charge transport, classically realized by wires and conductors between subunits. Molecular wires have been suggested and investigated as interconnectors on the nanometer scale. Saturated alkanes turned out to be poor conductors, but very useful models for both theoretical and experimental investigations.<sup>[55, 65, 68, 71, 76, 88, 89]</sup> To improve electronic communication over larger distances, delocalized  $\pi$ -systems with smaller HOMO–LUMO gaps are more promising.<sup>[5]</sup> Increased electron mobility, in the range of classical semiconductors, have been observed for delocalized  $\pi$ -systems.<sup>[12, 27, 54, 57, 68]</sup> Arranged with increasing complexity in terms of electronic functions, the next basic electronic feature is rectification, followed by bistable switching devices providing two different transparencies for the electronic current which can be altered by a stimulus. Even though numerous other electronic devices based on molecules such as insulators<sup>[90]</sup> or transistors<sup>[91, 92]</sup> showing either Coulomb blockade<sup>[46]</sup> or the Kondo effect<sup>[46, 93]</sup> have been proposed and investigated, the next part of the introduction will focus on molecular rectifiers and switches.

#### 1.1.3.1 Molecule Based Rectifying Systems

Rectification is a process of an electronic device which shows an asymmetric current response upon an applied bias voltage. It is one of the fundamental electronic functions which are used in electronic circuitry. A rectifier allows the current to pass in one direction better than in the other. In industry, vacuum tube diodes or nowadays p-/n-doped silicon semiconductor diodes are important parts in devices used to convert alternating current (AC) to direct current (DC), as components of power supplies or as detectors, respectively. In the field of molecular electronics metal-molecule-metal junctions are considered as molecular rectifiers. Inspired by the solid-state semiconductor industry where p-n-junctions consisting of electron poor (p-type) and electron rich (n-type) subunits are used as rectifiers, Aviram and Ratner proposed a molecular rectifier with an acceptor-bridge-donor (A- $\sigma$ -D) geometry (Figure 18).<sup>[20]</sup> Electron withdrawing groups (EWG) or electron donating groups (EDG) can be placed in a molecule such, that acceptor (A) and donor (D) sites result.

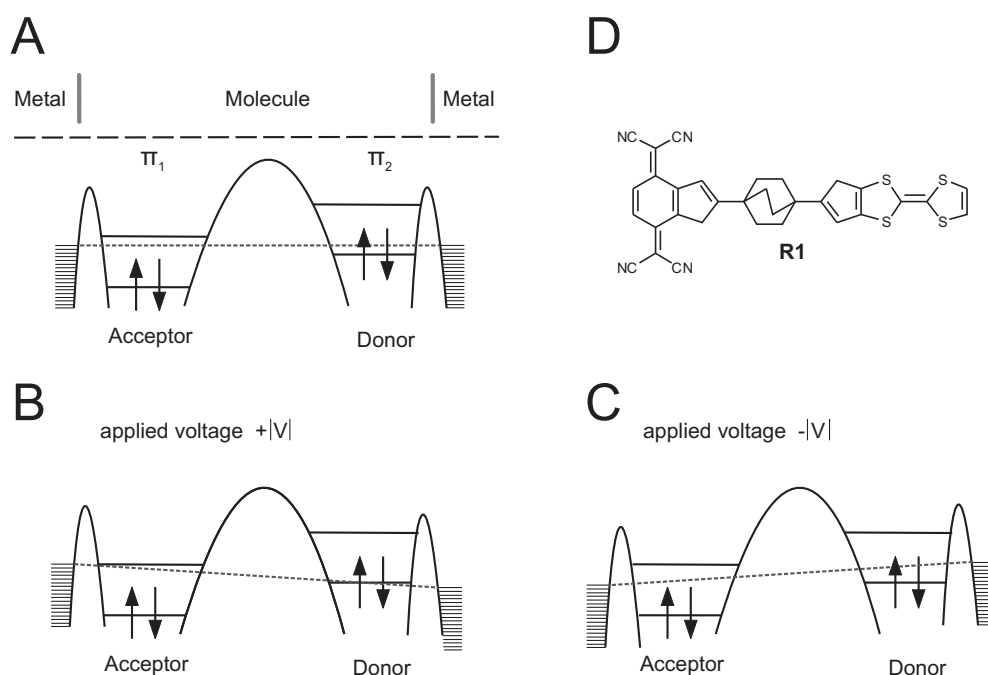
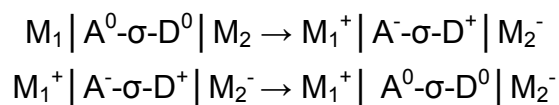


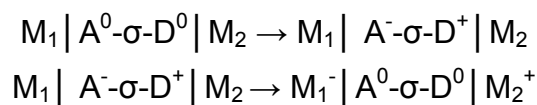
**Figure 18:** Proposed molecular rectifier (D) and a schematic representation of the energy levels without applied potential (A) and with applied potential (B and C).

The proposed molecular rectifier **R1** consists of a tetracyanoquinodimethane (TCNQ) acceptor site and a tetrathiafulvalene (TTF) donor site (Figure 18 D). As separators of the A- and D- $\pi$ -levels, sigma-electron systems should be feasible, however to assure rigidity, a 1,4-disubstituted bicyclo[2.2.2]octane bridge was suggested. In Figure 18 A a schematic representation of the energy levels of **R1** without applied voltage is depicted. Having a metal |A- $\sigma$ -D| metal junction electrons are allowed to pass from a cathode to the acceptor site and from the donor to the anode, but not in the other direction (B and C in Figure 18). The bridge is needed to separate the A and D. If the two units are connected too close to each other only one single donor level exists, however if they are too far apart no communication between the acceptor and the donor takes place. In a Gedankenexperiment, the proposed molecular rectifier **R1** was fixed between two metallic electrodes to form a metal-molecule-metal junction and the response to an applied field was calculated. The calculations proposed that the current flows at a lower voltage from one electrode  $M_1$  to the other electrode  $M_2$  than in the other direction (from  $M_2$  to  $M_1$ ), hence rectifying properties were predicted. Their semiquantitative calculations involve a mechanism where the electron transported between the metal electrodes  $M_1$  (e.g. cathode) and

$M_2$  (e.g. anode) first induces the formation of an excited state. After relaxation, the electron has moved, in this case, from electrode  $M_1$  to electrode  $M_2$ .



An alternative mechanism referred to as “Anti-Aviram-Ratner”<sup>[29, 94, 95]</sup> mechanism involves first the formation of the excited state of the molecule followed by the transfer of the electrons, which leads to current flow in opposite directions. However, in these first calculations by Aviram and Ratner, the “Anti-Aviram-Ratner” mechanism was believed to be a minor process.



The feasibility of molecules as building blocks in electronic devices, postulated in this pioneering work encouraged many scientists to search for suitable molecular systems and experimental integration setups. Indeed, several examples of molecular rectifiers, either investigated as molecular films prepared from self assembled monolayers (SAMs) or Langmuir-Blodgett (LB) films, or even as single molecules (unimolecular rectifiers) were reported and will be discussed in the following.

In all of the reported molecular rectifiers, rectification is found as a result of three possible processes.<sup>[29, 96]</sup> Chemisorbed molecules form bonds to the metal electrodes which lead to formation of Schottky barriers. When the two anchor groups are not the same or if different metal electrodes are used, the arising dipole moments are different which results in an asymmetric current. A second mechanism leading to rectification is asymmetric alignment of the chromophore between the two electrodes. This is often the case in physisorbed methods, as e.g. alkyl chains are used to form stable LB-films but then force the molecule to be asymmetrically placed between electrodes. Unimolecular Rectification, a third process, occurs when the electron transfers between orbitals with asymmetrically placed significant probability amplitudes.<sup>[97]</sup> While rectification in a metal-molecule-metal junction might arise from several described processes, unimolecular rectification remains the main goal to be achieved.

As mentioned above, several rectifying systems based on molecules have been reported. While organic rectifying junctions with evaporated molecular films (with a thickness of 200 – 2000 nm) were already investigated by Meinhard in the 1960's,<sup>[98]</sup>

it was Metzger who published the first example of molecular rectification.<sup>[21, 99]</sup> Metzger investigated hexadecylquinolinium tricyanoquinodimethanide ( $C_{16}H_{33}Q-3CNQ$ ), a molecule consisting of a positively charged quinolinium part and a negatively charged dicyanomethylene moiety, bridged by a twisted  $\pi$ -unit (**R2**, Figure 20). The alkyl groups are introduced to achieve LB-forming properties. Self-assembled LB-monolayers of  $C_{16}H_{33}Q-3CNQ$  were sandwiched between two metal electrodes and the electronic properties were investigated. As predicted, metal-molecule-metal junctions with aluminum electrodes showed rectification ratios (RR, defined as the current at a positive potential  $V$  divided by the absolute value of the current at the corresponding negative bias  $-V$ ) of about 27.<sup>[99]</sup>

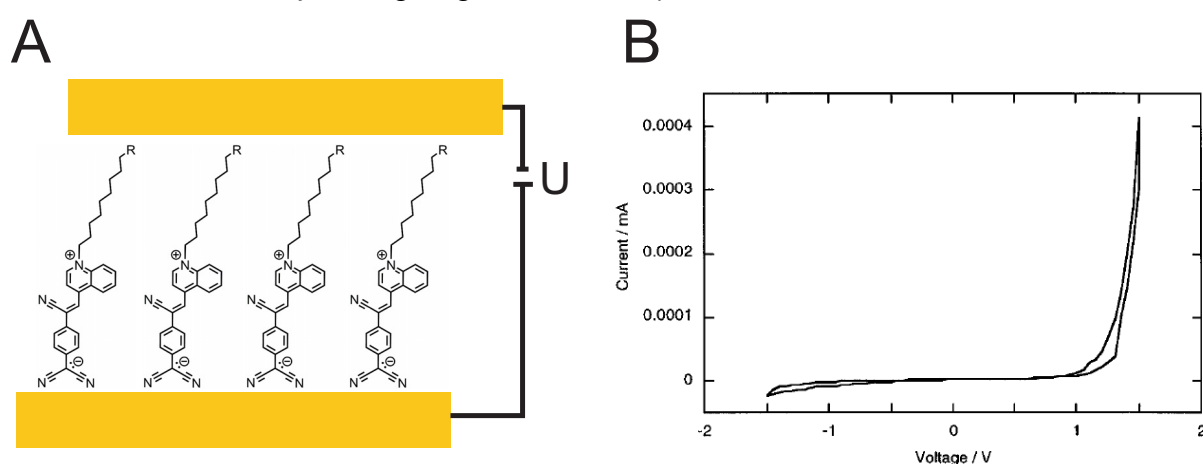


**Figure 19:** LB-monolayers of **R2** ( $R = (CH_2)_6CH_3$ ) were sandwiched between two alumina electrodes and revealed an asymmetric  $I/V$  behavior with a RR of 27.<sup>[99]</sup>

Similar values were obtained when using gold electrodes instead of aluminum.<sup>[100, 101]</sup> Due to rearrangement of the physisorbed molecules in the electric field upon repeated cycling, the  $I/V$ -curves show progressively less asymmetry and devices show very limited stability features. Even though the dipole moment of the zwitterion and the LB-forming properties of the alkyl chains were the main design criteria, rectification is rather explained by the asymmetric proximity of the  $\pi$ -chromophore to one electrode.<sup>[102]</sup>

After this proof of concept, several D- $\sigma$ -A based rectifiers prepared from LB films with different donor/acceptor systems based on aniline/fullerene,<sup>[103, 104]</sup> aniline/pyridinium,<sup>[105]</sup> perylenebisimide/ferrocene,<sup>[106]</sup> and TTF/fluorenone<sup>[96, 107]</sup> derivatives were reported. Further, monomolecular LB-films of amphiphilic conjugated diblock oligomers, consisting of an electron-rich oligo(3-alkylthiophene) as the donor block and an electron-poor oligo(4-alkylthiazole) as the acceptor block,

were investigated using scanning tunneling microscopy (STM) and scanning tunneling spectroscopy (STS) to induce rectification.<sup>[22]</sup>

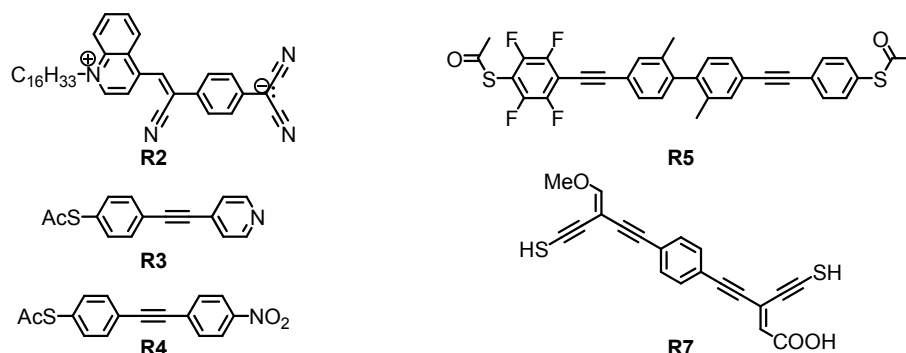


**Figure 20:** Investigated molecular rectifiers **R2** – **R5** and **R7** which are discussed in the text.

Exploiting different metal-molecule contacts, Kushmerick *et al.* investigated SAMs of oligo(phenylene ethynylene) (OPE) within a crossed-wire junction (**R3** & **R4**, Figure 20).<sup>[108]</sup> All investigated OPEs were fitted on one side with a thiol anchor group, whereas the opposite anchor group of the rod was either a nitro group or pyridine.

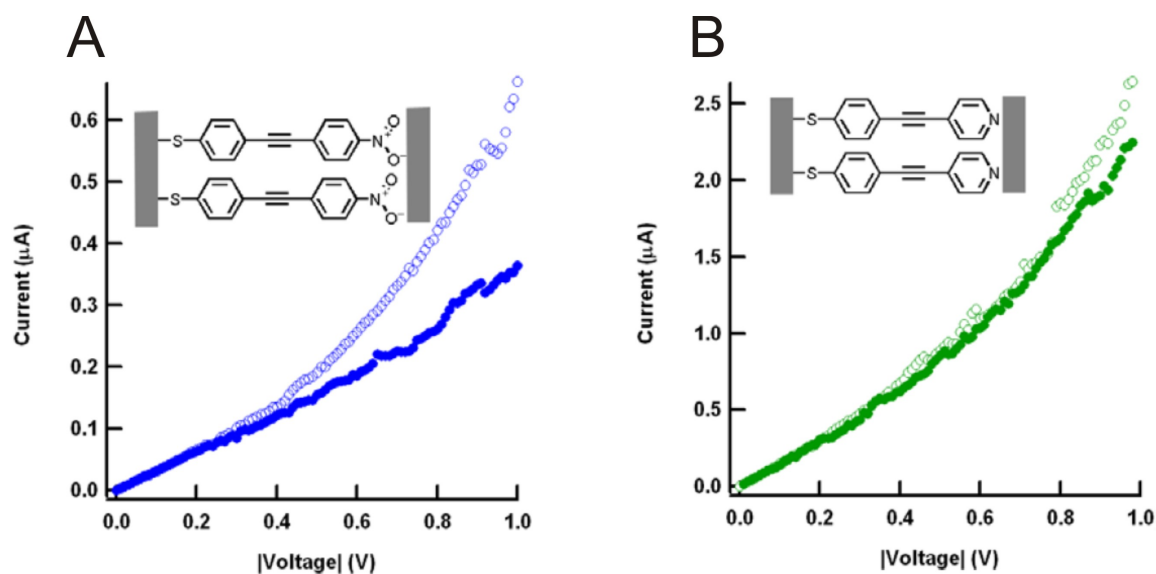


**Figure 21:** SAMs of OPE **R3** (B) and **R4** (A) were investigated in a crossed-wire junction. Transport characteristics of Au-**R3**-Au (B) and Au-**R4**-Au (A) were asymmetric. The open symbols correspond to electron injection of the gold-nitro (A) and gold-pyridine (B) interface, respectively. The close symbols correspond to electron injection of the gold-sulfur interface.

An advantage of crossed-wire junctions is, that the wires can be individually functionalized. Hence, the molecules were self assembled on the bottom electrode via SAM formation and then topped with the second wire. In doing so they were able

to know exactly on which contact the thiol and on which the pyridine/nitro anchor groups are bonded. Electrons were easily injected at the gold-nitro and gold-pyridine interface (open symbols in Figure 21 A and B) than in the other direction (full symbols in Figure 21 A and B). The asymmetric coupling to the electrodes resulted in asymmetric I/V-characteristics and rectification was obtained (Figure 21). Also in other systems it has been noted that asymmetric coupling to the electrodes leads to an increased rectification ratio.<sup>[109-112]</sup>

After the pioneering work of Aviram and Ratner in 1974 about molecular rectifiers,<sup>[20]</sup> several examples of molecular diodes have been reported. However, in all of the reported systems, assemblies of molecules were investigated, and it took over 30 years until a prototype of a single molecular rectifier was synthesized and investigated by Elbing *et al.*<sup>[113]</sup>

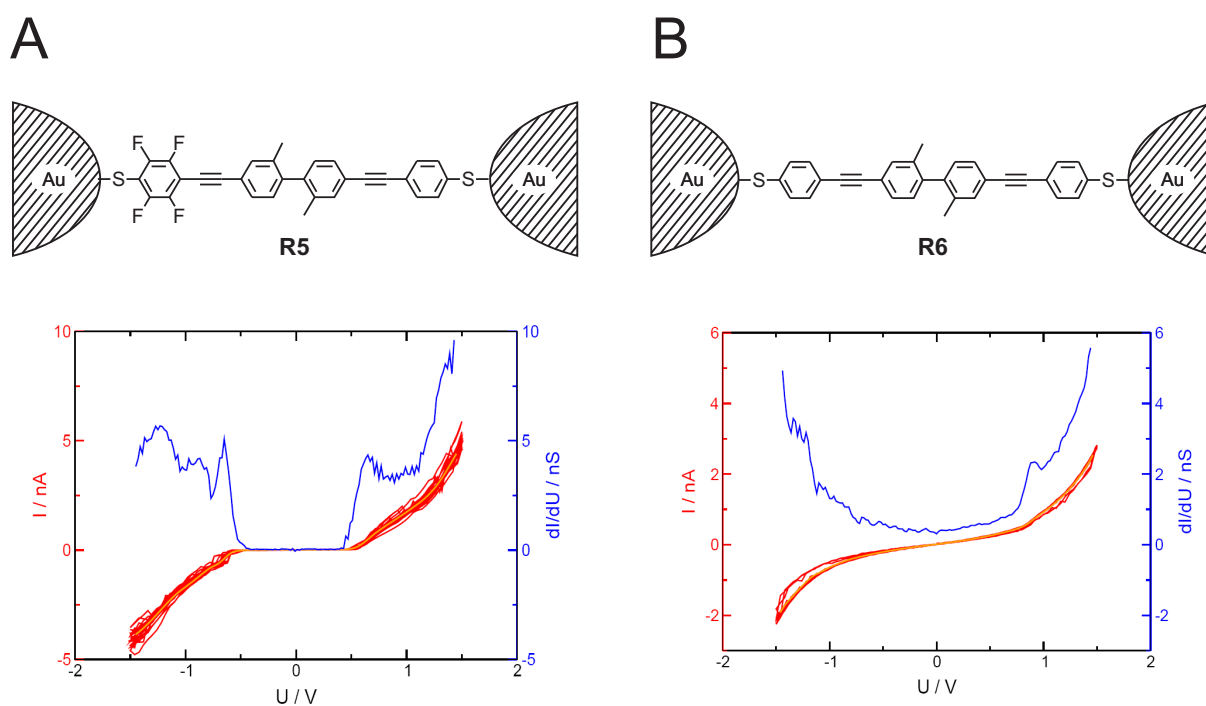


**Figure 22:** The molecular diode **R5** and the corresponding control molecule **R6** lacking the fluorine atoms were investigated in an MCBJ.<sup>[113]</sup> The asymmetric I/V characteristics of **R5** revealed an RR of about 5 at  $\pm 1.5$  V (A). The symmetric control molecule **R6** does not show any rectifying behavior (B).

The molecular rod is fitted with a sulfur anchor group on each side and consists of two weakly coupled  $\pi$ -systems (**R5**, Figure 20). One of the two  $\pi$ -systems is perfluorinated, and therefore shows a lower electron density (A), which leads to a broken symmetry in electron transport. The molecular rectifiers were investigated in an MCBJ setup and the I/V-characteristics of single molecules were recorded and indeed showed rectification with a RR of 5 at  $\pm 1.5$  V (Figure 22 A).

All the systems discussed so far showed  $RR \ll 100$ , far away from the values of diodes used in the semiconductor industry which show  $RR$ s in the range of  $10^5$ . The challenge of building molecular rectifiers is further confirmed by a theoretical study of Cortie and coworkers using the tunneling barrier model.<sup>[114]</sup> Corresponding to their calculations  $RR$  of molecular rectifiers will never overcome 100.

Ratner and coworkers recently reported a study on “Increasing Dynamic Range and Switching Speed Using Cross-Conjugated Species”.<sup>[115]</sup> Ideal transport behavior necessary for a molecule to function as a switch or as a rectifier was reported. The transmission probability of electrons tunneling through a molecule as a function of the energy results in transmission plots. The transmission probability of an ideal insulator is zero (blue in Figure 23 A), whereas the transmission probability of an ideal conductor is 1 (red in Figure 23 A). An ideal voltage switch is an insulator at the Fermi energy, but an ideal conductor when a voltage is applied (green in Figure 23 B). The conductance as a function of the voltage is plotted in Figure 23 C, and ideally, the conductance jumps from 0 to  $1 G_0$  when applying a distinct voltage.

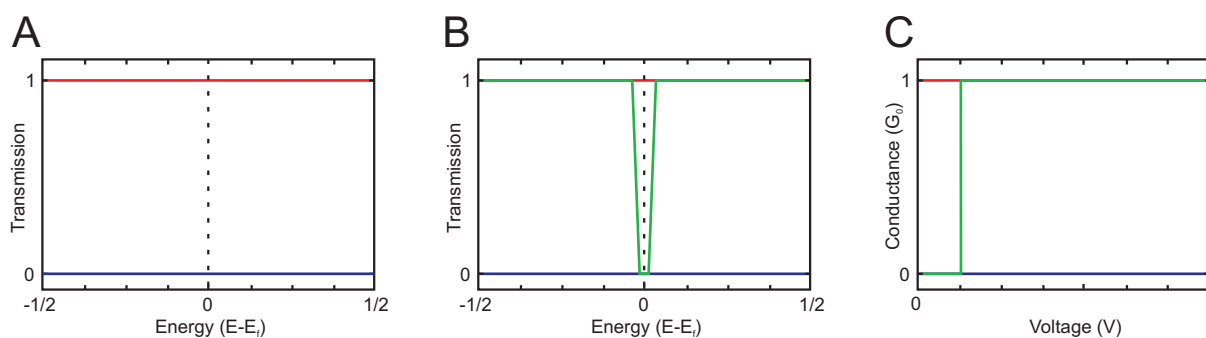


**Figure 23:** Transmission plots of an ideal insulator (blue) and an ideal conductor (red) are shown in the transmission plot A. B further shows the behavior of an ideal voltage switch. Without potential, the transmission probability is zero, when applying a distinct voltage the transmission probability is 1. C depicts the conductance as a function of the voltage of the ideal voltage switch.

Transport through single molecules in the Landauer-Imry low-bias tunneling regime was calculated, assuming the electron does not spend a significant amount of time on the molecule in the junction, leaving the molecule in the neutral state. It was found that cross-conjugated molecules show interesting dip like features in the transmission plots. It was further shown, that when electron donating (EDG) or electron withdrawing groups (EWG) were placed on the cross-conjugation point, the position of the dip is shifted (Figure 24). The direction of shifting is directed by the EDG and

EWG, respectively, and the amount of shifting depends on the strength of the electron donating or withdrawing character, respectively.

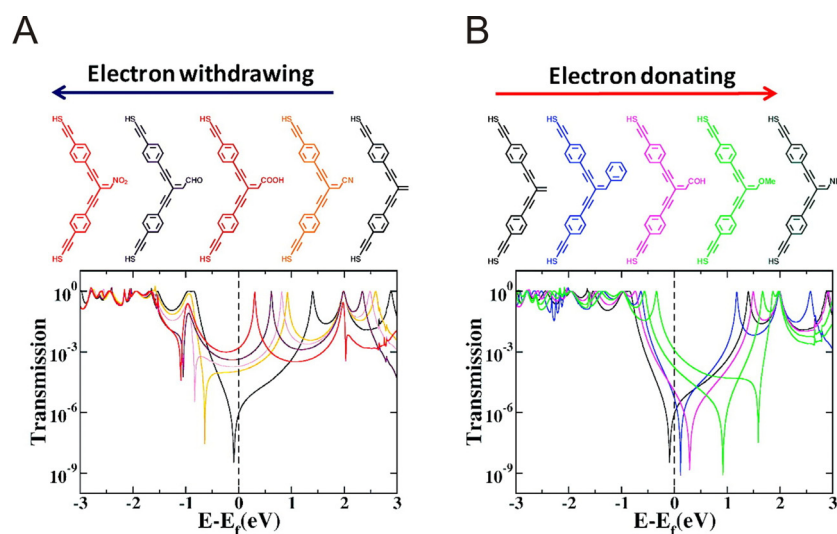


**Figure 24:** Cross-conjugated molecules show interesting dip-like interference features in the transmission plots. The position of the dip can be shifted by fitting the cross-conjugated spots with either EDGs or EWGs.<sup>[115]</sup>

When a molecule is fitted with two cross-conjugated spots, two dips occur in the transmission plots. The position and intensity of the dips depends on the nature and strength of the EDG and EWG. Ratner and coworker proposed a molecular rectifier (B) in Figure 25 comprising a cross-conjugated site fitted with a carboxylic acid as EWG and another cross-conjugated site fitted with a methoxy group as EDG. The transmission plot shows two dips which are asymmetrically aligned (Figure 25 C). At 1.2 V the proposed molecule has an RR of 249.



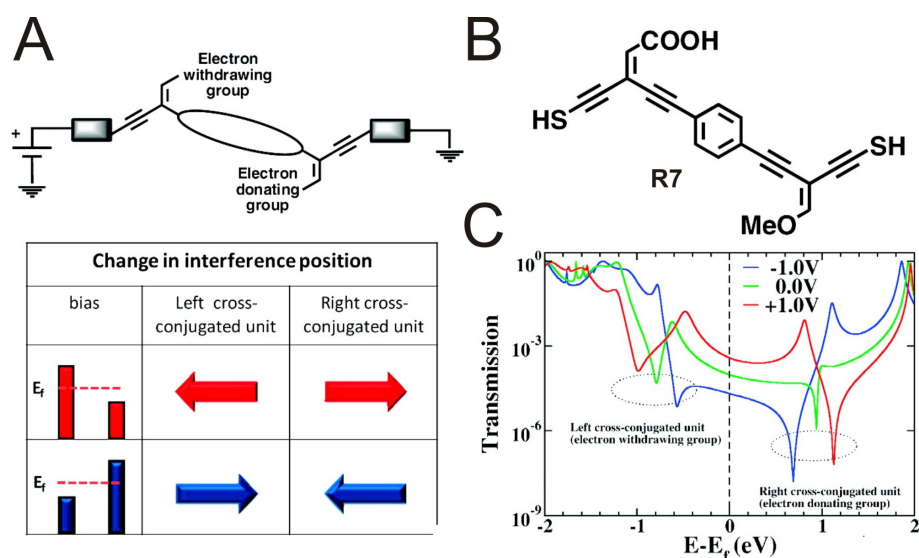


**Figure 25:** Two cross-conjugated spots reveal two interference dips in the transmission plots (C). The shift and intensity of the dips depends on the EWGs and EDGs (A). The proposed molecular rectifier (B) shows an RR of 249 at 1.2 V.<sup>[115]</sup>

Even though an RR of 249 is still orders of magnitudes below  $10^5$ , it is higher than RRs usually obtained from single molecules so far. For other more extended structures RRs of up to 10'000 were predicted.<sup>[115]</sup>

### 1.1.3.2 Molecular Switches

In order to realize electronic devices based on molecules, it is necessary to develop molecular switches. A molecular switch can be converted from one state to another by external stimuli such as light, electricity or a chemical reaction. In general, several molecular switches have been reported based on fulgides, azobenzenes, azulenes, alkylidenes cycloanones, overcrowded alkenes, spiropyran, diarylethenes, redox-systems and others finding applications in optics, data storage, nanomechanics and electronics.<sup>[116]</sup> However, here it is focused on conductance switches. A conductance switch has two different conductance levels, depending on its state, considered as an Off-state and an On-state. Upon the external trigger, the molecule is switched from one isomer to the other, the conformation is changed or the oxidation state is altered. These factors result in a change of conductance arising from differently aligned HOMO-LUMO levels to the Fermi-levels of the electrodes, change in conjugation of the molecule, variation of the electron transport distance or formation of multiple pathways for electron transport. In the following, examples of molecular switches considered for molecular electronics are discussed. Light

triggered molecular switches based on azobenzene or diarylethene systems and electrically triggered switches such as redox switches or voltage-triggered hysteretic switches are reported.

### 1.1.3.2.1 Light Triggered Switches

Photochromism is defined as a light-driven reversible transformation between two isomers possessing different absorption spectra.<sup>[116]</sup> Besides the different absorption spectra, the two isomers may further differ in their conformation and physical properties. When molecules possessing a function are fitted with a chromophore, the function can be switched upon irradiation. Photochromic chromophores are divided into two categories based on the thermal stability of the photogenerated isomers. T-type (thermally reversible type) chromophores have unstable photogenerated isomers and switch back to the initial isomer state in the dark. P-type (photochemically reversible type) chromophores are thermally irreversible and the photogenerated isomers are thermally stable and can only be switched back to the ground state upon irradiation with the corresponding wavelength.

#### 1.1.3.2.1.1 Azobenzene Based Switches

An example of a T-type photochromic switch is azobenzene. Azobenzene is a widely investigated molecular switch finding various applications such as switching elements for microelectronics, high density data storage, and nonlinear optics.<sup>[117]</sup> It can be switched from the thermally more stable trans-isomer to the cis-isomer by irradiating with UV-light. It then thermally isomerizes back to the trans-isomer or it can be switched back by irradiation with visible light (Figure 26).

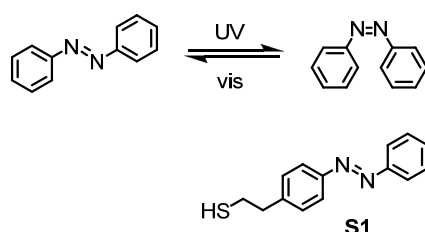


**Figure 26:** Azobenzene switches while irradiating with UV light from the thermally more stable trans-form to the cis-form. The cis-isomer is thermally unstable and reacts back to the trans-isomer. **S1** was investigated as an azobenzene based molecular switch.<sup>[118]</sup>

Kontturi and coworkers used an alkylthiol functionalized azobenzene derivative **S1** as a switch. Mixed self-assembled monolayers of an alkylthiol phenyl spacer molecule mixed with the alkylthiol functionalized azobenzene derivative **S1** were investigated.<sup>[118]</sup> Upon irradiation with 436 nm and 366 nm either the *trans*- or *cis*-form was obtained, respectively. The thicknesses of the SAMs were determined by ellipsometry. The barrier properties of the SAMs were then investigated by scanning electrochemical microscopy (SECM) under a constant irradiation to maintain the *cis*- or *trans*-conformation, respectively. An effect of the conformation of the azobenzene derivative **S1** was analyzed and showed strong correlation with the thicknesses of the SAMs. When the molecule is in its *trans*-form, the SAMs were thicker and showed higher tunnel barriers, whereas when the molecules are switched to the *cis*-form, thinner SAMs with lower tunnel barriers were obtained.

A fully conjugated rigid biphenyl azobenzene derivative **S2**, on one side fitted with a thiol anchor group, was designed to form SAMs on a gold substrate and to show packing features due to  $\pi$ - $\pi$ -interactions.<sup>[26]</sup> Indeed, highly packed and ordered SAMs were obtained, and after irradiation, switching of the entire molecular 2D crystalline domain is observed, which is ruled by the interactions between nearest neighbors. The complete switching of a domain is attributed to a so far unexplored cooperative effect. The collective switching of whole domains of a monolayer is of great interest for the design of high-density data storage devices.

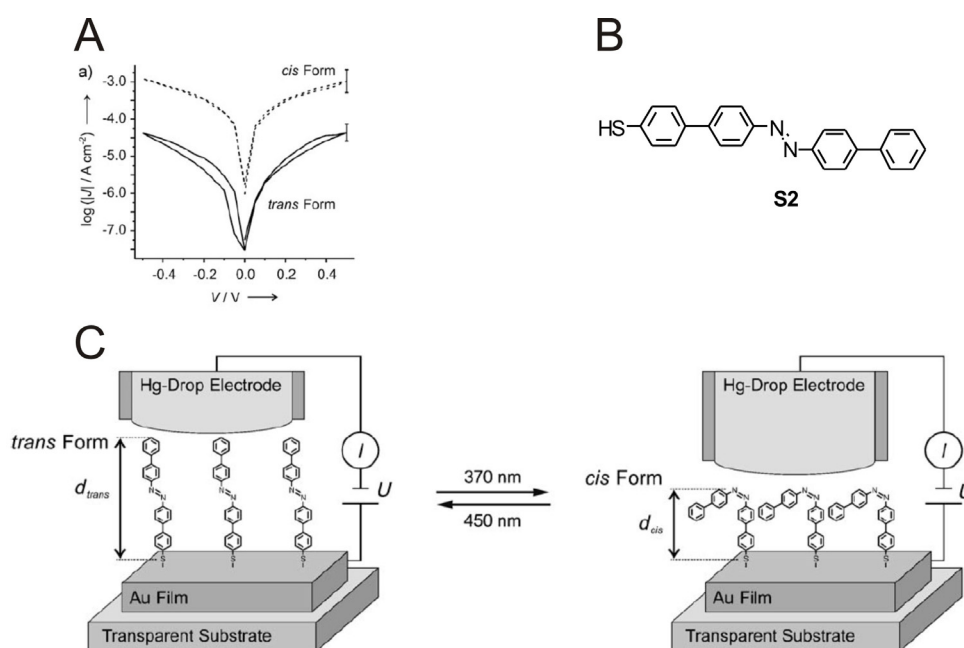


**Figure 27:** Azobenzene derivative **S2** (B), immobilized in a Hg-droplet junction (C) and the obtained I/V curves (A).<sup>[40]</sup>

It was further shown that the photoisomerization process of the biphenyl azobenzene derivative **S2** in a SAM can express work.<sup>[119]</sup> SAMs were investigated in a mercury droplet junction and it was shown that upon irradiation of the SAM isomerization occurs (Figure 27 C). The isomerization is reversible which means that the isomerization process is strong enough to lift the Hg-drop. I/V-curves were measured (Figure 27 A) and the cis-form was found to be 25 times more conductive than the trans-form. It was shown that films of azobenzene based molecules can be reversibly photoswitched.

Metal-molecule-metal junctions of the azobiphenyl derivative **S2** were produced by contacting SAMs on a gold substrate with a metal-coated AFM tip.<sup>[25]</sup> Depending on the tip size 30-90 molecules were contacted with the tip, therefore the measurement was performed on a single domain level and not as previously described with a whole film. I/V-curves were recorded and depending on the cis- and trans-state, altered upon irradiation with the corresponding wavelength, different resistances were obtained. The cis-form turned out to be 30 times more conducting than the trans-state. This change in conductance is attributed to a longer tunneling distance in the trans-state. This was the first example of switching upon an external stimulus using a conducting AFM approach.

#### 1.1.3.2.1.2 Diarylethene Based Switches

Diarylethene based switches and furylfulgides are the only reported P-type switches. In contrast to furylfulgides, diarylethenes are stable and can be photo induced switched repeatedly. The thermal stability and the stability upon cycling are important properties for future implementations into photoswitching applications and memory devices.

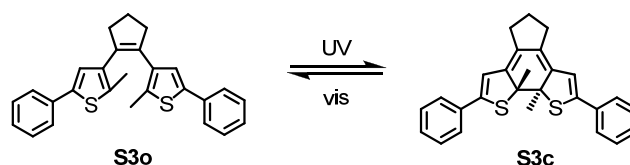


**Figure 28:** Photo driven rearrangement reaction of a diarylethene **S3**. The open isomer **S3o** undergoes cyclisation when irradiating with UV-light which yields in closed isomer **S3c**.

Figure 28 displays the switching behavior of a diarylethene example. Upon irradiation with UV light a carbon-carbon bond is formed and the open isomer **S3o** is rearranged

to the closed isomer **S3c**. The closed isomer **S3c** is thermally stable but it can be switched back to the open isomer **S3o** while irradiating with visible light.

In photochromic reactions, bonds are rearranged and undesired side reaction may take place. Even if the yield of the reaction is very high, side products can be accumulated upon repeated cycling. The resistivity of a switch to form side products upon repeated cycling is referred to as fatigue resistance. Fatigue resistance is a measure of how many times a switch can be cycled. Varying the substituents, the fatigue resistance properties can be tuned and when the thiophene-phenyl units in **S3** are replaced by benzothiophenes the fatigue resistance increases enormously and more than  $10^4$  cycles can be performed while forming less than 20% side products. The open-ring isomers of all reported diarylethenes are thermally stable. The stability of the closed-ring isomers is dependant on the nature of the aryl groups - furan, thiophene or thiazole aryl based diarylethene switches all show thermally stable closed-ring isomers. Thermal instability is only observed when the thiophenes are substituted with very strong electron-withdrawing groups. The response times for both isomerization reactions are very short and below 10 ps. Absorption spectra of the closed form are shifted towards longer wavelengths, suggesting delocalization of  $\pi$ -electrons over the entire structure (Figure 29 F). In the open form the conjugation is broken and restricted to one half of the molecule. A molecular switch with two optically addressable subunits which differ remarkably in the delocalization of the  $\pi$ -electrons is a very appealing candidate to be investigated in light triggered electronic circuits. Therefore if the diarylethene **S3** is fitted with adequate anchor groups and immobilized in a metal-molecule-metal junction, the open form would be referred to as the OFF-state and the closed form would be referred to as the ON-state.

Diarylethene switches have been exhaustively investigated in solution,<sup>[120]</sup> however it is not obvious that a molecule conserves its functionality when attached to a macroscopic surrounding. Feringa and coworker investigated a diarylethene molecule with two thiophene rings on each side and two acetyl protected thiol units (**S4**).<sup>[121]</sup> To measure electronic transport properties the molecules were investigated in an MCBJ setup. The molecule was trapped in its closed form between the two electrodes of the MCBJ (A in Figure 29) and I/V-curves were recorded (C in Figure 29). The resistance was then measured as a function of time while irradiating with

visible light. With a switching time of 10 s to 6 min the resistance suddenly increased by three orders of magnitude from the M $\Omega$  to the G $\Omega$  regime (E in Figure 29).

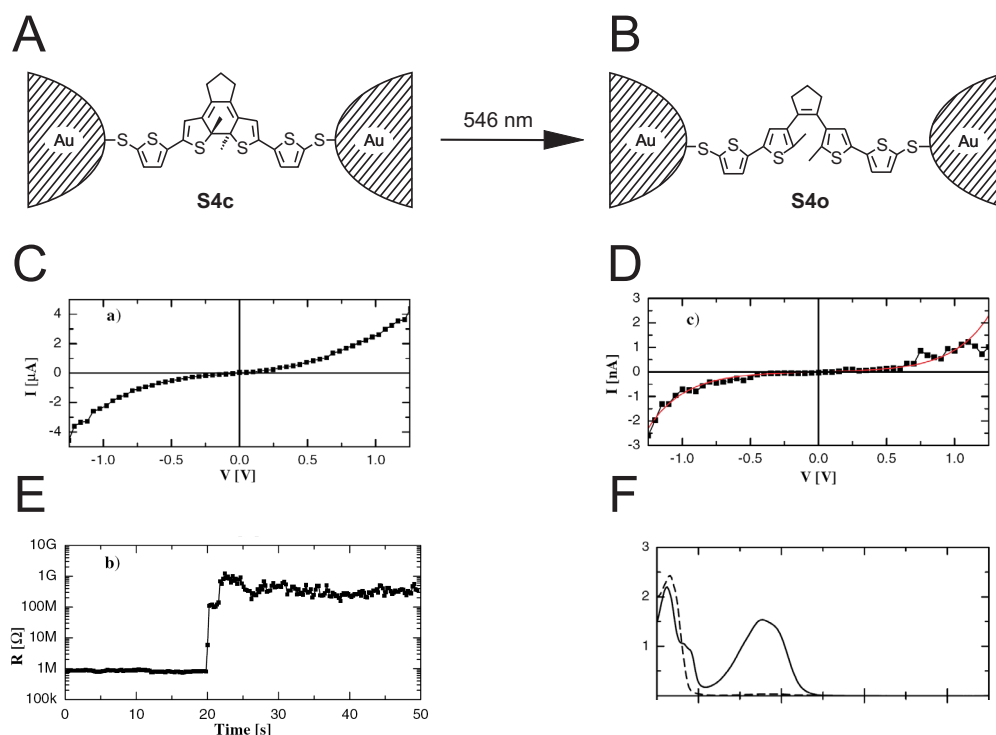


**Figure 29:** The closed form of a diarylethene derivative **S4c** was immobilized in an MCBJ (A) and I/V curves were measured (C). The sample was then irradiated with 546 nm (set  $t = 0$  s). After about 20 s the resistance drastically increases from the M $\Omega$  to the G $\Omega$  regime (E). I/V curves of the open form **S4o** (D) were recorded, but the switching was irreversible. (F) Absorption spectra of the molecular switches in toluene. Solid line: closed form (**S4c**); dashed line: open form (**S4o**).

This change in resistance is attributed to switching from the ON-state (closed form, **S4c**) to the OFF-state (open form, **S4o**) and resistance values are supported by calculations. However, the switching was found to be irreversible and the molecules can only be switched from the closed to the open state, and not the other way round. In solution the switching from the open state to the closed state (initiated by irradiating with UV-light) shows a very high quantum yield and is even faster than from the closed to the open state. Quenching of the open form excited state by the Fermi level of the gold electrode was proposed as an explanation of the inhibition of the closing reaction.

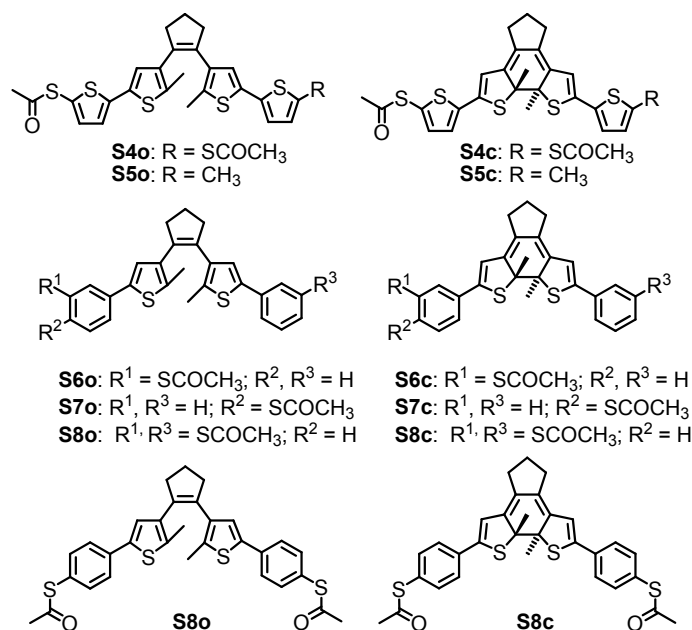


**Figure 30:** Examples of investigated diarylethenes.

As a control experiment UV/vis absorption measurements of the corresponding monothiol functionalized derivative **S5** were performed. The closed form shows an absorption maximum at 550 nm which completely disappears upon irradiating with visible light (546 nm). The process is completely reversible and upon irradiating with UV-light (313 nm) the absorption maximum at 550 nm is again obtained. The closed form isomer of the monothiolated compound **S5c** was then self-assembled on gold colloids which were subsequently suspended in toluene (Figure 31 C). Again an absorption maximum at 550 nm is obtained and decreases upon irradiating with visible light. However, even after three days of irradiating at 313 nm the absorption maximum is not recovered. Investigating switching properties of molecular switches absorbed on gold nanoparticles is a fast and reliable screening method to test the photochromic properties of molecules attached to a metal. It is in between ordinary solution-phase measurements and highly advanced molecular device techniques demanding expensive and time-consuming nanofabrications.

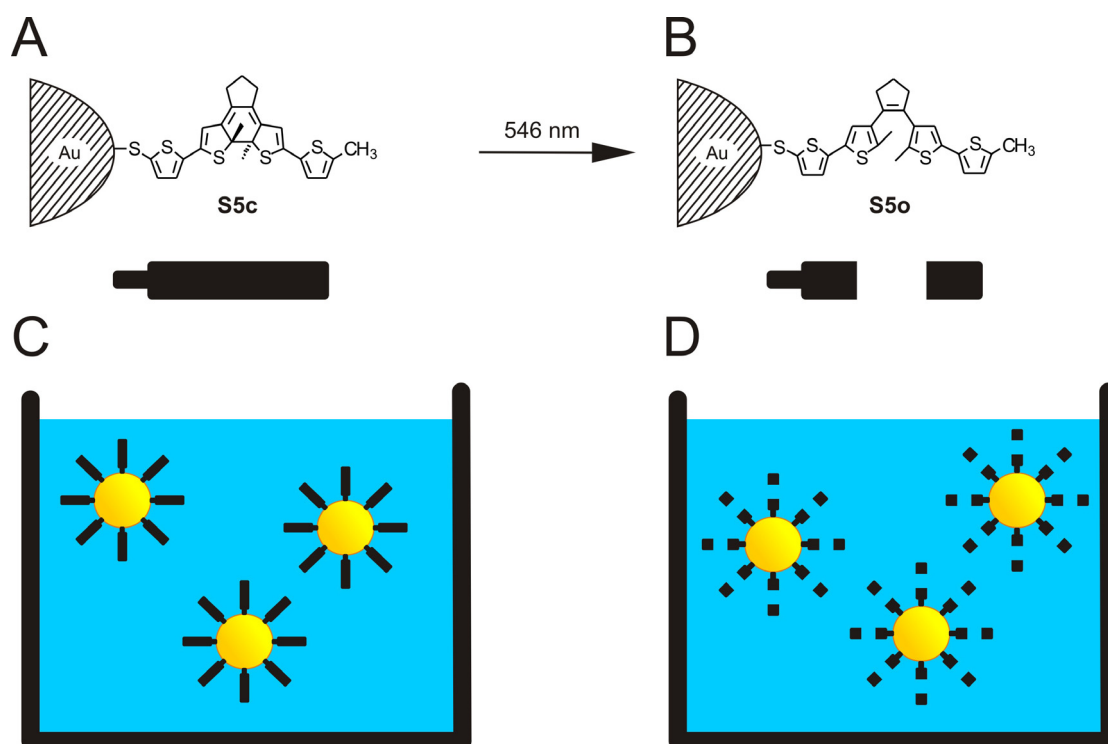


**Figure 31:** Switching properties of diarylethene switches **S5** absorbed on gold nanoparticle were investigated in solution. The state of the switch can be read from the absorption spectra.

As it was shown that switching behavior depends critically on the nature, length and position of the spacer linking the switching unit to the anchoring unit, diarylethene derivatives with different spacer groups were investigated on gold nanoparticles.<sup>[122]</sup> Absorption spectra of compound **S6** and **S7** bound to gold nanoparticles were recorded and the suspension was irradiated to trigger switching. In contrast to **S5**, reversible switching was obtained for both **S6** and **S7**. The quantum yield for the closed- to open-form isomerization is 0.07, which is lower than 0.4 in solution, but while introducing appropriate linker units bi-directional switching of photochromic molecules bound to metal can be obtained.

The knowledge obtained in this screening method was exploited and corresponding switches were designed to be investigated not only spectroscopically on gold nanoparticles in solution but also in a junction. SAMs of dodecanethiol on a Au(111) substrate were exposed to a solution of the dithiol functionalized switch **S6**. Hence, monolayers of dodecanethiols were doped with single diarylethene switches, and these SAMs were investigated by STM having the switches in the OFF-state (closed form) (STM-carpet approach, E in Figure 3). A regular pattern was obtained. However, upon irradiating the sample with UV-light leading to rearrangement to the ON-state (closed form, **S6c**) bright spots appear. These bright spots are attributed to



the molecule **S6c** in its ON-state and alter vastly from the OFF-state isomers **S6o**. STM measures apparent height that is in combination of electronic and topographic characteristics. However the difference in length of the ON- and OFF-state isomers is very small (0.1 nm), but the delocalization of the  $\pi$ -electrons in the two isomers differs strongly. Therefore the STM results are attributed to two different conductance states. Conductance switching is fundamentally different from length switching, such as observed in the previously described azobenzene systems. Optical-spectroscopy experiments further hold the conclusion that the high conductance state is attributed to the closed form and the low conductance state is attributed to the open form. The switching was reversible and both conversions from ON to OFF and from OFF to ON were obtained.

Diarylethene switches were further investigated in gold nanoparticle junctions.<sup>[123, 124]</sup> **S8** was investigated in 2D gold nanoparticle arrays (D in Figure 3).<sup>[125]</sup> The nanoparticles define a highly ordered 2D template, whereas the molecules contribute their functional properties. Via thiolate exchange the diarylethene switches **S8c** are brought into the junction (b in Figure 32). The conductance of the array after introduction of the closed-form isomer increases drastically from the initial conductance where only the alkylthiols are present. In a further experiment the conductance is measured as a function of time while irradiating alternately with UV and visible light, respectively (Figure 32). Indeed, the conductance changed in dependence of the wavelength of the irradiation. Hence a light sensitive device based on switchable diarylethene molecules, each coupled to two metal electrodes was created.

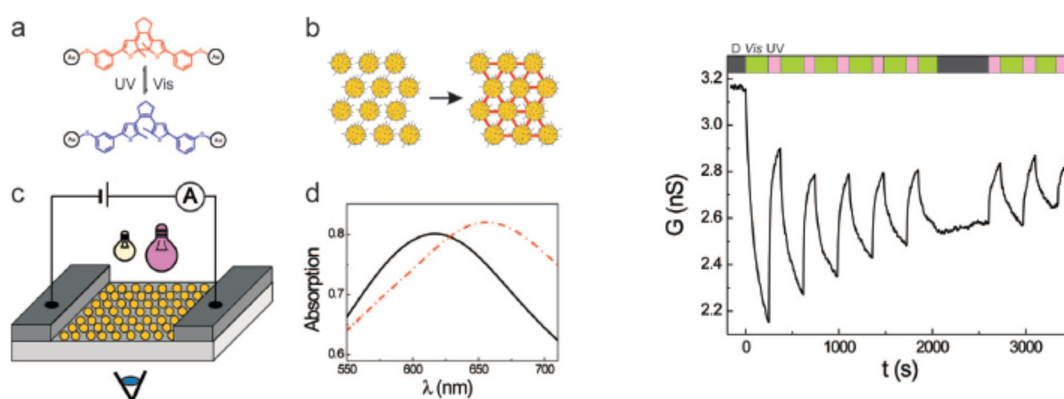


**Figure 32:** Photoswitchable 2D-network of gold nanoparticles bridged with diarylethenes. **S8** was investigated as a photoactive molecular switch.<sup>[125]</sup>

Besides photochromic switching diarylethene derivatives also show electrochromic switching. The isomers can therefore not only be transformed by irradiating with light, but also electrochemically.<sup>[126, 127]</sup> As this is an additional function other than switching (write-erase), this property was exploited to investigate information storage devices (read-write-erase). A diarylethene derivative **S10** was chemisorbed on a transparent indium tin oxide (ITO) electrode (Figure 33).<sup>[128]</sup> The immobilized switch underwent multicyclic ring-opening and ring-closing reactions both electrochemically and photochemically and the state of the modified surface was read non-destructively by electrochemical means. Hence, diarylethene derivatives can be grafted on electrodes without loss of functionality providing a basis for read-write-erase systems.

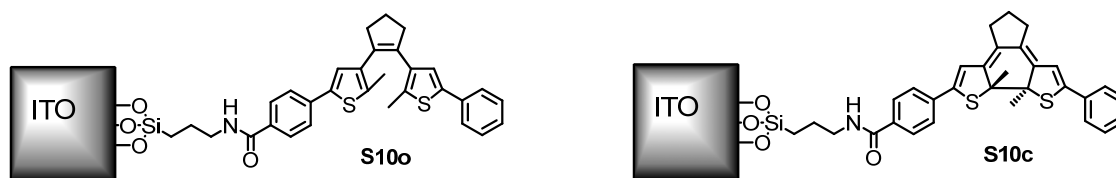


**Figure 33:** Electrochemical and photochemical switchable diarylethene derivative **S9** grafted on an ITO electrode.

Further, cysteamine modified gold electrodes were functionalized with carboxymethyl-pyridinium end-groups comprising diarylethene derivatives exploiting amide bond formation.<sup>[129]</sup> The corresponding electroactive and photoisomerizable monolayer was exploited as a read-write-erase information processing unit as well as a set-reset flip-flop memory element and the read-out signal amplification was accomplished by a secondary electrocatalytic process.

Photochromic diarylethenes are not only exciting for the investigation of fundamental switching and information storage concepts, they are also very attractive for numerous other devices such as; chiroptic applications,<sup>[130]</sup> photoregulation in metal catalysis<sup>[131]</sup> and photodelivery applications.<sup>[132]</sup> However, their integration into future electronic devices is questionable. In particular, light operated systems raise numerous issues like nature, size and integration of the light source into the circuit, control over the illuminated area and the number of illuminated molecules.

### 1.1.3.2.2 Electrically Triggered Switches

Electrically triggered molecules are basically divided into two types. As in a metal-molecule-metal junction the electrons are expected to flow through the frontier orbitals of a molecule (either HOMO or LUMO), and the electron population in the frontier orbitals is dependent on the oxidation state. Change of the oxidation state may directly result in a change of conductance. Therefore a first type of electrically triggered switches is considered to be a redox state dependant switch. Changing the redox state of a molecule can further lead to a change in the rate of delocalization in the electron pathway. In contrast to the electrochemically triggered switches, voltage triggered hysteretic switching has to be considered as a second type of electrically triggered switches. In voltage triggered switches the redox states of the two isomers are the same, but the conductance shows a hysteretic behavior.

#### 1.1.3.2.2.1 Redox Switches

To realize a molecular redox state driven molecular switch, a redox active core needs to be functionalized with two adequate spacers and two anchor groups. As a redox active molecule bipyridinium, also called viologen was investigated. Viologen can be switched from its dicationic  $V^{+2}$  state to the reduced radical cation state  $V^{+}$  and further to the neutral state  $V^0$  (Figure 34).

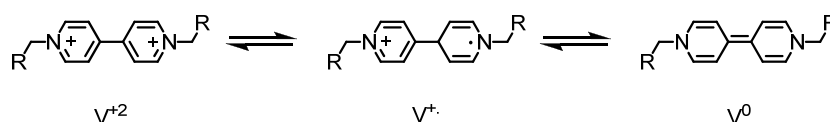


**Figure 34:** Redox reactions of viologen. The twofold positively charged ground stated  $V^{+2}$  can be reduced to the radical cation state  $V^{+}$  and further to the neutral state  $V^0$ .

Schiffrin and coworkers investigated a dialkyl dithiol functionalized viologen derivative **S10** ( $R = (CH_2)_5SAc$  in Figure 34), self assembled on a gold substrate.<sup>[133]</sup> Gold nanoparticles were placed on the SAM which were then addressed by an STM tip. In this manner they were able to indirectly address the viologens and form metal-molecule-nanoparticle-STM tip junctions. The oxidation state of the viologen was controlled with an electrochemical gate without affecting the bias. Monitoring the tunnel current through the junction by STS, an increased conductance was observed for the reduced form  $V^{+}$  compared to the dicationic state  $V^{+2}$ . Three years later the same group reported a method to directly address the viologen with an STM tip.<sup>[134]</sup>

The molecules were chemisorbed on a Au(111) substrate forming a low-coverage phase. The STM tip was then brought close to the SAM and subsequently gently lifted while holding the tip at a constant x-y-position. The current was measured as a function of the relative tip-sample distance. Besides fast exponential decay curves, less abrupt decay followed by a characteristic current plateau is observed, indicating that single metal-molecule-metal junctions are formed. These measurements were then performed within a liquid environment with an electrolyte. Measuring at a different potential it was possible to determine the conductance of single molecules as a function of the applied electrode potential. Reversible conductivity changes of a factor  $\approx 5$  were observed when the molecule was switched from its oxidized  $V^{+2}$  state to the reduced  $V^{+}$  state.

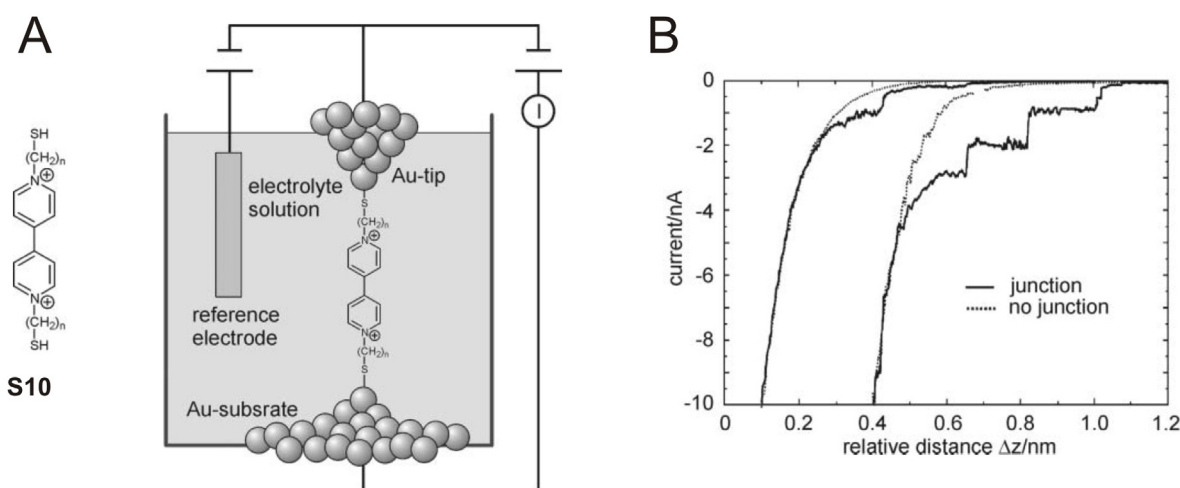


**Figure 35:** Viologen derivative **S10** ( $n=6$ ) has been investigated in several electrochemical STM setups like the sketched single molecule junctions (A)<sup>[134-136]</sup> or Au-nanoparticle covered junctions.<sup>[133]</sup> B displays typical pulling traces for **S10** during the electrochemical STM experiment reported by Wandlowski.<sup>[135]</sup>

Comprehensive investigations of viologen derivatives as electrochemical potential dependant structures were performed to gain information about the relationship between molecular and electronic structure.<sup>[135-137]</sup> In particular, self-assembly and redox properties of viologen derivatives, consisting of a viologen core functionalized with alkylthiol groups on gold electrodes was reported. Depending on the assembly conditions, different types of adlayers were found, low coverage (disordered), striped and high coverage monolayers. STM experiments were performed to explore electron-transport properties while forming substrate-molecule-STM tip junctions (Figure 35). The recorded current traces were statistically analyzed, showing redox

state dependant transport currents through single molecule junctions. The obtained sigmoidal potential dependence was attributed to the electronic structural change. Exploiting different alkyl spacer lengths ( $n = 5,6,7,8$ ) showed a surprisingly low tunneling decay constant calculated for the molecular system.<sup>[136]</sup> In this approach, using viologen as an electrochemically triggered active unit, the redox active core is rather isolated from the electrodes due to the poorly conducting alkyl spacer units. This was essential for the basic understanding of the electrochemical conductance switching. Therefore, systems where the redox core is directly coupled to the electrodes via conjugated spacers need to be investigated.

A molecular rod **S11** with a central tetrathiafulvalene (TTF) core was proposed as a molecular switch.<sup>[138]</sup> TTF has three stable redox states and can be oxidized from the neutral  $\text{TTF}^0$  to the cationic  $\text{TTF}^+$  and dicationic  $\text{TTF}^{2+}$  state (Figure 36).

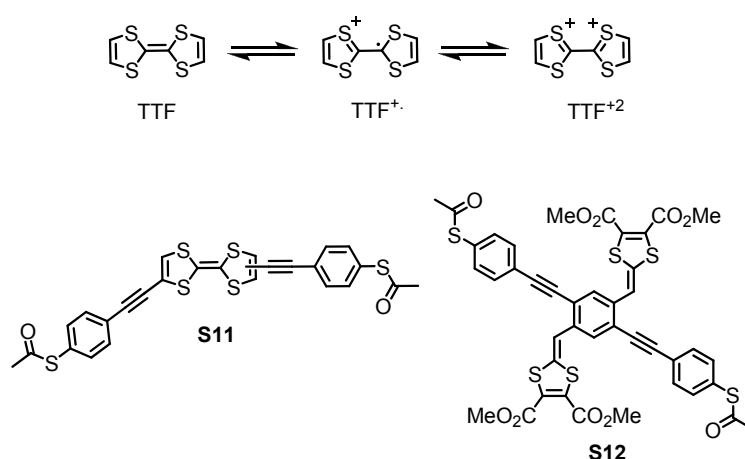


**Figure 36:** Redox reactions of TTF and proposed molecular switches **S11** and **S12** exploiting the redox character of TTF.

Indeed, cyclic voltammetry (CV) measurements of the rod **S11** in solution revealed two pairs of well-defined and reversible redox couples typical of TTF. Preliminary conductance measurements of single molecules using an STM setup were performed and stable  $I/V$ -characteristics recorded in an MCBJ setup reported. However, conductance measurements depending on the oxidation state have not been reported thus far. Extended TTFs implemented into molecular rods (**S12**) were also considered as redox switches. Similar to the principle previously described with the diarylethene switches, the conjugation of the  $\pi$ -system in the electron transport pathway is altered.<sup>[139]</sup> Upon oxidation of the extended TTF to the dicationic form, the

conjugation of the oligo(phenylene ethynylene) (OPE) rod is changed from conjugated to cross-conjugated. This change in conjugation was intended to be exploited in an electrochemically triggered molecular switch. CV measurements and computational calculations support the proposed switching mechanism, however, conductance measurements and switching behavior has not yet been reported

Another approach to address the conjugation of the  $\pi$ -system electrochemically was reported by Hummelen and coworkers.<sup>[140]</sup> The proposed switch **S13** consists of an OPE system with a central anthraquinone core and terminal acetyl protected sulfur anchor groups (Figure 37). The central anthraquinone group acts as a barrier for conjugation and divides the  $\pi$ -system apart. However, in its reduced hydroquinone form, the  $\pi$ -system is delocalized over the whole rod and an increased current is expected for this change when addressed with two electrodes.

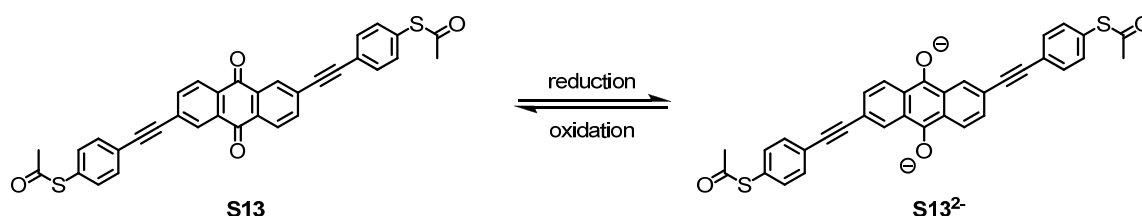


**Figure 37:** Anthracene based molecular rod **S13** proposed as potential electrochemically addressable molecular switch. While the conjugation is broken by the quinone in **S13**, the  $\pi$ -system is fully conjugated in the reduced form **S13**<sup>2-</sup>.

CV investigations display a two-step reversible redox process with a semiquinone intermediate upon reduction. The difference in delocalization of the  $\pi$ -systems of the two isomers is also reflected in the absorption spectra. The absorption band of the conjugated hydroquinone isomer undergoes a bathochromic shift of about 300 nm compared with the anthraquinone isomer. Molecular orbital calculations have supported the proposed switch, but conductance measurements of immobilized molecules have not yet been reported.

### 1.1.3.2.2 Voltage-Triggered Hysteretic Switches

In comparison to the previously described redox switches, voltage triggered switches bear the same oxidation state in both their ON- and OFF-state. This class of switches rather relies on hysteretic properties, a delayed response to a stimulus. Hysteresis, in general, is a property of a system not to respond instantly to an applied force, or not to return to its initial state immediately after applying the force. Therefore hysteretic systems remember their latest history. If the force is plotted against the state of a system, hysteretic systems show loop-like behavior. For applied forces within the region of the hysteretic loop, the system is bistable, and the state can be nondestructively read out. This feature makes hysteretic switches very interesting for logic applications or memory cells.

An elaborated system to approach hysteretic switching based on supramolecular architectures was investigated by Stoddart and coworkers.<sup>[13, 141, 142]</sup> They exploited bistable properties of mechanical interlocked molecules (MIM). Molecules can be programmed to form mechanically interlocked molecules such as catenanes or rotaxanes using template-directed synthesis. Catenanes consist of two interlocked rings whereas rotaxanes consist of a ring encircling a handle fixed with two appropriate stopper units. MIMs containing two different binding recognition sites with the ring component preferentially binding one of the stations are called bistable mechanically interlocked molecules. Upon application of an external stimulus, affinity of the ring component towards recognition sites can be reversed and the switching occurs. As an example, this supramolecular rearrangement reaction is explained with the rotaxane **S14** (Figure 38). The handle consists of an ethyl glycol chain comprising two binding sites, namely a TTF and a dioxynaphthalene (DNP) station, both being electron rich. In the ground state a tetracationic cyclobis(paraquat-*p*-phenylene) (CBQT<sup>4+</sup>) ring preferentially encircles the TTF station. This thermodynamically more stable coconformer is referred to as the ground state coconformer (GSCC). The handle is fitted with two sterically demanding stoppers, such that the ring can not slip off the rod. The TTF can be oxidized to its dicationic TTF<sup>+2</sup> form, resulting in a coulombic repulsion of the TTF<sup>+2</sup> and the CBQT<sup>4+</sup> ring. Relieving the coulombic strain, the ring shuttles to the second binding site, the DNP unit. However, when reducing the TTF<sup>+2</sup> back to its neutral state, the ring keeps binding to the DNP

station. This coconformer has the same oxidation state as the GSCC and is referred to as the metastable coconformer (MSCC). The two conformers are in equilibrium, however by an appropriate electrochemical stimulus one of the two states can be enriched.

The modular synthesis of MIMs allows varying the structure and therefore the properties. The stoppers can for example be fitted with groups supporting film formation or binding selectively to a distinct electrode.

These bistable molecular-mechanical switches have been investigated extensively in solution.<sup>[143-145]</sup> They are promising candidates for many technological applications, although few are likely to be liquid-phase based.

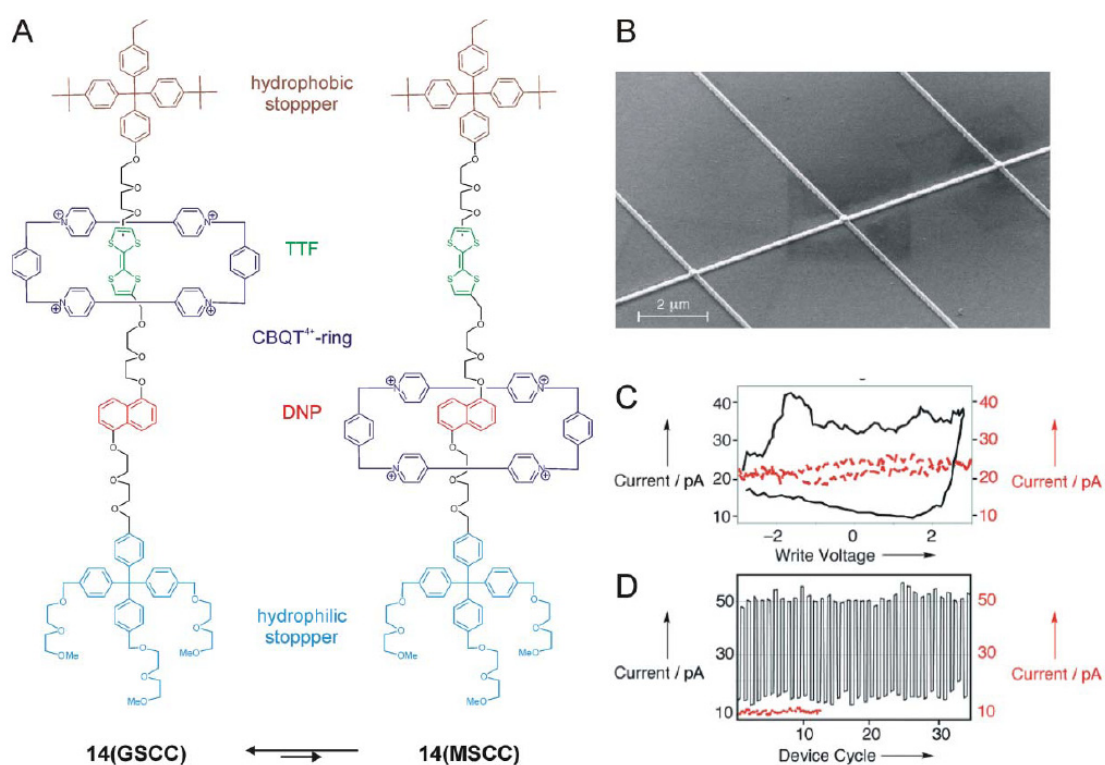


**Figure 38:** Rotaxane **S14** (A) In the ground state the CBQT<sup>4+</sup> ring encircles the TTF unit. Upon oxidation of the TTF the ring is shuttled to its preferential position at the DNP site. The two coconformers are in equilibrium, however upon an electrochemical stimulus one state can be enriched. **S14** was successfully immobilized in a crossbar-architecture (B) and hysteretic switching was obtained (D).

The feasibility of bistable MIMs as switches in solid-state applications was explored by integrating bistable [2]catenanes and [2]rotaxanes into solid-state polymer electrolytes.<sup>[146]</sup> While addressing with a microfabricated electrochemical cell, thermodynamic properties of the switches were quantified by time and



temperature dependent cyclovoltammetry. The position of the ring, and therefore the state of the switch can be determined by CV due to the considerably lower oxidation potential of the bare TTF in the MSCC (200 mV less positive). The shuttling mechanism in the solid-state polymer, which can be considered as a viscous liquid, remains the same as in solution, although remarkably slowed down. The mechanism was also proved in other environments such as Langmuir-Blodgett Films (LB)<sup>[147]</sup> and self-assembled monolayers (SAMs),<sup>[148]</sup> but the recovery rate from the MSCC to the GSCC was found to be dependant on the media.

Monolayers of [2]rotaxanes were investigated in molecular switch tunnel junctions (MSTJ) (Figure 38).<sup>[17, 36-38]</sup> Indeed, two different conductance states were found upon switching the rotaxanes. The switches were opened at +2 V, closed at -2 V and read at 0.1 V. Temperature dependent electrochemical and current-voltage measurements were performed to determine qualitatively and quantitatively the thermodynamic properties of the rotaxane. The high-conductance state (ON-state) corresponds to the MSCC and the low conductance state (OFF-state) is related to the MSCC/GSCC ratio at equilibrium.<sup>[38]</sup> The difference in conductivity depends on the spatial arrangement of the two conformers. The stability of the supermolecules in two different spatial arrangements is the origin of the bistability and hysteretic behavior.

As the MSTJs exhibit a hysteretic response to an applied voltage, they can serve as the basis of information storage. MSTJs are promising candidates for the active elements of two-dimensional memory circuits. Rotaxane **S14** was integrated into a two-dimensional crossbar architecture, and indeed, information could be stored in this memory device.<sup>[17]</sup> The crossbar architecture consists of two series of parallel electrodes between which a molecular film is sandwiched. As shown in Figure 39, the top electrodes are perpendicular to the bottom electrodes, defining a small area of the sandwiched molecular film, which consists of numerous molecules at each intersection, addressable by applying an electric current at the corresponding junction between the top and bottom electrodes. In an ideal case, the junction consists of a molecular monolayer comprising metastable molecular structures whose states may be defined (written) and altered by strong current pulses. The read-out of the state of the junction is accomplished by applying lower voltages, which does not alter the state of the junction.

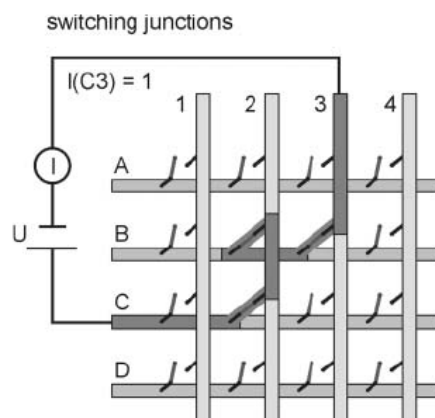


**Figure 39:** Crossbar architecture for the integration of molecular devices as potential memory cells.

The modular synthesis of these molecules allowed an adaption to electro engineering problems. Improved [2]rotaxane structures immobilized within a crossbar architecture led to a 160-kilobit molecular electronic memory, patterned at  $10^{11}$  bits per square centimeter.<sup>[149]</sup> The cross-bar geometry was made of 400 silicium nanowires as bottom electrodes. A LB monolayer of the [2]rotaxane was then placed on the nanowires which in turn was topped by 400 titanium nanowires at right angles as top electrodes. The 160000 (400 x 400) memory cells with a cell size of  $0.0011 \mu\text{m}^2$  can be switched to the ON-state by applying a +1.5 V pulse on the Si electrodes. At +0.2 V the state can be nondestructively read out. The circuit has large numbers of defects but they could be readily identified through electronic testing and isolated using software coding. About 50 % of the cells yielded some sort of switching response, but some of these responses may result from parasitic current pathways through the crossbar array. The drawback of the crossbar architecture wherein each junction is electrically connected to every other junction could be overcome by incorporating diodes at each cross point. Nevertheless, the density of these data storage elements is very high and is predicted to increase further.<sup>[149]</sup>

Hysteretic switching was also obtained for a rather simple molecular rod **S15** comprising a dinitro functionalized bipyridine core. Transport investigations of molecule **S15** were performed using STM and crossed-wire junctions.<sup>[150]</sup> STM studies were either performed with SAMs of **S15**, **S15** inserted into SAMs of alkanethiols with gold nanoparticles placed on top, or as **S15** inserted into SAMs of alkanethiols without nanoparticles. When a SAM of **S15** was addressed with an STM tip and a bias voltage from 0 V – 2 V was applied, the tunneling current suddenly

jumped to a better conductance at 1.6 V. The molecule is then in an ON-state being 30 times more conducting than in the initial OFF-state. The molecule remains at the higher conductance state until the applied bias voltage approaches 0 V. At this point the molecule switches back to its OFF-state and only reaches the high-conductance state when again pulsed with 1.6 V. Qualitatively similar results were obtained when isolated molecules in a SAM of alkylthiols were addressed with an STM tip (switching at 1.7 V) or with assemblies of **S15** in a crossed-wire junction (switching at 1.1 V). In the later method the system was stable for more than one hundred cycles. No hysteresis was obtained when SAMs of only alkylthiols were measured. Therefore it was concluded that voltage-triggered switching is a molecular phenomenon.

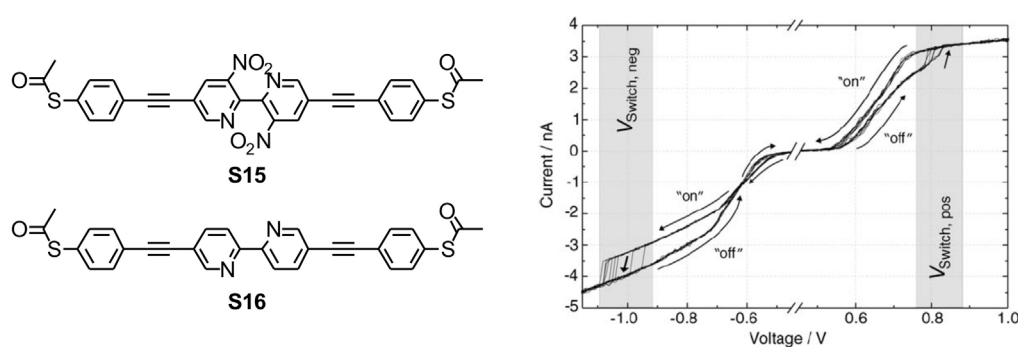


**Figure 40:** Compound **S15** displayed hysteretic switching whereas the control molecule lacking the nitro groups **S16** did not show any voltage triggered switching.<sup>[18]</sup>

Riel and coworkers investigated the hysteretic properties of the same molecule **S15** within an MCBJ setup.<sup>[18]</sup> Single molecules were connected to symmetric leads, and I/V-curves were recorded. The I/V-curves were symmetrical between  $\pm 1.2$  V showing hysteresis between  $\pm 0.9$  V (Figure 40). When a bias voltage was applied starting from 0 V the current traces showed an increased conductivity when sweeping above 0.8 V. The molecule stayed in this good-conductance state until it was switched back to the OFF-state by applying a negative bias of -1.0 V. This negative sweep resets the system to the OFF-state. A control experiment was performed with molecule **S16** lacking the two nitro functions. Symmetric I/V-curves were obtained but no hysteretic properties were found. This reversible and controllable voltage-triggered switching ability of **S15** has already been used as single molecule memory element.<sup>[18]</sup> The switching mechanism is not yet fully understood, but conformational change, electrostatic charging and tilting have been hypothesized.

With all the selected examples discussed in the introduction, it was shown that molecules are suitable to be integrated into electronic circuits. It was also pointed out that nowadays molecular electronic systems have particular drawbacks, and they need to be remarkably improved to find applications in industry. There is still a vast need of basic understanding of electron transport through single molecules to reach a level enabling the fabrication of molecular electronic circuits.

Our contribution to the field will be discussed in the following chapters. The goal of this thesis is to design and synthesize molecules such that the molecular properties result in functional materials.

## 2 Molecular Rods as Model Compounds for Electron Transport Investigations

Since the goal of molecular electronics is to embed molecules between two electrodes and let them perform electronic functions, we first consider conduction, the simplest electronic function. In an ideal molecular electronic device, not only the active part but also the contacts, interconnects and wires are made of molecules. Even though it is unrealistic to fabricate fully organic devices, and hybrid setups are much more promising, it is essential that transport properties through molecules are investigated starting from simple test systems. Several molecules comprising complex functions have been designed and synthesized. Subsequently, their transport properties have been investigated. However, the behavior of these complex systems often raised more questions than providing clarity. Therefore simple rod like structures were chosen as model compounds for these investigations. By systematically varying certain components, effects on different anchor groups and intermolecular interactions in molecular junctions will be discussed.

### 2.1 Design of Molecular Rods

We use oligo(phenylene ethynylene) (OPE) structures as model compounds to systematically investigate electron transport through molecules. OPEs are rod like structures consisting of modular and repetitive subunits. Compared to saturated alkane model systems discussed in the introduction, OPEs are expected to display improved electron transparencies due to their backbone conjugation. As a basic reference molecule, OPE **1** is proposed (Figure 41). With three phenyl units bridged by ethynyl groups it has an ideal length to be integrated between two electrodes. To provide stable binding and electronic coupling to the electrodes, OPE **1** is fitted with two thiol anchor groups.

In a first instance we investigate the role of contact. The effect on the electron transport when the anchor groups are changed from thiols to pyridine is explored. Therefore the terminal thiophenol subunits of **1** are systematically substituted by pyridines. OPE **2** comprises one thiol and one pyridine unit, OPE **3** comprises two terminal pyridine units where the thiophenol units are fully replaced.

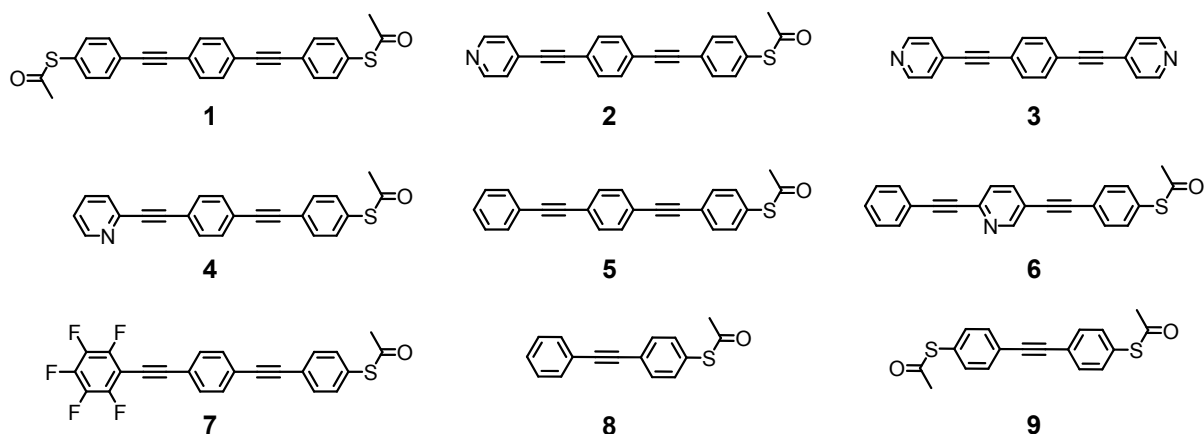


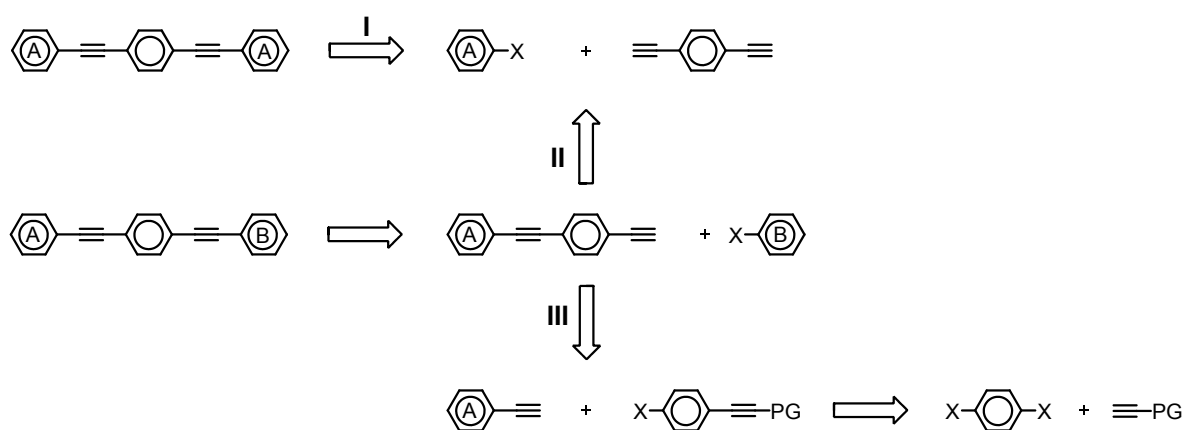
**Figure 41:** Molecular rods **1** – **9** were considered for investigation. All compounds consist of an OPE backbone. Rod **1** is the basic reference compound with two thiol anchor groups. Rod **2** has one thiol and one pyridine anchor group, rod **3** bears two pyridine anchor groups. Rod **4** – **8** comprise only one anchor group. OPE **8** and **9** comprise only two phenyl rings.

To connect molecules with two electrodes, two anchor groups are required. However, previous experimental findings in our measurements gave rise to the question whether  $\pi$ - $\pi$  stacking might be the origin of molecular junction formation.<sup>[50]</sup> According to the measurements it was not *a priori* obvious that **1** was bound to two electrodes with its two sulfur units, or if it was binding to one electrode and stacking with a second molecule binding to the other electrode. Therefore we systematically investigate the role of – so far unexplored – intermolecular interactions in molecular junctions. We examine the bridging of two electrodes by formation of a molecule-molecule junction.  $\pi$ - $\pi$  Stacking is envisaged as the predominant intermolecular force. Therefore molecular rods comprising only one anchor group are proposed (compound **4-8**). While compound **1** and **2** are designed to form two contacts to the electrodes, the pyridine group in compound **4** is hidden in the *ortho*-position. In compound **5** the pyridine is substituted with a phenyl unit and the OPE comprises only one anchor group. Placing the pyridine on the central unit provides similar electronic properties to compound **2** and **4** but also disables binding to two electrodes (compound **6**). The extent of  $\pi$ - $\pi$  stacking depends on the different electron densities of the stacking rings. Compound **7** comprises a perfluorinated electron poor phenyl unit as an alternative to pyridine. Further control molecules are the shortened OPEs **8** and **9** comprising only two phenyl rings and one and two thiol groups, respectively.

## 2.2 Synthesis of Molecular Rods

### 2.2.1 Synthetic Strategy

The synthetic strategy to assemble OPE **1-9** is based on *Sonogashira* coupling reactions. These coupling reactions allow a modular synthesis of the rigid OPE structures. In general, three different strategies are considered (SCHEME 1). The symmetrical OPEs **1** and **3** can be assembled in one step by a twofold coupling reaction of 1,4-bisethynylbenzene with the corresponding functionalized building block (route I in SCHEME 1, with A is either pyridine or a thiophenol). If A and B are different (OPE **2, 4 – 7**), the OPE loses its symmetry and a stepwise assembly becomes necessary. However, if A is a pyridine (**2** and **4**), it decreases the electron density in the conjugated  $\pi$ -system when monocoupled to 1,4-bisethynylbenzene, which decreases the reactivity of the free acetylene. This enables a selective monocoupling (route II in SCHEME 1). The third strategy is to build up the OPE (**5, 6** and **7**) stepwise by a coupling-deprotection sequence (route III in SCHEME 1). Trialkylsilane protection groups (PG) are considered to protect the acetylene. The silane PGs allow the basic reaction conditions of the *Sonogashira* reaction but can be mildly cleaved. The shorter OPEs **8** and **9** can be assembled in a single coupling reaction.



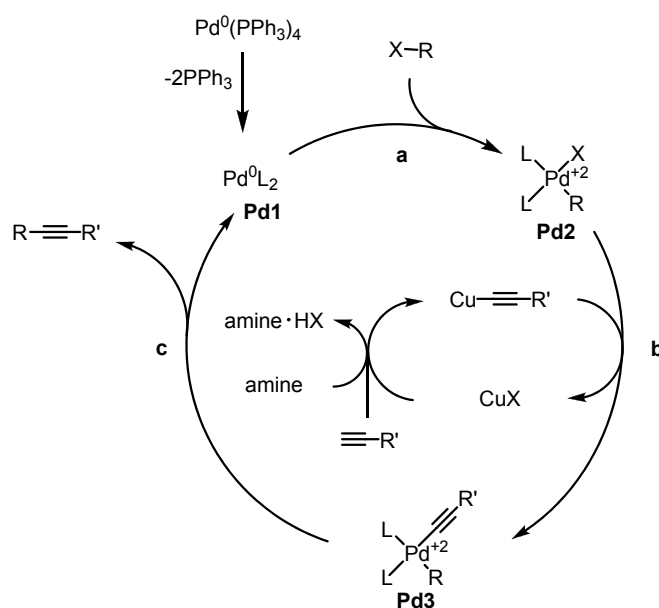
**SCHEME 1:** Synthetic Strategy for the assembly of OPE **1 – 9**.

The thiophenols are envisaged to be protected with acetyl protection groups. The acetyl groups allow the conditions of *Sonogashira* reactions but can mildly and efficiently be cleaved prior to the physical investigations in the MCBJ.

## 2.2.2 Synthesis and Characterization

All target structures **1-9** are assembled by *Sonogashira* reactions as key steps. The *Sonogashira* reaction is a transition metal catalyzed cross coupling reaction, and is an efficient method to build up OPE structures.<sup>[151-153]</sup> For the understanding of the outcome of the following reactions, the mechanism will be briefly discussed.

The *Sonogashira* reaction is a palladium catalyzed coupling reaction co-catalyzed by a copper(+I) salt.<sup>[154]</sup> The catalytic cycle is displayed in Scheme 2. The acetylene is deprotonated by the amine base forming an acetylide and an amine salt as side product. To stabilize the acetylide and increase its nucleophilicity, the copper salt is required as a co-catalyst while forming the copper acetylide. The first step in the main catalytic cycle is an oxidative addition (**a** in Scheme 2). The active catalyst is an electron deficient palladium(0) species (**Pd1**) to which the halide bearing reagent is introduced and the palladium is oxidized (**Pd2**). The oxidative addition is the rate limiting step of the reaction. In a transmetallation step (**b** in Scheme 2) the palladium complex **Pd3** is formed. Followed by the reductive elimination, the cross-coupled product is relieved and the active palladium catalyst is regenerated.



**Scheme 2:** Catalytic cycle of a *Sonogashira* reaction. **a:** oxidative addition, **b:** transmetallation, **c:** reductive elimination. R = aryl. R' = aryl, alkenyl, alkyl,  $\text{SiR}''_3$ . X = I, Br, OTf.

The most widely used catalysts are  $[\text{Pd}(\text{PPh}_3)_2\text{Cl}_2]$  and  $[\text{Pd}(\text{PPh}_3)_4]$ .  $\text{CuI}$  is used as co-catalyst. As base, amine bases are employed either directly as solvent or as reagents. There are many variables that dictate the overall efficiency of the catalytic cycle, including catalysts, amine base, solvent and the electronic and steric

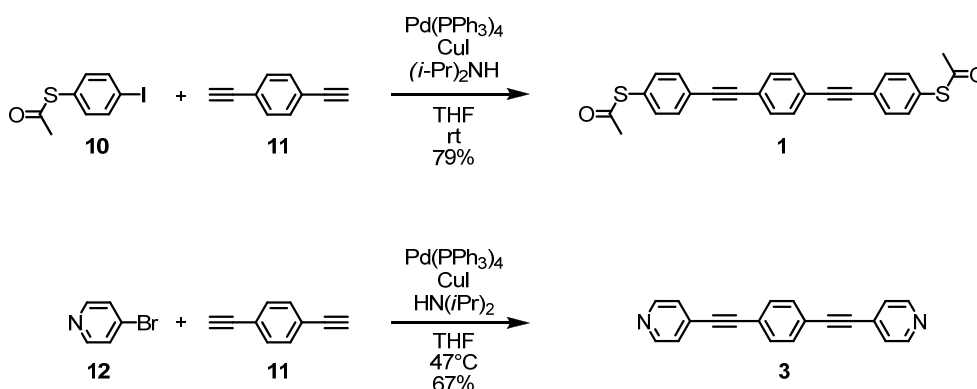


characteristics of the organic electrophile and alkyne. Electron-deficient organic halides are more reactive to cross-couplings than electron-rich, while the opposite is true for alkynes.<sup>[154-156]</sup> The general reactivity order of the  $sp^2$  species is aryl iodide > aryl triflate  $\geq$  aryl bromide  $\gg$  aryl chloride.<sup>[154, 157]</sup>

For the assembly of target structure **1-9**, several *Sonogashira* reactions were performed. The reaction conditions found to be generally applicable to most of these couplings were the following:

The acetylene and the aryl-iodide were dissolved in a 5:1 mixture of dry THF and diisopropylamine. 10 mol%  $[Pd(PPh_3)_4]$  and 10 mol% CuI were added and the reaction mixture was stirred until complete at room temperature. The extent of the reaction was followed by thin layer chromatography (TLC). The reaction mixture was then evaporated, absorbed on silica gel and purified by column chromatography (CC). To prevent oxidative diacetylene-formation, the solvent mixture was degassed before use, and the reaction was performed under an inert argon atmosphere. These reaction conditions are in the following referred to as the standard *Sonogashira* conditions and where no further clarification is stated these conditions were applied.

Applying synthetic strategy I the symmetric compounds **1** and **3** were assembled in a single *Sonogashira* reaction (Scheme 3). 1-Acetylsulfanyl-4-iodobenzene (**10**)<sup>[158]</sup> and 1-4-bisethynylbenzene (**11**) were treated with the standard conditions.<sup>[159]</sup> After workup the crude was purified by CC to yield compound **1** as a beige solid in 79% yield.



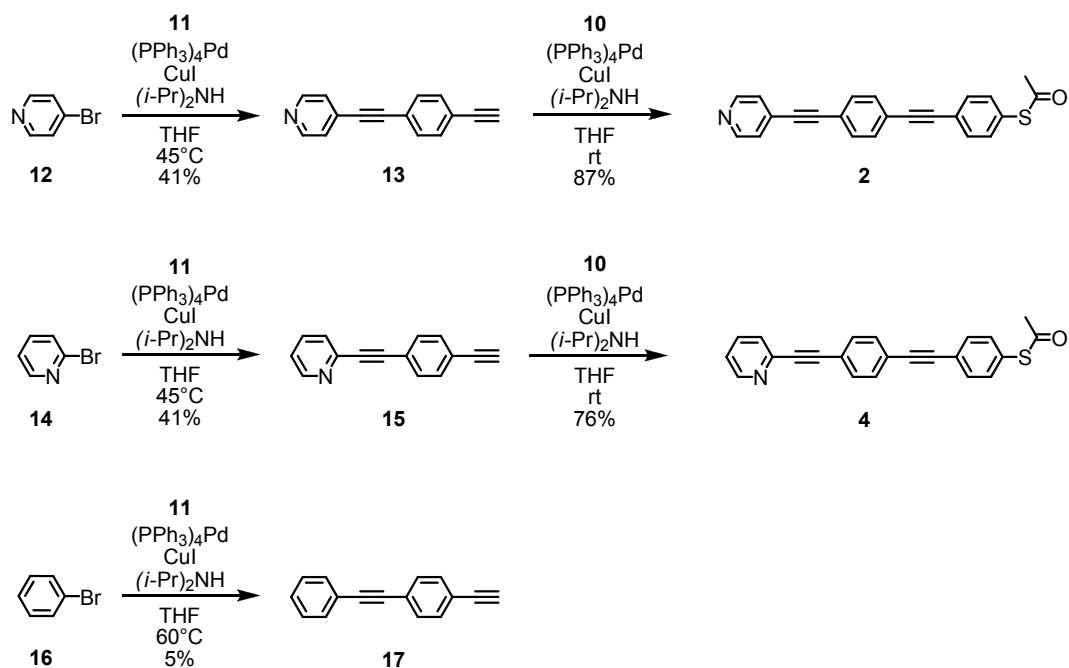
**Scheme 3:** Synthesis of symmetric rod **1** and **3** following synthetic strategy I.

The dipyridine functionalized OPE derivative **3** was synthesized applying the standard conditions to **11** and commercially available 4-bromo pyridine (HCl-salt) (**12**). The substitution of the bromide required elevated reaction temperatures and

therefore the reaction was performed at 47 °C. After workup and CC compound **3** was isolated in a 67 % yield.

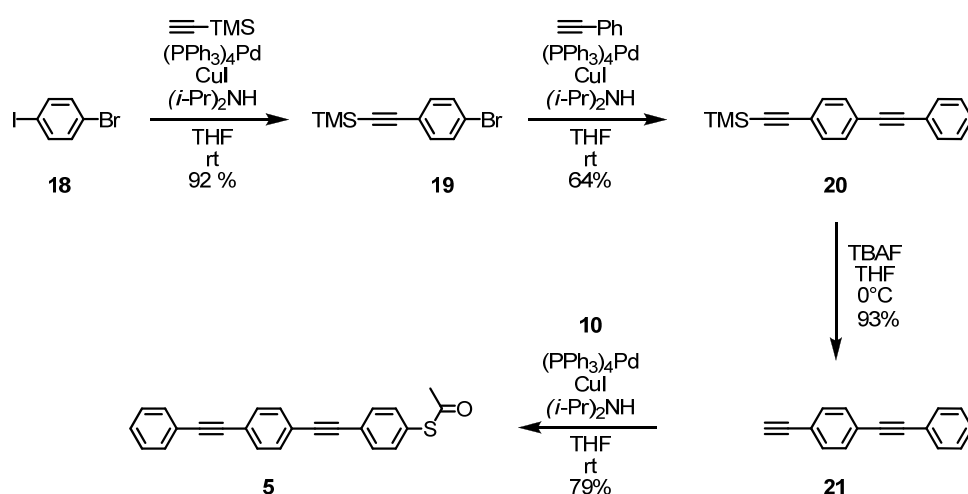
Target molecules **2** and **4** were synthesized applying synthetic strategy II. The electron withdrawing character of bromopyridines enabled monocoupling to 1,4-bisethynylbenzene (**11**). As the pyridines are electron poor aromatics, they withdraw electrons from the conjugated system which leads to a deactivation of the free acetylene in **13** and **15** and reduces the reactivity of a second coupling. Therefore **13** and **15** are achievable in acceptable yields in only one step. 4-Bromopyridine or 3-bromopyridine and 1,4-bisethynylbenzene were treated with the standard conditions at 45 °C. The mono coupled products **13** and **15** were isolated after workup and CC in 41% yield each. In a second *Sonogashira* reaction **13** and **15** were coupled with building block **10** and the two target molecules **2** and **4** were isolated in 87% and 76% yield as beige solids (Scheme 4).

The assembly of the monothiolated OPE **5** could not be performed efficiently by a comparable selective coupling strategy. For example, if bromo-benzene is reacted with 1,4-bisethynylbenzene (**11**) the monocoupled 1-ethynyl-4-(phenylethynyl)-benzene (**17**) was only isolated in 5 % yield. Therefore a stepwise synthesis is inevitable and synthetic strategy III was considered for the synthesis of **5**.



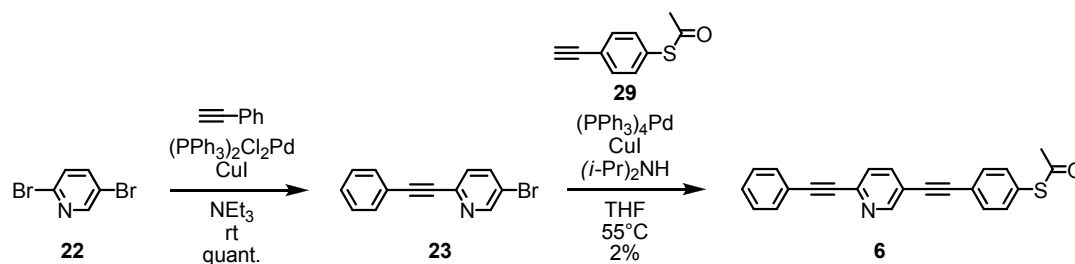
**Scheme 4:** Synthesis of compound **2** and **4**.

1-Bromo-4-iodobenzene (**18**) was treated with trimethylsilane-acetylene (TMS-acetylene) in a *Sonogashira* reaction using the standard conditions. The iodide-bromide selectivity in metal catalyzed coupling reactions is nicely reflected in this example, as 4-bromo-1-(2-trimethylsilyl-ethynyl)benzene (**19**) was isolated in 92% yield. **19** was then coupled with ethynylbenzene to give **20** in 64% yield. The TMS-protection group of the acetylene was cleaved with fluoride ions using tetrabutylammonium fluoride (TBAF). **20** was dissolved in THF and treated with a 1 M TBAF solution (in THF containing 5% water) at 0°C to yield the free acetylene **21** in good yield. In a final *Sonogashira* reaction **21** was coupled with **10** to give OPE **5** in a 79% yield as a beige solid.



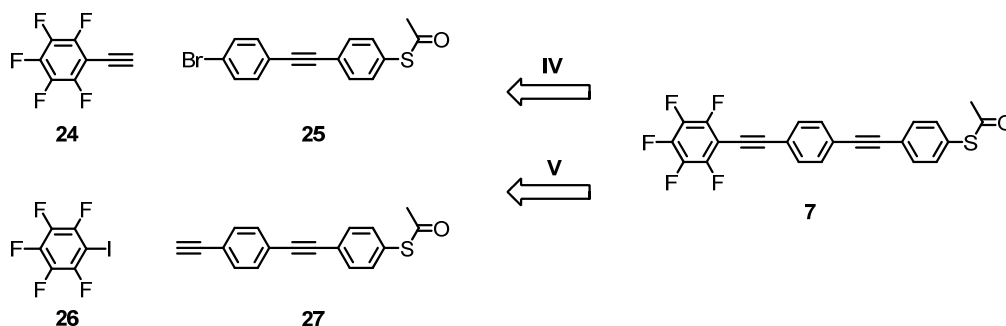
**Scheme 5:** Synthesis of compound **5**.

Compound **6** bears a 2,5-substituted pyridine as a central unit. The electron withdrawing character of pyridine towards the *ortho* and *para*-positions, activates the oxidative addition of 2,5-dibromopyridine in 2-position. Therefore, 2,5-dibromopyridine can be selectively substituted at the 2-position.<sup>[160]</sup> So if 2,5-dibromopyridine (**22**) is treated with ethynylbenzene in a *Sonogashira* reaction, **23** is observed as the main product in quantitative yields. The bromide **23** was coupled with 1-ethynyl-4-acetylsulfanylbenzene (**29**)<sup>[161]</sup> which directly led to the target structure **6**, but only in very low yield (Scheme 6). Elevated temperatures were required for the substitution of the bromide which led to decomposition of building block **29**. The acetyl protection group of the thiol is not stable under these harsher reaction conditions. To improve the outcome of this reaction, the thiol needs to be protected with a more stable protection group, or the bromide needs to be exchanged with iodide such that the reaction can be performed at room temperature.



**Scheme 6:** Synthesis of compound **5**. Pyridine activates the bromide in alpha position and therefore the compound **23** is selectively formed.

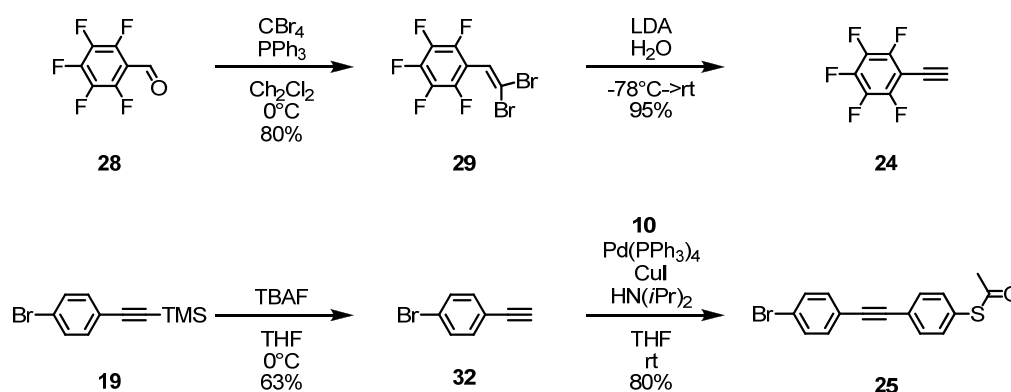
For the synthesis of target molecule **7** different strategies were envisaged. The most straightforward pathway would have been synthetic strategy II. However, coupling pentafluoroiodobenzene with 1,4-bisethynylbenzene did not lead to the desired mono-coupled building block 1-((4-ethynylphenyl)ethynyl)-pentafluorobenzene. Therefore a stepwise assembly was required and two different strategies (IV and V in Scheme 7) were considered. In the synthetic strategy IV the acetylene functionalized pentafluorobenzene **24**, which is available directly from a *Corey-Fuchs* reaction sequence from the commercially available corresponding aldehyde, is coupled with the corresponding halide **25**. On the other side, building block **27** can be assembled by a coupling-deprotecting sequence, and later coupled to the commercially available pentafluoroiodobenzene (**26**) (strategy V in Scheme 7).<sup>[162]</sup>



**Scheme 7:** Synthetic strategy IV and V for the assembly of target structure **7**.

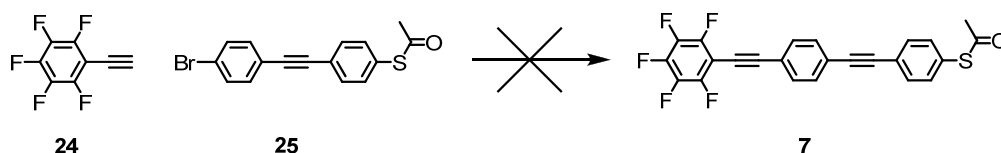
1-ethynyl-pentafluorobenzene (**24**) was synthesized with a *Corey-Fuchs* reaction starting from pentafluorobenzaldehyde (**28**) (Scheme 8)<sup>[163-165]</sup>. Therefore, carbontetrabromide and triphenylphosphine were dissolved in dichloromethane. The aldehyde was added at 0 °C and the reaction mixture was stirred for 30 minutes. To remove the salts that form, the reaction mixture was filtrated over a silica gel plug. After evaporation of the solvents, the mixture was purified by CC to obtain **29** as a colorless solid. **29** has a high vapor pressure and needs to be handled with care to

prevent sublimation on the rotary evaporator or at high vacuum. Therefore dichloromethane was chosen as the eluent for column chromatography. If hexane:ethylacetate is used as an eluent system, the product is lost while evaporating the solvents. In a second step the dibromo-olefine is treated with two equivalents of lithiumdiisopropylamine (LDA) which leads to formation of the vinylcarbenoid. After an H-shift, the acetylene is formed and immediately deprotonated with the second equivalent LDA and the lithium salt is formed. After aqueous workup the free acetylene is obtained. To form LDA, diisopropylamine was dissolved in dry THF, and *n*-BuLi was added as a 1.6 molar solution in hexane at -78 °C. The freshly formed LDA was then transferred by a cannula to a -78 °C cold solution of the dibromo-olefine in dry THF. After stirring for 40 minutes at -78 °C and one hour at room temperature the reaction mixture was quenched with water. After work up and CC, the acetylene **24** was obtained as a colorless solid in 95% yield. Again, pentafluoro-ethynyl (**24**) has to be handled with care to prevent sublimation.



**Scheme 8:** Synthesis of building block **24** and **25**.

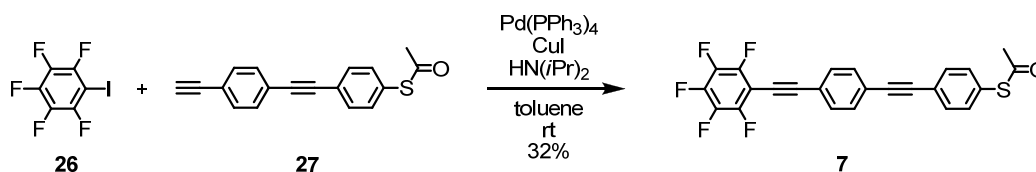
The corresponding building block **25** was synthesized starting from the previously described 1-bromo-4-(2-trimethylsilylethynyl)benzene (**19**). After deprotection with TBAF, **32** was coupled in a *Sonogashira* reaction to 1-acetylsulfanyl-4-iodobenzene (**10**) to afford building block **25** in 80% yield.



**Scheme 9:** Attempted synthesis of target structure **7**.

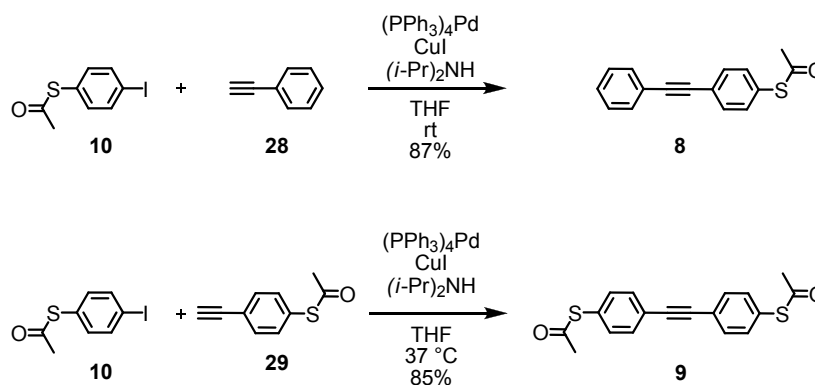
With both building blocks **24** and **25** in hand, the final *Sonogashira* coupling was aimed. However, all attempts for the synthesis of the fluorinated OPE through this

route failed (Scheme 9). One explanation could be that the perfluorinated benzene unit of **24** reduces the nucleophilicity of the acetylene, and disables it towards a *Sonogashira* reaction with a bromide.



**Scheme 10:** Synthesis of target structure **7**.

As an alternative pathway, synthetic strategy V was considered. Building block **27**<sup>[166, 167]</sup> was coupled with commercially available pentafluoroiodobenzene (**26**) in a *Sonogashira* reaction and indeed, the desired fluoro functionalized OPE **7** was obtained in 32 % yield (Scheme 10).<sup>[162]</sup>



**Scheme 11:** Synthesis of the short OPEs **8** and **9**.

The short OPEs **8** and **9** were readily accessible in one step. Coupling of 1-acetylsulfanyl-4-iodobenzene (**10**) to either ethynylbenzene (**28**) or 1-ethynyl-4-acetylsulfanylbenzene (**29**) led to the desired compounds **8** and **9** in 87 % and 85 %, respectively.

All compounds were fully characterized by melting point, TLC,  $^1\text{H}$ -NMR-spectra,  $^{13}\text{C}$ -NMR-spectra and mass spectroscopy (EI, MALDI-ToF or FAB). The elemental analysis of the OPE structures were off, therefore the purity of the compounds was further proved by gel permeation chromatography (GPC) in an HPLC setup. The absorption spectra recorded in dichloromethane are depicted in Figure 42.

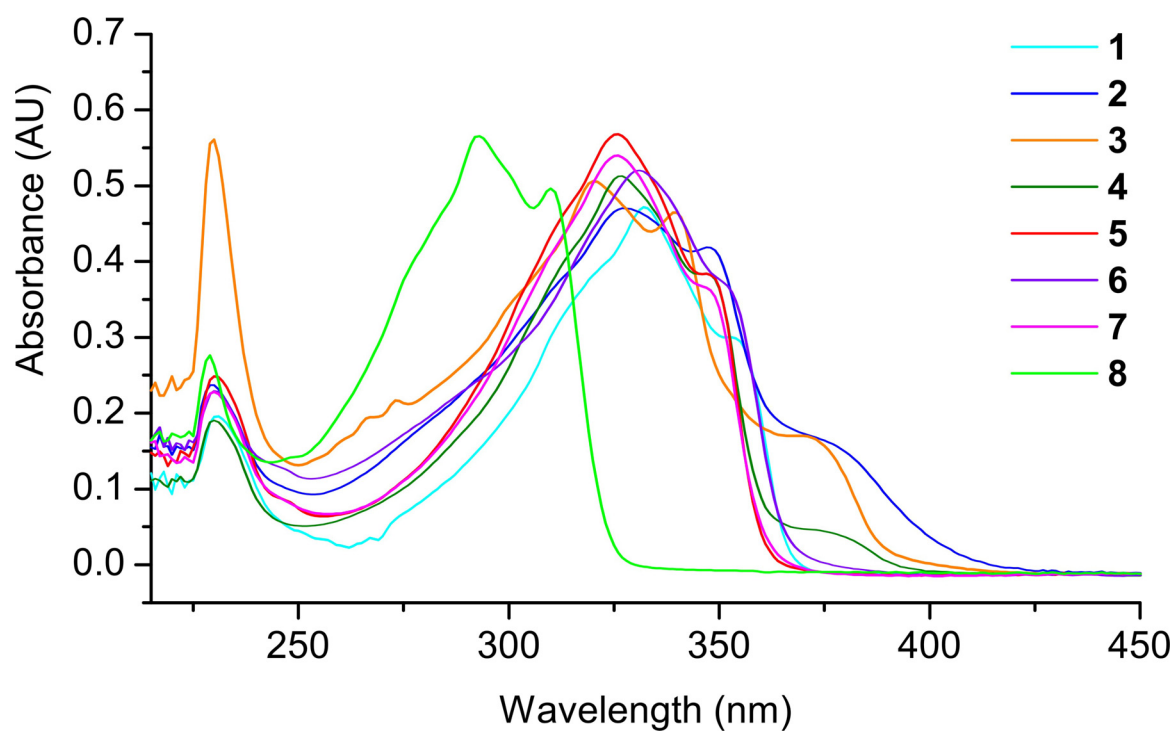


**Figure 42:** Absorption spectra of **1- 8** in dichloromethane.

All OPEs **1-7** have an absorption maximum between 320-332 nm with a shoulder at 340-351 nm. The pyridine containing compounds **2, 3, 4,** and **6** further show a shoulder at 374-378 nm. The short OPE **8** has an absorption maximum at 293 nm with a shoulder at 310 nm.

The transport investigation experiments of the synthesized compounds **1-8** will be discussed in the following sections.

## 2.3 Transport Investigations through Molecular Rods

### 2.3.1 Connecting Single Molecules to Two Electrodes

Electron transport investigations through molecular rods were performed in an MCBJ setup within a liquid environment. As a basic test and reference molecule, OPE **1** was initially investigated.

To immobilize molecules in the junction, the cell (cell volume: 3 ml) was flooded with a 0.25 mM solution of the OPE **1** in a degassed THF/mesitylene mixture (1/4). The acetyl protection groups of the thiophenol anchor groups were removed *in situ* by adding 50  $\mu\text{l}$  of a 10 mM solution of tetrabutylammonium hydroxide (TBAOH) in THF. Hereafter, the term solvent will refer to the degassed THF/mesitylene mixture (1/4) with the deprotection agent.

While measuring the conductance  $G(z)$  of only the solvent, the conductance decays after breaking the gold electrodes, but in presence of OPE **1** the current traces show plateaus with a value lower than  $G_0$  (Figure 43). The plateaus at the range of  $G \approx 10^{-4} G_0$  are attributed to single molecules immobilized between two electrodes.

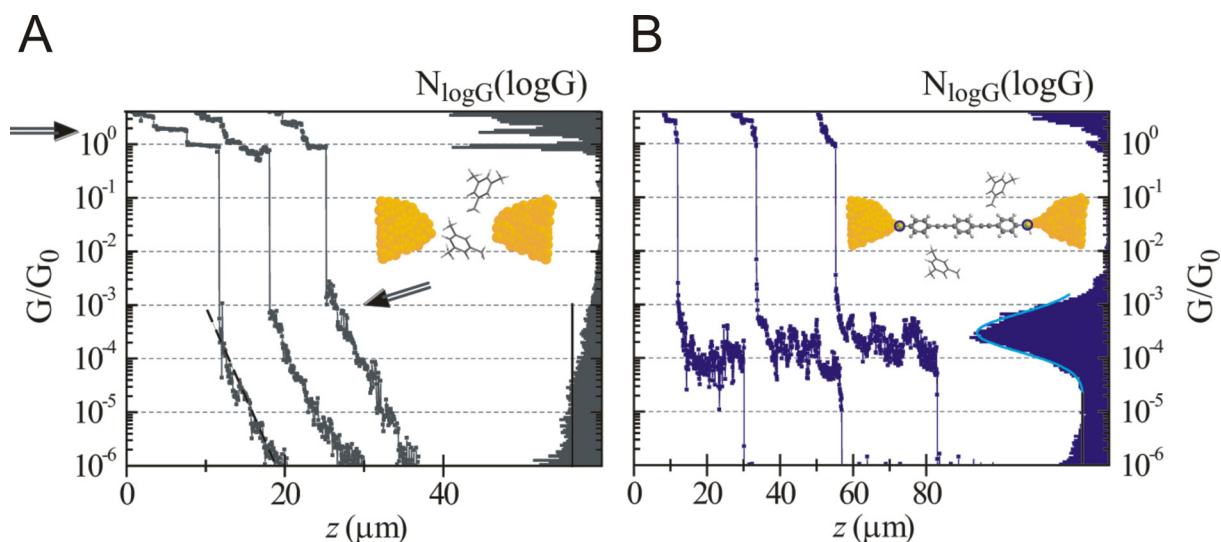


**Figure 43:** 3 conductance traces ( $G(z)$ ) of solvent molecules only are shown in A. The conductance traces are statistically analyzed by projecting hundreds of conductance traces towards the conductance axis revealed in histograms. When this is done with conductance traces of only solvent molecules, no molecular signature is obtained. 3 conductance traces of **1** are shown in B. In the histogram a pronounced conductance peak is obtained.



Histograms from 100 current traces were formed and are shown in Figure 44. Besides subtracting the background no data selection was performed. The clearest histograms are obtained in the logarithmic representation (B in Figure 44). Figure 44 shows a linear and a logarithmic representation of a histogram for OPE **1**. The histogram after subtraction of the tunneling background is shown in red. To deduce the conductance of a single molecule a Gaussian curve is fitted to the histogram. While determining the maximum of the Gaussian fit, the conductance of OPE **1** can be assigned to  $G = 1.2 \cdot 10^{-4} G_0$ . The peaks are centered at a different position in the two kinds of histograms. The peak appears at slightly lower values in the G-histogram compared to the  $\log(G)$  one.

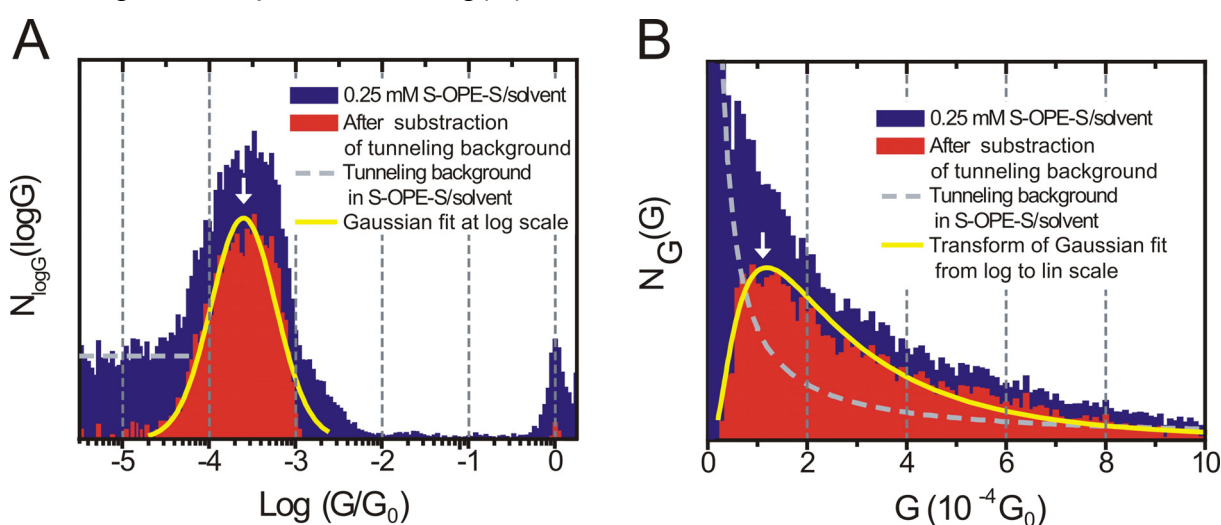


**Figure 44:** Logarithmic representation of a histogram obtained for OPE **1** (A) and the linear representation (B).

Using the MCBJ technique it was possible to trap single molecules comprising two anchor groups between two electrodes. The conductance of OPE **1** was deduced and has a value of  $G = 1.2 \cdot 10^{-4} G_0$ . These results are very reproducible, and therefore OPE **1** is often referred to as a standard molecule. Henceforth, the conditions applied for the immobilization of OPE **1** in an MCBJ setup within a liquid environment are referred to as the MCBJ standard conditions.

### 2.3.2 Exploring Different Contacts

To trap a molecule between two electrodes, the molecule needs to possess anchor groups. Sulfur forms strong covalent Au-S bonds and proved to be a good choice to fix molecules to metal electrodes and provide electronic coupling. In the introduction several anchor groups were mentioned, however here we are looking at binding properties of pyridines and thiols. The OPE backbone is kept the same for all three investigated molecules but the thiophenol subunits are systematically substituted with pyridines. The immobilized OPEs **1** - **3** are depicted in Figure 45.

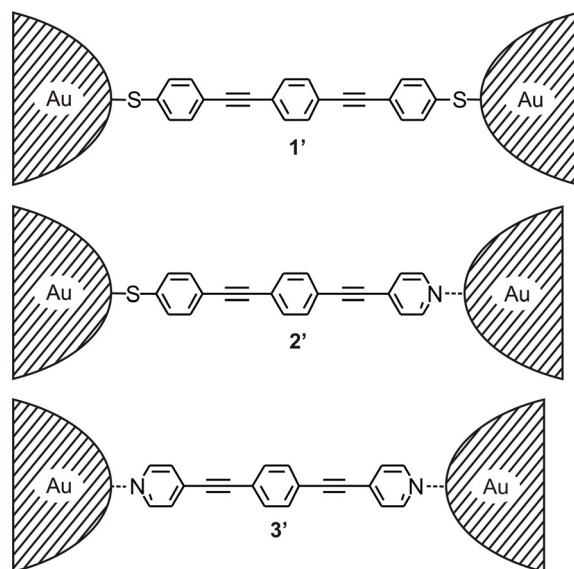


**Figure 45:** Immobilized target molecules possessing two thiol (**1'**), one thiol and one pyridine (**2'**) and two pyridine (**3'**) anchor groups, respectively.

The molecules **1** - **3** were immobilized in an MCBJ within a liquid environment applying the standard conditions described. In the case of the acetyl protected compound (**1** and **2**) a deprotection agent (TBAOH) was added prior to exposition to the setup, whereas the dipyridine functionalized OPE **3** was directly exposed to the setup. The recorded current traces of all three molecules show plateaus at a  $G$  value below  $G_0$  and the plateau formation probability is about the same for all molecules (40 – 50 %). Figure 46 shows the histograms obtained for the measurements of OPE **1** - **3**. Interestingly all three signals are comparable in height and width, however drastically vary in their position.

As the molecules become shorter when exchanging a thiol anchor group to a pyridine anchor group, one would expect the conductance to increase due to a shorter tunneling distance. However, the opposite is found to be the case. The dithiol

functionalized molecule **1** shows a conductance around  $G = 1.2 \cdot 10^{-4} G_0$ . By replacement of one thiol unit (**2**) the conductance decreases to  $G = 5.7 \cdot 10^{-5} G_0$ . By replacement of both thiol units to pyridine (**3**) the conductance decreases by nearly two orders of magnitude to  $G = 3.5 \cdot 10^{-6} G_0$ .

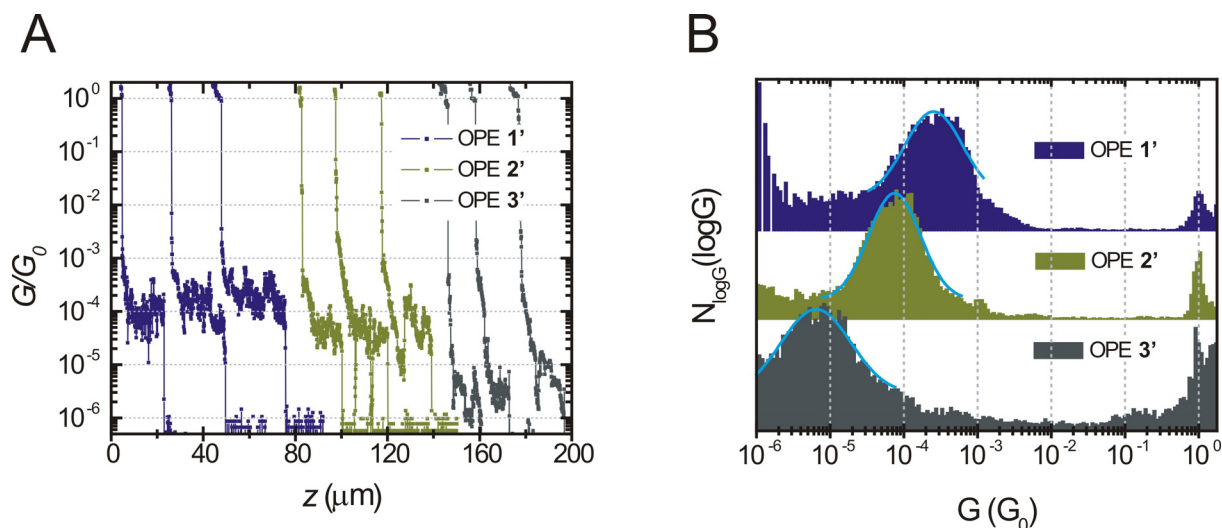


**Figure 46:** Conductance traces of **1'**, **2'** and **3'** (A) and the logG histogram (B).

Molecule	Conductance $G$ ( $G_0$ )	Distance ( $\text{\AA}$ )
<b>1'</b>	$(1.2 \pm 0.1) \cdot 10^{-4}$	20.7 (S,S)
<b>2'</b>	$(5.7 \pm 2.4) \cdot 10^{-5}$	18.7 (S, N)
<b>3'</b>	$(3.5 \pm 1.2) \cdot 10^{-6}$	16.6 (N,N)

**Table 1:** Average single molecule conductance. At least 4 samples were investigated each. The distance of the anchor groups was calculated using MM2 force field calculations (ChemDraw 3D).

Already discussed in the introduction, the conductance through a molecule with a distance  $d$  is described in the tunneling physics theory as:

$$G = A \cdot e^{-\beta d}$$

The decay constant  $\beta$  is determined by electronic parameters of the molecule backbone.  $A$  is the prefactor and depends on the electron density-of-states at the point where the molecule contacts an electrode and consists in our case (different anchor groups) of  $A = A_{left} \cdot A_{right}$ .  $A$  is considered as “contact conductance” and for a simple estimation we assume  $A$  to be independent of  $\beta$ . Due to a systematic variation of the anchor groups in OPE **1-3** we can calculate e.g.  $A_S$  and  $A_N$  from **1** and **3** and then compare the calculated  $A_{NS}$  with the  $A_{NS}$  experimentally obtained. For the decay constant  $\beta$  ( $=0.3 \text{ \AA}^{-1}$ ) of conjugated molecules and the length of the molecules as shown in table 1 we can calculate the “contact conductance”.

For compound **1** and **3**:

$$G_{SS} = A_S \cdot A_S \cdot e^{-\beta d_{SS}}$$

$$G_{NN} = A_N \cdot A_N \cdot e^{-\beta d_{NN}}$$

we can calculate the contact conductance for thiol:  $A_S = 0.24 G_0$ ; and pyridine nitrogen:  $A_N = 0.028 G_0$ .

From the two values we can calculate the contact conductance of OPE **2**

$$A_N \cdot A_S(\text{calc}) = 0.0067 G_0$$

However, assigning  $A_N A_S$  from the experimental values with:

$$G_{NS} = A_N \cdot A_S e^{-\beta d_{NS}}$$

we obtain  $A_N A_S(\text{exp}) = 0.019 G_0$  which is about three times larger. The fact that  $A_N A_S(\text{exp})$  is larger than  $A_N A_S(\text{calc})$  indicates that the transport is dominated by the thiol anchor. Therefore the model of independent “contact conductance” does not appear to hold true. The disagreement may arise from effects of the anchor group on the HOMO-LUMO gap or from a different alignment of the frontier orbitals with respect of the Fermi level of the electrodes. UV/vis investigations of OPE **1** - **3** show similar absorption spectra for all three molecules. The HOMO-LUMO gap only varies slightly. This suggests a different alignment of the HOMO-LUMO orbitals to the Fermi level of the gold contacts.

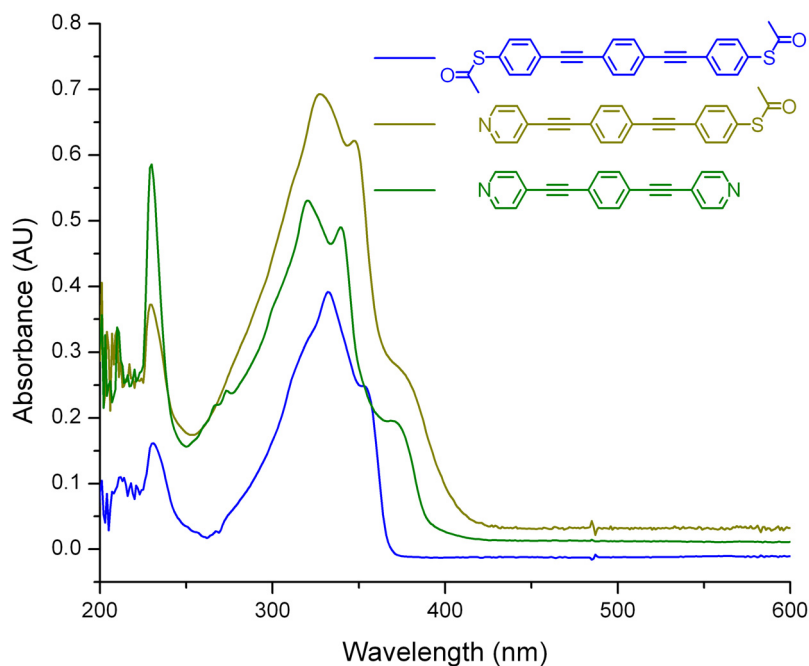


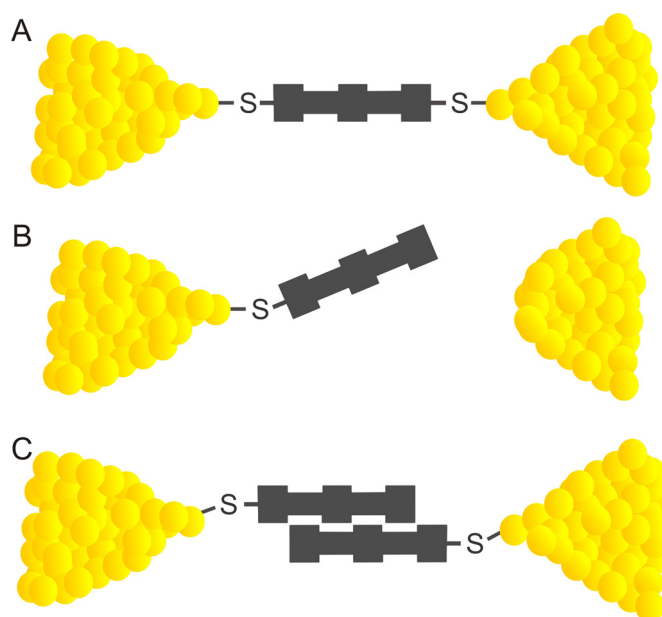
**Figure 47:** Absorption spectra of **1**, **2** and **3**.

We think that the low conductance value of **3** is due to misalignment of the frontier orbitals. For the asymmetric compound **2** the frontier molecular orbitals seem to be fixed by the coupling of thiol to gold.

In conclusion the role of contact in molecular junctions was investigated. The anchor groups in OPE model compounds were systematically varied with pyridines and thiophenols. The conductance of the molecule with one thiol and one pyridine anchor group is an order of magnitude larger than the conductance of the dipyridine functionalized OPE **3** but only half the conductance of the dithiol OPE **1**. The electron transport was found to be dominated by the thiol-contact. Contacts are very important components in molecular electronic systems and anchor groups have to be carefully selected.

### 2.3.3 Molecular Junctions Based on Aromatic Coupling

Molecules investigated between two electrodes usually are designed as rod-like systems with two anchor groups. Single molecules with two anchor groups can be bridged between the electrodes of an MCBJ setup (as already discussed in 2.3.2). Sulfur forms a covalent bond to gold which is more stable than the Au-Au bond.<sup>[168]</sup> Therefore if a molecule is immobilized in an MCBJ and the electrodes are further bended apart, the gold atoms migrate towards the tips until the junction breaks. For molecules with only one anchor group rather than two, one would not expect a stable metal-molecule-metal junction because the molecule can only attach to one side of the junction (B in Figure 48). However, this assumption ignores intermolecular interactions and, as we shall see, these interactions can be relevant to the behavior of molecular junctions. We investigate the formation of metal-molecule-molecule-metal junctions consisting of two molecules, each binding to one of the electrodes.<sup>[59]</sup>

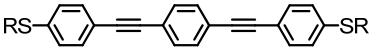
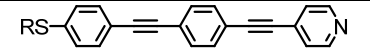
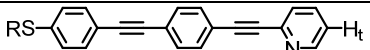
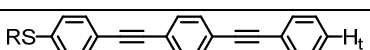
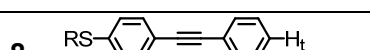


**Figure 48:** Molecules with two anchoring groups form metal-molecule-metal junctions (A). Molecular rods lacking a second anchor group are not expected to form a stable junction (B). However, we investigate whether it is possible to connect two electrodes with two molecules both fixed to one of the electrodes. It is postulated that intermolecular interactions such as  $\pi$ - $\pi$  stacking might be the origin of a stable junction formation (C).

Here we report MCBJ investigations on molecules with anchor groups on both ends, and the situation when one anchor group is removed. The influence of aromatic  $\pi$ - $\pi$  coupling between adjacent molecules on the formation of molecular junctions will be discussed.

### 2.3.3.1 Molecular Signals of OPEs with One Anchor Group

The rigid OPE systems are considered as molecular rods. While keeping a thiol anchor group on one side, we systematically vary the group on the other side of the rod. As a reference molecule we look at molecule **1** with two thiol anchor groups, one on each side, providing strong binding to both electrodes. This molecule does form single molecule junctions (chapter 2.3.1). In the OPE **2** one thiol anchor group is replaced by a pyridine unit in the *para*-position. Pyridine can form a coordination bond to gold, and one can still expect that OPE **2** forms single molecule junctions, although less stable with a lower conductance (chapter 2.3.2). In OPE **4** the position of the pyridine unit is changed to the *ortho*-position and therefore the pyridine anchor group is hidden. Providing very comparable electronic properties as in OPE **2**, the pyridine can hardly form a bond to gold due to its position. As a terminal atom of **4** the hydrogen atom of the terminal phenyl ring  $H_t$  has to be considered. In the molecule **5** the pyridine unit is completely removed, leaving a bare phenyl unit. Also here the opposite group to the thiol anchor group is a hydrogen atom  $H_t$ . No formation of a single metal-molecule-metal junction is expected for molecule **5** as it has only one anchor group on one side of the rod. As another control molecule the OPE comprising one thiol unit but only consisting of two phenyl rings **9** was designed.

Molecule	Length (Å)	No. of samples	Conductance ( $G_0$ )
<b>1</b> 	20.7 (S-S)	4	$(1.2 \pm 0.1) \cdot 10^{-4}$
<b>2</b> 	18.7 (S-N)	3	$(5.7 \pm 2.4) \cdot 10^{-5}$
<b>4</b> 	19.8 (S- $H_t$ )	3	$(6.6 \pm 1.3) \cdot 10^{-6}$
<b>5</b> 	19.8 (S- $H_t$ )	3	$(5.9 \pm 2.4) \cdot 10^{-6}$
<b>8</b> 	12.9 (S- $H_t$ )	4	

**Table 2:** The molecule **1**, **2**, **4**, **5** and **8** were synthesized in their acetyl protected form ( $R = \text{COCH}_3$ ) *In situ* deprotection leads to the free thiols which then bind to the gold electrodes ( $R = \text{Au}$ ).  $H_t$  denotes the terminal hydrogen atom. The length of each molecule is obtained after energy minimization using the MM2 force field (ChemDraw 3D). The single-molecule conductance value  $G$  was deduced from the peak that appears in the  $\log(G)$  histograms of 100 opening  $G(z)$  curves obtained from three to four different samples.

The results of the corresponding conductance measurements are shown in Figure 49. It is evident that for all the molecules **1** – **4** a pronounced conductance peak is obtained. It is surprising that both the height and the width of these peaks are similar for molecules **1** – **4**. The conductance value of molecule **2** is slightly reduced by approximately a factor of 2-3 as compared to the reference OPE **1**. This smaller value is due to weaker electronic coupling between nitrogen and Au atoms as discussed in section 2.3.3. Although we expect a peak in  $\log(G)$  for molecule **2**, a similar peak of equal magnitude for molecule **4** comes as a surprise. Because the nitrogen atom of the pyridine structure in molecule **4** is “hidden”, it may provide, if at all, a much less probable binding site to the electrode.

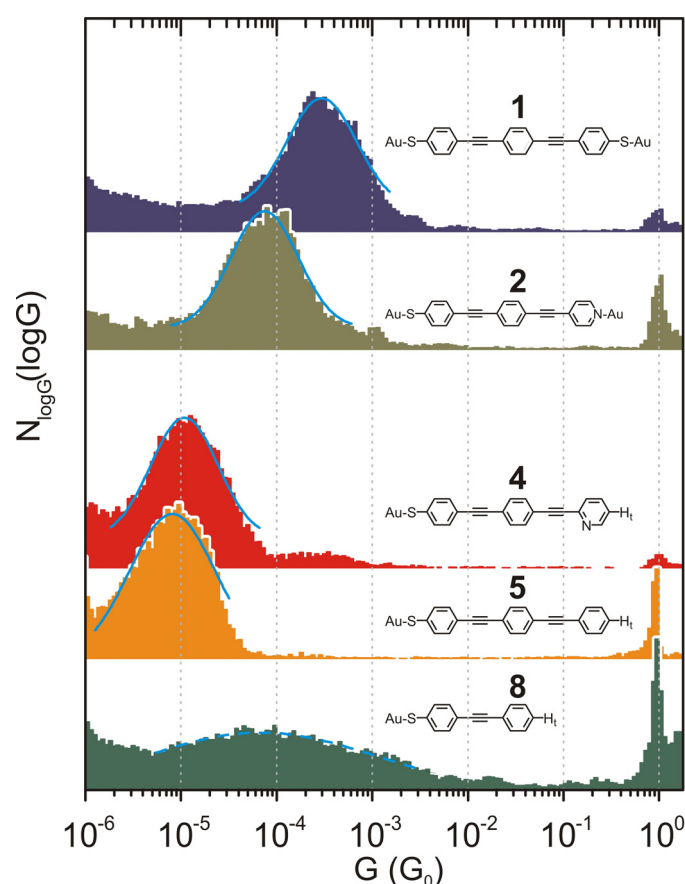


**Figure 49:** Conductance histograms for the different molecules. Molecule **1** and **2** have two anchor groups, whereas molecule **4**, **5** and **8** only comprise one anchor group. The histograms are formed from 100  $G(z)$  curves and the blue solid lines are the Gaussian fit curves.

In contrast to this, the identical magnitude and width of the peak in  $\log(G)$  suggest that molecule **4** also binds in the junction with a similar probability as molecules **1** and **2**. Hence, the observed strong binding must have another origin. This is further supported by the measurements for molecule **5**. Although the anchor group at one



end is now removed completely, we obtain very similar results for **3** and **4**. These results lead to the question why molecular junctions form, even with molecular rods having only a single linker group on one side of the rod.

We believe that the connection between the electrodes is made possible by a  $\pi$ - $\pi$  stacking interaction between a pair of molecules.<sup>[59, 169-171]</sup> If one molecule is anchored by means of its thiol linker group to, for example, the left electrode, another one bound to the right electrode can complete the mechanical assembly of the junction through  $\pi$ - $\pi$ -coupling through the phenyl rings. This interpretation is supported by the shift of the conductance peak to lower values by more than an order of magnitude. In this picture, a reduced G value is expected, because the pair of molecules will be longer than a single dithiol molecule anchored between gold electrodes. We observe that the junctions form with a similar probability, whether for dithiolated compounds or monothiolated compounds. As the strength of  $\pi$ - $\pi$  stacking depends strongly on the conjugation extent of the system and the overlap between adjacent compounds, one straightforward control experiment, without modifying the electronic structure of the molecules to a great extent, is to investigate an OPE compound with only two phenylene units (molecule **8**). Although this peak is shallow, single conductance traces are still clearly visible but noisier plateaus at values larger than the plateau values for molecules **4** and **5**. We believe that the peak for molecule **8** is less pronounced because of the reduced  $\pi$ - $\pi$ -interaction for these shorter molecules, leading to a mechanically less stable junction. A pair of molecules of **8** tends to have a higher conductance value than a pair of molecules of **5** because of the reduced distance the electrons have to tunnel between the gold electrodes through the molecular bridge. We also checked that for molecules where no aromatic stacking is possible, such as in monothiolated alkane chains, we do not observe the formation of molecular junctions. We also emphasize that without deprotecting the thiol function, no molecular signature can be detected. This permits the elimination of other unanticipated interactions except for intermolecular interactions to explain the signal observed for compounds **4**, **5** & **8**.

The different conductance values obtained for the metal-molecule-molecule-metal junctions compared to the metal-molecule-metal junctions can be qualitatively attributed to the difference in the distance that electrons have to tunnel between the gold electrodes. This distance is determined by the length of a  $\pi$ - $\pi$  stacked pair of molecules. The stacking of a pair of monothiol molecules **4** is illustrated in Figure

50 A. Figure 50 B-D present different stacking configurations of the same molecule and Figure 50 E shows the molecule with two anchor groups fixed on both sides to the electrodes. Due to electrostatic repulsion of the negative  $\pi$ -electron clouds, the aromatic rings will not sit directly on top of each other, but rather in a staggered configuration.<sup>[172]</sup> Despite working with diluted solutions, the molecules self-assemble at the surface of the gold electrodes, leading to a high local concentration. We therefore expect the molecules to form coplanar stacks as illustrated in Figure 50 A. Still, there are three possible arrangements, either one pair of phenyl rings stack (D in Figure 50), two pairs of phenyl rings stack (B in Figure 50) or three pairs of phenyl rings stack (C in Figure 50). We believe that Figure 50 B represents the actual stacking configuration of a pair of molecules of compound **5**.

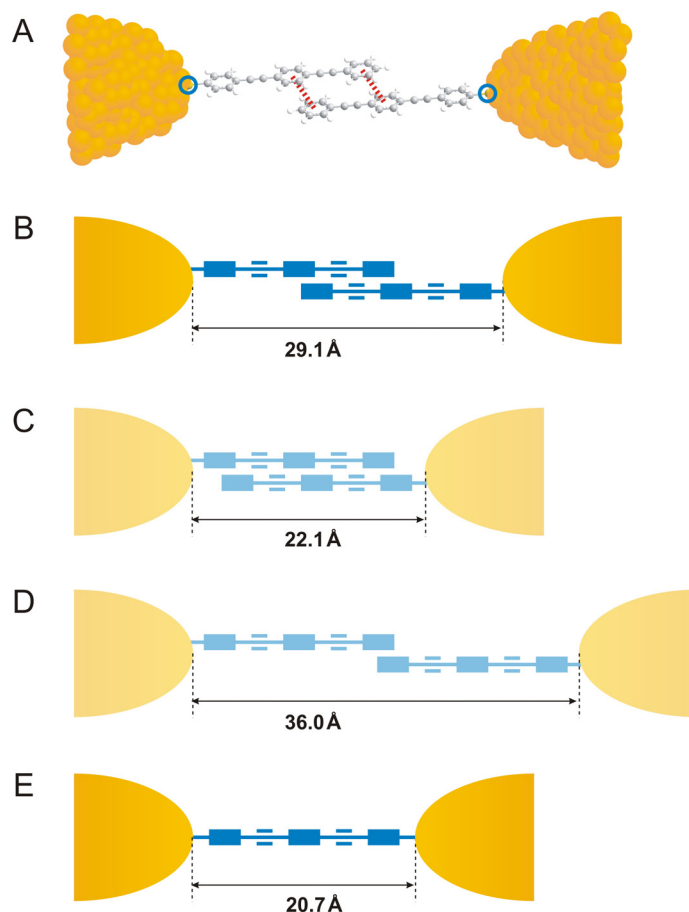


**Figure 50:** Staggered conformation of a molecular junction consisting of two molecules of **5** (A). Simplified schematic representation of different stacking configurations with either two pairs of phenyl rings stacking (B), three pairs of phenyl rings stacking (C) or one pair of phenyl rings stacking (D), respectively. Configuration B is the most probable one whereas the other configurations are believed to be less favored due to steric interactions (C) and reduced conjugation and overlap (D), respectively. The molecule bearing two anchor groups fixed to both electrodes is schematically represented in E. The lengths given are sulfur to sulfur distances calculated by MM2 minimization (ChemDraw 3D).

The structures in Figure 50 C & D are postulated to be less probable because of steric hindrance and because of weaker  $\pi$ - $\pi$  interactions due to the reduced overlap between the molecules, respectively. The two sulfur atoms in dithiol functionalized OPE **1** are 20.7 Å apart. In the proposed configuration B (in Figure 50), the two sulfur atoms are separated by 29.1 Å. In a simple tunneling picture where electrons tunnel through an effective medium over a distance  $d$ , the conductance  $G$  can be written as  $G = Ae^{-\beta d}$ . The decay constant  $\beta$  is determined by the electronic parameters of the effective medium (here, the molecules). For a given electrode material (here, gold), the prefactor  $A$  depends on the electron density-of-states at the point where the molecules contact the gold electrode. Because this is determined by thiol anchors both in a single molecule and a stacked pair of molecules, this factor can be taken as a constant. The longer tunneling distance of electrons in a junction based on two stacking molecules leads to a 12 times smaller conductance by estimation. This is in reasonable agreement with experiment which shows a 20-fold difference.

$\pi$ - $\pi$  Stacking is stronger with a larger difference in electron density of the two stacking phenyl units. Therefore the  $\pi$ - $\pi$  stacking is enhanced when an electron rich phenyl faces an electron poor phenyl. As pyridine reduces the electron density of its aromatic core, molecule **4** favors the overlap of two phenyl pairs and forces the molecules to stack in a slightly more planar fashion than in pairs of molecule **5**. This small shift slightly reduces the tunneling distance leading to a small increase in conductance by a factor of 1.11.

As a further control experiment molecule **6** comprising the pyridine unit as a central ring was designed and synthesized. The pyridine on the central ring disfavors stacking with two pairs of phenyl moieties, but it could still stack with one ring (D in Figure 50). However, no molecular signature was obtained for molecule **6** when the previously described immobilization conditions in an MCBJ were applied. These results further corroborate that the molecular junctions are best described by the schematic representation B in Figure 50.

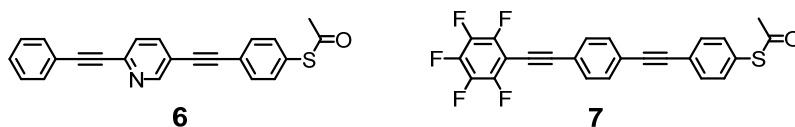


**Figure 51:** Molecule **6** comprises a pyridine ring as central unit.  $\pi$ - $\pi$  Stacking is therefore disfavored. On the other hand OPE **7** comprises a perfluorinated phenyl ring which should enhance the stacking properties.

To enhance stacking properties, OPE **7** with a perfluorinated terminal phenyl ring was synthesized. The fluorine atoms reduce the electron density of the ring which should increase the stacking properties. However, no pronounced peak was obtained for **7**. This might be attributed to the high local density of molecule leading to repulsion of the sterically more hindered perfluorinated phenyls when the two electrode tips come close together.

These results were further confirmed by calculations in a systematic first-principle study.<sup>[173]</sup>

In conclusion, the role of intermolecular interactions in molecular junctions was investigated. Whereas molecular rods commonly bear two anchor groups to provide stable binding to both electrodes, the molecules for these investigations were designed such that molecular junctions were solely formed due to  $\pi$ - $\pi$ -interactions. The intermolecular  $\pi$ - $\pi$  stacking interaction between monothiol molecules composed of alternating phenylene and ethynylene units was strong enough to induce the formation of molecular junctions. The conductance of the metal-molecule-molecule-metal junction was smaller than the conductance of reference OPE **1** due to longer electron tunneling distances, but interestingly the junction formation probability and the height and width of the peak in the logarithmic histogram were very comparable to OPE **1**. We also showed that  $\pi$ - $\pi$  stacking can be used as the dominant guiding force for the formation of molecular bridges in few-molecule electronic junctions.

### 2.3.4 From Single Junctions to Two-Dimensional Gold Nanoparticle Arrays

Described in section 2.3.1, it was possible to form single metal-molecule-metal junctions using the MCBJ technique and we were able to immobilize different molecular rods on a single molecule level. In this section we focus on the formation of networks of metal-molecule-metal junctions. Therefore two-dimensional gold nanoparticle arrays are anticipated to be linked by molecular conductors.<sup>[51]</sup> In previous investigations, an increased conductance of the gold nanoparticle arrays was observed when the thioalkanes were exchanged with OPE 1.<sup>[49, 50]</sup> The question arose whether the origin of the molecular junction formation was a covalent linking of the dithiol OPE 1 to two nanoparticles, or an aromatic coupling of two molecules, each bound to one of two bridging nanoparticles. In the following experiments molecules with one and two anchor groups were investigated in order to answer this question.

#### 2.3.4.1 Formation of Gold Nanoparticle Array Junctions

The gold nanoparticle arrays were prepared as described in the introduction (1.1.1.1 *D*). In doing so, highly ordered two-dimensional arrays of alkylthiol protected gold nanoparticles were obtained. These nanoparticle arrays display an ideal platform to form extended junctions. While evaporating gold pads onto the arrays, they become electronically addressable. Every pair of neighboring contact pads will be termed device and contains typically  $10^6$  molecular junctions between the metallic contacts. One sample contains a few tens of devices (B in Figure 52). Conjugated molecules can be introduced into the arrays using place-exchange while dipping a sample in a solution of the incoming molecule (A in Figure 52). The samples were immersed in a 1 mM solution of the OPE in THF with ammonium hydroxide as a deprotecting agent at 40 °C under an argon atmosphere. After 10 h the samples were taken out of solution, rinsed with THF and dried under a stream of nitrogen gas.

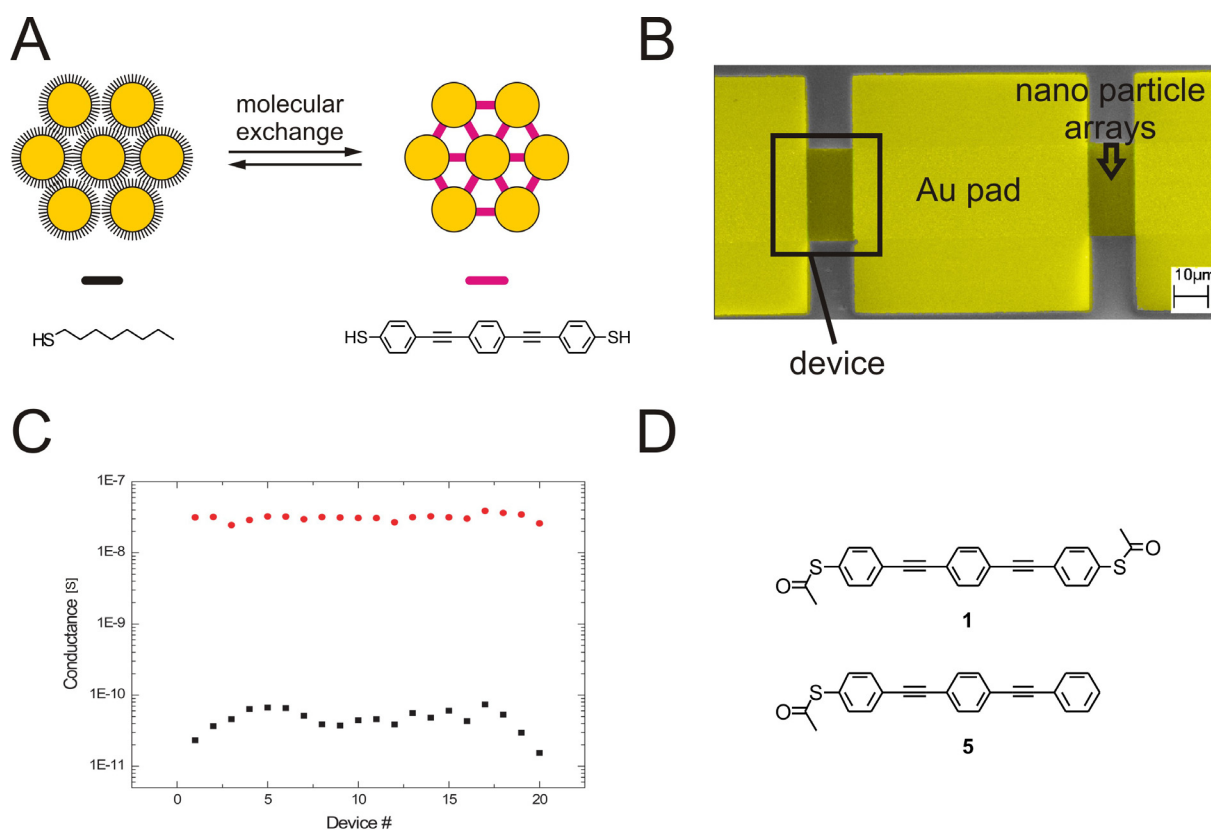


**Figure 52:** Gold nanoparticle arrays prepared as described in 1.1.1.1 D. Two neighboring gold pads form a device (B). Each sample contains a few tens of devices. Via place exchange the molecules of interest (D) are brought into the devices (A) which leads to a drastic increase in conductance (C).

Two different OPEs were investigated within these two-dimensional arrays (D in Figure 52). First, OPE **1** was studied. With its two thiol anchor groups, it is in principle able to covalently connect two gold nanoparticles. Second, OPE **5** was investigated. OPE **5** has the same OPE backbone as OPE **1** but lacks a second anchor group.

### 2.3.4.2 Results

Three samples were prepared for each compound, and the initial conductance  $G_i$  before exchange of the alkyl thiols and the final conductance  $G_f$  after exchange were measured for each device. Figure 52 C shows the sheet conductance  $G_{\square}$  for 20 devices measured before and after exchange for OPE **1**. Here,  $G_{\square} = G \cdot l / w$ , where  $w$  is the width of the printed nanoparticle line,  $l$  the distance between the two neighboring contact pads and  $G$  the measured conductance. It is clearly seen that the conductance of each device increases by a factor of 2-3 after introducing the conjugated OPEs. From Figure 52 C it is also obvious, that the conductance of the devices is not always the same. This device-to-device fluctuation is attributed to local

geometric variations emerging during sample preparation. Note, however, that the variation of the final conductance value  $G_f$  correlates very well with that of the  $G_i$ . This indicates that the structure of the arrays remains intact during the course of exchange, as also demonstrated by SEM images of the arrays taken before and after exchange. Given this observation, the ratio of conductances  $G_f/G_i$  before and after exchange was compared to investigate the differences emerging from the difference in anchoring groups between compound **1** and **5**.

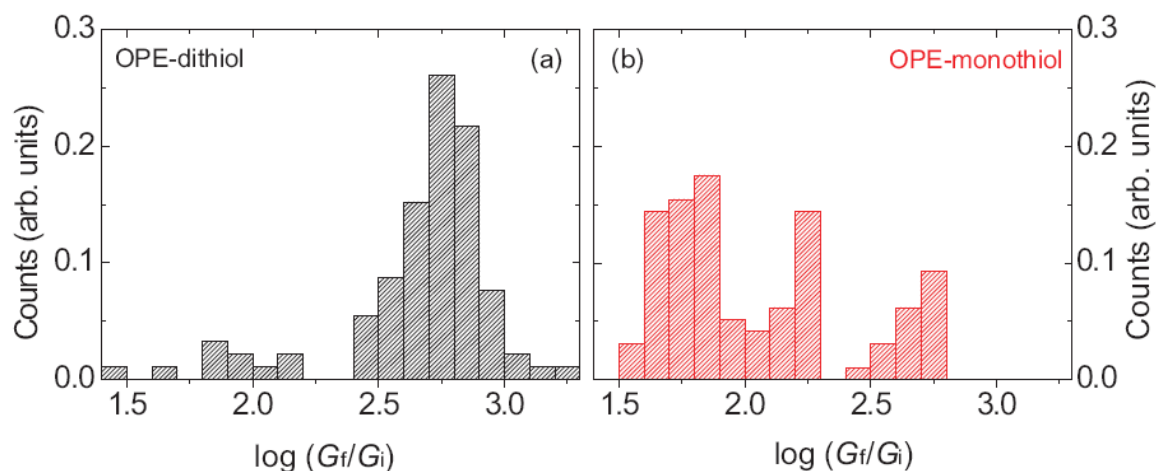


**Figure 53:** Histograms of  $\log(G_f/G_i)$  for OPE-dithiol **1** (a, black) and OPE-monothiol **5** (b, red).  $G_f$  is the final sheet conductance after exchange and  $G_i$  is the initial sheet conductance before exchange.

In Figure 53 the histograms of the logarithm of the conductance ratios ( $G_f/G_i$ ) for OPE-dithiol **1** and OPE-monothiol **5** are shown. These experimental results reveal that conductance increases is for both the conjugated compounds. This increase is, on average, larger for OPE-dithiol **1**. The distribution of the conductance ratios is broader for the monofunctionalized OPE **5** compared to the OPE **1** containing two anchor groups. Figure 54 shows a log-log plot of  $G_f$  as a function of  $G_i$  for all measured devices. Black symbols indicate data for the OPE-dithiol **1**, while red symbols are for OPE-monothiol **5**. The different symbol shapes represent different samples. The linear fit curves are shown as dotted lines. For any given initial conductance value, the final conductance of the arrays after insertion of the conjugated compounds is systematically larger for **1** than for **5**. The average ratio  $G_f/G_i$  is with 600 for **1** larger than 230 for **5**.

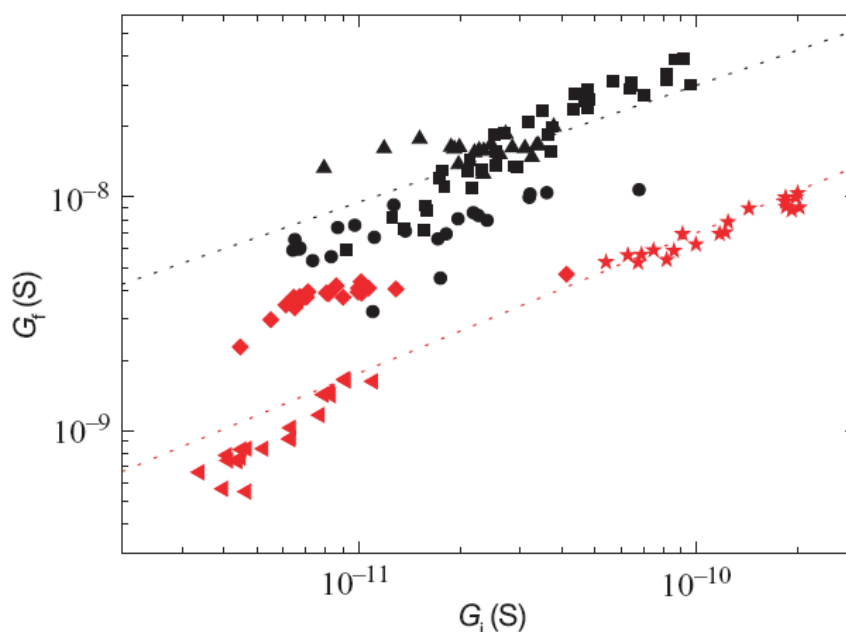


**Figure 54:** The log-log plot of the final conductance  $G_f$  as a function of the initial conductance  $G_i$  of all devices for **1** (black) and **5** (red). Different symbols indicate data from different samples. The dotted lines show the average slopes for both the molecular compounds of 0.5 (**1**) and 0.6 (**5**).

If we consider a simple tunneling model, the conductance can be described as  $G = A \cdot e^{-\beta d}$ , where  $d$  is the molecule's length, and the decay factor  $\beta$  is determined by the molecule between electrodes. The prefactor  $A$  accounts for the molecule-electrode contact conductance. From the slope of the linear fit in Figure 54 we can deduce the ratio of the two decay factors  $\beta_f/\beta_i$ . The ratios of the two decay factors are for **1** and **5** with  $0.5 \pm 0.2$  for **1** and  $0.6 \pm 0.2$  for **5** very similar. As the length  $d$  of both molecules **1** and **5** are very comparable, the prefactor  $A$  must be different for OPE-dithiol **1** and OPE-monothiol **5**. In the simple tunneling model considered, the prefactor  $A$  reflects the efficiency of charge transport across the contacts of the molecule to the Au electrode (here, the nanoparticles) and is proportional to the product of the density of states at both metal-molecule interfaces. The absence of a covalent bond between molecule and electrode leads to a reduced density of states at the molecule-metal interface and thus the prefactor will be reduced. Therefore we can associate the systematic lower conductance of molecular junctions formed by **5** to the absence of a metal-molecule covalent bond at one end of the molecule. These experiments provide strong evidence that the place exchange of dithiolated OPE **1** into a nanoparticle array leads to an interlinking of neighboring nanoparticles,



resulting in the formation of a chemically interconnected network of molecular junctions.

In conclusion we have seen with these experiments that molecular rods consisting of an OPE backbone can be used to form two-dimensional arrays of junctions. While molecules with one and two anchor groups were investigated, it was shown that for both molecules the conductance of the device increased drastically after exchanging the alkyl thiols, even though the increase was about a factor 2-3 higher for the OPE with two anchor groups. Comparing the conductance value before and after exchange for both molecules, the molecule **1** with two anchor groups is considered to covalently link two particles. This was not *a priori* obvious, because molecular junction formation based on aromatic coupling (as described in 2.3.3) was initially also considered as the origin of the junctions.

## 2.4 Conclusion

A row of model compounds based on an OPE backbone was synthesized. While varying certain components without changing the actual backbone, effects on the electron transport were investigated. It was possible to immobilize single molecules between two gold electrodes of a mechanically controllable break junction in a liquid environment.

The role of contact was investigated while systematically substituting the thiophenol anchor groups with pyridine anchor groups. It was found that the electron transport was dominated by the thiol anchor group.

Intermolecular interactions in molecular junctions were explored. Molecular rods which are not able to covalently bridge two electrodes were found to form stable molecular junctions based on aromatic coupling. Two molecules, each bound to one of the electrodes were interacting and therefore forming the junction by  $\pi$ - $\pi$  stacking.

In addition to the MCBJ investigations, molecular rods were investigated in highly ordered two dimensional systems of gold nanoparticle arrays and it was shown that dithiol functionalized molecules formed extended gold nanoparticle networks while covalently binding two nanoparticles.

It is essential to understand electron transport properties through single molecules. In the next chapters we expand the function of the molecules and investigate the scope of molecular switches and rectifiers. Furthermore, we explore how to obtain a spectroscopical signal from molecules bound to two electrodes.

### 3 Molecular Switches

Switching, as already described in the introduction is an appealing function which might be realized by molecules in electronic circuits. In particular hysteretic switching entails the promises of minute memory units based on molecules. To switch a molecule's state, an external trigger is required. This stimulus can either be light, an electrochemical potential or an applied electric field. For particular systems light was found to be a well suited trigger to switch a molecule by means of fatigue resistance or switching speed, respectively. However, from the point of view of device fabrication light is rather troublesome. In particular, light operated systems raise numerous issues such as nature, size and integration of the light source into the circuit, control over the illuminated area and the number of illuminated molecules. As an alternative, electrochemical triggers were investigated. Switching behavior was obtained upon changing the oxidation state of a redox-core fitted with linker and anchor groups,<sup>[133-137]</sup> and an electrochemical trigger was exploited to arrange the supramolecular arrangement of interlocked superstructures,<sup>[91]</sup> leading to a change in tunnel currents when immobilized between two electrodes.

We are investigating molecular rods comprising a redox active core and explore the influence of the conductance as a function of the oxidation state. Molecular rod type structures fitted with two terminal anchor groups were functionalized with a central ferrocene as electro active group. A 1,1'-dithioalkyl ferrocene switch was synthesized as a model compound. In addition, a 1,1'-divinylthiol ferrocene based switch was synthesized and electrochemically investigated. The latter switch was integrated into an MCBJ setup combined with an electrochemical cell and reversible conductance switching upon a redox reaction was observed.

Furthermore we propose a new switching concept based on the interplay of molecule and electrode. We propose cruciform structures consisting of two crossed rods which comprise different anchor groups. The potential dependent bonding strengths of different anchor groups to electrodes is exploited to establish and lock multiple pathways for electron transport. The molecular switch bears the same oxidation state in both, the ON-state and the OFF-state. In the following the principle of our new approach for molecular switches, such as the synthesis of cruciform structures and immobilization experiments will be described.

## 3.1 Coordination Induced Switches

### 3.1.1 Principle

We propose a new switching concept based on the interplay of molecule and electrodes. Having a cruciform type structure, consisting of two crossed rods, different pathways for electrons are considered. The two rods are fitted with different anchor groups which show potential dependent binding to gold. Exploiting the different bonding strengths of the anchor groups either both rods, or only one rod is bridging the electrodes. When the two rods have different conductances, a conductance switching behavior is expected when one or two rods of the cruciform structure bind to the electrodes.

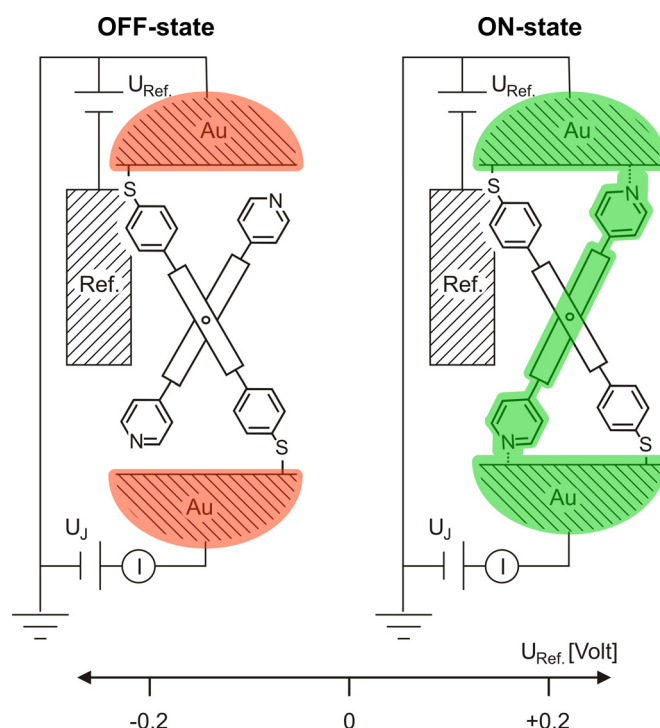


**Figure 55:** Proposed switching mechanism

Reversible potential dependent coordination of nitrogen containing heterocycles to metal substrates has been observed in electrochemical scanning probe investigations.<sup>[65, 174]</sup> Interestingly, upon coordination, the  $\pi$ -system of the heterocycle is expected to couple strongly with the electrode's Fermi level. In contrast to this, the sulfur noble metal bond is known to provide a considerable tunnel barrier for electronic transport.<sup>[76, 175]</sup> The extent of coupling of the sulfur anchor group strongly depends on the relative substitution position with respect to the molecule's backbone,<sup>[176]</sup> providing further tunability of the resistivity through the integrated

structure. The switching mechanism proposed here profits from the subtle interplay between molecule and electrode (Figure 55). The two rod-like  $\pi$ -systems crossing each other in the proposed cruciform structure (Figure 55) are both able to bridge the gap between the electrodes. However, they are expected to display different surface potential dependent behavior. While one of the rods bears terminal sulfur groups, the second transversal rod is functionalized terminally with pyridine subunits. The task of the sulfur functionalized rod is solely to fix the molecule in the junction. The perpendicular rod with terminal pyridine anchor groups is the active component of the switch. In an electrochemically controlled junction, the coordination of the pyridine nitrogen should depend on the surface potential of both electrodes with respect to a reference electrode ( $U_{\text{Ref}}$  in Figure 55).

At a negative electrode potential, both pyridine groups are not coordinated to the electrode surface due to the electrostatic repulsion between the electrode and the nitrogen lone-pair (**(OFF-state)** in Figure 55). The only connection between both electrodes is the backbone of the less conducting sulfur functionalized rod. Upon moving  $U_{\text{Ref}}$  into a positive potential regime, the pyridine nitrogens coordinate to the electrode surface. The strong coupling of the rod's  $\pi$ -system via the pyridine-nitrogens to both electrodes is expected to provide an efficient transport channel between both electrodes (**(ON-state)** in Figure 55). Thus, both states displayed in Figure 55 are expected to differ considerably in their current transport properties. Furthermore, the switching process is expected to be fully reversible, as the potential dependant surface coordination will be reversible and the active molecule has to remain in the junction, as it is immobilized by the less conducting sulfur terminated rod.

### 3.1.2 1<sup>st</sup> Generation Cruciform Structures

#### 3.1.2.1 Molecular Design and Synthetic Strategy

As the first generation of the proposed molecular switches, compound **30** and **31** are proposed. Both structures consist of two crossed rods. One rod consists of an oligo(phenylene ethynylene) (OPE) backbone and comprises two terminal pyridine units, one on each end. The perpendicular rod consists of an oligo(phenylene vinylene) (OPV) backbone and is fitted with two thiol anchor groups.

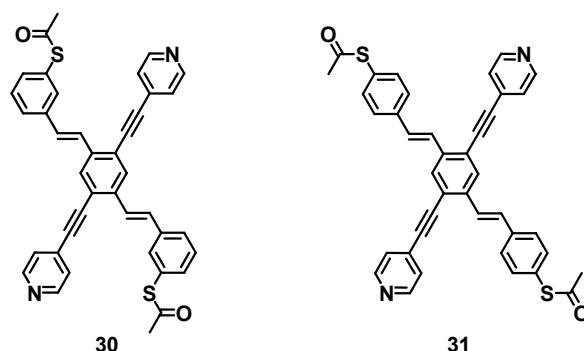
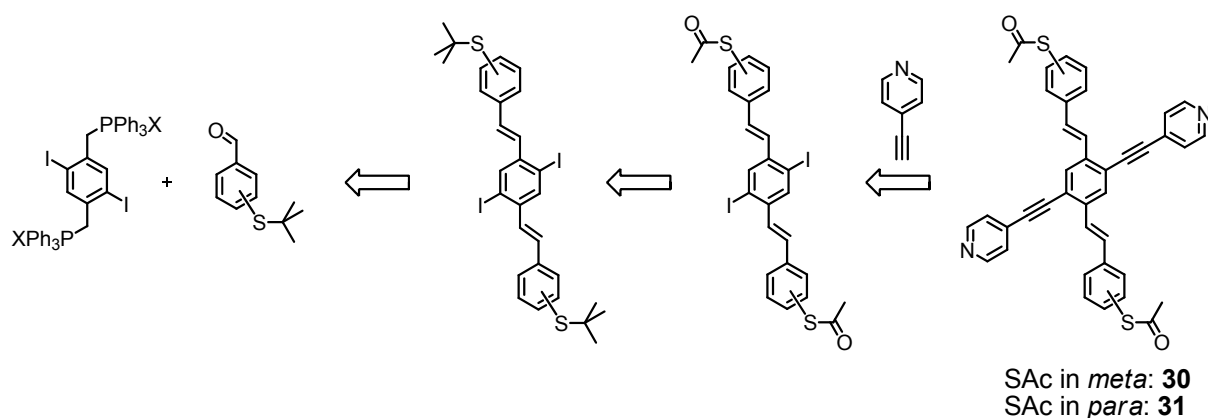


**Figure 56:** Proposed structures **30** and **31** as first generation cruciform switches

The pyridine unit is reported to form a potential dependant coordination bond to gold. While adjusting the surface potential of the electrode with a reference electrode, an efficient coupling of the pyridine, and therefore with the conjugated OPE rod and the electrode is expected. The sulfur functionalized rod should be less conducting than the pyridine functionalized one, and its task is solely to hold the molecule in its position. Sulfur is reported to form a strong covalent bond with gold, stable across a large potential window. In target structure **30** the position of the sulfur anchor group is placed in the *meta*-position with respect to the OPV backbone. This drastically reduces the conductivity of the corresponding rod subunit, due to decoupling of the  $\pi$ -system with the electrode by breaking the conjugation. Target structure **31** bears the sulfur anchor groups in the *para*-position. This increases the conductivity of the sulfur functionalized subunit, which on the one hand goes against the switching principle, but on the other makes it easier to detect single molecules trapped between two electrodes. As thiophenols tend to form disulfides, the sulfur units need to be suitably protected. As protection group, the acetyl group is considered, as it can be easily cleaved prior to exposure to the physical setup. However, during the synthesis of the cruciform structure a protection group resisting harsh reaction

conditions is required. Therefore the sulfur will be transprotected only in one of the last steps.

Both target structures **30** and **31** consist of a terminally acetylsulfanyl functionalized OPV rod and a terminally pyridine functionalized OPE rod. Both rods have the central benzene unit in common. Our synthetic strategy is to assemble the OPV rod in the first place by *Wittig*-type chemistry<sup>[177]</sup> (Scheme 12). Subsequently, the transversal OPE rod will be assembled by *Sonogashira* coupling reactions.<sup>[151, 154]</sup> In addition to the functional groups required for the *Wittig* reaction (aldehyde and triphenylphosphonium salt), a suitably functionalized building block for the cruciform's central phenyl ring already comprises leaving groups allowing the further assembly of the transversal rod, whereas an ideal building block of the terminal phenyl rings of the OPV rod would already comprise the sulfur anchor group. In this strategy, the sulfur group is introduced as a *tert*-butyl thioether for two reasons: namely its robustness in harsh basic conditions of the *Wittig* reaction and its efficient transprotection to the desired acetylsulfanyl group.<sup>[161, 178]</sup> Furthermore, acetyl protected thiophenols tolerate the mild basic conditions of the *Sonogashira* coupling reactions, in particular when efficient leaving groups like iodines are involved. Hence, iodine leaving groups are considered for the central phenyl ring and the plan is to transprotect the terminal sulfur groups prior to the assembly of the pyridine functionalized OPE rod substructure.



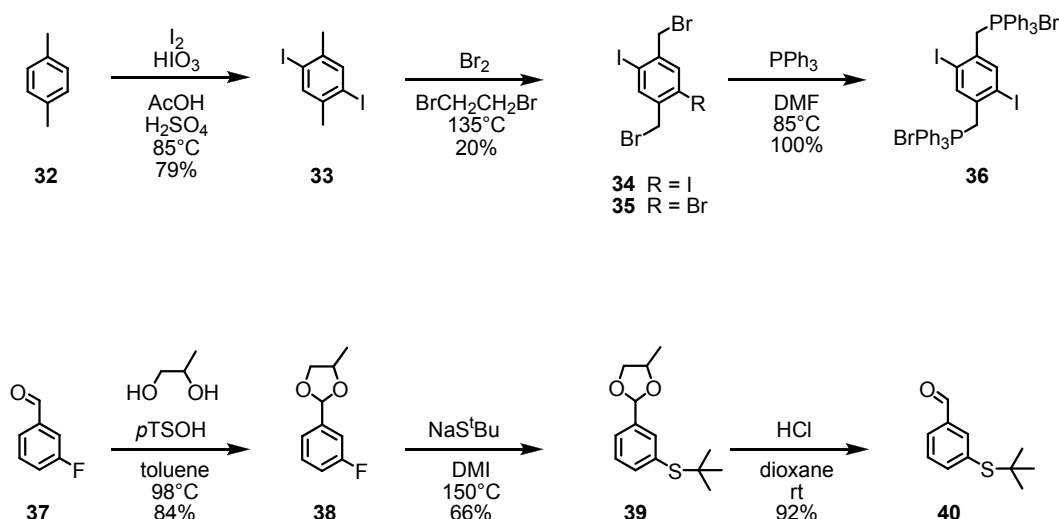
**Scheme 12:** Synthetic strategy for the assembly of cruciform structures **30** and **31**.

For the starting *Wittig* reaction the central phenyl ring can either bear the phosphonium salt or the aldehyde. The successfully applied strategy here was the route with the phosphonium salt as the central unit due to the straight forward synthetic availability of the required building blocks.

### 3.1.2.2 Synthesis of 1<sup>st</sup> Generation Cruciform Structures

For the *Wittig* reaction the phosphonium salt and the aldehyde is needed. Starting with commercially available *para*-xylene (**32**), the desired bromine salt of 2,5-diiodo-1,4-bis(triphenylphosphoniummethyl)benzene (**36**) as precursor of the cruciform's central phenyl ring was synthesized in three steps (Scheme 13). Following a literature procedure,<sup>[179]</sup> *para*-xylene was iodinated to 2,5-diiodo-*para*-xylene (**33**). The bromination of both methyl groups of **33** turned out to be challenging despite of several reported procedures.<sup>[180, 181]</sup> Besides the expected side reaction of double bromination of one methyl group, a halogen exchange was always observed, and one bromide was substituted with an iodide. This halogen exchange reaction is kinetically favored and therefore the bromo-iodo derivatives were always observed even though when working with small concentrations of the brominating agent. Several bromination methods such as with NBS in CCl<sub>4</sub> and light did not lead to the product in good yield. Bromination with bromine in 1,2-dibromoethane (C<sub>2</sub>H<sub>4</sub>Br<sub>2</sub>) provided the desired product **34**, but also considerable quantities of compound **35** where one iodide was substituted with a bromide in the halogen exchange reaction. However, as both reaction products can be separated by repeated recrystallization and derivative **35** is of particular interest as it enables the controlled assembly of asymmetric OPE rods due to the substantial difference in reactivity of both halogens in metal catalyzed cross coupling reactions, the protocol has been chosen for the assembly of the building block **34**. Thus, **33** was treated with three equivalents of bromine in C<sub>2</sub>H<sub>4</sub>Br<sub>2</sub> for 20 h at room temperature to provide a 1:1 mixture of **34** and **35** after precipitation and recrystallization from C<sub>2</sub>H<sub>4</sub>Br<sub>2</sub>. Repeated recrystallization from hot CHCl<sub>3</sub> provided 1,4-bis(bromomethyl)-2,5-diiodo benzene (**34**) as a colorless crystalline solid in 20% yield. Treating **34** with two equivalents of triphenylphosphine in dry DMF at 80°C provided the desired *Wittig* salt **36** in quantitative yield as a white precipitate.

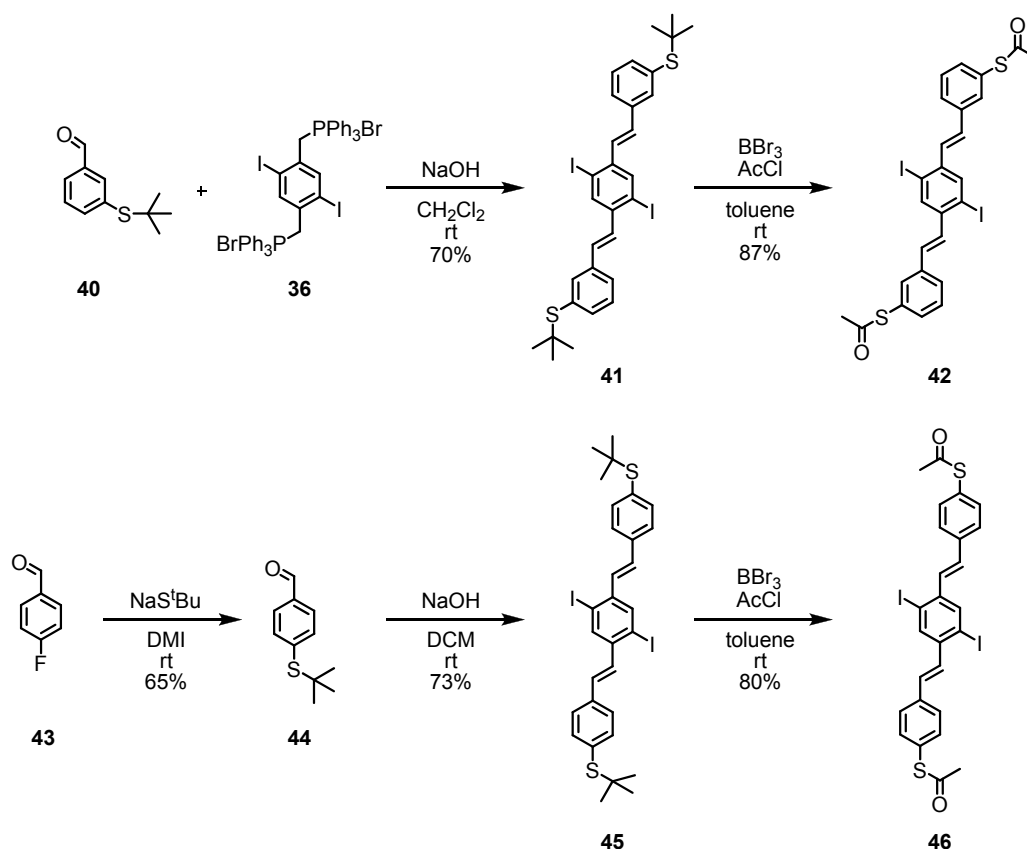




**Scheme 13:** Synthesis of the two building blocks required for the *Wittig* reaction. The phosphonium salt **36** was accessible in three steps starting from *para*-xylene. After iodination of *para*-xylene, the methyl groups were brominated, and the bromides were subsequently substituted with triphenylphosphine. The aldehyde **40** was available after protection-deprotection in a nucleophilic aromatic substitution reaction with sodium *tert*-butylthiolate.

The benzaldehyde **40** comprising a *tert*-butylsulfanyl group in the *meta*-position as the second precursor of the *Wittig* reaction was synthesized from the corresponding fluorine derivative **37**. With sodium *tert*-butylthiolate as nucleophile, the protected sulfur anchor group was introduced in an  $S_{\text{N}}\text{Ar}$  reaction. Because an aldehyde in the *meta*-position does not activate the aromatic nucleophilic substitution reaction, elevated temperatures were necessary. The aldehyde did not resist the nucleophilic conditions at elevated temperatures, therefore it needed to first be protected. The acetal was considered as protection group. Thus, **37** was treated with 1,2-propylenglycol in toluene in the presence of molecular sieves (3Å) and catalytic amounts of *para*-toluenesulfonic acid to provide the acetal **38** in 84% as a colorless liquid. Treating **38** with sodium *tert*-butylthiolate in DMI at 150°C provided the acetal **39** as colorless oil. Subsequent treatment of **39** with aqueous HCl in dioxane provided the desired aldehyde **40** in 92% yield as a yellowish liquid. The desired aldehyde for the assembly of target structure **31** with the thiol anchor group in the *para*-position can be synthesized starting from 4-fluoro-benzaldehyde (**42**). The substantially increased reactivity of aromatic systems with an electron withdrawing substituent in the *ortho*- or *para*-position with respect to the leaving group in  $S_{\text{N}}\text{Ar}$  reactions<sup>[182]</sup> is nicely reflected by both commercially available precursors **37** and **43**. While compound **37**, with the electron withdrawing aldehyde in the *meta*-position

relative to the fluorine substituent, required elevated temperatures for the substitution and therefore needed to be protected first. 4-Fluoro-benzaldehyde (**43**) bears an electron withdrawing group in the *para*-position and therefore activates the aromatic nucleophilic substitution reaction. Due to this activation, the fluorine atom is readily substituted at room temperature. These milder reaction conditions did not require a protection of the aldehyde and the functional aldehyde **44** was accessible in one step. Having all building blocks required for the *Wittig* reaction in hand, the assembly of the OPV-branches was envisaged. In a two phase *Wittig* reaction, two equivalents of the aldehyde (**40** or **44**) and the bisphosphonium salt **36** in dichloromethane (CH<sub>2</sub>Cl<sub>2</sub>) were vigorously stirred with an equal volume of a 50% aqueous sodium hydroxide (NaOH) solution.



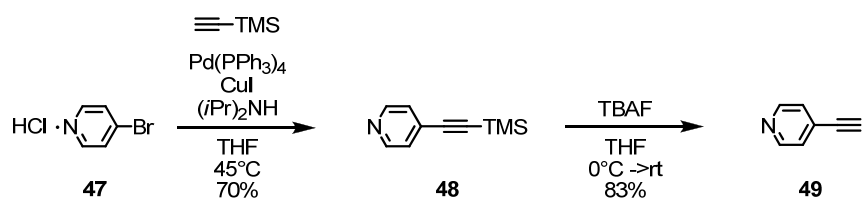
**Scheme 14:** Both OPV-bars **41** and **45** were synthesized in a *Wittig* reaction. The *tert*-butyl protection group of the thiol groups were cleaved by means of BBr<sub>3</sub> and acetyl sulfanyl groups were introduced *in situ*.

After work up, the crude reaction product was isolated as a yellow solid in 83% yield. By <sup>1</sup>H-NMR spectroscopy the crude product was proven to be a mixture of all possible isomers (EE, EZ, ZZ) which were distinguished by their different coupling constants of about 16 Hz for the E double bonds and of about 12 Hz for the Z double

bonds. Without further purification, the crude reaction mixture was exposed to an iodine addition-elimination reaction sequence to increase the fraction of the thermodynamically most stable EE-isomer. Thus, the crude reaction mixture was refluxed in toluene with traces of iodine. Subsequent recrystallization from hot toluene provided both desired EE-isomers **41** and **45** as yellow solids in yields of 70% and 73% respectively.

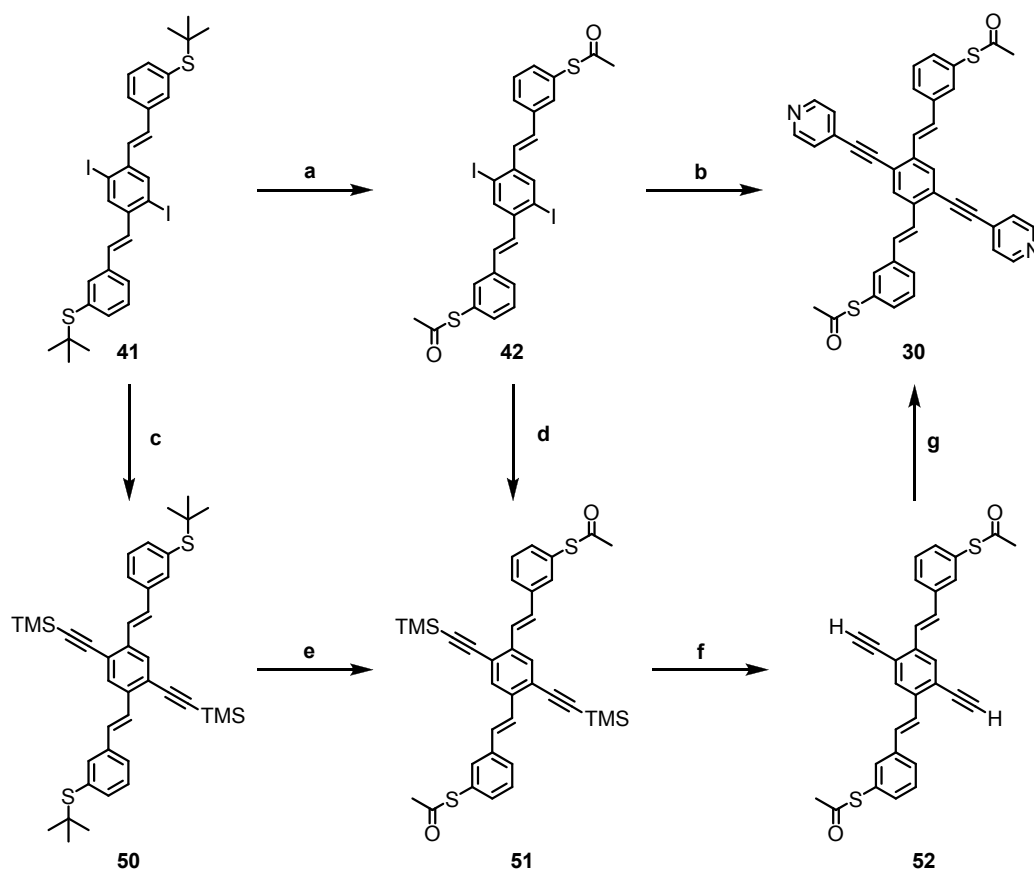
For the transprotection of the *tert*-butylsulfanyl groups of compounds **41** and **45** to acetylsulfanyl groups two alternative protocols have been reported.<sup>[161, 178]</sup> The rather poor solubility of both starting materials and reaction products favored the protocol based on *Lewis* acids<sup>[178]</sup> instead of catalytic amounts of bromine<sup>[161]</sup> as a reagent to cleave the *tert*-butyl group. Thus, the *tert*-butyl protected rods **41** and **45** were partially dissolved and partially suspended in a degassed mixture of toluene and acetyl chloride (toluene/AcCl = 5/1) and four equivalents of borontribromide (BBr<sub>3</sub>) in CH<sub>2</sub>Cl<sub>2</sub> were added in portions. After work up of the reaction mixture, the desired acetyl protected derivatives **42** and **46** were isolated by chromatography as yellow solids in yields of 87% and 80% respectively.

The assembly of 4-ethynyl-pyridine **49** as a required building block is based on a *Sonogashira* reaction. The commercially available HCl salt of 4-bromopyridine was treated with trimethylsilylacetylene in a mixture of THF and diisopropylamine (DIPA) with catalytic amounts of tetrakis(triphenylphosphine)palladium (Pd(PPh<sub>3</sub>)<sub>4</sub>) and copper iodide (CuI) at room temperature to provide the trimethylsilyl (TMS) protected 4-ethynyl-pyridine **48** as a brownish liquid in 70% yield.<sup>[183, 184]</sup> Subsequently, **48** was treated with tetra-butyl-ammonium fluoride (TBAF) in wet THF to provide the desired 4-ethynyl-pyridine **49** as a colorless solid in 83% yield.<sup>[183]</sup> Both derivatives **48** and **49** are light sensitive compounds and were stored in the dark at low temperature (-18°C).



**Scheme 15:** 4-Ethynylpyridine (**49**) was synthesized in a *Sonogashira* reaction followed by cleaving of the TMS group by means of TBAF.

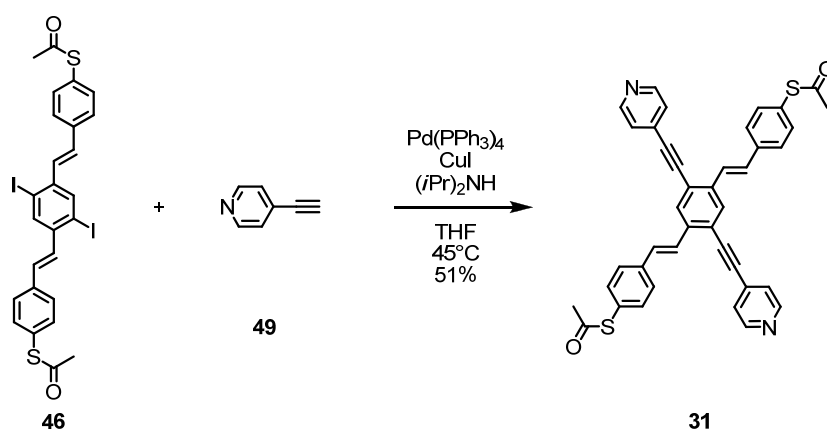
Having all required building blocks for the assembly of the cruciform structures in hand, their syntheses were tackled. To assemble the perpendicular OPE rod of the cruciform structures several alternative synthetic strategies were considered.



**Scheme 16:** Different explored pathways for the assembly of cruciform **30**. a)  $\text{BBr}_3$ ,  $\text{CH}_3\text{COCl}$ , toluene, rt, 2h, 87%. b) **49**,  $\text{Pd}(\text{PPh}_3)_4$ ,  $\text{CuI}$ , THF,  $i\text{-Pr}_2\text{NH}$ , 24h,  $45^\circ\text{C}$ , 51%. c) Trimethylsilylacetylene,  $\text{Pd}(\text{PPh}_3)_4$ ,  $\text{CuI}$ , THF,  $i\text{-Pr}_2\text{NH}$ , 2.5h, rt, 80%. d) Trimethylsilylacetylene,  $\text{Pd}(\text{PPh}_3)_4$ ,  $\text{CuI}$ , THF,  $i\text{-Pr}_2\text{NH}$ , 2h,  $60^\circ\text{C}$ , 80%. e)  $\text{BBr}_3$ , toluene,  $\text{AcCl}$ , 2h, rt, 11%. f) TBAF,  $\text{AcOAc}$ ,  $\text{AcOH}$ , THF, 40 min.,  $0^\circ\text{C}$ ->rt, 80%. g) 4-Iodopyridine,  $\text{Pd}(\text{PPh}_3)_4$ ,  $\text{CuI}$ , THF,  $i\text{-Pr}_2\text{NH}$ , 5h, rt, 50%.

For the target structure **30** with the acetyl protected sulfur anchor groups in the *meta*-position, the potential of the different synthetic routes has to some extent been investigated as displayed in Scheme 16. Both iodines of the *tert*-butyl protected rod **41** and of the acetyl protected rod **42** have been substituted by TMS-acetylene to provide the intermediates **50** and **51** in good yields of 80% in both cases. However, the yield of the subsequent transprotection of the *tert*-butyl sulfanyl group to the acetyl sulfanyl group was with 11% unacceptably low, disqualifying the route over the intermediate **50**. In the case of intermediate **51**, TBAF as reagent to remove the TMS protection groups of the acetylene also attacks the acetyl protection group of the terminal thiophenols. However, protocols based on *in situ* reprotection of the

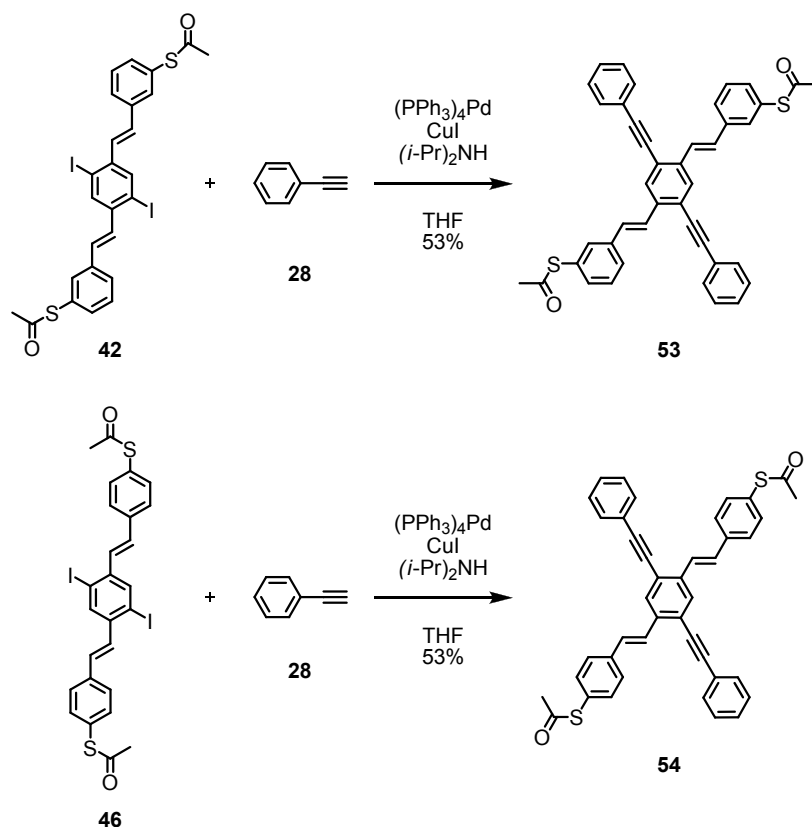
thiophenol by acetic acid anhydride ( $\text{Ac}_2\text{O}$ ) have been applied for systems comprising the same functional groups.<sup>[176]</sup> Treatment of **51** with TBAF,  $\text{Ac}_2\text{O}$  in THF and acetic acid provided the acetylene functionalized rod **52** in 80% yield. Coupling of two equivalents of 4-iodo pyridine to **52** provided the desired cruciform target structure **30** as yellow solid in a yield of 50% after work up and purification by precipitation. Alternatively, *Sonogashira* coupling between the diiodo OPV rod **42** and 4-ethynyl-pyridine building block **49** results in the desired cruciform structure **30** as well. It is noteworthy that this strategy has been reported by Bunz and coworkers for the assembly of OPV/OPE cruciform structures.<sup>[185, 186]</sup> Treating **42** with 2.2 equivalents of the pyridine acetylene **49** in a degassed THF/DIPA mixture containing catalytic amounts of  $\text{Pd}(\text{PPh}_3)_4$  and  $\text{CuI}$  at  $45^\circ\text{C}$  for 24h, provided the cruciform target structure **30** in 50% yield after work up and purification by precipitation. With a similar over all yield of 30% (taking into account the yields of the two steps for the synthesis of **49**) compared to 32% for the serial assembly (steps d, f and g in Scheme 16), but a considerable increase of the relative yield (51% for b compared to 32% for steps d, f and g in Scheme 16) only considering the elaborate precursor **42**, the parallel assembly of the cruciform was clearly the strategy of choice for further derivatization of the parent structure. Thus, similar reaction sequences have been applied for the assembly of the cruciform **31** with the acetyl sulfanyl groups in the *para*-position (Scheme 17).



**Scheme 17:** The target structure **31** was assembled in a *Sonogashira* reaction by coupling the thioacetyl OPV building block **46** with 4-ethynylpyridine (**49**).

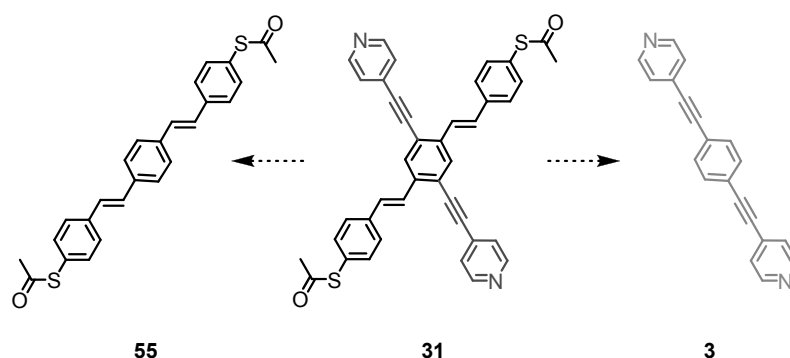
As control molecules, the two cruciform structures **53** and **54** lacking the pyridine function but comprising terminal phenyl units instead were synthesized applying the same conditions as described above (Scheme 18). Therefore the corresponding iodo

functionalized OPVs **42** and **46** were coupled with commercially available phenyl acetylene (**28**).



**Scheme 18:** The synthesis of the “naked” control molecules **53** and **54** respectively, was performed by coupling the building blocks **42** and **46** with phenylacetylene.

In addition, the two substructures of compound **31**, namely the OPV molecular rod **55** with terminal sulfur anchor groups in the *para*-position and the OPE molecular rod **3** with two terminal pyridine units were synthesized to trace the origin of the observed transport behavior in control experiments with the parent structural motives (Scheme 19).<sup>[187]</sup>



**Scheme 19:** Cruciform target structure **31** and its parent substructures the OPV **55** and the OPE **3**.

Having all structures of the 1<sup>st</sup> generation cruciform structures in hand, immobilization experiments could now be performed

### 3.1.2.3 Integration in a “wet” MCBJ and Transport Investigations

Due to their structural complexity and spatial extension, from the beginning it is unclear whether the cruciform structures **30**, **31**, **53** and **54** can be efficiently contacted for subsequent transport characterization. Before attempting any switching of these compounds, their immobilization on a single molecule level between contact electrodes has to be demonstrated. For this purpose, a mechanically controllable break junction (MCBJ) setup operated in a liquid environment has recently been developed.<sup>[60]</sup> The liquid environment will subsequently allow the extension of the setup to gain electrochemical control over the surface potential of both electrodes. A sample consists of a lithographically fabricated gold structure with a freely suspended 80 to 150 nm wide constriction in the central part. The substrate is a flexible spring steel foil with a several micrometers thick polyimide isolation layer. When mounted in a three-point bending mechanism, the suspended gold wire can be elongated in a controlled manner and, ultimately, broken. When broken in the presence of molecules with anchoring groups, the two tips of the broken wire form ideal electrodes to contact single molecules. A flexible viton tube mounted on a spring-loaded support serves as liquid cell to deliver the molecules *in situ*. During the breaking process, the conductance of the junction is monitored via a converter. To immobilize molecules in the junction, the cell (cell volume: 3 mL) was flooded with a 0.25 mM solution of the molecule under investigation in a degassed THF/mesitylene mixture (1/4). The acetyl protection groups of the thiophenol anchor groups were removed *in situ* by adding 50  $\mu$ l of a 10 mM solution of tetrabutylammonium-hydroxide (TBAOH) in THF. Hereafter, the term solvent will refer to the degassed THF/mesitylene mixture (1/4) with the deprotection agent. Conductance traces  $G(z)$  were recorded while breaking and opening the junction. After a plateau close to  $1G_0$  due to the breaking of a final monoatomic Au contact, the conductance drops abruptly, signaling the opening of a gap in the Au bridge. By repeatedly opening and closing the gap, we can collect numerous single molecule current traces providing a good statistics of the molecular junction formation. For this work, about 200 consecutive open-close cycles for each solution were recorded. Note that, during the

measurements, the liquid cell was kept under argon atmosphere to suppress any oxygen-promoted oxidation process such as disulfide formation.

From all individual measurements obtained for the solvent or a specific compound, conductance histograms have been made (Figure 55). Plateaus in the individual curves translate as peaks in the histograms, denoting the most favorable microscopic conformation for the molecular junction. The last peak in the conductance histogram is interpreted as the typical single molecule signature of a particular molecule.<sup>[64]</sup>

No molecular signature could be detected for cruciform **30**. Even though OPE rod-type structures with sulfur anchor groups in *meta*-position have been investigated in an MCBJ set-up in vacuum,<sup>[176]</sup> similar lock-in characteristics of the OPV backbone bearing sulfur anchor groups in the *meta*-position was not observed in the liquid environment. We foresee that the subunit investigated displayed a conductance below the detection threshold ( $\sim 10^{-6}$  G<sub>0</sub>) of the setup. To improve the transport properties of the OPV rod, the cruciform **31** with sulfur anchor groups in the *para*-position was designed and synthesized. As the conjugation from sulfur to sulfur in **31** is provided because they are placed in the *para*-position with respect to the OPE backbone, an increased current is expected through the sulfur functionalized bar in **31** compared to **30**. This is somehow a dilemma, as the conductance of the sulfur functionalized rod is supposed to remain below that of the pyridine functionalized OPE rod. However, the increased conductance of the rod substructure enables detecting the molecule between two electrodes.

All three molecules comprising the *para*-thiolated OPV backbone (**31**, **54** and **55**) have been integrated successfully in the MCBJ set-up in the liquid environment and their conductance histograms are displayed in Figure 57, together with the conductance histogram of the solvent solely containing the deprotection agent (TBAOH). Besides the peak at  $G_0 = 2e^2/h$  which corresponds to the breaking of the Au bridge, the measurement of the solvent (grey in Figure 57 a and b) does not show any peaks. In contrast to that, both cruciforms **31** (red in Figure 57a) and **54** (black in Figure 57a) display a clear molecular signature in the tunnel region ( $G \ll G_0$ ) of the conductance histogram.



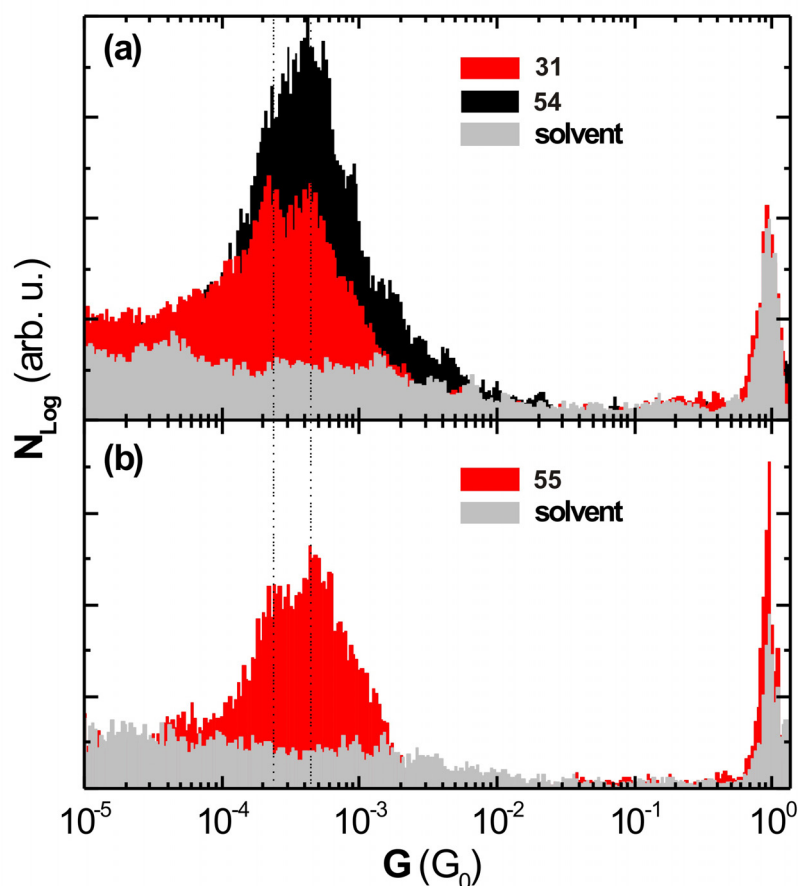


**Figure 57:** (a) Conductance histogram for the pure solvent (grey), compound **31** (red) and **54** (black). The histograms are made from 200 consecutive conductance curves. (b) Characterization of OPV **55** (red) as a reference compound. The histogram is made of 100 consecutive conductance curves. All histograms were normalized to allow a proper comparison. The solvent was a 0.17mM TBAOH solution in THF/mesitylene (1/4).

We assign this signature to the OPV substructure of these cruciforms, immobilized with their terminal sulfur groups in the *para*-position and forming a covalent S-Au bond. As a control experiment, the OPV rod **55** was inspected in the junction under the same conditions (red in Figure 57b). The similarity between the recorded histograms for **32** and **55** is quite striking. Both display two marked peaks at  $2.2 \cdot 10^{-4} G_0$  and  $4.4 \cdot 10^{-4} G_0$  (vertical dashed lines). The appearance of two peaks can be explained by different contact geometries, or that one and two molecules are immobilized in parallel in the junction.<sup>[64, 76, 188]</sup> The histogram recorded with the cruciform **54** also shows a clear molecular signature in the same conductance regime, with the first two peaks being more blurred, although a shoulder at  $2.2 \cdot 10^{-4}$

$G_0$  is still perceivable. These preliminary investigations demonstrate that designed molecular structures encompassing significant complexity can be successively immobilized in an MCBJ set-up in a liquid environment. This confirms the pertinence of developing molecular complexes with added functionality such as that proposed with these cruciforms. We additionally demonstrated that the molecules were anchored via the thiol end groups with the OPV subunit as the immobilized rod.

### 3.1.2.4 Conclusion 1<sup>st</sup> Generation

The fact that we are able to immobilize molecules already bearing the function necessary for the proposed switching behavior is very promising. It was not obvious from the beginning that such rather sterically demanding cruciform structures could be fixed between two electrodes on a single molecule level. Only few years ago it was not possible to immobilize single molecules, but we are with these experiments still at the border of technical limitations. The detection limit of the conductance which still allows a relatively well resolved molecular signature is very close to the conductance of the molecule of interest. The initially proposed target structure **30** bears the sulfur anchor groups in the *meta*-position, which significantly reduces the conductivity of a molecule while breaking its conjugation.<sup>[176]</sup> As we were not able to detect target structure **30** with the anchor groups in the *meta*-position, target structure **31** with anchor groups in the *para*-position was designed and synthesized. Indeed, single molecules of **31** were detected in the MCBJ setup. The principle of the proposed switching behavior relies on the different conductivities of the two crossed rods. The pyridine functionalized rod is supposed to be more conducting than the sulfur functionalized rod. Therefore the conductivity of the sulfur-functionalized rod has to be kept at a low value. However, we are in a dilemma of technical possibilities and chemical design. The conductivity of the sulfur branched rod needs to be small to provide the proposed switching behavior, but large enough that the immobilization of single molecules can be detected.

However, as these investigations are very interdisciplinary and demand a very close collaboration with physicists, the problem has to be approached from both sides, physics and chemistry. So far, the measurements were performed without controlling the electrochemical potential with respect to a reference electrode. To control an appropriate bond formation of pyridine to gold, the MCBJ measurements

---

need to be performed in an electrochemical environment. This is a considerable work, as many problems arise, such as increased leakage current upon applied potential due to the electrolyte. Further, the detection limit of the MCBJ setup needs to be reduced such that very poor conductors can still be detected. On the other hand from a chemical point of view, the design of the cruciform structures can be improved. The conductivity of the pyridine functionalized rod needs to be increased relative to the sulfur functionalized rod. However, the latter has still to be kept at a detectable value.

To investigate potential bar substructures of cruciforms investigations on the conductance of various molecular rods were performed.

### 3.1.3 Investigations on Rod Substructures

To improve the design of the proposed coordination induced molecular switch studies of molecular rods which are part of the attempted cruciform switches were performed.<sup>[58]</sup> Both the OPEs and OPVs with either sulfur anchor groups or terminal pyridine units were synthesized (Figure 58).

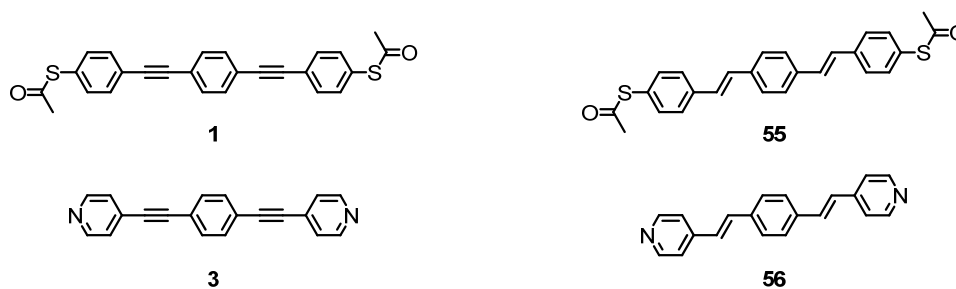


**Figure 58:** Molecular rods mimicking single struts of the cruciform structures.

OPE **1** and **3** and OPV **55** and **56** were investigated in an MCBJ setup and the  $\log(G)$  histograms are shown in Figure 59.

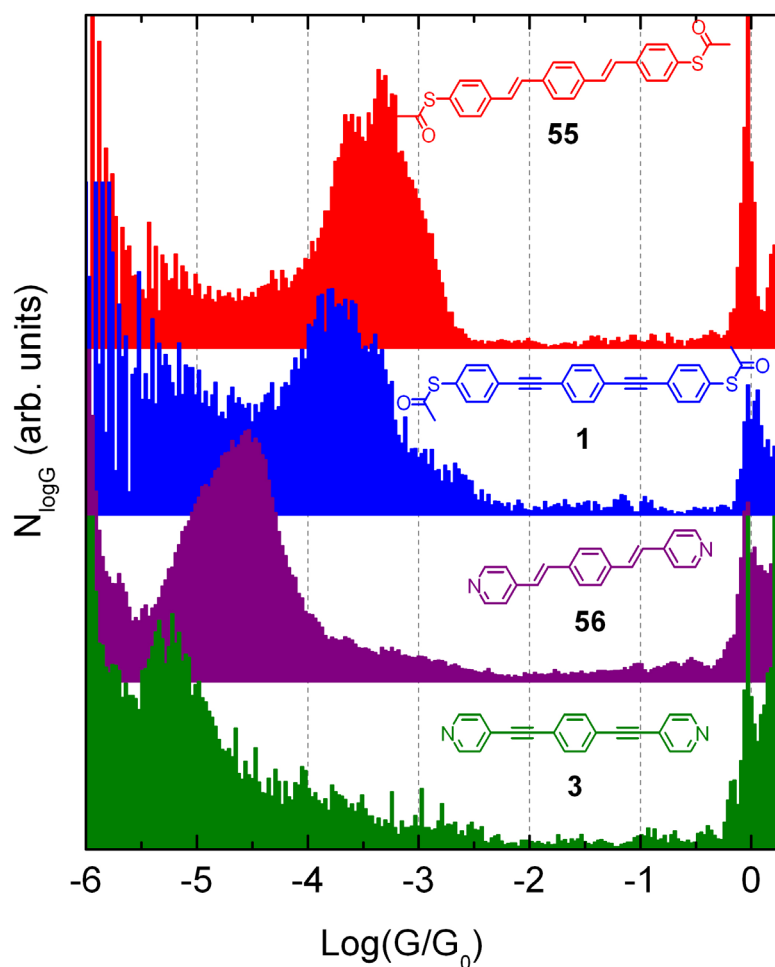


**Figure 59:**  $\log(G)$  histograms of molecular rods **55**, **1**, **56** and **3**.

For all molecules a pronounced conductance peak was observed. It turned out that the sulfur functionalized OPV **55** is the best conductor of the series with a single molecule conductance of  $2.1 \cdot 10^{-4} G_0$ . The conductance of the sulfur functionalized OPE **1** is lower by a factor of 1.75 ( $1.2 \cdot 10^{-4} G_0$ ). The same trend is observable with the pyridine functionalized rods **56** and **3**. Again the conductance of the dipyridine-OPV (1,4-bis((E)-2-(pyridin-4-yl)vinyl)benzene) (**56**) is about double the conductance of the dipyridine-OPE (1,4-bis(pyridin-4-ylethynyl)benzene) (**3**).

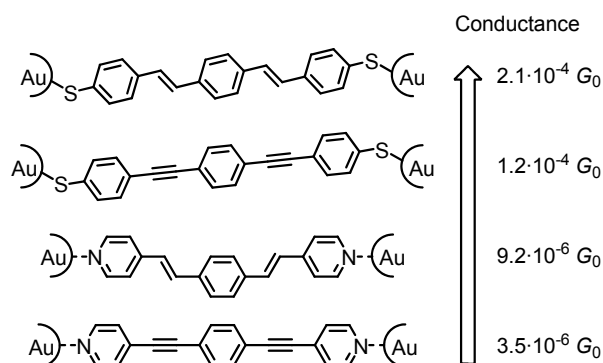


**Figure 60:** Qualitative trend in conductivity of the OPVs and OPEs, respectively.

Without applying a gate voltage, the conductance of the pyridine-anchor group bearing rods is lower than the conductance of the sulfur-anchor group bearing rods. But, in the OFF-state of the proposed switching mechanism, only the sulfur functionalized rod is bridging the electrodes, and in the ON-state both rods are connected (Figure 55). These findings led to a reconsideration of the design of the proposed molecular switches. The further advanced cruciform structures will be discussed in the following section.

### 3.1.4 2<sup>nd</sup> Generation Cruciform Structures

#### 3.1.4.1 Molecular Design and Synthetic Strategy

The results obtained while investigating molecular rods to mimic single struts of the cruciform structures led to a redesign of the initially proposed structures. As OPVs are more conductive than OPEs, the position of the two different anchor groups should be exchanged, to improve the switching effect.

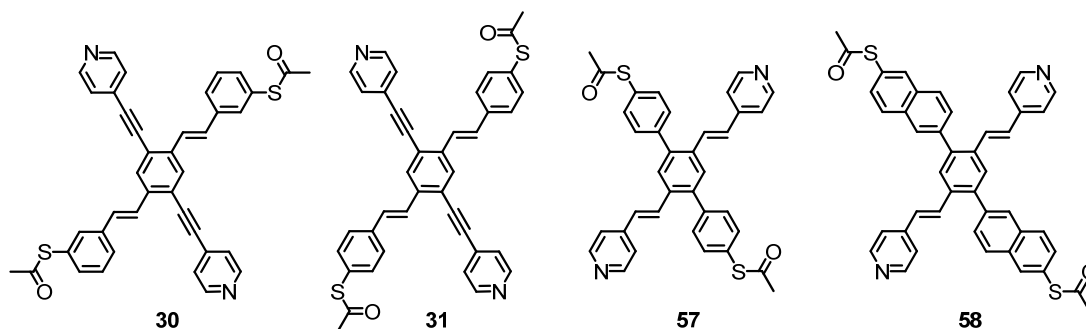
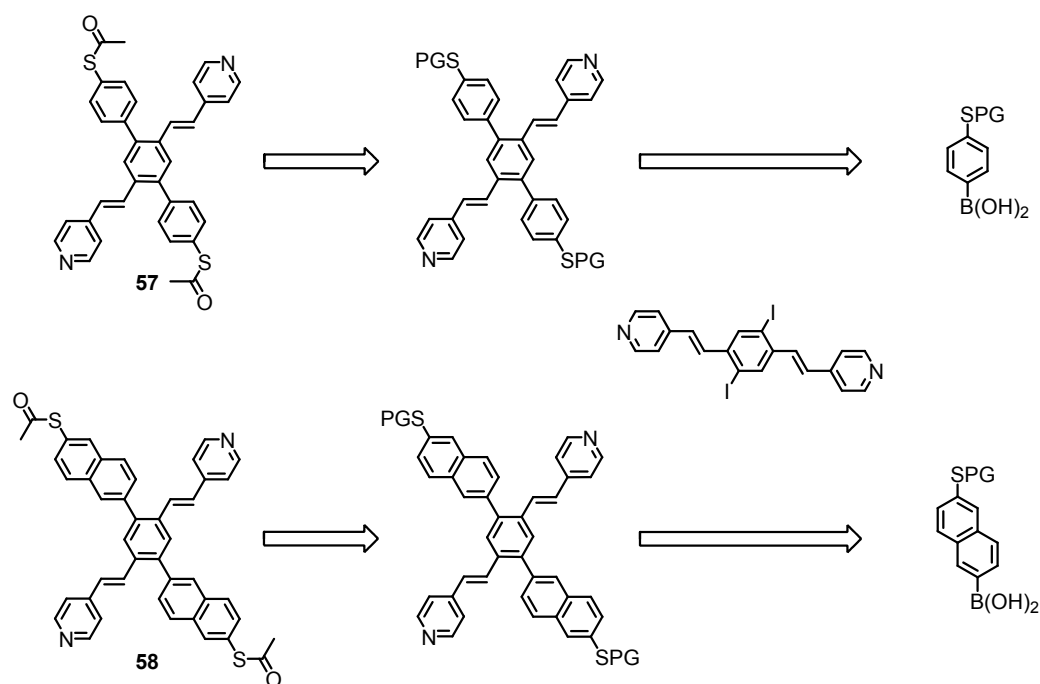


**Figure 61:** Originally proposed target structures **30** and **31** and the improved target structures **57** and **58**.

In Figure 61 the initial compounds **30** and **31** and the improved target structures **57** and **58** are displayed. In the improved structures **57** and **58** the position of the pyridine units is changed from the OPE-rod to the more conducting OPV unit. To maintain an ideal distance ratio of the two crossed rods the perpendicular rod of the pyridine functionalized OPV rod is no longer an OPE system but an oligophenyl (OP) unit (**57**). The OP-system is shorter than the OPV, but the twisted phenyl units reduce its conductivity. By introducing a naphthyl unit, the twist remains, but the system is elongated and therefore shows another rod-distance ratio (target structure **58**). Therefore we propose compound **57** and **58** as improved structures for a coordination induced switching system.

The synthetic strategy is to first build up the oligo(phenylene vinylene)-system by a *Horner-Wadsworth-Emmons* (HWE) reaction. The perpendicular oligophenylene-system will be assembled subsequently in a *Suzuki* reaction with the corresponding boronic acid (Scheme 20). At this time the sulfur is already introduced and needs to be suitably protected, allowing the basic conditions of the *Suzuki* reaction and the formation of the boronic acid. In a last step, the sulfur needs to be transprotected to have an easily cleavable protection group for the immobilization experiments, namely an acetyl protection group.

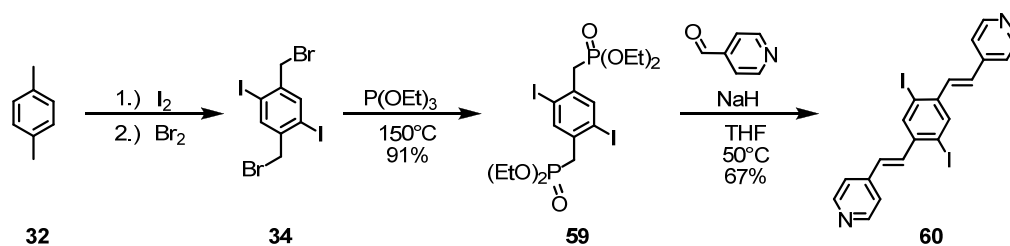


**Scheme 20:** Synthetic strategy for the assembly of target structure **57** and **58**.

The synthesis and characterization, such as the immobilization in an MCBJ-setup is described in the following

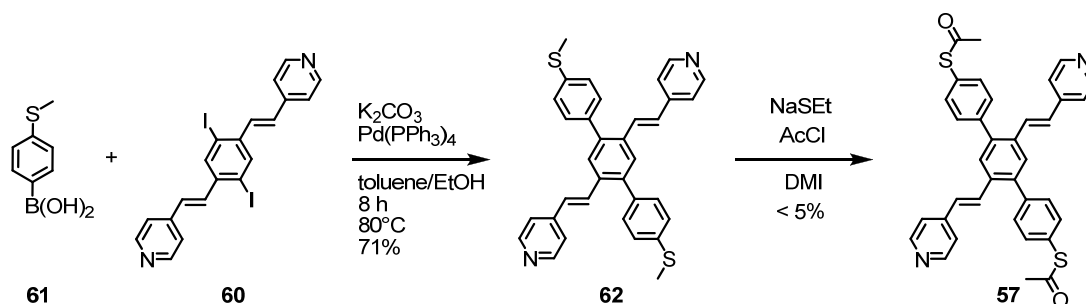
### 3.1.4.2 Synthesis of the 2<sup>nd</sup> Generation Cruciform Structures

The known building block **60** can be synthesized starting from *para*-xylene (**32**) (Scheme 21).<sup>[180]</sup> Iodination, followed by bromination provides compound **34** (As already described in 3.1.2.1).<sup>[187]</sup> For the assembly of the OPV-part of the cruciform structures a HWE reaction is considered. Compared to the *Wittig* reaction applied in the synthesis of the OPV-part of the first generation cruciform structures **30** and **31**, the HWE reaction directly leads to the *EE*-isomers. Therefore no isomerization reaction is required as was performed for the synthesis of the OPV-building blocks **41** and **45**. For the HWE reaction a phosphonate is required, and therefore the bromide **34** is treated with triethylphosphite at 150 °C for 12 hours to yield the bisphosphonate **59** in 91% yield. Having both building blocks, the aldehyde and the phosphonate in hand, the HWE reaction was tackled. The bisphosphonate **59** was dissolved in THF and sodium hydride was added at 45 °C to form the ylide. To this purple solution, commercially available 4-carboxaldehydepyridine was added dropwise over 1 hour. After workup, the iodinated OPV **60** was obtained in 67% yield (Scheme 21).



**Scheme 21:** Synthesis of building block **60**.

With its two iodine atoms as excellent leaving groups in palladium catalyzed coupling reactions, compound **60** is an ideal candidate for a *Suzuki* reaction to assemble the oligophenylene-system. Therefore, the corresponding sulfur bearing boronic acid is required. Initially, commercially available 4-(methylthio)phenylboronic acid (**61**) was envisaged. In a *Suzuki* coupling, the commercially available boronic acid **61** and the corresponding bisiodide **60** were treated in an toluene-ethanol solvent mixture using potassium carbonate as base and tetrakis(triphenylphosphine)palladium as catalyst. The new cruciform structure **62** was successfully isolated in 71% yield as a yellow solid after workup and purification by CC (Scheme 22).<sup>[189]</sup>

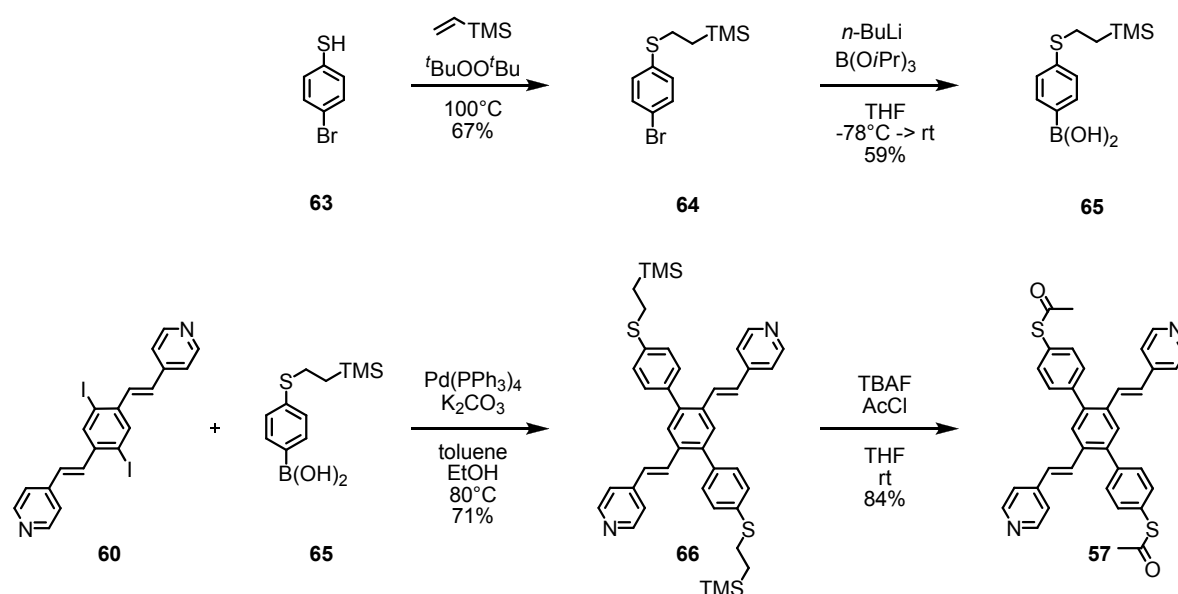


**Scheme 22:** Attempted synthesis of target structure **57** using commercially available boronic acid **9**.

However, the transprotection step turned out to be very challenging. To deprotect the methyl protection group of the thiol unit, a nucleophilic attack was considered.<sup>[190]</sup> Therefore, **62** was treated with sodium methane thiolate in DMI at elevated temperatures. After cooling to room temperature, acetyl chloride was added to the reaction mixture to provide acetylation of the thiol. Indeed, after workup and purification by CC, **57** could be isolated, but only with very poor yields of less than 5%. A <sup>1</sup>H-NMR and a mass spectrum were obtained, which in a first instance proved the existence of compound **57**. While no deprotection took place under ambient temperatures, decomposition of the compound was observed when treating **62** with nucleophiles at elevated temperatures. Therefore an alternative protection group for the sulfur was considered. A suitable protection group could be ethyl-trimethylsilane



(ethyl-TMS). It survives the introduction of the boronic acid, and is stable for the weak basic conditions of the *Suzuki* reaction. Further it can be easily cleaved by means of TBAF. Therefore the corresponding boronic acid **65** was synthesized starting from 4-bromothiophenol (**63**) (Scheme 23). The thiol **63** reacts in a radical addition reaction with vinyltrimethylsilane, using *tert*-butylperoxide as radical initiator to the ethyl-TMS protected thiol **64** in 67% yield.<sup>[191]</sup> In a next step the boronic acid was introduced by treating compound **64** with a 1.6 M solution of *n*-BuLi in hexane to perform a bromide lithium exchange.<sup>[191]</sup> Subsequently the lithiated intermediate was quenched with triisopropyl borate to provide boronic acid **65** after aqueous workup and purification by recrystallization in 59% yield (Scheme 23).



**Scheme 23:** Synthesis of target structure **4**.

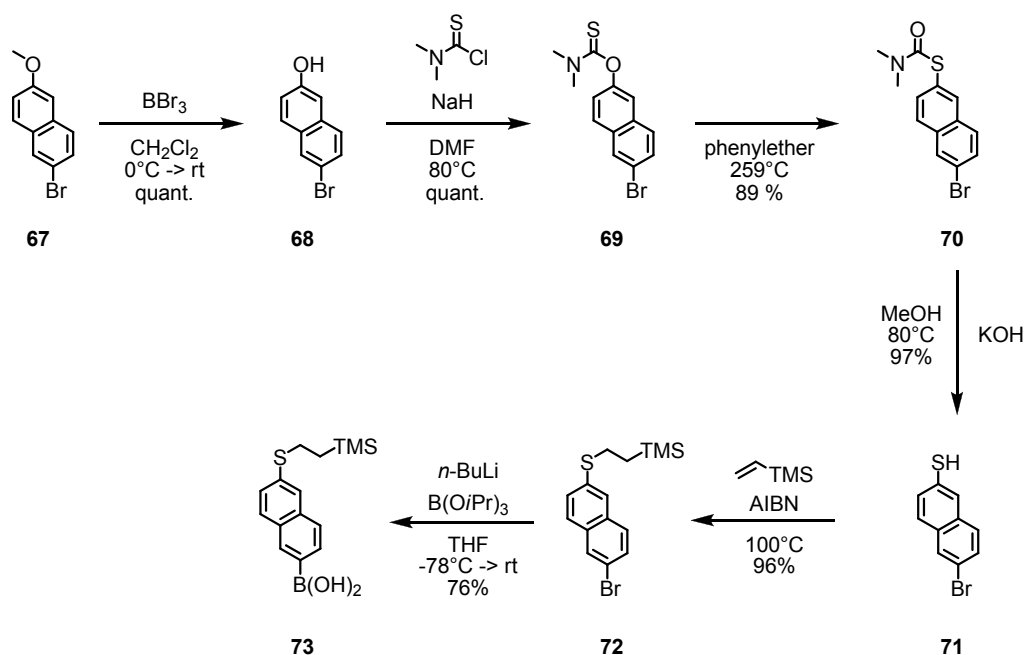
Having all building blocks for the assembly of the new cruciform structure **66** in hand, the *Suzuki* reaction was envisaged. Therefore the bisiodide **60** and the boronic acid **65** were dissolved in a toluene-ethanol mixture. As a catalyst tetrakis-(triphenylphosphine)palladium and as base potassium carbonate were added. The reaction mixture was stirred for 7.5 hours at  $80^\circ\text{C}$  and after the workup and purification by CC, the cruciform structure **66** was obtained in 71% yield. The final step is the transprotection from ethyl-TMS masked to acetyl protected sulfur anchor groups. While the ethyl-TMS group was easily cleaved by tetrabutylammonium fluoride (TBAF) the subsequent treatment with acetyl chloride resulted in the acetylation of both, the sulfur groups and the pyridine nitrogens. However, extensive studies of “Zur Kenntnis der Additionsprodukte von Carbonsäurechloriden an tertiäre

*Amine*” by Karl Freudenberg and Daniel Peters revealed that the acetylated pyridine units can be fast and effectively cleaved by treating the adduct in chloroform with ethanol.<sup>[192]</sup> Subsequently, the ethyl-TMS protected compound **66** was dissolved in THF and a TBAF solution was added. After stirring for one hour at room temperature, an excess of acetyl chloride was added at 0 °C. The reaction mixture was stirred for 30 minutes at room temperature, before chloroform and ethanol were added. After aqueous workup and purification by column chromatography, the cruciform target structure **57** was obtained in 84% yield.

For the synthesis of target structure **58** the boronic acid **73** was required (Scheme 24). As oxygen naphthyl derivatives with the required substitution pattern are available, a *Newman-Kwart* rearrangement (NKR) reaction was considered to introduce the sulfur anchor group. The *Newman-Kwart* reaction is a thermally activated rearrangement reaction, where an *O*-thiocarbamate rearranges to the *S*-thiocarbamate.<sup>[193-195]</sup> It is therefore a useful method to convert phenols into thiophenols.

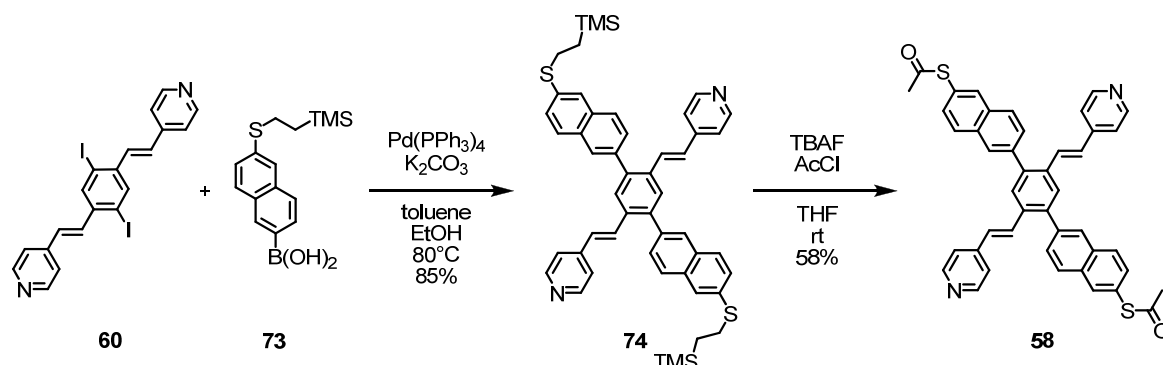
Commercially available 2-bromo-6-methoxynaphthalene (**67**) was deprotected by means of BBr<sub>3</sub> to give 6-bromonaphthalen-2-ol (**68**) in quantitative yields. The *O*-thiocarbamate **69** was then synthesized by reacting 6-bromonaphthalen-2-ol (**68**) with dimethylcarbonylchloride using sodium hydride as base.<sup>[196]</sup> For the NKR reaction, the *O*-thiocarbamate **69** was dissolved in diphenylether and heated to reflux (259 °C). Therefore a silicon oil bath (AP 100) was brought to 300 °C while heating with a heating plate (Stuart – heat CB 160) without stirring. Monitored by thin layer chromatography (TLC), the *O*-thiocarbamate was fully converted after 1.5 hours. Due to the very high boiling point of the solvent (diphenyl ether, mp.: 26-30 °C, bp.: 259 °C) it could not be removed at the rotary evaporator. Therefore the product was separated from the solvent by column chromatography. Thus, the reaction mixture was directly exposed to column chromatography, after cooling to room temperature, to give the *S*-thiocarbamate **70** as a beige solid in 89% yield. The *S*-thiocarbamate was then transferred to the thiol by hydrolysis. **70** was therefore treated with KOH in methanol to provide 6-bromonaphthalene-2-thiol (**71**) after aqueous workup as a beige solid in 97% yield. A *Newman-Kwart* rearrangement (NKR) was therefore a suitable method to introduce thiol groups into such naphthalene systems. In the next to step, the thiol had to be protected with an ethyl-

TMS group and the boronic acid had to be introduced. Similar reaction conditions as previously described for the synthesis of the boronic acid **65** from **63** were considered.



**Scheme 24:** Synthesis of the boronic acid **73**, key building block for the assembly of target structure **58**.

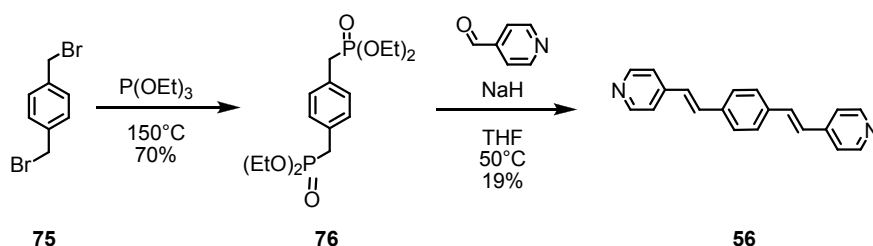
The thiol **71** was ethyl-TMS protected by heating it in vinyltrimethylsilane containing catalytic amounts of AIBN as radical initiator in a pressure tube. After complete reaction the reaction mixture was cooled to room temperature which led to precipitation of compound **72**. After washing with chloroform and drying at high vacuum, **72** was isolated in 96% yield as a beige solid. Treating **72** with *n*-BuLi and quenching with triisopropyl borate, followed by aqueous workup, and recrystallization from hexane, provided the desired boronic acid **73** in 76% yield.



**Scheme 25:** Synthesis of target structure **58**.

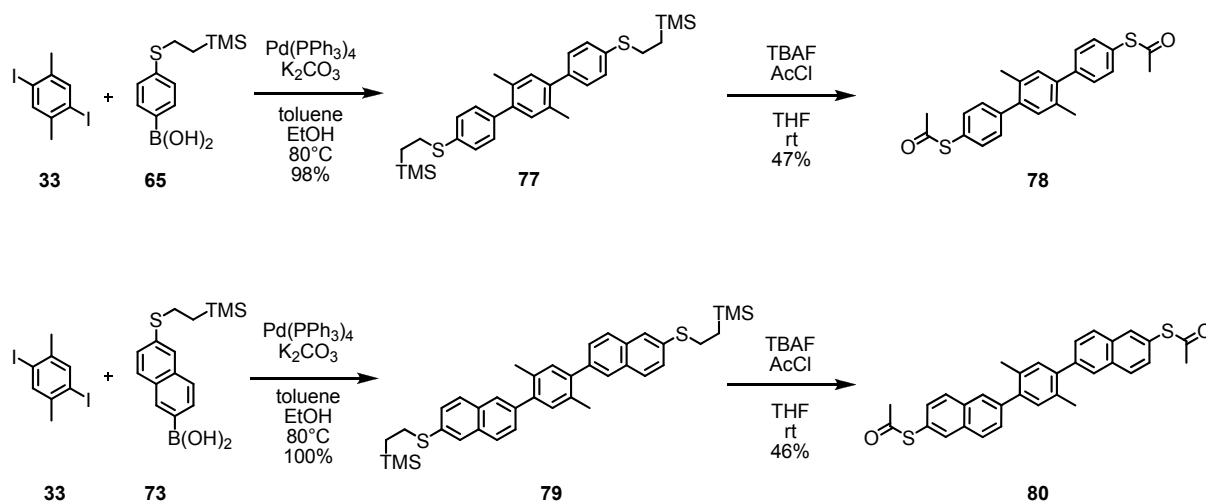
For the *Suzuki* coupling of the new boronic acid **73** with the diiodo derivative **60** similar reaction conditions were applied as described previously for the boronic acid **65**. The new cruciform structure **74** was obtained as a yellow solid in 85% yield after aqueous workup and purification by CC. After deprotection with TBAF and subsequent treatment with acetyl chloride, followed by hydrolysis of the acetylated pyridines, workup and purification by column chromatography, the acetylated cruciform **58** was obtained as a yellow solid in 58% yield (Scheme 25). Both target structures **57** and **58** were successfully synthesized, and fully characterized.

To be able to relate particular transport characteristics to the rod-like subunits of the cruciforms, several control compounds consisting of either a single bar of the cruciform structure or lacking the coordinating pyridine nitrogen atoms have also been synthesized. The OPV with two pyridine anchor groups **56** was synthesized starting from 1,4-bis(bromomethyl)benzene (**75**) which was first converted to the phosphonate **76**. In a HWE-reaction the phosphonate **76** reacts with 4-carboxaldehydepipridine to the desired OPV **56** (Scheme 26).<sup>[197]</sup>



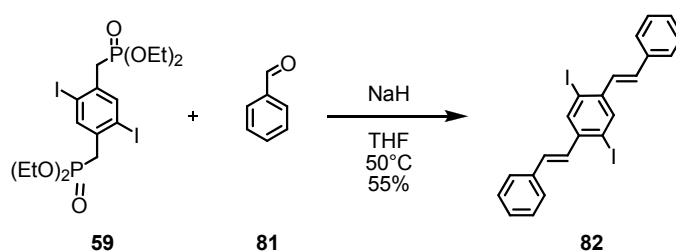
**Scheme 26:** Synthesis of OPV **56**.

Furthermore, the corresponding oligoaryl-rods **78** and **80**, were assembled to mimic the terminal sulfur functionalized bar substructure. Therefore, **78** and **80** were assembled via a *Suzuki* reaction. The corresponding boronic acid was treated with 2,6-diiodo-*para*-xylene (**33**) to give the rods **77** and **79**, respectively. Transprotection of the sulfur was performed using TBAF and acetyl chloride in THF. The reaction mixture was quenched with water and aqueously worked up. The crude was purified by CC to afford the acetylated control molecules **78** and **80** as colorless solids in 47%, and 46% yield, respectively (Scheme 27).



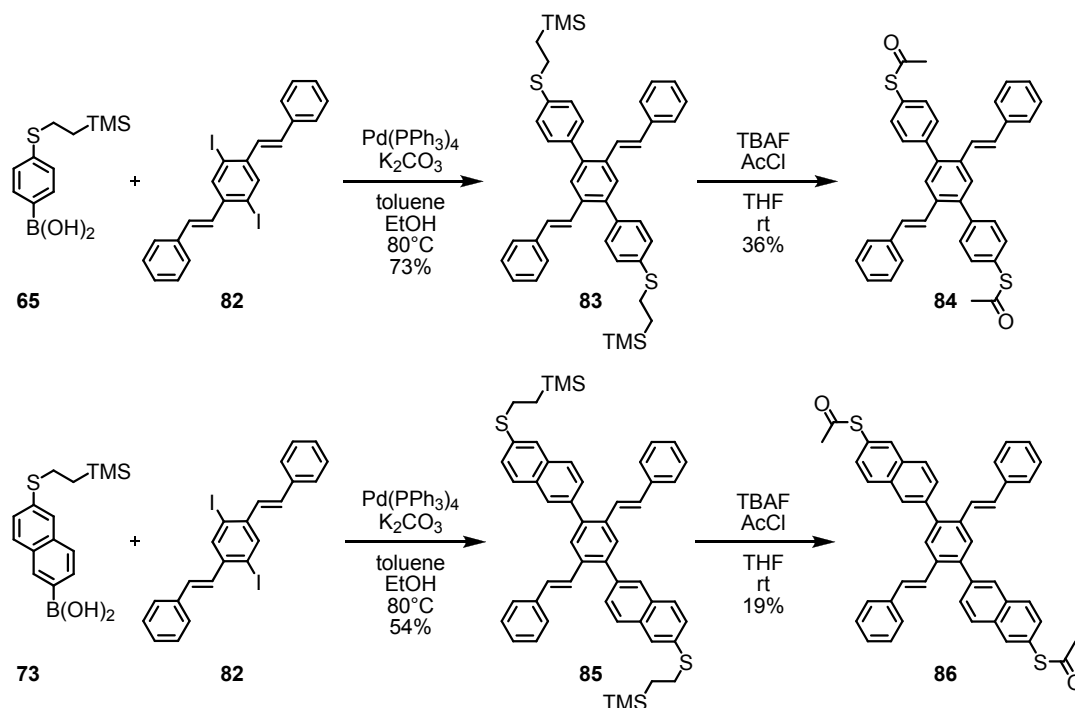
**Scheme 27:** Synthesis of control molecules **78** and **80**.

The two cruciform structures without a pyridine anchor group but only a benzene unit **84** and **86** were synthesized. Therefore the iodinated OPV bar **82** was synthesized using a HWE reaction (Scheme 28).<sup>[198]</sup> Phosphonate **59** was reacted with benzaldehyde and sodium hydride as base in THF to give compound **82** in 55% yield.



**Scheme 28:** Synthesis of OPV building block **82**.

Having all building blocks, the iodide **82** and the boronic acid **65** and **73** in hand, the assembly of the control cruciforms was achieved using similar protocols as previously described. Again, a *Suzuki* coupling followed by a transprotection of the sulfur unit yielded the desired control molecules **84** and **86** (Scheme 29).



**Scheme 29:** Synthesis of control molecules **84** and **86**.

All new compounds were analyzed by determination of the melting point (if a solid), determination of the  $R_f$ -value,  $^1\text{H-NMR}$ ,  $^{13}\text{C-NMR}$ , mass spectrometry and elemental analysis (EA). UV/vis-spectra of all cruciform structures such as of the corresponding rods were recorded. The purity of the cruciform structures was further determined by gel permeation chromatography (GPC) in a HPLC setup because their EA were slightly off the desired range. For the molecular rod **78** crystals suitable for X-ray analysis were obtained.

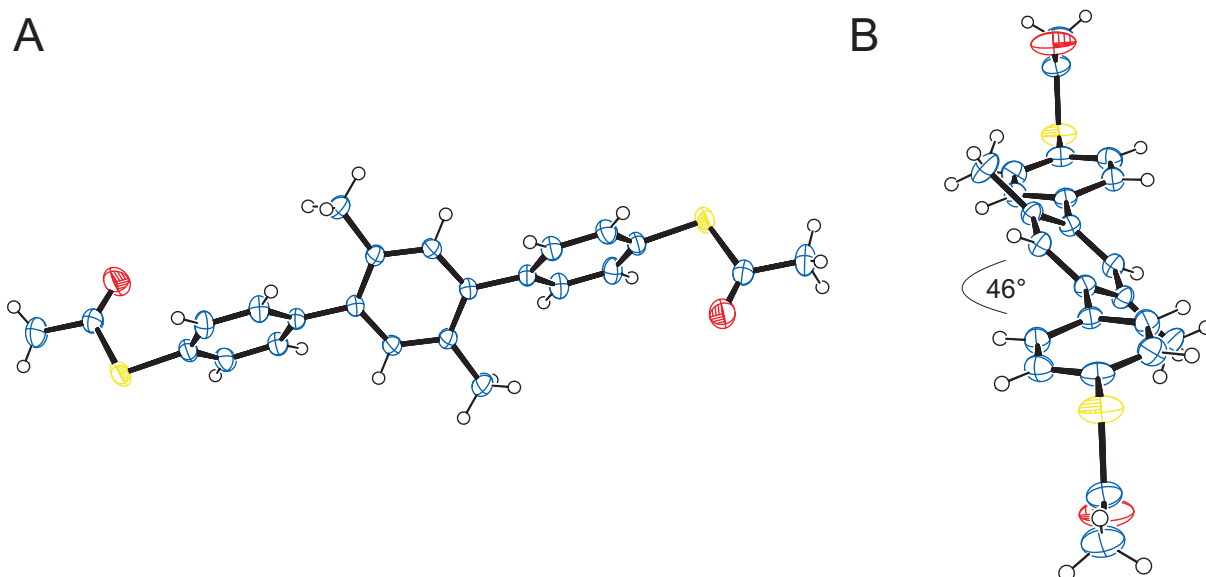


**Figure 62:** Crystal structure of molecular rod **78**. In the front view (B) it is clearly seen that the phenyl rings are twisted by about  $46^\circ$ . The S-S distance is 1.49 nm.

In the solid state structure the central phenyl unit is twisted with respect to the terminal phenyl groups. The twist angle (the angle between the planes fitted to the rings) is  $46^\circ$ . The sulfur-sulfur distance is 1.49 nm. Even though this distance is shorter than the S-S distance of the OPV **55** (1.95 nm), the conductance is expected to be reduced by the twisted backbone.<sup>[199]</sup>

Having all target molecules and the corresponding control molecules in hand, single molecule transport measurements were investigated and will be described in the following.

### 3.1.4.3 Immobilization of the 2<sup>nd</sup> Generation Cruciform Structures

The above described target structures were investigated in a mechanically controllable break junction (MCBJ) setup in a liquid environment described previously (3.1.2.3).<sup>[58, 64, 187]</sup> First, cruciform **57** was exposed to the break junction without adding any deprotection agent (Figure 4a). Quite remarkably, the signature of compound **57** shows two distinct peaks. In contrast, when compound **57** is deprotected in the liquid cell, then only one peak is observed (Figure 4b). While we may expect a spontaneous deprotection of the sulfur rod in presence of the Au electrodes, the observed behavior seems to indicate that a deprotection step strongly favors the sulfur-Au binding versus the pyridine-Au coordination. To clarify this point, we further investigated the building blocks of compound **57** and characterized the sulfur functionalized rod (OP unit) **78** and the pyridine-OPV strand **56** *separately* (Figure 63 c and Figure 63 d, respectively). These experiments support the view that the two peaks observed in Figure 63 a for the protected compound **57** stem from the two rods forming the cruciform structure. We expect that the pyridine-OPV rod of compound **57** can be immobilized between the two electrodes, giving rise to the peak at lower conductance. However, in this situation, the protected sulfur end comes close to the Au electrodes as well. Because the OP rod cannot diffuse freely in solution, the probability of having a spontaneous deprotection of the sulfur groups increases and will sometimes form a sulfur-Au covalent bond at both ends of the OP rod. Spontaneous hydrolysis of acetyl-sulfanyl groups has been reported in the literature and was exploited to form adsorption layers of thiophenols on gold surfaces.<sup>[90, 176, 200-205]</sup> If this spontaneous deprotection happens frequently enough, we expect the system to present two possible stable local conformations for the

molecular-junction: one where the pyridine OPV rod dominates transport and one where the thiolated OP rod dominates. By deprotecting the sulfur end groups, we simply shift the equilibrium of the system towards the situation dominated by the OP rod. This interpretation is qualitatively supported by the control measurements performed for the rods taken separately. Indeed, the peak for the pyridine-OPV **56** appears clearly at a substantially lower conductance than that for the deprotected OP unit **78**, the latter being close to the peak exhibited by the deprotected compound **57**. Note also that measurements of the OP unit **78** when still protected do not exhibit a molecular signature: the probability for spontaneous deprotection is here too low to result in a clear signal. The conductance histogram in this case is similar to that for the pure solvent (Figure 63 h).

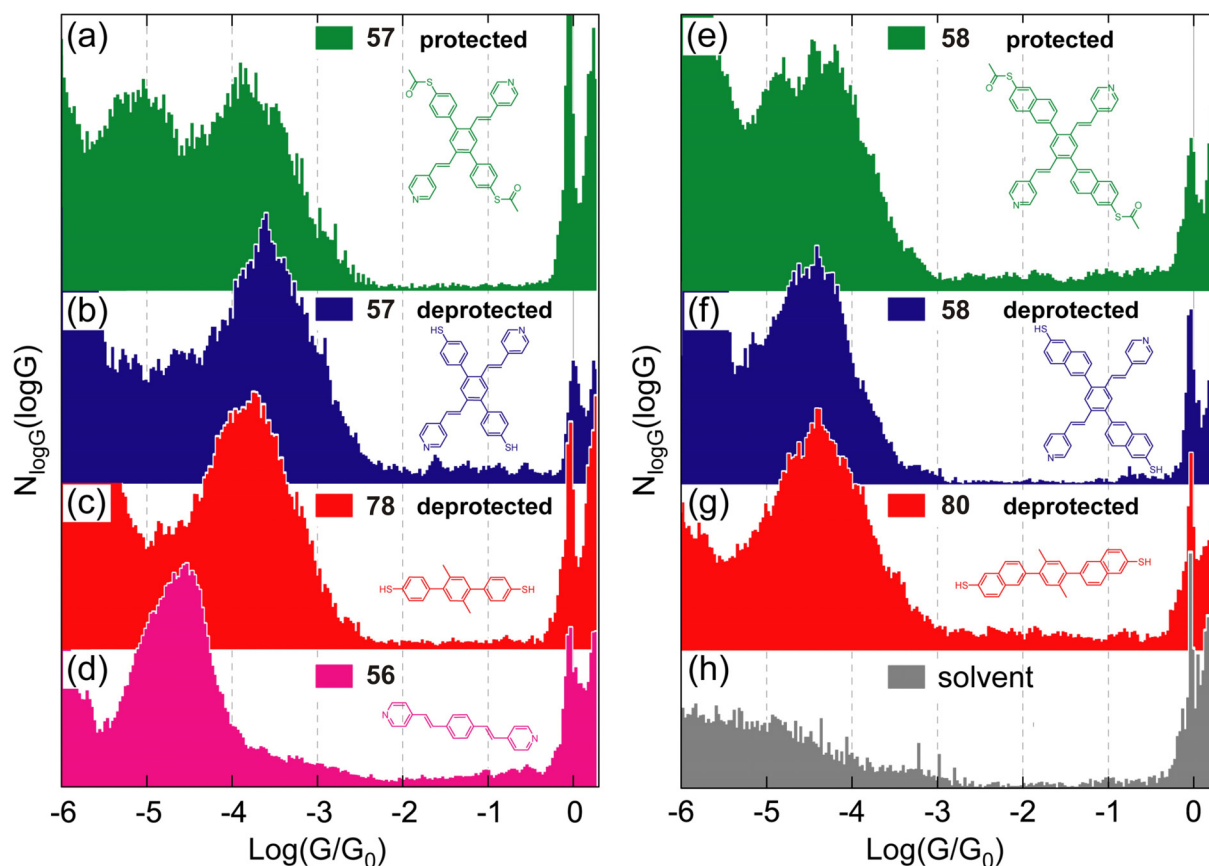


**Figure 63:** Measured conductance histograms for compounds **57** and **58** without and with deprotection agent (a), (b) and (e), (f), respectively. The measured reference conductance histograms for compounds **56**, **78**, **80**, as well as for the solvent alone are shown in (c), (d), (g) and (h), respectively.

An overview of the peak conductance values in the  $\log(G)$  histograms is provided in Table 3 showing a summary of the measured conductance values of the different target molecules.  $G_{\log\text{-low}}$  and  $G_{\log\text{-high}}$  are obtained by a Gaussian fit of the molecular



peak in the  $\log(G)$ -conductance histograms.  $G_{\text{lin-low}}$  and  $G_{\text{lin-high}}$  are the same conductance values transformed to a linear scale. Due to the width of the peaks and the log scale, the  $G_{\text{lin}}$  values are slightly shifted to lower conductances.<sup>[58]</sup>

Cruciform **58** was also investigated in the MCBJ and a similar pattern in the histogram is observed. When no deprotection agent is added (Figure 63 e), two peaks appear, while when the cruciform is first deprotected, only one distinct peak is observed (Figure 63 f). The lower peak corresponds well to that of the pyridine-OPV **56** (Figure 63 d) and the higher peak to that of the single rod **80** (Figure 63 g). We can notice that the two peaks in Figure 63 e are less clearly separated than was observed for compound **57**. This correlates well with the fact that the peak for the dithiolated rod **80** is at lower conductance than rod **78**, used for compound **57**. It is therefore not surprising that cruciform **58** shows a slightly lower conductance than the previously investigated cruciforms **30** and **31**.

Molecule	$G_{\text{log-low}} [G_0]$	$G_{\text{log-high}} [G_0]$	$G_{\text{lin-low}} [G_0]$	$G_{\text{lin-high}} [G_0]$
<b>57</b> – protected	-5.1	-3.8	$3.3 \cdot 10^{-6}$	$9.8 \cdot 10^{-5}$
<b>57</b> – deprotected		-3.6		$1.5 \cdot 10^{-4}$
<b>58</b> – protected	-4.8	-4.3	$9.9 \cdot 10^{-6}$	$2.6 \cdot 10^{-5}$
<b>58</b> – deprotected		-4.5		$1.9 \cdot 10^{-5}$
<b>56</b>	-4.7		$9.2 \cdot 10^{-6}$	
<b>78</b> – deprotected		-3.8		$6.2 \cdot 10^{-5}$
<b>80</b> – deprotected		-4.4		$1.6 \cdot 10^{-5}$

**Table 3:** Conductance values of the measured compounds.  $G_{\text{log}}$  denote the values derived from a Gaussian fit of the molecular signature in the  $\text{Log}(G)$  histogram.  $G_{\text{lin}}$  denotes the corresponding maximum in a linear representation which results slightly shifted to lower values, depending on the width of the peak in log scale.<sup>[58]</sup>

However, the conductance of the cruciform structure is still dominated by the thiol comprising rod-substructure.

### 3.1.4.4 Conclusions

Two new structures were proposed as potential coordination induced single molecule switches. The cruciform structures are based on a crossed OPV/oligo-aryl system. The oligoaryl system of target structure **57** consists of an oligophenyl structure, whereas target structure **58** comprises naphthyl subunits to elongate the oligo-aryl substructure. The OPV substructure was assembled by a HWE reaction directly leading to the desired EE-isomer. The perpendicular oligoaryl structures were assembled using *Suzuki* cross couplings. In addition, all of the corresponding control molecules, the pyridine bearing OPV, the two sulfur bearing single bars and the cruciform structure without any pyridine units but only benzene units were synthesized. Furthermore, transport investigations were performed in an MCBJ setup in a liquid environment. The new cruciform structures, such as all rods comprising suitable anchor groups were immobilized on a single molecule level between two electrodes. It was demonstrated that both rod substructures of the cruciform are functional and can be used for immobilization. However, under these immobilization conditions the electron transport is dominated by the rods, or rod substructures with thiol anchor groups. Detailed investigations of the behavior of the cruciform in presence of a control potential within an electrochemical break junction setup are currently underway. To observe a switching behavior, the conductance of the pyridine functionalized rod-substructure needs to be increased relative to the conductance of the thiol comprising rod-substructure. We may see an increase of conductance due to a stronger coordination bond of pyridine to gold when a positive potential is applied. On the other hand, the design of the structure could be further improved to tune the conductances of the rod-substructures towards each other. The conductivity of the thiol comprising rod could be reduced by breaking the conjugation of the rod substructures, but it is very delicate not to get below the detection limit of the setup. On the other side, to improve the conductance of the nitrogen-heterocycle-comprising rod, the pyridine could be exchanged with pyrroles. The binding lone-pair of pyrrole is part of the aromatic system which might provide direct coupling of the gold electrodes with the molecule's  $\pi$ -system leading to an increased conductance. Investigations on pyrrole functionalized molecular rods are currently in progress.

### 3.2 Redox Switches

In the above proposed coordination induced switch, an electrochemical trigger is required. The binding properties of distinct anchor groups are altered while adjusting the electrode's surface potential in respect to a reference electrode. The proposed switch consists of two crossed rods, and depending on the applied potential either two or only one rod connect both the source and drain electrodes, respectively. However, the oxidation state of the molecule is the same, in both the ON-state and the OFF-state.

In this chapter we focus on redox switches. A redox switch consists of a redox active core fitted with adequate linker and anchor groups. We investigate the influence of the oxidation state of an integrated molecule on its conductivity. Therefore two model compounds were synthesized. As a redox active unit ferrocene was chosen. Ferrocene is an organo-metallic complex consisting of two cyclopentadienyl rings sitting on opposite sides of an  $\text{Fe}^{2+}$  core.<sup>[206]</sup> It is also known as sandwich complex and it is a prototypical member of the metallocene family. The ferrocene (+II) can be oxidized reversibly from its neutral +II state to the positively charged +III state named ferrocenium. The oxidation potential of ferrocene is 0.35 V vs. Ag/AgCl which is in an accessible range for probing a redox switch in integration setups.

First, we synthesized a ferrocene derivative fitted with two thioalkyl groups in the 1,1'-position. Each linker is connected to one of the two decks sandwiching the iron. Hence, the iron atom as an electroactive part is the intersection of the molecule. Similar to previously reported viologen switches we envisage investigating the switching properties of such redox active switches. In the fully organic viologen redox system, the structure is changed considerably between the two oxidation states. However, as ferrocene bears a metal centre the structure is not affected remarkably upon oxidation.

Second, a switch was proposed based on a ferrocene unit functionalized in the 1,1'-position with two conjugated thiovinyl groups to provide efficient coupling with the electrodes. We report the synthesis of the ferrocene comprising OPV-type rod, its electrochemical characteristics and we demonstrate conductance switching in an MCBJ setup.

### 3.2.1 A 1,1'-Dithioalkyl Functionalized Ferrocene as Model Compound for Redox Switches

Wandlowski and coworkers recently published an electrochemical approach to switch single molecules consisting of a viologen core in a metal-molecule-metal junction (Figure 64).<sup>[135-137]</sup> The viologen core can be reduced from its initial state  $V^{+2}$  to the reduced state  $V^{+}$  and further to  $V^0$ . The viologen was functionalized with alkyl chains bearing terminal sulfur anchor groups. The molecules were immobilized in an STM-break junction and a change in conductivity was observed upon changing the oxidation state of the viologen.

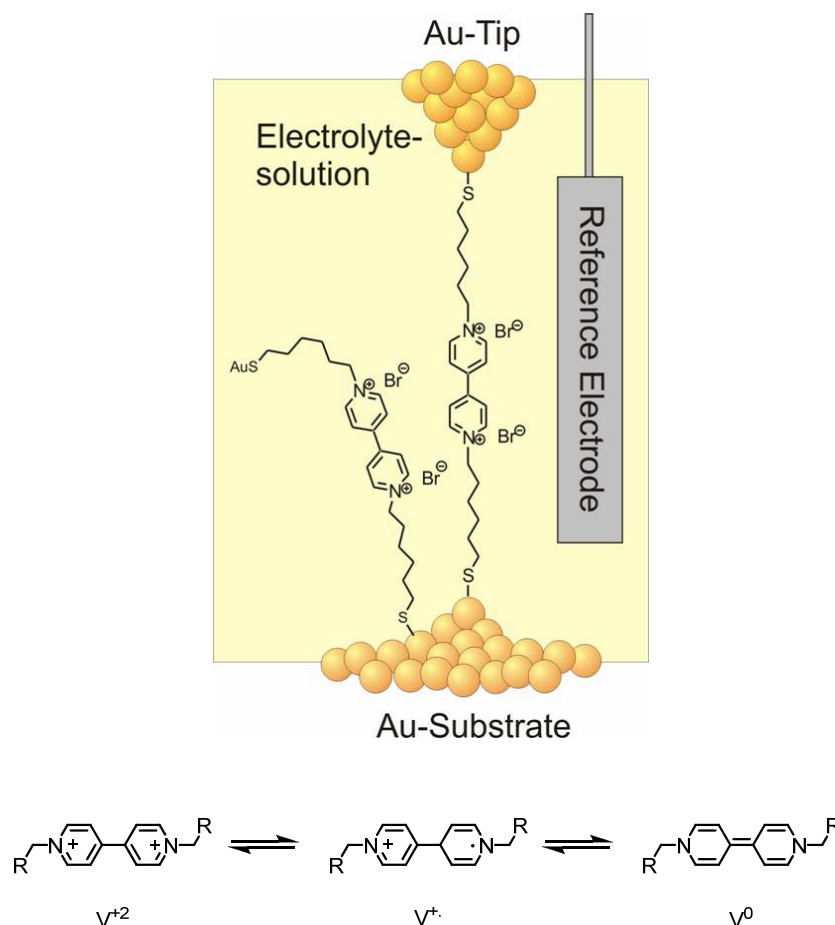


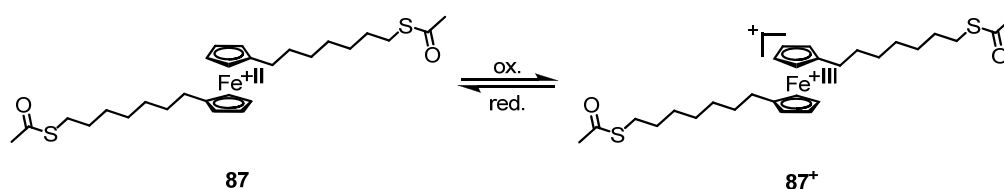
**Figure 64:** Schematic picture of a viologen derivative trapped in a junction. Lower part: Redox reactions of viologen.

To complement these studies of redox active subunits integrated in molecules, ferrocene was chosen as an electroactive unit. With its low and distinct reversible redox behavior, ferrocene is an ideal redox core to investigate in an analogous way

to the viologen system, and then obtain information about the reorganization processes in redox-reactions and the change of conductivity upon oxidation state.

### 3.2.1.1 Molecular Design and Synthetic Strategy

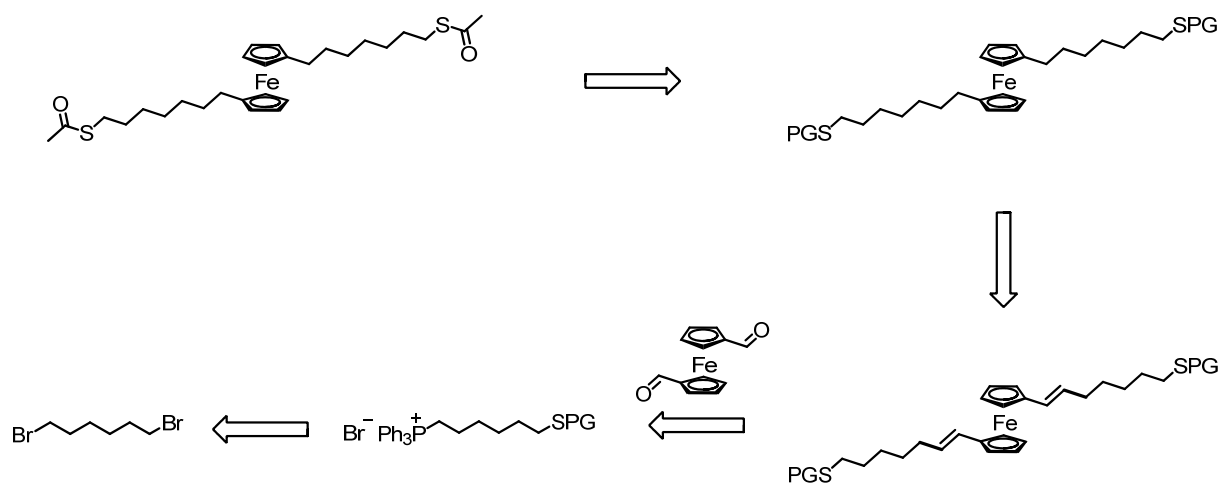
Scheme 30 shows the target molecule **87** and its oxidized state **87<sup>+</sup>**. The target structure **87** contains a ferrocene unit which is fitted with two alkyl chains in 1,1'-position which are functionalized with two terminal sulfur groups. The sulfur is protected with an acetyl unit, which can be mildly cleaved before exposing the molecule to the physical setup and therefore is an ideal protection group.



**Scheme 30:** Reversible redox reaction of the target structure from the +II state to the +III state.

However, the acetyl protection group needs to be introduced in a last step in the synthesis as it does not allow the reaction conditions needed to assemble the target molecule. The synthetic strategy is to introduce the alkyl groups via a *Wittig*-type reaction, which leads to the olefin, and then reduce the double bonds (Scheme 31). Therefore 1,1'-dicarboxaldehydeferrocene, available in one step,<sup>[207]</sup> and the corresponding phosphonium salt are required. The sulfur needs to be protected at this stage with a protection group (PG) which is stable to the basic conditions of the *Wittig* reaction and the subsequent reduction conditions. Further it needs to be cleavable and transprotected to the final thioacetyl groups without affecting the ferrocene unit. The *tert*-butyl group was proven to survive harsh reaction conditions as it was reported to be a stable protection group for *Wittig*-type reactions.<sup>[187]</sup> However, the transprotection is expected to be troublesome in the presence of a ferrocene due to the oxidizing transprotection conditions. Therefore the strategy is to use the methyltriphenyl (trityl) protection group which is stable under the basic *Wittig* reaction conditions but which can be subsequently mildly cleaved under acidic conditions. The synthetic strategy is therefore to profit from tritylthiol as the sulfur source and to statistically introduce it in a substitution reaction with 1,6-dibromohexane and triphenylmethanethiol. The remaining bromide of the mono-

substituted building block can then be substituted with triphenylphosphine to give the phosphonium salt required for the *Wittig* reaction.



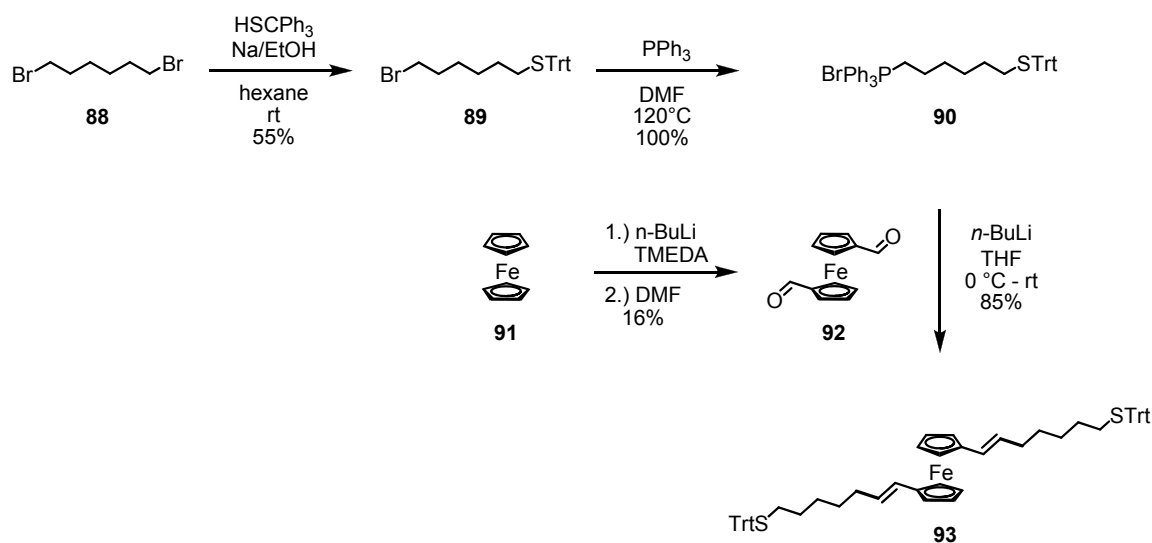
**Scheme 31:** Synthetic strategy for the synthesis of target molecule **87**. PG = protection group.

The *Wittig* reaction is not selective towards formation of the E- or Z-isomers. However, as the strategy is to reduce the double bonds, a separation of the isomers is not necessary. To reduce the double bonds a hydrogenation reaction is envisaged. Both the ferrocene and the trityl group are usually stable under hydrogenation conditions. In a last step the sulfur needs to be transprotected to the final acetyl protected compound.

### 3.2.1.2 Synthesis and Discussion

The phosphonium salt required for the *Wittig* reaction was synthesized starting from 1,6-dibromohexane (**88**). The sulfur was introduced in a statistical substitution reaction of tritylthiolate with dibromoalkane **88**. Therefore one equivalent of triphenylmethanethiol was treated with ethanolate and dropped slowly to a solution of one equivalent of 1,6-dibromohexane in hexane (Scheme 32).<sup>[208]</sup> After stirring for six hours the reaction mixture was filtrated and evaporated. Purification of the crude by column chromatography provided the mono-substituted compound **89** as a colorless oil which solidified foam-like upon drying under high vacuum. After recrystallization from hexane analytically pure compound **89** was obtained. The 55% yield is satisfying, as the product is only statistically formed. Similar reaction conditions were applied for the reaction of sodium *tert*-butylthiolate with 1,6-dibromohexane yielding

only 28% of the mono substituted product.<sup>[208]</sup> In this case intramolecular ring formation, forming the sulfonium salt, further decreased the yield. The sterically demanding trityl-group avoids this side reaction and further helps to form the monosubstituted product. The bromide **89** was then treated with triphenylphosphine in DMF at 120 °C for 13 hours. The DMF was distilled off and the residue was taken up in small amounts of dichloromethane and dropped into rapidly stirring hexane which led to precipitation of the phosphonium salt **90** which was obtained after drying under high vacuum as a colorless powder in quantitative yield.



**Scheme 32:** Synthesis of an E-/Z-isomer mixture of compound **93**. Trt = trityl

The corresponding 1,1'-dicarboxaldehydeferrocene (**92**) as counterpart for the *Wittig* reaction was synthesized following a reported procedure.<sup>[207]</sup> Ferrocene was treated with  $n\text{-BuLi}$  and TMEDA<sup>[207]</sup> leading to lithiation of the ferrocene in the 1,1'-position.<sup>[207]</sup> By treating this lithiated intermediate with dimethylformamide, followed by aqueous workup and recrystallization from cyclohexane, 1,1'-dicarboxaldehydeferrocene (**92**) is obtained as a red solid in 16%. This yield is low due to considerable loss during the recrystallization. Having both building blocks in hand the *Wittig* reaction was envisaged. Therefore  $n\text{-BuLi}$  was added to a suspension of the phosphonium salt **90** in THF.<sup>[209]</sup> The color changed from colorless to orange to dark-black-reddish, pointing at the formation of the ylide. Then a solution of the aldehyde was added dropwise. After stirring for three hours, the reaction mixture was worked up and purified by column chromatography to give the dialkene **93** as red solid in 85% yield. According to its  $^1\text{H-NMR}$  spectrum, the isolated compound **93** was an expected E/Z-mixture. However, a clear  $^{13}\text{C-NMR}$  spectrum was obtained as all the

E/E, E/Z and Z/Z isomers do not differ in their  $^{13}\text{C}$ -NMR signals. The mass was found both by ESI and with MALDI-ToF mass spectrometry. Furthermore, the elemental analysis confirmed the chemical constitution of the compound.

As a next step the reduction of the double bonds of compound **93** was envisaged. Being the most straight forward route, hydrogenation was chosen. Ferrocene is an often used spacer in ligands used for hydrogenations. It is reported to be stable to hydrogenation conditions and should not affect the catalytic system.<sup>[210]</sup> Sulfur could also cause problems as sulfur is reported to poison the catalyst. However, there are reported procedures where sulfur containing compounds were hydrogenated.<sup>[211-214]</sup> Furthermore, transition metal catalyzed reactions other than hydrogenations are reported where sulfur does not disturb the catalytic systems.<sup>[187]</sup>

Initially, heterogeneous hydrogenation with palladium on charcoal was envisaged. The starting material **93** was dissolved in a methanol-dichloromethane 1:1 mixture and treated over night under one atmosphere of hydrogen in presence of 10 mol% palladium on charcoal (Table 4, entry 1). Monitored by thin layer chromatography (TLC) only starting material was observed. Mass spectrometry and  $^1\text{H}$ -NMR-spectroscopy further proved that no conversion took place. The solvent was changed to ethyl acetate (EtOAc) which is known to be a suitable solvent for such hydrogenation reaction (Table 4, entry 2)<sup>[215]</sup> and the same conditions were applied, nevertheless no product was obtained, only starting material. Obviously the hydrogenation of compound **93** is more challenging than initially expected. Therefore harsher reaction conditions were chosen.

Using again a heterogeneous catalyst, the starting material **93** dissolved in EtOAc with 10 mol% palladium on charcoal was stirred at room temperature under an atmosphere of 50 bar of hydrogen overnight. No conversion was observed and only starting material was obtained (Table 4, entry 3).

As these heterogeneous conditions were not successful, homogeneous hydrogenation was attempted. Compound **93** contains no directing groups, a feature which is often required in homogenous hydrogenation. Therefore the most promising catalysts are iridium based catalysts, such as the *Crabtree* catalyst (Table 4, entry 4).<sup>[216, 217]</sup> A series of four iridium catalysts (Table 4, entry 4-7) were screened.<sup>[218]</sup> As a solvent dichloromethane was chosen, the reaction was loaded with 10 mol% of the catalyst and it was stirred under an atmosphere of 50 bar of

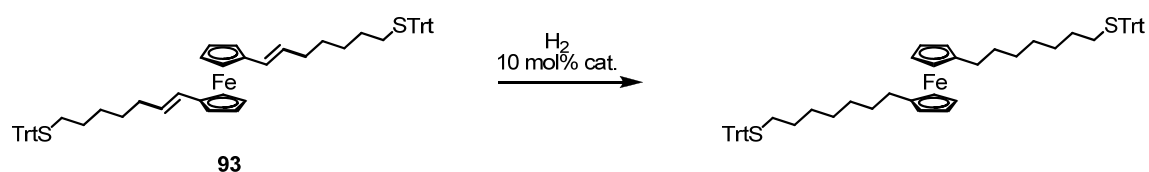


hydrogen overnight. The reactions were monitored by TLC and mass spectroscopy, but undesirably no product was formed and the starting material was recovered after CC.

As a next step in the search for suitable catalysts a range of different heterogeneous catalysts were screened. Palladium on calcium carbonate and palladium on barium sulfate were inactive catalysts as well (Table 4, entry 8 & 9). Also platinum oxide in ethyl acetate did not provide any conversion (Table 4, entry 10). As it is often attested to the poisoning character of sulfur towards catalysts, already poisoned catalysts were used, such as the Lindlar catalyst (Table 4, entry 11).<sup>[219]</sup> In this case the reaction mixture was even heated to 50 °C under an atmosphere of 100 bar of hydrogen. But even under these harsh conditions no product was obtained.

Ruthenium oxide was reported to be a suitable catalyst for hydrogenation reactions of unsaturated sulfides.<sup>[214]</sup> But also these conditions were found to be inapplicable for the reduction of compound **93** (Table 4, entry 12).

All the hydrogenation attempts are summarized in table 3. Several transition metal catalyzed hydrogenation reactions proved to be inapplicable for the reduction of compound **93** (Table 4, entry 1-12). Therefore alternative reduction pathways were investigated.



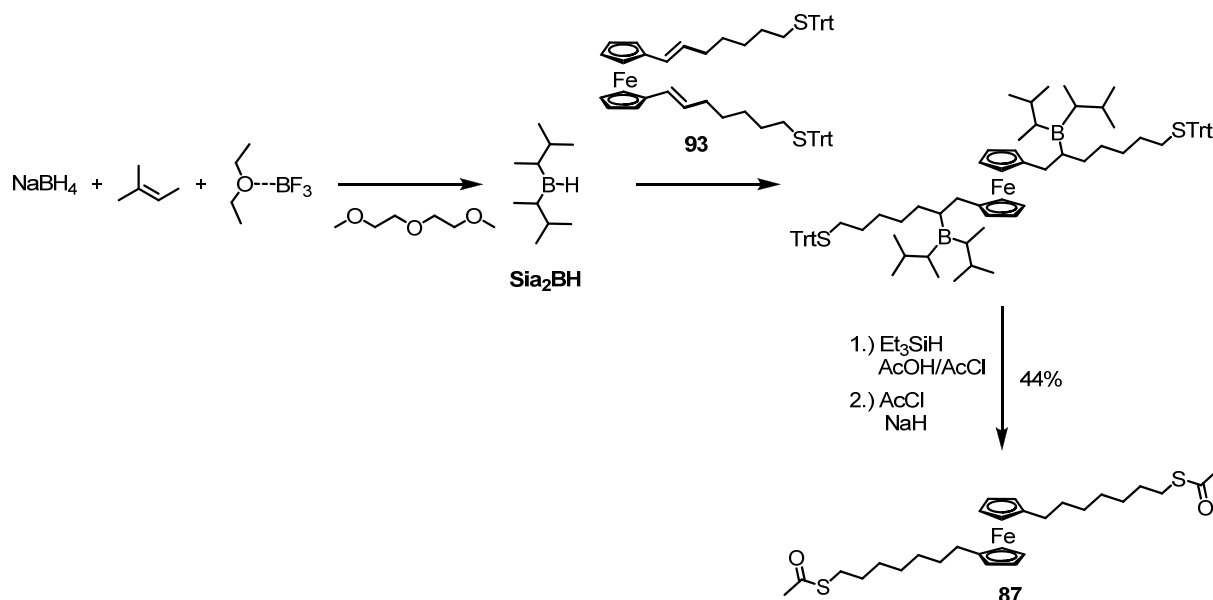
Entry	Catalyst	H <sub>2</sub> (bar)	Temp. (°C)	solvent	time (h)	conversion (%)
1	Pd/C	1	rt	DCM/MeOH	12	0
2	Pd/C	1	rt	EtOAc	12	0
3	Pd/C	50	rt	EtOAc	12	0
4		50	rt	DCM	12	0
5		50	rt	DCM	12	0
6		50	rt	DCM	12	0
7		50	rt	DCM	12	0
8	Pd/CaCO <sub>3</sub>	50	rt	EtOAc	12	0
9	Pd/BaSO <sub>4</sub>	50	rt	EtOAc	12	0
10	PtO <sub>2</sub>	50	rt	EtOAc	12	0
11	Pd/CaCO <sub>3</sub> *Pb (Lindlar)	100	50	EtOAc	72	0
12	RuO <sub>2</sub>	50	60	EtOAc	48	0

**Table 4:** Reaction conditions for the attempted hydrogenation reactions. The conversion was determined by TLC.

Hydrazine is a reported reduction agent, or reduction agent precursor, respectively.<sup>[220]</sup> A convenient system for the reduction of unsaturated compounds with hydrazine are hydrazine-oxygen-copper ion systems.<sup>[221]</sup> Therefore compound **93** was treated with hydrazine in the presence of copper sulfate, but no conversion

was observed, monitored by TLC and MALDI-ToF-spectroscopy. Sodium hydrazide is also reported to be an active reduction agent, for example used in the selective reduction of stilbene to 1,2-diphenylethane.<sup>[222]</sup> But also this system did not show activity towards reduction of compound **93** to the desired product **87**. As a further alternative pathway a hydroboration-protonolysis sequence was envisaged. A study about organoboranes for synthesis revealed that the protonolysis of trialkylboranes takes place under very mild conditions and it tolerates various groups such as active sulfur, halogens and nitrogen functionalities.<sup>[223]</sup> The first group of trialkylboranes is readily cleaved with carboxylic acids at ambient temperatures. The second and the third group require elevated temperatures and stronger acids. Steric requirements of the alkyl groups attached to the boron play an important role in the rate of protonolysis. Indeed, relative rate studies showed that steric hindrance is the most important factor in the protonolysis of trialkylboranes. Therefore partially alkylated borane derivatives such as bis(3-methyl-2-butyl)borane ( $\text{Si}_2\text{BH}$ ) can be used to form mixed organoboranes. Exploiting the selective protonolysis of the less hindered group of a mixed trialkylborane, such species become applicable in organic synthesis and show enhanced regioselectivity and functional group tolerance. As tolerance towards the sulfide and towards the ferrocene is required for the hydrogenation of compound **93**, this procedure is promising, at least for the hydroboration of the olefin **93**. However, the trityl group will not be stable under the protonolysis conditions, using acetic acid. As the acetic acid will protonolyse the mixed borane and also cleave the trityl group, the thiol might be *in situ* trapped with an acetyl source and therefore this pathway could directly lead to the desired target structure **87**. The dialkylborane was therefore *in situ* prepared by suspending sodium borohydride in dry dimethylethyl glycol (diglyme) which was previously stored for two days over calcium chloride and then distilled over sodium/benzophenone (Scheme 33). Then borontrifluoride etherate was added at 0 °C dropwise. A solution of the olefin **93** was then added dropwise. Gas evolution was observed when a drop of the olefin was mixed with the dialkylborane solution. When the gas evolution decreased the next drop of the olefin was added. Initially the orange color of the olefin disappeared upon touching the surface of the  $\text{Si}_2\text{BH}$  solution but after a while the color remained. The temperature was always kept at 0 – 10 °C. After complete addition of the olefin the reaction mixture was stirred additionally for 30 minutes at room temperature and for 45 minutes at 35 °C. Then triethylsilane – a cation scavenger needed to trap the trityl

cation – and a 1:1 mixture of acetic acid and acetyl chloride was added simultaneously. The reaction mixture was kept for 10 minutes at 38 °C and then heated to 100 °C for one hour. To be sure that all of the thiol was acetylated, the reaction mixture was cooled to 0 °C, acetyl chloride and sodium hydride were added and it was stirred for 15 minutes at room temperature.



**Scheme 33:** Final synthesis of target structure **1**, following a hydroboration-protonolysis sequence.

After quenching the reaction mixture, aqueous workup and purification by column chromatography, the desired hydrogenated compound **87** was obtained in 44 % yield as yellowish oil which tends to crystallize. The instability of the trityl protection group towards the protonolysis conditions was exploited to perform two reaction simultaneously.

All compounds were fully characterized by melting point determination (if a solid at room temperature),  $^1\text{H-NMR}$ -spectra,  $^{13}\text{C-NMR}$ -spectra, mass spectroscopy (EI, MALDI-ToF or FAB) and elemental analysis. It remains to be stated that no exact mass-peak was obtained for **89**, only the trityl cation peak was observed as main peak. Furthermore, the elemental analysis of the phosphonium salt **90** was not within the desired range.

### 3.2.1.3 Conclusion

A ferrocene based molecular switch was proposed as model compound to investigate redox switching behavior of single molecules. The ferrocene was functionalized in the 1,1'-position with two thioalkyl groups. The central electro active ferrocene core is rather isolated due to the poorly conducting alkyl linkers, reducing effects from the linker groups on the switching behavior.

The proposed target structure **87** was synthesized with a *Wittig* reaction as the key step. In a hydroboration-protonolysis sequence the double bonds were reduced and the trityl-protection groups of the sulfur were replaced with acetylsulfanyl groups. The molecule is currently under investigation in the group of Prof. Thomas Wandlowski at the University of Berne. The molecules are investigated in an electrochemically controlled STM break junction which already proved its potential during the investigation of the viologen derivatives.<sup>[136]</sup> The correlation between the transport features of the single molecule junction and the redox state of the integrated molecule will be of particular interest.

### 3.2.2 A 1,1'-Distyrene-Ferrocene Based Redox Switch

In the approach described in the chapter above, using ferrocene as an electrochemically triggerable unit, the redox active core is rather isolated from the electrodes due to poorly conducting alkyl spacers. This is essential for the basic understanding of electrochemical conductance switching; however, systems where the redox core is directly coupled to the electrodes via conjugated spacers are very important to be investigated. The conductance of a ferrocene functionalized molecular wire was reported to be  $0.7 G_0$  which is close to the maximal possible conductance through a molecule.<sup>[224]</sup> We report investigations on a molecular rod consisting of an OPV-type backbone comprising an electro-active centre. We propose to use ferrocene as redox subunit, functionalized in the 1,1'-position with two styrenes terminated with sulfur anchor groups. The synthesis, the electrochemical characterization and the immobilization of single molecules between two electrodes will be discussed. Conductance measurements in an MCBJ setup were performed and conductance switching was successfully obtained.

#### 3.2.2.1 Molecular Design and Synthetic Strategy

##### *Molecular Design*

The proposed molecular switch **94** consists of a central ferrocene subunit functionalized with two linker groups in the 1,1'-position (Figure 65). To provide effective coupling of the electro-active core with the electrodes, thiol functionalized styrenes were considered as conjugated linkers.

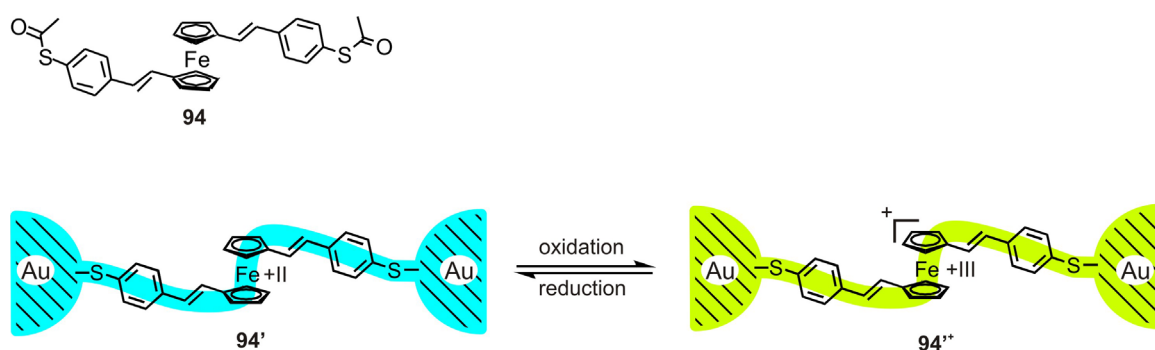


**Figure 65:** Electrochemical active molecular rod containing a 1,1'-functionalized ferrocene.

Figure 65 displays the target structure **94** and its anticipated reversible switching when immobilized between two gold-electrodes (**94'**, **94'+**). The iron atom of

ferrocene is the centre of the electron pathway as the linkers are placed in the 1,1'-position. We expect an effect of the oxidation state on the conductance, as the redox reaction alters the electron population of the frontier orbitals, through which the electron transport is presumed. Placing the linker groups in the 1,1'-position further provides rotational freedom, as the two cyclopentadienyl rings of ferrocene can freely rotate. On one hand this is an advantage as it provides flexibility of the structure, on the other hand it might challenge the immobilization experiments as both sulfur groups of one molecule could bind to one electrode when the molecule is in a U shape.

We are interested to further compare the effect of oxidation state on conductance in a comparable structure where the ferrocene is functionalized in the 1,3-position (Figure 66).

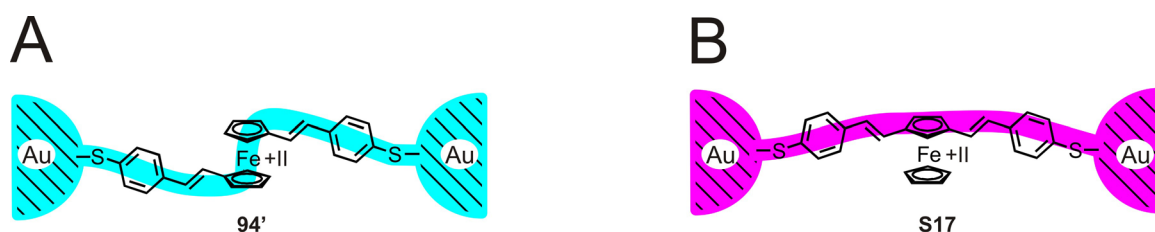


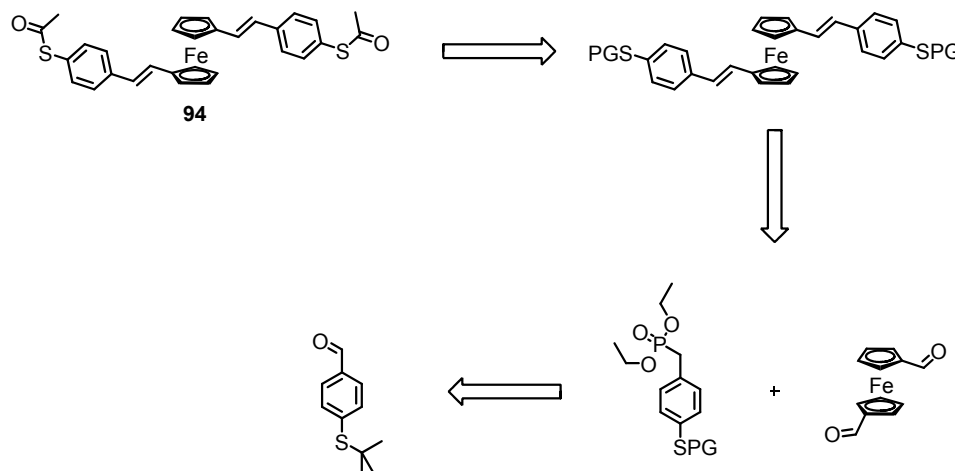
**Figure 66:** Proposed molecular redox switches. The ferrocene is functionalized either in the 1,1'-position for compound **94** (A) or in 1,3-position for compound **S17** (B).

Compound **S17** has the same chemical constitution as compound **94** and only differs in the position of the linkers on the ferrocene. As both linkers are bound on the same cyclopentadienyl ring of ferrocene, the structure is more rigid. The comparison of the effect of oxidation state on conductance of the two isomers could reveal very interesting insights into electronic properties of molecules integrated between two electrodes. The molecular switch **S17** is currently being synthesized in our group, and no results will be discussed within this thesis.

### *Synthetic strategy*

The synthetic strategy is to assemble the OPV backbone of compound **94** in a *Horner-Wadsworth-Emmons* reaction (HWE), leading directly to the EE-isomers (Scheme 34). The two thiols in **94** are protected with acetyl groups. The acetyl sulfanyl group can be mildly cleaved prior to exposition to the MCBJ. However during the synthesis a more stable protection group of the sulfur is required, as the acetylsulfanyl groups will not survive the harsh conditions of the HWE reaction and

the formation of the phosphonate. Therefore the *tert*-butyl protected thiol is envisaged, and the sulfur will not be transprotected prior to the assembly of the OPV unit.



**Scheme 34:** Synthetic strategy for the synthesis of target structure **94**. PG = protection group.

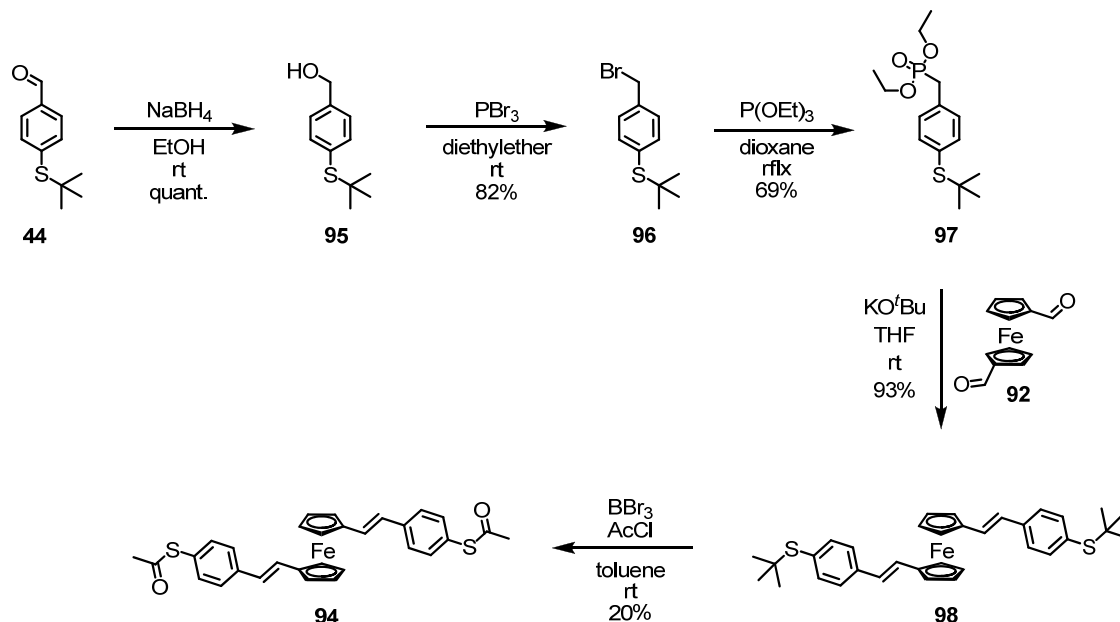
For the HWE reaction an aldehyde and a phosphonate are required. We plan to fit the ferrocene core with two aldehyde groups in the 1,1'-position and the phosphonate on the outer building block, due to the ready availability of 1,1'-dicarboxaldehydeferrocene in one step. The phosphonate is envisaged to be synthesized starting from 4-*tert*-butylsulfanyl-benzaldehyde. After reduction of the aldehyde and substitution of the alcohol with a bromide, it should be possible to introduce the phosphonate.

### 3.2.2.2 Synthesis

The synthesis of 1,1'-dicarboxaldehydeferrocene (**92**) was already described in chapter 3.2.1.2. The corresponding building block to the aldehyde **92** for the HWE reaction is the phosphonate **97**. The phosphonate **97** was synthesized starting from 4-fluorobenzaldehyde (Scheme 14).<sup>[225]</sup> The electron-withdrawing aldehyde group in the *para*-position relative to the fluoride is activating the aromatic nucleophilic substitution reaction. Therefore the fluoride was treated with sodium-*tert*-butyl thiolate in DMI at room temperature to give the functionalized aldehyde **44** in 74% yield (as already discussed in 3.1.2.2).<sup>[187]</sup> Reduction of the aldehyde with sodium borohydride yielded the alcohol **95** as a colorless oil in quantitative yield (Scheme 35).<sup>[226]</sup> In a next step the alcohol needs to be converted to a leaving group. Therefore, the alcohol **95** was treated with  $\text{PBr}_3$  in diethylether at room temperature to give the bromide **96** after aqueous workup and recrystallization from hexane/EtOAc in 82%



yield.<sup>[226]</sup> The phosphonate was then introduced by refluxing the bromide **96** with triethylphosphite in dioxane. After evaporation of the solvent, the crude was purified by distillation. The thio-functionalized phosphonate **97** was obtained as a colorless liquid in 69% yield.<sup>[226]</sup>



**Scheme 35:** Synthesis of target structure **94**.

For the assembly of the OPV **98** several conditions were investigated. It was found that potassium *tert*-butoxide is a good choice as a base.<sup>[227]</sup> Therefore, the aldehyde **92** and the phosphonate **97** were treated with potassium *tert*-butoxide in THF for three hours at room temperature. The reaction mixture was aqueously worked up and the crude was purified by CC to give the EE-isomer **98** as a red solid in 93% yield. Even though transprotection of the *tert*-butyl protected sulfur to the acetylated sulfur of a ferrocene containing molecule has been described, this step was found to be very challenging.<sup>[228]</sup> Only two methods for the conversion of the *tert*-butyl moiety on a thiophenyl have been described, either by means of  $\text{BBr}_3$ <sup>[178]</sup> or by means of bromine.<sup>[161]</sup> Bromine was found to be troublesome, because ferrocene is too easily oxidized by the bromine as oxidizing agent. The oxidation of the ferrocene also perturbs the transprotection using  $\text{BBr}_3$ . The reaction conditions, such as reaction time, temperature, and  $\text{BBr}_3$  concentration were vastly altered and investigated. However, the acetylated target structure **94** was only obtained in low yields of 16-27%. Reproducible conditions were found when the *tert*-butyl protected starting material was dissolved in a well degassed mixture of toluene and acetyl chloride (4:1). 2.4 equivalents of a 1 M solution of  $\text{BBr}_3$  in dichloromethane were added

dropwise at room temperature. The reaction mixture was stirred for two hours at room temperature before quenching with water at 0°C. After the aqueous work up and purification by column chromatography, the product was obtained as red solid in 20% yield. By cooling down a saturated solution of compound **94** in CDCl<sub>3</sub> in an NMR tube to -15°C, crystals suitable for X-ray analysis were obtained (Figure 67).

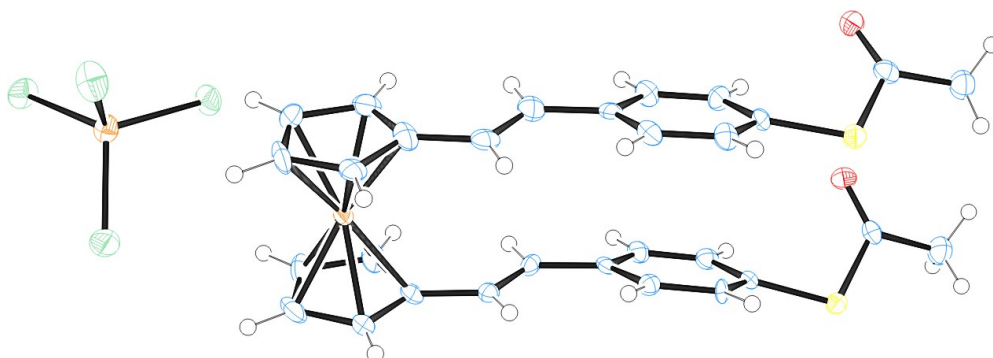


**Figure 67:** X-ray structure of **94**.

Most of the crystals were too thin, however one little red crystal, different in color compared to the other crystals, was suitable for the X-ray analysis. The compound **94** was cocrystallizing together with another substance (left in Figure 67). On the first instance the substance was believed to be [BBr<sub>4</sub>]<sup>-</sup> arising from the deprotection agent of the reaction. However, the obtained electron density of the central atom did not accord with the expected electron density for boron. Alternatively, it could consist of [FeBr<sub>4</sub>]<sup>-</sup> or [FeCl<sub>4</sub>]<sup>-</sup>.<sup>[229, 230]</sup> The iron might arise from decomposed **92** or ferrocene containing intermediates. This would also corroborate the low yield of the transprotection reaction. As ligands (green in Figure 67) of the iron both bromides and chlorides are considered, arising either from boron tribromide or acetyl chloride. The measured electron density of the X-ray analysis pointed more towards chlorides, therefore the substance is rather [FeCl<sub>4</sub>]<sup>-</sup>. However, the fact that the ferrocene derivative **94** bears a counter ion points to that the ferrocene is charged (ferrocenium) which means that it is in its oxidized Fe(+III)-state. Ferrocenium is reported to be blue-green in color. However, the fact that the color of the measured crystal was red, points to that the compound is in its neutral Fe(+II) state, but it can not be excluded that the compound of the measured crystal is in its oxidized state. However, it was proven that the isolated compound **94** after the transprotection reaction is in its neutral reduced form by <sup>1</sup>H-NMR-spectroscopy, electrochemistry and spectroelectrochemistry. Ferrocene is a diamagnetic compound whereas ferrocenium

is paramagnetic; however sharp signals were obtained in the  $^1\text{H-NMR}$  spectrum of **94** which would not be expected for a paramagnetic substance.<sup>[231]</sup> A solution of **94** in acetonitrile does not show a reduction curve within the electrochemical window of ferrocene/ferrocenium when ramped to a negative voltage in an electrochemical cell, but shows an oxidation when ramped to a positive potential. This further indicates that compound **94** is already in its reduced form. Furthermore, the UV/vis absorption spectra of **94** were compared with the spectra of electrochemically reduced **94** and oxidized **94**<sup>+</sup> (See next section) and were according to the absorption spectrum of the reduced form. From these findings we conclude, that either the crystals were from an impurity, or that the cocrystallizing substance is not the counter ion of a charged ferrocenium species.

In any case, the X-ray analysis of **94** shown in Figure 67 nicely reflects the structure of the compound **94**. The linker groups are both oriented in the same direction and the molecule is aligned in its U shape in the solid state. This might give rise challenges to immobilize compound **94** between two electrodes, as both thiols could bind to the same electrode. However, this is only the solid state structure and the molecule is expected to freely rotate in solution.

### 3.2.2.3 Electrochemical Characterization

To screen the feasibility of the target structure as a molecular switch, its redox behavior was investigated by cyclic voltammetry and spectroelectrochemistry. Both the acetyl protected compound **94** and the more stable *tert*-butyl protected compound **98** were inspected.

#### Cyclic Voltammetry

Cyclic voltammograms (CV) were measured on the two target structures. CVs of **94** and **98** are shown in Figure 68. A 1.0 mM solution of the target compounds in acetonitrile was investigated using tetrabutylammonium hexafluorophosphate (TBAPF<sub>6</sub>) as electrolyte and Ag/AgCl as reference electrode, in a classical three electrode electrochemical cell. As TBAPF<sub>6</sub> is a base and is able to affect the acetyl sulfanyl groups of **94**, the *tert*-butyl protected derivative **98** was investigated as a model compound. Compound **98** shows a fully reversible oxidation wave with a half-wave potential ( $E^{1/2}$ ) at 0.365 V (vs Ag/AgCl). The criteria for reversibility were a separation of 70 mV between cathodic and anodic peaks, a ratio of  $1.0 \pm 0.1$  for the intensities of the cathodic and anodic currents  $I_c/I_a$ , and no shift of the half-wave potentials with varying scan rates. The half-wave potential of **98** is shifted to a higher potential compared to parent ferrocene (0.35 V vs Ag/AgCl), which corresponds to a small shift of the LUMO towards higher energy. Obviously, substitution in the 1,1'-position with styrene subunits does not seem to affect the switching properties of ferrocene, which is an interesting feature for the design of a molecular switch.

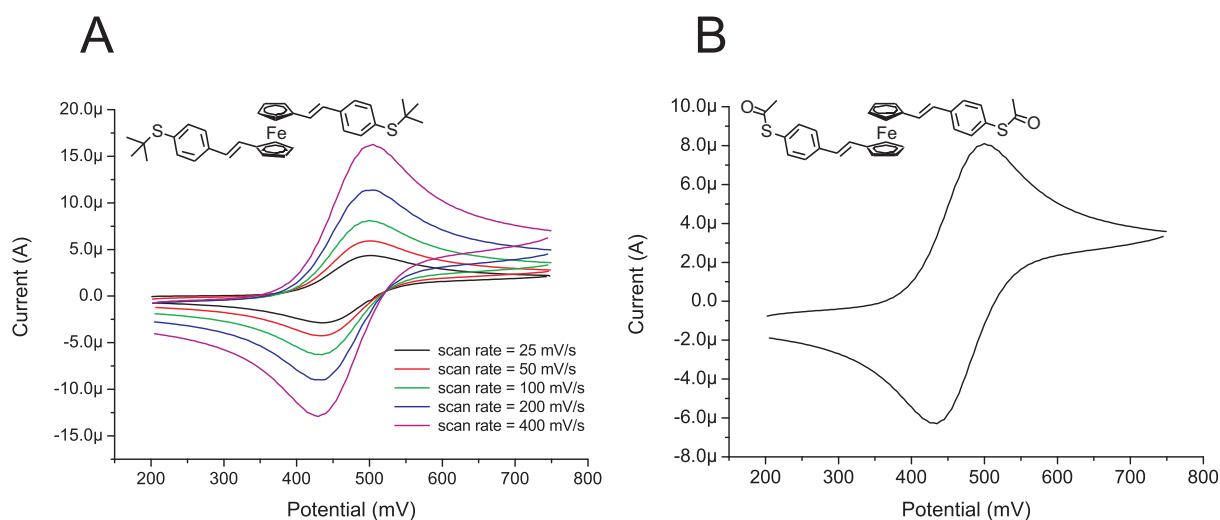
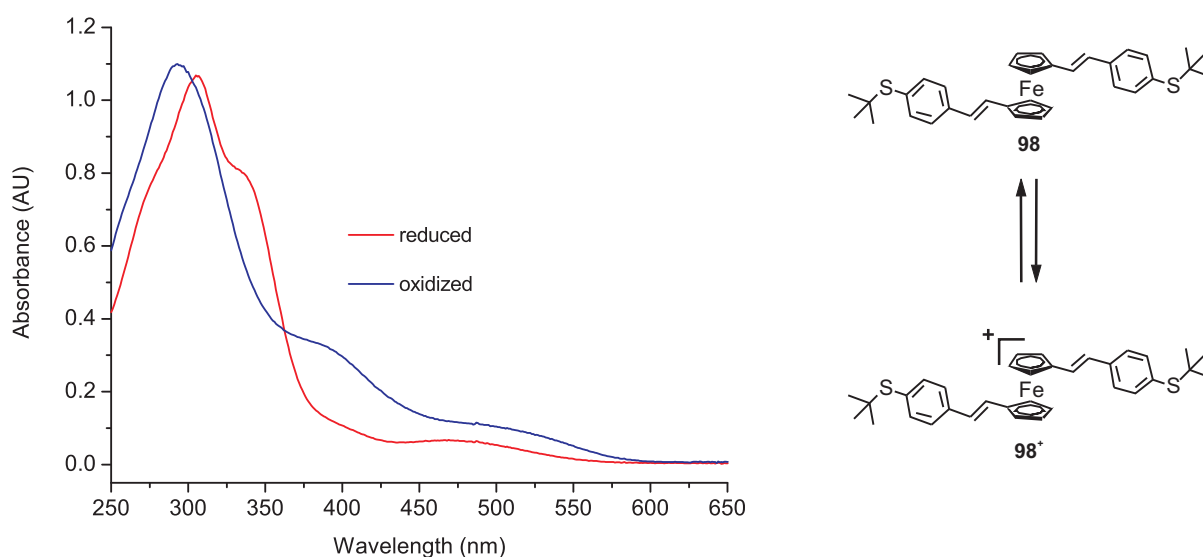


Figure 68: CVs of **94** (B) and **98** (A).

The acetyl protected target compound **94** shows a similar redox behavior. However, the system seems to be less stable in time, probably due to the more labile sulfur protection group in the presence of the electrolyte.

### Spectroelectrochemistry

To correlate electronic properties with photophysical properties the spectroelectrochemical investigations of **94** and **98** were of particular interest. A commercially available quartz UV-cuvette with a three electrode setup was used to record spectroelectrochemical data. UV/vis absorption spectra were recorded while changing the redox state of the molecule by an electrochemical potential.



**Figure 69:** UV/vis absorption spectra of compound **98** and the electrochemically oxidized **98<sup>+</sup>** in acetonitrile.

The UV/vis absorption spectra of compound **98** (red) and the electrochemically oxidized compound **98<sup>+</sup>** (blue) are shown in Figure 69. The reduced compound **98** shows an absorption maximum at 304 nm with a shoulder at 337 nm. In addition a shallow, broad absorption peak is observed at 483 nm. The bands of the absorption spectrum were not assigned to its transitions; therefore it is vague to conclude on changes in the absorption spectra of the reduced and the oxidized compounds **98** and **98<sup>+</sup>**, respectively. However, it was qualitatively observed that the main absorption maximum at 304 nm was hypsochromically shifted to 292 nm and the shoulder at 337 nm disappeared upon oxidation. A new shoulder at 390 nm, which was only weakly present in the oxidized form, appeared. Further, a slight increase in intensity and hypsochromic shift of the weak broad peak at 483 nm was observed.

The extent of the redox reaction was qualitatively followed by spectroelectrochemistry (Figure 70 A).

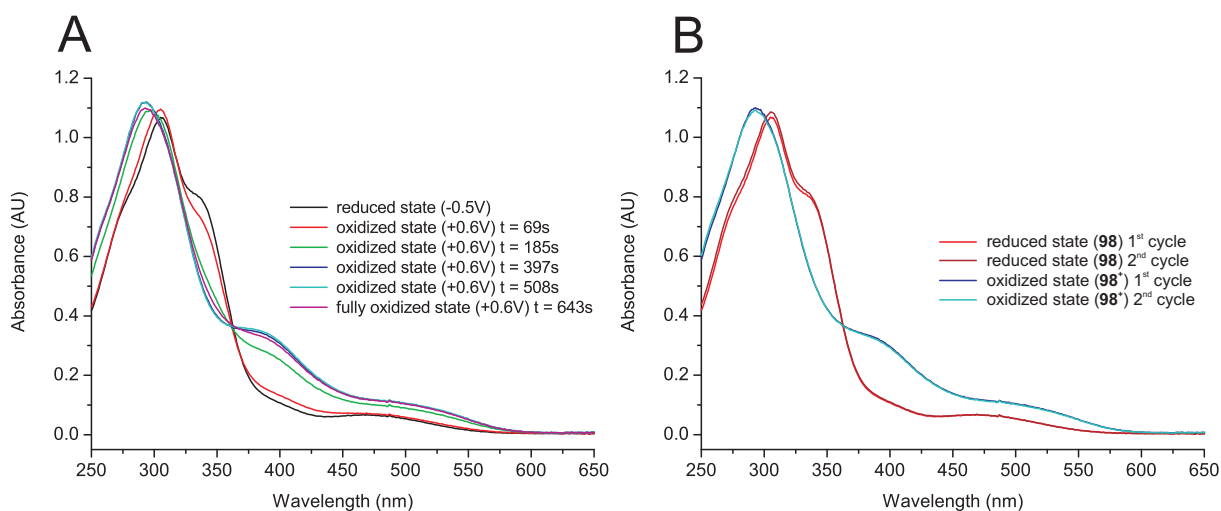


**Figure 70:** Spectroelectrochemistry of **98**.

In its initial state, compound **98** is in the neutral form ( $\text{Fe}^{\text{II}}$ ). However, a potential of  $-0.5\text{ V}$  was applied for 5 minutes, to be sure that all molecules are in the reduced state (black curve in Figure 70 A). A potential of  $+0.6\text{ V}$  was applied and UV/vis-spectra were recorded after 1 minute, 3 minutes, 6 minutes, 9 minutes and 11 minutes (Figure 70). The absorption spectra taken after 6, 9, and 11 minutes overlap, denoting that all molecules in solution are oxidized. Subsequently, the solution of  $\mathbf{98}^+$  was reduced to **98** while applying  $-0.2\text{ V}$ . The oxidation followed by reduction is referred to as one cycle. The reversibility of the redox process is reflected in Figure 70 B. The absorption spectra of the reduced state recorded in the first and second cycle, such as the absorption spectra of the oxidized state recorded in the first and second cycle overlap well.

The spectroelectrochemical behavior of the acetyl protected compound **94** was also investigated (Figure 71), but, monitored by TLC, the thioacetyl protection group was not sufficiently stable during the redox reaction in the presence of the electrolyte ( $\text{TBAPF}_6$ ). The positions of the absorption maxima of the reduced form in the first and second cycle remain the same, but the intensity drastically increases (Figure 15 B).

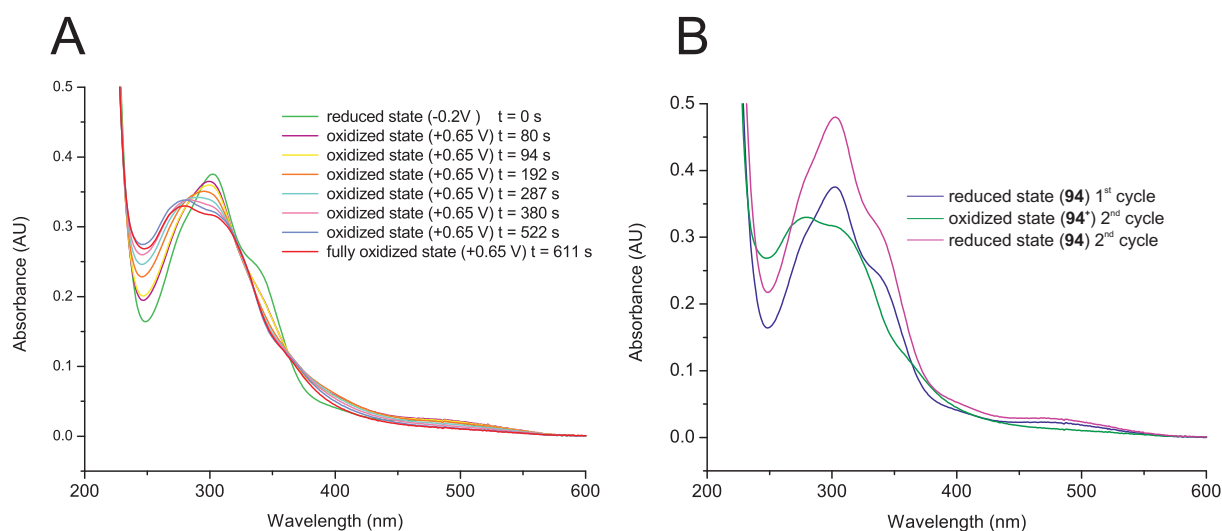


**Figure 71:** Spectroelectrochemistry of **94**.

While applying a negative potential, the absorption spectra of the *tert*-butyl protected compound **98** did not change, a change in the absorption spectra of the acetyl protected compound **94** was observed. It is likely that the redox reaction of the acetyl protected compound **94** is reversible but the acetyl protection groups of the thiol are not stable under these conditions.

### 3.2.2.4 Integration Experiments

Compound **94** displays a distinct redox behavior and a change in the UV/vis-absorption spectra upon changing the oxidation state in solution. As a next step the integration of compound **94** into an electronic device and a potential controlled electron transport investigation is envisaged. To immobilize the molecule between two electrodes, an MCBJ setup is considered. To measure transport properties in relation to a controlled potential, an electrochemical cell needs to be combined with the MCBJ setup. The MCBJ setup which was used for the previous integration experiments described in this thesis is ideally suited for these experiments as it allows transport investigations within a liquid environment. To provide a classical three electrode electrochemical cell as discussed in the electrochemical characterization section, the setup of the MCBJ needs to be enriched with a counter electrode and a reference electrode, while the source and drain electrodes act as working electrodes (Figure 72). This setup is similar to a bipotentiostat.<sup>[232]</sup>

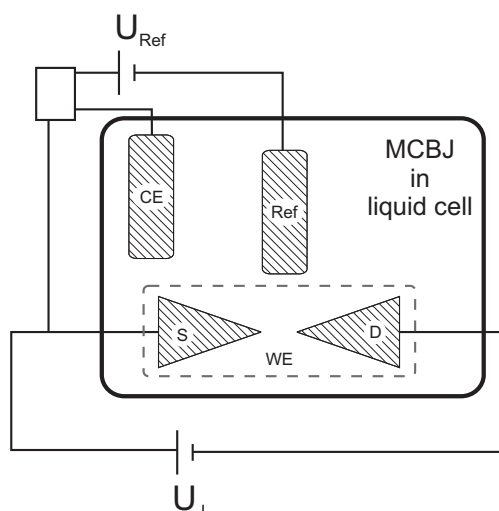


**Figure 72:** A simplified schematics of the circuit of the MCBJ combined with a potentiostat. The setup combines the MCBJ with a three electrode electrochemical cell. The source (S) and drain (D) electrodes become the working electrode (WE). The potential drop ( $U_{Ref}$ ) between source-and-drain-electrodes (WE) and a reference electrode (Ref) is adjusted with a potentiostat. The counter electrode (CE) completes the cell circuit.

The MCBJ setup needed to be adapted to some extent. As quasi-reference electrode (Pt/Ppy), a platinum wire coated with partially oxidized polypyrrole (Ppy) was fabricated and added to the setup (referred to as gate electrode). The voltage between source-and-drain and reference electrodes, referred to as gate voltage, was applied through a potentiostat (for details see Ref.<sup>[233]</sup>) In order to measure the signal of a single molecule, it is required to reduce the faradic electrochemical cell current which is efficiently done by reducing the electrodes' surface.<sup>[234]</sup> Therefore, the Au electrodes are spincoated with a polyimide photoresist layer (Figure 73). The sample was then irradiated with UV using a 10  $\mu\text{m}$  mask. The sample was developed, baked and under-etched to provide an MCBJ sample with reduced electrodes' surface. An SEM image of the covered junction is shown in Figure 73 B.



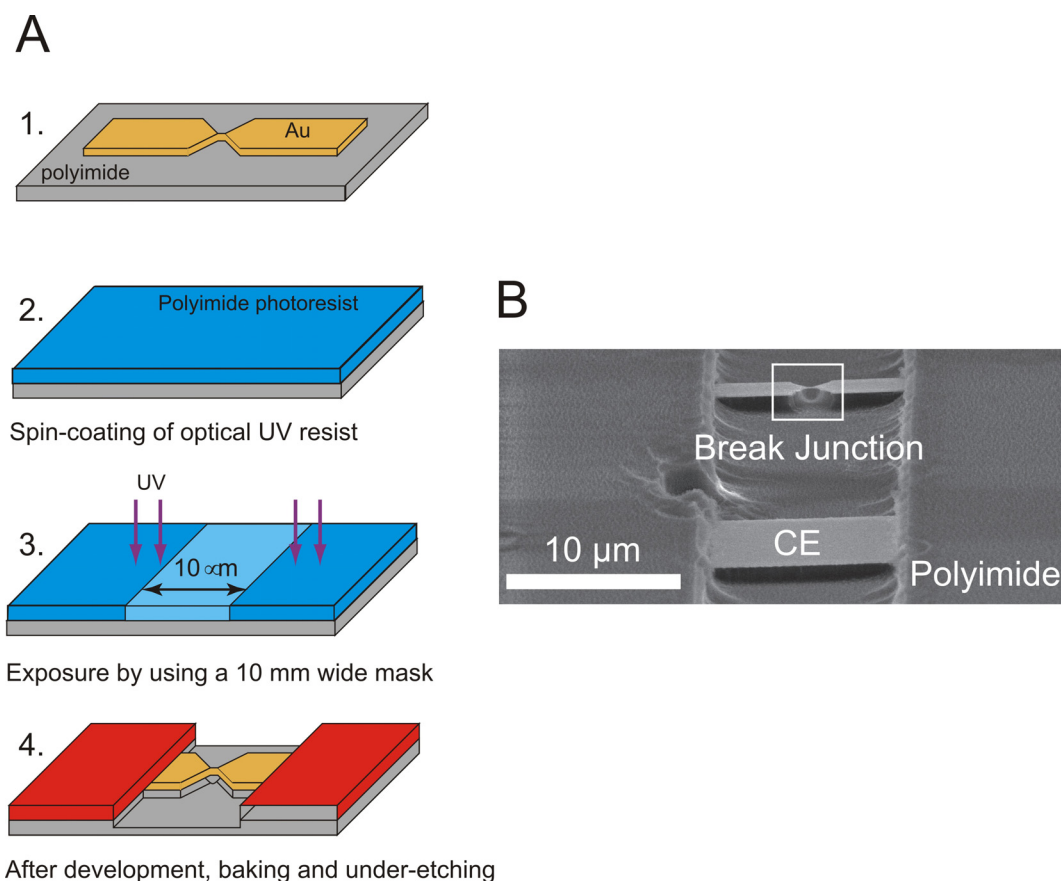


**Figure 73:** A) Protection of Au electrodes' surface with a polyimide layer. The normal break junction sample (1.) is protected with a polyimide photoresist (2). The spin coated sample was exposed to UV irradiation with a 10  $\mu$ m mask (3). The sample was then developed and under-etched to give the protected break junction sample with reduced electrodes' surface (4). B) SEM image of the protected break junction.

As a first experiment, it was tried to immobilize the molecule **94** without controlling the potential (potentiostat off). A solution of **94** in dichloromethane and an electrolyte (TBAPF<sub>6</sub>) was deprotected *in situ* (TBAOH) and exposed to the MCBJ.  $G(z)$  curves were recorded. Histograms of 100 current traces are shown in Figure 74 B. The grey histogram in Figure 74 B corresponds to the control molecule OPV **55** and the red histogram in Figure 74 B corresponds to conductance measurements of **94**. A pronounced conductance peak was observed. Even though the conductance value of compound **94** is more than a magnitude lower than for the control molecule OPV **55**, these results are very promising as it was not obvious from the beginning that it is possible to integrate compound **94** due to its U shape in the solid state structure.

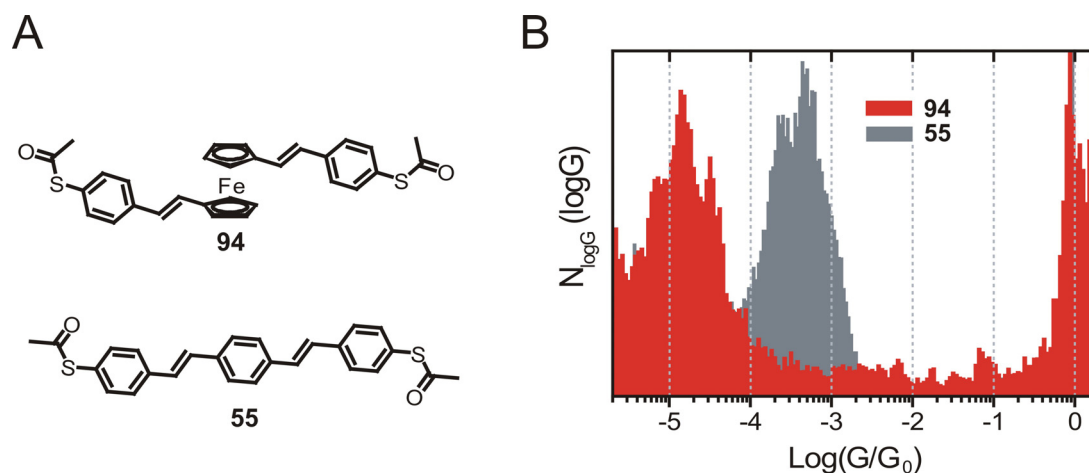


**Figure 74:** Classical MCBJ measurement of compound **94**. No potential was applied with respect to the reference electrode.

These promising results were very motivating to further investigate the switching properties of the target molecule. Therefore as a next step, the MCBJ measurements were performed while controlling the gate voltage and the histograms are shown in Figure 75 A. When applying a gate voltage of 0 V, the yellow histogram was obtained. The position of the peak of the histogram is marked with a yellow arrow and has a value of  $G_{Fc} = 3.72 \cdot 10^{-5} G_0$ , thus a pronounced peak was observed. The gate voltage was then moved to a positive value. A gate voltage of +0.2 V vs. Pt/Ppy was applied and conductance traces were recorded. The histogram of the oxidized form **94**<sup>+</sup> is shown in pink in Figure 75 A. The peak of the histogram is clearly shifted to a higher conductance value and marked with a pink arrow. The conductance of the oxidized species has a value of  $G_{Fc^+} = 1.29 \cdot 10^{-4} G_0$ . A clear shift of the conductance was obtained with a factor of 3.5. By again applying a gate voltage of 0 V the conductance peak is shifted back to the position where it was initially (olive histogram in Figure 75 A). The olive histogram and yellow histogram overlap quite well and are considered to be at the same conductance value. However, when a negative gate voltage was applied, the position of the conductance peak is shifted towards a smaller value (blue histograms in Figure 75). This shift is not fully understood and can not be explained by the proposed redox switching mechanism.

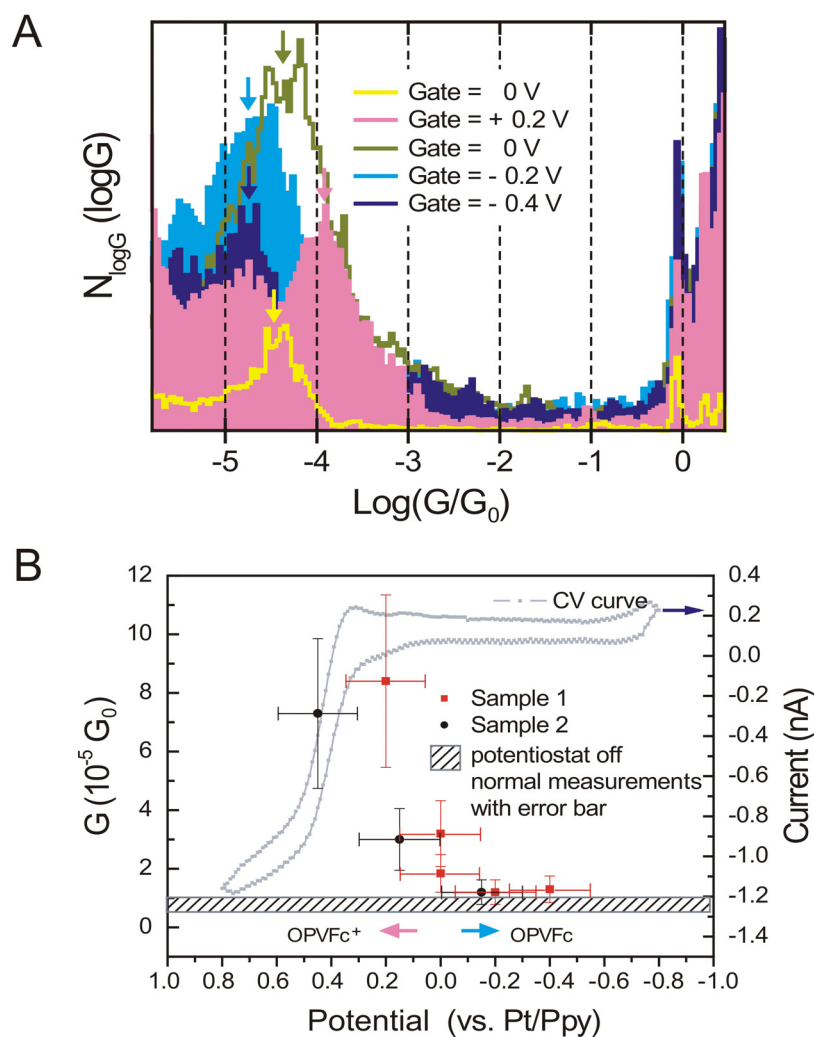


**Figure 75:** A) Histograms of **94** are shown. The initial yellow histogram at a gate voltage of 0 V is shifted when applying a positive gate voltage of +0.2 V corresponding to oxidation of the ferrocene (pink histogram). Setting the potential back to 0 V the ferrocenium is reduced and the conductance peak is shifted back to its initial value (olive). When a negative gate voltage of -0.2 V and -0.4 V is applied the position of the histogram peak is shifted to a smaller value attributed to decomposition of the investigated molecules. In graph B the conductance values are plotted as a function of the potential. The dashed line is the conductance of **94'** when the potentiostat is turned off. An *in situ* CV was recorded and shown as grey curve. A clear conductance jump is observed when setting the gate voltage to a value close to the oxidation potential of **94**. Two samples were investigated (red and black) which both revealed the same results.

An *in situ* CV was measured within the MCBJ setup (Figure 75 B). Overlaid are the conductance values of **94'** and **94'**<sup>+</sup> as a function of the applied potential. The dashed bar shows the conductance of **94'** when the potentiostat is turned off. The conductance values are slightly higher at 0 V gate voltage compared to when the potentiostat is turned off. A jump in conductance was observed when setting the gate

voltage to a positive value. The position of the current jump fits well with the position of the oxidation potential of the CV recorded *in situ*. Figure 75 B nicely reflects the correlation of the conductance and the oxidation state of **94'**.

The shift of the conductance to a smaller value when setting a negative gate voltage has not been clarified yet. A possible hypothesis considers decomposition of compound **94**. As already shown in the spectroelectrochemical investigations, molecule **94** is not stable when applying a negative potential which can be observed as a change in the UV/vis-absorption spectra. The histograms shown in Figure 75 were made from transient conductance traces. Hence, each metal-molecule-metal junction might be made of different molecules. This means that a trapped molecule was before in solution under a negative gate voltage and was treated with very similar conditions as in the spectroelectrochemical investigations. A possible side reaction which might take place is an electrophilic aromatic substitution reaction. The cyclopentenyl rings of ferrocene are nucleophilic and readily react in electrophilic substitution reactions such as *Friedel Crafts* acylations.<sup>[231, 235-237]</sup> This could be one of the possible side reactions which might take place when a negative gate voltage is applied. As the acetyl sulfanyl groups were deprotected prior to the MCBJ measurements, there is an acetyl source in solution. When applying a negative gate voltage to an immobilized molecule, the nucleophilicity of the cyclopentadienyl rings is even enlarged and a *Friedel Crafts* reaction might take place. Having additional acetyl units on the cyclopentadienyl rings of the ferrocene derivatives reduces the electron density of the system which could be an explanation of the decrease in conductance. However, these are at the moment only speculations on possible decomposition mechanisms. Nevertheless, reversible shifting of the conductance peak of the log(G) histograms was observed when applying a positive gate voltage and a zero gate voltage.

### 3.2.2.5 Conclusion

A new redox switch was proposed. The switch is based on a ferrocene unit, functionalized in the 1,1'-position with conjugated vinyl thiol linker groups to provide electronic coupling with the electrodes. Each linker is bonded to one of the two cyclopentenyl rings sandwiching the electroactive iron atom. The target structure **94** was synthesized with a HWE reaction as a key step. In the solid state structure obtained by X-ray diffraction, both linker groups are oriented in the same direction and the molecule is in a U shape. The target structure was electrochemically characterized and a fully reversible redox system was observed in solution. Qualitative spectroelectrochemical investigations were performed and a change in the UV/vis-absorption spectra of the two oxidation states was observed. It was possible to integrate single molecules between two electrodes of an MCBJ in a liquid environment. The conductance was deduced and found to be lower than the conductance of the OPV control molecule **55**. The near-perfect conductance of  $0.7 G_0$  which was found for a similar molecule was not verified.<sup>[224]</sup> Furthermore, the target compound was investigated in an MCBJ setup combined with an electrochemical cell, enabling single molecule measurements under electrochemical control. Indeed a change in conductance was obtained corresponding to a change in oxidation state of the molecule. A better conductance was observed for the oxidized species **94<sup>+</sup>** than for the neutral compound **94**.

It was shown that the change of oxidation state can be exploited as a conductance switching mechanism. Even though the difference in the conductance of a factor of 3.5 is low compared to switches used in modern switching devices, it is a proof of concept, and single molecules were able to switch a current between two different conductance values.



## 4 Rectifiers

As already discussed in the introduction, several molecular rectifiers have been synthesized and rectifying properties of monomolecular films and even of single molecules have been observed.<sup>[96]</sup> However, obtained rectifying ratios (RRs) of molecular rectifiers are smaller than 100, which is way below the values of solid-state rectifiers nowadays used in electronic circuits which show  $RRs > 10^5$ . Theoretical calculations recently claimed that cross-conjugated molecules might show RRs of up to 10'000.<sup>[115]</sup> Therefore we propose a first cross-conjugated molecule comprising an electron rich and an electron poor unit to investigate the potential of cross-conjugated structures as molecular rectifiers.

### 4.1 Cross-Conjugated Molecular Rectifiers

#### 4.1.1 Molecular Design and Synthetic Strategy

A proposed molecular switch **R6** from Ratner and coworkers, displayed in Figure 76, consists of two cross-conjugated spots, each functionalized with either an electron donating (EDG), namely a methoxy group, or an electron withdrawing, namely a carboxylic acid group (EWG).<sup>[115]</sup> The molecule **R6** is terminated with two thiol units, directly bound to the acetylenes. From the point of view of stability of immobilized molecules **R6** and from a synthesis point of view, the target molecule **R6** shows drawbacks. We want to profit from *meta*-substituted benzenes as cross-conjugated units. *meta*-Substituted benzenes show similar features as the cross-conjugated units in molecule **R6** because benzene units show conjugation in *ortho*- and *para*-direction, but not in *meta*-direction. For these reasons we propose a molecule comprising two *meta*-substituted benzene units to investigate its potential as a molecular rectifier. One *meta*-substituted benzene unit is functionalized with an EDG group, whereas the other unit is functionalized with an EWG group. One can think of using several different EDGs and EWGs, however, as a prototype we chose to use a nitro-group as an EWG and a tertiary amine as an EDG (**99** and **100** in Figure 76). The electron withdrawing and donating character of the two groups is very strong, and both the nitro and amine are synthetically accessible.

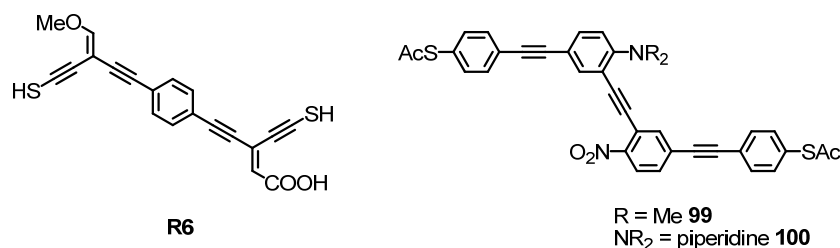


**Figure 76:** Proposed rectifier **R6**, and the *meta*-substituted benzene based rectifiers **99** and **100**.

The target structures **99** and **100** are not conjugated between both terminal anchor groups (A in Figure 77). However, one sulfur is conjugated with respect to the EWG group, whereas the other is conjugated with respect to the EDG group (B in Figure 77). Further the EWG and the EDG are also conjugated towards each other (C in Figure 77)

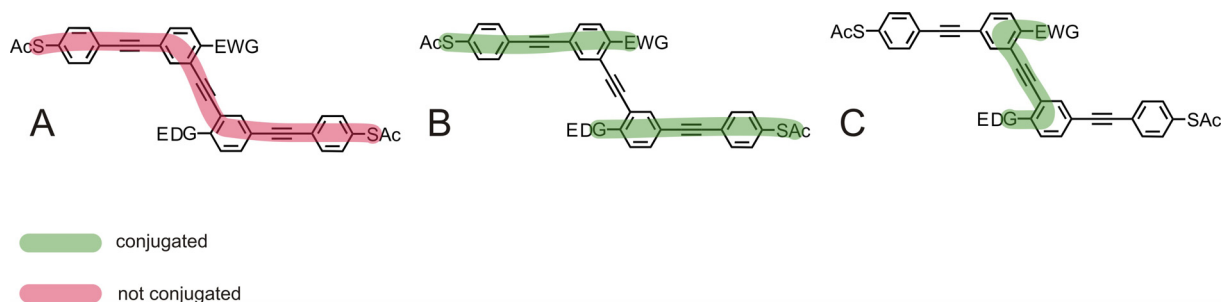
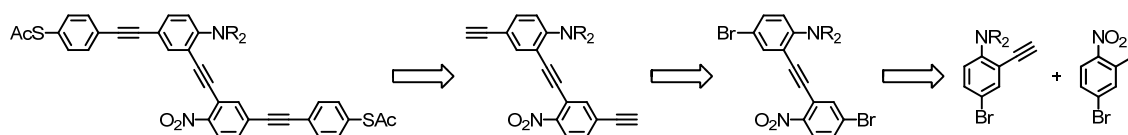


**Figure 77:** Conjugation in target structure **99/100**. A: The two terminal sulfurs are not conjugated towards each other. B: One sulfur is conjugated towards the EWG whereas the other end is conjugated towards the EDG. C: The EWG and the EDG groups are conjugated towards each other.

The synthetic strategy is to first assemble the cross-conjugated handle (Scheme 36). Therefore the two *meta*-substituted benzenes have to be synthesized. If the benzene derivative comprising the nitro or the amine group are functionalized with an iodine in the 2-position and a bromine in the 4-position the selectivity of iodine over bromines in *Sonogashira* reactions can be exploited to assemble the cross-conjugated handle. In a further coupling step the acetylenes are supposed to be introduced. In a last coupling reaction with 4-iodo-thioacetylbenzene the target structure is envisaged to be assembled directly in the desired acetylated compound, therefore no transprotection is required with this strategy.

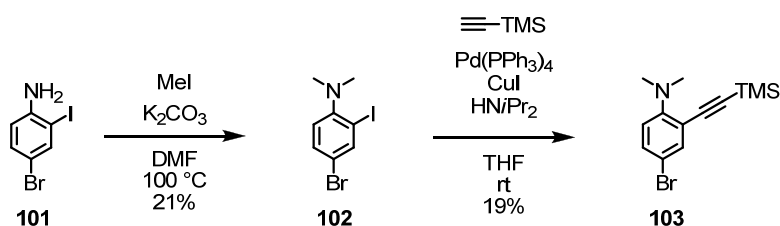


**Scheme 36:** Synthetic strategy towards target structures **99/100**.



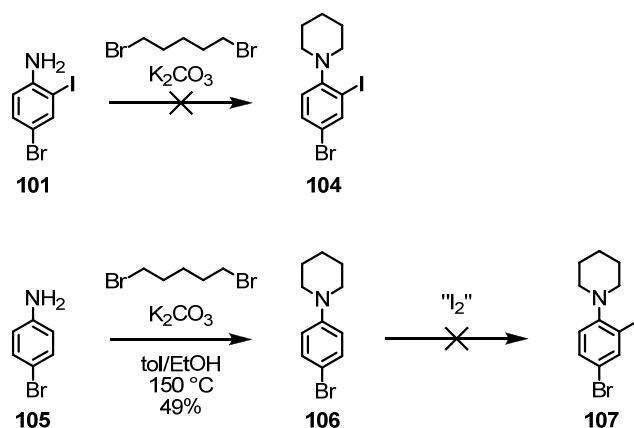
### 4.1.2 Synthesis

Initially it was envisaged to introduce the dimethyl aniline derivative as EDG. Therefore 2-iodo-4-bromoaniline was synthesized following a reported procedure.<sup>[238]</sup> Dimethylation of the aniline derivative using methyl iodide and potassium carbonate in DMF yielded 4-bromo-2-iodo-*N,N*-dimethylaniline in rather low yields (Scheme 37).<sup>[239]</sup> In a next step 4-bromo-2-iodo-*N,N*-dimethylaniline was treated with TMS-acetylene in a *Sonogashira* reaction to selectively substitute the iodide. However, the yield was with 19% low which was attributed to instability of the product **103**. The fact that already this rather small building block is not very stable is discouraging.



**Scheme 37:** Synthesis of building block **103**.

The instability of the dimethyl-aniline derivative led to a small change in the molecular design, namely the exchange of the EDG. As a more stable tertiary amine the methyl groups were exchanged to a cyclic alkyl protection – and donating – group, namely a piperidine. First we envisaged to introduce the piperidine via a twofold substitution reaction from the corresponding aniline derivative **101** with 1,5-dibromopentane (Scheme 38). Common conditions, using potassium carbonate as base and water as a solvent and exposure to microwaves were applied, however unsuccessfully.<sup>[240]</sup> Also changing the solvent to a toluene/ethanol mixture and heating to 150 °C by exposure to microwaves did not yield any product. A possibility to overcome these problems to introduce the piperidine unit – most probably steric hindrance – could be to change the reaction sequence and therefore introduce the piperidine first and then iodinate in a second step.

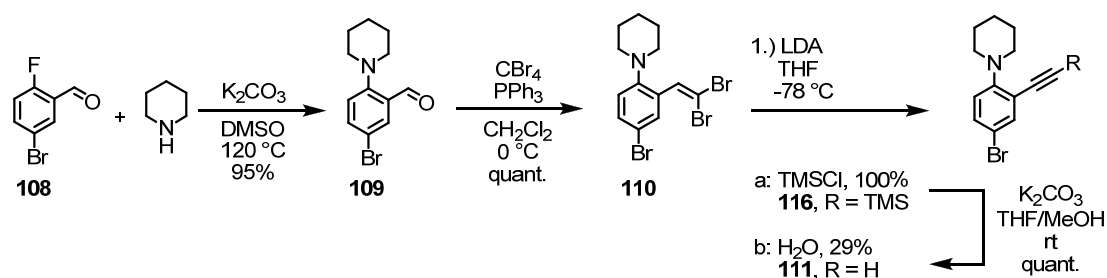


**Scheme 38:** Attempted but unsuccessful pathway towards the 2-iodo-4-bromo-substituted aniline derivative **107**.

Therefore 4-bromo-aniline was reacted with 1.1 equivalents 1,5-dibromopentane and potassium carbonate in a toluene/ethanol mixture while exposing to microwaves. The reaction mixture was aqueously worked up and the crude was purified by CC to give the piperidine derivative **106** as a brownish solid in 49% yield. In a next step compound **106** needs to be iodinated in the *ortho*-position to the piperidine. The piperidine-group has to be in its neutral state, as a protonated species would change the electronic properties and therefore no longer direct the electrophilic aromatic substitution reaction in *ortho*- and *para*-position, respectively. Hence no acidic conditions can be applied. Therefore compound **106** was suspended in water and stirred in the presence of iodine and sodium bicarbonate at room temperature, but no product was formed. Common iodination methods for 4-bromo-substituted aniline derivatives using a refluxing ether/water solvent mixture, iodine and sodium bicarbonate were applied, however unsuccessfully.<sup>[238]</sup> As these iodination methods were not harsh enough,  $ICl_2$  was chosen as an electrophile. But even these strong electrophilic conditions did not afford any product, and mostly starting material was obtained.<sup>[241]</sup> Benzyltrimethylammonium dichloriodate (BTMA  $ICl_2$ ) is reported to be an excellent iodination agent, and is often used to iodinate aniline derivatives in *ortho*- and *para*-position, respectively.<sup>[242-244]</sup> However, mostly starting material was recovered when compound **106** was treated with BTMA  $ICl_2$  and no iodinated product was obtained.

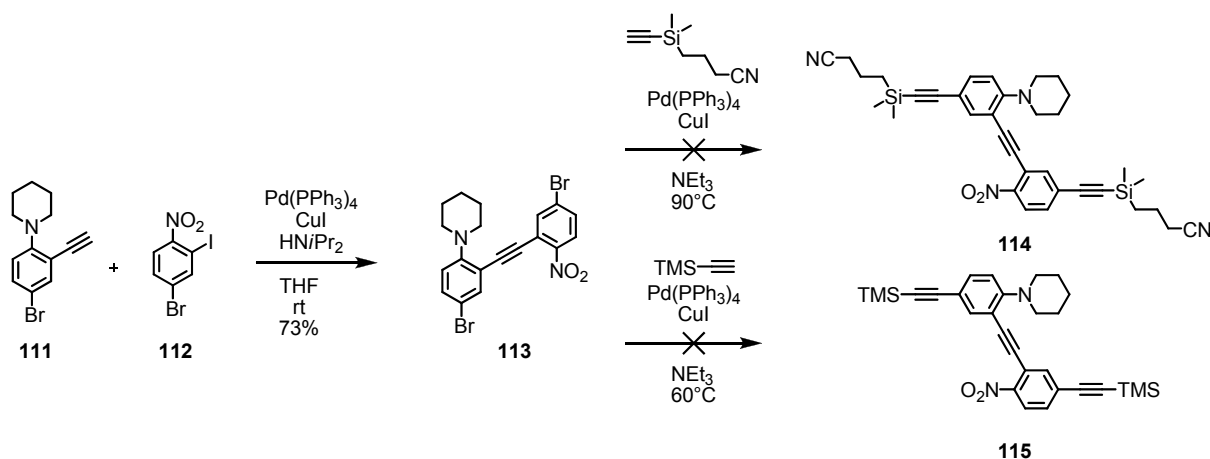
Probably steric hindrance is too dominating and does not allow assembling the building block in the desired fashion. An alternative route to introduce acetylenes is to

perform a *Corey-Fuchs* reaction sequence. With a *Corey-Fuchs* reaction sequence an aldehyde can be converted to an acetylene via a dibromoolefin derivative.<sup>[165]</sup>



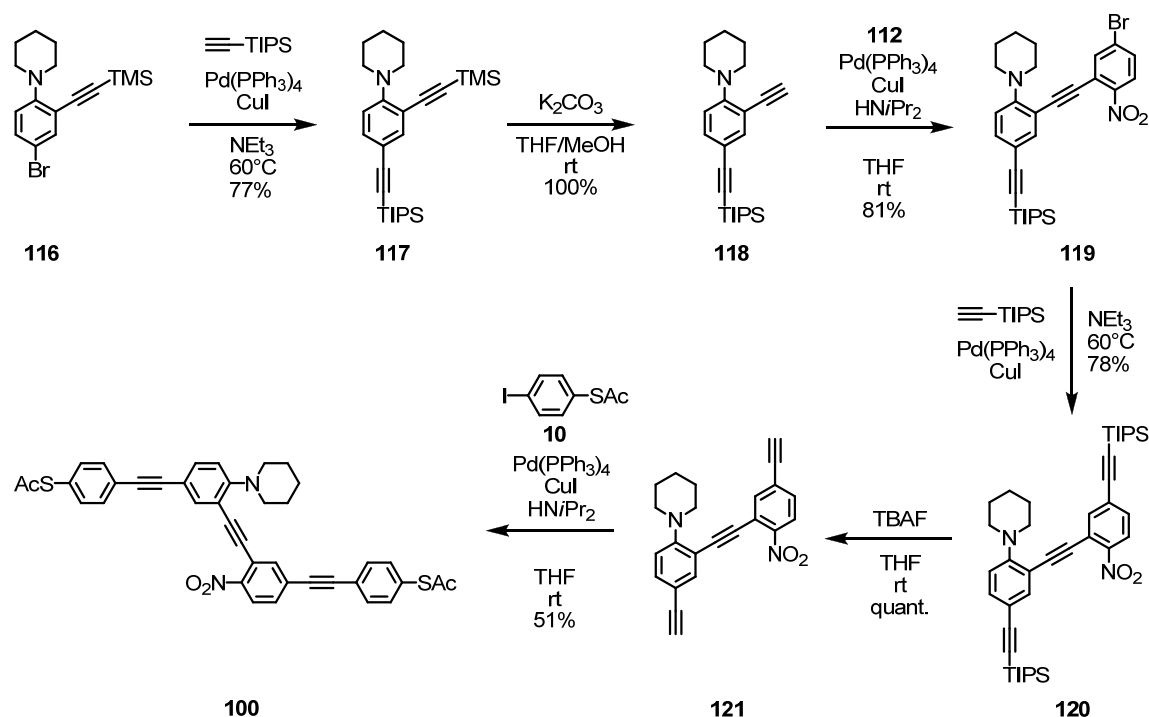
**Scheme 39:** Synthesis of building block **111**.

3-Bromo-5-fluorobenzaldehyde was treated in an aromatic nucleophilic substitution reaction with piperidine and potassium carbonate as base. The reaction mixture was worked up aqueously and dried at high vacuum to give the aldehyde **109** as brownish oil in 95% yield (Scheme 39).<sup>[245, 246]</sup> Compound **109** comprises the desired piperidine functional group and an aldehyde function which was then treated in a *Corey-Fuchs* reaction sequence. Carbontetrabromide was added to a solution of the aldehyde **109** and triphenylphosphine in dichloromethane which immediately led to a precipitation. The formed salts were filtrated off and the filtrate was evaporated to give the dibromoolefin **110** in quantitative yield as a colorless oil which solidified upon drying at high vacuum. A solution of freshly prepared lithium diisopropylamine (LDA) was then added to the dibromoolefin **110** in THF. The reaction mixture was quenched with water and after aqueous workup the free acetylene **111** was isolated in 29% yield. This low yield is attributed to instability of the free acetylene. Therefore instead of forming directly the free acetylene, the intermediate of the *Corey-Fuchs* reaction was trapped with chlorotrimethylsilane to give the TMS-protected acetylene **116** in quantitative yield as a colorless liquid after aqueous workup and purification by CC.<sup>[247, 248]</sup> The TMS-group of compound **116** was in a next step removed using potassium carbonate to give the free acetylene **111** in quantitative yield. Having the ethynyl-functionalized push-building block **111** ready, the assembly of the push-pull-handle **113** was attempted. Therefore the acetylene **111** was reacted in a *Sonogashira* reaction with the corresponding 2-iodo-4-bromo-nitrobenzene **112** which was synthesized following a reported procedure.<sup>[249]</sup> The iodide was selectively substituted and the push-pull-handle **113** was obtained after aqueous workup and purification by CC and recrystallization from hexane in 74% yield as an orange solid.



**Scheme 40:** Synthesis of the push-pull handle **113** together with unsuccessful follow up steps.

In a next step the system was intended to be enlarged with two acetylene units using a *Sonogashira* coupling. As an acetylene source [(3-Cyanopropyl)-dimethylsilyl]acetylene, a polar analogue of (trimethylsilyl)acetylene (TMS-acetylene) was chosen to improve the separation features of the expected products.<sup>[250]</sup> However, the desired product **114** was not obtained. The same coupling reaction was repeated, but using TMS-acetylene. Also this reaction turned out to be troublesome and no product was obtained. As the rate determining step in a *Sonogashira* reaction is the oxidative addition and as the oxidative addition is activated by having an EWG-group in *para*-, and *ortho*-position, respectively, the reaction to substitute both bromides of **113** was expected to be challenging. Indeed the mono-coupled product in which only the bromide in *para*-position to the nitro group was substituted was isolated in 76% yield. Even if the monocoupled product was treated in a further coupling reaction with a fresh catalyst system, and even when the reaction was performed in refluxing triethylamine, only traces of the product were obtained, monitored by MALDI-ToF mass spectrometry, but corresponding to the TLC most of the starting material did not react. Obviously it is very challenging to introduce the acetylene unit at the deactivated *para*-position to the amine at this stage of the synthesis. Therefore the new strategy was to fit the push-building block with both the acetylenes before assembling the push-pull-handle. To provide a selective assembly of the handle the acetylenes of the push-building block need to be equipped with two different protection groups, such that the protected-acetylene in *ortho*-position to the amine can be selectively deprotected. A selective deprotection can be exploited using trimethylsilyl (TMS) and triisopropylsilyl (TIPS) protection groups, respectively.<sup>[251]</sup>



**Scheme 41:** Final synthesis of the target structure **100**. The bromide *para* to the piperidino-moiety was substituted in an early stage (**117**). After that the push-pull handle **119** was assembled. After introduction of the second TIPS-acetylene the TIPS groups were removed to give the free acetylene **121** which then was treated in a last *Sonogashira* reaction to give the target molecule **100**.

The bromide of compound **116** was substituted with TIPS-acetylene in a *Sonogashira* reaction with tetrakis(triphenylphosphine)palladium and copper iodide in triethylamine at 60 °C. The reaction mixture was aqueously worked up and the crude was purified by CC to give compound **117** as colorless oil which was crystallizing with time in a yield of 77%. Compound **117** comprises two protected acetylenes, the acetylene in *ortho*-position to the amine is protected with TMS whereas the acetylene in *para*-position to the amine is protected with TIPS. The TMS-group was selectively cleaved with potassium carbonate.<sup>[252]</sup> Therefore the TMS-protected species **117** was dissolved in a THF/MeOH mixture and treated with 0.5 equivalents of an aqueous 1 M potassium carbonate solution. After stirring for 2 hours the reaction mixture was extracted and the crude was purified by column chromatography (CC) to give the desired free acetylene **118** in 100% yield as a pale yellowish oil. The acetylene **118** was then coupled with the push-building block **112** in a *Sonogashira* reaction with tetrakis(triphenylphosphine)palladium and copper iodide as catalysts in a THF/diisopropylamine mixture. The reaction mixture was evaporated and purified by

CC to give the mono-acetylene-comprising push-pull-handle **119** as an orange solid in 81% yield. The nitro group of **119** activates the oxidative addition reaction and therefore the bromide was efficiently substituted in a *Sonogashira* reaction. Therefore, the bromide **119** was treated with TIPS-acetylene and tetrakis(triphenylphosphine)palladium and copper iodide as catalysts in triethylamine at 60 °C. The reaction mixture was aqueously worked up and purified by CC to give the diacetylene functionalized compound **120** in a yield of 75% as an orange solid. The TIPS groups of **120** were then quantitatively removed using tetrabutylammonium fluoride (TBAF) to give the free acetylene **121** as a red solid. In a last *Sonogashira* reaction the acetylenes of **121** were coupled with 4-iodo-thioacetylphenyl (**10**). As catalysts tetrakis(triphenylphosphine)palladium and copper iodide were used and the reaction was performed in a THF/diisopropylamine mixture. The reaction mixture was quenched with water and extracted with dichloromethane. The crude was purified by CC and by precipitation from dichloromethane into rapidly stirring hexane. The target molecule **100** was obtained as a red solid in 51% yield. That way the synthesis of the desired target structure was successfully performed, even though some detours had to be taken.

The target structure such as all the precursors were characterized by TLC, melting point, <sup>1</sup>H-NMR, <sup>13</sup>C-NMR, mass spectrometry and elemental analysis. It remains to be stated that the elemental analysis of the target structure was marginally not in the desired range.

### 4.1.3 Conclusion

A new molecular rectifier was proposed. The design of the rectifier is based on cross-conjugated systems which are postulated to show RRs more than one hundred times larger than RRs obtained so far from molecular rectifiers. To increase synthetic accessibility and stability, *meta*-substituted benzenes were chosen as cross-conjugated joints. The structure comprises two *meta*-substituted benzene units, one functionalized with an electron donating and the other one with an electron withdrawing group. The synthesis and characterization of the target structure was successfully performed.

Currently we are looking for an ideal setup to immobilize target structure **100**. To determine the RR I/V-curves have to be measured. The MCBJ setup we were using

---

to measure the rods and the switches measure transient conductance curves at a constant potential. A metal-molecule-metal contact is formed and broken in a repeated fashion. However, to measure  $I/V$ -curves, a molecule has to be fixed between electrodes and the voltage has then to be changed while monitoring the current. To provide a stable molecular junction an ideal integration setup for the investigations of the rectifying properties of compound **100** should operate at low temperatures. The MCBJ setup used to investigate hysteretic switches<sup>[253]</sup> (see introduction) could be a suitable setup to investigate rectifying properties of compound **100**.





## 5 Molecules “Waving” Inside the Gap: Electroluminescence in a Single-Walled Carbon Nanotube Junction

### 5.1. Introduction

If molecules are considered as the smallest units in electronic devices, their tininess is on the one hand a great advantage as it reduces the feature size down to a very small scale, but on the other hand makes them very challenging to handle.<sup>[1]</sup> Since it was understood what molecules are made of, a particular challenge of synthetic chemistry is to master the structure of molecules and thereby their functions. Also thanks to a great development of analytical tools, it is nowadays possible to assemble very complex molecules.<sup>[254]</sup>

The field of molecular electronics was in its origins limited to theoretical investigations, and only a large improvement of physical setups to address small assemblies of molecules and even single molecules made it possible to approach the field experimentally.<sup>[3, 6, 255]</sup> From a molecule bound to two electrodes, the response of an electric input can be measured. Molecules were designed such, that when immobilized between electrodes, rectification or switching was obtained. However, it would be very appealing to get an additional signal from a molecule different than the electrical response. The additional signal from an integrated molecule would offer information that molecules are bridging the electrodes, thus help to understand the behavior of integrated molecules to a level enabling the design and assembly of molecular electronic devices.

Nongjian Tao and coworkers developed a setup which combined surface-enhanced Raman scattering (SERS) and mechanically controllable break junction (MCBJ) to measure SERS signals of molecules located inside the nanogap between two electrodes.<sup>[256]</sup> An incident laser was focused onto the top of a molecular junction and the scattered light was collected with a lens and directed to a spectrometer. They used 1,4-dithiol as a molecule because it forms two strong covalent bonds to the gold electrodes, and strong SERS signals are expected. Indeed, an SERS signal was obtained, the intensity of which depends on the gap width and the incident light polarization, indicating that the signals came from the molecules inside the gap. However, like other spectroscopic tools, it cannot be easily distinguished if the signal

originates from the particular molecules that are responsible for the current between the electrodes.

Optical emission signals from integrated molecules are considered as a promising alternative spectroscopic method other than SERS. Light is an attractive media, as it can be detected with a very high sensitivity. The emission from single molecules has already been detected.<sup>[257-261]</sup> Furthermore, the emission spectra of molecules are very characteristic giving additional insights concerning their structures.<sup>[257, 262, 263]</sup> To promote emission of a fluorophore, the molecule needs to be excited. This is commonly realized by irradiation with photons with a corresponding wavelength. Relaxation of the excited electrons to the ground state is then accompanied by the emission of photons. Besides photons, an electric current passing through a fluorophore or a strong applied electric field can be exploited to excite a molecule to subsequently emit light, referred to as electroluminescence.<sup>[263-265]</sup> Electroluminescence is the result of radiative recombination of electrons and holes, which are separated prior to recombination.

However, it is challenging to investigate optical properties of molecules connected to metal-electrodes, as the excited state of the molecule is often quenched by the metal. In all of the previously described attempts to connect molecules to electrodes in this thesis and in most of the reports in literature, metal-electrodes are used (see chapter 1.1.1). Despite many advantages of metal electrodes, these methods suffer from some limitations such as unstable anchor groups of the immobilized molecules, laborious electrode fabrication and precise control over the contact geometry. An alternative strategy is to use single-walled carbon nanotubes (SWNTs) as electrodes.

### **5.1.1 Single-Walled Carbon Nanotubes as Potential Electrodes for Molecular Electronic Devices**

Since the discovery of carbon nanotubes,<sup>[266]</sup> they have been regarded as an exceptional material.<sup>[267-269]</sup> They are hollow molecular nanostructures made of a monoatomic wall of  $sp^2$ -bonded carbons and are the equivalent of a rolled-up graphene sheet. Single-walled carbon nanotubes (SWNTs) have elementary chemical composition but exhibit a high diversity. SWNTs can be either metallic or semiconducting leading to a wide electrical versatility.<sup>[269]</sup> SWNTs are quasi

one-dimensional ballistic nanowires that are intrinsically molecular.<sup>[268, 269]</sup> They can be processed and their  $\pi$ -bonding provides useful electrical behavior. Compared to ordinary metal electrodes, SWNTs are molecularly sized in their width but infinitely long. SWNTs are very promising materials for several applications,<sup>[268]</sup> however, for the realization of electronic circuits based on carbon nanotubes there are considerable challenges to overcome. Namely, separation of metallic from semiconducting tubes and positioning and contacting of carbon nanotubes are two of the main issues.

#### *Separation of metallic and semiconducting SWNTs.*

During the common preparation procedures of SWNTs, metallic and semiconducting SWNT are usually grown together as bundles.<sup>[268]</sup> However, for potential applications either metallic or semiconducting SWNTs are required, leading to a grand challenge of sorting metallic from semiconducting SWNTs. Ralph Krupke and coworkers developed a nanotube separation method based on alternating current (AC) dielectrophoresis.<sup>[270, 271]</sup> SWNTs develop an induced dipole moment when subjected to an electric field, which is different for metallic and semiconducting SWNTs. The induced dipole moment allows aligning and moving suspended tubes in a specific manner by designing an appropriate inhomogeneity of the electric field. In doing so, semiconducting and metallic SWNTs were separated. Alternative methods based on chemical selectivity towards metallic tubes,<sup>[272]</sup> or selection via ion exchange chromatography<sup>[273]</sup> were exploited to separated suspensions of metallic and semiconducting nanotubes.<sup>[271]</sup>

#### *Contacting SWNT with electrodes*

Krupke extended the dielectrophoresis technique developed for the separation of SWNTs to trap SWNTs between prefabricated metal electrodes.<sup>[274]</sup> The dielectrophoretic deposition technique even allows parallel manufacturing of carbon nanotube devices (Figure 78 A).<sup>[275]</sup> The dielectrophoretic force is attractive in all regions in the absence of deposited nanotubes, but becomes repulsive between the electrodes once a nanotube has been deposited (Figure 78 B and C). This enables control of the number of trapped nanotubes.

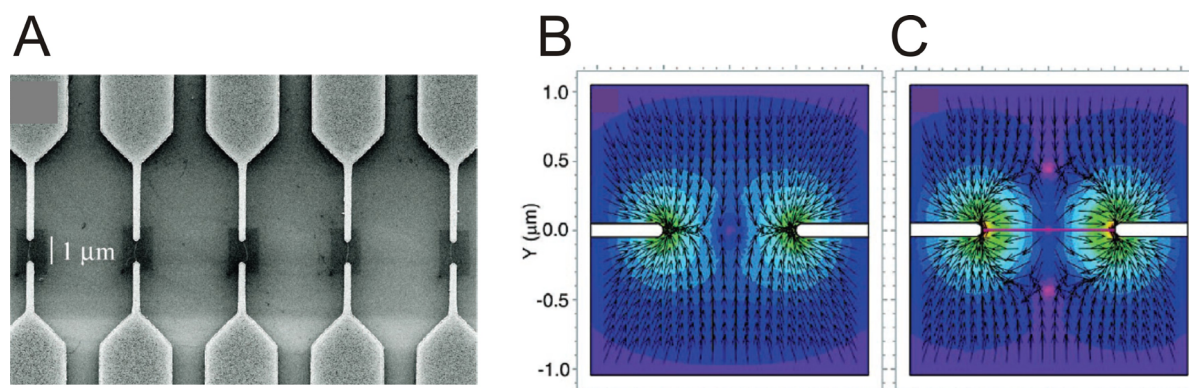


**Figure 78:** A) An SEM image of the electrode arrays in ref<sup>[275]</sup> showing five adjacent devices, with each electrode pair bridged by one CNT visible as fine white lines. B) Simulation of dielectrophoretic force fields. The arrows indicate the direction of the force acting on a nanotube and, hence, the direction of nanotube motion. The force is attractive in the absence of deposited nanotubes (B) but becomes repulsive between the electrodes once a nanotube has been deposited (C).

To control the fabricated devices, the electrode pairs were contacted with submicrometer probes mounted inside a SEM and electronic transport through the nanotubes was measured (Figure 79). Initially the contact resistance is with 2-5 M $\Omega$  high but can be significantly lowered to 500-1000 k $\Omega$  by annealing the devices at 200°C. This process leads to an improved metal-nanotube interface and desorption of residual surfactants from the nanotube surface.

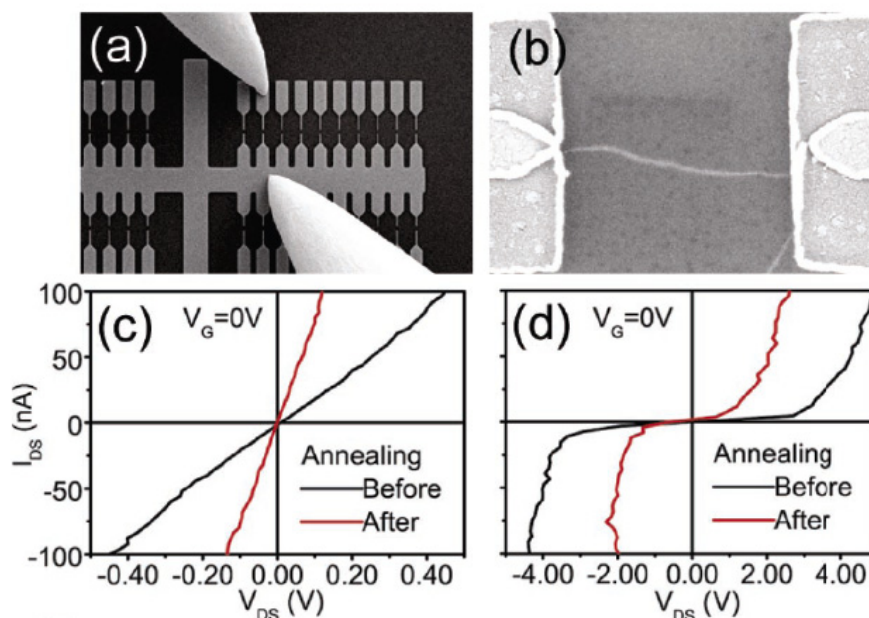


**Figure 79:** a) Contacting of distinct devices with two submicrometer probes. b) SEM of an annealed device. c) and d) I/V-curves of the device before (black) and after (red) annealing.

*Formation of SWNT-electrodes.*

While AC dielectrophoresis turned out to be a very powerful tool to immobilize SWNTs between two electrodes, it remains to form the actual SWNT electrodes. Only then, molecular electronic devices based on single walled carbon nanotubes can be investigated. Since Krupke and coworkers were able to bridge electrodes with single SWNTs, they developed a method to “cut” the tubes providing two freestanding SWNT contacts (Figure 80).

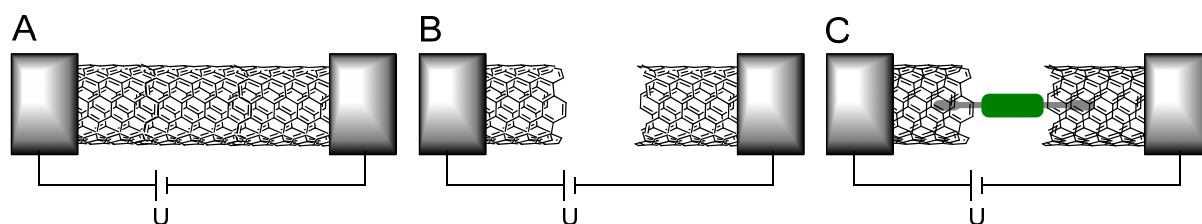


**Figure 80:** Schematic Illustration of the formation of a CNT device. The SWNT is contacted with two palladium electrodes (A). A voltage is applied leading to a break down and a nanogap is produced (B). The gap is then considered as a platform to immobilize molecules (green) (C).

Palladium electrodes were fabricated by electron-beam lithography. The surface between the electrodes was edged to provide a 50 nm wide trench. After electrically contacting the electrodes, metallic SWNT were deposited between the electrodes using AC dielectrophoresis. In doing so free standing SWNT contacted with two electrodes were provided. The immobilized nanotubes were then characterized by I/V-measurements. A voltage was applied to the contacted metallic SWNTs until the tubes break. Initially the size of the gaps formed could not be controlled and was large with more than 20 nm. However, after extensive investigations and optimizations of parameters such as applied voltage or partial oxygen-pressure, the formation of nanogaps became reproducible and gaps of down to 5 nm can be formed. SEM is a well established technique for imaging carbon nanotubes,<sup>[276, 277]</sup> however in this stage it is delicate to use SEM as characterization tool, because the electron-beam causes damage to the free-standing SWNT, and the devices can no longer be used for experiments after taking a SEM image. However, an SEM image of one sample comprising a nanogap is depicted in Figure 81 B. To non-destructively analyze the SWNT-gaps, I/V-characteristics of the devices are measured.

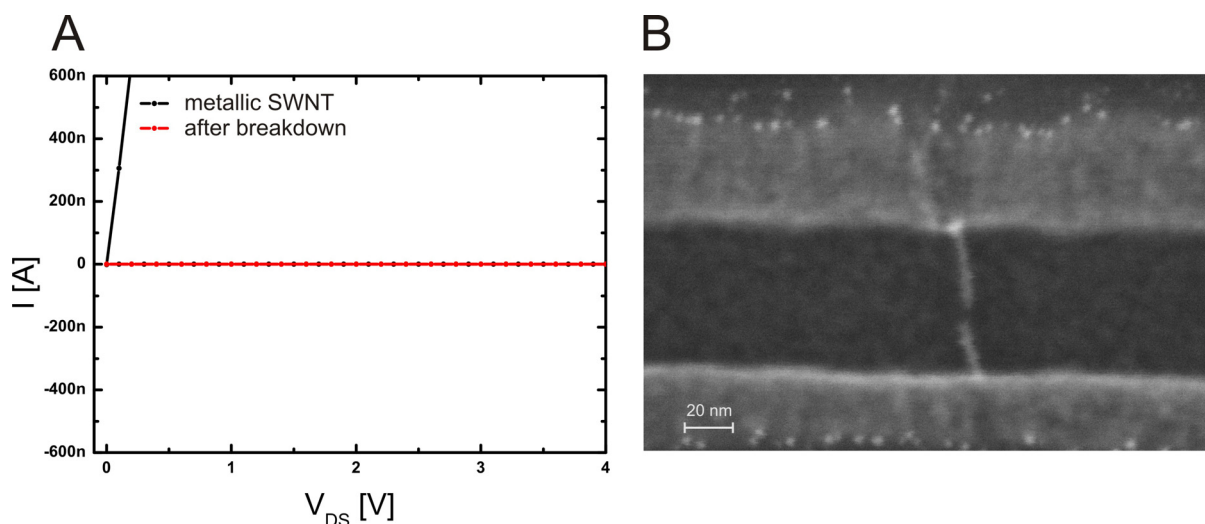


**Figure 81:** A: I/V-characteristics of a SWNT contacted with two Pd-electrodes before (black line) and after (red) breakdown. B: SEM image of a contacted SWNT after breakdown. A nanogap of about 5 nm is formed.

Figure 81 A shows the I/V-plot of a SWNT-junction. The metallic SWNT response is depicted in black. After cutting the SWNT, the red curve is obtained. It is clearly seen that the conductance of the device decreased drastically.

Other techniques to prepare molecular electronic systems based on SWNTs have also been reported. Nuckolls and coworkers were edging gaps into SWNTs with an oxygen plasma.<sup>[269]</sup> The acid functionalized borders of the SWNT-gap were covalently bridged with amine terminated molecules via amide bond formation. While immobilizing appropriate molecules, pH sensing, metal-ion recognition and DNA hybridization sensors were realized.<sup>[269]</sup>

We want to profit from the freestanding SWNT electrodes prepared by Krupke and coworkers. The SWNT gap offers a nice interface for molecular electronic devices.



## 5.2 Project Description

The possibility of forming distinct gaps in a SWNT offers the manufacture of molecular electronic junctions based on SWNT electrodes. The two borders of the gap can be considered as contacts and therefore we propose to bridge the nanogap with a molecule to form a SWNT-molecule-SWNT junction. To provide a driving force of the molecule to bridge the nanogaps it needs to be polarizable such that it moves, similar to the SWNTs into the gap. If the molecule bears two anchor groups with affinity towards carbon rich materials, it is possible to form a stable SWNT-molecule-SWNT junction. We propose long rigid molecules comprising a central fluorophore to be immobilized in the nanotube junction. The fluorophore will be excited by applying a voltage, and the emitted light is envisaged to be detected to obtain a characteristic spectroscopic signal of a molecule connected to two contacts. An illustration of one of the proposed target structures in a SWNT-molecule-SWNT junction is shown in Figure 82. The design, synthesis and characterization of the proposed molecules and the electroluminescence of a SWNT-molecule-SWNT junction will be reported in the following sections.

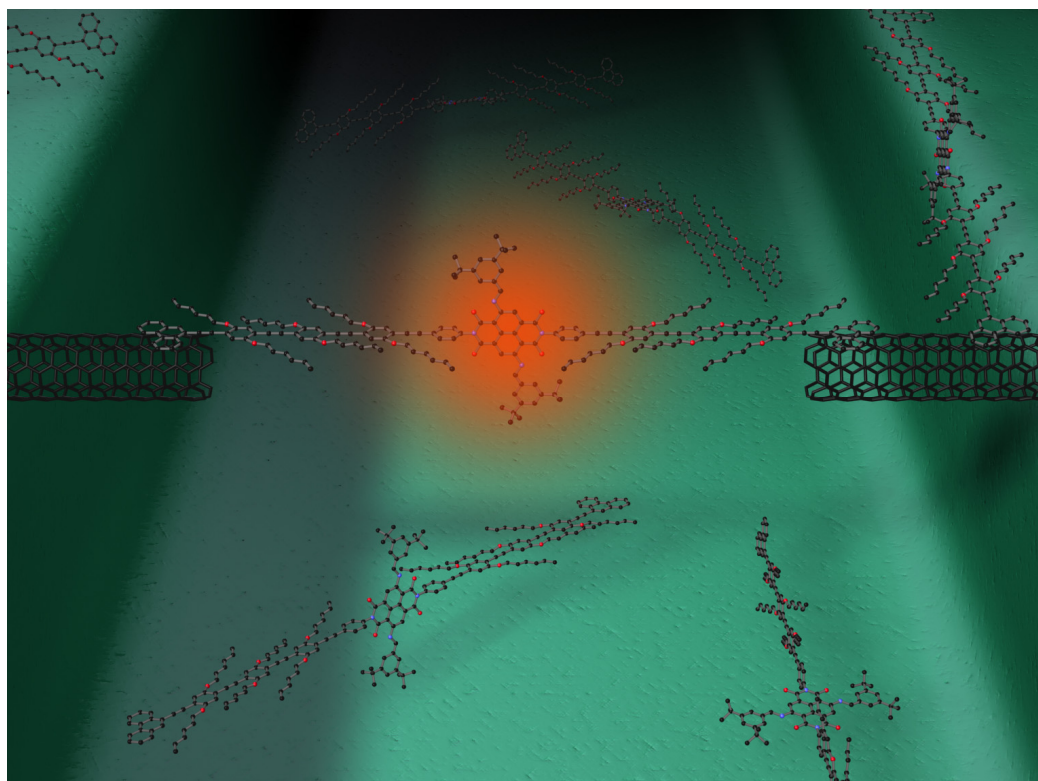


**Figure 82:** Illustration of a SWNT-molecule-SWNT junction. The emission of the fluorophore is depicted in red.

### 5.3 Molecular Design and Synthetic Strategy

To bridge the carbon nanotube gap, a molecule with a length longer than 5 nm is required. To provide a stable junction, the molecule needs to be polarizable and rigid. The central fluorophore is substituted with two rigid linkers, on which end anchor groups are placed. The design of the target molecules and the certain substructures is described in the following.

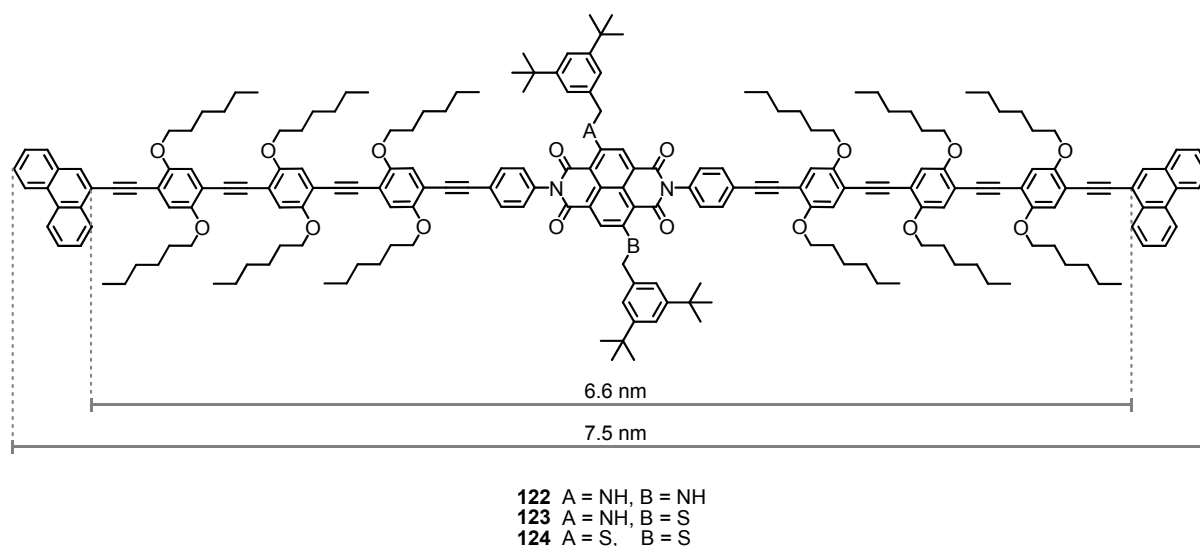


**Figure 83:** Proposed target structure. The core substituents are systematically varied to tune the photophysical properties. The displayed lengths are calculated by force field minimization (ChemDraw 3D).

#### *Fluorophore*

Naphthalene diimides (NDI) were considered as rigid linear chromophores. NDIs draw several advantages for the targeted experiments. They show different absorption and emission properties as a function of lateral substituents, without changing the actual rod-type backbone.<sup>[278, 279]</sup> The color is reported to be tunable by the 2,6-core-substituents and also the fluorescence depends to some extent on the core-substituents. Introduction of benzylic hetero atom subunits as core substituents leads to fluorescent dyes.<sup>[280]</sup> 2,6-Dibenzyl amine substituted NDIs are reported to be blue in color and strongly fluorescent with an absorption maximum at 610 nm. Substitution of 2,6-dibenzyl sulfides is reported to lead to a hypsochromic shift with an absorption maximum at 528 nm. The mixed-substituted NDIs show an absorption maximum at 567 nm and they are pink in color. The possibility to tune the optical properties of the fluorophore is very appealing, as for the attempted experiment, the emitted light would be characteristic for the immobilized molecule. Therefore we



propose three different fluorophores, one disubstituted with (3,5-di-tert-butylphenyl)methanamine (in target structure **122**), one disubstituted with (3,5-di-tert-butylphenyl)methansulfide (in target structure **124**) and one fluorophore with two different core-substituents (3,5-di-tert-butylphenyl)methanamine and (3,5-di-tert-butylphenyl)methansulfide (in target structure **123**). A considerable change concerning the optical properties is expected for the three compounds (Figure 83).

The fluorophore is expected to be electrically excited. From one electrode electrons are injected whereas from the other electrode holes are injected. The electrons and holes are recombined on the central fluorophore while exciting it. However, to provide the radiative recombination of electrons and holes they need to be separated. The linkers are placed on the diimide nitrogens of the NDIs providing the required separation due to breaking of the electronic communication.<sup>[281]</sup>

Furthermore, NDIs are polarizable providing the desired alignment in a dielectrophoretic field. For all these reasons NDIs appeared ideally suited for the envisaged experiments.

#### *Anchor groups*

As anchor groups, a unit with high affinity to carbon rich materials is required. We chose polyaromatic hydrocarbons (PAH) as anchor groups as they show high affinity to carbon rich materials such as SWNTs due to van der Waals interactions of the flat  $\pi$ -systems. We chose phenanthrene as PAH due to the commercial availability of the 9-bomophenanthrene derivative. The anchor groups are not covalently bound to the electrodes, and the target structures is rather immobilized by a supramolecular approach between the electrodes.

#### *Linkers*

The task of the linkers is to connect the anchor groups with the fluorophore. The linkers afford the communication from the anchor groups to the central unit. Furthermore they provide the desired length of the molecule. For these reasons we propose an oligo(phenylene ethynylene) (OPE) backbone as linkers as OPEs are well conjugated and rigid systems. In addition, the phenyl units of the OPE backbone are fitted with alkoxy groups to provide solubility for the long target structures.

With all these design criteria, target structures **122-124** are proposed. The length of the molecules is estimated to be 7.5 nm (MM2 force field minimization, ChemDraw 3D). Due to systematic variation of the core-substituents of the NDI fluorophore, characteristic optical properties are expected.

### Synthetic strategy

The synthetic strategy is to assemble the OPE backbone by *Sonogashira* coupling reactions.<sup>[151]</sup> This is a very efficient method to assemble long OPE systems.<sup>[154, 282, 283]</sup> The target molecules **122** and **124** are symmetric, and **123** is considered pseudo-symmetric as the different core substituents are not expected to affect the linker's assembly. Therefore a symmetric assembly is considered. There are two possible strategies, either a stepwise assembly or a parallel assembly. Due to the improved relative yields of a parallel assembly and due to the enhanced modularity, the parallel assembly was clearly the strategy of choice. Therefore we planed to assemble the target structure **X** by coupling in a last step the bis-ethynyl-functionalized NDI derivative **Z** with two equivalents of the iodine functionalized rods **Y** in a *Sonogashira* coupling reaction (Figure 84).

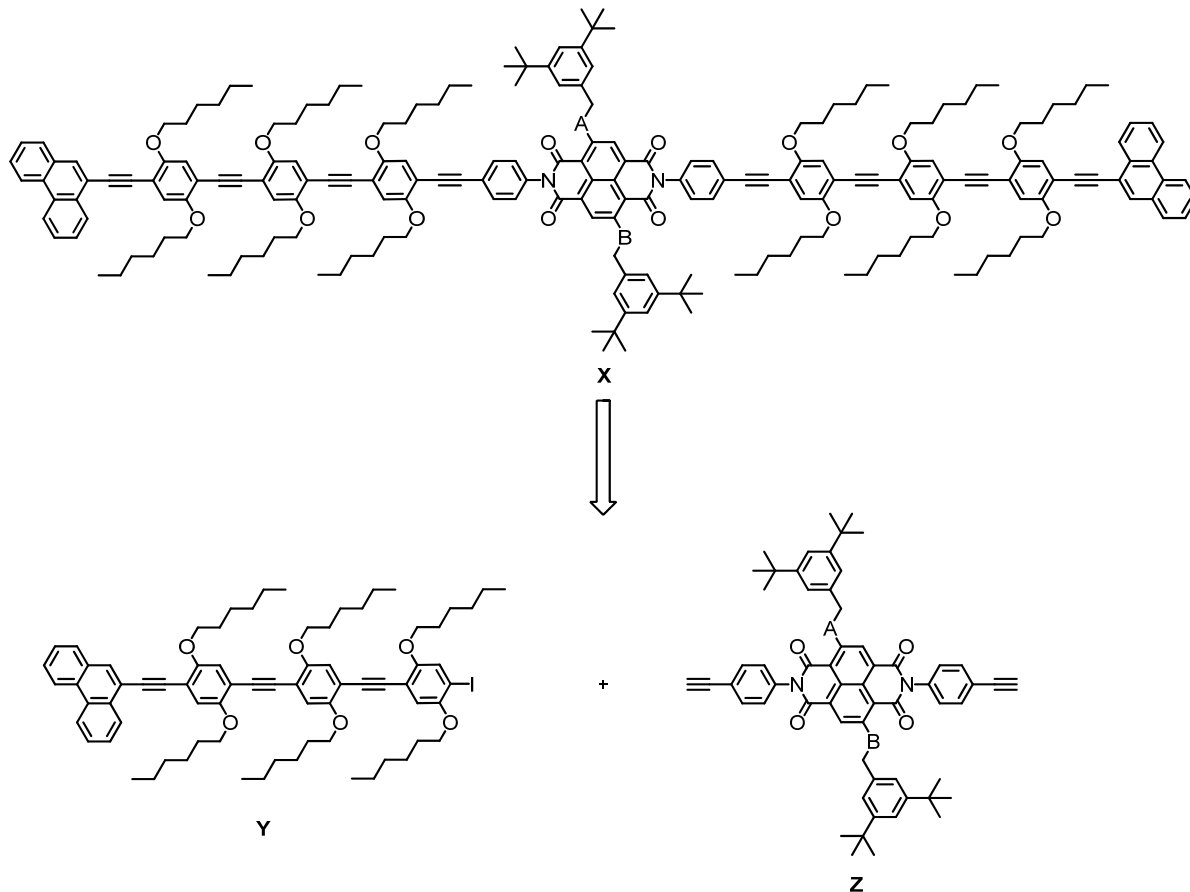


**Figure 84:** Synthetic strategy for the assembly of target structure **Z**.

The precursor **U** allows a modular synthesis of the different core-substituted NDI building block **Z** (Figure 85). Compound **U** is available in a reaction of 2,6-dichloro-1,4,5,8-naphthalene tetracarboxylic acid anhydride (**W**) with 4-((tri/isopropylsilyl)ethynyl)-aniline (**N**). The acetylene is protected by silane protection groups, which will be cleaved after introduction of the core-substituents. The chlorides of compound **U** can be modularly substituted with building block **V**. By varying A in compound **V** from being either NH<sub>2</sub> or SH, all three building blocks **Z** (with A = B = NH; A = B = S; A = NH, B = S) will be available.

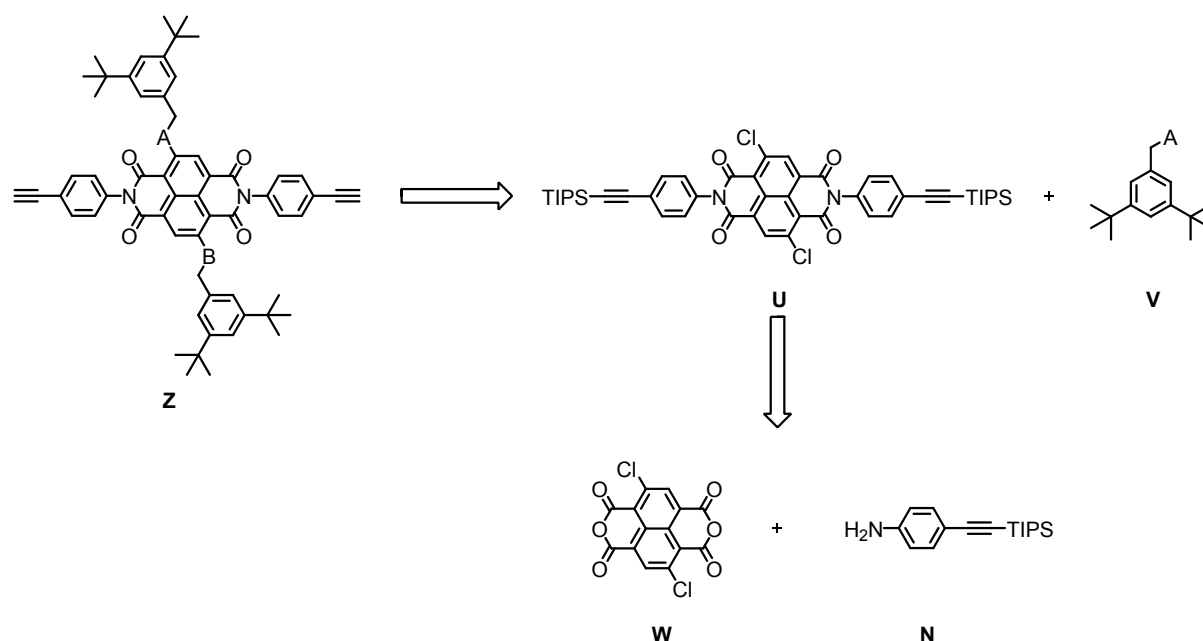


**Figure 85:** Synthetic strategy for the assembly of NDI buildingblock **Z**.

The synthetic strategy to assemble the molecular rod **Y** is a repeated coupling-deprotection sequence (Figure 86). The smallest unit of the OPE-backbone is the diiodo compound **O**. To reduce the number of steps for the total assembly of **Y** building block **Q** is envisaged, already comprising a protected ethynylene unit. Building block **Q** can be coupled to a free acetylene, and after cleaving of the protection group (PG) the next free acetylene is provided, which can subsequently be coupled to the building block **Q**.

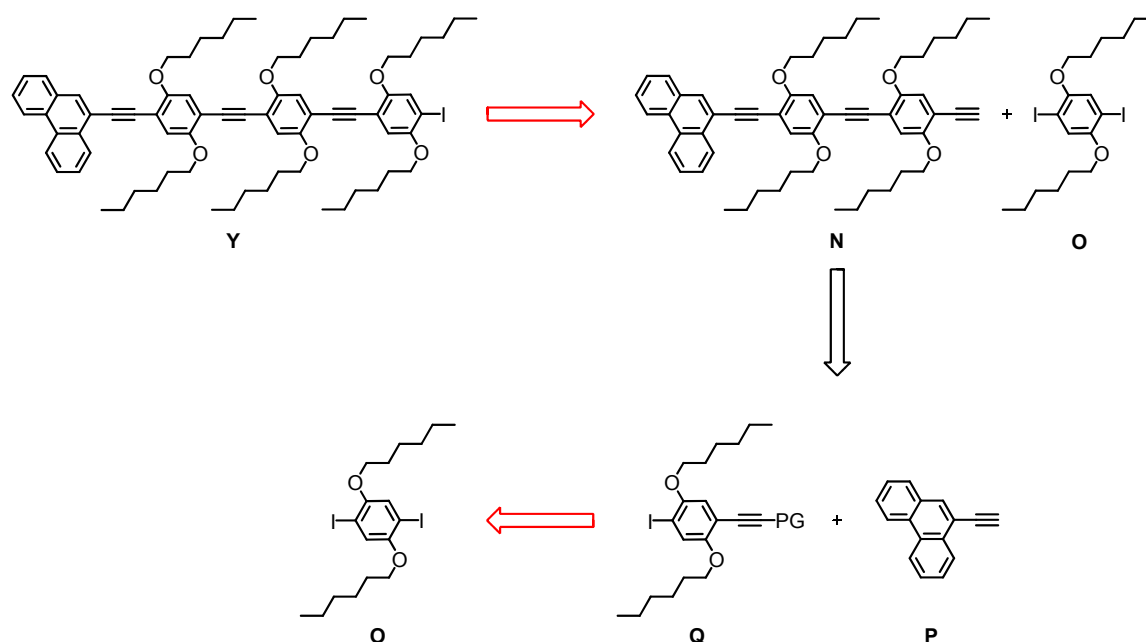


**Figure 86:** Synthetic strategy for the synthesis of the molecular rod building block **Y**.

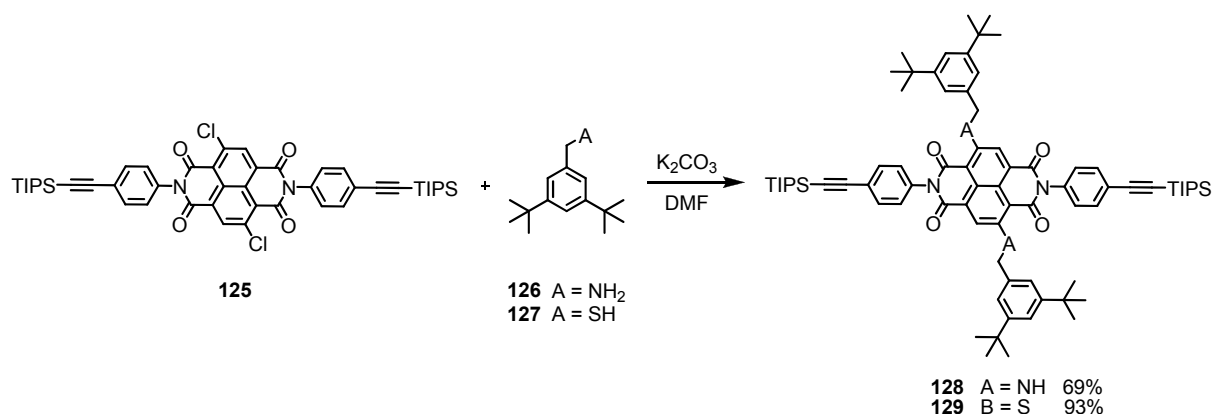
The synthetic strategy draws on two statistical steps expected to be challenging, which are depicted with red arrows in Figure 86. The final building block **Y** bears a terminal iodide, and therefore compound **O** is supposed to be coupled to the acetylene **N**. However, compound **O** comprises with its two iodides two active sites for a *Sonogashira* reaction, and therefore the disubstituted product is expected to be formed as well. However, the statistical limitations can be overcome when **O** is applied in a large excess. The second challenging step in the synthetic strategy is the synthesis of building block **Q**. By inserting a protected acetylene into the structure of building block **O**, again one or both iodides can be substituted in a *Sonogashira* reaction. Therefore the reaction mixture is expected to consist of the starting material (**O**), the monosubstituted compound (**Q**) and the disubstituted compound. As trialkylsilane-protected acetylenes have a very comparable  $R_f$  value like halides, when substituted at an aromatic core, it will not be possible to separate the mixture of the three compounds. However, by profiting from a polar silane as protection group, considerable differences in  $R_f$  values are expected, whilst maintaining the deprotection chemistry of a silyl protection group. Thus, the mixtures will be chromatographically separable.

With this promising synthetic strategy we started to investigate the synthesis of target structure **122**, **123** and **124**.

## 5.4 Synthesis and Characterization

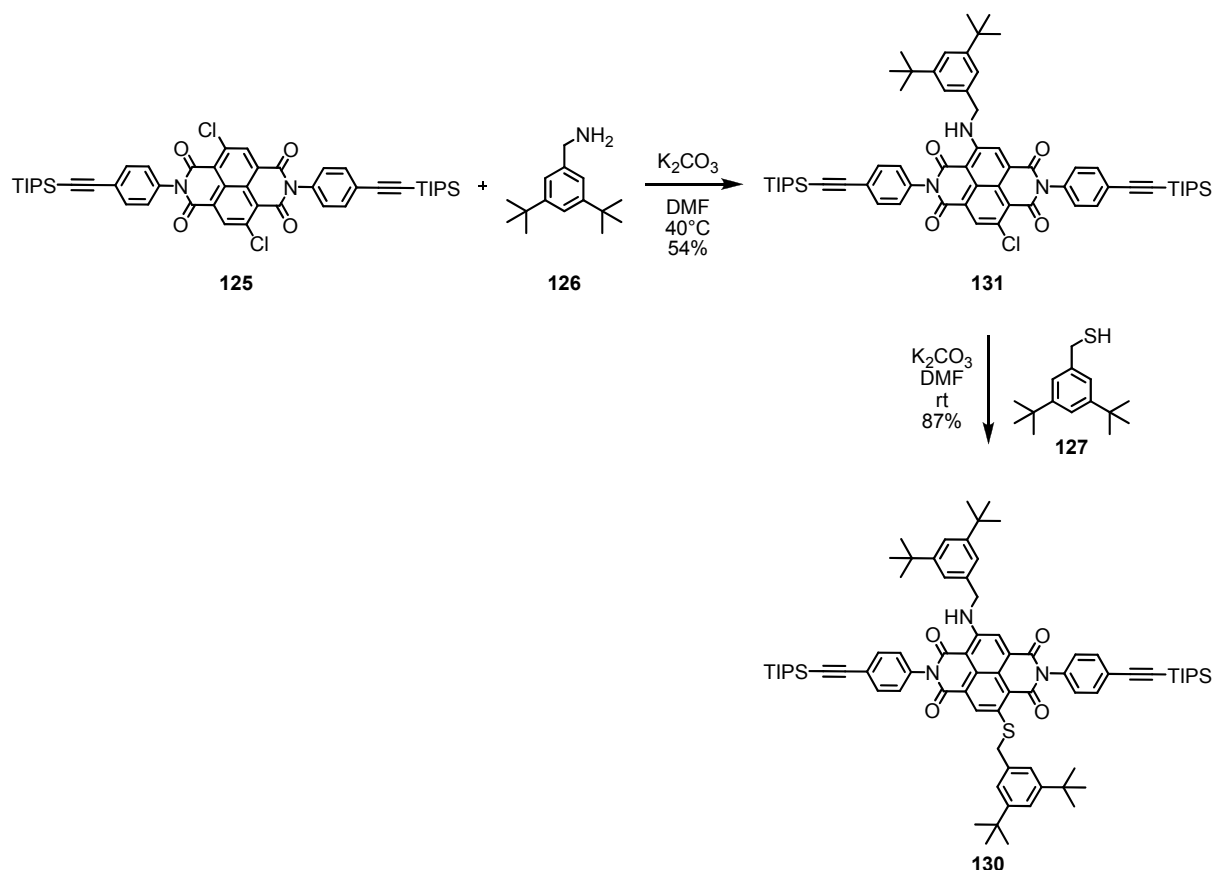
### *Synthesis of the NDI building blocks 132-134*

The synthesis of the NDI-building blocks **132-134** was started with compound **125** (Scheme 42).<sup>[284]</sup> The chlorides of **125** were substituted with the corresponding amine **126** or thiol **127** to give the core functionalized NDI derivatives **128-130**. The symmetric NDIs **128** and **129** are provided in one step, by dissolving the chloride **125**, and the nucleophile **126** or **127**, respectively, in DMF and stirring the solution in presence of potassium carbonate. As the sulfur is a better nucleophile, the substitution reactions with **127** readily took place at room temperature, the substitution reaction with the amine **126** required elevated temperatures (Scheme 42). Hence, the symmetrically functionalized NDI derivatives were obtained after aqueous workup and purification by column chromatography (CC) as a blue solid in 69% yield (**128**) and as a violet solid in 93% yield (**129**), respectively.



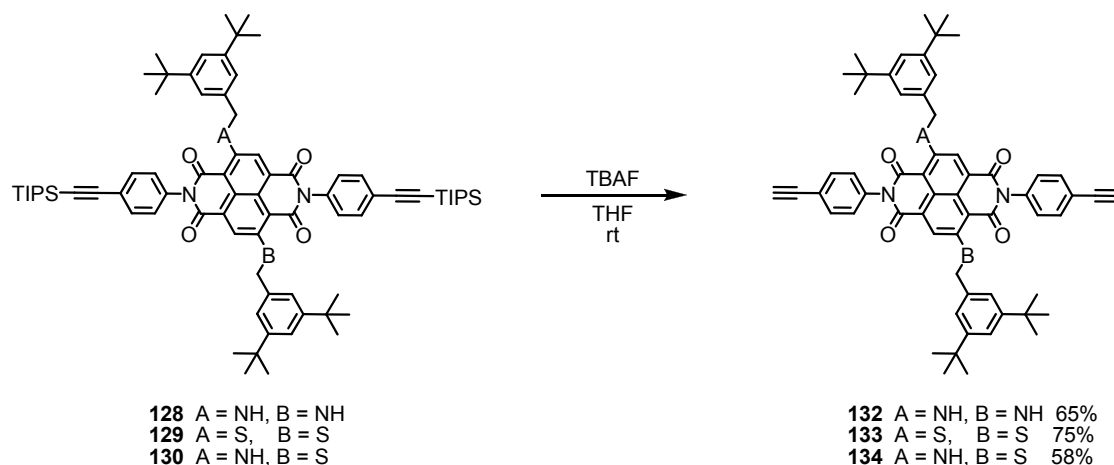
**Scheme 42:** Synthesis of the symmetric NDI building blocks **128** and **129**.

The asymmetric derivative **130** was synthesized in a stepwise manner (Scheme 43). A 1:1 mixture of **125** and **126** was dissolved in DMF with potassium carbonate as base and the reaction mixture was heated to 40°C. After aqueous workup and purification by CC, the monosubstituted compound **131** was isolated as red solid in 54% yield. In a next step, the thiol **127** was introduced applying the same reaction conditions as described for compound **129**, and the mixed NDI **130** was isolated after purification by column chromatography as a violet solid in 87% yield.



**Scheme 43:** Synthesis of the mixed NDI-building block **130**. A stepwise assembly was required due to the asymmetry of **130**.

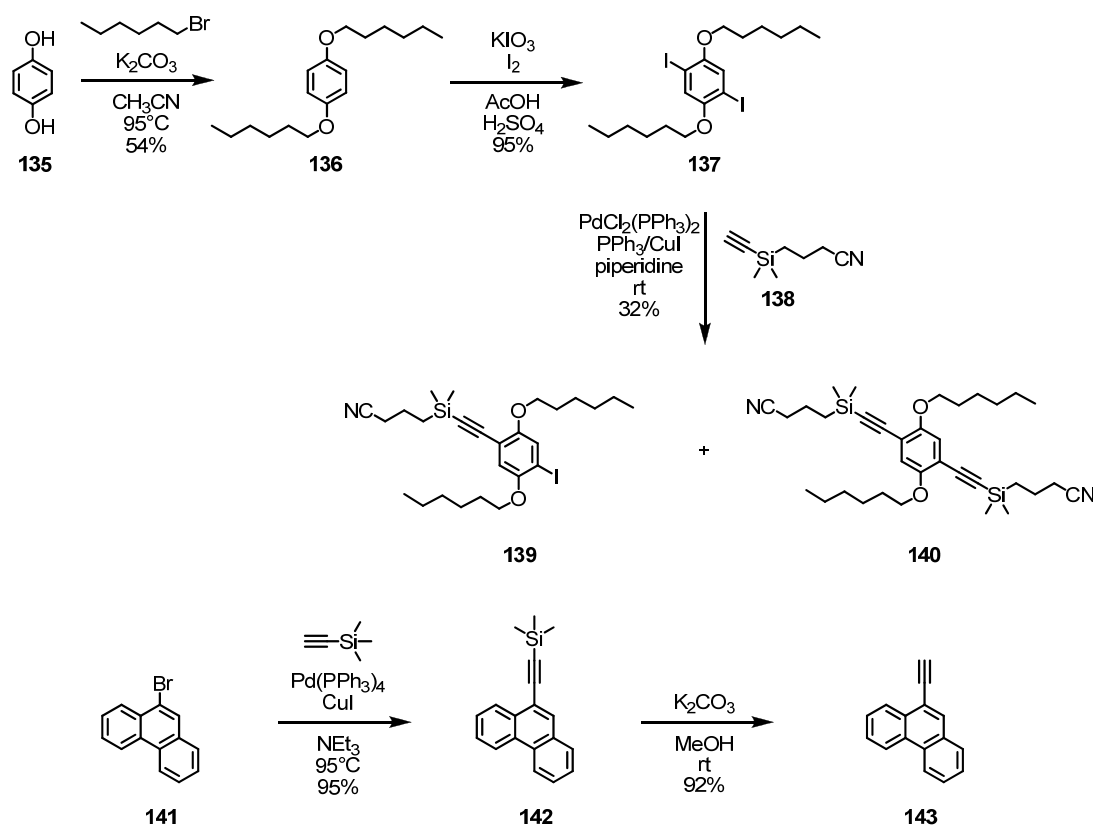
The TIPS protection groups of the acetylenes in compounds **128-130** were deprotected using tetrabutylammonium fluoride (TBAF). Therefore the starting materials **128-130** were dissolved in THF and treated with a 1 M TBAF solution in THF containing 5% water. After aqueous workup and purification by column chromatography, the free acetylenes **132**, **133** and **134** were obtained in 65%, 75%, and 58% yield, respectively (Scheme 44). The free acetylenes are less stable than their TIPS-protected forms, and therefore they were only deprotected prior to their use. The NDIs substituted with amines, both the compounds **128** and **132**, are deep blue in color and fluorescence was already observed during the reaction and the purification steps (excited with daylight or with 254 nm). The mixed NDIs **130** and **134** are violet in color and the disulfur functionalized NDIs **129** and **133** are pink in color.



**Scheme 44:** The TIPS-protection groups were cleaved by means of TBAF to obtain the NDI building blocks **132-134**.

#### *Synthesis of the linker and anchor building block*

The building block (**139**) of the repeating unit of the OPE backbone was synthesized starting from hydroquinone (**135**) (Scheme 45). Hydroquinone was suspended in acetonitrile. After addition of 1-bromohexane and potassium carbonate, the reaction mixture was heated to reflux for one day. The insoluble material was filtrated off (hot) and while cooling the filtrate to room temperature, 1,4-bis(hexyloxy)benzene crystallized as colorless crystals in 53% yield. Iodination of the alkylated hydroquinone derivative **136** by standard iodination conditions with potassium iodate and iodine in a 10:1 mixture of concentrated acetic acid and concentrated sulfuric acid, followed by an aqueous workup and purification by recrystallization from hot ethanol provided compound **137** as colorless solid in 95% yield on a 100-gram scale.<sup>[285]</sup> Building block **139** was synthesized by reacting the diiodo compound **137** with one equivalent of an acetylene. To overcome separation problems of the statistical mixture of products discussed in the synthetic strategy, polar [(3-cyanopropyl)dimethylsilyl] was chosen as protection group of the acetylene. [(3-cyanopropyl)dimethylsilyl]acetylene (**138**) was prepared in one step from (3-cyanopropyl)dimethylsilyl chloride and ethynylmagnesium bromide in a Grignard-type reaction.<sup>[250]</sup> [(3-cyanopropyl)dimethylsilyl]acetylene (**138**) was coupled to **137** in a *Sonogashira* reaction. Therefore, **137** and **138** were dissolved in degassed piperidine. As catalytic system PdCl<sub>2</sub>(PPh<sub>3</sub>)<sub>2</sub>, PPh<sub>3</sub> and CuI were added and the reaction mixture was stirred at room temperature. The statistical mixture of **137**, **139** and **140** which was observed after aqueous workup was purified by column chromatography to give the desired building block **139** as beige solid in 32% yield.

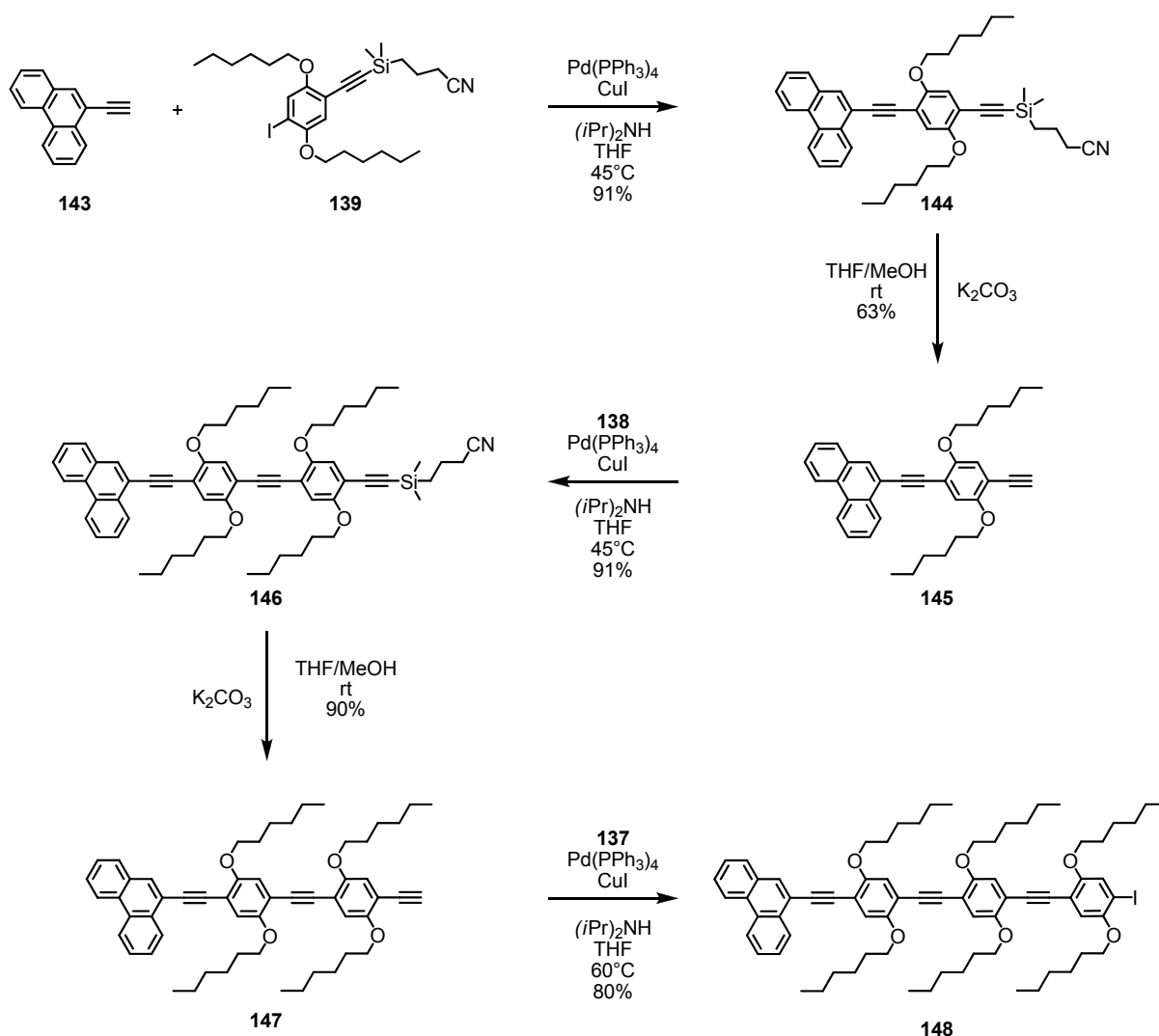


**Scheme 45:** Synthesis of the phenylene ethynylene repeating unit building block **139**. The terminal phenanthrene anchor group is introduced as 9-ethynyl-phenanthrene (**143**)

9-Ethynylphenanthrene (**143**) was synthesized on a gram scale starting from commercially available 9-bromophenanthrene (**141**).<sup>[286]</sup> In a *Sonogashira* reaction with TMS-acetylene and tetrakis(triphenylphosphine)palladium and copper iodide in triethylamine, the TMS-protected acetylene **142** was obtained after aqueous workup and purification by CC as beige solid in 95% yield. The TMS-group was subsequently cleaved using potassium carbonate. Therefore potassium carbonate was added to a solution of **142** in methanol, and after stirring for 2.5 hours at room temperature the solvent was evaporated. After an aqueous workup, pure acetylene **143** was obtained in 92% yield as beige solid. The two building blocks acetylene **143** and iodide **139** were then coupled in a *Sonogashira* reaction (Scheme 46). Tetrakis-(triphenylphosphine)palladium and copper iodide were used as catalysts. The reaction was performed in a 5:1 mixture of THF/diisopropylamine at 45°C. These conditions were found to be well suited for the forthcoming *Sonogashira* reactions as well, and are therefore referred to as standard *Sonogashira* conditions. The reaction was stirred for 20 hours at 45 °C, and then the solvents were evaporated. The crude



was purified by column chromatography to give the compound **144** as beige solid in 91% yield. The (3-cyanopropyl)trimethylsilyl protection group is base labile and therefore, compound **144** was dissolved in a THF/methanol mixture (1:1) and treated with two equivalents potassium carbonate to give after aqueous workup and purification by column chromatography the free acetylene **145** as beige solid in 63% yield. The acetylene **145** was again coupled with building block **139** using the standard *Sonogashira* conditions to give the compound **146** as yellow solid in 91% yield. The (3-cyanopropyl)-trimethylsilyl protection group was removed applying the same conditions as for compound **144**, and the free acetylene **147** was obtained as yellow solid in 90% yield.



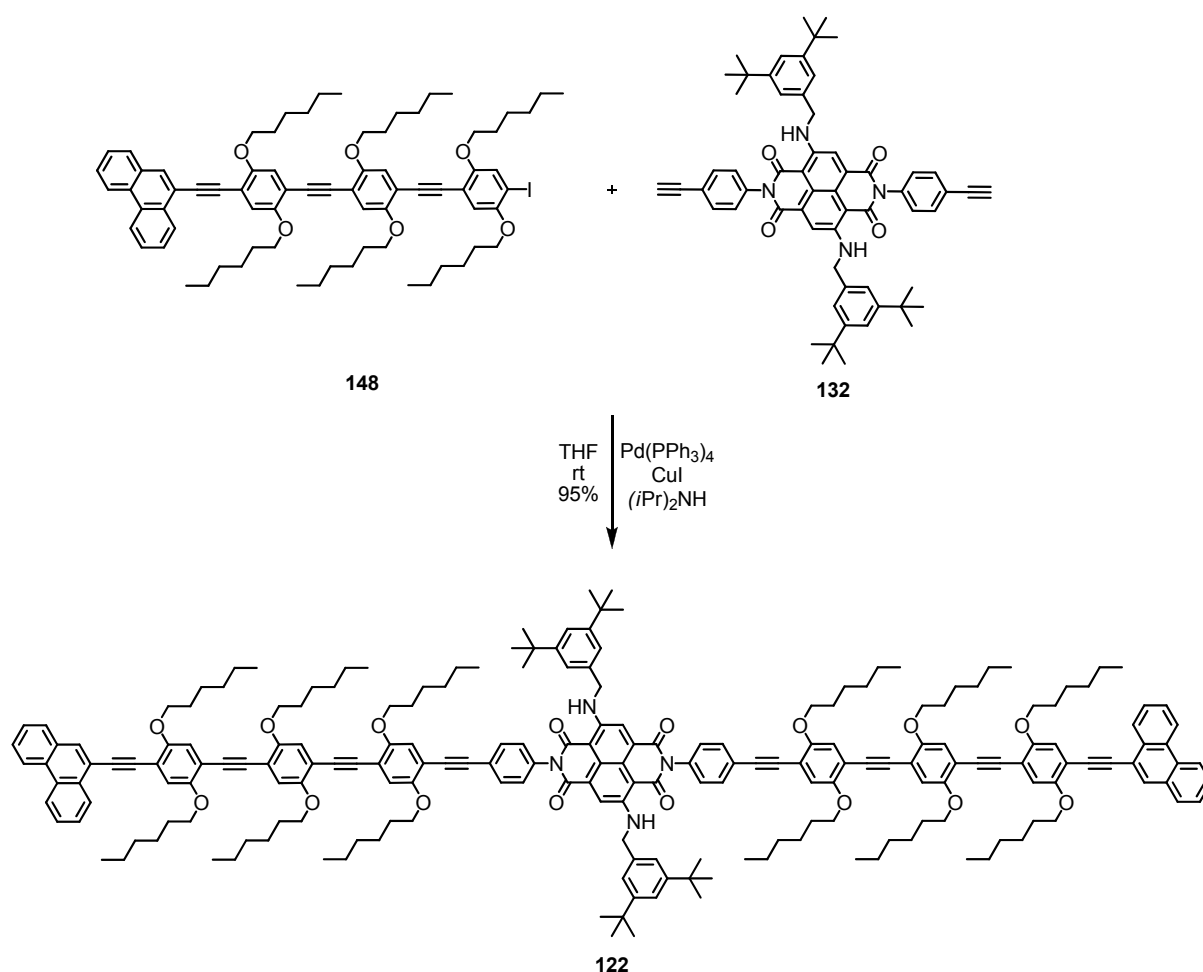
**Scheme 46:** Synthesis of the OPE-building block **148** via a multiple *Sonogashira* reaction sequence.

In a next step the compound **147** is expected to be expanded by another phenyl unit. However, for the final assembly of the target structures, the rod building block needs

to comprise a terminal iodide function. Therefore it was envisaged to couple 1,4-bis(hexyloxy)-2,5-diiodobenzene (**137**) to the acetylene **147**. However, as **137** bears two iodide functions which readily react in *Sonogashira* reactions, not only the target compound **148**, but also the disubstituted compound where both iodides of **137** have reacted is expected to be formed. However, by applying a large excess of compound **137**, the formation of the desired compound **148** was expected to be favored. Therefore, 10 equivalents of the diiodo compound **137** and one equivalent of the acetylene **147** were dissolved in a mixture of THF and diisopropylamine (5:1). Tetrakis(triphenylphosphine)palladium and copper iodide were added and the reaction mixture was stirred for three hours at 60°C. After aqueous workup and purification by column chromatography, the compound **148** was isolated as a yellow solid in remarkable 80% yield.

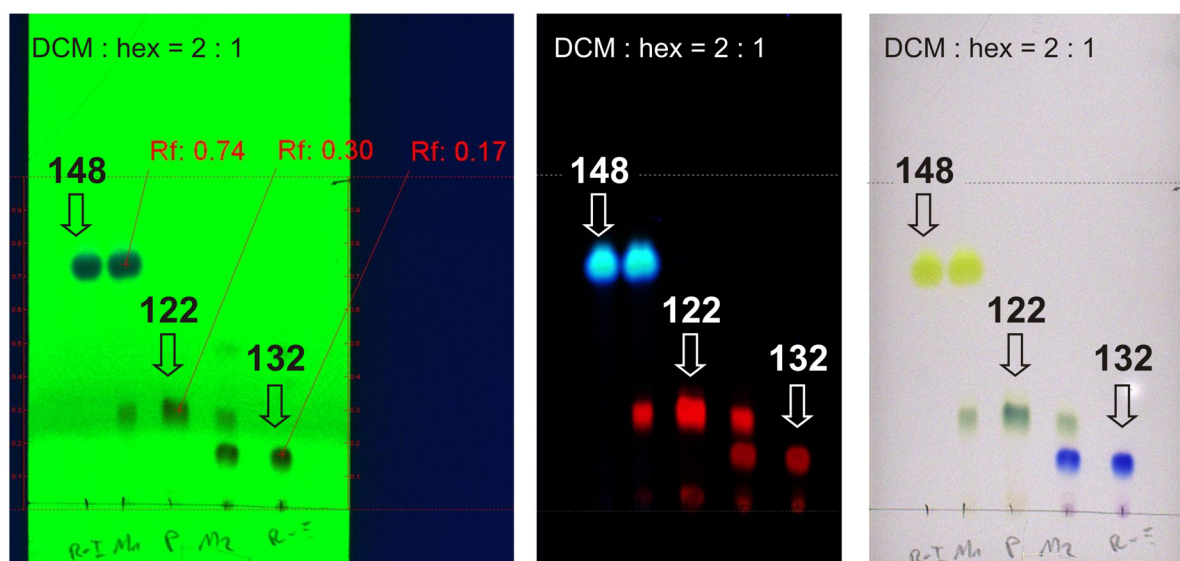
#### *Assembly of target structure 122*

Having both building blocks, the iodide **148** and the acetylene **132** in hand, the synthesis of the first target structure **122** was envisaged (Scheme 47). Therefore, one equivalent of the acetylene and 2.04 equivalent of the iodide were dissolved in a THF/diisopropylamine (25:2) mixture. As catalysts tetrakis(triphenylphosphine)-palladium and copper iodide were added. The reaction mixture was stirred for 23 hours at room temperature and the extent of the reaction was monitored by thin layer chromatography (TLC). Both starting materials are chromophores. While the rod building block **148** is a yellow solid and shows a blue emission (when irradiated by day light, 254 nm or 366 nm, visible by eye), the NDI building block **132** is a blue solid with a red emission (when irradiated by day light, 254 nm or 366 nm, visible by eye). The color of the compounds is very nicely reflected on the TLC as the yellow spot of **148** and the blue spot of **132** are well visible by eye. If the TLC-plate is irradiated with 366 nm, the corresponding blue and red fluorescent spots are visible. After an hour a new greenish spot (monosubstituted intermediate) appears, followed by a second new green spot (product). The first greenish spot disappears and the product spot is observed as a main spot. The reaction mixture was then evaporated and purified by column chromatography to give the product **122** as a green solid in 95% yield.



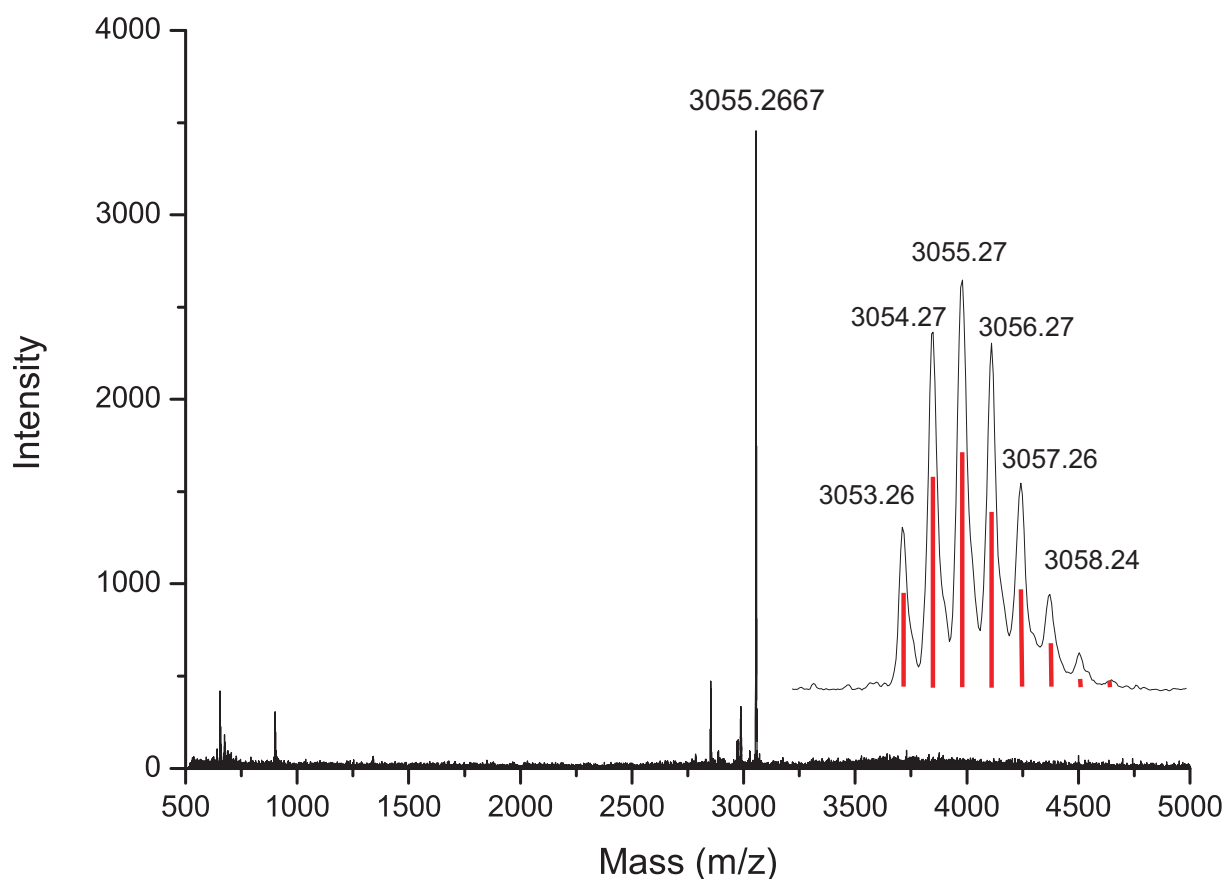
**Scheme 47:** The target structure **122** is assembled with a final *Sonogashira* reaction.

Figure 87 shows photographs of the developed TLC plates. The two starting materials, and the product were spotted on a TLC plate (silica gel, on a glass plate) and developed using dichloromethane/hexane 2:1 as eluent (Note, the isolated compounds were spotted on the TLC, not the reaction mixture). The left picture was taken while irradiating with 254 nm. The iodide **148** has an  $R_f$  value of 0.74, the acetylene **132**  $R_f = 0.17$ , and the product **122** has a  $R_f$  value of 0.30. The picture in the middle was taken while irradiating with 366 nm. The blue fluorescence of the OPE-building block **132** is nicely reflected. The NDI building block **148** shows a reddish fluorescence, and the strong red fluorescence of the product **122** is nicely reflected. The picture of the TLC plate on the right side was taken while irradiating with white light.



**Figure 87:** The two starting materials **132** and **148** such as the product **122** are spotted on a TLC plate and developed with DCM:hex = 2:1. A picture is taken from the same plate at 254 nm irradiation (left), at 366 nm irradiation (middle) and when irradiating with white light (right). The  $R_f$  values are calculated and shown in the left picture.

After being able to obtain the target structure **122**, the compound was fully characterized by mass spectrometry,  $^1\text{H}$ -NMR-spectroscopy and  $^{13}\text{C}$ -NMR spectroscopy. Compound **122** has a molecular weight of 3056.18 g/mol and constitutes of  $\text{C}_{208}\text{H}_{244}\text{N}_4\text{O}_{16}$ . The molecule is too large to be analyzed by electron ionization (EI) or electron spray ionization (ESI) mass spectrometry methods. However, matrix assisted laser desorption/ionization time of flight (MALDI-ToF) mass spectrometry was found to be suitable to measure mass spectra of **122**. 1,8,9-anthracenol was used as matrix. The molecular mass of **122** was found by MALDI-ToF to be 3055.2667 which fits well with 3055.8469 calculated for  $\text{C}_{208}\text{H}_{244}\text{N}_4\text{O}_{16}$ . Figure 88 shows the MALDI-ToF mass spectra of **122**. The spectrum is well resolved, depicted in the zoomed in peak (inset in Figure 88). The calculated isotopic distribution is overlaid (red in the inset in Figure 88) and matches very well with the isotopic distribution found with MALDI-ToF spectrometry.



**Figure 88:** MALDI-ToF spectra of **122**. The inset shows the enlarged peak. The calculated isotopic distribution is overlaid in red.

The compound was further characterized by NMR-spectroscopy. All peaks were assigned by HMBC, HMQC, TOCSMY, COSY, and  $^{13}\text{C}$ -NMR methods. A  $^1\text{H}$ -NMR spectra of **122** recorded at 600 MHz is shown in Figure 89. The color code shows the assignment of the protons in structure **122** to the observed  $^1\text{H}$ -NMR peaks.

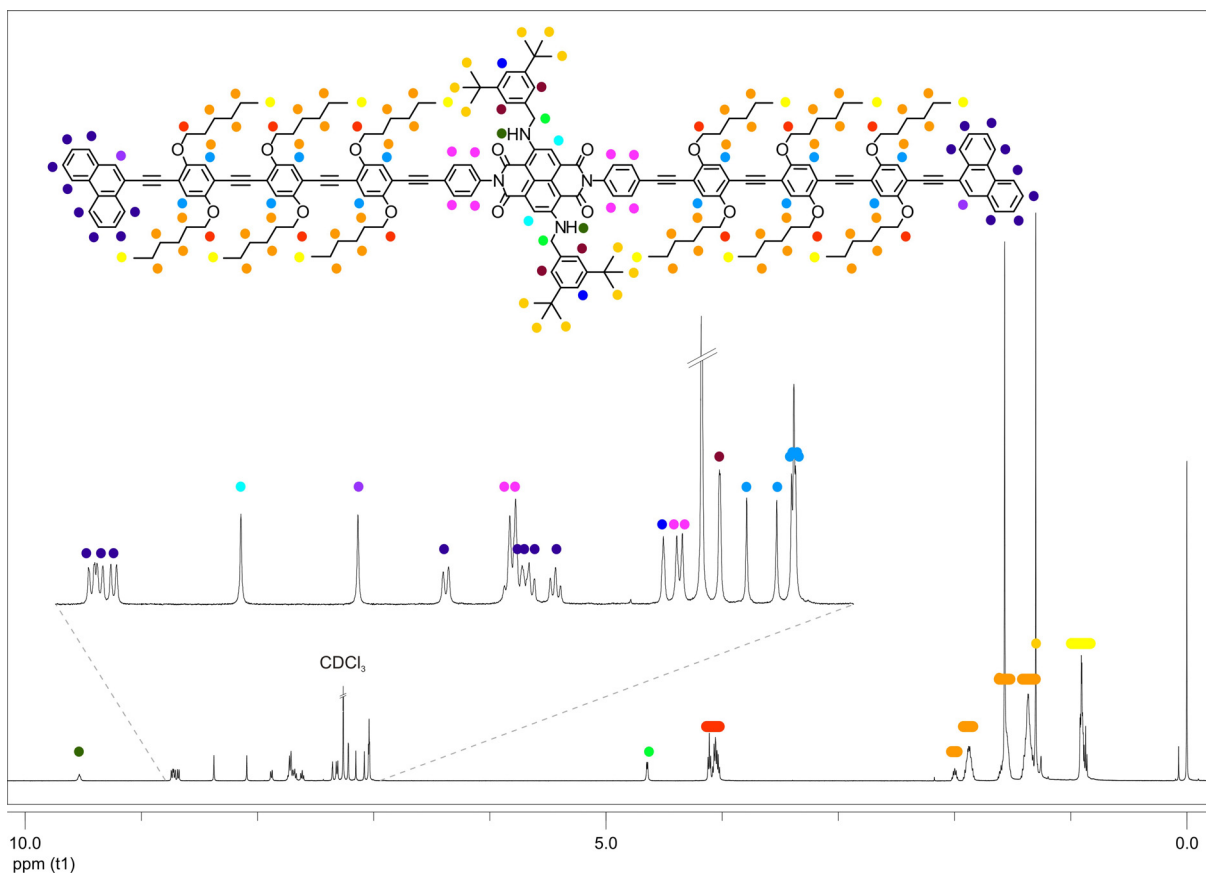


**Figure 89:**  $^1\text{H}$ -NMR spectrum of **122** in  $\text{CDCl}_3$  at room temperature. The signals were assigned to the different protons depicted by the color code.

In the  $^{13}\text{C}$ -NMR, 94 different carbon peaks are expected.  $^{13}\text{C}$ -NMR-spectra were recorded on a 600 MHz machine with enlarged pulse lengths, however, not all peaks were observed. It is known that it is challenging to obtain ethynyl-carbons in long conjugated structures and indeed, the quaternary ethynyl peaks were not observed. Figure 90 shows a 600 MHz  $^{13}\text{C}$ -NMR spectra of **122**, with a bar indicating the region where the eight different ethynyl carbons were expected. But in this region of 70-100 ppm, no distinct  $^{13}\text{C}$ -NMR peaks were present. Therefore 2-D NMR spectra were recorded. The resolution of two dimensional NMR is higher, and peaks which are not obtained in standard 1D experiments emerged.

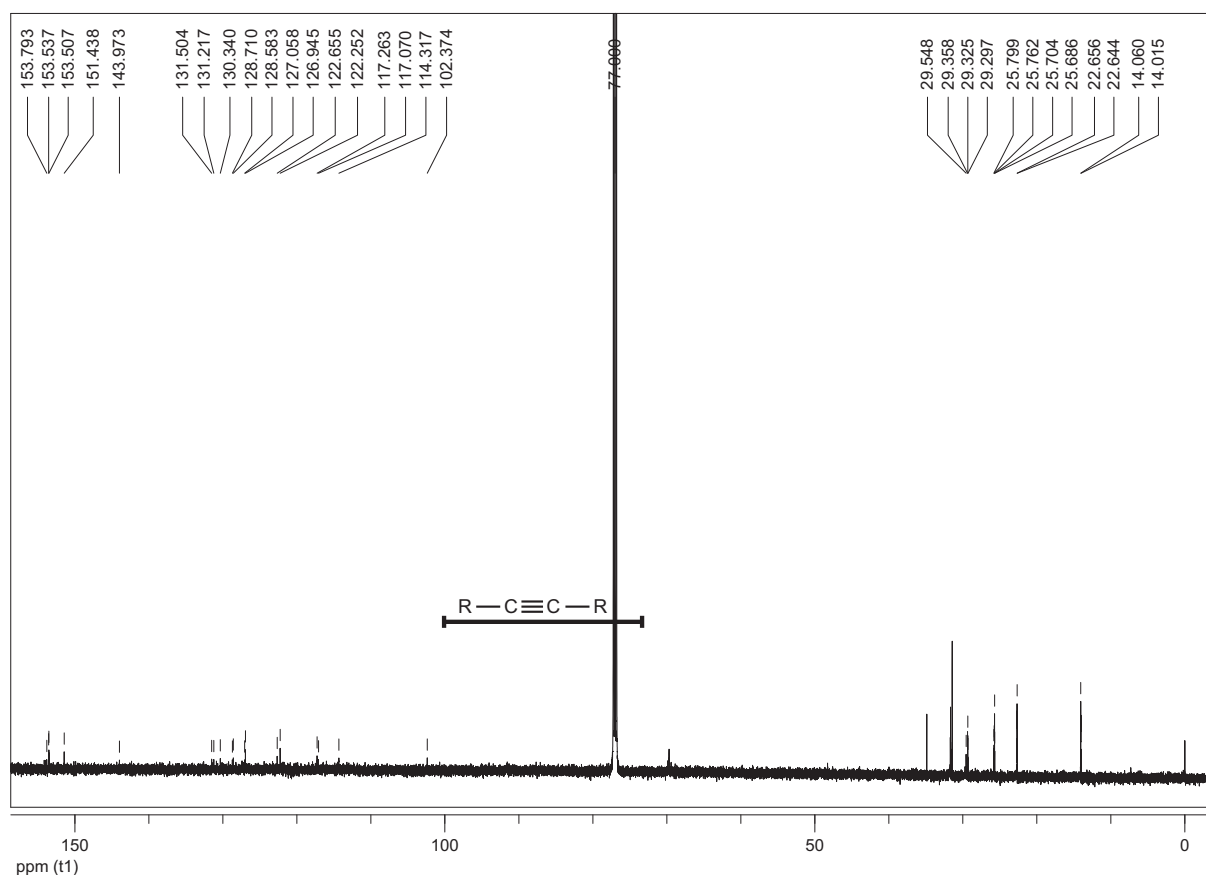


**Figure 90:**  $^{13}\text{C}$ -NMR spectra of **122**. The bar indicates the region where acetylene-carbon peaks are expected.

To characterize the ethynyl peaks, HMBC (heteronuclear multiple bond coherence) spectra were recorded. In HMBC NMR spectroscopy, coupling of protons with carbon nuclei is observed. A strong  $^1\text{H}$ - $^{13}\text{C}$  coupling is obtained over three bonds. This is therefore ideal to detect the ethynyl peaks while they couple with the proton in *ortho*-position of the substituted phenyl units (Figure 91). Figure 91 shows the region of the HMBC spectra in which the ethynyl peaks of compound **122** are expected. On the x-axis, the  $^1\text{H}$ -NMR is plotted, on the y-axis the  $^{13}\text{C}$ -NMR spectra is plotted. The inset shows the coupling of the ethynyl carbon nucleus with the proton in *ortho*-position (green in Figure 91). A coupling of protons with 8 ethynyl carbons is obtained and all 8 ethynyl carbon nuclei can be assigned to an NMR signal.

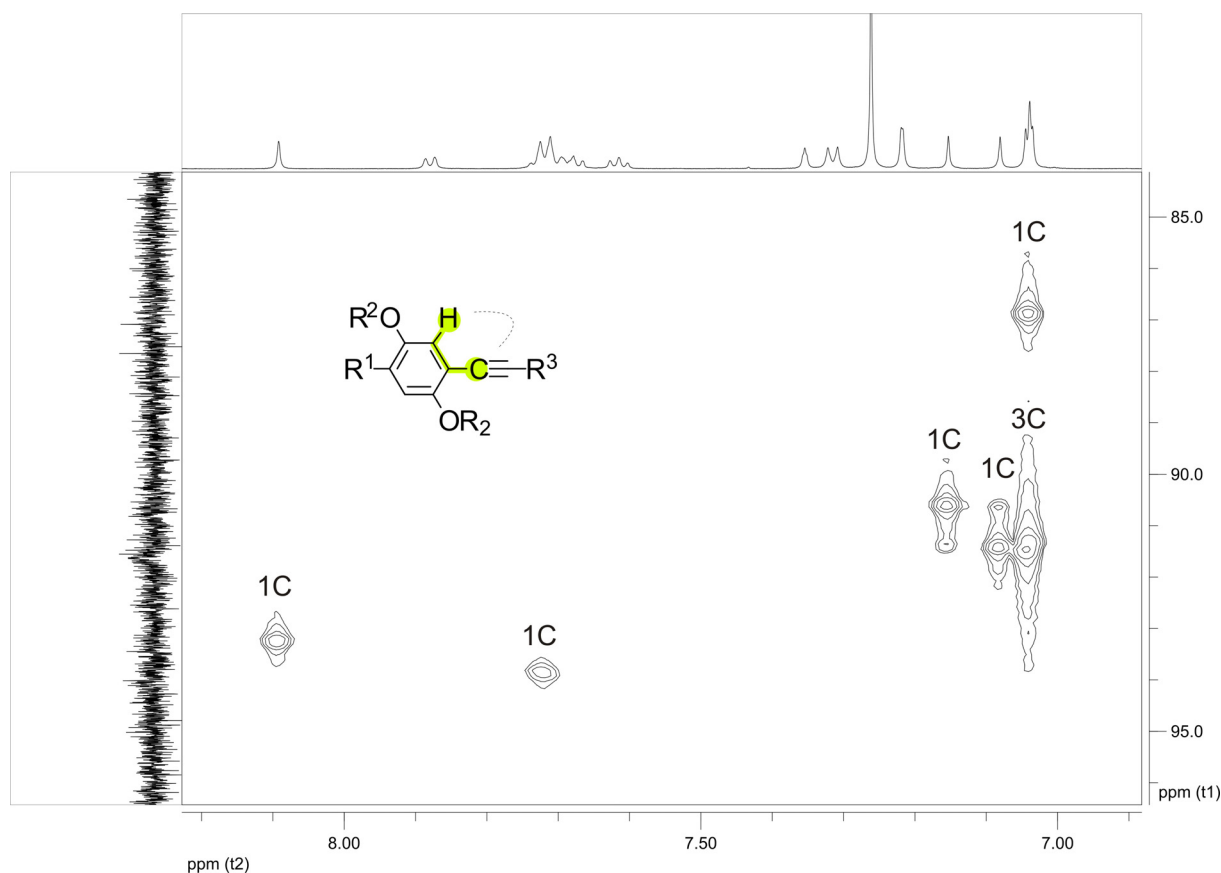


**Figure 91:** HMBC spectra of **122**.  $^{13}\text{C}$ - $^1\text{H}$  coupling over 3 bonds is observed in HMBC spectroscopy. This is ideal to assign the acetylene carbons of **122**, as they show a coupling over three bonds with a proton (Depicted green in the inset). 6 peaks are observed, in one of the peaks three carbon signals overlap.

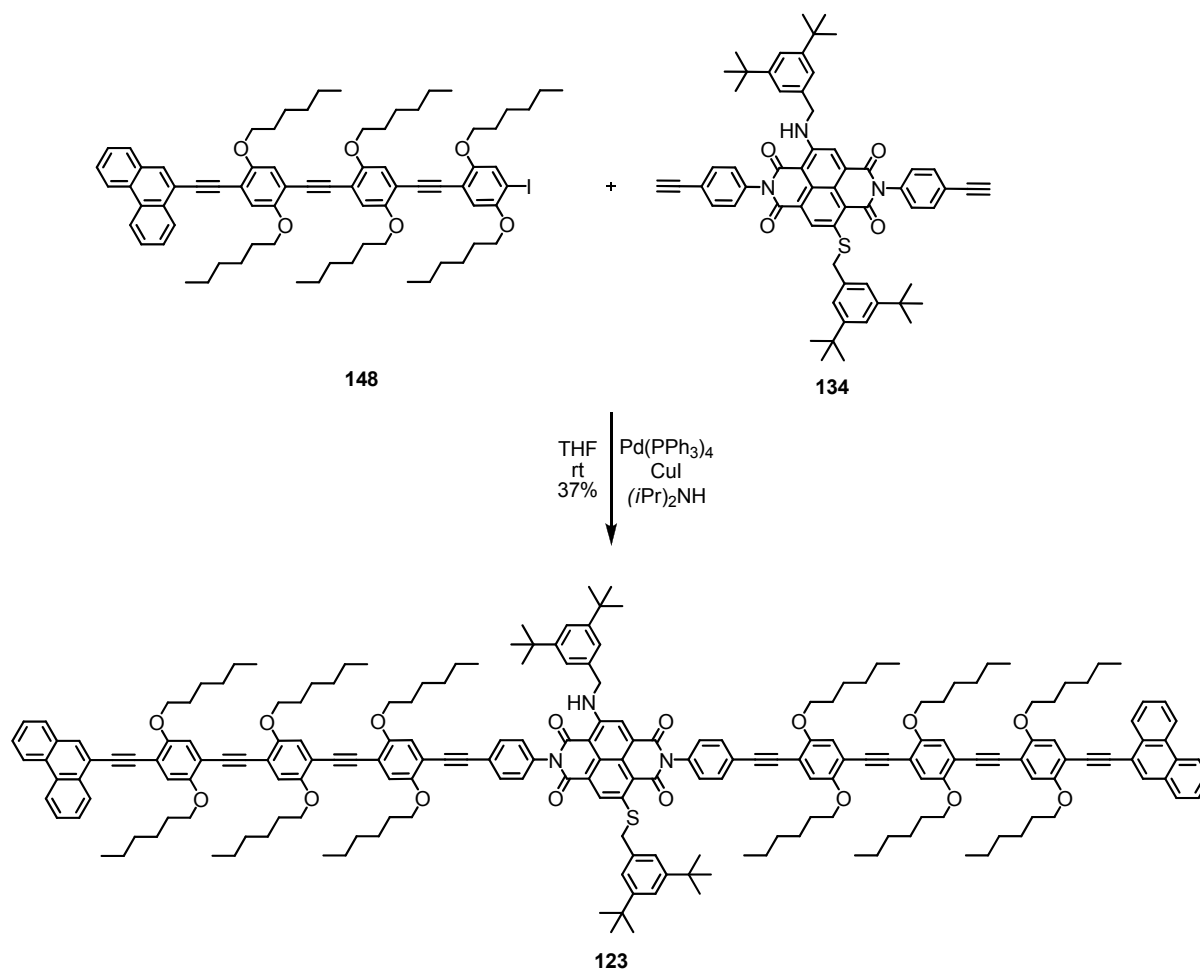
2D NMR spectroscopy is therefore an ideal tool to assign all peaks of **122**. For the complete assignment see the experimental section.

Compound **122** was further photophysically characterized by absorption and emission spectroscopy. This is discussed in the next section 5.5. The purity of all the intermediates and of the target compounds was in addition shown by GPC.

#### *Assembly of target structure 123*

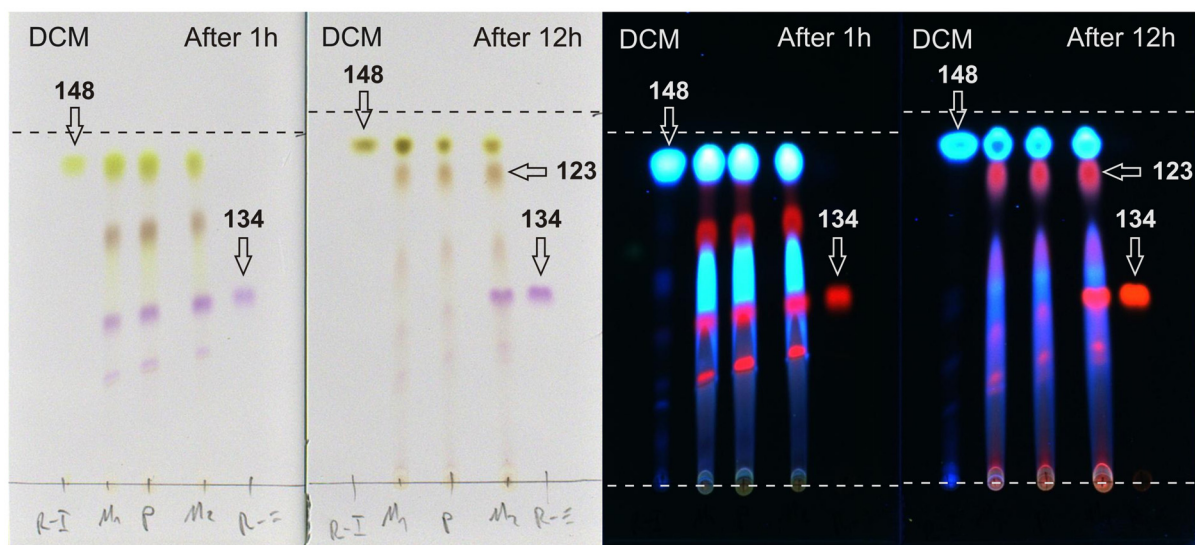
For the synthesis of the mixed target structure **123** comprising the NDI core with an amine and a thiol substituent, one equivalent of the violet NDI building block **134**, and 2.07 equivalent of the yellow molecular rod building block **148** were dissolved in a THF/diisopropylamine mixture (Scheme 48). As catalysts, tetrakis-(triphenylphosphine)palladium and copper iodide were added and the reaction mixture was stirred for 15 hours at room temperature and was then evaporated.





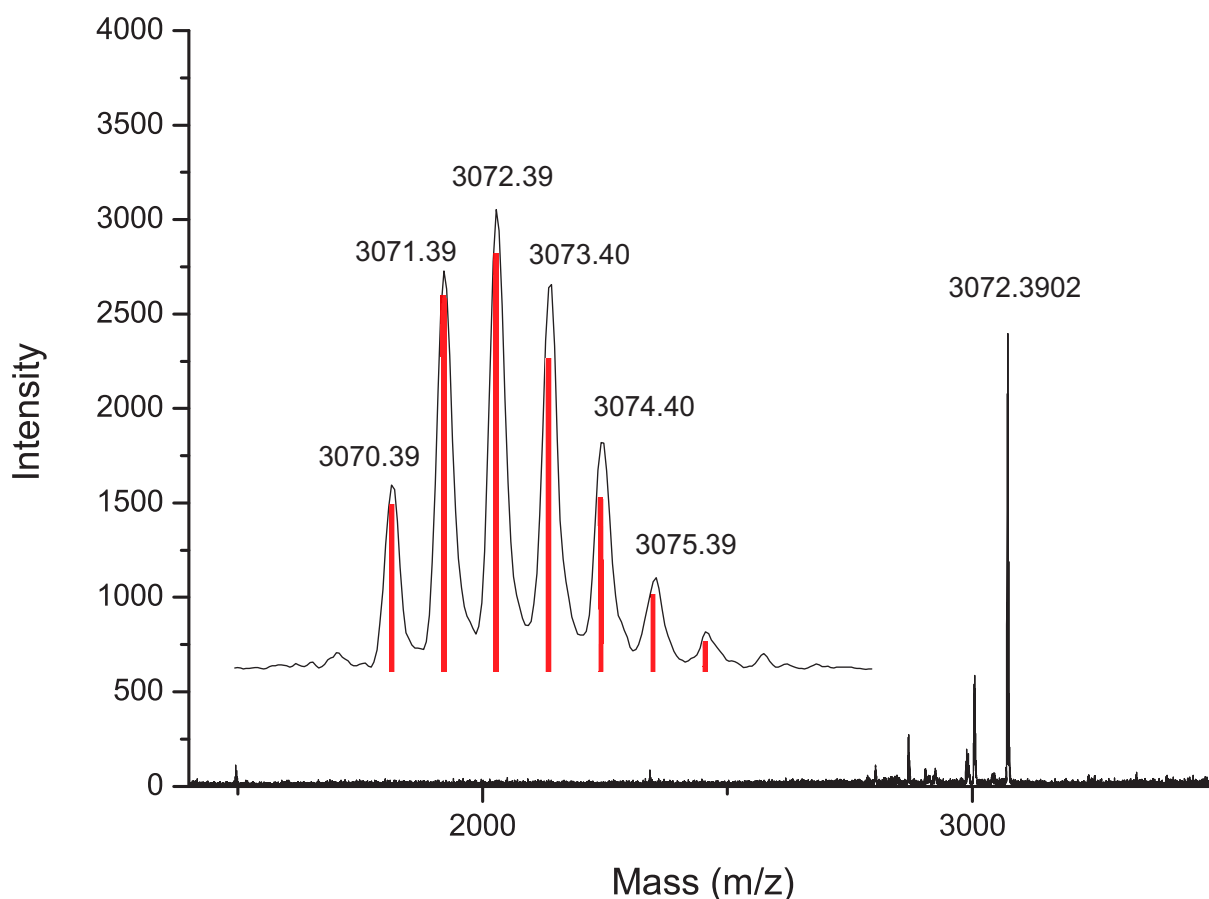
**Scheme 48:** Synthesis of the target structure **123**.

The reaction mixture was monitored by TLC, and after 1 hour a new orangish spot occurred. After stirring overnight, the spot disappeared mostly and a new dark orangish spot was observed, which proved to be the product. Figure 92 shows the image of two TLC taken from the reaction mixture after 1 hour and 12 hours, respectively. Appearance of the product **123** as an orangish, reddish fluorescent spot is clearly seen.



**Figure 92:** TLC of the reaction mixture of the *Sonogashira* reaction yielding **123** after 1 hour and after 12 hours. The picture of the TLC plates were taken when irradiating with white light (left) and 366 nm (right), respectively.

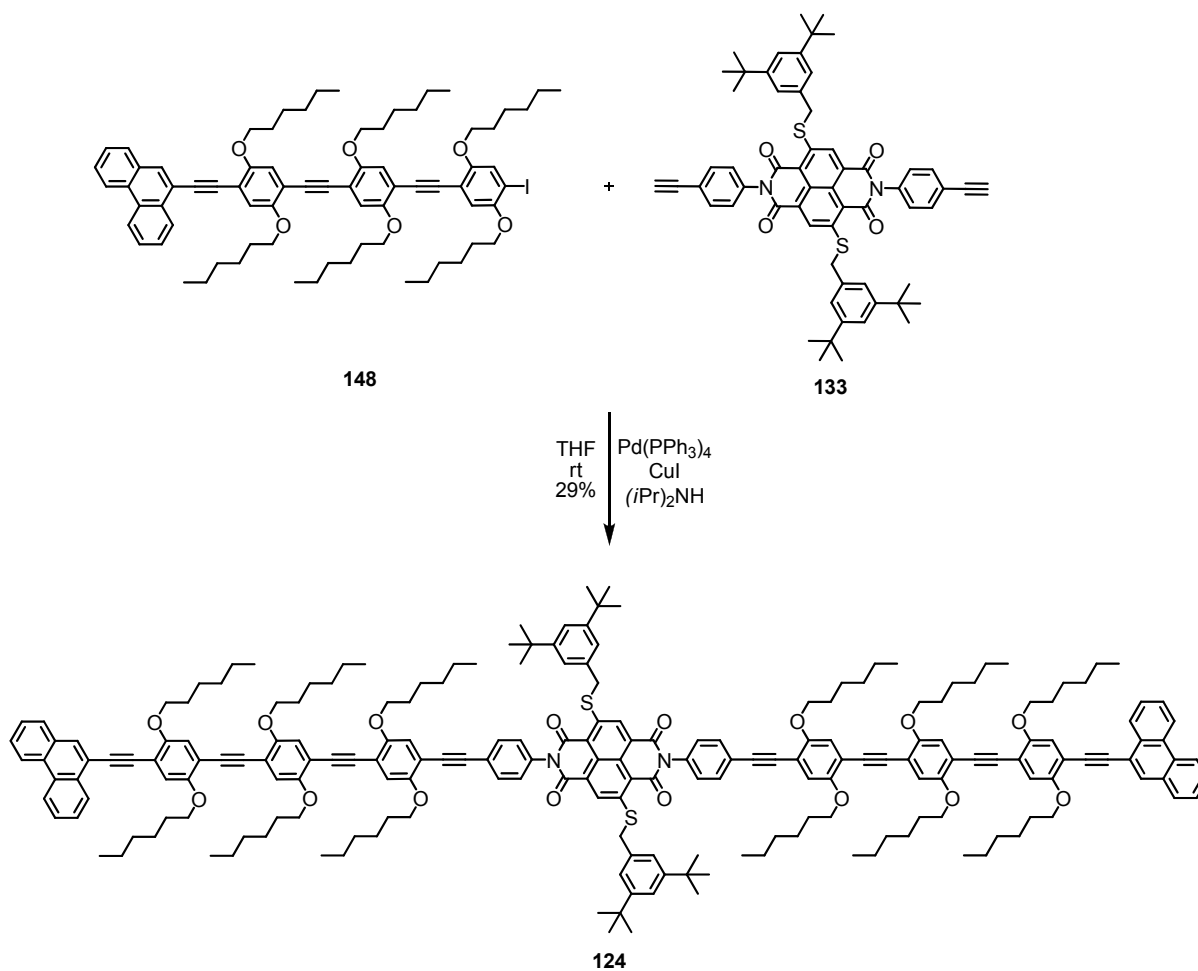
The product was isolated as an orange solid after two columns in 37% yield. This yield is much lower than 95% yield for target structure **122**. During the column chromatography the product was sticking on the column and was spread over many fractions. Considerable amounts of **123** were lost in the purification steps which drastically reduced the yield. However, the compound **123** was isolated as a pure compound and was characterized fully by TLC, MALDI-ToF mass spectrometry and by NMR-spectroscopy ( $^1\text{H-NMR}$ , HMBC, HMQC, TOCSMY, COSY and  $^{13}\text{C-NMR}$ ). The absorption and emission spectroscopic analysis will be discussed in the section 5.5. The MALDI-ToF mass spectrum of compound **123** is shown in Figure 93. The calculated isotopic distribution (red) matches very well with the obtained isotopic distribution. The calculated mass peak with 100% intensity for  $\text{C}_{208}\text{H}_{243}\text{N}_3\text{O}_{16}\text{S}$  is 3072.8081, found was 3072.3902 with MALDI-ToF mass spectrometry using 1,8,9-anthracentriol as matrix.



**Figure 93:** MALDI-ToF spectra of **123** using anthracenol as matrix. The calculated isotopic distribution (red) fits well with the obtained isotopic distribution.

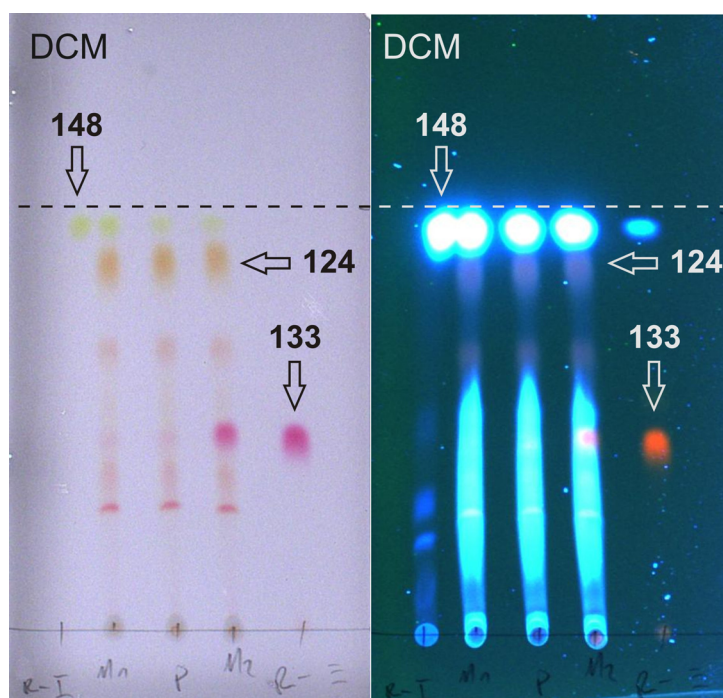
#### *Assembly of target structure 124*

Target structure **124** was synthesized applying the same conditions, while coupling one equivalent of the pink NDI derivative **133** comprising two terminal acetylenes with 2.07 equivalent of the iodide comprising OPE-building block **148** in a THF/diisopropylamine mixture (Scheme 49). As catalysts, again tetrakis-(triphenylphosphine)palladium and copper iodide were chosen. The reaction was monitored by TLC, and the product occurred as an orange-red spot. The reaction mixture was stirred for 21 hours at room temperature and was then evaporated. The crude was purified by column chromatography. The product **124** was isolated as a reddish solid in 29% yield. Considerable amounts of the product were lost during the purification steps.



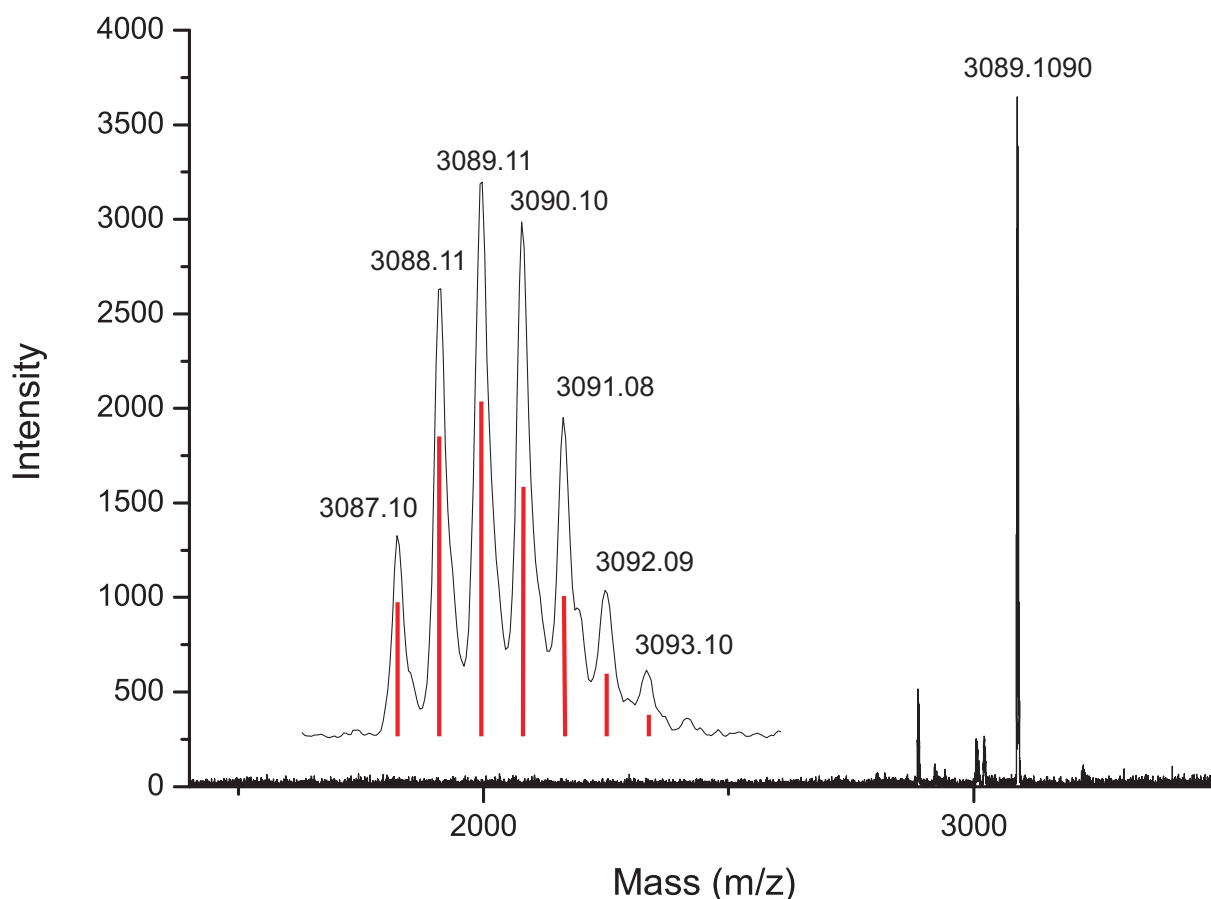
**Scheme 49:** Synthesis of target structure **124**.

Figure 94 shows an image of the TLC of the reaction mixture (developed with dichloromethane). **124** appears as an orange red spot on the TLC. The fluorescence is, corresponding to the TLC only very weak, but the product is still visible when irradiating with 366 nm.



**Figure 94:** TLC of the reaction mixture of the *Sonogashira* reaction yielding **124**. The pictures of the TLC plates were taken when irradiating with white light (left) and 366 nm (right), respectively.

Compound **124** was fully analyzed by TLC, MALDI-ToF mass spectrometry and by NMR-spectroscopy ( $^1\text{H}$ -NMR, HMBC, HMQC, TOCSY, COSY,  $^{13}\text{C}$ -NMR). The absorption and emission spectroscopic analysis will be discussed in the section 5.5. Figure 95 shows the MALDI-ToF mass spectrum. The calculated isotopic distribution (red) fits very well with the obtained isotopic distribution. The calculated mass peak with 100% intensity for  $\text{C}_{208}\text{H}_{242}\text{N}_2\text{O}_{16}\text{S}_2$  is 3089.7693, found was 3089.1090.



**Figure 95:** MALDI-ToF spectra of **124** using anthraceniol as matrix. The calculated isotopic distribution (red) fits well with the obtained isotopic distribution.

Despite several attempts to obtain crystals of the target structures suitable for X-ray analysis, it was not yet possible to obtain a solid state structure. However, crystals of the OPE building block **148** suitable for X-ray scattering were obtained. The solid state structure of **148** is displayed in Figure 96. Figure 96 A shows a front view of the building block. The length bar indicates the length of the molecule (as the distance of the two terminal carbon atoms), which is 2.55 nm. Figure 96 B shows the building block from the side and displays its rigidity. The molecule has a rod like arrangement and the phenyl units are rather in one plane, indicating the conjugated system. One of the solubilizing, flexible hexyl chains is distorted and the crystal structure could not be perfectly solved. However, the crystal structure shows that the molecule is rigid and well conjugated as designed.

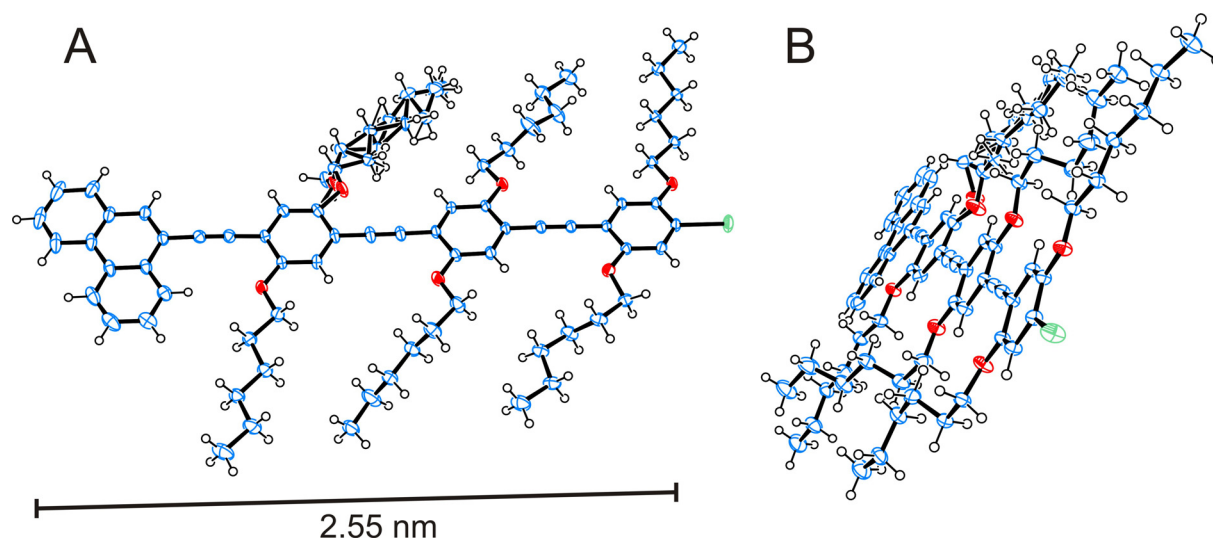


**Figure 96:** Solid state structure of **148**. The length of the molecule, corresponding to the two terminal carbon atoms, is 2.55 nm. Figure B shows the rigidity of the molecule. The structure is aligned flat and the phenyl units are rather not twisted.

## 5.5 Photophysical Characterization

Further, optical properties were investigated. UV/vis-spectra of building block **148** and of the TIPS protected NDI building block **128**, such as of target structure **122** are shown in Figure 97. The spectra were recorded at room temperature in  $\text{CH}_2\text{Cl}_2$ . The OPE-building block **148** shows an absorption maximum at 407 nm. The NDI building block shows an absorption maximum at 609 nm with a shoulder at 563 nm. The absorption spectrum of target structure **122** is the sum of the two UV/vis-spectra of the building blocks with absorption maxima at 609, 563 and 415 nm. The absorption maxima arising from the OPE part at 415 nm is slightly shifted to the red compared to the absorption maxima of the OPE buildingblock **128** at 407 nm. This bathochromic shift is due to the elongation of the conjugated OPE-system about one phenyl unit.

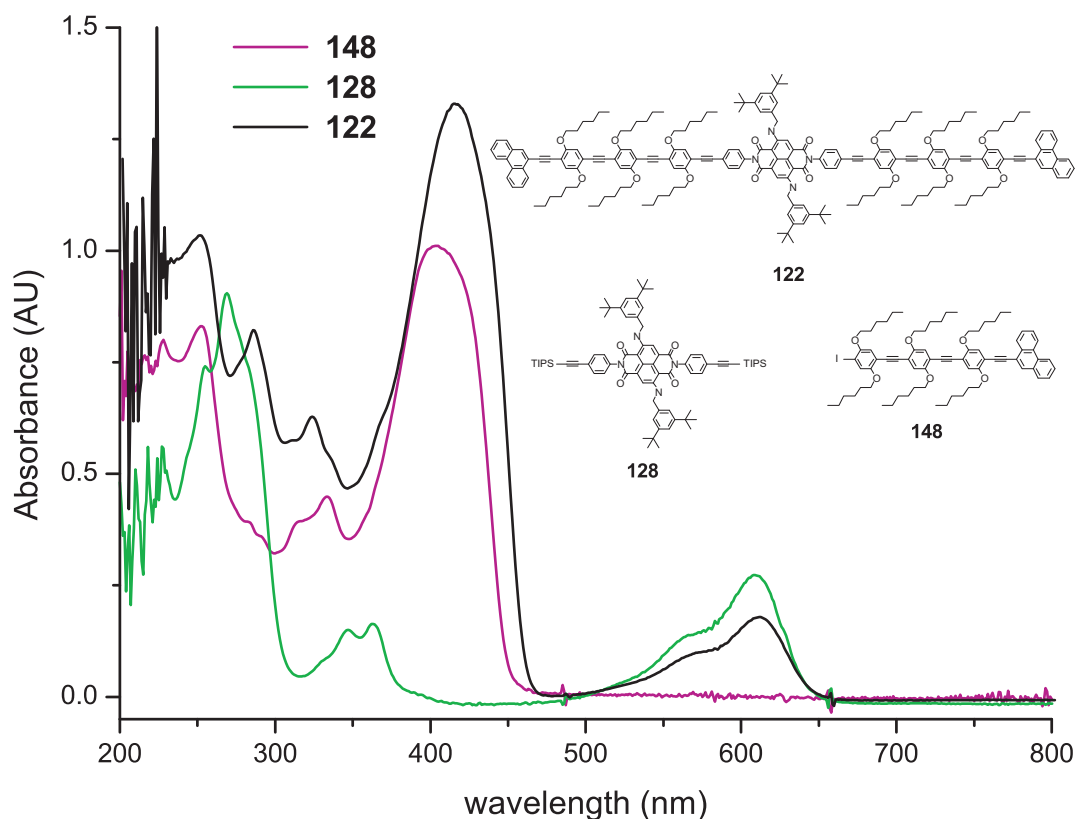
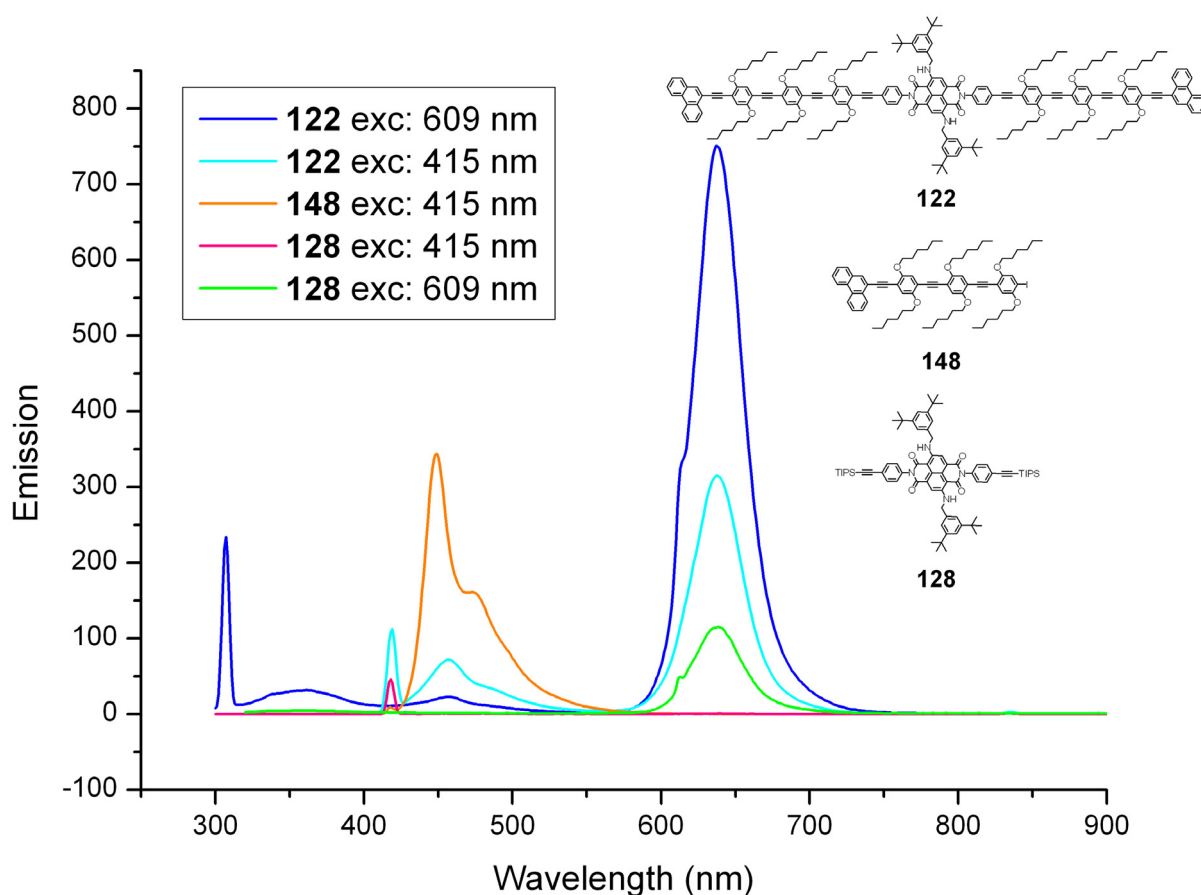


**Figure 97:** Absorption spectra of OPE building block **148** (pink), NDI building block **128** (green) and target structure **122** (black).

Emission spectra of compounds **122**, **128** and **148**, recorded in  $\text{CH}_2\text{Cl}_2$  at room temperature, are shown in Figure 98. The OPE-building block (**148**) shows an emission at 449 nm with a shoulder at 474 nm when excited with 415 nm (orange in Figure 98). The NDI-buildingblock (**128**) shows an emission maximum at 638 nm

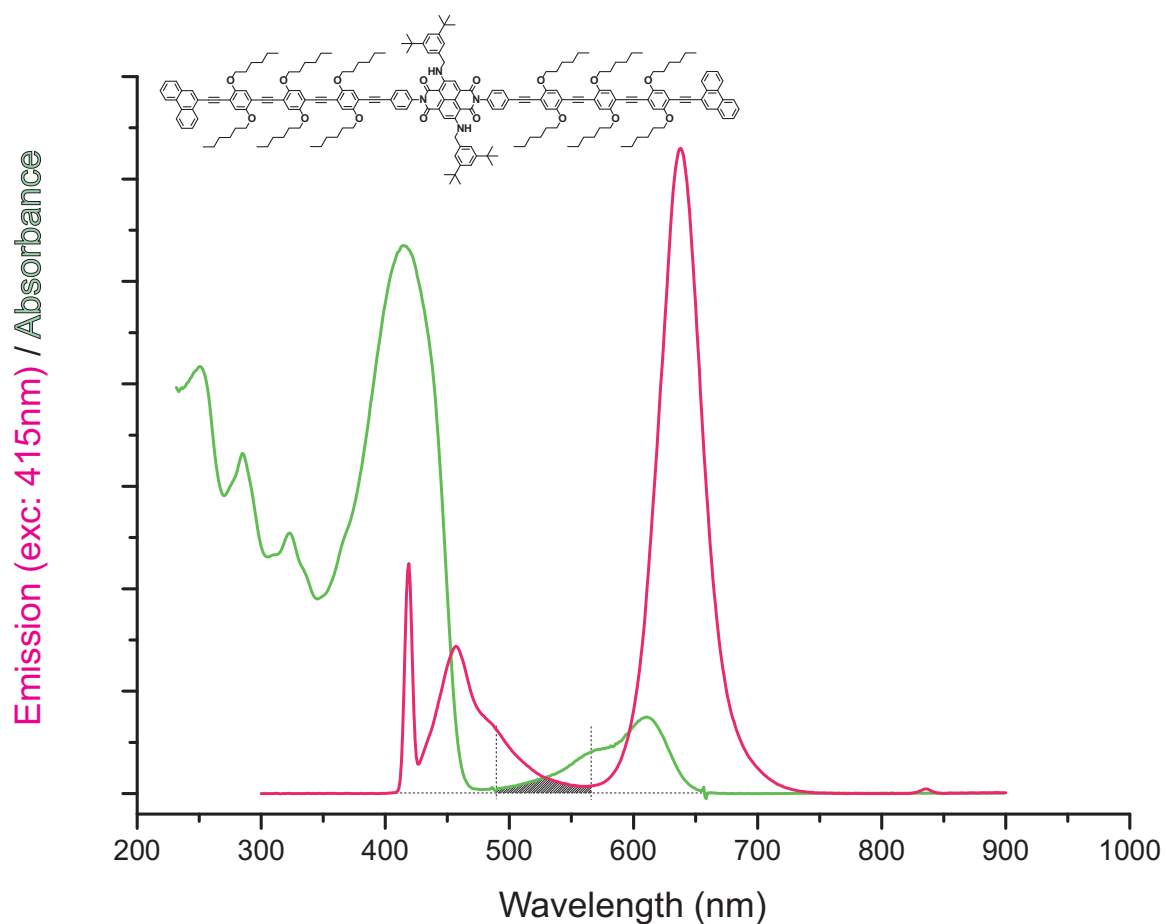


when excited at 609 nm. However, when **128** is irradiated with 415 nm, no emission is observed (pink in Figure 98). The emission spectra of target structure **122** show interesting properties. When **122** is excited at 609 nm, a strong emission maximum is observed at 637 nm (dark blue in Figure 98). However, when **122** is excited at 415 nm, not only an emission at 457 nm arising from the OPE-part is observed, but also a strong emission maximum at 637 nm is obtained (cyan in Figure 98). This emission peak is obviously arising from the NDI part of the molecule. However, as it was shown before, that the NDI unit is not excited at 415 nm, an energy transfer from the OPE part to the NDI central unit does occur, leading to an emission at 637 nm when exciting at 415 nm.



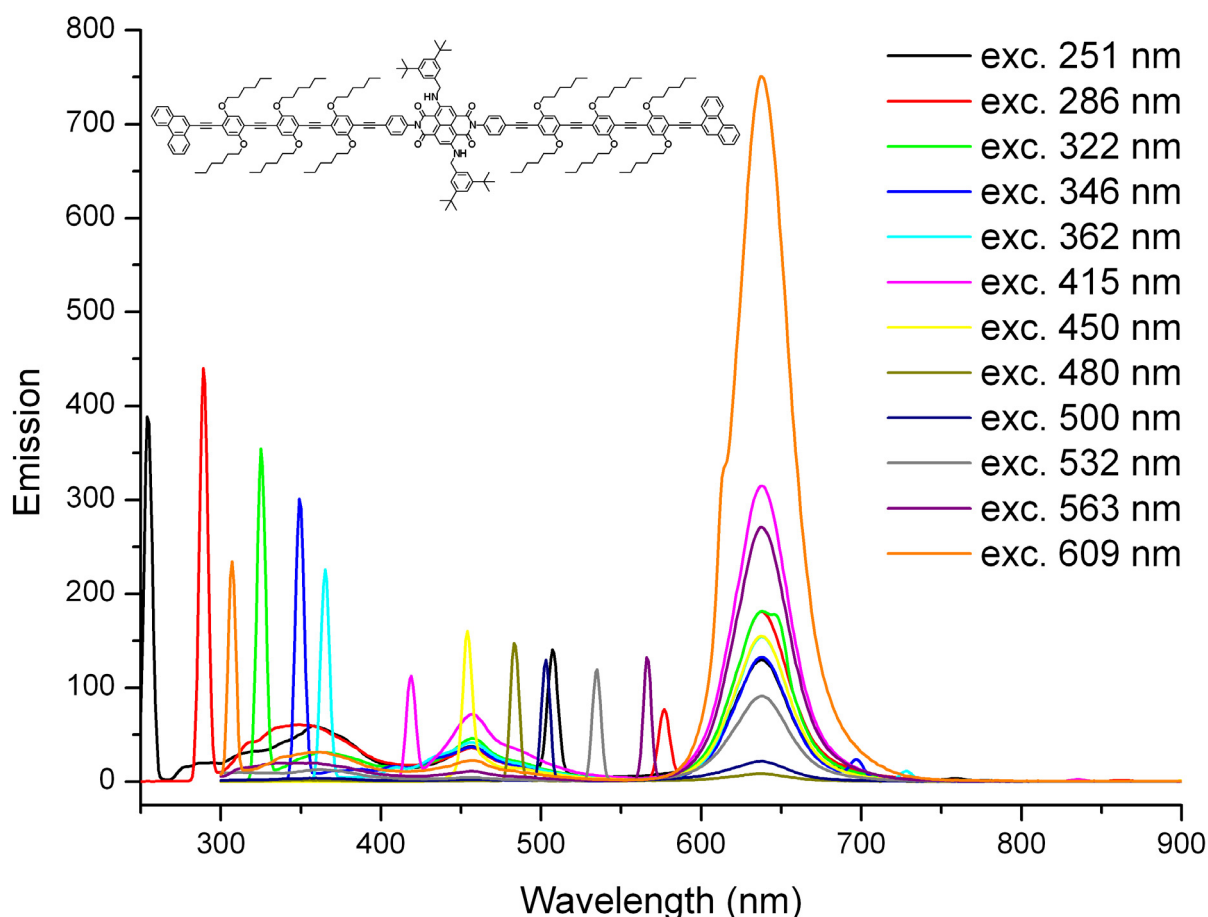
**Figure 98:** Emission spectra of **122** ( $6.5 \cdot 10^{-7} \text{M}$ ), **128** ( $2.2 \cdot 10^{-6} \text{M}$ ) and **148** ( $1.2 \cdot 10^{-6} \text{M}$ ) in  $\text{CH}_2\text{Cl}_2$  at room temperature.

As a possible energy transfer Förster resonance energy transfer (FRET)<sup>[287]</sup> is considered. One criteria for a FRET is the overlap of emission spectra from the donor with the absorption spectra of the acceptor. The overlapping of the emission and the absorption curves is displayed in Figure 99 and pointed out with the dashed area. The yield of the energy transfer has not been analyzed quantitatively.



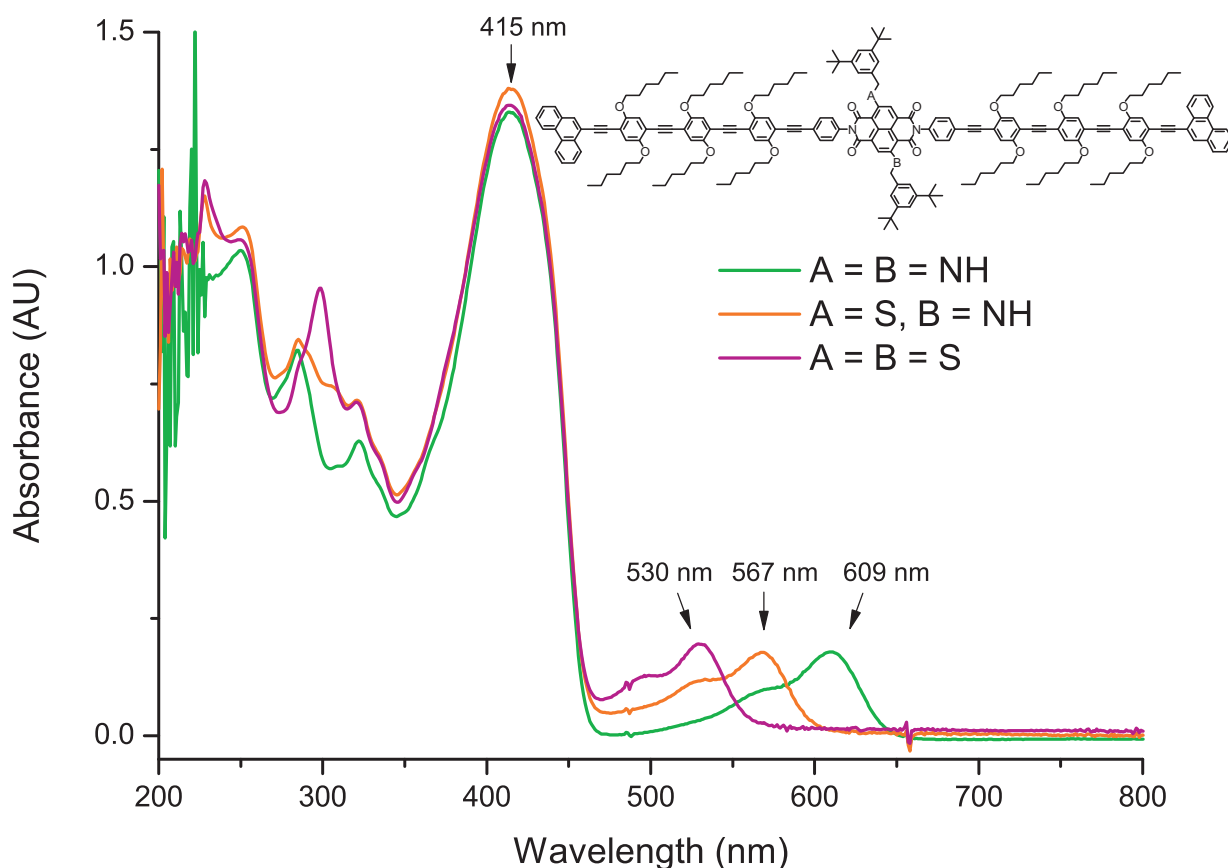
**Figure 99:** Absorption and emission spectra of **122**. The dashed area displays the overlapping area of the emission and absorption curves.

Figure 100 shows the emission spectra of **122** exciting at several wavelengths. Independent of the excitation wavelength, an energy transfer to the NDI-core leading to an emission at 637 nm is observed.



**Figure 100:** Emission spectra of **122** in  $\text{CH}_2\text{Cl}_2$ , excited at several wavelengths.

After investigation of the absorption and emission properties of **122**, the optical properties of **123** and **124** were investigated and compared to **122**. Therefore the absorption spectra of **123** and **124** were recorded in dichloromethane and compared to the absorption spectra of **122** (Figure 101). The diamine functionalized target structure **122** shows an absorption maximum at 415 nm and 609 nm. The mixed compound **123** has an absorption maximum at 415 nm and 567 nm. The dithiol functionalized compound **124** has absorption maxima at 415 nm and 530 nm. While the absorption band arising from the OPE-part is at 415 nm for all three compounds **122-124**, the NDI absorption band was shifted 79 nm hypsochromically by systematically changing the core substituents from amines (**122**) to sulfides (**124**). The compound **123** with mixed core-substituents has an absorption maximum at 567 nm.



**Figure 101:** Absorption spectra for compound **122**, **123**, **124** in dichloromethane. The NDI band is progressively hypsochromically shifted when exchanging the amines with thiol core substituents.

This blue shift is also obtained in the emission spectra (Figure 102). The emission maxima are shifted from 637 nm (NN, **122**), to 593 nm (NS, **123**), to 557 nm (SS, **124**). However, the intensity of the fluorescence is also drastically reduced. While the emission of the NN-substituted compound **122** is readily observed at daylight, the intensity of the emission in the mixed compound **123** is much weaker. For the disulfur functionalized compound **124** the fluorescence nearly vanished, and is hardly obtained. The overlap of emission and absorption is even more pronounced in compound **123** and **124** than in compound **122**, but the amount of energy transfer is drastically reduced. While in compound **122** most of the energy is transferred and most of the excited light has a wavelength of 638 nm when irradiating at 415 nm, the energy is only partially transferred in **123** and **124** when irradiating at 415 nm and most of the light is emitted at 455 nm. Even though these are only qualitative findings and the quantum yield of the energy transfer has not been quantitatively determined it gives information about emission properties of **122-124**.

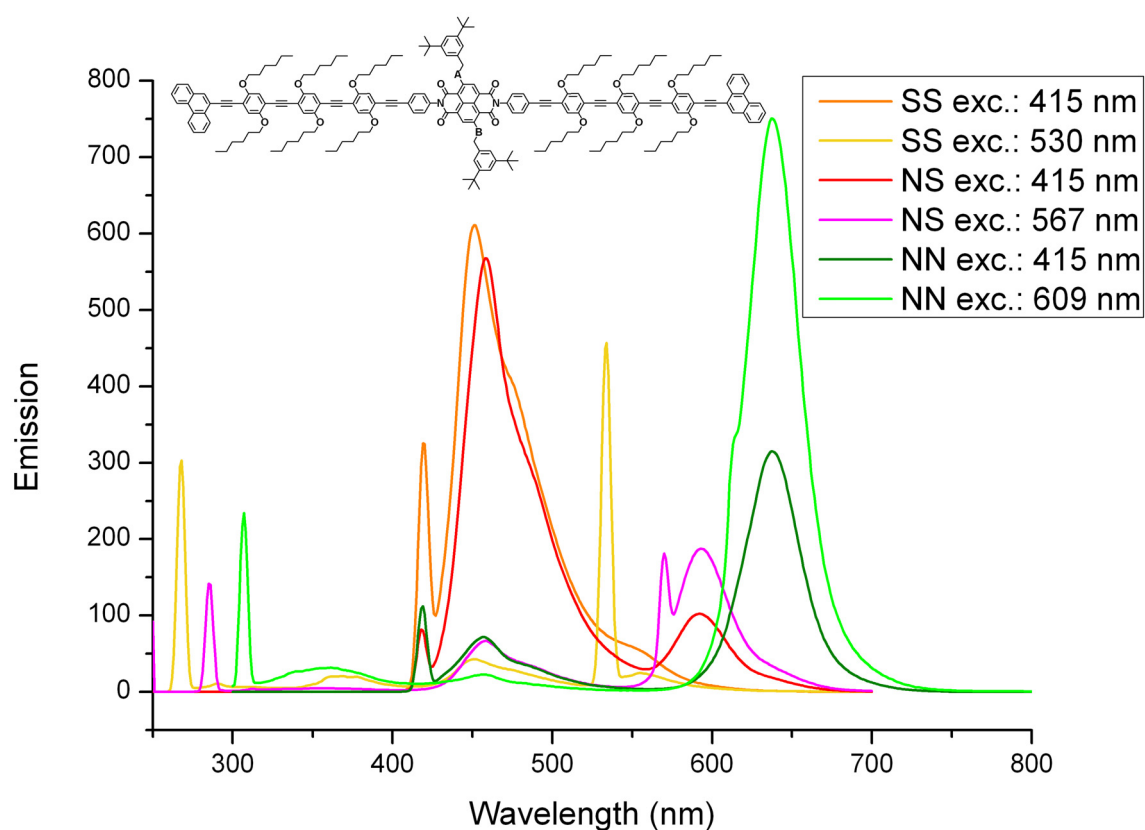


**Figure 102:** Emission spectra of compounds **122**, **123**, **124** in dichloromethane.

In summary, the three target compounds bearing different core substituents were qualitatively analyzed by their absorption and emission spectroscopic behavior. The characterization revealed interesting features and is important for the coming physical experiments. The photophysical properties of the three target structures **122-124** are summarized in Table 5.

Compound	Abs. Max OPE-part	Abs. Max NDI-part	Emission exc. OPE	Emission exc. NDI	Emission max
<b>122</b> (NN)	415 nm	609 nm	457/637 nm	637 nm	637 nm
<b>123</b> (NS)	415 nm	567 nm	458/593 nm	593 nm	458 nm
<b>124</b> (SS)	415 nm	530 nm	451 nm	557 nm	451 nm

**Table 5:** The measurements were performed in dichloromethane. Abs. Max OPE-part is the absorption maximum obtained from the OPE-subunits. Abs. Max. NDI-part is the emission maximum obtained from the NDI subunits. Emission exc. OPE is the emission maximum obtained when irradiated at the absorption maximum of the OPE subunit (415 nm for all compounds). The emission exc. NDI-part is the emission maximum obtained when irradiated at the absorption maximum of the NDI-subunit (609 nm, 567 nm and 530 nm). Emission max is the main emission when irradiated at 415 nm.

## 5.6 Investigations in a SWNT Junction

The synthesized and characterized target compounds bear all the required design criteria and seem ideally suited for the attempted experiments. Compounds **122-124** were investigated in a SWNT junction. First, the setup of the experiment will be described and then, the obtained results will be discussed.

### 5.6.1 Setup

The setup of the experiment is displayed in Figure 103. The measurements were performed in an optical cryostat at high vacuum. With a cooling finger the temperature can be cooled down with liquid helium to 4.2 K. The emitted light is collected with a microscope and analyzed with a spectrometer.

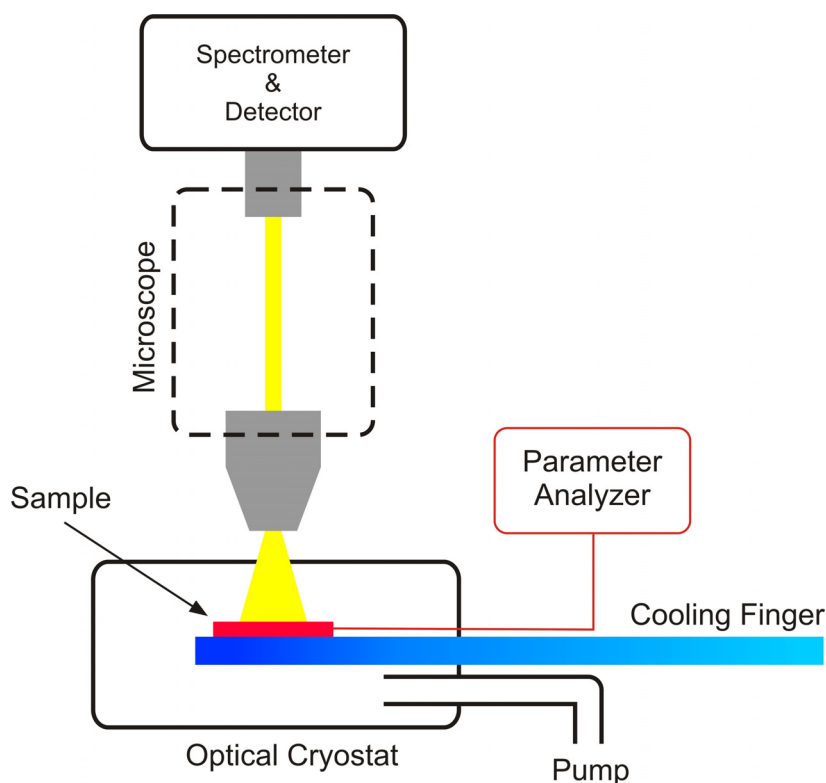


**Figure 103:** Setup of the experiment. The optical cryostat is cooled down with a cooling finger to liquid helium temperatures. The light is collected with a microscope and analyzed with a spectrometer. The sample is fitted with a feedthrough to address the electrodes.

### 5.6.2 Fiat Lux

Gaps of  $\approx 5$  nm in metallic SWNTs were produced as described in 5.1.1 to provide the freestanding SWNT electrodes. It was then investigated to bridge the gap with molecules. A solution of **122** in mesitylene was exposed to the sample. To align and immobilize the molecules between the two SWNT electrodes, a voltage bias was applied while pumping vacuum. To analyze the device, I/V-curves were measured as shown in Figure 104. The black curve corresponds to the metallic SWNT before breakdown. The red curve was recorded after breakdown. After exposition of the molecules, I/V curves were recorded and are shown in blue. After exposing the molecules to the broken SWNT, the conductance is increasing significantly, which indicates that molecules are bridging the two electrodes.

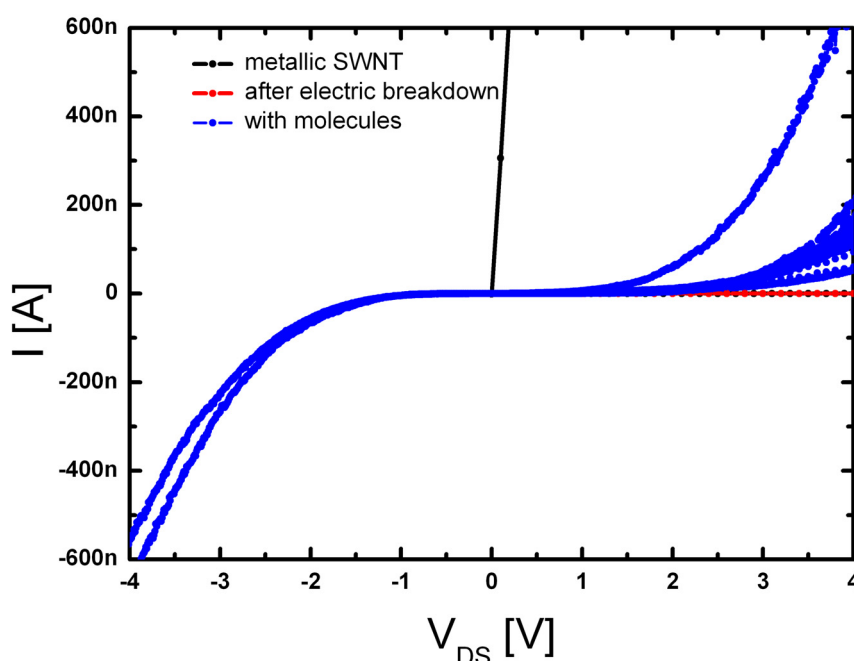


**Figure 104:** I/V-characteristics of a SWNT device before (black), after breakdown (red) and after the exposure of **122** to a broken sample (blue).

The sample is cooled down with liquid helium to 4.2 K. A voltage bias of 4V was then applied to induce electroluminescence of immobilized molecules and the emitted light was detected. Indeed, a light spot was observed with the microscope. Figure 105 A shows an image of the sample, with the light spot in the middle. The image consists of two overlaid pictures. First the light picture, in which only the lighting point is visible and the rest is dark, and the second overlaid image is a picture of the probe in which the contacts are visible. Figure 105 A nicely demonstrates, that single, or few

molecules can be electrically excited to emit light which is detected with the microscope.

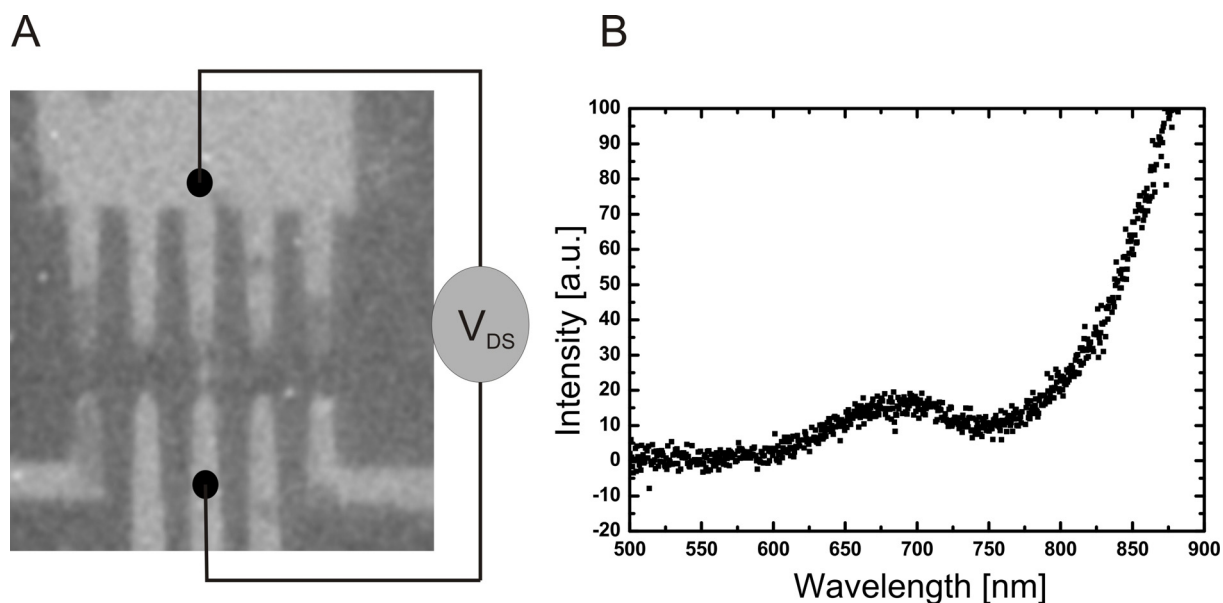


**Figure 105:** A: SEM image of the probe consisting of a light picture in which only the lighting point is visible with the rest being black, and the picture of the setup to visualize the contacts. B: Integrated emission spectra of **122** immobilized in a SWNT-junction. The molecule is excited while applying a constant bias voltage of 4V. The data points are collected over 50 minutes.

The light of the lighting spot was spectroscopically analyzed. The emitted light was detected over 50 minutes while applying a constant voltage bias of 4V. The spectrum obtained is shown in Figure 105 B. The integrated emission spectra shows a clear maximum between at 685 nm, which is in the range of the emission maximum of compound **122** in dichloromethane (638 nm). The emission wavelength is dependent of several parameters such as surrounding or solvents. To mimic the conditions of a SWNT-junction, the photo-excited fluorescence of compound **122** was investigated on highly-ordered-pyrolytic-graphite (HOPG) under vacuum (Figure 106) while irradiating with a laser at 532 nm. Figure 106 shows the emission spectra recorded at different temperatures. Above 200 K the emission spectra look very similar to the electrically-excited spectrum recorded in the SWNT-junction, and an emission maximum at about 675 nm is observed. When the sample is cooled further down, the peak becomes more pronounced. Below 46.5 K the peak is very pronounced with an emission maximum at 675 nm. The shape of the peak fits well with the mirror image of the absorption peak, which indicates that the obtained fluorescence arises from the molecules.



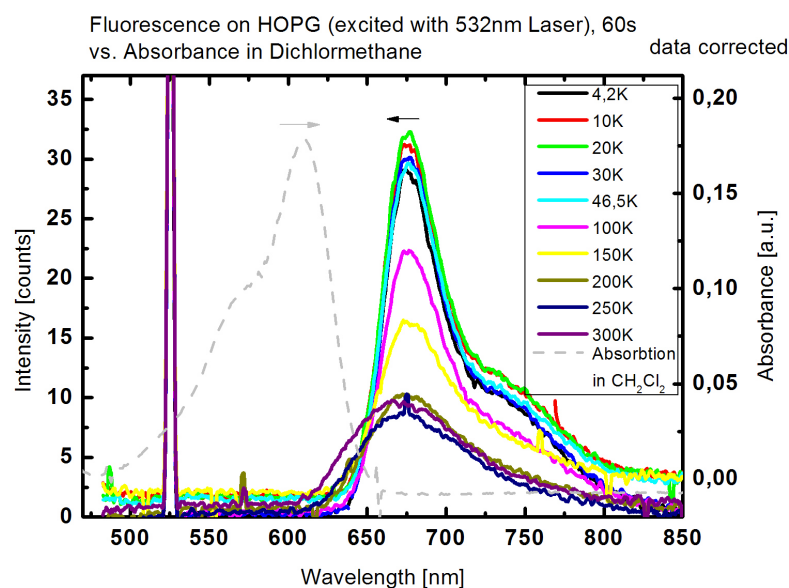


**Figure 106:** Fluorescence spectra of compound **122** on HOPG excited with a laser at 532 nm. The peaks become more pronounced while cooling down and show an emission maxima at 675 nm. The grey dashed line is the absorbance spectra of **122** in dichloromethane. The shape of the emission spectra is the mirror image of the absorbance spectrum.

The electroluminescence occurs after exciting electrons by recombination of electrons and holes in the fluorophore. Electrons and holes are injected from opposite electrodes. Therefore, only molecules bridging the electrodes are expected to be excited. Furthermore, the detected light arising from the emission is characteristic for compound **122**. Regarding the size of the junction and the size of the molecules, we conclude that single (or few) molecules are immobilized in the SWNT junction.

### 5.6.3 Changing the Core-Substituent

To gain further prove that the emission arises from the investigated molecule, we systematically changed the photophysical properties of the molecules while changing the core substituents of the NDI core. Doing so, the emission of the molecule can be shifted from 638 nm (NN, **122**) to 593 nm (NS, **123**) to 557 nm (SS, **124**) in dichloromethane. However, the intensity of the fluorescence also drastically decreases and the observed FRET diminishes as well. The fluorescence of the disulfur functionalized molecule is too weak to be observed in the setup. The mixed-derivative **123** is currently under investigation. The intensity of the fluorescence is weaker than for **122**, therefore the setup has to be improved. The emitted light has to

be collected from all sites and must be directed with mirrors to the lens of the microscope such that enough light can be observed to be spectroscopically analyzed.

## 5.7 Conclusion

Three target compounds were proposed to bridge a single-walled carbon nanotube junction. The design carefully considered several aspects of the device and its function. The molecule needs to be long and rigid to bridge the nanotube gap of about 5 nm. It needs to be polarizable to provide a driving force for locating it in between the gap of the nanotube electrodes. Furthermore, the target compounds are functionalized with a central electrically excitable fluorophore to get a spectroscopic signal from molecules contacted with two electrodes.

The synthesis of the target compounds was successfully performed and the compounds were properly analyzed. The compounds were further characterized by their absorption and emission properties. By systematically varying the core-substituents of the NDI-fluorophore, the color and the emission of the target compound was tuned.

The diamine core-substituted target compound was in addition successfully immobilized between two nanotube electrodes to form a SWNT-molecule-SWNT junction. Supramolecular interaction of the anchor groups of the target compound with the single-walled carbon nanotubes stabilized the molecular junction. While injecting electrons from one side and holes from the other side which meet on the fluorophore, immobilized molecules were excited and the emission of a single molecule at low temperature was analyzed with a spectrometer. Interestingly, a perfect match between the electroluminescence emission spectrum and the photoluminescence emission spectrum of the molecule absorbed on a graphene surface was found.

Hence, a characteristic spectroscopic signal from a molecule connected with two electrodes was obtained. This is a new approach to gain additional spectroscopic information of molecules fixed between two electrodes. The setup is not only interesting from a molecular electronics point of view, but also from a single molecule spectroscopic viewpoint. Variations of the chromophore will allow to investigate the number of immobilized molecules in further details.

## 6 Summary and Conclusions

The goal of this thesis is the design and synthesis of new functional molecules for molecular junctions. In the introduction, a motivation for the research in the field of molecular electronics is given, methods and integration setups are discussed, and selected examples are presented to provide an overview of what has been achieved in this field. Molecular electronics is a very interdisciplinary field and requires a close collaboration of researchers from different backgrounds in of science such as physics, electro engineering and chemistry. Although most of the results discussed in this thesis are obtained in collaboration with physicists, it is written from a chemist's point of view with a focus on the design and synthesis of molecules.

To achieve molecular electronic devices, molecules need to perform functions. Among them the most appealing ones are rectification and switching. However, to enable the design of electronic functions on a molecular level, it is equally important to develop a thorough comprehension of the relationship between the molecules structure and its transport properties. The contents of this thesis thus contributes to various aspects of molecular electronics.

A series of model compounds consisting of a conjugated oligo(phenylene ethynylene) (OPE) backbone is synthesized and subsequently investigated in a mechanically controllable break junction (MCBJ) in a liquid environment (Figure 107). As a reference molecule, OPE **1** is inspected. It is possible to connect a single molecule to two electrodes and its conductance is deduced to be  $G = 1.2 \cdot 10^{-4} G_0$ . Certain components are systematically varied to examine the role of contacts and intermolecular interactions in molecular junctions.

It is found that both thiol and pyridine terminated OPEs form stable junctions using MCBJ. The HOMO-LUMO gaps of both the thiol and pyridine functionalized rods are very comparable, however, the conductance of the dipyridine functionalized OPE **3** is found to be two orders of magnitudes lower than the conductance of the dithiol functionalized OPE **1**. Based on systematic variations of the integrated structure the current hypothesis is that the reduced conductance of the pyridine anchor group bearing rods is not due to a low "contact conductance", but rather due to misalignment of the frontier molecular orbitals to the Fermi level of the electrodes.

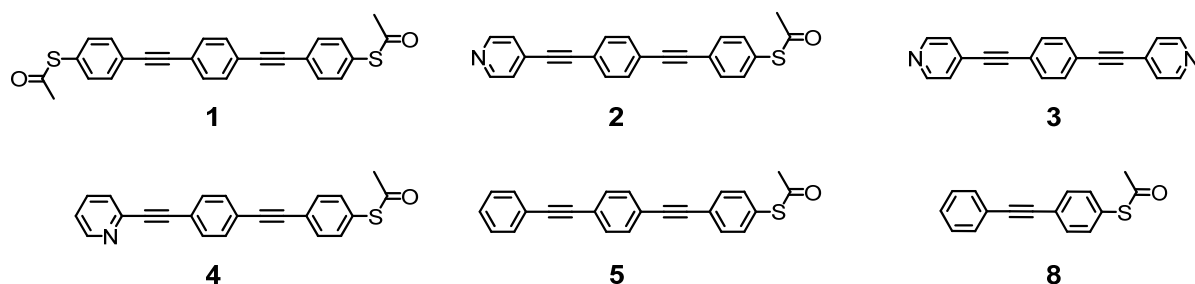


**Figure 107:** A series of OPE model compounds. The role of contact is investigated by systematically varying the anchor groups from thiophenols to pyridines (**1-3**). Intermolecular interactions in molecular junctions are investigated by inspecting molecules with two anchor groups (**1** and **2**) and molecules which can only covalently bind to one electrode (**4**, **5** and **8**) in an MCBJ liquid environment.

Unexplored effects of intermolecular interactions in molecular junctions are examined. It is questioned if it is possible to form molecular junctions based on intermolecular interactions. Therefore, molecular rods are designed and synthesized such that they can only covalently bind to one electrode (compound **4**, **5** and **8**). Investigating these compounds in an MCBJ in a liquid environment reveals that molecular junctions based on aromatic coupling are formed. The metal-molecule-molecule-metal junction formation is interpreted as  $\pi$ - $\pi$  stacked molecules, each binding to one of the electrodes. The conductance is smaller due to a longer tunnelling distance. Interestingly, the possibility of junction formation is similar to the reference molecule OPE **1** covalently binding both electrodes.

The molecular rod model compounds **1** and **5** are further investigated in highly ordered two-dimensional gold nanoparticle arrays. Extended networks of molecular junctions are formed based on compound **1** covalently binding two gold nanoparticles.

After these basic investigations the molecule's function is further enriched and molecular switches and molecule based rectifiers move into the focus of interest. Two redox switches based on ferrocene are proposed (Figure 108). In both switches, the ferrocene is functionalized in the 1,1'-position with two linkers comprising thiol anchor groups. Whereas in the first model compound **87** the linkers consist of rather poor conducting alkyl groups, the linkers of the second switch **94** are conjugated vinyl groups to provide an efficient electronic coupling to the electrodes.

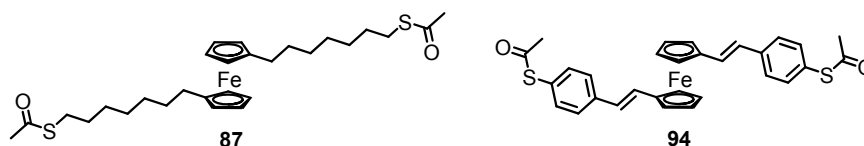


**Figure 108:** Proposed ferrocene based redox switches **87** and **94**. Both structures bear a 1,1'-functionalized ferrocene core. The alkyl linkers in target structure **87** are rather isolated leaving the ferrocene subunit as a hopping island for electrons. The conjugated linkers in target structure **94** provide electronic coupling of the ferrocene to the electrodes.

The switch **94** is electrochemically characterized and a fully reversible redox reaction is observed. It is possible to immobilize single molecules of the switch in an MCBJ setup. The conductance is lower than the conductance of a comparable OPV control molecule **55** and the near-perfect conductance of a literature reported similar molecule can not be confirmed. Combining the MCBJ setup with an electrochemical cell, the conductance of the immobilized molecule is investigated in relation to an applied potential with respect to a reference electrode. The applied potential between the source-and-drain-electrode and the reference electrode is considered as a gate voltage. The molecule is immobilized in its neutral reduced state (potentiostat set to 0 V) and the gate voltage is then increased. The conductance increases and at one point jumps to a larger conductance, attributed to the oxidation of the ferrocene subunit in the switch. The oxidation is reversible and while reducing the molecule, the initial conductance is maintained. Thus, the integration of the ferrocene derivative **94** comprising junction in an electrochemical setup can be considered as a reversible single molecule redox switch.

Furthermore a new switching concept based on the interplay of electrode and molecule is proposed. Therefore, different pathways for electrons in a cruciform type structure consisting of two crossed rods are considered. One of the rods bears terminal sulfur groups, whereas the second transversal rod is functionalized terminally with pyridine subunits. The active component of the switch is the pyridine terminated rod, in an electrochemically controllable MCBJ the coordination of the pyridine nitrogen is expected to bind to the gold surface in dependence of the surface potential of the electrodes. The task of the sulfur functionalized rod is solely to fix the molecule within the junction. Initially, compounds **30** and **31** are proposed (Figure 109). Both target structures consist of an oligo(phenylene vinylene) (OPV) and an OPE substructure. In compound **30** the sulfur is placed in the *meta*-position to reduce

the electronic transparency through the sulfur functionalized rod, whereas the anchor groups are placed in the *para*-position in compound **31** to facilitate the detection on a single molecule level.

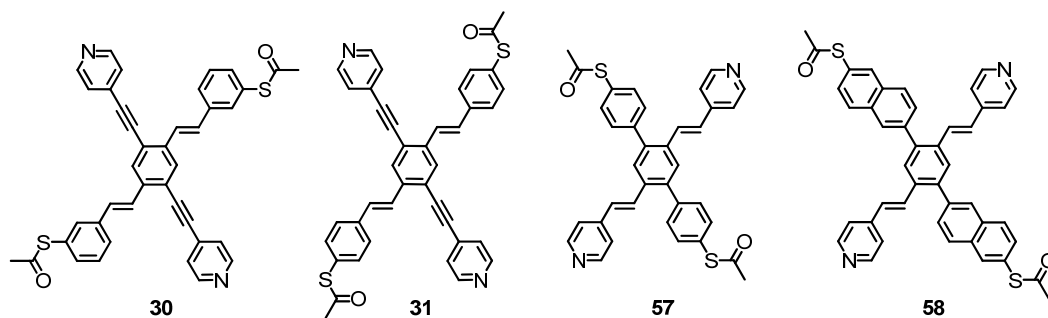


**Figure 109:** Proposed cruciform structure **30**, **31**, **57** and **58** as model compounds for coordination induced single molecule switches.

The synthesis and characterization of compound **30** and **31** including their inspection in an MCBJ setup within a liquid environment is discussed.<sup>[288]</sup> The conductivity of the sulfur bearing rod substructure of compound **30** is below the detection limit, and therefore only compound **31** can be integrated in an MCBJ. This is a first proof of principle that molecules carrying the necessary function can be integrated between two electrodes. However, electron transport investigations on single rod substructures reveal that OPVs are in general more conducting than OPEs.<sup>[58]</sup> This leads to a reconsideration of the design and the place of the anchor groups is exchanged. To maintain a proper distance ratio, the OPE substructure is replaced with an oligo aryl substructure. The oligo aryl structure in target structure **57** consists of an oligo phenylene (OP) structure and in target compound **58** naphthyl units are introduced to elongate the oligo aryl rod (Figure 109). The synthesis of the two novel oligoaryl cruciform structures **57** and **58** is discussed. The OPV substructure is built up with a *Horner-Wadsworth-Emmons* reaction, whereas the perpendicular oligo-aryl substructures are assembled by *Suzuki* cross couplings. Having the target structures in hand they are both immobilized in an MCBJ. Interestingly, two molecular signatures are obtained in the logarithmic histograms when no deprotection agent is added to the compounds bearing acetyl protected sulfurs. One peak in the histogram is attributed to molecular junctions which are formed via the pyridine functionalized rod, whereas the second peak is attributed to molecular junctions bound via spontaneously deprotected thiols. These findings reveal that the molecule is functional and that electron transport is possible through both of the crossed rods.

However, the electron transport is still dominated by the sulfur functionalized rod. To observe a switching behavior, the conductance of the pyridine functionalized rod-substructure needs to be increased relative to the conductance of the thiol comprising rod-substructure. The challenge is currently attacked from two directions, physics and chemistry. On the one hand detailed investigations of the behavior of the cruciform in the presence of a control potential within an electrochemical break junction setup is underway. On the other hand, investigations on nitrogen-heterocycle (other than pyridine) functionalized rod model compounds which might provide a larger electronic transparency are in progress.

Due to the interfacial challenges between molecules and electrodes, electronic functions realizable with two terminal structures are particularly appealing for single molecule experiments. The extent of rectification arising from integrated molecule is thus of particular interest. The rectification ratios (RRs) of molecule based rectifiers reported so far are all below one hundred which is orders of magnitudes below RRs of diodes used in modern circuits. Calculations predicted that cross-conjugated systems show RRs of up to 10'000.

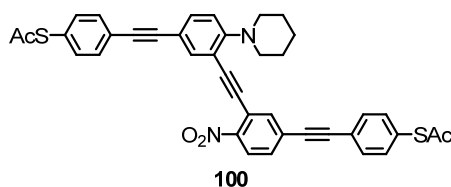


**Figure 110:** Proposed molecular rectifier **100** based on “cross-conjugated” *meta*-substituted benzene units.

We propose a molecular rectifier **100** based on two *meta*-substituted benzene units, one functionalized with an electron donating tertiary-amine group, the other with an electron withdrawing nitro-group (Figure 110). The synthesis is successfully performed, but no integration experiments to prove its rectifying properties have yet been performed.

So far we are able to integrate single molecules between two electrodes and characterize the molecular junction by detecting the current as a response on the applied voltage. An additional signal from a molecule other than the electrical

response would be very appealing to obtain information that molecules are bridging the electrodes.

We propose to profit from electroluminescence of a molecule connected to two electrodes. Electroluminescence as signal from molecules is very appealing as it indicates that molecules are bridging the electrodes (only then are they excited) and the emitted light is characteristic for the fluorophore. Three target structures **122-124** possessing fluorophores are designed to bridge a 5 nm gap of two single-walled carbon nanotube electrodes (Figure 111). As fluorophores naphthalene diimides (NDIs) are considered. While keeping the actual fluorophores the same, small changes in the fluorophore's core substituents allow tuning the optical properties of the target structures without affecting the overall structure and thus the physical chemical deposition features.

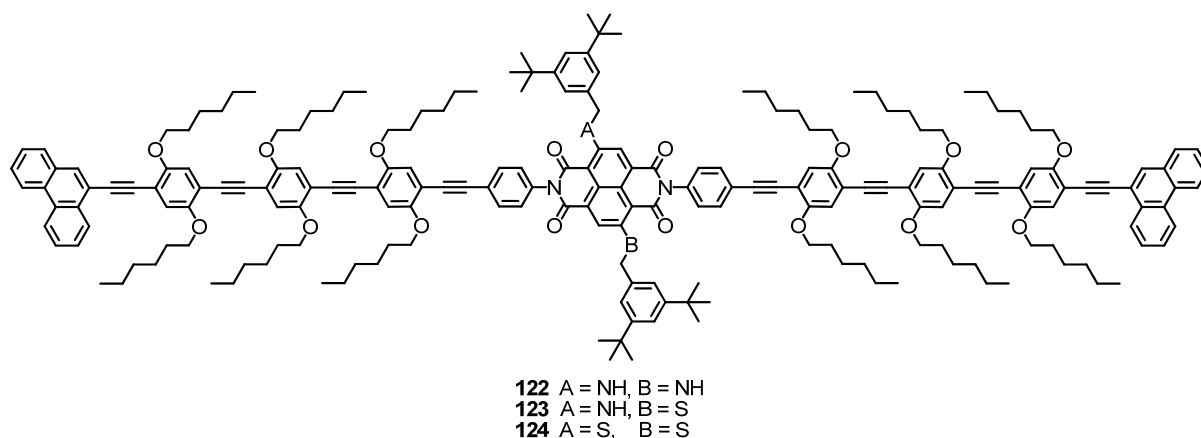


**Figure 111:** The proposed target structures **122-124**

Phenanthrene groups are considered as anchor group to provide fixation of the molecule to the electrodes via supramolecular interactions. As linker groups an OPE backbone is considered. The OPE backbone provides on the one hand electronic coupling with the anchor group and the NDI core, and on the other hand the required length. The successful synthesis and characterization of the three target structures with a length of around 7.5 nm is described. The photophysical investigations in solution confirm the possibility of tuning the absorption and emission bands. The longest wavelength emission maxima of the three target structures cover a range of 79 nm. The integration into a single-walled carbon nanotube device is successfully performed and the nanotube-molecule-nanotube junction is characterized by its  $I/V$ -characteristics. Furthermore, the characteristic emission signal of integrated molecules is detected upon electrical excitation.



---

An additional characteristic signal in this electroluminescence experiment (I/V and electroluminescence) of a molecule connected with two electrodes is obtained. This new approach is very interesting from a molecular electronics point of view, but also from the aspect of single molecule emission. Investigations with varied fluorophores will provide more insights onto the exact number of integrated molecules.



## 7 Experimental Section

### 7.1 Materials and Methods

#### *Reagents and solvents*

All chemicals were directly used for the synthesis without further purification as received from *Fluka AG* (Buchs, Switzerland), *Acros AG* (Basel, Switzerland), *Merck* (Darmstadt, Germany), *ABCR* (Karlsruhe, Germany) and *Aldrich* (Buchs, Switzerland) unless otherwise stated. The solvents for chromatography and crystallization were distilled once before use, the solvents for extraction were used in technical grade. Dry tetrahydrofuran (THF) was dispensed from a Pure Solv MD Solvent Purification System or distilled over Na/benzophenone. Dry dichloromethane (DCM) was dispensed from a Pure Solv MD Solvent Purification System. Dry toluene was distilled over Na/benzophenone. Dry DMF was purchased over molecular sieves from *Fluka*.

#### *Synthesis*

All reactions with reagents which are sensitive to air or moisture were performed under an argon atmosphere using Schlenk-technique, only dry solvents were used and the glassware was heated out. For an inert atmosphere *Argon 4.8* from *PanGas AG* (Dagmersellen, Switzerland) was used.

#### *<sup>1</sup>H-Nuclear Magnetic Resonance (NMR)*

*Bruker DPX-NMR* (400 MHz) and *Bruker BZH-NMR* (250 MHz) instruments were used to record the spectra. Chemical shifts ( $\delta$ ) are reported in parts per million (ppm) relative to residual solvent peaks ( $\text{CDCl}_3$ : 7.26 ppm) or trimethylsilane (TMS), and coupling constants (J) are reported in Hertz (Hz). NMR solvents were obtained from *Cambridge Isotope Laboratories, Inc.* (Andover, MA, USA). The measurements were done at room temperature. The multiplicities are written as: s = singlet, d = doublet, q = quartet, quin = quintet, m = multiplet and b = broad.

#### *<sup>13</sup>C-Nuclear Magnetic Resonance (NMR)*

*Bruker DPX-NMR* (101 MHz) and *Bruker DRX-600 NMR* (151 MHz) instruments were used to record the spectra. Chemical shifts ( $\delta$ ) are reported in parts per million (ppm)

relative to residual solvent peaks ( $\text{CDCl}_3$ : 77.0 ppm). The measurements were done at room temperature. Carbon valency is given as: Cp (primary carbon), Cs (secondary carbon), Ct (tertiary carbon) and Cq (quaternary carbon).

### **Mass spectrometry (MS)**

Mass spectra were recorded on a *Bruker esquire 3000 plus* for Electron Spray Ionization (ESI), a *finnigan MAT 95Q* for Electron Impact (EI), a *finnigan MAT 8400* for Fast Atom Bombardment (FAB), or a *Voyager-De™ Pro* for MALDI-TOF (using 1,8,9-anthracenetriol as matrix). Important signals are given in mass units per charge ( $m/z$ ) and the relative intensities are given in brackets.

### **Elementary Analysis (EA)**

Elementary analyses were measured by W. Kirsch on a *Perkin-Elmer Analysator 240*. The values are given in mass percent.

### **Melting points (Mp)**

Melting points (Mp) were determined in °C using a *Stuart SMP3* apparatus and are uncorrected.

### **Ultraviolet Spectroscopy (UV)**

UV/vis-spectra were recorded on an *Agilent 8453* diode array detector spectrophotometer using optical 114-QS *Hellma* cuvettes (10 mm light path) under an oxygen atmosphere.

### **Fluorescence Spectroscopy**

Emission spectra were recorded on a *Shimadzu RF-5301 PC* spectrofluorophotometer under an oxygen atmosphere.

### **Gel Permeation Chromatography (GPC)**

*Shimadzu LC-8A* was used to record the chromatogram. The measurements were done at room temperature with an *OligoPore* 300 x 7.5 mm column (particle size 6  $\mu\text{m}$ ) from *Polymer Laboratories*, eluting with toluene, with a flow rate of 0.5 ml/min at  $\lambda = 220$  nm.

**Column Chromatography (CC)**

For CC *silica gel 60* (40-63  $\mu\text{m}$ ) from *Merck* or *silica gel 60* (40-63  $\mu\text{m}$ ) from *Fluka* was used.

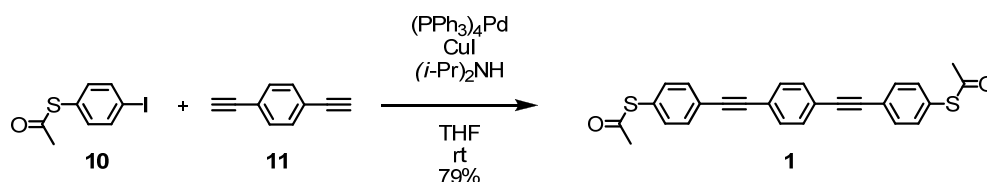
**Thin Layer Chromatography (TLC)**

*Silica gel 60 F<sub>254</sub>* glass plates with a thickness of 0.25 mm from *Merck* were used. The detection was observed with a UV-lamp at 254 nm or 366 nm.

## 7.2 Synthetic Procedures

### 7.2.1 Molecular Conductors

#### 1,4-bis[(4-acetylsulfanylphenyl)ethynyl]benzene (**1**)



**10** (326 mg, 1.17 mmol, 2.2 eq.) and **11** (67 mg, 0.53 mmol, 1.0 eq.) were dissolved in a well degassed mixture of 15 ml dry THF and 3 ml diisopropylamine. It was degassed for another 10 minutes before Pd(PPh<sub>3</sub>)<sub>4</sub> (61 mg, 10 mol%) and CuI (10 mg, 10 mol%) were added. The reaction mixture was stirred for 7 hours at room temperature and then evaporated, absorbed on silica and chromatographed (silica gel, 2x12 cm, hex:EtOAc 5:1 → 1:1) to give a beige solid (179 mg, 79%).

TLC R<sub>f</sub> = 0.15 (hexane:EtOAc = 5:1).

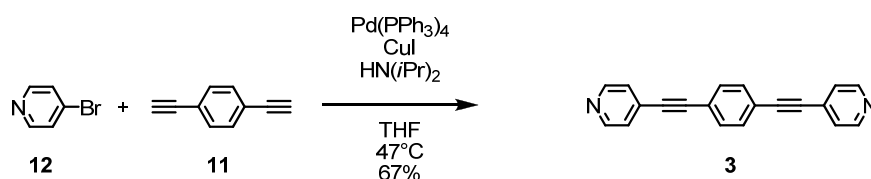
<sup>1</sup>H-NMR (250 MHz, CDCl<sub>3</sub>, 25 °C): δ = 7.58-7.52 (8H, m), 7.41 (4H, d, <sup>3</sup>J<sub>HH</sub> = 8.8 Hz), 2.44 (6H, s) ppm.

<sup>13</sup>C-NMR (101 MHz, CDCl<sub>3</sub>, 25 °C): δ = 193.8, 134.7, 132.6, 132.1, 128.7, 124.7, 123.4, 91.1, 91.0, 30.7 ppm.

UV/Vis: λ<sub>max</sub> 332 nm;

MS (EI): *m/z* (%) =: 426.1 (M<sup>+</sup>, 29%), 384.1 (33%), 342.1 (100%).

#### 1,4-bis(4-pyridinylethynyl)benzene (**3**)



4-Bromopyridine (HCl salt) (339 mg, 1.74 mmol, 2.2 eq.), diethynylbenzene (100 mg, 0.793 mmol, 1.0 eq), Pd(PPh<sub>3</sub>)<sub>4</sub> (60 mg, 0.08 mmol, 10 mol%) and CuI (15 mg, 0.08 mmol, 10 mol%) were suspended in a well degassed mixture of 10 ml dry THF and 1.5 ml diisopropylamine. The reaction mixture was stirred for 3.75 h at 47 °C and then extracted with 10 % aq. NaHSO<sub>3</sub> and toluene. The organic phase was washed with water, dried over Na<sub>2</sub>SO<sub>4</sub>, evaporated and chromatographed (silica gel, 2x12

cm, hexane: ethyl acetate 1:1 with 5% NEt<sub>3</sub>) to give a colorless solid (128 mg, 0.457 mmol, 67%).

TLC R<sub>f</sub> = 0.64 (hexane : ethyl acetate 1:1).

Mp: 189-191°C.

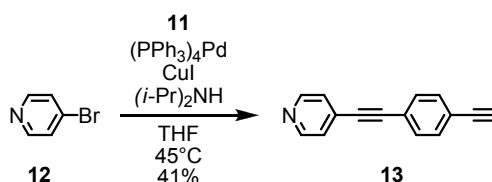
<sup>1</sup>H NMR (250 MHz, CDCl<sub>3</sub>, 25 °C): δ = 8.63 (4H, d, <sup>3</sup>J<sub>HH</sub> = 5.83 Hz); 7.56 (4H, s); 7.39 (4H, d, <sup>3</sup>J<sub>HH</sub> = 6.05 Hz) ppm.

<sup>13</sup>C NMR (101 MHz, CDCl<sub>3</sub>, 25 °C): δ = 159.3, 132.3, 131.4, 125.9, 123, 3, 93.6, 89.2 ppm.

MS (EI): *m/z* (%) = 280 (100 %, M<sup>+</sup>).

IR(neat, ν, cm<sup>-1</sup>): 3087.3, 3053.1, 2228.6.

#### 4-((4-ethynylphenyl)ethynyl)pyridine (**13**)



4-bromopyridine (HCl-salt) (585 mg, 3.01 mmol, 0.95 eq.) and 1,4-bisethynylbenzene (400 mg, 3.17 mmol, 1.0 eq.) were suspended in a degassed mixture of 150 ml dry THF and 15 ml diisopropylamine in a 250-ml-3-neck-flask with condenser. Pd(PPh<sub>3</sub>)<sub>4</sub> (5 mol%, 173 mg) and CuI (5 mol%, 29 mg) were added and it was stirred for 4 hours at 45°C. The volatile compounds were removed by rotary evaporation. The crude was dissolved in dichloromethane, absorbed on silica gel, evaporated and chromatographed (silica gel, 2x12 cm, hexane:ethyl acetate = 1:1) to give **13** as a pale yellow solid (252 mg, 41%).

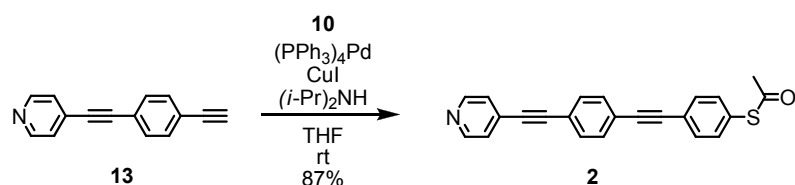
Mp.: 178-180°C (lit.<sup>9</sup> 180-181°C).

TLC R<sub>f</sub> = 0.32 (EtOAc:hexane = 1:1).

<sup>1</sup>H NMR (400 MHz, CDCl<sub>3</sub>, 25 °C): δ = 8.62 (2H, d, <sup>3</sup>J<sub>HH</sub> = 5.6 Hz), 7.50 (4H, s), 7.38 (2H, d, <sup>3</sup>J<sub>HH</sub> = 5.9 Hz), 3.21 (1H, s) ppm.

<sup>13</sup>C NMR (101 MHz, CDCl<sub>3</sub>, 25 °C): δ = 150.3, 132.6, 132.2, 131.5, 125.9, 123.4, 122.9, 93.6, 88.8, 83.4, 79.9 ppm.

MS (EI): *m/z* (%) = 203.1 (M<sup>+</sup>, 100%), 204.1 (16.5%).

**1-[(4-acetylsulfanylphenyl)ethynyl]-4-(pyridine-4-ylethynyl)benzene (2):**


4-((4-ethynylphenyl)ethynyl)pyridine (**13**) (211 mg, 1.04 mmol, 1.0 eq.) and 1-acetylsulfanyl-4-iodobenzene (**10**) (290 mg, 1.04 mmol, 1.0 eq.) were dissolved in a degassed mixture of 10 ml dry THF and 3 ml diisopropylamine in a 50-ml-3-neck-flask. Pd(PPh<sub>3</sub>)<sub>4</sub> (8 mol%, 86 mg) and Cul (8 mol%, 20 mg) were added and it was stirred for 2 hours at room temperature. The volatile compounds were removed by rotary evaporation. The crude was dissolved in dichloromethane, absorbed on silica gel, evaporated and chromatographed (silica gel, 2x12 cm, hexane:ethyl acetate = 2:1) to give a pale yellow solid (258 mg, 73%).

Mp.: 190 -192°C.

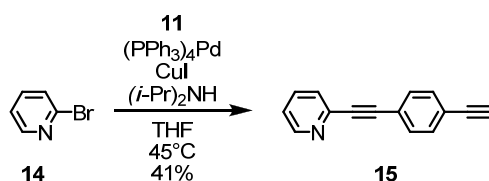
TLC R<sub>f</sub> = 0.31 (EtOAc:hexane = 1:1).

<sup>1</sup>H NMR (400 MHz, CDCl<sub>3</sub>, 25 °C): δ = 8.61 (2H, d, <sup>3</sup>J<sub>HH</sub> = 6.1 Hz), 7.56 (2H, d, <sup>3</sup>J<sub>HH</sub> = 8.6 Hz), 7.53 (4H, s), 7.41 (2H, d, <sup>3</sup>J<sub>HH</sub> = 8.1 Hz), 7.38 (2H, d, <sup>3</sup>J<sub>HH</sub> = 6.1 Hz), 2.44 (3H, s, CH<sub>3</sub>) ppm.

<sup>13</sup>C NMR (101 MHz, CDCl<sub>3</sub>, 25 °C): δ = 193.7, 150.3, 134.7, 132.6, 132.3, 132.1, 131.6, 128.9, 125.9, 124.5, 124.2, 122.5, 93.9, 91.4, 90.9, 88.9, 30.7 ppm.

UV/Vis: λ<sub>max</sub> 328, 348 nm;

MS (EI): *m/z* (%) = 353 (M<sup>+</sup>, 22%), 311 (100%), 43 (9%).

**2-((4-ethynylphenyl)ethynyl)pyridine (15)**


2-bromopyridine (476 mg, 294 μl, 3.01 mmol, 0.95 eq.) and 1,4-bisethynylbenzene (400 mg, 2.17 mmol, 1.0 eq.) were dissolved in a well degassed mixture of 50 ml dry THF and 6 ml diisopropylamine in a 100-ml-3-neckflask in the absence of light. Pd(PPh<sub>3</sub>)<sub>4</sub> (4.6 mol%, 170 mg) and Cul (4.5 mol%, 27 mg) were added and it was heated to 45°C for two hours. The reaction mixture was then evaporated, absorbed on silica and chromatographed (silica gel, 3x12 cm, hex:EtOAc 1:1) to give compound **15** as a colorless solid (252 mg, 41 %).



Mp.: decomp. >124°C.

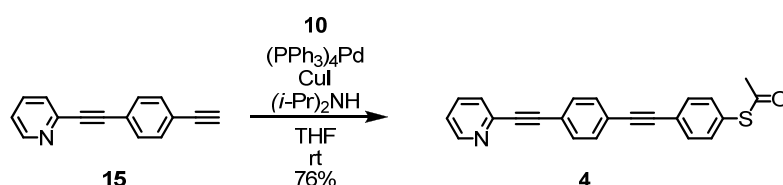
TLC  $R_f$  = 0.39 (EtOAc:hexane = 1:1).

$^1\text{H}$  NMR (400 MHz,  $\text{CDCl}_3$ , 25 °C):  $\delta$  = 8.64-8.63 (1H, m), 7.70-7.67 (1H, m), 7.56-7.47 (5H, m), 7.28-7.24 (1H, m), 3.19 (1H, s) ppm.

$^{13}\text{C}$  NMR (101 MHz,  $\text{CDCl}_3$ , 25 °C):  $\delta$  = 150.6, 143.6, 136.6, 132.5, 132.2, 127.7, 123.4, 123.10, 123.08, 90.8, 88.9, 83.5, 79.7 ppm

MS (EI): 203.1 ( $\text{M}^+$ , 100%), 204.1 (15.7%).

### 1-[(4-acetylsulfanylphenyl)ethynyl]-4-(pyridine-2-ylethynyl)benzene (**4**):



2-((4-ethynylphenyl)ethynyl)pyridine (**15**) (101 mg, 0.50 mmol, 1.0 eq.) and 1-acetylsulfanyl-4-iodobenzene (**10**) (138 mg, 0.50 mmol, 1.0 eq.) were dissolved in a well degassed mixture of 10 ml dry THF and 1.5 ml diisopropylamine in a 50-ml-3-neckflask.  $\text{Pd}(\text{PPh}_3)_4$  (7.3 mol%, 42 mg) and CuI (8.4 mol%, 8 mg) were added and it was stirred at room temperature for 4 hours. The reaction mixture was then evaporated, absorbed on silica and chromatographed (silica gel, 2x12 cm, hex:EtOAc 1:1) to give a beige solid (133 mg, 76%).

mp: 168-169°C;

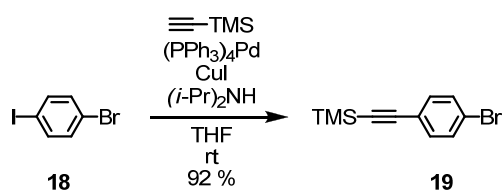
TLC (EtOAc:hexane, 1:1, v/v):  $R_f$  = 0.33.

$^1\text{H}$  NMR (400 MHz,  $\text{CDCl}_3$ , 25 °C):  $\delta$  = 8.64 (1H, m), 7.70 (1H, td,  $^3J_{\text{HH}}$  = 7.7 Hz,  $^4J_{\text{HH}}$  = 1.8 Hz), 7.60-7.51 (7H, m), 7.41 (2H, d,  $^3J_{\text{HH}}$  = 8.5 Hz), 7.26 (1H, m), 2.44 (3H, s) ppm.

$^{13}\text{C}$  NMR (101 MHz,  $\text{CDCl}_3$ , 25 °C):  $\delta$  = 193.8, 150.6, 143.7, 136.6, 134, 132.6, 132.4, 132.1, 128.8, 127.7, 124.6, 123.9, 123.4, 122.7, 91.2, 91.0, 30.7 ppm.

UV/Vis:  $\lambda_{\text{max}}$  327, 347 nm.

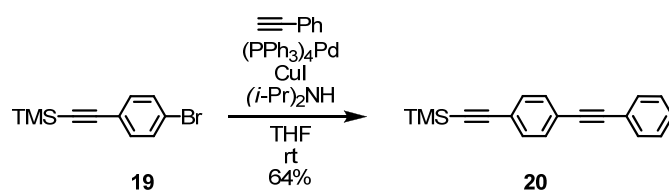
MS (EI): 353 ( $\text{M}^+$ , 21%), 311 (100%), 43 (8%).

**((4-bromophenyl)ethynyl)trimethylsilane (19)**

1-bromo-4-iodobenzene (2.38g, 8.4 mmol, 1.0 eq.) and TMS-acetylene (1.3 ml, 897 mg, 9.1 mmol, 1.09 eq.) were dissolved in a well degassed mixture of 20 ml dry THF and 3.5 ml diisopropylamine in a 100-ml-3-neckflask. Pd(PPh<sub>3</sub>)<sub>4</sub> (300 mg, 3 mol%) and CuI (50 mg, 3 mol%) were added and it was stirred for 17 hours at room temperature. The reaction mixture was then evaporated, absorbed on silica and chromatographed (silica gel, 3x12cm, hex:EtOAc 20:1) to give the product (2.04 g, 91.6%).

TLC R<sub>f</sub> = 0.61 (EtOAc:hexane = 20:1).

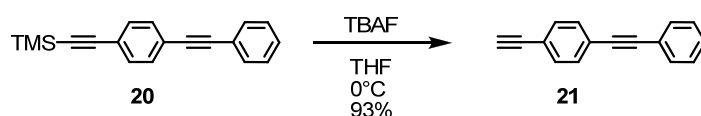
<sup>1</sup>H NMR (400 MHz, CDCl<sub>3</sub>, 25 °C): δ = 7.43 (2H, d, <sup>3</sup>J<sub>HH</sub> = 8.7 Hz); 7.32 (2H, d, <sup>3</sup>J<sub>HH</sub> = 8.7 Hz); 2.43 (9H, s) ppm.

**trimethyl((4-(phenylethynyl)phenyl)ethynyl)silane (20)**

1-bromo-4-TMS-acetylenebenzene (**19**) (1.26 g, 4.96 mmol, 1.0 eq.) was dissolved in 20 ml dry THF and 4 ml diisopropylamine in a 250-ml-3-neckflask. The mixture was degassed for 15 minutes and then phenylacetylene (1.09 ml, 1.01 g, 9.9 mmol, 2.0 eq.), Pd(PPh<sub>3</sub>)<sub>4</sub> (286 mg, 5 mol%) and CuI (47 mg, 5 mol%) were added. The reaction mixture was stirred for 3.5 hours at 60°C and was then filtrated, evaporated, absorbed on silica and chromatographed (silica gel, 4x12 cm, hex:EtOAc 20:1) (790 mg, 64%).

TLC R<sub>f</sub> = 0.57 (EtOAc:hexane=20:1).

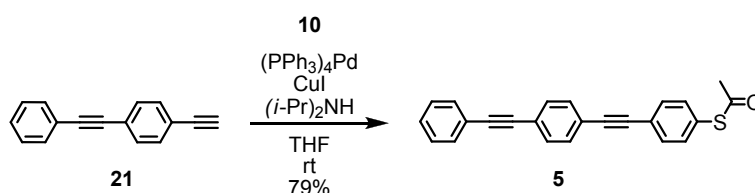
<sup>1</sup>H NMR (400 MHz, CDCl<sub>3</sub>, 25 °C): δ = 7.54-7.50 (2H, m); 7.46-7.45(4H, m); 7.36-7.34 (3H, m); 0.26 (9H, s) ppm.

**1-ethynyl-4-(phenylethynyl)benzene (21)**

**20** (785 mg, 2.86 mmol, 1.0 eq.) was dissolved in 20 ml THF. A TBAF solution (6 ml, 6 mmol, 1M in THF, contains 5% water) was added at 0°C. The ice bath was taken away and it was stirred for 40 minutes. The reaction mixture was then evaporated, absorbed on silica and chromatographed (silica gel, 2x10 cm, hex:EtOAc 20:1) to give the product (535 mg, 93%).

TLC  $R_f$  = 0.40 (EtOAc:hexane = 20:1).

$^1\text{H NMR}$  (400 MHz,  $\text{CDCl}_3$ , 25 °C):  $\delta$  = 7.59-7.55 (2H, m); 7.51 (4H, s); 7.40-7.38 (3H, m); 3.21 (1H, s) ppm.

**1-[(4-acetylsulfanylphenyl)ethynyl]-4-(phenylethynyl)benzene (5)**

**21** (480 mg, 2.37 mmol, 1.0 eq.) and 1-acetylsulfanyl-4-iodobenzene (**10**) (660 mg, 2.37 mmol, 1.0 eq.) were dissolved in a degassed mixture of 20 ml dry THF and 4 ml, diisopropylamine. It was degassed for another ten minutes before  $\text{Pd}(\text{PPh}_3)_4$  (136 mg, 5 mol%) and  $\text{CuI}$  (22 mg, 5 mol%) were added. The reaction mixture was stirred for five hours at room temperature and was then evaporated, absorbed on silica and chromatographed (3x12 cm,  $\text{CH}_2\text{Cl}_2$ :hexane 1:1) to give **4** as a beige solid (659 mg, 79%)

Mp.: 191-193°C.

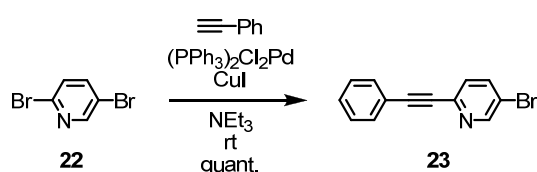
TLC  $R_f$  = 0.17 (hexane:EtOAc = 20:1).

$^1\text{H NMR}$  (400 MHz,  $\text{CDCl}_3$ , 25 °C):  $\delta$  = 7.57-7.51 (8H, m), 7.41-7.35 (5H, m), 2.44 (3H, s) ppm.

$^{13}\text{C NMR}$  (101 MHz,  $\text{CDCl}_3$ , 25 °C):  $\delta$  = 193.8, 134.7, 132.6, 132.1, 132.0, 132.0, 128.9, 128.8, 128.7, 124.7, 123.8, 123.4, 123.1, 91.8, 91.2, 90.8, 89.5, 30.7 ppm.

UV/Vis:  $\lambda_{\text{max}}$  325, 347 nm.

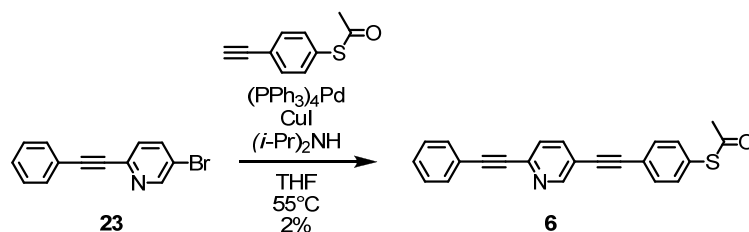
MS (EI):  $m/z$  (%) = 352.1 ( $\text{M}^+$ , 34%); 310.1 (100%).

**5-bromo-2-(phenylethynyl)pyridine (23)**<sup>[160]</sup>

2,5-dibromopyridine (**22**) (1.10 g, 4.50 mmol, 1.0 eq.) and phenylacetylene (459 mg, 494  $\mu$ l, 1.0 eq.) were dissolved in 13.5 ml Et<sub>3</sub>N. Pd(PPh<sub>3</sub>)<sub>2</sub>Cl<sub>2</sub> (63 mg, 2 mol%) and CuI (17 mg, 2 mol%) were added and it was stirred for 1.5 hours at room temperature. The reaction mixture was evaporated and chromatographed to give **23** as a beige solid (1.16 g, 100%).

TLC R<sub>f</sub> = 0.77 (EtOAc:hexane=1:1).

<sup>1</sup>H NMR (400 MHz, CDCl<sub>3</sub>, 25 °C):  $\delta$  = 8.69-8.67 (1H, m); 7.84-7.80 (1H, m); 7.61-7.58 (2H, m); 7.44-7.38 (4H, m) ppm.

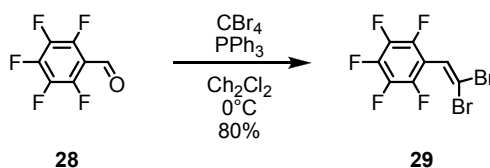
**S-4-((6-(phenylethynyl)pyridin-3-yl)ethynyl)phenyl ethanethioate (5)**

5-bromo-2-(phenylethynyl)pyridine (**23**) (112 mg, 0.434 mmol, 1.0 eq.) was dissolved in a well degassed mixture of 20 ml dry THF and 4 ml diisopropylamine in a 50-ml-3-neckflask with condenser. 1-acetylsulfanyl-4-ethynylbenzene (180 mg, 1.02 mmol, 2.4 eq.), Pd(PPh<sub>3</sub>)<sub>4</sub> (50mg, 10 mol%) and CuI (10 mol%, 8 mg) were added and the reaction mixture was stirred for 29 hours at 55°C. The reaction mixture was then evaporated and chromatographed (silica gel, 2x12 cm, CH<sub>2</sub>Cl<sub>2</sub>) (3 mg, 2 %).

TLC R<sub>f</sub> = 0.27 (CH<sub>2</sub>Cl<sub>2</sub>).

<sup>1</sup>H NMR (400 MHz, CDCl<sub>3</sub>, 25 °C):  $\delta$  = 8.77-8.76 (1H, m); 7.82-7.78 (1H, m); 7.63-7.50 (5H, m); 7.45-7.37 (5H, m); 2.45 (3H, s) ppm.

MS (Maldi-TOF): *m/z* (%) = 355 (M<sup>+</sup>).

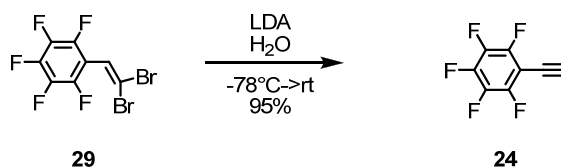
**1-(2,2-dibromovinyl)- pentafluorobenzene (29)**<sup>[163, 164]</sup>

CBr<sub>4</sub> (10.74g, 32.4 mmol, 2.0 eq.) and triphenylphosphine (17.00 g, 64.8 mmol, 4.0 eq.) were dissolved in 60 ml dichloromethane (crown cap) at 0°C in a 250-ml-2-neck flask. Pentafluorobenzaldehyde (3.178 mg, 2.0 ml, 16.2 mmol, 1.0 eq.) was added and it was stirred for 30 minutes at 0°C. The reaction mixture was then filtrated through a 3x3 cm silica plug, washed with hex:EtOAc (5:1), evaporated and chromatographed (silica gel, 5x10 cm, CH<sub>2</sub>Cl<sub>2</sub>) (4.54 g, 80%).

TLC R<sub>f</sub> = 0.64 (hex:EtOAc 5:1).

<sup>1</sup>H NMR (400 MHz, CDCl<sub>3</sub>, 25 °C): δ = 7.18 (1H, s) ppm.

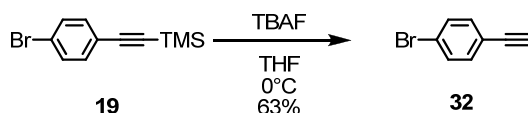
<sup>19</sup>F-NMR (376 MHz, CDCl<sub>3</sub>, 25 °C): δ = -138.4—138.5 (2F, m), -153.9 (1F, t, J = 20.3 Hz) -162.5—162.6 (2F, m) ppm.

**1-ethynyl-pentafluorobenzene (24)**

Diisopropylamine (4.97 g, 49.1 mmol 4.0 eq.) was dissolved in 20 ml dry THF. *n*-BuLi (1.6M in hexane, 30.7 ml, 49.1 mmol, 4.0 eq.) was added at -78°C. The mixture was stirred for 15 minutes and was then transferred with a cannula to a -78° cold solution of **29** (4.33 g, 12.3 mmol, 1.0 eq.) in 20 ml THF. It was stirred for 40 minutes at -78 °C and 1 hour at room temperature. Then water was added and the reaction mixture was extracted with TBME. The combined organic phases were washed twice with water, dried over Na<sub>2</sub>SO<sub>4</sub>, filtrated, evaporated and chromatographed (silica gel, 4x12 cm, hex:EtOAc 5:1) to give the product (2.29 g, 97%).

TLC: R<sub>f</sub> = 0.63 (hex:EtOAc 5:1).

<sup>1</sup>H NMR (400 MHz, CDCl<sub>3</sub>, 25 °C): δ = 4.29(1H, m) ppm.

**1-bromo-4-ethynylbenzene (32)**

The TMS-protected acetylene **19** (1.148 g, 4.53 mmol, 1.0 eq.) was dissolved in 20 ml THF. The TBAF solution (1M in THF, 18 ml, 18 mmol, 4.0 eq.) was added at 0 °C. It was stirred for one hour at 0 °C, then the ice bath was taken away and it was stirred for another 15 minutes. The reaction mixture was then evaporated, absorbed on silica and chromatographed (silica gel, 4x12 cm, hex:EtOAc 20:1) to give the product (436 mg, 63%).

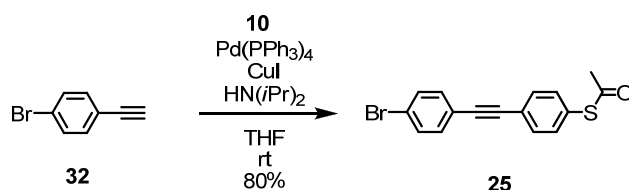
TLC  $R_f$  = 0.50 (hex:EtOAc 20:1).

$^1\text{H}$  NMR (250 MHz,  $\text{CDCl}_3$ , 25 °C):  $\delta$  = 7.46 (2H, dt,  $^3J_{\text{HH}} = 8.7$  Hz,  $^3J_{\text{HH}} = 2.0$  Hz), 7.35 (2H, dt,  $^3J_{\text{HH}} = 8.7$  Hz,  $^3J_{\text{HH}} = 2.0$  Hz), 3.12 (1H, s) ppm.

$^{13}\text{C}$  NMR (101 MHz,  $\text{CDCl}_3$ , 25 °C):  $\delta$  = 134.0, 132.0, 123.6, 121.5, 83.0, 78.8 ppm.

MS (EI):  $m/z$  (%) = 181.9(97%,  $\text{M}^+$ ); 179.9 (100%).

EA: calculated: C = 53.08, H = 2.78, found: C = 52.72, H = 2.73.

**S-4-((4-bromophenyl)ethynyl)phenyl ethanethioate (25)**

1-bromo-4-ethynylbenzene (**32**) (406 mg, 2.25 mmol, 1.0 eq.) and 1-acetylsulfanyl-4-iodobenzene (**10**) (625 mg, 2.25 mmol, 1.0 eq.) were dissolved in a well degassed mixture of 20 ml dry THF and 3.5 ml diisopropylamine. It was degassed for another 10 minutes before Pd(PPh<sub>3</sub>)<sub>4</sub> (220 mg, 8.5 mol%) and CuI (42 mg, 10 mol%) were added. It was stirred for 3.5 hours at room temperature. The reaction mixture was then evaporated, absorbed on silica and chromatographed (silica gel, 3x12 cm, hex:EtOAc = 20:1). (598 mg, 80%)

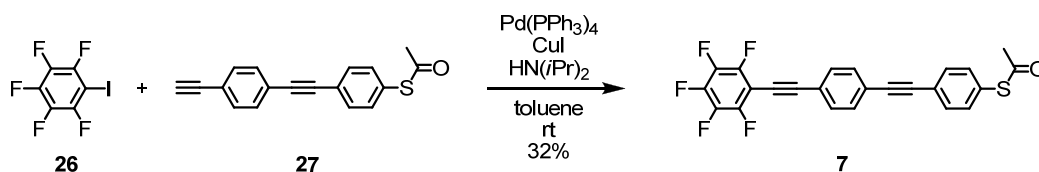
TLC: R<sub>f</sub> = 0.17 (hex:EtOAc = 20:1).

<sup>1</sup>H NMR (400 MHz, CDCl<sub>3</sub>, 25 °C): δ = 7.54 (2H, dt, <sup>3</sup>J<sub>HH</sub> = 8.6 Hz, <sup>4</sup>J<sub>HH</sub> = 2.0 Hz), 7.49 (2H, dt, <sup>3</sup>J<sub>HH</sub> = 8.6 Hz, <sup>3</sup>J<sub>HH</sub> = 2.0 Hz), 7.41-7.38 (4H, m) ppm.

<sup>13</sup>C NMR (101 MHz, CDCl<sub>3</sub>, 25 °C): δ = 193.8, 134.7, 133.5, 132.6, 132.1, 128.8, 124.6, 123.2, 122.3, 90.3, 90.1, 30.7 ppm.

MS (EI): *m/z* (%) = 332.0 (19%, M<sup>+</sup>); 330.0 (18%); 290.0 (100%); 288.0 (97%).

EA: calculated: C = 58.02, H = 3.35, found: C = 58.29, H = 3.44.

**1-[(4-acetylsulfanylphenyl)ethynyl]-4-((perfluorophenyl)ethynyl)benzene (7)**

**27** (18 mg, 0.065 mmol, 1.0 eq.) and pentafluoroiodobenzene (**26**) (30 μl, 68 mg, 0.173 mmol, 2.7 eq.) were dissolved in a well degassed mixture of 5 ml toluene (crown cap) and 1.5 ml diisopropylamine. Then Pd(PPh<sub>3</sub>)<sub>4</sub> (7.5 mg, 10 mol%) and CuI (1.2 mg, 10 mol%) were added and it was stirred for 23 hours at room temperature. The reaction mixture was then evaporated and chromatographed (silica gel, 1x12 cm, toluene) to give a colorless solid (9.1 mg, 32 %).

TLC R<sub>f</sub> = 0.57 (toluene).

<sup>1</sup>H NMR (400 MHz, CDCl<sub>3</sub>, 25 °C): δ = 7.58-7.53 (6H, m), 7.42 (2H, d, <sup>3</sup>J<sub>HH</sub> = 8.1 Hz), 2.45 (3H, s) ppm.

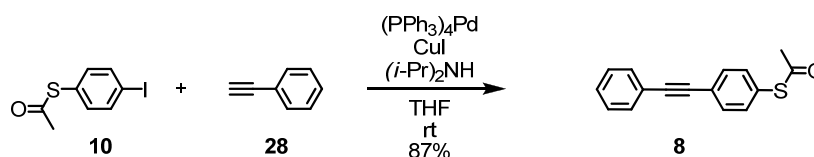
$^{19}\text{F}$ -NMR (376 MHz,  $\text{CDCl}_3$ ,  $\delta$ /ppm, 25 °C): -136.9—137.0 (2F, m); -153.4 (1F, t,  $J$ = 20 Hz); -162.7—162.9 (2F, m) ppm

$^{13}\text{C}$  NMR (101 MHz,  $\text{CDCl}_3$ , 25 °C):  $\delta$  = 193.8, 134.7, 132.6, 132.3, 132.1, 129.0, 124.7, 124.4, 121.9, 91.6, 90.8, 30.7 ppm.

MS (Maldi-TOF):  $m/z$  (%) = 443.9 ( $\text{M}^+$ ).

UV/Vis:  $\lambda_{\text{max}}$  326, 347 nm.

### 1-acetylsulfanyl-4-phenylethynylbenzene (**8**)<sup>8</sup>



**10** (126 mg, .45 mmol, 1.0 eq.) and **28** (59.7  $\mu\text{l}$ , 55.5 mg, 0.54 mmol, 1.2 eq.) were dissolved in a well degassed mixture of 5 ml dry THF and 1ml diisopropylamine.  $\text{Pd}(\text{PPh}_3)_4$  (52 mg, 10 mol%) and  $\text{CuI}$  (9 mg, 10 mol%) were added. The reaction mixture was stirred at room temperature for three hours and was then evaporated, absorbed on silica and chromatographed (silica gel, 1x15cm, hex:EtOAc 5:1) to give a beige solid (99 mg, 87%).

Mp.: 99-101 °C (lit.<sup>8</sup> 84-86°C).

TLC  $R_f$  = 0.42 (hexane:EtOAc = 5:1).

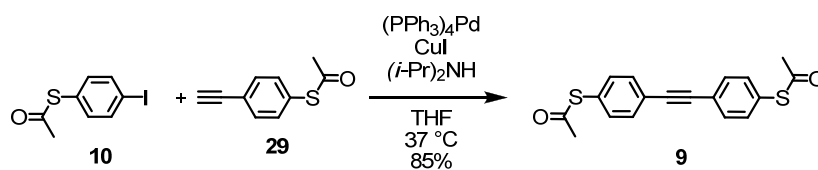
$^1\text{H}$  NMR (250 MHz,  $\text{CDCl}_3$ , 25 °C):  $\delta$  = 7.57-7.52 (4H, m), 7.41-7.34 (5H, m), 2.43 (3H, s) ppm.

$^{13}\text{C}$ -NMR (101 MHz,  $\text{CDCl}_3$ ):  $\delta$ = 193.9, 134.6, 132.6, 132.1, 129.0, 128.8, 128.4, 125.0, 123.3, 91.5, 89.0, 30.7 ppm.

UV/Vis:  $\lambda_{\text{max}}$  293, 310 nm; MS (EI): 252 ( $\text{M}^+$ , 18%), 210 (100%).

EA (calcd, found for  $\text{C}_{16}\text{H}_{12}\text{OS}$ ): C (76.16, 76.12), H (4.79, 4.88,).



**1,2-bis(4-acetylsulfanyl-phenyl)ethyne (9)**

The iodide **10** (238 mg, 0.856 mmol, 1.0 eq.) and the acetylene **29** (155 mg, 0.880 mmol, 1.03 eq.) were dissolved in a degassed mixture of 12 ml dry THF and 3 ml diisopropylamine in a 25-ml-Schlenktube. Pd(PPh)<sub>3</sub> (22.0 mg, 0.019 mmol, 2.2 mol%) and CuI (3.4 mg, 0.019 mmol, 2.2 mol%) were added and the reaction mixture was stirred for 4 hours at room temperature and three hours at 37 °C. The reaction mixture was then evaporated and the crude was purified by column chromatography (silica gel, 3x12 cm, hex:EtOAc = 5:1 -> 2 :1) to give the product **9** as colorless solid (236 mg, 0.723 mmol, 85%).

TLC R<sub>f</sub> = 0.24 (hexane:EtOAc = 5:1).

<sup>1</sup>H NMR (250 MHz, CDCl<sub>3</sub>, 25 °C): δ = 7.56 (4H, d, <sup>3</sup>J<sub>HH</sub> = 8.3 Hz), 7.41 (4H, d, <sup>3</sup>J<sub>HH</sub> = 8.3 Hz), 2.44 (s, 6H) ppm.

<sup>13</sup>C-NMR (101 MHz, CDCl<sub>3</sub>): δ = 193.3, 134.2, 132.2, 128.4, 124.1, 90.2, 30.3 ppm.

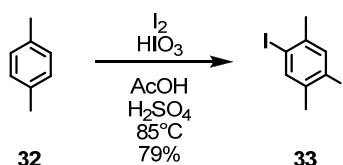
MS (Maldi-TOF): *m/z* (%) = 326.24 (M<sup>+</sup>).

## 7.2.2 Molecular Switches

### 7.2.2.1 Coordination Induced Switches

#### 7.2.2.1.1 1<sup>st</sup> Generation Cruciform Structures

##### 2,5-diiodo-*para*-xylene (**33**)



*p*-Xylene (12.24 ml, 10.60 g, 100 mmol, 1.0 eq.), iodine (20.3 g, 0.08 mol, 0.8 eq.) and iodic acid (HIO<sub>3</sub>, 7.8 g, 0.044 mol, 0.44 eq.) were dissolved in 50 ml glacial acetic acid, 5 ml concentrated sulfuric acid, 5 ml water and 5 ml chloroform. It was stirred at 85 °C for 4 hours. The reaction mixture was poured into 200 ml 10 % aq. NaHSO<sub>3</sub>. The insoluble material was filtered off and washed with methanol. The solid was recrystallized from ethyl acetate/methanol to give **33** as colorless crystals (28.33 g, 79.2 mmol, 79 %).

TLC: R<sub>f</sub> = 0.64 (hexane : ethyl acetate 20:1).

<sup>1</sup>H-NMR (250 MHz, CDCl<sub>3</sub>, δ/ppm): 7.65 (2H, s); 2.34 (6H, s).

<sup>13</sup>C-NMR (101 MHz, CDCl<sub>3</sub>, δ/ppm): 141.1, 139.7, 101.0, 27.3.

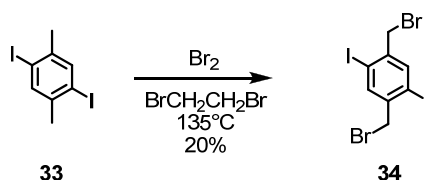
MS (FAB): 357 (100 %, M<sup>+</sup>); 230 (22 %); 104 (31 %).

EA: calculated: C = 26.84, H = 2.25, found: C = 26.87, H = 2.26.

Mp: 102-104°C.

Ir: 2972.1, 2910.4, 1433.0.

##### 1,4-bis(bromomethyl)-2,5-diiodobenzene (**34**)



2,5-diiodo-*p*-xylene (17.72 g, 49.5 mmol, 1.0 eq.) was dissolved in 200 ml 1,2-dibromoethane. Bromine (15.83 g, 5.07 ml, 99 mmol, 2.0 eq.) was added and it was heated to 135 °C for 6 hours. Another equivalent of Br<sub>2</sub> was added (2.5 ml, 49.5 mmol, 1.0 eq.). The mixture was stirred over night at 135 °C, cooled to room

temperature, poured into 200 ml 10 % aq. NaHSO<sub>3</sub> and extracted. In the organic phase a precipitate was formed that was filtered off and recrystallized from chloroform to give colorless needles (5.1 g, 10.0 mmol, 20%).

TLC: R<sub>f</sub> = 0.15 (hexane)

<sup>1</sup>H-NMR (250 MHz, CDCl<sub>3</sub>, δ/ppm): 7.90 (2H, s); 4.48 (4H, s).

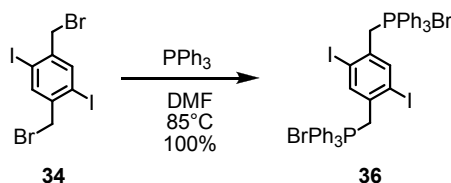
MS (EI): 515 (22 %, M<sup>+</sup>); 434 (100 %); 388 (14 %); 355 (69 %); 228 (7 %).

EA: calculated: C = 18.63, H = 1.17, found: C = 18.79, H = 1.10.

Mp: 221-222 °C

IR(neat, ν, cm<sup>-1</sup>): 3066.6, 3028.0, 1431.1, 1045.4.

### 1,4-bis(bromidetriphenylphosphinemethyl)-2,5-diiodobenzene (36)



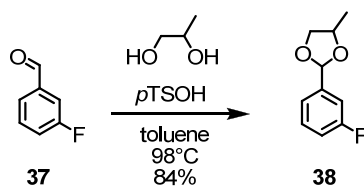
1,4-bis(bromomethyl)-2,5-diiodobenzene (1.960 g, 3.82 mmol, 1.0 eq.) was dissolved in 36 ml dry DMF at 85 °C. PPh<sub>3</sub> (2.002 g, 7.64 mmol, 2.0 eq.) was added. The homogeneous solution was stirred at 85 °C. After 5 minutes a white precipitate was formed. The reaction mixture was cooled to room temperature. The precipitate was filtered off washed with toluene and dried under high vacuum to give **36** as a white powder (3.97 g, 3.82 mmol, 100 %).

<sup>1</sup>H-NMR (250 MHz, CDCl<sub>3</sub>, δ/ppm): 7.69 (32H, m), 5.70 (4H, sb).

MS (FAB): 440 (38%, M<sup>2+</sup>), 307 (15%), 262 (100%).

Mp: 276-277 °C.

IR(neat, ν, cm<sup>-1</sup>): 2823.6, 1666.4, 1434.9, 1099.4.

**2-(3-fluorophenyl)-4-methyl-1,3-dioxolane (38)**

3-fluorobenzaldehyde (2.00 ml, 19.0 mmol, 1.0 eq) was dissolved in 30 ml toluene. Molecular sieves (3 Å) and *para*-toluenesulfonic acid (1.70 g, 9 mmol, 50 mol%) was added. It was stirred over night at 100°C. The reaction mixture was filtrated over 1 cm silica gel, washed with CH<sub>2</sub>Cl<sub>2</sub> and evaporated. The product was purified by column chromatography (CC) (silica gel, 3 x 5 cm, CH<sub>2</sub>Cl<sub>2</sub>) to get a colorless liquid (2.73 g, 15.0 mmol, 79 %).

TLC: R<sub>f</sub> = 0.51 (CH<sub>2</sub>Cl<sub>2</sub>/hexane, 1:1);

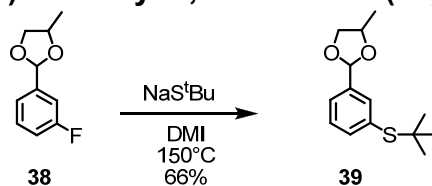
<sup>1</sup>H-NMR (250 MHz, CDCl<sub>3</sub>, δ/ppm): 7.39-7.16 (3H, m), 7.05 (1H, m), 5.95-5.80 (1H, 2s), 4.2-4.31 (1H, m), 4.27-4.10 (1H, m), 3.62-3.53 (1H, m), 1.41-1.34 (3H).

<sup>13</sup>C-NMR (101 MHz, CDCl<sub>3</sub>, δ/ppm): 164.4, 162.0, 141.7, 141.0, 130.4, 130.3, 122.7, 122.4, 116.4, 116.2, 113.8, 113.5, 103.5, 102.6, 74.1, 72.9, 72.4, 18.9, 18.7.

MS (FAB): 181 (100 %, M<sup>+</sup>), 137 (24 %), 123 (94 %).

EA: calculated: C = 65.92, H = 6.09, found: C = 65.59, H = 6.16.

IR (neat, ν, cm<sup>-1</sup>): 2977.9, 2877.6, 1593.1, 1454.2, 1091.6.

**2-(3-(tert-butylthio)phenyl)-4-methyl-1,3-dioxolane (39)**

2-(3-fluorophenyl)-4-methyl-1,3-dioxolane (**38**) (11.22 g, 61.6 mmol, 1.0 eq.) was dissolved in 120 ml DMI. Sodium 2-methyl-2-propanethiolate (13.8 g, 123.2 mmol, 2.0 eq.) was added and the reaction was stirred over night at 150°C. The reaction mixture was extracted with water and toluene. The organic phase was washed with water. The aqueous phase was washed three times with toluene. The combined organic phases were dried over Na<sub>2</sub>SO<sub>4</sub> and evaporated. The crude was purified by CC (silica gel, 5 x 12 cm, toluene/CH<sub>2</sub>Cl<sub>2</sub>, 3:2) to give **39** as a colorless liquid (10.24 g, 40.6 mmol, 66%).

TLC: R<sub>f</sub> = 0.45 (toluene/CH<sub>2</sub>Cl<sub>2</sub>, 3:2).

$^1\text{H-NMR}$  (250 MHz,  $\text{CDCl}_3$ ,  $\delta/\text{ppm}$ ): 7.68-7.19 (4H, m), 5.99-5.84 (1H, 2s), 4.46-4.13 (2H, m), 3.67-3.57 (1H, m), 1.40-1.35 (3H, m), 1.32 (9H, s).

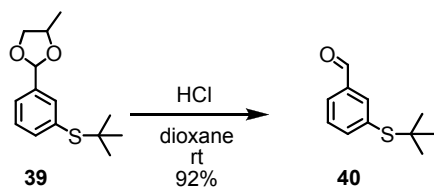
$^{13}\text{C-NMR}$  (101 MHz,  $\text{CDCl}_3$ ,  $\delta/\text{ppm}$ ): 139.5, 138.8, 138.4, 133.2, 128.9, 127.4, 127.2, 104.1, 103.1, 74.0, 72.8, 72.4, 71.8, 46.4, 31.4, 19.0, 18.8.

MS (EI): 252 (32 %,  $\text{M}^+$ ), 196 (100 %), 163 (7%), 137 (30 %).

EA: calculated: C = 66.63, H = 7.99, found: C = 66.66, H = 7.94.

IR(neat,  $\nu$ ,  $\text{cm}^{-1}$ ): 2939.3, 2862.2, 1685.7, 1504.3, 1442.7, 1396.37.

### 3-(*tert*-butylthio)benzaldehyde (**40**)



**39** (8.98 g, 35.6 mmol) was dissolved in 100 ml dioxane. 70 ml 0.5 M HCl was added. The reaction mixture was stirred at room temperature for one hour and was then extracted with water and toluene. The organic phase was dried over  $\text{Na}_2\text{SO}_4$ , filtrated and evaporated. The crude product was purified by CC (silica gel, 5x13 cm, hexane: ethyl acetate 20:1) to give **40** as a yellow liquid (6.345 g, 32.7 mmol, 92 %).

TLC:  $R_f$  = 0.21 (hexane: ethyl acetate 20:1).

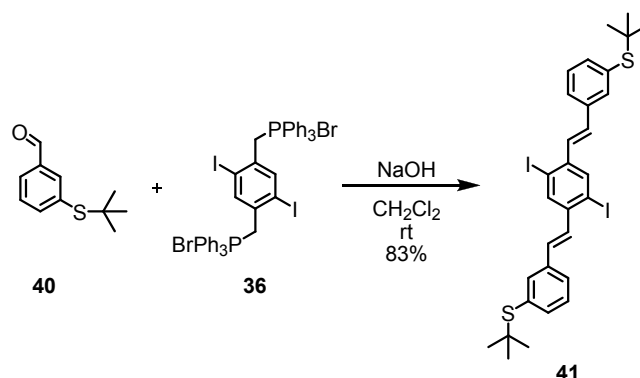
$^1\text{H-NMR}$  (250 MHz,  $\text{CDCl}_3$ ,  $\delta/\text{ppm}$ ): 10.05 (1H, s), 8.04 (1H, st,  $^4J_{\text{HH}} = 1.84$  Hz); 7.91 (1H, dt,  $^3J_{\text{HH}} = 7.70$  Hz,  $^4J_{\text{HH}} = 1.34$  Hz); 7.82 (1H, dt,  $^3J_{\text{HH}} = 7.70$  Hz,  $^4J_{\text{HH}} = 1.34$  Hz); 7.53 (1H, t,  $^3J_{\text{HH}} = 7.70$  Hz); 1.33 (9H, s).

$^{13}\text{C-NMR}$  (101 MHz,  $\text{CDCl}_3$ ,  $\delta/\text{ppm}$ ): 192.2, 143.6, 138.9, 137.1, 134.8, 130.0, 129.6, 46.8, 31.4.

MS (FAB): 194 (19 %,  $\text{M}^+$ ), 138 (100 %), 109 (11 %).

EA: calculated: C = 68.00, H = 7.26, found: C = 68.04, H = 7.41.

IR(neat,  $\nu$ ,  $\text{cm}^{-1}$ ): 2962.5, 2862.2, 1701.1, 1570.0, 1199.6.

**1,4-bis(3-thio-*tert*-butyl-styryl)-2,5-diiodobenzene (41)**

**40** (1.68 g, 8.65 mmol, 3.0 eq.) was dissolved in 150 ml  $\text{CH}_2\text{Cl}_2$ . The phosphonium salt **36** (3.00 g, 2.88 mmol, 1.0 eq.) was added. 100 ml aq. 50 % NaOH were added and it was stirred for 2.5 days at room temperature. The reaction mixture was then extracted. The aqueous phase was washed twice with dichloromethane. The combined organic phases were dried over  $\text{Na}_2\text{SO}_4$ , filtrated and evaporated. The crude was chromatographed (silica gel, 3x12 cm,  $\text{CH}_2\text{Cl}_2$ ) to give an isomeric mixture in 83% yield. The isomers were refluxed in toluene containing iodine in catalytic amount over night. The EE-product was precipitating. It was filtrated off and washed with hexane to give a yellow solid. (1.43 g, 2.01 mmol, 70%).

TLC:  $R_f = 0.30$  (hexane: ethyl acetate 20:1).

$^1\text{H-NMR}$  (250 MHz,  $\text{CDCl}_3$ ,  $\delta/\text{ppm}$ ): 8.12 (2H, s); 7.74 (2H, s), 7.60 (2H, d,  $^3J_{\text{HH}} = 7.70$  Hz), 7.51 (2H, d,  $^3J_{\text{HH}} = 7.70$  Hz), 7.39 (2H, t,  $^3J_{\text{HH}} = 7.70$  Hz), 7.25 (2H, d,  $^3J_{\text{HH}} = 16.06$  Hz), 7.00 (2H, d,  $^3J_{\text{HH}} = 15.73$  Hz), 1.36 (18H, s).

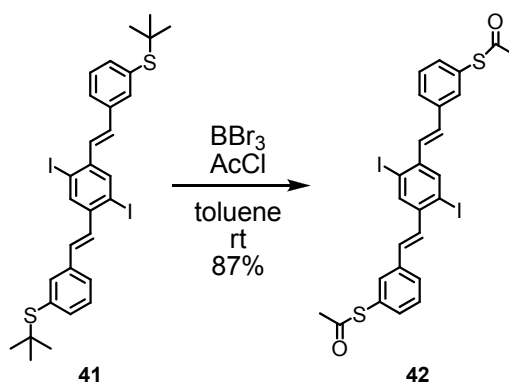
$^{13}\text{C-NMR}$  (101 MHz,  $\text{CDCl}_3$ ,  $\delta/\text{ppm}$ ): 141.2, 137.6, 137.4, 136.8, 136.4, 133.8, 132.2, 131.5, 129.3, 127.4, 100.7, 46.5, 31.4.

MS (EI): 710 (15 %,  $\text{M}^+$ ); 653 (11 %); 598 (46 %); 551 (12 %); 469 (5 %).

EA: calculated: C = 50.71, H = 4.54, found: C = 50.24, H = 4.46.

Mp: 247-248°C.

IR(neat, v,  $\text{cm}^{-1}$ ): 3055.0, 2958.6, 2858.3, 1809.1, 1566.1, 1454.2.

**1,4-bis(3-thio-acetyl-styryl)-2,5-diiodobenzene (42)**

1,4-bis(3-thio-*tert*-butyl-styryl)-2,5-diiodobenzene (**41**) (2.13 g, 3.00 mmol, 1.0 eq.) was dissolved in a degassed mixture of 500 ml dry toluene and 100 ml acetyl chloride. 6 ml of a 1M solution of  $\text{BBr}_3$  in  $\text{CH}_2\text{Cl}_2$  (1.408 mol, 2.0 eq.) was added. The reaction was stirred for one hour at room temperature. Another 4.5 ml of the 1M solution of  $\text{BBr}_3$  solution in  $\text{CH}_2\text{Cl}_2$  was added and it was stirred for another hour at room temperature. While cooling with an ice-bath, the reaction mixture was quenched with water. The product precipitated as a yellow solid, which was filtrated off and washed with water. The organic phase was washed with water, evaporated and recrystallized from toluene to give more of product **52** (1.75 g, 2.56 mmol, 87%).

TLC:  $R_f = 0.43$  ( $\text{CH}_2\text{Cl}_2$ );

$^1\text{H-NMR}$  (250 MHz,  $\text{CDCl}_3$ ,  $\delta/\text{ppm}$ ): 8.06 (2H, s), 7.59 (2H, d,  $^3J_{\text{HH}} = 7.58$  Hz), 7.58 (2H, d,  $^4J_{\text{HH}} = 1.52$  Hz), 7.44 (2H, t,  $^3J_{\text{HH}} = 7.58$  Hz), 7.35 (2H, d,  $^3J_{\text{HH}} = 7.58$  Hz), 7.19 (2H, d,  $^3J_{\text{HH}} = 15.66$  Hz), 6.96 (2H, d,  $^3J_{\text{HH}} = 16.17$  Hz), 2.46 (6H, s).

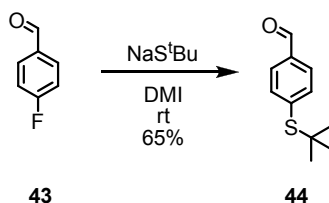
$^{13}\text{C-NMR}$  (101 MHz,  $\text{CDCl}_3$ ,  $\delta/\text{ppm}$ ): 194.2, 141.2, 138.1, 136.9, 134.6, 133.3, 131.9, 131.8, 130.0, 129.1, 128.2, 100.7, 30.7.

MS (EI) : 681 (84%,  $\text{M}^+$ ), 639 (34%), 597 (49%).

EA: calculated: C = 45.76, H = 2.95, found: C = 46.20, H = 2.95.

Mp: 214-215°C.

IR(neat, v,  $\text{cm}^{-1}$ ): 3051.1, 2958.6, 1890.1, 1697.2, 1118.6.

**4-(*tert*-butylthio)benzaldehyde (44)**

4-fluoro-benzaldehyde (174mg, 1.85 mmol, 1.0 eq.) was dissolved in 15 ml DMI. NaS<sup>t</sup>Bu (312mg, 2.78 mmol, 1.5 eq.) was added and it was stirred for 20 hours at room temperature. The reaction mixture was then extracted with water and TBME, the combined organic phases were dried over Na<sub>2</sub>SO<sub>4</sub>, filtrated, evaporated and chromatographed (silica gel, 3x12 cm, TBME:hexane 1:3) to give a colorless liquid that tends to crystallize (266mg, 1.37 mmol, 74%).

TLC: R<sub>f</sub> = 0.47 (TBME:hexane, 1:3).

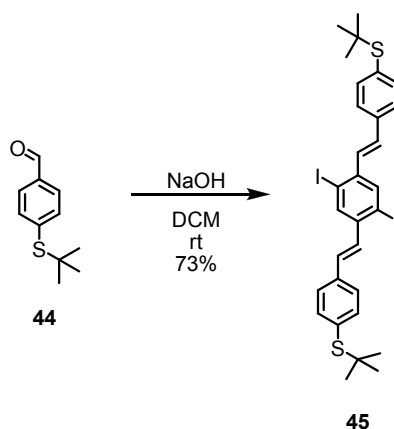
<sup>1</sup>H-NMR (250 MHz, CDCl<sub>3</sub>, δ/ppm): 10.01 (1H, s); 7.81 (2H, d, <sup>3</sup>J<sub>HH</sub> = 8.59 Hz); 7.66 (2H, d, <sup>3</sup>J<sub>HH</sub> = 8.08 Hz); 1.32 (9H, s).

<sup>13</sup>C-NMR (101 MHz, CDCl<sub>3</sub>, δ/ppm): 192.1, 141.7, 137.4, 136.2, 129.8, 47.6, 31.5.

MS (EI): 194.0 (18.5%, M<sup>+</sup>); 138.0 (94.9%); 109.0 (13.8%).

EA: calculated: C = 68.00, H = 7.26, found: C = 68.21, H = 7.41.

IR(neat, ν, cm<sup>-1</sup>): 2962.5, 1701.1, 1593.1, 1164.9.

**1,4-bis(4-thio-*tert*-butyl-styryl)-2,5-diiodobenzene (45)**

**44** (190 mg, 0.98 mmol, 3.0 eq.) and the phosphonium salt (**36**) (340mg, 0.33 mmol, 1.0 eq.) were dissolved in 7 ml CH<sub>2</sub>Cl<sub>2</sub>. 6ml 50% aq. NaOH were added and it was stirred vigorously for 69 hours. The reaction mixture was then extracted with water/toluene. The combined organic phases were dried over Na<sub>2</sub>SO<sub>4</sub>, filtrated, evaporated and chromatographed (silica gel, 2x12 cm, CH<sub>2</sub>Cl<sub>2</sub>). The isomeric mixture



was then refluxed in toluene with catalytic amounts of iodine over night. It was then extracted with 10% aq. NaHSO<sub>3</sub>, washed with water, dried over Na<sub>2</sub>SO<sub>4</sub>, evaporated and recrystallized from toluene to get **45** as a yellow solid (170 mg, 0.24 mmol, 73%).

TLC: R<sub>f</sub> = 0.74 (CH<sub>2</sub>Cl<sub>2</sub>).

<sup>1</sup>H-NMR (250 MHz, CDCl<sub>3</sub>, δ/ppm): 8.08 (2H, s), 7.53 (8H, m), 7.24 (2H, d, <sup>3</sup>J<sub>HH</sub> = 16.06 Hz), 6.98 (2H, d, <sup>3</sup>J<sub>HH</sub> = 16.06 Hz), 1.32 (18H, s).

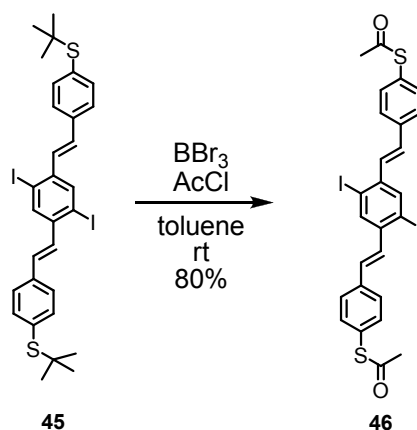
<sup>13</sup>C-NMR (101 MHz, CDCl<sub>3</sub>, δ/ppm): 141.1, 138.2, 137.2, 136.8, 133.5, 132.1, 131.7, 127.3, 100.8, 46.8, 31.4.

MS (EI): 710.0 (42.3%, M<sup>+</sup>); 597.8 (100%).

EA: calculated: C = 50.71, H = 4.54, found: C = 50.74, H = 4.55;

IR(neat, ν, cm<sup>-1</sup>): 3018.9, 2954.7, 2858.3, 1892.5, 1356.3.

Mp: 232-233 °C.

**1,4-bis(4-thio-acetyl-styryl)-2,5-diiodobenzene (46)**

**45** (356 mg, 0.521 mmol, 1.0 eq.) was dissolved in a degassed mixture of 85 ml dry toluene and 15 ml concentrated AcCl.  $\text{BBr}_3$  (1M in  $\text{CH}_2\text{Cl}_2$ , 3.6 ml, 3.6 mmol, 6.9 eq.) was added portion wise during 2.5 hours at room temperature. The reaction mixture was quenched with water at  $0^\circ\text{C}$ . A precipitate was formed which was filtered off and recrystallized from toluene to give **46** as a yellow solid (283 mg, 0.41 mmol, 80%).

TLC:  $R_f = 0.48$  ( $\text{CH}_2\text{Cl}_2$ ).

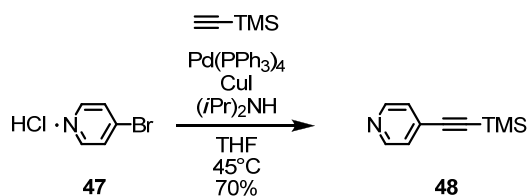
Mp:  $253\text{-}255^\circ\text{C}$ .

$^1\text{H-NMR}$  (250 MHz,  $\text{CDCl}_3$ ,  $\delta/\text{ppm}$ ): 8.08 (2H, s), 7.59 (4H, d,  $^3J_{\text{HH}} = 8.37$  Hz), 7.43 (4H, d,  $^3J_{\text{HH}} = 8.37$  Hz), 7.24 (2H, d,  $^3J_{\text{HH}} = 16.06$  Hz), 6.97 (2H, d,  $^3J_{\text{HH}} = 16.16.40$  Hz), 2.45 (6H, s).

MS (EI) : 681.8 (76%,  $\text{M}^+$ ), 639.8 (56%), 597.8 (100%).

EA: calculated: C = 45.76, H = 2.95, found: C = 45.81, H = 2.97.

IR(neat,  $\nu$ ,  $\text{cm}^{-1}$ ): 2920.0, 2854.5, 1905.5, 1689.5, 1122.5.

**4-(2-(trimethylsilyl)ethynyl)pyridine (48)**

4-bromo-pyridine (1.00 g, 5.14 mmol, 1.0 eq.) and 2-(trimethylsilyl)ethynyl (1.3 ml, 9.26 mmol, 1.8 eq.) were suspended in a well degassed solution of 50 ml dry THF and 5 ml diisopropylamine. It was degassed for another 20 minutes.  $\text{Pd}(\text{PPh}_3)_4$  (300 mg, 0.26 mmol, 5 mol%) and  $\text{CuI}$  (95 mg, 0.51 mmol, 10 mol%) were added. It was stirred for 2.5 hours at room temperature. The reaction mixture was filtrated over

2 cm silica gel, washed with THF, evaporated and chromatographed (silica gel, 3x12 cm, hexane:ethyl acetate = 5:1) to give a yellowish liquid that tends to crystallize (635 mg, 3.62 mmol, 70%). The reaction was performed in absence of light.

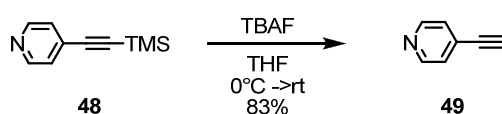
TLC:  $R_f = 0.15$  (EtOAc:hexane=1:5).

$^1\text{H-NMR}$  (250 MHz,  $\text{CDCl}_3$ ,  $\delta/\text{ppm}$ ): 8.58 (2H, d,  $^3J_{\text{HH}} = 6.02$  Hz); 7.33 (2H, d,  $^3J_{\text{HH}} = 6.36$  Hz); 0.29 (9H, s).

$^{13}\text{C-NMR}$  (101 MHz,  $\text{CDCl}_3$ ,  $\delta/\text{ppm}$ ): 150.1, 131.6, 126.2, 102.3, 100.4, 0.1.

MS(EI): 175 ( $\text{M}^+$ ), 160 ( $\text{M}^+ - \text{CH}_3$ ), 130 ( $\text{M}^+ - (\text{CH}_3)_3$ ).

#### 4-(ethynyl)pyridine (**49**)

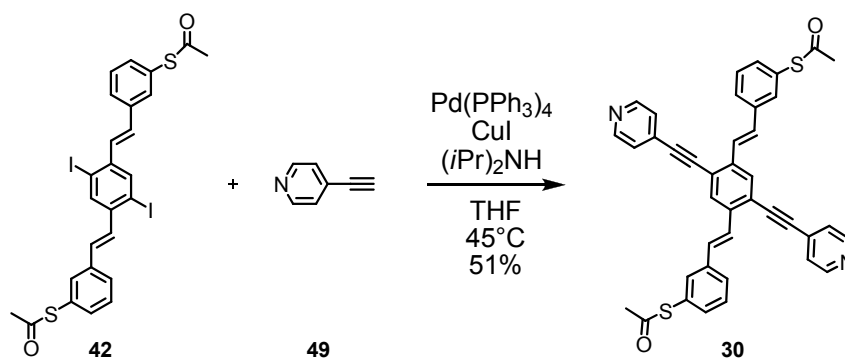


4-(2-(trimethylsilyl)ethynyl)pyridine (**48**) (516 mg, 2.94 mmol, 1.0 eq.) was dissolved in 20 ml dry THF. 12 ml 1M TBAF-solution (12 mmol, 4.1 eq.) in THF was added at 0°C. The reaction mixture was allowed to come to room temperature, stirred for 1 hour and was then evaporated, dissolved in  $\text{CH}_2\text{Cl}_2$ , absorbed on silica gel, evaporated and chromatographed in the dark (silica gel, 2x12cm, hex:EtOAc 1:1) to give **49** as a light sensitive colorless solid (251 mg, 2.43 mmol, 83%).

$^1\text{H-NMR}$  (400 MHz,  $\text{CDCl}_3$ ,  $\delta/\text{ppm}$ ): 8.60 (2H, d,  $^3J_{\text{HH}} = 6.06$  Hz); 7.35 (2H, d,  $^3J_{\text{HH}} = 6.06$  Hz); 3.30 (1H, s).

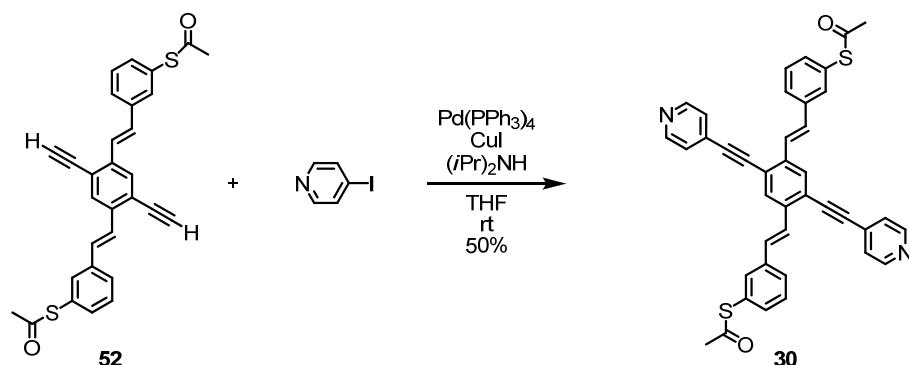
$^{13}\text{C-NMR}$  (101 MHz,  $\text{CDCl}_3$ ,  $\delta/\text{ppm}$ ): 150.2, 130.7, 126.4, 82.2, 81.3.

MS(EI): 103 ( $\text{M}^+$ ).

**1,4-bis(3-thio-acetyl-styryl)-2,5-bis(ethynyl-4-pyridine)benzene (30)**

4-(Ethynyl)pyridine (**49**) (2.2 eq., 1.65 mmol, 170 mg), 1,4-bis(3-thio-acetyl-styryl)-2,5-diiodobenzene (**42**) (1.0 eq., 0.76 mmol, 520 mg),  $\text{Pd}(\text{PPh}_3)_4$  (10 mol%, 87 mg) and  $\text{CuI}$  (10 mol%, 14 mg) were dissolved in a well degassed mixture of 90 ml dry THF and 10 ml diisopropylamine. The reaction mixture was stirred for 24 hours at  $45^\circ\text{C}$  and was then poured to a mixture of 250 ml hexane and 250 ml aq. 5%  $\text{NH}_4\text{OH}$ . The precipitated solid was collected, dissolved in a minimum amount of  $\text{CH}_2\text{Cl}_2$  and dropped to 250 ml rapidly stirring hexane. The precipitate was collected and recrystallized from toluene/ $\text{CH}_2\text{Cl}_2$  to give **30** as a yellow solid (246 mg, 0.39 mmol, 51%).

f)



1,4-bis(3-Thio-acetyl-styryl)-2,5-bis(ethynyl)benzene (**52**) (1.0 eq., 0.167 mmol, 80 mg) was dissolved in a degassed mixture of 15 ml dry THF and 2.5 ml diisopropylamine. Then 4-iodo-pyridine (75 mg, 2.2 eq., 0.368 mmol),  $\text{Pd}(\text{PPh}_3)_4$  (10 mol%, 42 mg) and  $\text{CuI}$  (10 mol%, 7 mg) was added. The reaction mixture was stirred for 24 hours room temperature respectively and was then poured to a mixture of 100 ml hexane and 100 ml aq. 5%  $\text{NH}_4\text{OH}$ . The precipitated solid was collected, dissolved in a minimum amount of  $\text{CH}_2\text{Cl}_2$  and dropped to 200 ml rapidly stirring hexane. The precipitate was collected and recrystallized from toluene/ $\text{CH}_2\text{Cl}_2$  to give **30** as a yellow solid. (52 mg, 50%).

$^1\text{H-NMR}$  (250 MHz,  $\text{CDCl}_3$ ,  $\delta/\text{ppm}$ ): 8.67 (4H, d,  $^3J_{\text{HH}} = 6.06$  Hz), 7.92 (2H, s), 7.64 (2H, s), 7.61 (2H, d,  $^3J_{\text{HH}} = 16.67$  Hz), 7.58 (2H, d,  $^3J_{\text{HH}} = 8.08$  Hz), 7.46 (4H, d,  $^3J_{\text{HH}} = 6.06$  Hz), 7.45 (2H, t,  $^3J_{\text{HH}} = 8.08$  Hz), 7.35 (2H,  $^3J_{\text{HH}} = 7.58$  Hz), 7.26 (2H, d,  $^3J_{\text{HH}} = 16.67$  Hz), 2.47 (6H, s).

$^{13}\text{C-NMR}$  (101 MHz,  $\text{CDCl}_3$ ,  $\delta/\text{ppm}$ ): 194.4, 150.4, 138.5, 138.1, 134.3, 133.1, 131.3, 131.0, 130.1, 129.8, 129.2, 128.2, 126.5, 125.9, 122.5, 93.7, 92.1, 30.8;

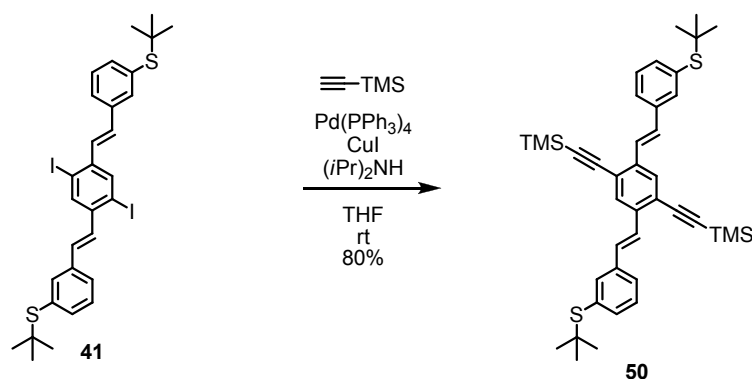
MS (MALDI): 632 ( $\text{M}^+$ ).

Mp: 227.7-228.7°C (melting followed by decomposition).

IR(neat,  $\nu$ ,  $\text{cm}^{-1}$ ): 3049.7, 3008.3, 2201.1, 1699.2, 1588.3, 953.7.

GPC (oligopore  $6\mu\text{m}$ , toluene, UV/VIS photodiode array detector): area: 99.6%.

### 1,4-bis(3-thio-*tert*-butyl-styryl)-2,5-bis(ethynyltrimethylsilyl)benzene (**50**)



1,4-bis(3-thio-*tert*-butyl-styryl)-2,5-diodobenzene (**41**) (140 mg, 0.197 mmol, 1.0 eq.) and trimethylsilylacetylene (96.8 mg, 0.985 mmol, 5.0 eq.) were dissolved in a well degassed solution of 20 ml dry THF and 7 ml diisopropylamine. It was degassed for another 20 minutes.  $\text{Pd(PPh}_3)_4$  (23 mg, 0.020 mmol, 10 mol%) and  $\text{CuI}$  (4 mg, 0.020 mmol, 10 mol%) were added and it was stirred at room temperature for 1.5 hours. Another two equivalents of trimethylsilylacetylene (38.7 mg, 0.394 mmol, 2.0 eq) were added and it was stirred for one hour. The reaction mixture was then evaporated. The crude was dissolved in  $\text{CH}_2\text{Cl}_2$ , absorbed on silica gel, evaporated and chromatographed (silica gel, 1x12 cm, toluene) to give a yellow solid (102 mg,  $\text{C}_{40}\text{H}_{50}\text{S}_2\text{Si}_2$ , 651.13 g/mol, 79.8%).

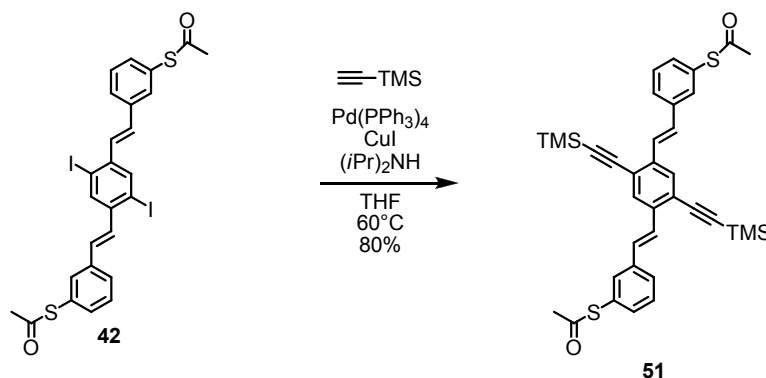
TLC:  $R_f = 0.69$  (toluene).

$^1\text{H-NMR}$  (250 MHz,  $\text{CDCl}_3$ ,  $\delta/\text{ppm}$ ): 7.85 (2H, s); 7.75 (2H, s); 7.64 (2H, d,  $^3J_{\text{HH}} = 16.40$  Hz); 7.56 (2H, d,  $^3J_{\text{HH}} = 7.70$  Hz); 7.49 (2H, d,  $^3J_{\text{HH}} = 7.04$  Hz); 7.37 (2H, t,  $^3J_{\text{HH}} = 7.53$  Hz); 7.23 (2H, d,  $^3J_{\text{HH}} = 16.40$  Hz); 1.36 (18 H, s); 0.37 (12 H, s).

$^{13}\text{C}$ -NMR (101 MHz,  $\text{CDCl}_3$ ,  $\delta/\text{ppm}$ ): 138.5 (2C, s, Cq); 147.9 (2C, s, Cq); 137.7 (2C, s, Cq); 134.8 (2C, s, Cq); 134.6 (2C, s, Ct); 133.1 (2C, s, Ct); 131.4 (2C, s, Ct); 129.7 (2C, s, Ct); 128.9 (2C, s, Ct); 128.7 (2C, s, Ct); 103.4 (2C, s, Cq); 101.2 (2C, s, Cq); 46.4 (2C, s, Cq); 31.5 (6C, s, Cp); 0.5 (6C, s, Cp).

MS (MALDI): 650, 651 ( $\text{M}^+$ ), 652.

### 1,4-bis(3-thio-acetyl-styryl)-2,5-bis(ethynyltrimethylsilyl)benzene (**51**)



1,4-bis(3-thio-acetyl-styryl)-2,5-diodobenzene (**42**) (285 mg, 0.418 mmol, 1.0 eq.) was suspended in a well degassed solution of 75 ml dry THF and 30 ml  $(i\text{-Pr})_2\text{NH}$ . Ethynyltrimethylsilane (0.3 ml, 2.09 mmol, 5.0 eq.) was added and it was degassed for another 20 minutes.  $\text{Pd}(\text{PPh}_3)_4$  (48 mg, 0.042 mmol, 10 mol%) and  $\text{CuI}$  (4 mg, 0.042 mmol, 10 mol%) were added and it was stirred for 2 hours at  $60^\circ\text{C}$ . The reaction mixture was then evaporated and chromatographed (silica gel,  $2 \times 12\text{cm}$ ,  $\text{CH}_2\text{Cl}_2$ ) to give **51** as a yellow solid (209 mg, 0.335 mmol, 80%).

TLC:  $R_f = 0.56$  ( $\text{CH}_2\text{Cl}_2$ ).

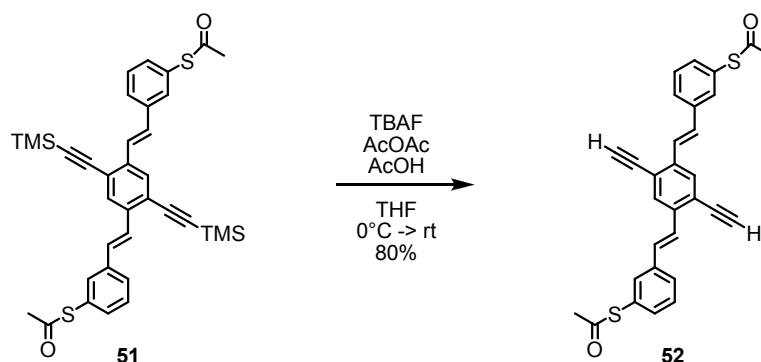
$^1\text{H}$ -NMR (250 MHz,  $\text{CDCl}_3$ ,  $\delta/\text{ppm}$ ): 7.83 (2H, s); 7.64 (2H, d,  $^3J_{\text{HH}} = 16.40$  Hz); 7.63 (2H, s); 7.57 (2H, d,  $^3J_{\text{HH}} = 8.00$  Hz); 7.45 (2H, t,  $^3J_{\text{HH}} = 7.53$  Hz); 7.36 (2H, d,  $^3J_{\text{HH}} = 7.70$  Hz); 7.21 (2H, d,  $^3J_{\text{HH}} = 16.40$  Hz); 2.47 (6H, s); 0.36 (18H, s).

$^{13}\text{C}$ -NMR (101 MHz,  $\text{CDCl}_3$ ,  $\delta/\text{ppm}$ ): 194.2, 138.9, 137.9, 134.2, 132.95, 129.96, 129.8, 129.2, 129.0, 128.2, 127.1, 122.9, 103.3, 101.9, 30.6, 0.4.

MS (EI): 622 (93%,  $\text{M}^+$ ); 580 (34%); 538 (9%).

IR (neat,  $\nu$ ,  $\text{cm}^{-1}$ ): 3061.3, 2957.2, 2156.8, 1705.4, 1246.4.

Mp:  $184\text{--}187^\circ\text{C}$ .

**1,4-bis(3-thio-acetyl-styryl)-2,5-bis(ethynyl)benzene (52)**

**51** (260 mg, 0.417 mmol, 1.0 eq.) was dissolved in 25 ml dry THF, 1.5 ml glacial acetic acid and 2.5 ml acetic anhydride. The solution was degassed before 10 ml of a 1M TBAF solution in THF (10 mmol, 55 eq.) was added at 0°C. The reaction was allowed to come to room temperature. After 20 minutes 5 ml acetic anhydride was added in one portion and it was stirred for another 20 minutes. The reaction mixture was extracted with toluene and water. The organic phase was washed with water, evaporated and chromatographed (silica gel, 2x12 cm, CH<sub>2</sub>Cl<sub>2</sub>) to give a yellow solid (188 mg, 0.393 mmol, 94%).

TLC:  $R_f = 0.75$  (CH<sub>2</sub>Cl<sub>2</sub>).

<sup>1</sup>H-NMR (250 MHz, CDCl<sub>3</sub>,  $\delta$ /ppm): 7.83 (2H, s); 7.58 (2H, d, <sup>3</sup> $J_{HH} = 7.58$  Hz); 7.57 (2H, s); 7.55 (2H, d, <sup>3</sup> $J_{HH} = 16.06$  Hz); 7.43 (2H, dt, <sup>3</sup> $J_{HH} = 7.58$  Hz, <sup>4</sup> $J_{HH} = 1.40$  Hz); 7.34 (2H, d, <sup>3</sup> $J_{HH} = 7.58$  Hz); 7.16 (2H, d, <sup>3</sup> $J_{HH} = 16.06$  Hz); 3.49 (2H, s); 2.45 (6H, s).

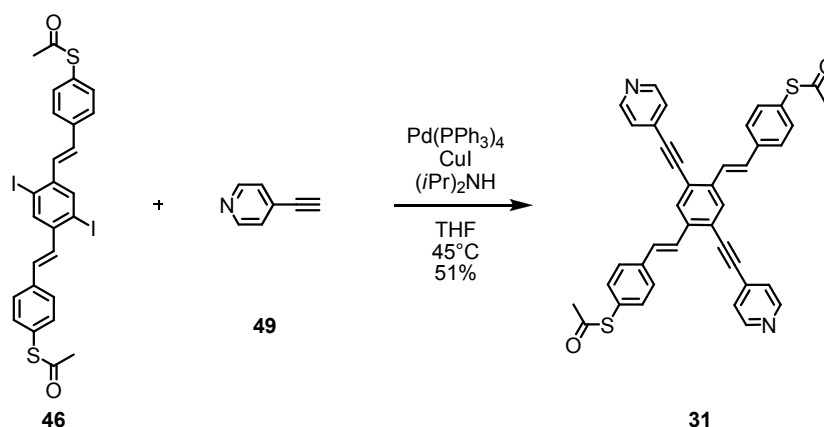
<sup>13</sup>C-NMR (101 MHz, CDCl<sub>3</sub>,  $\delta$ /ppm): 194.3, 138.6, 138.2, 134.4, 133.2, 130.6, 129.9, 128.9, 128.2, 126.6, 122.2, 84.1, 81.8, 30.7.

MS (MALDI) : 478 (M<sup>+</sup>).

IR(neat,  $\nu$ , cm<sup>-1</sup>): 3055.0, 1704.0, 1350.1.

2920.0, 2854.5, 1905.5, 1689.5, 1122.5.

Mp: 214-219°C (followed by decomposition).

**1,4-bis(4-thio-acetyl-styryl)-2,5-bis(ethynyl-4-pyridine)benzene (31)**

**46** (155 mg, 0.227 mmol, 1.0 eq.) was dissolved in a well degassed mixture of 20 ml dry THF and 2.5 ml diisopropylamine. **49** (58.6 mg, 0.568 mmol, 2.5 eq.), Pd(PPh<sub>3</sub>)<sub>4</sub> (20 mg, 0.017 mmol, 7.6 mol%) and CuI (8 mg, 0.042 mmol, 18.5 mol%) were added and it was stirred 7 hours at room temperature and 15 hours at 50°C. The reaction mixture was then poured to a mixture of 50 ml 5% aq. NH<sub>4</sub>OH and 50 ml hexane. The precipitate was filtrated off, dissolved in CH<sub>2</sub>Cl<sub>2</sub> and precipitated into 60 ml rapidly stirring hexane. The insoluble material was collected and recrystallized from toluene to give a yellow solid (75 mg, 0.119 mmol, 52%).

<sup>1</sup>H-NMR (250 MHz, CDCl<sub>3</sub>, δ/ppm): 8.71 (4H, d, <sup>3</sup>J<sub>HH</sub> = 6.36 Hz), 7.97 (2H, s), 7.80 (2H, d, <sup>3</sup>J<sub>HH</sub> = 16.40 Hz), 7.63 (4H, d, <sup>3</sup>J<sub>HH</sub> = 8.34 Hz), 7.48 (4H, d, <sup>3</sup>J<sub>HH</sub> = 6.02 Hz), 7.47 (4H, d, <sup>3</sup>J<sub>HH</sub> = 8.03 Hz), 7.31 (2H, d, <sup>3</sup>J<sub>HH</sub> = 16.06 Hz), 2.48 (6H, s).

<sup>13</sup>C-NMR (101 MHz, CDCl<sub>3</sub>, δ/ppm): 194.3, 150.4, 138.4, 138.4, 138.1, 135.3, 131.3, 131.2, 129.9, 128.2, 127.9, 126.7, 125.8, 122.5, 93.6, 92.0, 30.7.

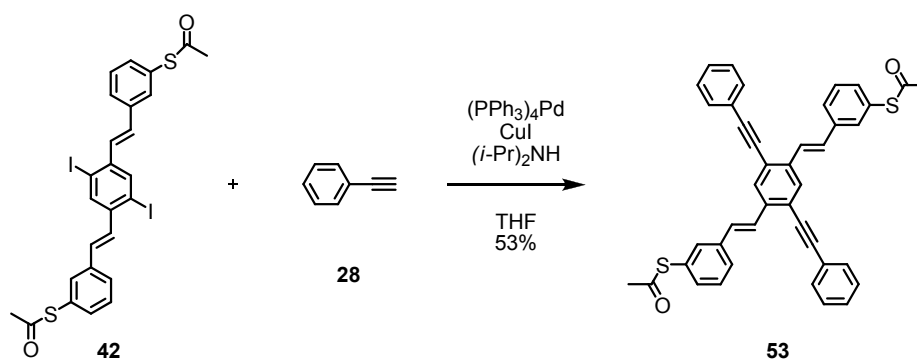
MS(MALDI): 633.6 (100%, M<sup>+</sup>).

IR(neat, ν, cm<sup>-1</sup>): 3046.4, 2217.5, 1699.2, 1588.3.

Mp: decomposition at 192.2°C-199.5°C.

GPC (oligopore 6μm, toluene, UV/VIS photodiode array detector): area: 100 %.



**1,4-bis(3-thio-acetyl-styryl)-2,5-bis(ethynylbenzene)benzene (53)**

**42** (120 mg, 0.176 mmol, 1.0 eq.) was suspended in a well degassed mixture of 10 ml dry THF and 2 ml diisopropylamine. Ethynylbenzene (90 mg, 0.879 mmol, 5.0 eq.),  $\text{Pd}(\text{PPh}_3)_4$  (20 mg, 0.018 mmol, 10 mol%) and  $\text{CuI}$  (4 mg, 0.018 mmol, 10 mol%) were added and it was stirred for 3.5 hours at 40°C, before the reaction mixture was evaporated and chromatographed (silica gel, 2x12 cm,  $\text{CH}_2\text{Cl}_2$ ) to give a yellow solid (58.9 mg, 0.093 mmol, 53%).

$^1\text{H-NMR}$  (250 MHz,  $\text{CDCl}_3$ ,  $\delta/\text{ppm}$ ): 7.90 (2H, s); 7.69 (2H, d,  $^3J_{\text{HH}} = 16.25$  Hz); 7.62 (8H, m); 7.41 (10H, m); 7.26 (2H, d,  $^3J_{\text{HH}} = 16.50$  Hz); 2.45 (6H, s).

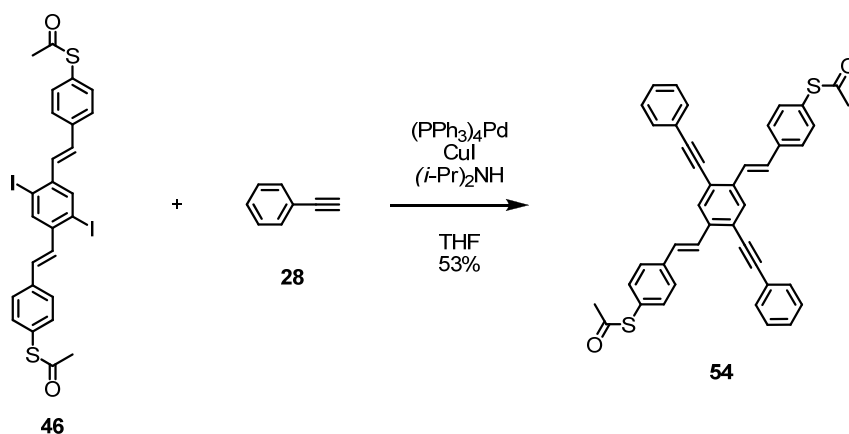
$^{13}\text{C-NMR}$  (101 MHz,  $\text{CDCl}_3$ ,  $\delta/\text{ppm}$ ): 194.2, 138.9, 137.7, 134.1, 133.2, 132.1, 130.2, 130.0, 129.4, 129.1, 129.0, 128.9, 128.0, 127.2, 123.4, 122.9, 96.3, 88.0, 30.7.

MS(EI): 630.2 ( $\text{M}^+$ , 55%); 588 (93%); 546(100%).

IR(neat,  $\nu$ ,  $\text{cm}^{-1}$ ): 3061.8, 3025.4, 2196.7, 1694.8, 1588.3, 959.5.

Mp: melting followed by decomposition at 224.0 – 225.0°C.

GPC (oligopore 6 $\mu\text{m}$ , toluene, UV/VIS photodiode array detector): area: 98.8 %.

**1,4-bis(4-thio-acetyl-styryl)-2,5-bis(ethynylbenzene)benzene (54)**

**46** (14 mg, 0.021 mmol, 1.0 eq.) was suspended in a well degassed mixture of 5 ml dry THF and 0.5 ml diisopropylamine. Ethynylbenzene (10.5mg, 0.103 mmol, 5.0 eq.),  $\text{Pd}(\text{PPh}_3)_4$  (2.5 mg, 0.002 mmol, 10 mol%) and  $\text{CuI}$  (0.5 mg, 0.002 mmol, 10 mol%) were added and it was stirred for 3 hours at room temperature, before the reaction mixture was evaporated and chromatographed (silica gel, 2x12 cm,  $\text{CH}_2\text{Cl}_2$ ) to give a yellow solid (5.6 mg, 0.0089 mmol, 43.3%).

TLC:  $R_f = 0.63$  ( $\text{CH}_2\text{Cl}_2$ ).

$^1\text{H-NMR}$  (250 MHz,  $\text{CDCl}_3$ ,  $\delta/\text{ppm}$ ): 7.93 (2H, s), 7.72 (2H, d,  $^3J_{\text{HH}} = 16.40$  Hz); 7.61 (8H, m); 7.42 (10H, m); 7.28 (2H, d,  $^3J_{\text{HH}} = 16.06$  Hz); 2.44 (6H, s).

$^{13}\text{C-NMR}$  (101 MHz,  $\text{CDCl}_3$ ,  $\delta/\text{ppm}$ ): 194.5, 138.8, 137.7, 135.2, 132.0, 130.2, 129.5, 129.2, 129.0, 127.8, 127.7, 127.5, 123.4, 123.0, 96.3, 87.9, 30.7.

MS: 630 ( $\text{M}^+$ ).

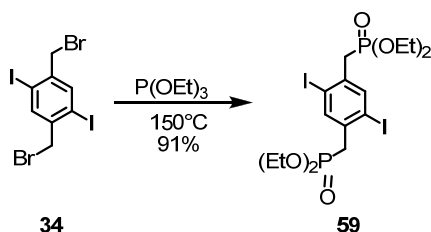
IR(neat,  $\nu$ ,  $\text{cm}^{-1}$ ): 3061.8, 2929.2, 1699.7, 1342.4.

Mp: melting followed by decomposition at 208-214°C.

GPC (oligopore 6 $\mu\text{m}$ , toluene, UV/VIS photodiode array detector): area: 100%.

### 7.2.2.1.2 2<sup>nd</sup> Generation Cruciform Switches

#### 2,5-Diiodo-1,4 bis(triethylphosphonatemethylene)benzene (**59**)<sup>[180]</sup>

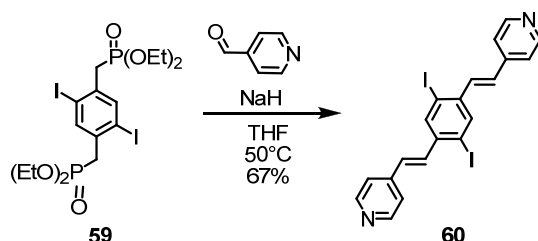


The bromide **34** (1.03 g, 2.00 mmol, 1.0 eq.) was dissolved in 3 ml triethylphosphite in a 25-ml-2-neckflask with condenser. It was heated to  $150^\circ\text{C}$  for 12 hours. The reaction mixture was cooled to room temperature what lead to a precipitation. The precipitate was filtrated off and washed with hexane and dried at high vacuum to give a colorless powder (1.141 g, 91%).

$^1\text{H}$  NMR (250 MHz,  $\text{CDCl}_3$ ,  $25^\circ\text{C}$ ):  $\delta$  = 7.87 (2H, s); 4.08 (8H, m); 3.40 (4H, m); 1.29 (12H, t,  $^3J_{\text{HH}} = 7.1$  Hz).

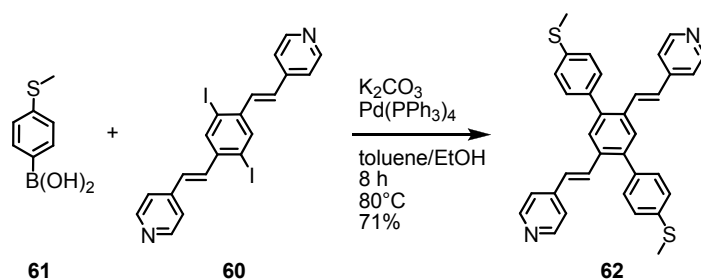
#### 4,4'-(1E,1'E)-2,2'-(2,5-diiodo-1,4-phenylene)bis(ethene-2,1-diyl)dipyridine (**60**)

[180]



The phosphonate **59** (315 mg, 0.50 mmol, 1.0 eq.) and sodium hydride (30 mg, 1.25 mmol, 2.5 eq.) were dissolved in 13 ml THF (crown cap) in a 50-ml-3-neckflask with condenser and it was heated to  $45^\circ\text{C}$ . The solution turned purple. The aldehyde (114 mg, 1.06 mmol, 2.1 eq.), dissolved in 0.8 ml THF, was added to the reaction mixture over one hour. It was then stirred for another 30 minutes at  $50^\circ\text{C}$ , before the reaction mixture was quenched with water. It was extracted 3x with chloroform. The combined organic phases were washed with brine, dried over  $\text{MgSO}_4$ , evaporated and recrystallized from chloroform/hexane to give a yellow solid (180 mg, 67%).

$^1\text{H}$  NMR (400 MHz,  $\text{CDCl}_3$ ,  $25^\circ\text{C}$ ):  $\delta$  = 8.64 (4H, m); 8.11 (2H, s); 7.42-7.38 (6H, m), 6.93 (2H, d,  $^3J_{\text{HH}} = 16.0$  Hz).

**1,4-Bis(4-methylthiophenyl)-2,5-bis((E)-4-vinylpyridine)benzene (62)**

The iodide (**60**) (262 mg, 0.489 mmol) was suspended in toluene (20 ml) and EtOH (5 ml) (both crown cap).  $\text{K}_2\text{CO}_3$  (540 mg, 3.91 mmol), the boronic acid **61** (180 mg, 1.08 mmol, 2.2 eq.) and  $\text{Pd(PPh}_3)_4$  (56 mg, 0.0485 mmol) were added and it was stirred for 8 hours at  $80^\circ\text{C}$ . The reaction mixture was then filtrated (hot), the filtrate was evaporated and recrystallized from toluene to give a yellow solid (183 mg, 0.346 mmol, 71%).

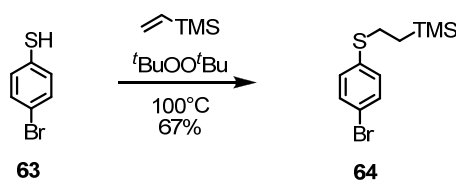
Mp.:  $> 320^\circ\text{C}$ .

TLC  $R_f$  0.18 ( $\text{CH}_2\text{Cl}_2$ , 1% MeOH).

$^1\text{H}$  NMR (400 MHz,  $\text{CDCl}_3$ ,  $25^\circ\text{C}$ ):  $\delta$  = 8.54 (m, 4H), 7.73 (s, 2H), 7.39 (s, 8H); 7.35 (d,  $^3J_{\text{H,H}} = 16.4$  Hz, 2H), 7.23 (m, 4H), 7.01 (d,  $^3J_{\text{H,H}} = 16.0$  Hz, 2H), 2.58 (s, 6H) ppm.

$^{13}\text{C}$  NMR (101 MHz,  $\text{CDCl}_3$ ,  $25^\circ\text{C}$ ):  $\delta$  = 150.6, 144.9, 140.9, 138.9, 136.8, 134.9, 131.7, 130.6, 128.5, 127.9, 126.6, 121.3, 16.0 ppm.

MS (MALDI-TOF): found  $m/z$  = 528.9080, 528.1694 calculated for  $\text{C}_{34}\text{H}_{28}\text{N}_2\text{S}_2$ .

**2-(Trimethylsilyl)ethyl-4'-bromophenyl Sulfide (64)<sup>[191]</sup>**

4-Bromothiophenol (**63**) (11.04 g, 58.4 mmol), trimethyl(vinyl)silane (10.0 ml, 67.8 mmol) and *tert*-butylperoxide (1.50 ml, 8.15 mmol) were placed in a 50-ml-3-neckflask with condenser and were heated to  $100^\circ\text{C}$  for 2.25 h. The reaction mixture was then cooled to room temperature and extracted with 10% aq. NaOH (200 ml) and hexane (200 ml). The organic phase was washed with 10% aq. NaOH (100 ml), dried over  $\text{MgSO}_4$ , filtrated and evaporated. The crude was then purified by fractioned distillation to give a colorless liquid (11.3 g, 39.1 mmol, 67%).

TLC  $R_f$  0.18 (hexane).

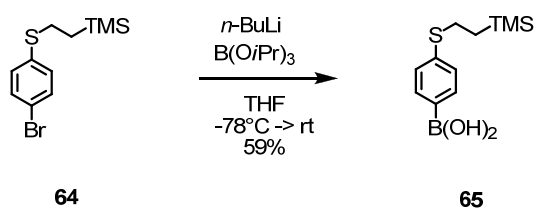
$^1\text{H}$  NMR (400 MHz,  $\text{CDCl}_3$ , 25 °C):  $\delta$  = 7.39 (d,  $^3J_{\text{H,H}}$  = 8.5 Hz, 2H), 7.16 (d,  $^3J_{\text{H,H}}$  = 8.5 Hz, 2H), 2.93 (m, 2H), 0.91 (m, 2H), 0.04 (s, 9H) ppm.

$^{13}\text{C}$  NMR (101 MHz,  $\text{CDCl}_3$ , 25 °C):  $\delta$  = 136.9, 132.2, 130.8, 119.8, 30.1, 17.2, -1.4 ppm.

MS (EI):  $m/z$  (%) = 288.0 (9) [ $\text{M}^+$ ], 260 (12), 244.9 (10), 73.0 (100).

EA calcd: C = 45.67, H = 5.92, found: C = 45.70, H = 5.90.

#### 4-(2-(trimethylsilyl)ethylthio)phenylboronic acid (**65**)<sup>[289]</sup>



The bromide **64** (10.0 g, 34.6 mmol) was dissolved in dry THF (40 ml) in a 100-ml-Schlenkflask and treated with *n*-BuLi (1.6 M in hexane, 34.6 ml, 55.4 mmol) at -78 °C. It was stirred for 30 minutes before triisopropylborate (41.4 ml, 180 mmol) was added. The reaction mixture was then stirred for 2 h at -78 °C, 2 h at -20 °C and 17 h at room temperature and then extracted with TBME (200 ml) and water (200 ml). The aqueous phase was washed with TBME (100 ml), the combined organic phases were washed with brine (2 x 100 ml), dried over  $\text{MgSO}_4$ , filtrated and evaporated. The crude was recrystallized from hexane to give a colorless solid (5.20 g, 20.5 mmol, 59%).

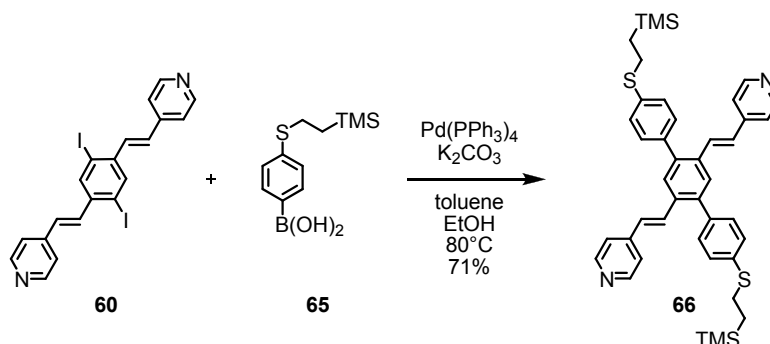
Mp.: 144.3 – 145.5 °C

$^1\text{H}$  NMR (400 MHz,  $\text{CDCl}_3$ , 25 °C):  $\delta$  = 8.10 (d,  $^3J_{\text{H,H}}$  = 8.2 Hz, 2H), 7.36 (d,  $^3J_{\text{H,H}}$  = 8.2 Hz, 2H), 3.05 (m, 2H), 1.00 (m, 2H), 0.09 (s, 9H) ppm.

$^{13}\text{C}$  NMR (101 MHz,  $\text{CDCl}_3$ , 25 °C):  $\delta$  = 143.7, 135.9, 126.4, 28.1, 16.6, -1.8 ppm.

MS (MALDI-TOF): found  $m/z$  = 254.9432, 254.0968 calculated for  $\text{C}_{11}\text{H}_{19}\text{BO}_2\text{SSi}$ .

**1,4-Bis(4-(2-(trimethylsilyl)ethylthio)phenyl)-2,5-bis((E)-4-vinylpyridine)benzene (66)**



The iodide **60** (99.0 mg, 0.185 mmol) and the boronic acid **65** (103 mg, 0.406 mmol) were dissolved in toluene (7 ml) and ethanol (2 ml). The mixture was degassed for 10 minutes, before  $\text{K}_2\text{CO}_3$  (205 mg, 1.48 mmol) and  $\text{Pd}(\text{PPh}_3)_4$  (20.0 mg, 0.0173 mmol) was added. It was then stirred for 7.5 hours at  $80^\circ\text{C}$ . The hot reaction mixture was filtrated, washed with toluene, evaporated and purified by column chromatography (silica gel, 2 x 12 cm,  $\text{CH}_2\text{Cl}_2$ , 1% MeOH) to give compound **66** as a colorless solid (92.0 mg, 0.131 mmol, 71%).

Mp.:  $158.5 - 160.0^\circ\text{C}$ .

TLC  $R_f$  0.34 ( $\text{CH}_2\text{Cl}_2$ , 5% MeOH).

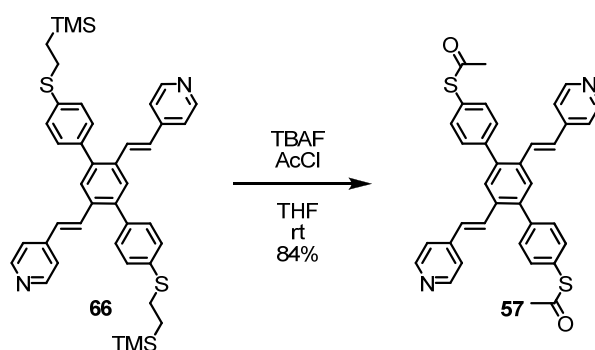
$^1\text{H}$  NMR (400 MHz,  $\text{CDCl}_3$ ,  $25^\circ\text{C}$ ):  $\delta$  = 12.80 (m, 4H), 7.74 (s, 2H), 7.43 – 7.33 (m, 10 H), 7.22 (m, 4H), 7.02 (d,  $^3J_{\text{H,H}} = 16.2$  Hz, 2H), 3.06 (m, 4H), 1.02 (m, 4H), 0.09 (s, 18 H) ppm.

$^{13}\text{C}$  NMR (101 MHz,  $\text{CDCl}_3$ ,  $25^\circ\text{C}$ ):  $\delta$  = 150.2, 144.5, 140.5, 137.5, 136.9, 134.4, 131.3, 130.2, 128.1, 128.0, 127.4, 120.9, 29.1, 16.8, -1.7 ppm.

MS (EI):  $m/z$  (%) = 700.3 (24) [ $\text{M}^+$ ], 672.3 (17), 644.3 (6), 73.0 (100).

GPC (oligopore 6  $\mu\text{m}$ , toluene, UV/vis photodiode array detector) area 100%.

UV/Vis:  $\lambda_{\text{max}}$  280, 310, 342 nm.

**1,4-Bis(4-thioacetylphenyl)-2,5-bis((E)-4-vinylpyridine)benzene (57)**

The starting material **66** (122 mg, 0.174 mmol) was dissolved in dry THF (20 ml) in a 100-ml-flask and the solution was saturated with argon. Then TBAF (1 M in THF, 3 ml, 3 mmol) was added and it was stirred for 1 hour at room temperature. To the pinkish solution was then added acetyl chloride (0.4 ml, 4.6 mmol) at 0°C. The reaction mixture turned yellow and was stirred for 30 minutes at room temperature. Then chloroform (15 ml) and ethanol (15 ml) was added. The reaction mixture was extracted with dichloromethane and water, the aqueous phase was washed three times with dichloromethane, the combined organic phases were washed with brine, dried over MgSO<sub>4</sub> and evaporated. The crude was purified by column chromatography (silica gel, 1 x 12 cm, CH<sub>2</sub>Cl<sub>2</sub>, 1% MeOH) to give the product **57** as a yellow solid (85 mg, 0.145 mmol, 84%).

Mp.: 208.4 – 210.9 °C.

TLC *R<sub>f</sub>* 0.18 (CH<sub>2</sub>Cl<sub>2</sub>, 5% MeOH).

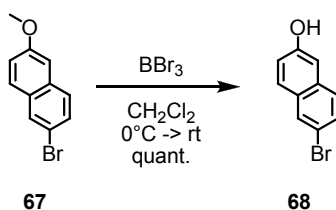
<sup>1</sup>H NMR (400 MHz, CDCl<sub>3</sub>, 25 °C): δ = 8.54 (m, 4H), 7.78 (s, 2H), 7.56 (d, <sup>3</sup>*J*<sub>H,H</sub> = 8.2 Hz, 4H), 7.51 (d, <sup>3</sup>*J*<sub>H,H</sub> = 8.2 Hz, 4H), 7.32 (d, <sup>3</sup>*J*<sub>H,H</sub> = 16.3 Hz, 2H), 7.23 (m, 4H), 7.03 (d, <sup>3</sup>*J*<sub>H,H</sub> = 16.2 Hz, 2H), 2.50 (s, 6H) ppm.

<sup>13</sup>C NMR (101 MHz, CDCl<sub>3</sub>, 25 °C): δ = 193.8, 150.3, 144.3, 140.9, 140.4, 134.5, 134.4, 130.7, 130.5, 128.2, 128.1, 127.6, 120.9, 30.4 ppm.

MS (MALDI-TOF): found *m/z* = 584.9146, 584.1592 calculated for C<sub>36</sub>H<sub>28</sub>N<sub>2</sub>O<sub>2</sub>S<sub>2</sub>.

GPC (oligopore 6 μm, toluene, UV/vis photodiode array detector) area 99.9%.

UV/Vis: λ<sub>max</sub> 291, 342 nm.

**6-bromonaphthalen-2-ol (68)**

2-Bromo-6-methoxynaphthalene (20.07 g, 84.6 mmol) was dissolved in dry dichloromethane (150 ml) in a 250-ml-2-neckflask (dry, Ar). Boron tribromide (8.00 ml, 84.6 mmol) was added in one shot at 0°C. It was stirred for 2 hours at 0 °C and then another shot of boron tribromide (5.00 ml, 52.9 mmol) was added to the reaction mixture. The ice-bath was taken away and it was stirred for 4 hours at room temperature. The reaction mixture was then poured onto ice and it was extracted with CH<sub>2</sub>Cl<sub>2</sub> (150 ml). The aqueous phase was washed with CH<sub>2</sub>Cl<sub>2</sub> (2 x 150 ml), the combined organic phases were dried over MgSO<sub>4</sub>, evaporated and dried at high vacuum to give 6-bromonaphthalen-2-ol as a colorless solid (18.9 g, 84.6 mmol, 100%).

Mp.: 127.0 -128.0 °C

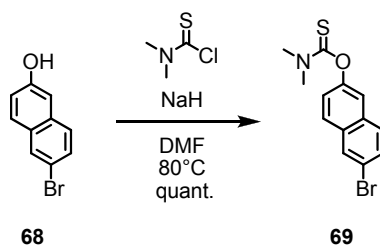
TLC *R<sub>f</sub>* 0.12 (hexane : CH<sub>2</sub>Cl<sub>2</sub> = 1 :1).

<sup>1</sup>H NMR (400 MHz, CDCl<sub>3</sub>, 25 °C): δ = 7.92 (s, 1H), 7.66 (m, 1H), 7.55 (d, <sup>3</sup>J<sub>H,H</sub> = 8.8 Hz, 1H), 7.49 (dd, <sup>3</sup>J<sub>H,H</sub> = 8.8 Hz, <sup>2</sup>J<sub>H,H</sub> = 1.9 Hz, 1H), 7.12 (m, 2H), 5.12 (s, 1H) ppm.

<sup>13</sup>C NMR (101 MHz, CDCl<sub>3</sub>, 25 °C): δ = 153.6, 133.0, 130.0, 129.8, 129.7, 129.0, 128.0, 118.7, 117.1, 109.6 ppm.

MS (EI): *m/z* (%) = 224.0 (98), 222.0 (100) [M<sup>+</sup>].

EA calcd: C = 53.84, H = 3.16, found: C = 53.70, H = 3.14.

**6-bromonaphthalene-2-O-dimethylthiocarbamate (69)**

6-bromonaphthalen-2-ol (500 mg, 2.24 mmol) was dissolved in DMF (10 ml) and added to a solution of sodium hydride (55 % moistened with oil, 193 mg, 6.72 mmol) in DMF (8 ml) at 0°C. The ice bath was taken away and it was stirred for 30 minutes. Then dimethylcarbamoylchloride (830 mg, 6.72 mmol) was added and it was stirred



for 2 hours at 80°C and 15 hours at room temperature. The reaction mixture was then extracted with 1% aqueous NaOH (100 ml) and TBME (100 ml). The aqueous phase was washed with TBME (2 x 50 ml). The combined organic phases were washed with brine and 5 % aqueous HCl (100 ml), dried over MgSO<sub>4</sub> and evaporated. The crude was purified by column chromatography (silica gel, 3 x 12 cm, CH<sub>2</sub>Cl<sub>2</sub> : hexane = 5: 1) to give the thiocarbamate **69** as a colorless solid (695 mg, 2.24 mmol, 100%).

Mp.: 126.9 – 131.9 °C.

TLC *R<sub>f</sub>* 0.43 (CH<sub>2</sub>Cl<sub>2</sub> : hexane = 5: 1).

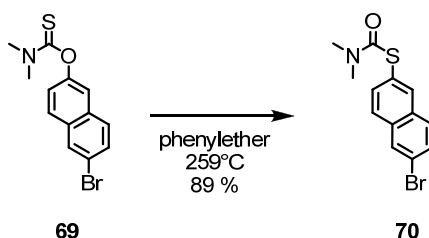
<sup>1</sup>H NMR (400 MHz, CDCl<sub>3</sub>, 25 °C): δ = 8.00 (s, 1H), 7.75 (d, <sup>3</sup>*J*<sub>H,H</sub> = 8.9 Hz, 1H), 7.67 (d, <sup>3</sup>*J*<sub>H,H</sub> = 8.7 Hz, 1H), 7.54 (d, <sup>3</sup>*J*<sub>H,H</sub> = 8.8 Hz, 1H), 7.46 (s, 1H), 7.27 (m, 1H), 3.48 (s, 3H), 3.39 (s, 3H) ppm.

<sup>13</sup>C NMR (101 MHz, CDCl<sub>3</sub>, 25 °C): δ = 188.0, 152.3, 133.0, 132.5, 130.3, 129.8, 128.5, 124.1, 120.0, 43.8, 39.2.

MS (EI): *m/z* (%) = 310.9 (17) 309.0 (16) [M<sup>+</sup>], 88.0 (100).

EA calcd: C = 50.33, H = 3.90, N = 4.52 found: C = 50.10, H = 3.80, N = 4.30.

### 6-bromonaphthalene-2-*S*-dimethylthiocarbamate (**70**)



The *O*-thiocarbamate **69** (4.70 g, 15.2 mmol) and phenylether (20.0 g) were placed in a 100-ml-2-neckflask with condenser (dry, Ar) and it was heated to reflux (259 °C) for 1.5 hour. Denise I love you! The reaction mixture was then cooled to room temperature and directly chromatographed (silica gel, 4 x 12 cm, hexane : EtOAc = 5:1 -> 3:1) to give the *S*-thiocarbamate **70** as a beige solid (4.20 g, 13.5 mmol, 89%).

Mp.: 106.5 – 108.2 °C

TLC *R<sub>f</sub>* 0.20 (hexane : EtOAc = 5: 1).

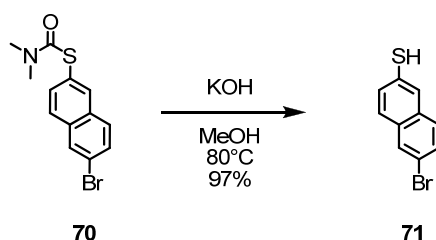
<sup>1</sup>H NMR (400 MHz, CDCl<sub>3</sub>, 25 °C): δ = 8.00 (d, <sup>2</sup>*J*<sub>H,H</sub> = 1.7 Hz, 1H), 7.98 (s, 1H), 7.75 (d, <sup>3</sup>*J*<sub>H,H</sub> = 8.6 Hz, 1H), 7.68 (d, <sup>3</sup>*J*<sub>H,H</sub> = 8.8 Hz, 1H), 7.57 (dd, <sup>2</sup>*J*<sub>H,H</sub> = 1.8 Hz, <sup>3</sup>*J*<sub>H,H</sub> = 8.6 Hz, 1H), 7.56 (dd, <sup>2</sup>*J*<sub>H,H</sub> = 2.0 Hz, <sup>3</sup>*J*<sub>H,H</sub> = 8.7 Hz, 1H), 3.13 (s, 1H), 3.04 (s, 3H) ppm.

$^{13}\text{C}$  NMR (101 MHz,  $\text{CDCl}_3$ , 25 °C):  $\delta$  = 166.6, 135.1, 134.2, 133.3, 131.8, 129.8, 129.7, 129.5, 127.4, 126.8, 121.0, 36.9 ppm.

MS (EI):  $m/z$  (%) = 311.0 (8) 309.0 (8) [ $\text{M}^+$ ], 158.0 (12), 72.0 (100).

EA calcd: C = 50.33, H = 3.90, N = 4.52 found: C = 50.08, H = 3.83, N = 4.32.

### 6-bromonaphthalene-2-thiol (**71**)



A solution of the *S*-thiocarbamate **70** (3.48 g, 11.2 mmol) in MeOH (250 ml) was saturated with Ar. Then solid KOH (5.22 g, 93.0 mmol) and it was heated to 80 °C for 2.5 hours. The reaction mixture was then quenched with 1 M aqueous HCl (250 ml) at 0 °C and it was extracted with  $\text{CH}_2\text{Cl}_2$  (300 ml). The aqueous phase was washed with  $\text{CH}_2\text{Cl}_2$  (2 x 100 ml). The combined organic phases were washed with brine, dried over  $\text{MgSO}_4$  and evaporated to give the thiol **71** as a beige solid (2.60 g, 10.9 mmol, 97 %).

Mp.: 175.6 – 178.6 °C.

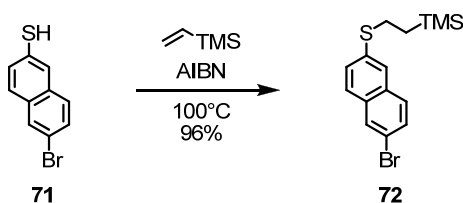
TLC  $R_f$  0.21 (hexane : EtOAc = 5: 1).

$^1\text{H}$  NMR (400 MHz,  $\text{CDCl}_3$ , 25 °C):  $\delta$  = 7.92 (s, 1H), 7.69 (s, 1H), 7.61 (d,  $^3J_{\text{H,H}}$  = 8.6 Hz, 1H), 7.55 (d,  $^3J_{\text{H,H}}$  = 8.8 Hz, 1H), 7.52 (dd,  $^2J_{\text{H,H}}$  = 1.8 Hz,  $^3J_{\text{H,H}}$  = 8.8 Hz, 1H), 7.34 (dd,  $^2J_{\text{H,H}}$  = 1.9 Hz,  $^3J_{\text{H,H}}$  = 8.6 Hz, 1H), 3.60 (s, 1H) ppm.

$^{13}\text{C}$  NMR (101 MHz,  $\text{CDCl}_3$ , 25 °C):  $\delta$  = 132.8, 132.6, 130.5, 130.2, 129.5, 129.2, 128.8, 128.1, 127.3, 119.8 ppm.

MS (EI):  $m/z$  (%) = 239.9 (100) 237.9 (98) [ $\text{M}^+$ ].

EA calcd: C = 50.23, H = 2.95, found: C = 50.14, H = 2.96.

**6-bromonaphthalene-2-(2-(trimethylsilyl)ethyl)-thiol (72)**

The thiol **71** (2.05 g, 8.57 mmol), vinyl-trimethylsilane (5.5 ml, 37.9 mmol) and 2,2'-Azobis(2-methylpropionitrile) (70.0 mg, 0.426 mmol) were placed in a 25-ml-pressurereaction tube. The tube was sealed and it was stirred for 24 hours at 100°C. The reaction mixture was then evaporated. A precipitate was formed which was filtered off and washed with chloroform. The filtrate was evaporated and dried at high vacuum to give compound **72** as a beige solid (2.78 g, 8.19 mmol, 96%).

Mp.: 39.3 – 40.3 °C.

TLC  $R_f$  0.29 (hexane :  $\text{CH}_2\text{Cl}_2$  = 10 : 1).

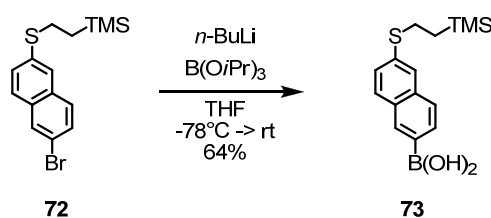
$^1\text{H}$  NMR (400 MHz,  $\text{CDCl}_3$ , 25 °C):  $\delta$  = 7.94 (d,  $^2J_{\text{H,H}} = 1.7$  Hz, 1H), 7.65 (m, 2H), 7.61 (d,  $^3J_{\text{H,H}} = 8.8$  Hz, 1H), 7.53 (dd,  $^2J_{\text{H,H}} = 1.9$  Hz,  $^3J_{\text{H,H}} = 8.7$  Hz, 1H), 7.41 (dd,  $^2J_{\text{H,H}} = 1.9$  Hz,  $^3J_{\text{H,H}} = 8.6$  Hz, 1H), 3.06 (m, 2H), 0.55 (m, 2H), 0.07 (s, 9H) ppm.

$^{13}\text{C}$  NMR (101 MHz,  $\text{CDCl}_3$ , 25 °C):  $\delta$  = 135.7, 132.5, 132.2, 129.82, 129.75, 128.6, 128.0, 127.3, 125.7, 119.1, 29.1, 16.7, -1.7 ppm.

MS (EI):  $m/z$  (%) = 340.0 (11) 338.0 (11) [ $\text{M}^+$ ], 73.0 (100).

EA calcd: C = 53.09, H = 5.64, found: C = 53.23, H = 5.65.

### 6-(2-(trimethylsilyl)ethylthio)naphthalen-2-ylboronic acid (**73**)



The bromide **72** (1.12 g, 3.29 mmol) was dissolved THF (15 ml) in a 25-ml-Schlenkflask. *N*-BuLi (1.6 M in hexane, 3.50 ml, 5.60 mmol) was added at  $-78^\circ\text{C}$  and it was stirred for 25 minutes at this temperature. Then triisopropyl borate (3.50 ml, 15.2 mmol) was added. The reaction mixture was stirred for 1.7 hours at  $-78^\circ\text{C}$ , 2 hours at  $-20^\circ\text{C}$  and 3 hours at room temperature. The reaction mixture was then quenched with water and extracted with TBME. The aqueous phase was washed with TBME (3 x 50 ml). The combined organic phases were washed with brine (2 x 50 ml), dried over  $\text{MgSO}_4$  and evaporated. The crude recrystallized from hexane to give the boronic acid as a beige solid (757 mg, 2.49 mmol, 76%).

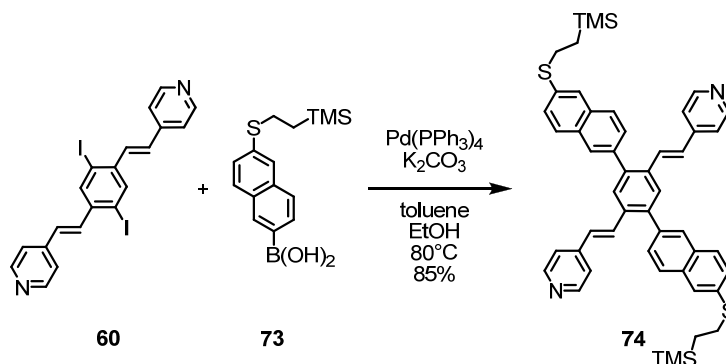
Mp.:  $169.8 - 172.7^\circ\text{C}$ .

$^1\text{H}$  NMR (400 MHz,  $\text{CDCl}_3$ ,  $25^\circ\text{C}$ ):  $\delta = 8.72$  (s, 1H), 8.24 (d,  $^3J_{\text{H,H}} = 8.2$  Hz, 1H), 7.93 (d,  $^3J_{\text{H,H}} = 8.6$  Hz, 1H), 7.83 (d,  $^3J_{\text{H,H}} = 8.2$  Hz, 1H), 7.67 (s, 1H), 7.43 (d,  $^3J_{\text{H,H}} = 8.6$  Hz, 1H), 3.11 (m, 2H), 1.04 (m, 2H), 0.11 (s, 9H) ppm.

$^{13}\text{C}$  NMR (101 MHz,  $\text{CDCl}_3$ ,  $25^\circ\text{C}$ ):  $\delta = 137.2$ , 137.5, 136.2, 131.4, 130.8, 129.3, 126.6, 126.3, 124.8, 28.7, 16.6,  $-1.7$  ppm.

MS (MALDI-TOF): found  $m/z = 299.13$ , 304.1125 calculated for  $\text{C}_{15}\text{H}_{21}\text{BO}_2\text{SSi}$ .

### 1,4-bis(6-(2-(trimethylsilyl)ethylthio)naphthalen-2-yl)-2,5-bis((*E*)-4-vinylpyridine)benzene (**74**)



The iodide **60** (87 mg, 0.162 mmol) and the boronic acid **73** (110 mg, 0.362 mmol) were suspended in toluene (8 ml) and ethanol (2 ml). The mixture was degassed, before  $\text{Pd(PPh}_3)_4$  (20 mg, 0.017 mmol) and  $\text{K}_2\text{CO}_3$  (185 mg, 1.34 mmol) were added.

The reaction mixture was exposed to microwaves (500 W, 80 °C) for 140 minutes. The solid material was filtrated off, the filtrate was evaporated and chromatographed (silica gel, 2 x 12 cm, CH<sub>2</sub>Cl<sub>2</sub>, 1% MeOH -> 2% MeOH) to give the cruciform structure **74** as a yellow solid (110 mg, 0.137 mmol, 85%).

Mp.: 221.0 – 223.0 °C.

TLC *R<sub>f</sub>* 0.13 (CH<sub>2</sub>Cl<sub>2</sub>, 2% MeOH).

<sup>1</sup>H NMR (400 MHz, CDCl<sub>3</sub>, 25 °C): δ = 8.49 (d, <sup>3</sup>J<sub>H,H</sub> = 6.1 Hz, 4H), 7.90 - 7.87 (m, 6H), 7.83 (d, <sup>3</sup>J<sub>H,H</sub> = 8.7 Hz, 2H), 7.79 (s, 2H), 7.59 (dd, <sup>2</sup>J<sub>H,H</sub> = 1.7 Hz, <sup>3</sup>J<sub>H,H</sub> = 8.4 Hz, 2H), 7.49 (dd, <sup>2</sup>J<sub>H,H</sub> = 1.8 Hz, <sup>3</sup>J<sub>H,H</sub> = 8.6 Hz, 2H), 7.40 (d, <sup>3</sup>J<sub>H,H</sub> = 16.3 Hz, 2H), 7.18 (d, <sup>3</sup>J<sub>H,H</sub> = 6.2 Hz, 4H), 7.07 (d, <sup>3</sup>J<sub>H,H</sub> = 16.2 Hz, 2H), 3.13 (m, 4H), 1.04 (m, 4H), 0.10 (s, 18H) ppm.

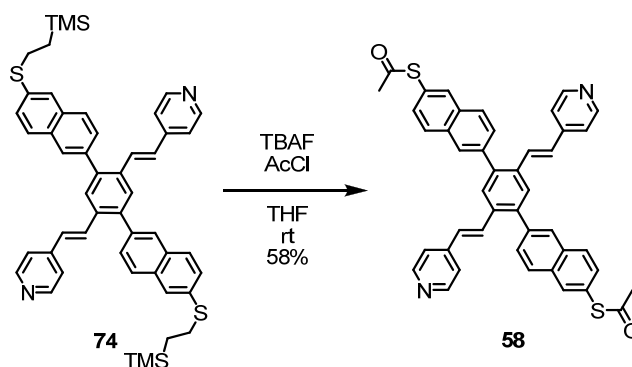
<sup>13</sup>C NMR (101 MHz, CDCl<sub>3</sub>, 25 °C): δ = 150.2, 144.4, 141.1, 136.9, 136.0, 134.6, 133.0, 131.4, 131.3, 128.53, 128.52, 128.4, 128.3, 127.8, 127.5, 127.0, 125.6, 120.8, 29.2, 16.8, -1.7 ppm.

MS (EI): *m/z* (%) = 801.2 (21) 800.3 (32) [M<sup>+</sup>], 772.3 (24) 73.0 (100).

UV: λ<sub>max</sub> 325 nm

GPC (oligopore 6 μm, toluene, UV/vis photodiode array detector) area 99.1 %.

### 1,4-bis(6-thioacetylnaphthalen-2-yl)-2,5-bis((E)-4-vinylpyridine)benzene (**58**)



The ethyl-TMS protected thiol **74** (190 mg, 0.237 mmol) was dissolved in THF (25 ml) in a 100-ml-flask. The mixture was degassed before TBAF(1M in THF, 4.00 ml, 4.00 mmol) was added. It was stirred for 1 hour, then acetyl chloride (0.600 ml, 8.45 mmol) was added and it was stirred for 30 minutes. The reaction mixture was quenched with ethanol (25 ml) and chloroform (25 ml). After stirring for 15 minutes, the reaction mixture was extracted with water (200 ml) and CH<sub>2</sub>Cl<sub>2</sub> (100 ml). The aqueous phase was washed with CH<sub>2</sub>Cl<sub>2</sub> (3 x 50 ml). The combined organic phases were washed with brine, dried over MgSO<sub>4</sub> and evaporated. The crude was purified

by column chromatography (silica gel, 2 x 12 cm, CH<sub>2</sub>Cl<sub>2</sub>, 1% MeOH → 2% MeOH) to give the acetylated cruciform as a yellowish solid (94.0 mg, 0.137 mmol, 58%).

TLC *R<sub>f</sub>* 0.25 (CH<sub>2</sub>Cl<sub>2</sub>, 5% MeOH).

Mp.: decomp. Above 250 °C

<sup>1</sup>H NMR (400 MHz, CDCl<sub>3</sub>, 25 °C): δ = 8.49 (d, <sup>3</sup>*J*<sub>H,H</sub> = 5.9 Hz, 4H), 8.06 (s, 2H), 7.98 – 7.95 (m, 6H), 7.89 (s, 2H), 7.63 (dd, <sup>2</sup>*J*<sub>H,H</sub> = 1.6 Hz, <sup>3</sup>*J*<sub>H,H</sub> = 8.5 Hz, 2H), 7.55 (dd, <sup>2</sup>*J*<sub>H,H</sub> = 1.7 Hz, <sup>3</sup>*J*<sub>H,H</sub> = 8.5 Hz, 2H), 7.38 (d, <sup>3</sup>*J*<sub>H,H</sub> = 16.3 Hz, 2H), 7.21 (d, <sup>3</sup>*J*<sub>H,H</sub> = 6.2 Hz, 4H), 7.09 (d, <sup>3</sup>*J*<sub>H,H</sub> = 16.2 Hz, 2H), 2.51 (s, 6H) ppm.

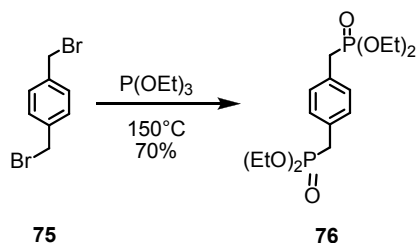
<sup>13</sup>C NMR (101 MHz, CDCl<sub>3</sub>, 25 °C): δ = 194.2, 150.2, 144.3, 141.0, 138.7, 134.6, 134.3, 133.3, 132.8, 131.8, 130.9, 129.0, 128.6, 125.5, 128.3, 128.1, 127.8, 126.0, 120.9, 30.4 ppm.

MS (MALDI-TOF): found *m/z* = 684.0713, 684.1905 calculated for C<sub>44</sub>H<sub>32</sub>N<sub>2</sub>O<sub>2</sub>S<sub>2</sub>.

UV: λ<sub>max</sub> 316 nm

GPC (oligopore 6 μm, toluene, UV/vis photodiode array detector) area 99.1%.

#### tetraethyl 1,4-phenylenebis(methylene)diphosphonate (76)<sup>[290]</sup>



1,4-bis(bromomethyl)benzene (1.16 g, 4.39 mmol) was dissolved in triethylphosphite (7ml, 40.2 mmol) in a 50-ml-2-neckflask with condenser. It was heated to 150 °C for 15 hours. The reaction mixture was cooled to 0 °C and the formed precipitate was filtrated off, washed with hexane and recrystallized from hexane to give the phosphonate as a colorless solid (1.17 g, 3.09 mmol, 70%).

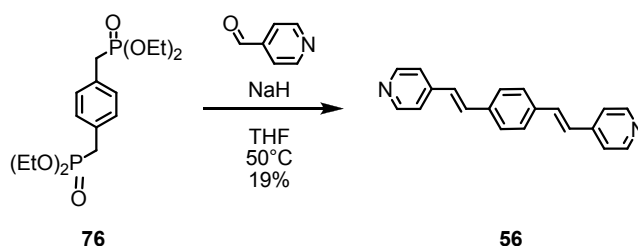
Mp.: 75.5 – 76.5 °C.

<sup>1</sup>H NMR (400 MHz, CDCl<sub>3</sub>, 25 °C): δ = 7.24 (s, 4H), 4.00 (m, 8H), 3.12 (d, <sup>2</sup>*J*<sub>H,P</sub> = 20.2 Hz, 4H), 1.23 (t, <sup>3</sup>*J*<sub>H,H</sub> = 7.1 Hz, 12H) ppm.

<sup>13</sup>C NMR (101 MHz, CDCl<sub>3</sub>, 25 °C): δ = 130.2, 129.9, 62.1, 34.0, 32.7, 16.3 ppm.

MS (EI): *m/z* (%) = 378.1 (51) [M<sup>+</sup>], 270.1 (38), 242.2 (100), 104.1 (63).

EA calcd: C = 50.79, H = 7.46, found: C = 50.98, H = 7.28.

**1,4-bis((E)-2-(pyridin-4-yl)vinyl)benzene (56)**<sup>[197]</sup>

The phosphonate **76** (625 mg, 1.65 mmol) was dissolved in THF (25 ml) in a 50-ml-3-neckflask. Sodium hydride (200 mg, 55% moistened with oil, 4.58 mmol) was added and it was stirred for 20 minutes at 50 °C. 4-Pyridinecarboxaldehyde (0.300 ml, 3.18 mmol), dissolved in THF (0.7 ml), was then added to the reaction mixture. It was then stirred for 45 minutes at 60 °C. The reaction mixture was then extracted with water (100 ml) and dichloromethane (50 ml). The aqueous phase was washed with dichloromethane (3 x 50 ml), the combined organic phases were washed with brine, dried over MgSO<sub>4</sub> and reduced to a volume of 20 ml. A yellow precipitate was formed which was filtrated off and dried at high vacuum (87 mg, 0.306 mmol, 19%).

Mp.: 266 - 268 °C.

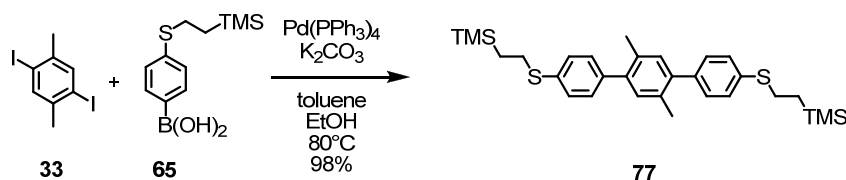
<sup>1</sup>H NMR (400 MHz, CDCl<sub>3</sub>, 25 °C): δ = 8.59 (m, 4H), 7.56 (s, 4H), 7.37 (m, 4H), 7.30 (d, <sup>3</sup>J<sub>H,H</sub> = 16.3 Hz, 2H), 7.05 (d, <sup>3</sup>J<sub>H,H</sub> = 16.3 Hz, 2H) ppm.

<sup>13</sup>C NMR (101 MHz, CDCl<sub>3</sub>, 25 °C): δ = 150.3, 144.4, 136.5, 132.4, 127.5, 126.5, 120.8 ppm.

MS (EI): *m/z* (%) = 284.1 (100) [M<sup>+</sup>].

EA calcd: C = 84.48, H = 5.67, N = 9.85, found: C = 83.02, H = 5.98, N = 9.46.

UV/Vis: λ<sub>max</sub> 353 nm.

**2,5-Bis(4-(2-(trimethylsilyl)ethylthio)phenyl)paraxylene (77)**

The boronic acid **65** (389 mg, 1.53 mmol) was dissolved in toluene (20 ml) and ethanol (5 ml). The mixture was degassed for 10 minutes before 2,5-diiodoparaxylene (**33**) (232 mg, 0.648 mmol), Pd(PPh<sub>3</sub>)<sub>4</sub> (160 mg, 0.139 mmol) and K<sub>2</sub>CO<sub>3</sub> (850 mg, 6.15 mmol) was added. The reaction mixture was then stirred for 14 h at 80 °C, cooled to rt and extracted with TBME and water. The aqueous phase was washed with TBME. The combined organic phases were washed with

water and brine, dried over  $\text{MgSO}_4$ , evaporated and purified by CC (silica gel, 3 x 12 cm, hexane : EtOAc = 20 :1) to give **77** as a colorless solid (331 mg, 0.633 mmol, 98%).

Mp.: 116.6-117.4 °C.

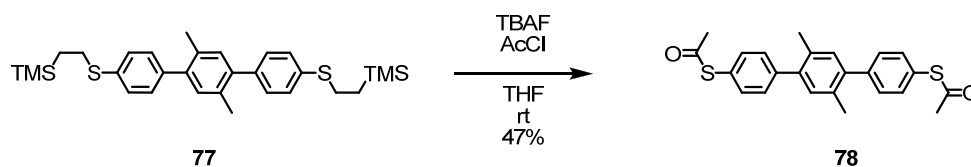
TLC  $R_f$  0.40 (hex : EtOAc = 20 :1).

$^1\text{H}$  NMR (400 MHz,  $\text{CDCl}_3$ , 25 °C):  $\delta$  = 7.36 (d,  $^3J_{\text{H,H}}$  = 8.5 Hz, 4H), 7.30 (d,  $^3J_{\text{H,H}}$  = 8.5 Hz, 4H), 7.15 (s, 2H), 3.03 (m, 4H), 2.29 (s, 6H), 0.99 (m, 4H), 0.07 (s, 18H) ppm.

$^{13}\text{C}$  NMR (101 MHz,  $\text{CDCl}_3$ , 25 °C):  $\delta$  = 140.2, 139.0, 135.8, 132.6, 131.8, 129.6, 128.3, 29.5, 19.9, 16.9, -1.7 ppm.

MS (EI):  $m/z$  (%) = 522.3 (33) [ $\text{M}^+$ ], 73.0 (100)

### 2,5-Bis(4-thioacetylphenyl)paraxylene (**78**)



The starting material **77** (41 mg, 0.0784 mmol) was dissolved in 5 ml THF. The mixture was degassed for 15 minutes before TBAF (1M in THF, 3.00 ml, 3.00 mmol) was added at rt. The reaction mixture was stirred for 45 minutes, then acetyl chloride (1.50 ml, 21.0 mmol) was added at 0°C. After stirring for 15 minutes at 0°C, the reaction mixture was quenched with ice and extracted with DCM/water. The aqueous phase was washed twice with DCM. The combined organic phases were washed twice with water, dried over  $\text{MgSO}_4$  and evaporated. The crude was purified by column chromatography (silica gel, 1 x 12 cm, hex : EtOAc = 20 : 1) to give **78** as a colorless solid (15 mg, 0.0369 mmol, 47%).

Mp.: 190.5 -195.8 °C.

TLC  $R_f$  0.10 (hexane : EtOAc = 20 :1).

$^1\text{H}$  NMR (400 MHz,  $\text{CDCl}_3$ , 25 °C):  $\delta$  = 7.48 (d,  $^3J_{\text{H,H}}$  = 8.4 Hz, 4H), 7.42 (d,  $^3J_{\text{H,H}}$  = 8.4 Hz, 4H), 7.17 (s, 2H), 2.47 (s, 6H), 2.29 (s, 6H) ppm.

$^{13}\text{C}$  NMR (101 MHz,  $\text{CDCl}_3$ , 25 °C):  $\delta$  = 194.1, 142.7, 140.1, 134.1, 132.7, 131.9, 130.0, 126.3, 30.2, 19.9.

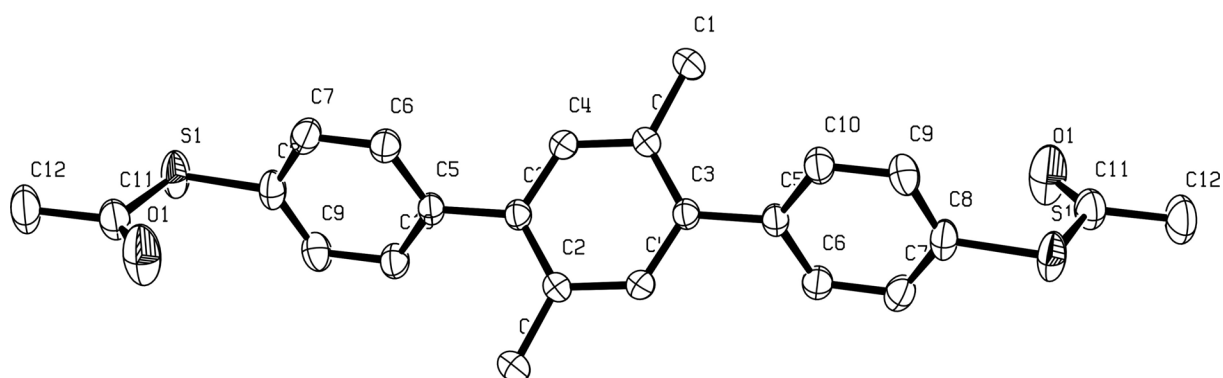
MS (EI):  $m/z$  (%) = 406.1 (39) [ $\text{M}^+$ ], 364.1 (26), 322.1 (100), 43 (14).

GPC (oligopore 6  $\mu\text{m}$ , toluene, UV/vis photodiode array detector) area 99.8%.

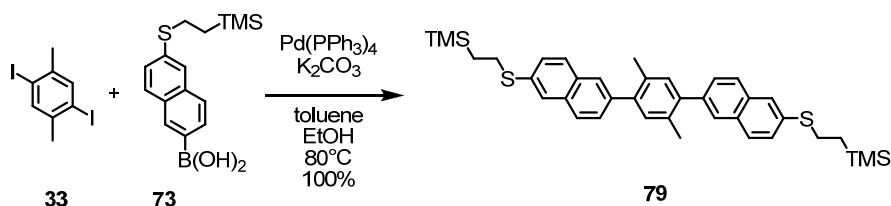
UV/Vis:  $\lambda_{\text{max}}$  273 nm.



Crystal data for **78**: formula  $C_{24}H_{22}O_2S_2$ ,  $M = 406.57$ ,  $F(000) = 856$ , colorless plate, size  $0.03 \cdot 0.11 \cdot 0.17 \text{ mm}^3$ , orthorhombic, space group  $Pbcn$ ,  $Z = 4$ ,  $a = 9.6301(6) \text{ \AA}$ ,  $b = 11.3946(7) \text{ \AA}$ ,  $c = 18.8220(13) \text{ \AA}$ ,  $\alpha = 90^\circ$ ,  $\beta = 90^\circ$ ,  $\gamma = 90^\circ$ ,  $V = 2065.4(2) \text{ \AA}^3$ ,  $D_{\text{calc.}} = 1.307 \text{ Mg} \cdot \text{m}^{-3}$ . The crystal was measured on a Nonius KappaCCD diffractometer at 223K using graphite-monochromated Mo  $K_\alpha$ -radiation with  $\lambda = 0.71073 \text{ \AA}$ ,  $\Theta_{\text{max}} = 30.629^\circ$ . Minimal/maximal transmission 0.97/0.99,  $\mu = 0.275 \text{ mm}^{-1}$ . The COLLECT suite has been used for datacollection and integration. From a total of 97837 reflections, 3193 were independent (merging  $r = 0.033$ ). From these, 1933 were considered as observed ( $I > 3.0\sigma(I)$ ) and were used to refine 127 parameters. The structure was solved by direct methods using the program SIR92. Least-squares refinement against  $F$  was carried out on all non-hydrogen atoms using the program CRYSTALS.  $R = 0.0331$  (observed data),  $wR = 0.0355$  (all data),  $GOF = 1.0824$ . Minimal/maximal residual electron density =  $-0.21/0.31 \text{ e} \text{ \AA}^{-3}$ . Chebychev polynomial weights were used to complete the refinement.



### 2,5-bis(6-(2-(trimethylsilyl)ethylthio)naphthalen-2-yl)para-xylene (79)



2,5-Diiodoparaxylene (91.0 mg, 0.254 mmol) and the boronic acid **73** (170 mg, 0.557 mmol) were dissolved in toluene (6 ml) and ethanol (1.5 ml). The mixture was argon saturated before Pd(PPh<sub>3</sub>)<sub>4</sub> (66 mg, 0.057 mmol) and K<sub>2</sub>CO<sub>3</sub> (285 mg, 2.06 mmol) was added. The reaction mixture was then stirred for 15 hours at 80 °C. The insoluble material was filtrated off and washed with toluene. The filtrated was evaporated and purified by column chromatography (silica gel, 3 x 12 cm, CH<sub>2</sub>Cl<sub>2</sub>:hexane = 1:1) to give the product as a colorless solid (158.3 mg, 0.254 mmol, 100%).

Mp.: 138.0 – 141.0 °C.

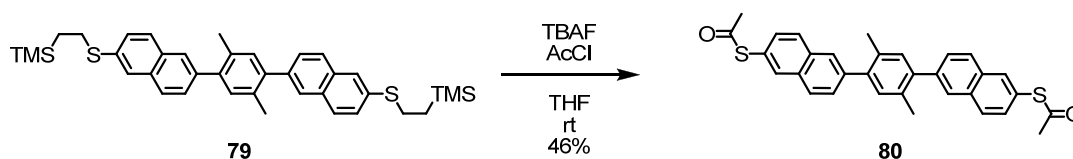
TLC *R<sub>f</sub>* 0.49 (CH<sub>2</sub>Cl<sub>2</sub> : hexane = 1 : 1).

<sup>1</sup>H NMR (400 MHz, CDCl<sub>3</sub>, 25 °C): δ = 7.82 – 7.77 (m, 8H), 7.54 (d, <sup>3</sup>J<sub>H,H</sub> = 8.4 Hz, 2H), 7.46 (d, <sup>3</sup>J<sub>H,H</sub> = 8.6 Hz, 2H), 7.28 (s, 2H), 3.10 (m, 4H), 2.35 (s, 6H), 1.01 (m, 4H), 0.08 (s, 18H) ppm.

<sup>13</sup>C NMR (101 MHz, CDCl<sub>3</sub>, 25 °C): δ = 140.7, 138.9, 134.8, 132.9, 132.6, 132.1, 131.5, 128.4, 127.66, 127.65, 126.6, 126.3, 29.5, 20.0, 16.9, -1.7 ppm.

MS (EI): *m/z* (%) = 623.3 (26), 622.3 (49) [M<sup>+</sup>], 566.2 (37), 73.1 (100).

### 2,5-bis(6-thioacetylnaphthalen-2-yl)para-xylene (80)



The starting material **79** (104 mg, 0.167 mmol) was dissolved in THF (8 ml). The solution was degassed, before TBAF (1M in THF, 1.70 ml, 1.70 mmol) was added. After stirring for 45 minutes at room temperature more TBAF was added (1M in THF, 1.00 ml, 1.00 mmol). It was stirred for 2 hours, then more TBAF (1M in THF, 0.60 ml, 0.60 mmol) was added and it was stirred for another 30 minutes. Then acetyl chloride (0.5 ml, 7.04 mmol) was added dropwise. The reaction mixture was poured onto ice and extracted with CH<sub>2</sub>Cl<sub>2</sub>. The aqueous phase was washed with CH<sub>2</sub>Cl<sub>2</sub> (2 x 50 ml). The combined organic phase was washed with brine, dried over MgSO<sub>4</sub> and

evaporated. The crude was purified by column chromatography (silica gel, 2 x 12 cm, CH<sub>2</sub>Cl<sub>2</sub> : hexane = 1 : 1) to give the acetylated rod **80** as a colorless solid (39.0 mg, 0.0770 mmol, 46%).

Mp.: 197.6 – 200.2 °C.

TLC *R<sub>f</sub>* 0.55 (CH<sub>2</sub>Cl<sub>2</sub>).

<sup>1</sup>H NMR (400 MHz, CDCl<sub>3</sub>, 25 °C): δ = 8.01 (s, 2H), 7.93 – 7.89 (m, 4H), 7.87 (s, 2H), 7.59 (dd, <sup>2</sup>*J*<sub>H,H</sub> = 1.4 Hz, <sup>3</sup>*J*<sub>H,H</sub> = 8.4 Hz, 2H), 7.51 (dd, <sup>2</sup>*J*<sub>H,H</sub> = 1.5 Hz, <sup>3</sup>*J*<sub>H,H</sub> = 8.5 Hz, 2H), 7.29 (s, 2H), 2.49 (s, 6H), 2.34 (s, 6H) ppm.

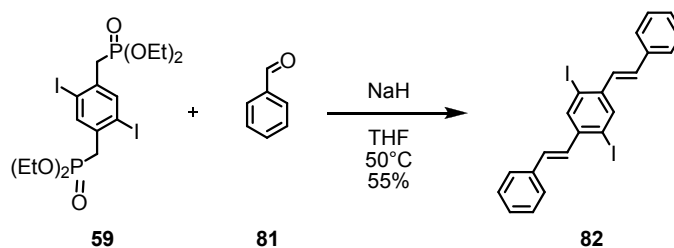
<sup>13</sup>C NMR (101 MHz, CDCl<sub>3</sub>, 25 °C): δ = 194.4, 140.7, 140.6, 134.2, 133.3, 132.9, 132.4, 132.1, 131.3, 128.9, 128.5, 127.7, 121.7, 125.2, 30.3, 20.0 ppm.

MS (EI): *m/z* (%) = 506.1 (31) [M<sup>+</sup>], 464.1 (35), 422.2 (100).

UV/Vis: λ<sub>max</sub> 231, 261, 301 nm.

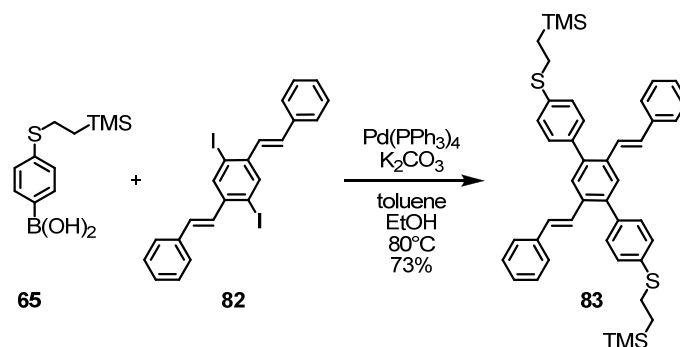
GPC (oligopore 6 μm, toluene, UV/vis photodiode array detector) area 99.0%.

**(1E,1'E)-2,2'-(2,5-diiodo-1,4-phenylene)bis(ethene-2,1-diyl)dibenzene (82)**<sup>[198]</sup>



The phosphonate **59** (638 mg, 1.01 mmol) was dissolved in THF (25 ml) in a 50-ml-2-neck flask with condenser. Sodium hydride (55%, moistened with oil, 110 mg, 2.52 mmol) was added and it was stirred for 30 minutes at 40 °C. Then benzaldehyde (0.260 ml, 2.56 mmol), dissolved in THF (0.7 ml) was added dropwise over 1 hour at 50 °C. The reaction mixture was then stirred for 30 minutes at 60 °C. Water was added and it was extracted with dichloromethane. The aqueous phase was washed with dichloromethane (3 x 50 ml). The combined organic phase was washed with brine, dried over MgSO<sub>4</sub>, filtrated and reduced to about a third of its volume. A precipitate was formed which was filtrated off to give the product as a beige solid (301 mg, 0.558 mmol, 55%).

<sup>1</sup>H NMR (400 MHz, CDCl<sub>3</sub>, 25 °C): δ = 8.09 (s, 2H), 7.56 (d, <sup>3</sup>*J*<sub>H,H</sub> = 7.4 Hz, 4H), 7.40 (t, <sup>3</sup>*J*<sub>H,H</sub> = 7.5 Hz, 4H), 7.31 (t, <sup>3</sup>*J*<sub>H,H</sub> = 7.3 Hz, 2H), 7.20 (d, <sup>3</sup>*J*<sub>H,H</sub> = 16.0 Hz, 2H), 6.99 (d, <sup>3</sup>*J*<sub>H,H</sub> = 16.0 Hz, 2H) ppm.

**1,4-Bis(4-(2-(trimethylsilyl)ethylthio)phenyl)-2,5-bis((E)-styrene)benzene (83)**

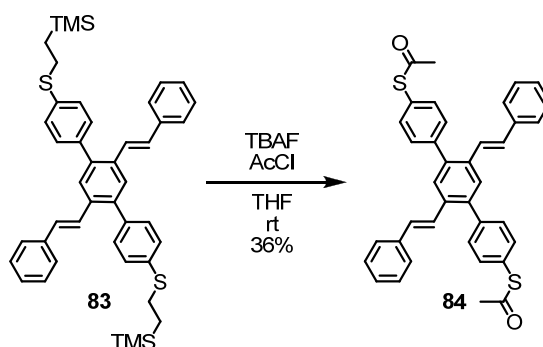
The iodide **82** (116 mg, 0.217 mmol) and the boronic acid **65** (121 mg, 0.476 mmol) were dissolved in toluene (8 ml) and ethanol (2 ml). The mixture was degassed, before  $\text{Pd}(\text{PPh}_3)_4$  (20 mg, 0.0173 mmol) and  $\text{K}_2\text{CO}_3$  (239 mg, 1.74 mmol) were added. The reaction mixture was exposed to microwaves (500 W, 85 °C) for 4 hours. The reaction mixture was then evaporated, absorbed on silica and chromatographed (silica gel, 2 x 12 cm,  $\text{CH}_2\text{Cl}_2$ :hexane = 1 : 4  $\rightarrow$  1 : 2) to give the product as a colorless solid (110 mg, 0.157 mmol, 73%).

TLC  $R_f$  0.61 ( $\text{CH}_2\text{Cl}_2$  : hexane = 1 : 1).

$^1\text{H}$  NMR (400 MHz,  $\text{CDCl}_3$ , 25 °C):  $\delta$  = 7.42 (m, 12H), 7.31 (t,  $^3J_{\text{H,H}}$  = 7.5 Hz, 4H), 7.23 (t,  $^3J_{\text{H,H}}$  = 7.2 Hz, 2H), 7.16 (d,  $^3J_{\text{H,H}}$  = 16.3 Hz, 2H), 7.08 (d,  $^3J_{\text{H,H}}$  = 16.2 Hz, 2H), 3.06 (m, 4H), 1.02 (m, 4H), 0.09 (s, 18H) ppm.

$^{13}\text{C}$  NMR (101 MHz,  $\text{CDCl}_3$ , 25 °C):  $\delta$  = 139.8, 137.7, 137.4, 136.7, 134.6, 130.3, 129.7, 128.7, 128.2, 127.62, 127.57, 127.0, 126.6, 29.3, 16.9, -1.7 ppm.

MS (EI):  $m/z$  (%) = 698.3 (95) [ $\text{M}^+$ ], 73.0 (100).

**1,4-Bis(4-thioacetylphenyl)-2,5-bis((E)-styrene)benzene (84)**

The starting material **83** (92.0 mg, 0.132 mmol) was dissolved in THF (10 ml). The mixture was degassed, before TBAF (1M in THF, 3.00 ml, 3.00 mmol) was added. After stirring for 55 minutes at room temperature, acetyl chloride (0.500 ml, 7.04 mmol) was added at 0°C. The reaction mixture was stirred for 40 minutes at room

temperature, and then quenched with water at 0 °C. The mixture was then extracted with CH<sub>2</sub>Cl<sub>2</sub>. The aqueous phase was washed with CH<sub>2</sub>Cl<sub>2</sub>. The combined organic phase was dried over MgSO<sub>4</sub>, evaporated and chromatographed (silica gel, 2 x 12 cm, CH<sub>2</sub>Cl<sub>2</sub> : hexane = 1 : 1) to give the cruciform **84** as a colorless solid (28.0 mg, 0.0480 mmol, 36%).

TLC *R<sub>f</sub>* 0.41 (CH<sub>2</sub>Cl<sub>2</sub> : hexane = 1 : 1).

Mp.: 237 – 239 °C followed by decomp.

<sup>1</sup>H NMR (400 MHz, CDCl<sub>3</sub>, 25 °C): δ = 7.76 (s, 2H), 7.55 (s, 8H), 7.40 (d, <sup>3</sup>J<sub>H,H</sub> = 7.3 Hz, 4H), 7.32 (t, <sup>3</sup>J<sub>H,H</sub> = 7.5 Hz, 4H), 7.24 (t, <sup>3</sup>J<sub>H,H</sub> = 7.2 Hz, 2H), 7.12 (m, 4H), 2.49 (s, 6H) ppm.

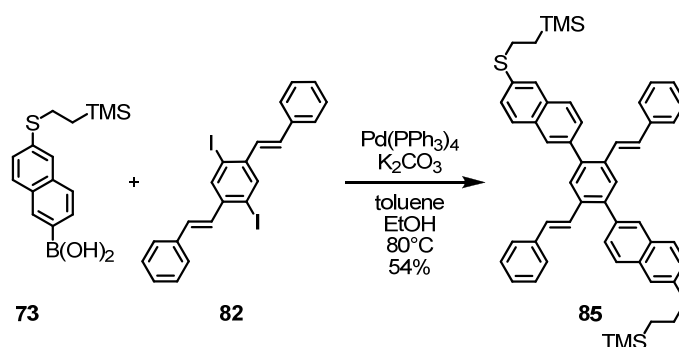
<sup>13</sup>C NMR (101 MHz, CDCl<sub>3</sub>, 25 °C): δ = 194.0, 141.6, 139.7, 137.2, 134.7, 134.2, 130.7, 130.3, 128.7, 127.8, 127.7, 127.0, 126.6, 126.4, 30.3 ppm.

MS (EI): *m/z* (%) = 582.2 (100) [M<sup>+</sup>], 540.2 (96), 498.1 (38).

UV/Vis: λ<sub>max</sub> 295, 347 nm.

GPC (oligopore 6 μm, toluene, UV/vis photodiode array detector) area 99.2%.

### 1,4-bis(6-(2-(trimethylsilyl)ethylthio)naphthalen-2-yl)-2,5-bis((E)-styrene)benzene (**85**)



The iodide **82** (91.0 mg, 0.170 mmol) and the boronic acid (107 mg, 0.352 mmol) were dissolved in toluene (8 ml) and ethanol (2 ml). The mixture was degassed, before Pd(PPh<sub>3</sub>)<sub>4</sub> (25 mg, 0.0217 mmol) and K<sub>2</sub>CO<sub>3</sub> (188 mg, 1.36 mmol) were added. The reaction mixture was exposed to microwaves (500 W, 85 °C) for 3 hours and then evaporated, absorbed on silica gel and chromatographed (silica gel, 2 x 12 cm, hexane : CH<sub>2</sub>Cl<sub>2</sub> = 5:1 → 1:1) to give the product as a colorless solid (73.0 mg, 0.0913 mmol, 54%).

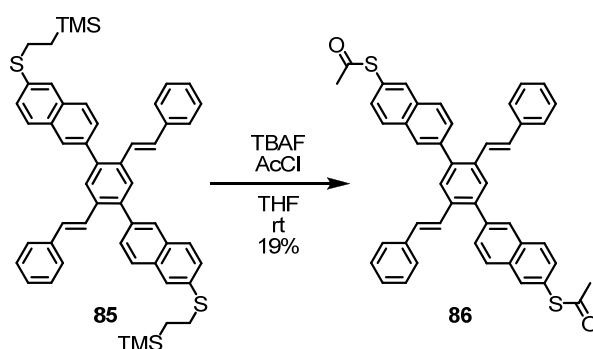
TLC *R<sub>f</sub>* 0.60 (CH<sub>2</sub>Cl<sub>2</sub>:hexane = 1:1).

$^1\text{H}$  NMR (400 MHz,  $\text{CDCl}_3$ , 25 °C):  $\delta$  = 7.94 (s, 2H), 7.87 -7.83 (m, 6H), 7.80 (s, 2H), 7.64 (dd,  $^2J_{\text{H,H}}$  = 1.7 Hz,  $^3J_{\text{H,H}}$  = 8.4 Hz, 2H), 7.48 (dd,  $^2J_{\text{H,H}}$  = 1.8 Hz,  $^3J_{\text{H,H}}$  = 8.5 Hz, 2H), 7.35 (d,  $^3J_{\text{H,H}}$  = 7.2 Hz, 4H), 7.27 (t,  $^3J_{\text{H,H}}$  = 7.4 Hz, 4H), 7.24 – 7.20 (m, 4H), 7.15 (d,  $^3J_{\text{H,H}}$  = 16.2 Hz, 2H), 3.13 (m, 4H), 1.04 (m, 4H), 0.10 (s, 18 H) ppm.

$^{13}\text{C}$  NMR (101 MHz,  $\text{CDCl}_3$ , 25 °C):  $\delta$  = 140.4, 137.7, 137.4, 135.4, 134.8, 132.9, 131.5, 129.8, 128.9, 128.6, 128.5, 128.4, 127.8, 127.7, 127.6, 127.0, 126.8, 126.6, 125.9, 29.3, 16.8, -1.7 ppm.

MS (EI):  $m/z$  (%) = 798.3 (100) [ $\text{M}^+$ ].

### 1,4-bis(6-thioacetylnaphthalen-2-yl)-2,5-bis((E)-styrene)benzene (**86**)



The ethyl-TMS protected cruciform **85** (55 mg, 0.070 mmol) was dissolved in 10 ml THF. It was degassed for 10 minutes before TBAF (1M in THF, 2.00 ml, 2.00 mmol) was added at room temperature. The reaction mixture was stirred for 55 minutes, then acetyl chloride (0.40 ml, 4.61 mmol) was added at 0°C. The mixture was stirred for 40 minutes. Then 5 ml ethanol was added and it was extracted with water and DCM. The aqueous phase was washed twice with DCM. The combined organic phases were washed with water, dried over  $\text{MgSO}_4$ , evaporated and purified by column chromatography (silica, 2x12 cm,  $\text{CH}_2\text{Cl}_2$ :hexane = 1:3 -> 1:1) to give the product **86** as a colorless solid (9.00 mg, 0.0132 mmol, 19%).

TLC  $R_f$  0.37 ( $\text{CH}_2\text{Cl}_2$ :hexane = 1:1).

Mp.: 301 – 304 °C.

$^1\text{H}$  NMR (400 MHz,  $\text{CDCl}_3$ , 25 °C):  $\delta$  = 8.05 (s, 2H), 8.01 (s, 2H), 7.96 (m, 4H), 7.86 (s, 2H), 7.68 (dd,  $^2J_{\text{H,H}}$  = 1.7 Hz,  $^3J_{\text{H,H}}$  = 8.5 Hz, 2H), 7.53 (dd,  $^2J_{\text{H,H}}$  = 1.7 Hz,  $^3J_{\text{H,H}}$  = 8.5 Hz, 2H), 7.35 (d,  $^3J_{\text{H,H}}$  = 7.2 Hz, 4H), 7.28 (m, 4H), 7.21 (m, 2H), 7.17 (s, 4H), 2.51 (s, 6H) ppm.

$^{13}\text{C}$  NMR (126 MHz,  $\text{CDCl}_3$ , 25 °C):  $\delta$  = 194.3, 140.3, 139.5, 137.3, 134.8, 134.3, 133.3, 132.7, 131.5, 130.1, 129.1, 129.0, 128.7, 128.5, 127.9, 127.7, 126.6 (6C), 125.6 ppm.

MS (EI):  $m/z$  (%) = 682.2 (7) [ $\text{M}^+$ ], 640.2 (41), 598.2 (100).

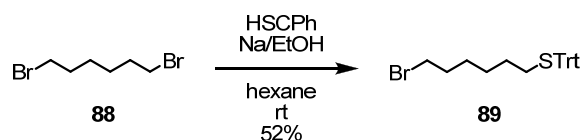
UV/Vis:  $\lambda_{\text{max}}$  317, 354 nm.

GPC (oligopore 6  $\mu\text{m}$ , toluene, UV/vis photodiode array detector) area 99.6%.

## 7.2.2.2 Redox Switches

### 7.2.2.2.1 1,1'-Dithioalkyl Functionalized Ferrocene

#### (6-bromohexyl)(trityl)sulfane (**89**)



Sodium (2.53 g, 0.110 mol, 4.3 eq.) was dissolved in 100 ml ethanol in a 250-ml-2-neckflask. Triphenylmethanthiol (6.36 g, 23.0 mmol, 1.0 eq.) was added and the suspension was stirred for 40 minutes at room temperature before adding via dropping funnel to a solution of 1,6-dibromohexane (5.60 g, 23.0 mmol, 1.0 eq.) in 200 ml hexane in a 500-ml-3-neckflask. The reaction mixture was stirred for six hours at room temperature and then filtrated. The filtrate was evaporated, absorbed on silica and chromatographed (silica gel, 5 x 12 cm, hexane : EtOAc = 20 : 1) to give **89** as a colorless oil which solidifies foam like upon drying on high vacuum to give a colorless solid (5.53 g, 12.6 mmol, 55%).

Mp.: 85.0 – 87.7 °C.

TLC  $R_f$  0.45 (EtOAc : hexane = 1 : 20).

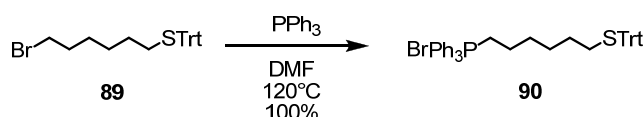
$^1\text{H}$  NMR (400 MHz,  $\text{CDCl}_3$ , 25 °C):  $\delta$  = 7.43 (d,  $^3J_{\text{H,H}}$  = 7.8 Hz, 6H), 7.29 (t,  $^3J_{\text{H,H}}$  = 7.8 Hz, 6H), 7.22 (t,  $^3J_{\text{H,H}}$  = 7.2 Hz, 3H), 3.35 (t,  $^3J_{\text{H,H}}$  = 6.8 Hz, 2H), 2.16 (t,  $^3J_{\text{H,H}}$  = 7.2 Hz, 2H), 1.77 (quin,  $^3J_{\text{H,H}}$  = 7.2 Hz, 2H), 1.40 (quin,  $^3J_{\text{H,H}}$  = 7.1 Hz, 2H), 1.29 (4H, m) ppm.

$^{13}\text{C}$  NMR (101 MHz,  $\text{CDCl}_3$ , 25 °C):  $\delta$  = 145.0, 129.6, 127.8, 126.5, 66.4, 33.8, 32.5, 31.8, 28.3, 28.0, 27.6 ppm.

MS (EI):  $m/z$  (%) = 243.1 (100) [Trt].

EA calcd: C = 68.33, H = 6.19, N = 0.00 found: C = 68.35, H = 6.20, N = 0.00.



**triphenyl(6-(tritylthio)hexyl)phosphonium bromide (90)**

The bromide **89** (1.63 g, 3.71 mmol, 1.0 eq.) and triphenylphosphine (973 mg, 3.71 mmol, 1.0 eq.) were dissolved in 10 ml DMF in a 25-ml-3-neckflask with condenser. The reaction mixture was stirred for 13 hours at 120 °C. DMF was then directly distilled off ( $8 \times 10^{-2}$  mbar, oil bath: 100 °C). The residue was taken up in dichloromethane and precipitated into rapidly stirring hexane. The hexane was decanted off and the sticky-oily residue was dried at vacuum which led to foam formation. After drying at high vacuum the phosphonium salt **90** was obtained as a colorless powder (2.60 g, 3.71 mmol, 100%).

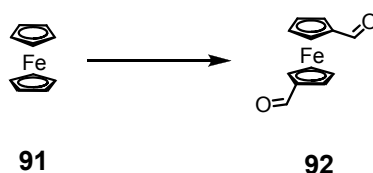
Mp.: 74-76 °C.

$^1\text{H}$  NMR (400 MHz, DMSO, 25 °C):  $\delta$  = 7.90 (m, 3H), 7.77 (m, 12H), 7.31 (m, 12H), 7.23 (m, 3H), 3.51 (m, 2H), 2.05 (m, 2H), 1.43 (m, 2H), 1.30 (m, 2H), 1.20 (m, 4H) ppm.

$^{13}\text{C}$  NMR (101 MHz, DMSO, 25 °C):  $\delta$  = 145.4 (Cq, s), 135.7 (Ct, d,  $^4J_{\text{C,P}} = 2.8$  Hz), 134.4 (Ct, d,  $^2J_{\text{C,P}} = 10.1$  Hz), 131.1 (Ct, d,  $^3J_{\text{C,P}} = 12.4$  Hz), 129.9 (Ct, s), 128.9 (Ct, s), 127.5 (Ct, s), 119.4 (Cq, d,  $^1J_{\text{C,P}} = 85.6$  Hz), 66.9 (Cq, s), 32.1 (Cs, s), 28.7 (Cs, s), 28.4 (Cs, s) ppm (the  $\text{CH}_2$  carbons in  $\alpha$ -,  $\beta$ - and  $\gamma$ -position to the phosphor couple with the phosphor and their peaks are not seen in the spectra).<sup>[206]</sup>

MS (FAB):  $m/z$  (%) = 621.3 (100) [ $\text{M}^+$ ].

EA calcd: C = 73.60, H = 6.03, N = 0.00 found: C = 70.98, H = 6.33, N = 0.16.

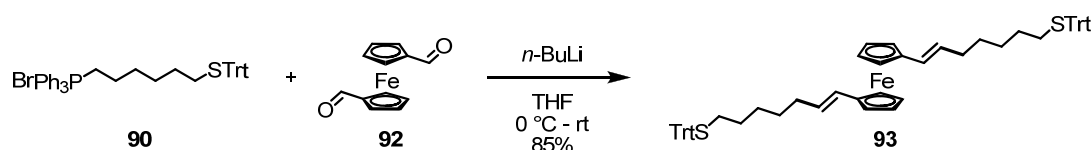
**1, 1'-dicarboxaldehydeferrocene (92)<sup>[207]</sup>**

Ferrocene (5.0 g, 26.9 mmol, 1.0 eq.) was dissolved in 60 ml diethylether (crown cap) in a 250-ml-3-neckflask (dry, Ar). *n*-BuLi (35.3 ml, 1.6 M in hexane, 57.0 mmol, 2.1 eq.) was added at -78 °C. Then tetramethylethylenediamin (TMEDA) (8.5 ml) was added. It was stirred at room temperature for 17 hours. Then 6.5 ml DMF was added (freshly distilled) dropwise over 20 minutes at -78°C. It was stirred for 2.5 hours at

-78 °C and then quenched with water. The reaction mixture was extracted with dichloromethane. The aqueous phase was washed twice with dichloromethane, the combined organic phases were washed with water, dried over MgSO<sub>4</sub>, filtrated and evaporated. The crude was dissolved in 200 ml cyclohexane. The insoluble black shit was filtrated off. The filtrated was evaporated and recrystallized from cyclohexane to give the dialdehyde **92** as a red solid (1.07 g, 16%).

<sup>1</sup>H-NMR (250 MHz, CDCl<sub>3</sub>, 25 °C): δ = 9.94 (2H, s), 4.78 (8H, m) ppm.

### 1,1'-(di(1-(7-tritylsulfanyl)hepten))ferrocene (**93**)



The phosphonium salt **90** (795 mg, 1.13 mmol, 1.0 eq.) was dissolved in 44 ml dry THF in a 100-ml-2-neckflask. *n*-BuLi (1.6 M in hexane, 650 μl, 1.04 mmol, 0.92 eq.) was added at 0 °C dropwise. The color changed from colorless to orange to dark brown-reddish. It was stirred for 40 minutes at 0 °C, then 1,1'-dicarboxaldehydeferrocene (**92**) (88 mg, 0.364 mmol, 0.32 eq.), dissolved in 25 ml dry THF was added over 20 minutes. The reaction mixture was then stirred for three hours at room temperature and it was then quenched with saturated aqueous sodium bicarbonate. It was then extracted twice with TBME. The combined organic phases were washed with brine, dried over MgSO<sub>4</sub> and evaporated. The crude was purified by column chromatography (silica gel, 4 x 12 cm, CH<sub>2</sub>Cl<sub>2</sub> : hexane = 1 : 1) to give the olefin **93** as an orange oil (286 mg, 0.309 mmol, 85%).

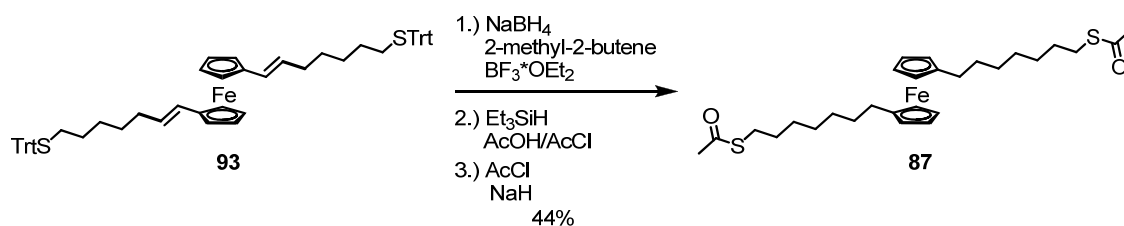
TLC *R<sub>f</sub>* 0.40 (CH<sub>2</sub>Cl<sub>2</sub>: hexane = 1 : 1).

<sup>1</sup>H NMR (400 MHz, CDCl<sub>3</sub>, 25 °C): δ = 7.42 (m, 12H), 7.28 (m, 12H), 7.20 (m, 6H), 5.96-5.89 (m, 2H), 5.42-5.35 (m, 2H), 4.24-4.13 (m, 8H), 2.15 (m, 8H), 1.41 (m, 4H), 1.30 (m, 8H) ppm.

<sup>13</sup>C NMR (101 MHz, CDCl<sub>3</sub>, 25 °C): δ = 145.0, 129.62, 129.58, 127.8, 126.5, 125.4, 70.2, 69.61, 69.59, 66.4, 32.0, 29.3, 28.9, 28.8, 25.5 ppm.

MS (MALDI-TOF): found *m/z* = 926.6462, 926.3642 calculated for C<sub>62</sub>H<sub>62</sub>FeS<sub>2</sub>.

EA calcd: C = 80.32, H = 6.74, N = 0.00 found: C = 80.13, H = 6.55, N = 0.00.

**1,1'-(di(1-(7-thioacetyl)heptane))ferrocene (87)**

Sodium borohydride (46.2 mg, 1.22 mmol, 4.62 eq.) was suspended in 5 ml dry dimethylethyl glycole (previously stored 2 days over CaCl<sub>2</sub> and then distilled over Na/benzophenone). 2-Methyl-2-butene (344  $\mu$ l, 3.25 mmol, 12.3 eq.) was added. Then boron trifluoride etherate (196  $\mu$ l, 1.58 mmol, 6.0 eq.) was added dropwise at 0 °C over 10 minutes. Then the olefin **93** (245 mg, 0.264 mmol, 1.0 eq.) dissolved in 4 ml dry dimethylethyl glycole was added dropwise. Gas evolution was observed when a drop of the olefin was mixed with the dialkylborane solution. When the gas evolution decreased the next drop of the olefin was added. Initially the orange color of the olefin disappeared upon touching the surface of the colorless Sia<sub>2</sub>BH solution but after a while the color remained. The temperature was always kept at 0 – 10 °C. After complete addition of the olefin the reaction mixture was stirred additionally for 30 minutes at room temperature and for 45 minutes at 35 °C. Then triethylsilane (400  $\mu$ l, 0.250 mmol, 0.95 eq.) and 6 ml of an 1 : 1 mixture of acetyl chloride and acetic acid (previously stirred for 10 minutes) were added simultaneously at room temperature while cooling with an ice bath. The reaction mixture turned yellowish and was stirred for 10 minutes at 38 °C and one hour at 100 °C. It was then cooled to 0 °C and acetyl chloride (0.5 ml, 14.1 mmol, 53 eq.) and sodium hydride (35 mg, 55 % on petroleum, 0.802 mmol, 3.0 eq.) were added. The reaction mixture was stirred for 15 minutes at room temperature and was then quenched carefully with ice. It was extracted with water and TBME. The aqueous phase was washed with TBME. The combined organic phases were washed twice with brine, dried over MgSO<sub>4</sub> and evaporated. The crude was absorbed on silica and purified by column chromatography to give the target molecule **87** as yellow oil which tends to crystallize (62.0 mg, 0.117 mmol, 44%).

TLC *R<sub>f</sub>* 0.33 (EtOAc: hexane = 1 : 5), yellow when stained with KMnO<sub>4</sub> dip.

<sup>1</sup>H NMR (400 MHz, CDCl<sub>3</sub>, 25 °C):  $\delta$  = 3.96 (m, 4H), 3.95 (m, 4H), 2.86 (t, <sup>3</sup>*J*<sub>H,H</sub> = 7.3 Hz, 4H), 2.29 (t, <sup>3</sup>*J*<sub>H,H</sub> = 7.8 Hz, 4H), 1.56 (quin, <sup>3</sup>*J*<sub>H,H</sub> = 7.3 Hz, 4H), 1.47 (m, 4H), 1.37 – 1.30 (m, 12H) ppm.

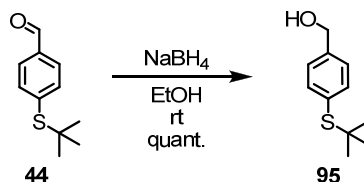
$^{13}\text{C}$  NMR (101 MHz,  $\text{CDCl}_3$ , 25 °C):  $\delta$  = 196.0 (Cq), 89.2 (Cq), 68.6 (Ct), 67.7 (Ct), 31.2 (Cs), 30.6 (Cp), 29.5 (Cs), 29.40 (Cs), 29.37 (Cs), 29.1 (Cs), 29.0 (Cs), 28.7 (Cs) ppm.

MS (MALDI-TOF): found  $m/z$  = 530.6976, 530.1976 calculated for  $\text{C}_{28}\text{H}_{42}\text{FeO}_2\text{S}_2$ .

EA calcd: C = 63.38, H = 7.98, N = 0.00 found: C = 63.56, H = 8.06, N = 0.00.

### 7.2.2.2.2 1,1'-Distyrene-Ferrocene Based Redox Switch

#### (4-(tert-butylthio)phenyl)methanol (**95**)<sup>[226]</sup>



In a 100 mL oven dried two-neck flask 4-(tert-butylthio)benzaldehyde (7.00 g, 36.0 mmol, 1.0 eq.) and dry EtOH (100 mL) was furnished and cooled with an ice bath. NaBH<sub>4</sub> (1.51 g, 39.9 mmol, 1.1 eq.) was added in portions during 10 min. while stirring. The reaction mixture was stirred for 70 min. and then poured over ice (100 g) containing HCl (4M, 60 mL). Saturated NaCl (300 mL) was added and then extracted with tBME (4x60 mL). The combined organics were washed with water (1x50 mL), dried over MgSO<sub>4</sub> and concentrated in vacuo. Removal of the staying solvent on the high vacuum gave the alcohol **95** as a colorless oil (7.11 g, 36.2 mmol, quant., Lit.<sup>[226]</sup>: 92 %).

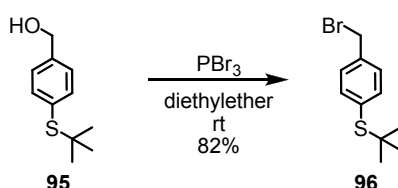
TLC R<sub>f</sub> = 0.11 (TBME:hexane, 1:4).

<sup>1</sup>H NMR (400 MHz, CDCl<sub>3</sub>, 25 °C): δ = 7.55-7.48 (m, 2H), 7.36-7.29 (m, 2H), 4.71 (s, 2H), 1.28 (s, 9H) ppm.

<sup>13</sup>C NMR (101 MHz, CDCl<sub>3</sub>, 25 °C): δ = 141.4, 137.6, 131.8, 126.9, 64.8, 45.9, 30.9.

MS(EI): *m/z* (%) = 196 (M<sup>+</sup>, 22), 140 (100), 107 (33), 77 (12), 57 (28) ppm.

EA: calculated: C = 67.30, H = 8.22, found: C = 67.24, H = 8.18.

**(4-(bromomethyl)phenyl)(tert-butyl)sulfane (96)**<sup>[226]</sup>

In a 250 mL oven dried three-neck flask (Ar) the alcohol (6.56 g, 33.4 mmol, 1.0 eq.) and dry diethylether (65 mL) was added and cooled with an ice bath. PBr<sub>3</sub> (3.50 mL, 36.7 mmol, 1.1 eq.) was added dropwise while stirring for about 15 min. The reaction mixture was stirred at rt. For 90 min. and water (200 mL) was added slowly while cooling. The layers were separated and the aqueous phase was extracted with dry diethylether (3x60 mL). The combined organics were washed with brine (1x50 mL), dried over MgSO<sub>4</sub> and filtered. Removal of the solvent gave a crystalline, white and solid raw product (7.80 g, 30.1 mmol, 90 %). A recrystallization from hexane/EtOAc did not afford more pure product and therefore the benzyl-bromide (7.10 g, 27.4 mmol, 82 %) was not purified any more for the next step.

TLC (SiO<sub>2</sub>, TBME:hexane, 1:4, UV): R<sub>f</sub> = 0.59.

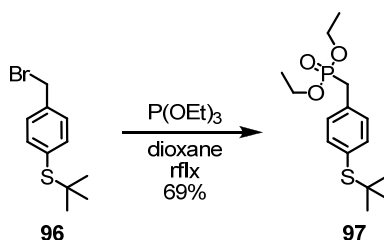
Mp: 54.5-54.9 °C (Lit.<sup>[3]</sup>: 59-60°C)

<sup>1</sup>H NMR (400 MHz, CDCl<sub>3</sub>, 25 °C): δ = 7.53-7.47 (m, 2H), 7.38-7.31 (m, 2H), 4.49 (s, 2H), 1.29 (s, 9H) ppm.

<sup>13</sup>C NMR (101 MHz, CDCl<sub>3</sub>, 25 °C): δ = 138.2, 137.7, 133.1, 129.0, 46.2, 32.8, 31.0 ppm.

MS(EI): *m/z* (%) = 260 (M<sup>+</sup>, 7), 204 (13), 179 (8), 123 (100), 78 (5), 57 (38).

EA: calculated: C = 50.97, H = 5.83, found: C = 51.87, H = 5.66.

**diethyl 4-(tert-butylthio)benzylphosphonate (97)**<sup>[226]</sup>

In a 100 mL oven dried two-neck flask (Ar) a solution of 4-(*tert*-butylthio)benzyl-bromide (5.18 g, 20.0 mmol, 1.0 eq.) and triethyl-phosphite (4.40 mL, 27.3 mmol, 1.37 eq.) in dry dioxane (30 mL) was refluxed under argon over night. The solvent was evaporated and the liquid crude product was transferred in a 25 mL flask. A

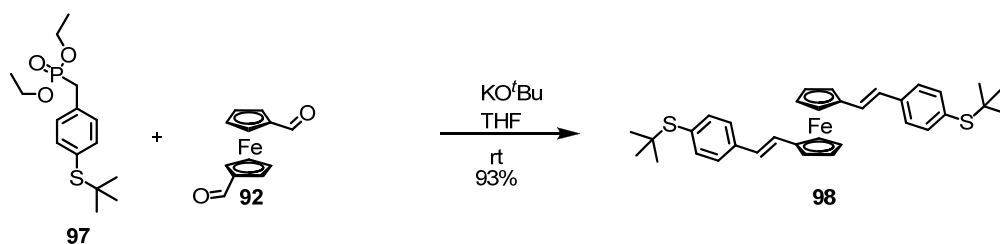
vacuum distillation was done ( $145^{\circ}\text{C}$ ,  $2.8 \cdot 10^{-2}$  mbar) to give the desired, oily and colorless phosphonate (4.34 g, 13.7 mmol, 68.7 %).

$^1\text{H}$  NMR (400 MHz,  $\text{CDCl}_3$ ,  $25^{\circ}\text{C}$ ):  $\delta$  = 7.48-7.44 (m, 2H), 7.28-7.24 (m, 2H), 4.05-3.94 (m, 4H), 3.18 (s, 1H), 3.12 (s, 1H), 1.26 (s, 9H), 1.22 (t,  $^3J_{\text{HH}} = 7.07$  Hz, 6H) ppm.

$^{13}\text{C}$  NMR (101 MHz,  $\text{CDCl}_3$ ,  $25^{\circ}\text{C}$ ):  $\delta$  = 137.5, 132.5, 131.2, 129.9, 62.2, 45.8, 34.2, 32.9, 30.9, 16.4 ppm.

MS(EI):  $m/z$  (%) = 316 ( $\text{M}^+$ , 14), 260 (100), 232 (25), 204 (27), 123 (56), 81 (9), 57 (18).

EA: calculated: C = 56.94, H = 7.96, found: C = 55.51, H = 7.83.

**1,1'-di(4-*tert*-butylthio-*E*-styrene)ferrocene (**98**)**

1,1'-ferrocenedicarboxaldehyde (75.0 mg, 0.310 mmol, 1.0 eq.) and the phosphonate **97** (215 mg, 0.680 mmol, 2.2 eq.) were dissolved in dry THF (5 ml) in a 25-ml-2-neckflask (dry, Ar). Potassium *tert*-butoxide (187 mg, 1.67 mmol, 5.4 eq.) was then added portion wise over 10 minutes at 0 °C. It was stirred for 3 hours at room temperature. The reaction mixture was then extracted with water and dichloromethane. The aqueous phase was washed three times with dichloromethane. The combined organic phases were dried over MgSO<sub>4</sub>, evaporated, absorbed on silica and chromatographed (silica gel, 2x12 cm, hexane:EtOAc = 5:1) to give the product as a red solid (163 mg, 0.288 mmol, 93%).

Mp.: 163.5 – 167.4 °C.

TLC *R<sub>f</sub>* 0.52 (hexane : EtOAc = 5 : 1).

<sup>1</sup>H NMR (400 MHz, CDCl<sub>3</sub>, 25 °C, grunder.445): δ = 7.43 (d, <sup>3</sup>*J*<sub>H,H</sub> = 8.2 Hz, 4H), 7.28 (d, <sup>3</sup>*J*<sub>H,H</sub> = 8.2 Hz, 4H), 6.84 (d, <sup>3</sup>*J*<sub>H,H</sub> = 16.2 Hz, 2H), 6.64 (d, <sup>3</sup>*J*<sub>H,H</sub> = 16.2 Hz, 2H), 4.42 (m, 4H), 4.29 (m, 4H), 1.31 (s, 18H) ppm.

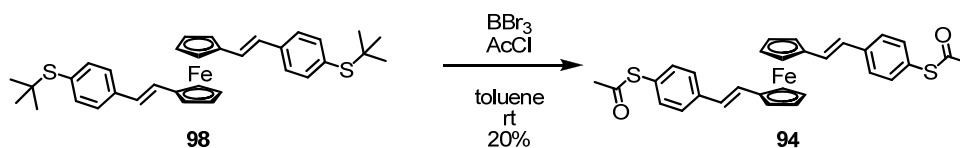
<sup>13</sup>C NMR (101 MHz, CDCl<sub>3</sub>, 25 °C): δ = 138.0, 137.7, 130.9, 127.3, 125.7, 83.8, 70.3, 68.2, 46.0, 31.0 ppm.

MS (ESI): *m/z* (%) = 566.4 [M<sup>+</sup>].

EA calcd: C = 72.07, H = 6.76, found: C = 71.83, H = 6.82.

UV/Vis: λ<sub>max</sub> 306, 335 nm.



**1,1'-di(4-thioacetyl-E-styrene)ferrocene (94)**

The starting material **98** (95 mg, 0.168 mmol, 1.0 eq.) was dissolved in a well degassed mixture of 30 ml dry toluene and 7.5 ml acetyl chloride in a 100-ml-2-neckflask (dry, Ar). Then Borontribromide (1 M in DCM, 0.400 ml, 0.400 mmol, 2.38 eq.) was added dropwise over 10 minutes at room temperature. The reaction mixture was then stirred for 2 hours at room temperature and then quenched with ice/water at 0°C. The reaction mixture was extracted with toluene and water. The aqueous phase was washed with 3 x 30 ml toluene. The combined organic phases were washed with brine, dried over MgSO<sub>4</sub> and evaporated. The crude was purified by column chromatography (silica gel, 2 x 12 cm, hexane : EtOAc = 5 : 1), to give the product as a red solid (14 mg, 0.0260 mmol, 16%).

Mp.: 145.5 – 146.8 °C.

TLC *R<sub>f</sub>* 0.25 (hexane : EtOAc = 5 : 1).

<sup>1</sup>H NMR (500 MHz, CDCl<sub>3</sub>, 25 °C): δ = 7.28 (d, <sup>3</sup>*J*<sub>H,H</sub> = 8.4 Hz, 4H), 7.25 (d, <sup>3</sup>*J*<sub>H,H</sub> = 8.3 Hz, 4H), 6.77 (d, <sup>3</sup>*J*<sub>H,H</sub> = 16.1 Hz, 2H), 6.59 (d, <sup>3</sup>*J*<sub>H,H</sub> = 16.2 Hz, 2H), 4.43 (m, 4H), 4.29 (m, 4H), 2.44 (s, 6H) ppm.

<sup>13</sup>C NMR (126 MHz, CDCl<sub>3</sub>, 25 °C): δ = 194.3, 138.8, 134.6, 127.7, 126.3, 125.6, 83.8, 70.3, 68.2, 30.2 ppm.

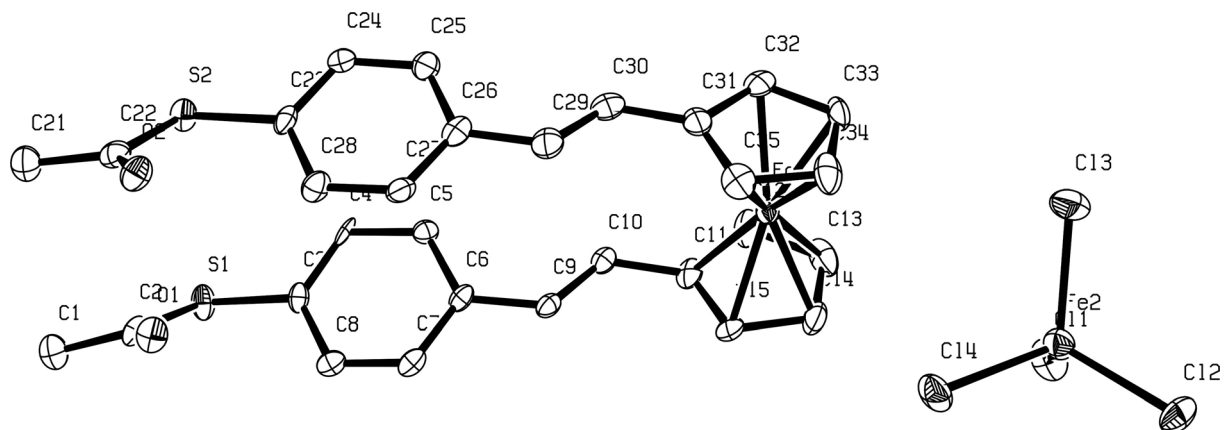
MS (ESI): *m/z* (%) = 538.3 [M<sup>+</sup>].

EA calcd: C = 66.91, H = 4.87, found: C = 65.62, H = 4.85.

UV/Vis: λ<sub>max</sub> 302, 339 nm.

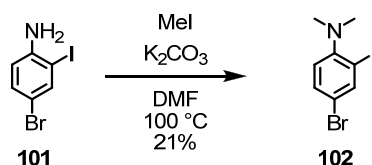
Crystal data for **94**: formula C<sub>30</sub>H<sub>26</sub>Cl<sub>4</sub>Fe<sub>2</sub>O<sub>2</sub>S<sub>2</sub>, M = 736.17, F(000) = 748, red plate, size 0.04 · 0.13 · 0.21 mm<sup>3</sup>, triclinic, space group P -1, Z = 2, a = 10.5400(8) Å, b = 11.4409(10) Å, c = 14.5335(11) Å, α = 84.736(4)°, β = 71.076(4)°, γ = 67.903(4)°, V = 1535.1(2) Å<sup>3</sup>, D<sub>calc.</sub> = 1.593 Mg · m<sup>-3</sup>. The crystal was measured on a Nonius KappaCCD diffractometer at 173K using graphite-monochromated Mo K<sub>α</sub>-radiation with λ = 0.71073 Å, Θ<sub>max</sub> = 26.443°. Minimal/maximal transmission 0.83/0.94, μ = 1.457 mm<sup>-1</sup>. The COLLECT suite has been used for datacollection and integration. From a total of 18669 reflections, 6188 were independent (merging r = 0.058). From these, 3717 were considered as observed (I > 1.8σ(I)) and were used to refine 361 parameters. The structure was solved by direct methods using the program SIR92.

Least-squares refinement against  $F$  was carried out on all non-hydrogen atoms using the program CRYSTALS.  $R = 0.0550$  (observed data),  $wR = 0.1721$  (all data),  $GOF = 1.1351$ . Minimal/maximal residual electron density =  $-0.68/0.96 \text{ e } \text{\AA}^{-3}$ . Chebychev polynomial weights were used to complete the refinement.



### 7.2.3. Cross-Conjugated Molecular Rectifier

#### 4-bromo-2-iodo-*N,N*-dimethylaniline (**102**)<sup>[239]</sup>



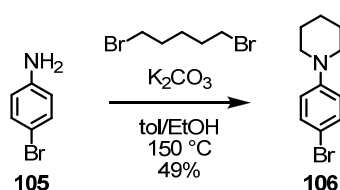
4-Bromo-2-iodo-aniline (511 mg, 1.72 mmol, 1.0 eq.) was suspended in 5 ml DMF (crown cap) in a 25-ml-2-neck flask. K<sub>2</sub>CO<sub>3</sub> (1.19 g, 8.60 mmol, 5.0 eq.) and methyl iodide (322  $\mu$ l, 732 mg, 5.16 mmol, 3.0 eq.) were added and it was heated to 100 °C for 12 hours. The reaction mixture was then quenched with water and extracted with TBME. The aq. phase was washed three times with ether. The combined organic phases were washed twice with brine, dried over MgSO<sub>4</sub> and evaporated. The crude was purified by column chromatography (CC) to give the product **102** (116 mg, 0.356 mmol, 21%).

TLC *R<sub>f</sub>* 0.32 (EtOAc : hexane = 1 : 20).

<sup>1</sup>H NMR (400 MHz, CDCl<sub>3</sub>, 25 °C):  $\delta$  = 7.95 (s, 1H), 7.41 (d, <sup>3</sup>*J*<sub>H,H</sub> = 8.5 Hz, 1H), 6.93 (d, <sup>3</sup>*J*<sub>H,H</sub> = 8.5 Hz, 1H), 2.74 (s, 6H) ppm.

<sup>13</sup>C NMR (101 MHz, CDCl<sub>3</sub>, 25 °C):  $\delta$  = 147.3, 140.2, 132.1, 110.8, 108.4, 84.9, 31.0 ppm.

#### 1-(4-Bromophenyl)piperidine (**106**)<sup>[240]</sup>

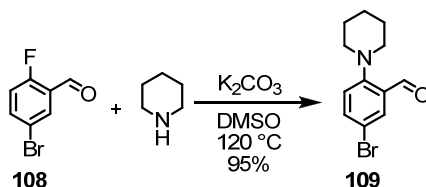


4-Bromoaniline (1.00 g, 5.81 mmol, 1.0 eq.) and K<sub>2</sub>CO<sub>3</sub> (883 mg, 6.39 mmol, 1.10 eq.) were suspended in 20 ml water in a 40-ml-pressure tube. 1,5-dibromopentane (874  $\mu$ l, 1.47 g, 6.39 mmol, 1.10 eq.) was added, the tube was sealed and exposed to microwaves (200 W, 120 °C) for 20 minutes. The reaction mixture was cooled to rt and extracted with water and ethyl acetate. The aq. phase was washed twice with ethyl acetate. The combined organic phases were washed with brine, dried over MgSO<sub>4</sub> and evaporated. The crude was purified by CC (silica gel, 4 x 12 cm, hex:EtOAc = 20 : 1) to give the product in 49% yield (680 mg, 2.83 mmol, 49%).

TLC  $R_f$  0.48 (EtOAc : hexane = 1 : 20).

$^1\text{H}$  NMR (400 MHz,  $\text{CDCl}_3$ , 25 °C):  $\delta$  = 7.31 (d,  $^3J_{\text{H,H}}$  = 9.0 Hz, 2H), 6.79 (d,  $^3J_{\text{H,H}}$  = 9.0 Hz, 2H), 3.12 (m, 4H), 1.68 (m, 4H), 1.59 (m, 2H) ppm.

### 5-Bromo-2-piperidinobenzaldehyde (109)<sup>[245]</sup>



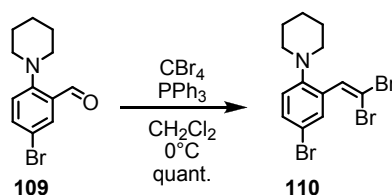
2-Fluoro-5-bromobenzaldehyde (7.18 g, 35.4 mmol, 1.0 eq.) was dissolved in 20 ml DMSO (crown cap) in a 50-ml-3-neck flask with condenser. Piperidine (3.84 ml, 3.31 g, 38.9 mmol, 1.1 eq.) and  $\text{K}_2\text{CO}_3$  (5.43 g, 39.3 mmol, 1.11 eq.) were then added. The reaction mixture was stirred for 8.5 hours at 120 °C, then cooled to rt and extracted with water and TBME. The aq. phase was washed three times with TBME. The combined organic phases were washed three times with water, dried over  $\text{MgSO}_4$ , evaporated and dried at high vacuum to give the product as a brownish oil (8.98 g, 33.5 mmol, 95%).

TLC  $R_f$  0.49 (EtOAc : hexane = 1 : 10).

$^1\text{H}$  NMR (400 MHz,  $\text{CDCl}_3$ , 25 °C):  $\delta$  = 10.19 (s, 1H), 7.88 (d,  $^4J_{\text{H,H}}$  = 2.5 Hz, 1H), 7.56 (dd,  $^3J_{\text{H,H}}$  = 8.7 Hz,  $^4J_{\text{H,H}}$  = 2.5 Hz, 1H), 6.97 (d,  $^3J_{\text{H,H}}$  = 8.7 Hz, 1H), 3.02 (m, 4H), 1.75 (m, 4H), 1.60 (m, 2H) ppm.

$^{13}\text{C}$  NMR (101 MHz,  $\text{CDCl}_3$ , 25 °C):  $\delta$  = 190.2, 155.7, 137.3, 131.7, 129.9, 121.0, 115.0, 55.6, 26.1, 23.9 ppm.

MS (EI):  $m/z$  (%) = 269.0 (99), 267.0 (100) [ $\text{M}^+$ ].

**5-Bromo-2-piperidino-(2,2-dibromovinyl)benzene (110)**

Triphenylphosphine (1.33 g, 5.07 mmol, 4.0 eq.) and 5-bromo-2-piperidino-benzaldehyde (340 mg, 1.27 mmol, 1.0 eq.) were dissolved in 6 ml dichloromethane (crown cap) in a 10-ml-schlenkflask. Carbontetrabromide (298  $\mu\text{l}$ , 841 mg, 2.54 mmol, 2.0 eq.) was then added drop wise at 0 °C which led to a precipitation. It was stirred for 30 minutes at 0 °C and then filtrated over a 2 x 3 cm silica plug, eluting with hexane : ethyl acetate = 5 : 1. The filtrate was evaporated to give an colorless oil which solidified upon drying at high vacuum (538 mg, 1.27 mmol, 100%).

Mp.: 90.9 – 91.8 °C

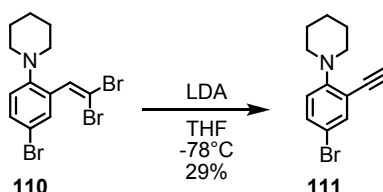
TLC  $R_f$  0.66 (EtOAc : hexane = 1 : 5).

$^1\text{H}$  NMR (400 MHz,  $\text{CDCl}_3$ , 25 °C):  $\delta$  = 7.77 (d,  $^4J_{\text{H,H}} = 2.0$  Hz, 1H), 7.46 (s, 1H), 7.38 (dd,  $^3J_{\text{H,H}} = 8.6$  Hz,  $^4J_{\text{H,H}} = 2.3$  Hz, 1H), 6.84 (d,  $^3J_{\text{H,H}} = 8.6$  Hz, 1H), 2.85 (t,  $^3J_{\text{H,H}} = 5.2$  Hz, 4H), 1.71 (m, 4H), 1.57 (m, 2H) ppm.

$^{13}\text{C}$  NMR (101 MHz,  $\text{CDCl}_3$ , 25 °C):  $\delta$  = 151.4, 134.5, 132.0, 131.8, 131.4, 120.1, 114.4, 89.9, 53.6, 26.4, 24.1 ppm.

MS (EI):  $m/z$  (%) = 424.9 (30), 422.9 (31) [ $\text{M}^+$ ], 344.0 (47), 341.9 (31), 264.0 (100).

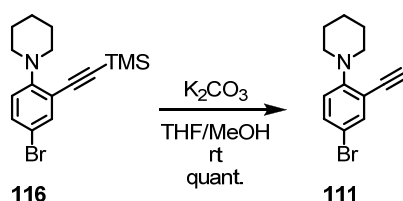
EA calcd: C = 36.83, H = 3.33, N = 3.30 found: C = 36.86, H = 3.33, N = 3.08.

**5-Bromo-2-piperidino-1-(ethynyl)benzene (111)**

*n*-BuLi (1.6 M in hexane, 1.50 ml, 2.41 mmol, 4.0 eq.) was added to diisopropylamine (183  $\mu\text{l}$ , 244 mg, 2.41 mmol, 4.0 eq.) in 2 ml dry THF (crown cap) at -78 °C. It was stirred for 10 minutes, and then transferred via syringe to a -78 °C solution of the dibromoolefin **110** in 4 ml THF in a 10-ml-Schlenkflask. The pale brownish solution turned immediately black. The cooling-bath was removed and it was stirred for one hour. The reaction mixture was then quenched with water and extracted with TBME. The aq. Solution was washed twice with TBME. The combined organic phases were

washed twice with brine, dried over  $\text{MgSO}_4$  and evaporated. The crude was purified by CC (silica gel, 2 x 12 cm, hexane : ethyl acetate = 10 : 1) to give the product as a colorless oil (46.0 mg, 0.174 mmol, 29%). Caution: The product is instable and needs to be handled with care. It was directly used after isolation.

Alternative route:



The TMS-protected acetylene **116** (225 mg, 0.669 mmol, 1.0 eq.) was dissolved in 10 ml THF and 10 ml MeOH in a 25-ml-Schlenkflask protected with an alumina foil to avoid light irradiation. Then  $\text{K}_2\text{CO}_3$  (102 mg, 0.736 mmol, 1.1 eq.) was added and it was stirred for 3.5 hours at room temperature. The reaction mixture was then quenched with water and extracted with dichloromethane. The aq. phase was washed twice with dichloromethane. The combined organic phases were dried over  $\text{MgSO}_4$ , evaporated and dried at the high vacuum to give a yellowish oil (177 mg, 0.669 mmol, 100%).

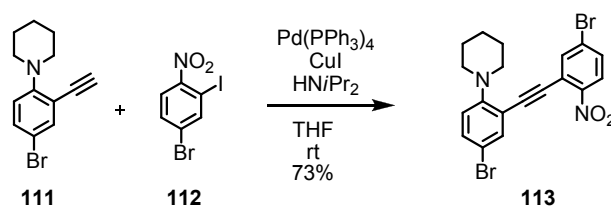
TLC  $R_f$  0.57 (EtOAc : hexane = 1 : 10).

$^1\text{H}$  NMR (400 MHz,  $\text{CDCl}_3$ , 25 °C):  $\delta$  = 7.58 (d,  $^4J_{\text{H,H}}$  = 2.5 Hz, 1H), 7.38 (dd,  $^3J_{\text{H,H}}$  = 8.7 Hz,  $^4J_{\text{H,H}}$  = 2.5 Hz, 1H), 6.81 (d,  $^3J_{\text{H,H}}$  = 8.7 Hz, 1H), 3.44 (s, 1H), 3.11 (m, 4H), 1.76 (m, 4H), 1.60 (m, 2H) ppm.

$^{13}\text{C}$  NMR (125.8 MHz,  $\text{CDCl}_3$ , 25 °C): 155.2, 136.7, 132.6, 119.5, 117.6, 113.0, 83.1, 81.1, 52.7, 26.1, 21.1 ppm.

MS (EI):  $m/z$  (%) = 265.0 (67), 264.0 (100), 263.0 (69) [ $\text{M}^+$ ], 262.0 (94), 236.0 (54), 234.0 (55).

EA calcd: C = 59.11, H = 5.34, N = 5.30 found: C = 59.21, H = 5.31, N = 5.17.

**4-Bromo-6-(2-(3-bromo-6-piperidino)ethynyl)-1-(nitro)benzene (113)**

The acetylene **111** (150 mg, 0.568 mmol, 1.0 eq.) was dissolved in 25 ml dry THF and 10 ml dry diisopropylamine in a 50-ml-2-neckflask. It was degassed for 15 minutes, before 4-bromo-2-iodonitrobenzene (**112**) (186 mg, 0.568 mmol, 1.0 eq.), Pd(PPh<sub>3</sub>)<sub>4</sub> (66.0 mg, 0.0571 mmol, 10.1 mol%) and CuI (11.0 mg, 0.0578 mmol, 10.2 mol%) were added at 0 °C. The reaction mixture was stirred for 18 hours at room temperature and then quenched with water and extracted with dichloromethane. The aq. Phase was washed twice with dichloromethane. The organic phase was dried over MgSO<sub>4</sub>, evaporated, absorbed on silica gel and purified by CC (silica gel, 3 x 12 cm, hexane : ethyl acetate = 20 : 1) to give the product **113** as an orange solid which was further recrystallized from hexane (193 mg, 0.416 mmol, 73%).

Mp.: 86.6 – 88.6 °C

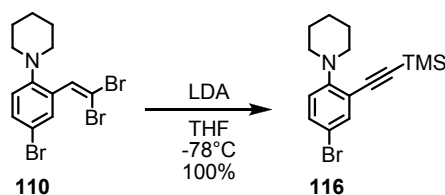
TLC *R<sub>f</sub>* 0.29 (EtOAc : hexane = 1 : 20).

<sup>1</sup>H NMR (400 MHz, CDCl<sub>3</sub>, 25 °C): δ = 7.99 (d, <sup>3</sup>*J*<sub>H,H</sub> = 8.8 Hz, 1H), 7.84 (d, <sup>4</sup>*J*<sub>H,H</sub> = 2.1 Hz, 1H), 7.65 (d, <sup>4</sup>*J*<sub>H,H</sub> = 2.5 Hz, 1H), 7.59 (dd, <sup>3</sup>*J*<sub>H,H</sub> = 8.8 Hz, <sup>4</sup>*J*<sub>H,H</sub> = 2.1 Hz, 1H), 7.39 (dd, <sup>3</sup>*J*<sub>H,H</sub> = 8.8 Hz, <sup>4</sup>*J*<sub>H,H</sub> = 2.5 Hz, 1H), 6.83 (d, <sup>3</sup>*J*<sub>H,H</sub> = 8.8 Hz, 1H), 3.17 (t, <sup>3</sup>*J*<sub>H,H</sub> = 5.3 Hz, 4H), 1.76 (m, 4H), 1.60 (m, 4H) ppm.

<sup>13</sup>C NMR (101 MHz, CDCl<sub>3</sub>, 25 °C): δ = 154.9, 147.7, 137.1, 136.9, 133.5, 131.6, 127.7, 126.2, 120.7, 119.6, 116.9, 113.0, 96.5, 89.4, 52.9, 26.2, 24.1 ppm.

MS (EI): *m/z* (%) = 466.0 (29), 464.0 (63) [M<sup>+</sup>], 462.0 (30), 449.0 (38), 447.0 (81), 445.0 (38), 418.0 (50), 416.0 (94), 414.0 (45), 169.1 (100).

EA calcd: C = 49.17, H = 3.47, N = 6.04 found: C = 49.40, H = 3.46, N = 5.94.

**5-Bromo-2-piperidino-1-(2-trimethylsilane-ethynyl)benzene (116)**

The dibromoolefin **110** (1.34 g, 3.16 mmol, 1.0 eq.) was dissolved in 30 ml dry THF in a 100-ml-3-neckflask. Lithium diisopropylamide (LDA) (2 M in THF/*n*-heptane/ethanebenzene, 6.33 ml, 12.7 mmol, 4.0 eq.) was added dropwise at -78 °C. The reaction mixture was stirred for two hours, then trimethylsilanechloride (2.70 ml, 21.1 mmol, 6.7 eq.) was added. It was stirred for one hour at -78 °C, and one hour at room temperature. The reaction mixture was then quenched with water and extracted with TBME. The aqueous phase was washed twice with TBME. The combined organic phases were washed with water and brine, dried over MgSO<sub>4</sub> and evaporated. The crude was purified by CC (silica, 4 x 12 cm, hexane : CH<sub>2</sub>Cl<sub>2</sub> = 1 : 1) to give the TMS-protected acetylene **116** as a colorless liquid (1.025 g, 3.05 mmol, 97 %).

TLC *R<sub>f</sub>* 0.62 (hexane : CH<sub>2</sub>Cl<sub>2</sub> = 1 : 1).

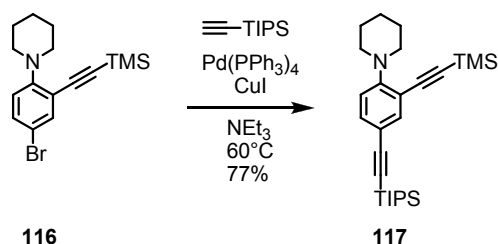
<sup>1</sup>H NMR (400 MHz, CDCl<sub>3</sub>, 25 °C): δ = 7.53 (d, <sup>4</sup>*J*<sub>H,H</sub> = 2.5 Hz, 1H), 7.31 (dd, <sup>3</sup>*J*<sub>H,H</sub> = 8.8 Hz, <sup>4</sup>*J*<sub>H,H</sub> = 2.5 Hz, 1H), 6.74 (d, <sup>3</sup>*J*<sub>H,H</sub> = 8.8 Hz, 1H), 3.11 (t, <sup>3</sup>*J*<sub>H,H</sub> = 5.2 Hz, 4H), 1.73 (m, 4H), 1.58 (m, 2H), 0.26 (s, 9H) ppm.

<sup>13</sup>C NMR (101 MHz, CDCl<sub>3</sub>, 25 °C): δ = 154.8, 136.5, 132.3, 119.2, 118.2, 112.8, 102.3, 100.7, 52.5, 26.2, 24.2, 0.0 ppm.

MS (EI): *m/z* (%) = 337.1 (20) [M<sup>+</sup>], 335.1 (20), 308.0 (37), 306.0 (36), 264.0 (100).

EA calcd: C = 57.14, H = 6.59, N = 4.16 found: C = 57.33, H = 6.51, N = 3.97.



**5-(2-triisopropylsilylacetylene)-2-piperidino-1-(2-trimethylsilane-ethynyl)benzene (117)**

The bromide **116** (985 mg, 2.93 mmol, 1.0 eq.) was dissolved in 35 ml triethylamine in a 100-ml-3-neckflask. It was degassed for 15 minutes, then triisopropylsilylacetylene (1.31 ml, 5.86 mmol, 2.0 eq.), Pd(PPh<sub>3</sub>)<sub>4</sub> (338 mg, 10 mol%) and CuI (55 mg, 10 mol%) were added. The reaction mixture was heated to 60 °C and stirred for 18 hours. After cooling to room temperature, water was added and it was extracted with TBME. The aqueous phase was washed twice with TBME. The combined organic phases were washed with water and brine, dried over MgSO<sub>4</sub> and evaporated. The crude was purified by CC (silica, 4 x 12 cm, hexane : CH<sub>2</sub>Cl<sub>2</sub> = 2 : 1) to give the product **117** as a colorless oil which is crystallizing upon standing (991 mg, 2.26 mmol, 77 %).

Mp.: 82.0 – 83.2 °C

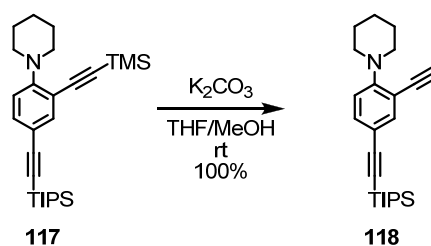
TLC *R<sub>f</sub>* 0.50 (hexane : CH<sub>2</sub>Cl<sub>2</sub> = 2 : 1).

<sup>1</sup>H NMR (400 MHz, CDCl<sub>3</sub>, 25 °C): δ = 7.54 (d, <sup>4</sup>*J*<sub>H,H</sub> = 2.0 Hz, 1H), 7.32 (dd, <sup>3</sup>*J*<sub>H,H</sub> = 8.5 Hz, <sup>4</sup>*J*<sub>H,H</sub> = 2.0 Hz, 1H), 6.78 (d, <sup>3</sup>*J*<sub>H,H</sub> = 8.5 Hz, 1H), 3.16 (t, <sup>3</sup>*J*<sub>H,H</sub> = 5.2 Hz, 4H), 1.73 (m, 4H), 1.58 (m, 2H), 1.11 (s, 21H), 0.26 (s, 9H) ppm.

<sup>13</sup>C NMR (101 MHz, CDCl<sub>3</sub>, 25 °C): δ = 155.9, 138.4, 133.6, 117.7, 116.3, 116.1, 107.0, 103.5, 100.1, 89.5, 52.7, 26.6, 24.7, 19.1, 11.8, 0.5 ppm.

MS (EI): *m/z* (%) = 437.3 (100) [M<sup>+</sup>], 364.3 (60).

EA calcd: C = 74.07, H = 9.90, N = 3.20 found: C = 74.12, H = 9.66, N = 2.90.

**5-(2-triisopropylsilylacetylene)-2-piperidino-1-(ethynyl)benzene (118)**

Compound **117** (738 mg, 1.69 mmol, 1.0 eq.) was dissolved in 40 ml THF and 40 ml MeOH. It was degassed before a 1 M aqueous  $K_2CO_3$  solution (0.850 ml, 0.850 mmol, 0.5 eq.) was added. It was stirred for 4 hours at room temperature. The reaction mixture was then quenched with water and extracted with TBME. The aqueous phase was washed twice with TBME. The combined organic phases were washed with water and brine, dried over  $MgSO_4$  and evaporated and dried at high vacuum to give the free acetylene **118** as a yellowish oil (616 mg, 1.69 mmol, quant.).

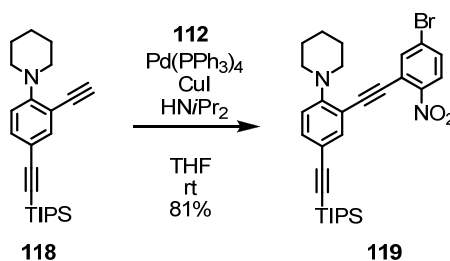
TLC  $R_f$  0.42 (hexane :  $CH_2Cl_2$  = 2 : 1).

$^1H$  NMR (400 MHz,  $CDCl_3$ , 25 °C):  $\delta$  = 7.57 (d,  $^4J_{H,H}$  = 2.0 Hz, 1H), 7.36 (dd,  $^3J_{H,H}$  = 8.5 Hz,  $^4J_{H,H}$  = 2.1 Hz, 1H), 6.82 (d,  $^3J_{H,H}$  = 8.5 Hz, 1H), 3.37 (s, 1H), 3.14 (t,  $^3J_{H,H}$  = 5.2 Hz, 4H), 1.73 (m, 4H), 1.58 (m, 2H), 1.12 (s, 21H) ppm.

$^{13}C$  NMR (101 MHz,  $CDCl_3$ , 25 °C):  $\delta$  = 155.8, 138.2, 133.4, 117.6, 115.9, 115.2, 106.4, 89.4, 82.3, 81.8, 52.5, 26.0, 24.2, 18.7, 11.3 ppm.

MS (EI):  $m/z$  (%) = 365.3 (100)  $[M^+]$ , 322.2 (90) 280.2 (57).

EA calcd: C = 78.84, H = 9.65, N = 3.83 found: C = 78.88, H = 9.48, N = 3.96.

**4-Bromo-6-(2-(3-(2-triisopropylsilylacetylene)-6-piperidino)ethynyl)-1-(nitro)benzene (119)**

The acetylene **118** (480 mg, 1.31 mmol, 1.03 eq.) and the iodide **112** (420 mg, 1.28 mmol, 1.00 eq.) were dissolved in 50 ml dry THF and 20 ml diisopropylamine in a 100-ml-2-neckflask. It was degassed for 15 minutes, then  $Pd(PPh_3)_4$  (145 mg, 9.81%) and  $CuI$  (24 mg, 9.8 mol%) were added. The reaction mixture was stirred

16 hours at room temperature and was then quenched with water and extracted with  $\text{CH}_2\text{Cl}_2$ . The aqueous phase washed twice with  $\text{CH}_2\text{Cl}_2$ . The combined organic phases were dried over  $\text{MgSO}_4$  and evaporated. The crude was absorbed on silica and purified by CC (silica gel, 4 x 12 cm, hexane : ethyl acetate = 20 : 1) to give compound **119** as an orange solid (585 mg, 1.04 mmol, 81%).

Mp.: 90.1 – 91.9 °C.

TLC  $R_f$  0.52 (hexane :  $\text{CH}_2\text{Cl}_2$  = 1:1).

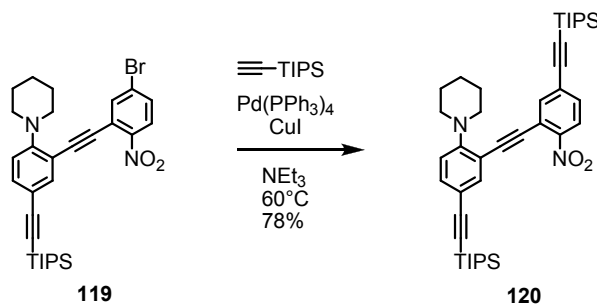
$^1\text{H}$  NMR (400 MHz,  $\text{CDCl}_3$ , 25 °C):  $\delta$  = 7.98 (d,  $^3J_{\text{H,H}}$  = 8.5 Hz, 1H), 7.85 (d,  $^4J_{\text{H,H}}$  = 2.1 Hz, 1H), 7.65 (d,  $^4J_{\text{H,H}}$  = 2.0 Hz, 1H), 7.57 (dd,  $^3J_{\text{H,H}}$  = 8.8 Hz,  $^4J_{\text{H,H}}$  = 2.1 Hz, 1H), 7.40 (dd,  $^3J_{\text{H,H}}$  = 8.5 Hz,  $^4J_{\text{H,H}}$  = 2.1 Hz, 1H), 6.87 (d,  $^3J_{\text{H,H}}$  = 8.6 Hz, 1H), 3.23 (t,  $^3J_{\text{H,H}}$  = 5.4 Hz, 4H), 1.76 (m, 4H), 1.61 (m, 2H), 1.13 (s, 21H) ppm.

$^{13}\text{C}$  NMR (101 MHz,  $\text{CDCl}_3$ , 25 °C):  $\delta$  = 155.5, 147.7, 138.3, 137.2, 134.4, 131.4, 127.6, 126.1, 121.0, 117.7, 116.0, 114.6, 106.1, 97.4, 89.7, 88.7, 52.7, 26.1, 24.2, 18.7, 11.3 ppm.

MS (EI):  $m/z$  (%) = 566.2 (56), 564.2 (52) [ $\text{M}^+$ ], 549.2 (100), 547.2 (92).

EA calcd: C = 63.70, H = 6.59, N = 4.95 found: C = 63.70, H = 6.55, N = 4.91.

**4-(2-triisopropylsilylacetylene)-6-(2-(3-(2-triisopropylsilylacetylene)-6-piperidino)ethynyl)-1-(nitro)benzene (120)**



The bromide **119** (282 mg, 0.500 mmol, 1.0 eq.) was dissolved in 40 ml triethylamine. The solution was degassed for 15 minutes. Then triisopropylsilylacetylene (224  $\mu\text{l}$ , 1.00 mmol, 2.0 eq.),  $\text{Pd(PPh}_3)_4$  (60.0 mg, 10.4 mol%) and  $\text{CuI}$  (10 mg, 10.5 mol%) were added and it was heated to 60 °C and stirred at this temperature for 14 hours. The reaction mixture was cooled to room temperature and extracted with water and  $\text{CH}_2\text{Cl}_2$ . The aqueous phase was washed three times with  $\text{CH}_2\text{Cl}_2$ . The combined organic phases were dried over  $\text{MgSO}_4$  and evaporated. The crude was absorbed on silica and purified by CC (silica gel, 4 x 12 cm, hexane : ethyl acetate = 20 : 1) to give the product **120** as a orange solid (258 mg, 0.387 mmol, 77%).

Mp.: 74.5 -76.5 °C.

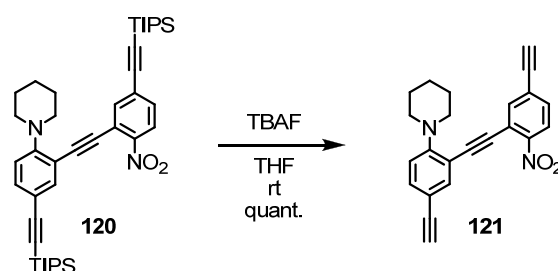
TLC  $R_f$  0.66 (hexane : ethyl acetate = 10 : 1).

$^1\text{H NMR}$  (400 MHz,  $\text{CDCl}_3$ , 25 °C):  $\delta$  = 8.06 (d,  $^3J_{\text{H,H}}$  = 8.6 Hz, 1H), 7.80 (d,  $^4J_{\text{H,H}}$  = 1.8 Hz, 1H), 7.67 (d,  $^4J_{\text{H,H}}$  = 2.0 Hz, 1H), 7.48 (dd,  $^3J_{\text{H,H}}$  = 8.6 Hz,  $^4J_{\text{H,H}}$  = 1.8 Hz, 1H), 7.40 (dd,  $^3J_{\text{H,H}}$  = 8.5 Hz,  $^4J_{\text{H,H}}$  = 2.0 Hz, 1H), 6.87 (d,  $^3J_{\text{H,H}}$  = 8.6 Hz, 1H), 3.23 (t,  $^3J_{\text{H,H}}$  = 5.4 Hz, 4H), 1.77 (m, 4H), 1.59 (m, 2H), 1.14 (m, 42 H) ppm.

$^{13}\text{C NMR}$  (101 MHz,  $\text{CDCl}_3$ , 25 °C):  $\delta$  = 155.5, 147.5, 138.3, 134.2, 131.2, 128.8, 125.0, 119.6, 117.7, 116.0, 115.0, 106.2, 104.1, 97.5, 96.4, 89.6, 89.4 ppm.

MS (EI):  $m/z$  (%) = 666.4 (28) [ $\text{M}^+$ ], 649.4 (100).

EA calcd: C = 73.82, H = 8.76, N = 4.20 found: C = 73.62, H = 8.65, N = 4.13.

**4-(ethynyl)-6-(2-(3-(ethynyl)-6-piperidino)ethynyl)-1-(nitro)benzene (121)**

The TIPS-protected compound **120** (179 mg, 0.269 mmol, 1.0 eq.) was dissolved in 20 ml THF. TBAF (1M in THF, 100  $\mu$ l, 0.100 mmol, 0.37 eq.) was added in four portions in a 30 minute interval at room temperature. The reaction mixture was stirred for another 30 minutes and then quenched with water and extracted with dichloromethane. The aqueous phase was washed three times with dichloromethane, dried over MgSO<sub>4</sub> and evaporated. The crude was absorbed on silica and purified by column chromatography (silica gel, 3 x 12 cm, hexane : ethyl acetate = 20 : 1) to give **121** as a red solid (95 mg, 0.269 mmol, 100%).

Mp.: 108.7 - 110.0 °C.

TLC  $R_f$  0.13 (hexane : ethyl acetate = 20 : 1).

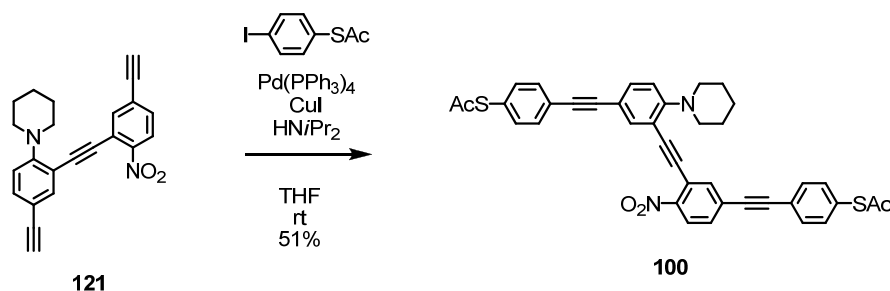
<sup>1</sup>H NMR (400 MHz, CDCl<sub>3</sub>, 25 °C):  $\delta$  = 8.06 (d, <sup>3</sup> $J_{H,H}$  = 8.5 Hz, 1H), 7.77 (d, <sup>4</sup> $J_{H,H}$  = 1.8 Hz, 1H), 7.68 (d, <sup>4</sup> $J_{H,H}$  = 2.1 Hz, 1H), 7.51 (dd, <sup>3</sup> $J_{H,H}$  = 8.5 Hz, <sup>4</sup> $J_{H,H}$  = 1.8 Hz, 1H), 7.40 (dd, <sup>3</sup> $J_{H,H}$  = 8.5 Hz, <sup>4</sup> $J_{H,H}$  = 2.1 Hz, 1H), 6.87 (d, <sup>3</sup> $J_{H,H}$  = 8.6 Hz, 1H), 3.34 (s, 1H), 3.25 (t, <sup>3</sup> $J_{H,H}$  = 5.4 Hz, 4H), 3.02 (s, 1H), 1.76 (m, 4H), 1.61 (m, 2H) ppm.

<sup>13</sup>C NMR (101 MHz, CDCl<sub>3</sub>, 25 °C):  $\delta$  = 155.6, 148.3, 138.7, 137.9, 134.2, 131.6, 127.5, 125.0, 119.5, 117.7, 114.8, 114.2, 96.5, 89.2, 82.9, 82.2, 80.9, 76.5, 52.6, 26.1, 24.2 ppm.

MS (EI):  $m/z$  (%) = 354.1 (59) [M<sup>+</sup>], 337.1 (100).

EA calcd: C = 77.95, H = 5.12, N = 7.90 found: C = 77.77, H = 5.15, N = 7.60.

**4-(2-(4-thioacetylphenyl)-ethynyl)-6-(2-(3-(ethynyl)-6-piperidino)-(2-(4-thioacetylphenyl)-ethynyl)-1-(nitro)benzene (100)**



The diacetylene **121** (76.0 mg, 0.214 mmol, 1.0 eq.) and the 4-iodo-thioacetophenyl (145 mg, 0.521 mmol, 2.44 eq.) were dissolved in 12 ml dry THF and 5 ml diisopropylamine in a 50-ml-2-neckflask. It was degassed for 15 minutes, and then Pd(PPh<sub>3</sub>)<sub>4</sub> (60.0 mg, 0.0519 mmol, 10 mol%) and CuI (10.0 mg, 0.0525 mmol, 10 mol%) were added. The reaction mixture was stirred for four hours at room temperature and 30 minutes at 40 °C and then quenched with water and extracted with dichloromethane. The aqueous phase was washed three times with dichloromethane, dried over MgSO<sub>4</sub> and evaporated. The crude was purified by column chromatography and then dissolved in small amounts of dichloromethane and precipitated into rapidly stirring hexane. The precipitate was filtrated of and dried at high vacuum to give target compound **100** as a red solid (99.6 mg, 0.152 mmol, 71%).

Mp.: 175 °C followed by decomposition.

TLC *R<sub>f</sub>* 0.40 (hexane : ethyl acetate = 2 : 1).

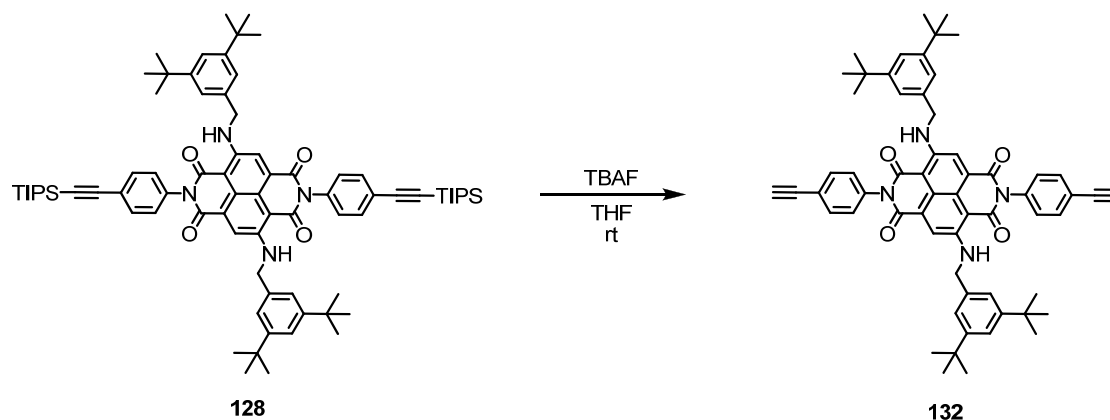
<sup>1</sup>H NMR (400 MHz, CDCl<sub>3</sub>, 25 °C): δ = 8.12 (d, <sup>3</sup>*J*<sub>H,H</sub> = 8.6 Hz, 1H), 7.83 (d, <sup>4</sup>*J*<sub>H,H</sub> = 1.7 Hz, 1H), 7.75 (d, <sup>4</sup>*J*<sub>H,H</sub> = 2.1 Hz, 1H), 7.59 (d, <sup>3</sup>*J*<sub>H,H</sub> = 8.5 Hz, 2H), 7.57 – 7.53 (m, 3H), 7.50 – 7.43 (m, 3H), 7.38 (d, <sup>3</sup>*J*<sub>H,H</sub> = 8.4 Hz, 2H), 6.92 (d, <sup>3</sup>*J*<sub>H,H</sub> = 8.6 Hz, 1H), 3.29 (t, <sup>3</sup>*J*<sub>H,H</sub> = 5.4 Hz, 4H), 2.45 (s, 3H), 2.43 (s, 3H), 1.79 (m, 4H), 1.63 (m, 2H) ppm.

<sup>13</sup>C NMR (101 MHz, CDCl<sub>3</sub>, 25 °C): δ = 193.6, 193.1, 155.4, 147.8, 138.3, 137.4, 134.3, 134.2, 133.7, 132.4, 132.0, 131.0, 129.5, 128.4, 127.6, 125.1, 124.8, 123.1, 119.7, 117.8, 115.0, 114.9, 96.6, 93.6, 90.5, 89.5, 88.3, 88.1, 52.6, 30.4, 30.3, 26.1, 24.2 ppm.

MS (MALDI-TOF): found *m/z* = 654.7626, 654.1647 calculated for C<sub>39</sub>H<sub>30</sub>N<sub>2</sub>O<sub>4</sub>S<sub>2</sub>.

### 7.2.4 A Characteristic Emission Signal from a Single Molecule Contacted With Two Electrodes

#### *N,N'*-bis(4-ethynylphenyl)-2,6-di-((3,5-di-*tert*-butylphenyl)methanamine)-1,4,5,8-tetracarboxylic acid diimide (**132**)



The TMS-protected starting material (91 mg, 0.075 mmol, 1.0 eq.) was dissolved in 20 ml THF in a 100-ml-2-neckflask (not dry, Ar). Then TBAF (1M in THF, 20  $\mu$ l, 0.02 mmol, 0.27 eq.) was added and it was stirred at room temperature. Then more TBAF (1M in THF) was added after 30 minutes (15  $\mu$ l, 0.015 mmol, 0.2 eq.) and after 1 hour (40  $\mu$ l, 0.04 mmol, 0.5 eq.). The reaction mixture was then stirred for 2 hours and then filtrated over a silica plug, evaporated and chromatographed (silica gel, 1 x 12 cm, CH<sub>2</sub>Cl<sub>2</sub>) to give the free acetylene **132** as a dark blue, red fluorescent solid (45 mg, 0.050 mmol, 67%).

TLC  $R_f$  0.55 (CH<sub>2</sub>Cl<sub>2</sub>).

Mp.:  $\geq 350^\circ\text{C}$

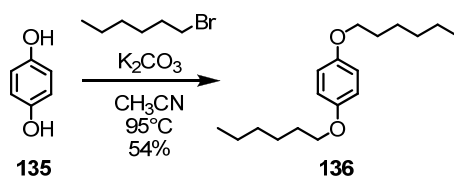
<sup>1</sup>H NMR (400 MHz, CDCl<sub>3</sub>, 25 °C):  $\delta$  = 9.48 (m, 2H), 8.34 (s, 2H), 7.67 (d, <sup>3</sup> $J_{\text{H,H}}$  = 8.5 Hz, 4H), 7.34 (t, <sup>4</sup> $J_{\text{H,H}}$  = 1.7 Hz, 2H), 7.28 (d, <sup>3</sup> $J_{\text{H,H}}$  = 8.5 hz, 4H), 7.19 (d, <sup>4</sup> $J_{\text{H,H}}$  = 1.8 Hz, 4H), 4.61 (d, <sup>3</sup> $J_{\text{H,H}}$  = 4H), 3.14 (s, 2H), 1.29 (s, 36H) ppm.

<sup>13</sup>C NMR (101 MHz, CDCl<sub>3</sub>, 25 °C):  $\delta$  = 166.6, 163.3, 151.9, 149.8, 136.3, 136.0, 133.7, 129.2, 126.7, 124.6, 123.4, 122.7, 122.5, 122.4, 119.7, 102.7, 90.7, 48.7, 35.3, 31.8 ppm.

MS (FAB):  $m/z$  (%) = 900.4 (26) [M<sup>+</sup>], 203.2 (100).

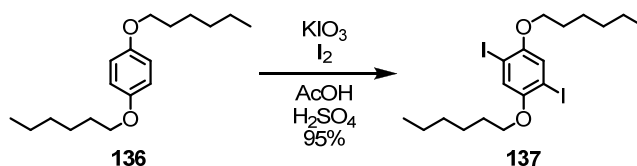
UV/Vis:  $\lambda_{\text{max}}$  566, 609 nm.

GPC (oligopore 6  $\mu$ m, toluene, UV/vis photodiode array detector) area 99.9% (at 16.46 min.)

**1,4-bis(hexyloxy)benzene (136)**

Hydroquinone (**135**) (37.8 g, 343 mmol, 1.0 eq.) was suspended in acetonitrile (400 ml) in a 1000-ml-3-neckflask with condenser. 1-Bromohexane (100 ml, 712 mmol, 2.1 eq.) and  $\text{K}_2\text{CO}_3$  (110 g, 795 mmol, 2.3 eq.) were then added and it was refluxed for 25 hours. The hot reaction mixture was then filtrated and washed with acetonitrile. While cooling with an ice-bath, the product **136** was crystallizing. The crystals were filtrated off, washed with acetonitrile and dried at high vacuum to give compound **136** as colorless crystals (51.0 g, 183 mmol, 53%).

$^1\text{H}$  NMR (250 MHz,  $\text{CDCl}_3$ , 25 °C):  $\delta$  = 6.82 (s, 4H), 3.90 (t,  $^3J_{\text{H,H}}$  = 6.6 Hz, 4H), 1.75 (q,  $^3J_{\text{H,H}}$  = 6.6 Hz, 4H), 1.44 (m, 4H), 1.34 (m, 8H), 0.90 (m, 6H) ppm.

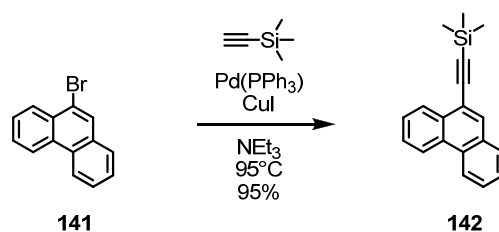
**1,4-bis(hexyloxy)-2,5-diiodobenzene (137)**<sup>[285]</sup>

1,4-bis(hexyloxy)benzene (**136**) (48.1 g, 173 mmol, 1.0 eq.),  $\text{KIO}_3$  (14.9 g, 69.5 mmol, 0.4 eq.) and iodine (48.7 g, 192 mmol, 1.1 eq.) were suspended in concentrated acetic acid (1000 ml) and 10% aqueous sulfuric acid (100 ml) in a 2-l-3-neckflask with condenser. It was heated to reflux (115°C) for 6 hours. Then 20% aqueous  $\text{Na}_2\text{S}_2\text{O}_4$  (~800 ml) was added to the hot reaction mixture until the brown-red color disappeared. The reaction mixture was cooled to room temperature what led to precipitation of the product. The precipitate was filtrated off, washed with ethanol and recrystallized from ethanol to give compound **137** as a colorless solid (87.5 g, 165 mmol, 95%).

$^1\text{H}$  NMR (400 MHz,  $\text{CDCl}_3$ , 25 °C):  $\delta$  = 7.17 (s, 2H), 3.92 (t,  $^3J_{\text{H,H}}$  = 6.4 Hz, 4H), 1.79 (tt,  $^3J_{\text{H,H}}$  = 6.5 Hz, 4H), 1.50 (m, 4H), 1.35 (m, 8H), 0.91 (m, 6H) ppm.

$^{13}\text{C}$  NMR (101 MHz,  $\text{CDCl}_3$ , 25 °C):  $\delta$  = 152.8, 122.7, 86.3, 70.3, 31.5, 29.1, 25.7, 22.6, 14.0 ppm.



**9-Trimethylsilylethynyl-phenanthren (142)**<sup>[286]</sup>

9-Bromophenanthren (5.26 g, 20.5 mmol, 1.0 eq.) was dissolved in  $\text{NEt}_3$  (60 ml) in a 100-ml-2-neckflask. It was degassed for 15 minutes, then trimethylsilylacetylene (5.00 ml, 36.1 mmol, 1.80 eq.),  $\text{Pd}(\text{PPh}_3)_4$  (760 mg, 0.658 mmol, 3.2 mol%) and  $\text{CuI}$  (120 mg, 0.630 mmol, 3.1 mol%) were added. The reaction mixture was stirred for hours at  $95^\circ\text{C}$ . The insoluble material was filtrated off (hot) and washed with hexane. The filtrate was evaporated and purified by column chromatography (silica gel, 4x12 cm, hex  $\rightarrow$  hex:DCM = 5:1) to give the product **142** as a yellowish oil (5.37 g, 19.6 mmol, 95%).

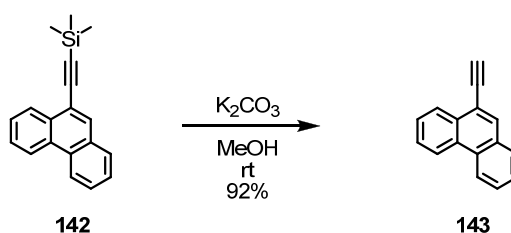
TLC  $R_f$  0.22 (hexane).

$^1\text{H}$  NMR (400 MHz,  $\text{CDCl}_3$ ,  $25^\circ\text{C}$ ):  $\delta$  = 8.69-8.64 (m, 2H), 8.46 (m, 1H), 8.05 (s, 1H), 7.85 (d,  $^3J_{\text{H,H}} = 7.9$  Hz, 1H), 7.72-7.65 (m, 3H), 7.59 (m, 1H), 0.38 (s, 9H) ppm.

$^{13}\text{C}$  NMR (101 MHz,  $\text{CDCl}_3$ ,  $25^\circ\text{C}$ ):  $\delta$  = 132.8, 131.5, 130.8, 130.4, 129.0, 128.0, 127.50, 127.46, 127.4, 127.3, 123.1, 123.0, 119.9, 103.6, 99.6, 0.6 ppm.

MS (EI):  $m/z$  (%) = 274.1 (62) [ $\text{M}^+$ ], 259.1 (100).

EA calcd: C = 83.16, H = 6.61, found: C = 83.10, H = 6.69.

**9-ethynyl-phenanthren (143)**<sup>[286]</sup>

The TMS-protected compound **142** (1.94 g, 7.07 mmol, 1.0 eq.) was dissolved in methanol (50 ml) in a 500-ml-flask. It was degassed, before  $\text{K}_2\text{CO}_3$  (200 mg, 1.44 mmol, 0.20 eq.) was added. The reaction mixture was stirred for 2.5 hours at room temperature. The solvent was then evaporated and the residue was taken up in dichloromethane and extracted with aqueous  $\text{NaHCO}_3$ . The organic phase was dried over  $\text{MgSO}_4$  and evaporated to give the product **143** as beige solid (1.32 g, 6.53 mmol, 92%).

Mp.: 64.0-66.0 °C

TLC  $R_f$  0.78 (hexane:CH<sub>2</sub>Cl<sub>2</sub> = 1:1).

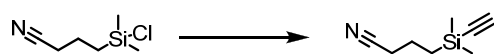
<sup>1</sup>H NMR (400 MHz, CDCl<sub>3</sub>, 25 °C): δ = 8.71-8.65 (m, 2H), 8.48 (m, 1H), 8.08 (s, 1H), 7.86 (d, <sup>3</sup>J<sub>H,H</sub> = 7.9 Hz, 1H), 7.71-7.66 (m, 3H), 7.61 (m, 1H), 3.49 (s, 1H) ppm.

<sup>13</sup>C NMR (101 MHz, CDCl<sub>3</sub>, 25 °C): δ = 133.4, 131.5, 131.4, 130.9, 130.4, 129.0, 128.2, 127.6, 127.4, 127.2, 123.2, 123.0, 119.0 ppm.

MS (EI):  $m/z$  (%) = 202.1 (100) [M<sup>+</sup>].

EA calcd: C = 95.02, H = 4.98, found: C = 94.46, H = 5.13.

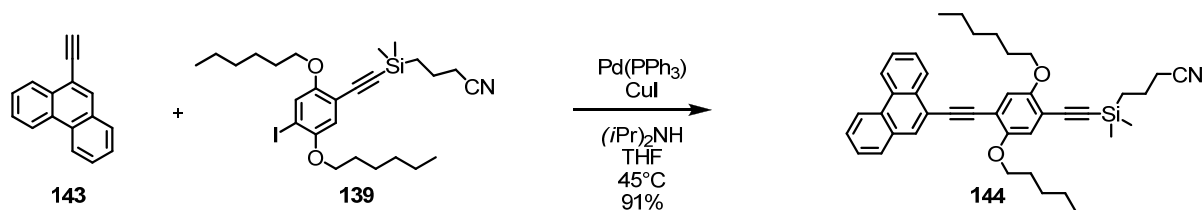
### [3-Cyanopropyl]dimethylsilyl]acetylene (138) <sup>[291]</sup>



(3-cyanopropyl)dimethylsilyl chloride (8.20ml, 45.0 mmol, (0.9 eq.) was dissolved in THF (30 ml) in a dry 250-ml-2-neck flask with dropping funnel. Ethynylmagnesium bromide (0.5 M in THF, 100 ml, 50.0 mmol) was added at -20 °C dropwise over 80 minutes. The reaction mixture was allowed to warm to room temperature and it was stirred over night. Then water was slowly added and it was extracted with TBME. The aqueous phase was washed with TBME. The combined organic phase was washed with brine, dried over MgSO<sub>4</sub>, evaporated and dried at high vacuum to give a brownish oil (7.30 g, 45 mmol, 100%).

<sup>1</sup>H NMR (400 MHz, CDCl<sub>3</sub>, 25 °C): δ = 2.41 (m, 3H), 1.78 (2H), 0.79 (m, 2H), 0.20 (s, 6H) ppm.

<sup>13</sup>C NMR (101 MHz, CDCl<sub>3</sub>, 25 °C): δ = 119.6, 94.5, 88.1, 20.4, 15.4, -2.1 ppm.

**9-((4-((3-cyanopropyl)dimethylsilyl)ethynyl)-2,5-dihexyloxyphenyl)ethynyl)phenanthrene (144)**

The acetylene **143** (390 mg, 1.93 mmol, 1.09 eq.) and the iodide **139** (983 mg, 1.78 mmol, 1.0 eq.) were dissolved in THF (40 ml) and diisopropylamine (7 ml) in a 100-ml-2-neckflask with condenser. The mixture was degassed for 15 minutes, then Pd(PPh<sub>3</sub>)<sub>4</sub> (200 mg, 0.173 mmol, 9.7 mol%) and CuI (33 mg, 0.173 mmol, 9.8 mol%) were added. The reaction mixture was stirred for 20 hours at 45°C. The reaction mixture was then evaporated and the crude was purified by column chromatography (silica gel, 3 x 12 cm, hexane:DCM = 1:2) to give the product **144** as a yellow solid (1.01 g, 1.61 mmol, 91%).

Mp.: 87.6-89.0 °C

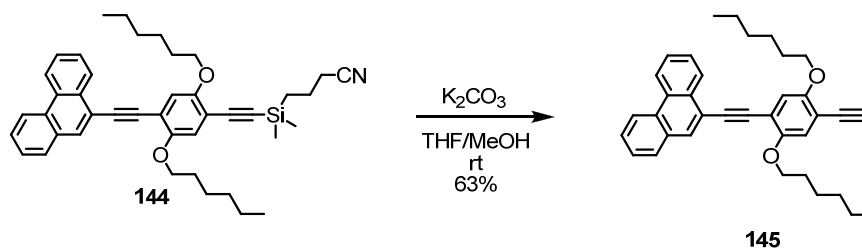
TLC *R<sub>f</sub>* 0.45 (hexane : CH<sub>2</sub>Cl<sub>2</sub> = 1 :2).

<sup>1</sup>H NMR (400 MHz, CDCl<sub>3</sub>, 25 °C): δ = 8.73-8.66 (m, 3H), 8.08 (s, 1H), 7.87 (d, <sup>3</sup>J<sub>H,H</sub> = 7.8 Hz, 1H), 7.74-7.65 (m, 3H), 7.61 (m, 1H), 7.10 (s, 1H), 7.00 (s, 1H), 4.09 (t, <sup>3</sup>J<sub>H,H</sub> = 6.6 Hz, 2H), 4.04 (t, <sup>3</sup>J<sub>H,H</sub> = 6.5 Hz, 2H), 2.45 (t, <sup>3</sup>J<sub>H,H</sub> = 7.0 Hz, 2H), 1.98 (quin, <sup>3</sup>J<sub>H,H</sub> = 7.1 Hz, 2H), 1.86 (m, 4H), 1.58 (m, 4H), 1.43-1.27 (m, 8H), 0.94 (m, 3H), 0.88 (m, 5H), 0.29 (s, 6H) ppm.

<sup>13</sup>C NMR (101 MHz, CDCl<sub>3</sub>, 25 °C): δ = 154.2, 153.7, 131.6, 131.3, 131.2, 130.3, 130.1, 128.6, 127.5, 127.3, 127.1, 126.9, 122.7, 122.6, 119.9, 119.7, 116.6, 116.5, 114.4, 113.2, 102.7, 97.9, 93.6, 90.6, 69.41, 69.36, 31.64, 31.59, 29.5, 29.3, 25.8, 25.7, 22.7, 22.6, 20.7, 20.5, 15.7, 14.1, 14.0, -1.8 ppm.

MS (EI): *m/z* (%) = 627.3 (100) [M<sup>+</sup>].

GPC (oligopore 6 μm, toluene, UV/vis photodiode array detector) area 99.9% (at 17.32 min.)

**9-((4-ethynyl-2,5-dihexyloxy-phenyl)ethynyl)phenanthrene (145)**

The starting material (**144**) (865 mg, 1.38 mmol, 1.0 eq.) was dissolved in THF (40 ml) and methanol (40 ml). The mixture was degassed for 15 minutes, then  $\text{K}_2\text{CO}_3$  (390 mg, 2.82 mmol, 2.04 eq.) was added. The reaction mixture was stirred for 30 minutes at room temperature and 1 hour at  $0^\circ\text{C}$ . It was then quenched with water and extracted with dichloromethane. The aqueous phase was washed twice with dichloromethane. The combined organic phases were washed with water, dried over  $\text{MgSO}_4$  and evaporated. The crude was absorbed on silica and purified by column chromatography (silica gel, 3 x 12 cm, hexane:DCM = 5:1  $\rightarrow$  1:1) to give the product **145** as yellow solid (440 mg, 0.875 mmol, 63%).

Mp.: 79.5-81.5  $^\circ\text{C}$

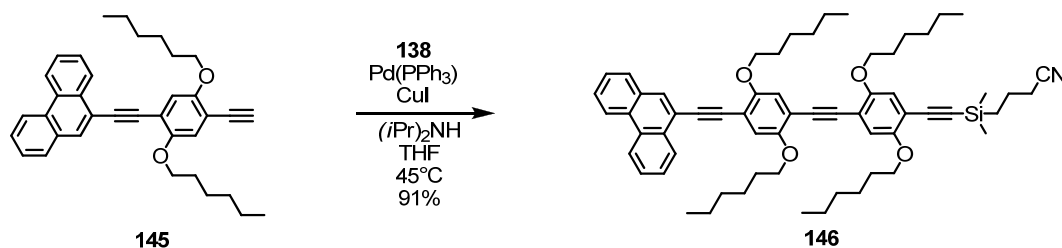
TLC  $R_f$  0.20 (hexane :  $\text{CH}_2\text{Cl}_2$  = 5 : 1).

$^1\text{H}$  NMR (400 MHz,  $\text{CDCl}_3$ , 25  $^\circ\text{C}$ ):  $\delta$  = 8.73-8.66 (m, 3H), 8.09 (s, 1H), 7.87 (d,  $^3J_{\text{H,H}}$  = 7.8 Hz, 1H), 7.74-7.63 (m, 3H), 7.61 (m, 1H), 7.13 (s, 1H), 7.04 (s, 1H), 4.07 (m, 4H), 3.38 (s, 1H), 1.97 (quin,  $^3J_{\text{H,H}}$  = 7.1 Hz, 2H), 1.86 (quin,  $^3J_{\text{H,H}}$  = 7.1 Hz, 2H), 1.55 (m, 4H), 1.38 (m, 8H), 0.93 (m, 3H), 0.86 (t,  $^3J_{\text{H,H}}$  = 7.2 Hz, 3H) ppm.

$^{13}\text{C}$  NMR (101 MHz,  $\text{CDCl}_3$ , 25  $^\circ\text{C}$ ):  $\delta$  = 154.6, 154.1, 132.0, 131.7, 131.6, 130.8, 130.5, 129.0, 127.9, 127.8, 127.5, 127.4, 123.11, 123.07, 120.3, 117.54, 117.51, 117.2, 114.9, 113.1, 93.9, 90.9, 82.8, 80.5, 70.1, 69.9, 32.1, 32.0, 29.9, 29.6, 26.2, 26.0, 23.1, 23.0, 14.5, 14.4 ppm.

MS (EI):  $m/z$  (%) = 502.3 (100) [ $\text{M}^+$ ].

GPC (oligopore 6  $\mu\text{m}$ , toluene, UV/vis photodiode array detector) area 99.0% (at 18.66 min.)

**9-((4-(4-((3-cyanopropyl)dimethylsilyl)ethynyl)-2,5-dihexyloxy-phenyl)ethynyl)-2,5-dihexyloxy-phenyl)ethynyl)phenanthrene (146)**

The acetylene **145** (355 mg, 0.706 mmol, 0.98 eq.) and the iodide **138** (400 mg, 0.723 mmol, 1.00 eq.) were dissolved in THF (20 ml) and diisopropylamine (5 ml) in a 50-ml-flask. It was degassed for 15 minutes, then Pd(PPh<sub>3</sub>)<sub>4</sub> (92 mg, 0.0796 mmol, 11 mol%) and CuI (13.8 mg, 0.0723 mmol, 10 mol%) were added. The reaction mixture was stirred for 16 hours at 45 °C, was then cooled to room temperature, quenched with water and extracted with dichloromethane and water. The aqueous phase was washed twice with dichloromethane. The combined organic phases were dried over MgSO<sub>4</sub> and evaporated. The crude was purified by column chromatography (silica gel, 4 x 12 cm, DCM:hex = 2:1 -> 5:1) to give **146** as yellow solid (590 mg, 0.701 mmol, 91%).

Mp.: 85.8-86.5 °C

TLC *R<sub>f</sub>* 0.28 (hexane : CH<sub>2</sub>Cl<sub>2</sub> = 1 :2).

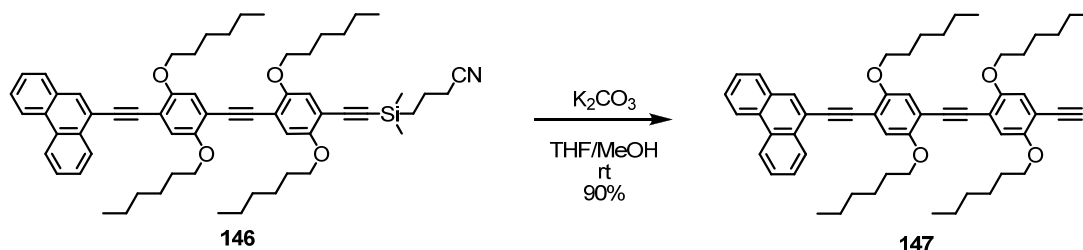
<sup>1</sup>H NMR (400 MHz, CDCl<sub>3</sub>, 25 °C): δ = 8.75-8.66 (m, 3H), 8.09 (s, 1H), 7.88 (d, <sup>3</sup>J<sub>H,H</sub> = 7.8 Hz, 1H), 7.74-7.65 (m, 3H), 7.61 (m, 1H), 7.15 (s, 1H), 7.07 (s, 1H), 7.00 (s, 1H), 6.96 (s, 1H), 4.10 (t, <sup>3</sup>J<sub>H,H</sub> = 6.6 Hz, 4H), 4.04 (t, <sup>3</sup>J<sub>H,H</sub> = 6.6 Hz, 2H), 4.00 (t, <sup>3</sup>J<sub>H,H</sub> = 6.5 Hz, 2H), 2.44 (t, <sup>3</sup>J<sub>H,H</sub> = 7.0 Hz, 2H), 1.99 (quin, <sup>3</sup>J<sub>H,H</sub> = 7.1 Hz, 2H), 1.87-1.78 (m, 8H), 1.63-1.48 (m, 8H), 1.42-1.30 (m, 16H), 0.91 (m, 14H), 0.28 (s, 6H) ppm.

<sup>13</sup>C NMR (101 MHz, CDCl<sub>3</sub>, 25 °C): δ = 154.2, 153.9, 153.5, 153.3, 131.5, 131.3, 131.2, 130.3, 130.1, 128.5, 127.41, 127.35, 127.0, 126.9, 122.7, 122.6, 120.0, 119.7, 117.4, 116.9, 116.7, 116.4, 114.9, 114.2, 113.9, 113.1, 102.6, 97.8, 93.5, 91.8, 91.4, 90.8, 69.74, 69.67, 69.3, 69.2, 31.64, 31.61, 31.59, 31.56, 29.5, 29.27, 29.25, 25.8, 25.7, 22.6, 20.6, 20.4, 15.7, 14.1, 14.03, 13.99, -1.8 ppm.

MS (EI): *m/z* (%) = 927.6 (100) [M<sup>+</sup>].

GPC (oligopore 6 μm, toluene, UV/vis photodiode array detector) area 99.9% (at 15.86 min.)

**9-((4-(4-ethynyl-2,5-dihexyloxy-phenyl)ethynyl-2,5-dihexyloxy-phenyl)ethynyl)phenanthrene (**147**)**



The dimethylcyanopropylsilane protected acetylene **146** (120 mg, 0.129 mmol, 1.0 eq.) was dissolved in 5 ml THF and 5 ml methanol.  $\text{K}_2\text{CO}_3$  (68 mg, 0.49 mmol, 3.8 eq.) was then added and it was stirred for 12 hours at room temperature. The reaction mixture was then extracted with water and TBME. The aqueous phase was washed with 3 x 20 ml TBME. The combined organic phases were washed with brine, dried over  $\text{MgSO}_4$  and evaporated. The crude was purified by column chromatography (silica gel, 2 x 12 cm,  $\text{CH}_2\text{Cl}_2$  : hexane = 1 : 2  $\rightarrow$  1 : 1) to give the compound **147** as a yellow solid (87.0 mg, 0.108 mmol, 90%).

TLC  $R_f$  0.46 ( $\text{CH}_2\text{Cl}_2$  : hexane = 1 : 1).

Mp.: 98.5 -100 °C

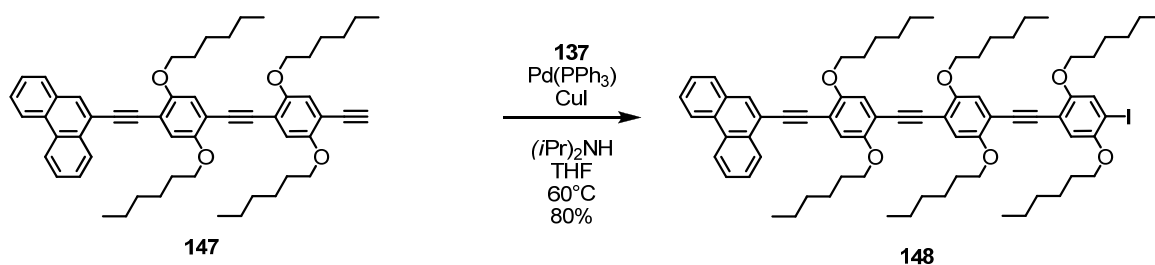
$^1\text{H}$  NMR (400 MHz,  $\text{CDCl}_3$ , 25 °C):  $\delta$  = 8.74-8.67 (m 3H), 8.09 (s, 1H), 7.87 (d,  $^3J_{\text{H,H}}$  = 3H, 3H), 7.61 (t,  $^3J_{\text{H,H}}$  = 7.9 Hz, 1H), 7.14 (s, 1H), 7.06 (s, 1H), 7.01 (s, 1H), 6.99 (s, 1H), 4.10 (t,  $^3J_{\text{H,H}}$  = 6.6 Hz, 4H), 4.02 (m, 8H), 3.35 (s, 1H), 1.99 (quin,  $^3J_{\text{H,H}}$  = 7.1 Hz, 2H), 1.92-1.79 (m, 6H), 1.63-1.47 (m, 6H), 1.41-1.25 (m, 18H), 0.90 (m, 18H) ppm.

$^{13}\text{C}$  NMR (101 MHz,  $\text{CDCl}_3$ , 25 °C):  $\delta$  = 154.1, 153.9, 153.5, 153.3, 131.5, 131.3, 131.2, 130.3, 130.1, 128.6, 127.42, 127.37, 127.05, 126.9, 122.7, 122.6, 120.0, 117.9, 117.0, 116.5, 114.9, 114.3, 113.9, 112.6, 93.5, 91.6, 91.3, 90.8, 82.3, 80.1, 69.8, 69.7, 69.6, 69.4, 31.7, 31.62, 31.60, 31.5, 29.5, 29.3, 29.2, 29.1, 25.8, 25.68, 25.67, 25.6, 22.64, 22.58, 14.04, 14.01 ppm.

MS (EI):  $m/z$  (%) = 802.5 (100) [ $\text{M}^+$ ].

GPC (oligopore 6  $\mu\text{m}$ , toluene, UV/vis photodiode array detector) area 99.0% (at 16.69 min.)

**9-((4-(4-(4-iodo-2,5-dihexyloxy-phenyl)ethynyl)-2,5-dihexyloxy-phenyl)ethynyl)-2,5-dihexyloxy-phenyl)ethynylphenanthrene (**148**)**



The iodide **137** (530 mg, 1.00 mmol, 10.0 eq.) and the acetylene **147** (80.0 mg, 0.0996 mmol, 1.0 eq.) were dissolved in 10 ml THF and 2 ml diisopropylamine. It was degassed for 15 minutes, before Pd(PPh<sub>3</sub>)<sub>4</sub> (12.0 mg, 0.010 mmol, 10 mol%) and CuI (2 mg, 0.01 mmol, 10 mol%) were added. It was then stirred for 3 hours at 60°C. The reaction mixture was evaporated, absorbed on silica gel and chromatographed (silica gel, 2 x 12 cm, CH<sub>2</sub>Cl<sub>2</sub> : hexane = 1 : 2 -> 1 : 1) to give compound **148** as a yellow solid (96.0 mg, 0.0796 mmol, 80%).

Mp.: 119.9-120.9 °C

TLC *R<sub>f</sub>* 0.29 (CH<sub>2</sub>Cl<sub>2</sub> : hexane = 1 : 1).

<sup>1</sup>H NMR (400 MHz, CDCl<sub>3</sub>, 25 °C): δ = 8.75-8.67 (m, 3H), 8.09 (s, 1H), 7.88 (dd, <sup>4</sup>*J*<sub>H,H</sub> = 1.2 Hz, <sup>3</sup>*J*<sub>H,H</sub> = 7.9 Hz, 1H), 7.74-7.65 (m, 3H), 7.61 (td, <sup>4</sup>*J*<sub>H,H</sub> = 1.1 Hz, <sup>3</sup>*J*<sub>H,H</sub> = 7.4 Hz, 1H), 7.31 (s, 1H), 7.15 (s, 1H), 7.08 (s, 1H), 7.04 (s, 1H), 7.02 (s, 1H), 4.10 (t, <sup>3</sup>*J*<sub>H,H</sub> = 6.6 Hz, 4H), 4.06-3.99 (m, 6H), 3.96 (t, <sup>3</sup>*J*<sub>H,H</sub> = 6.5 Hz, 2H), 2.00 (quin, <sup>3</sup>*J*<sub>H,H</sub> = 7.1 Hz, 2H), 1.85 (m, 10H), 1.62-1.48 (m, 12H), 1.42-1.30 (m, 24H), 0.90 (m, 18H) ppm.

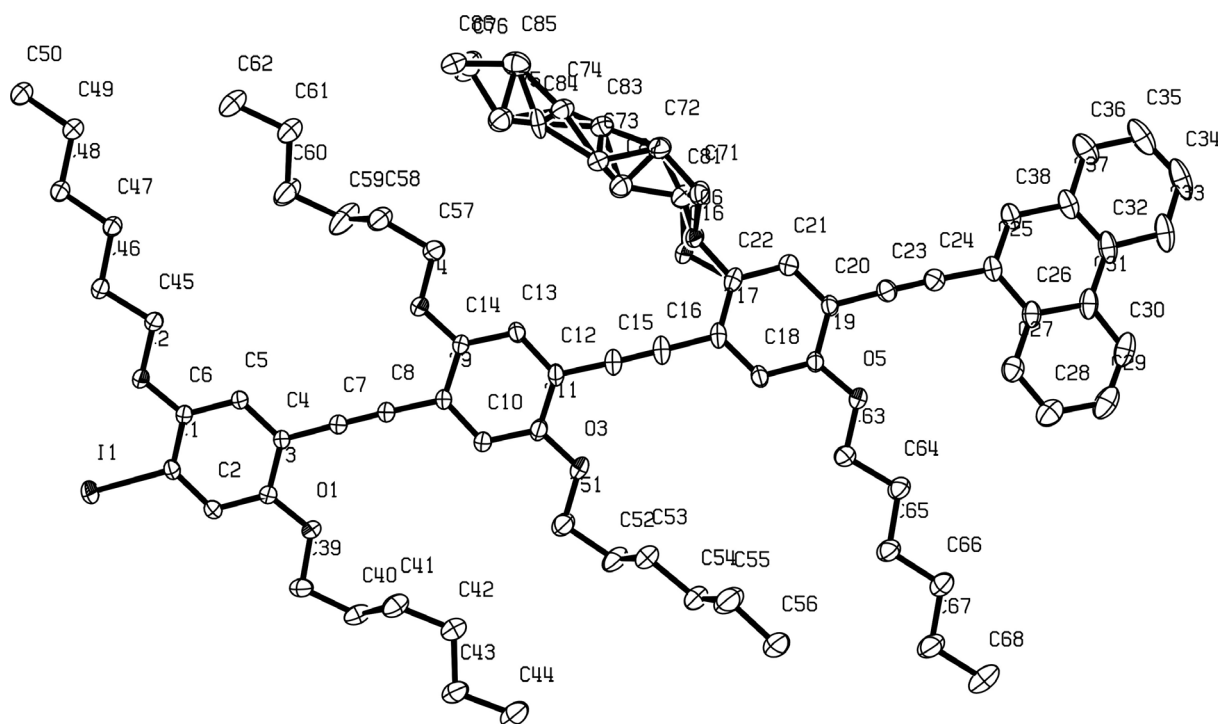
<sup>13</sup>C NMR (101 MHz, CDCl<sub>3</sub>, 25 °C): δ = 154.2, 153.9, 153.5, 153.47, 151.8, 131.5, 131.3, 131.2, 130.3, 130.1, 128.6, 127.42, 127.37, 127.1, 126.9, 124.0, 122.6, 120.0, 117.22, 117.2, 117.0, 116.4, 116.1, 114.4, 114.3, 114.2, 113.9, 113.8, 93.5, 91.64, 91.61, 91.1, 90.82, 90.79, 87.9, 70.06, 69.99, 69.8, 69.7, 69.6, 69.4, 31.7, 31.63, 31.61, 31.58, 31.5, 29.5, 29.3, 29.23, 29.16, 25.78, 25.75, 25.68, 25.67, 25.6, 22.7, 22.63, 22.59, 14.1, 14.03, 14.01 ppm.

MS (EI): *m/z* (%) = 1205.6 (29), 1204.6 (29) [M<sup>+</sup>], 77.0 (100).

UV/Vis: λ<sub>max</sub> 407 nm.

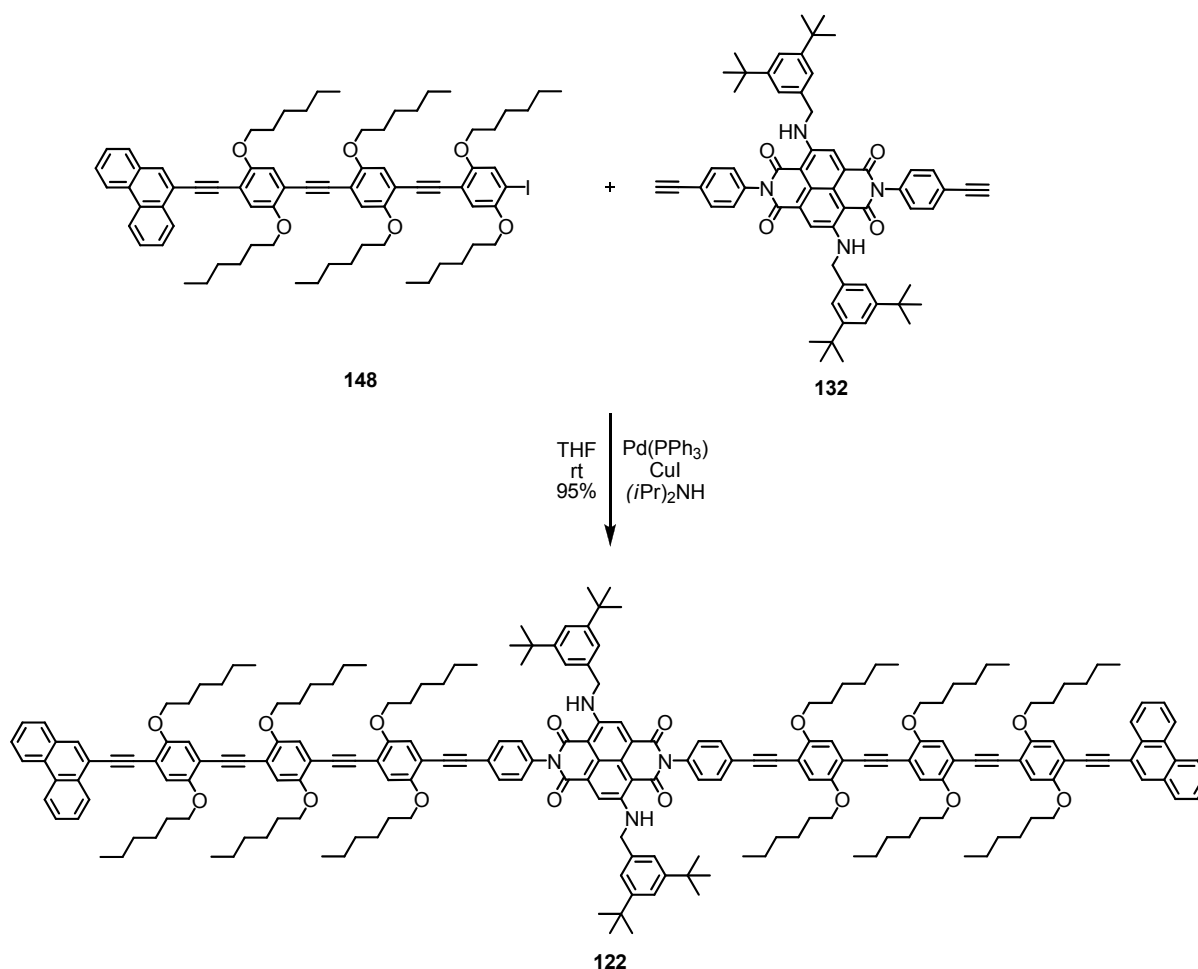
GPC (oligopore 6 μm, toluene, UV/vis photodiode array detector) area 99.0% (at 15.44 min.).

Crystal data for **148**: formula  $C_{74}H_{93}I_1O_6$ ,  $M = 1205.45$ ,  $F(000) = 1276$ , yellow block, size  $0.11 \cdot 0.14 \cdot 0.39 \text{ mm}^3$ , triclinic, space group  $P - 1$ ,  $Z = 2$ ,  $a = 14.2136(6) \text{ \AA}$ ,  $b = 14.9988(6) \text{ \AA}$ ,  $c = 16.9653(7) \text{ \AA}$ ,  $\alpha = 113.668(2)^\circ$ ,  $\beta = 93.579(2)^\circ$ ,  $\gamma = 97.560(2)^\circ$ ,  $V = 3257.2(2) \text{ \AA}^3$ ,  $D_{\text{calc.}} = 1.229 \text{ Mg} \cdot \text{m}^{-3}$ . The crystal was measured on a Area diffractometer at 123K using graphite-monochromated Mo  $K_\alpha$ -radiation with  $\lambda = 0.71073 \text{ \AA}$ ,  $\Theta_{\text{max}} = 33.207^\circ$ . Minimal/maximal transmission 0.93/0.94,  $\mu = 0.542 \text{ mm}^{-1}$ . The Apex2 suite has been used for datacollection and integration. From a total of 123417 reflections, 24657 were independent (merging  $r = 0.032$ ). From these, 17295 were considered as observed ( $I > 2.0\sigma(I)$ ) and were used to refine 793 parameters. The structure was solved by direct methods using the program SIR92. Least-squares refinement against  $F$  was carried out on all non-hydrogen atoms using the program CRYSTALS.  $R = 0.0435$  (observed data),  $wR = 0.0692$  (all data),  $\text{GOF} = 1.0863$ . Minimal/maximal residual electron density =  $-0.36/1.85 \text{ e \AA}^{-3}$ . Chebychev polynomial weights were used to complete the refinement.





***N,N'*-bis(9-((4-(4-(4-iodo-2,5-dihexyloxy-phenyl)ethynyl)-2,5-dihexyloxy-phenyl)ethynyl)-2,5-dihexyloxy-phenyl)ethynyl)phenanthrenyl)-2,6-di-((3,5-di-tert-butylphenyl)methanamine)-1,4,5,8-tetracarboxylicacid diimide (**122**)**



The blue acetylene **132** (20.7 mg, 0.0230 mmol, 1.0 eq.) and the yellow iodide **148** (57 mg, 0.0470 mmol, 2.04 eq.) were dissolved in 25 ml THF and 2 ml diisopropylamine in a 50-ml-2-neckflask (dry, Ar). It was degassed for 15 minutes, then Pd(PPh<sub>3</sub>)<sub>4</sub> (6 mg, 23 mol%) and CuI (1 mg, 23 mol%) were added. It was then stirred for 23 hours at room temperature. The reaction mixture was evaporated and chromatographed (silica gel, 1 x 12 cm, CH<sub>2</sub>Cl<sub>2</sub>) to give compound **122** as a green, red fluorescent solid (67 mg, 0.0219, 95 %).

TLC *R<sub>f</sub>* 0.31 (CH<sub>2</sub>Cl<sub>2</sub> : hexane = 2 : 1).

<sup>1</sup>H NMR (600 MHz, CDCl<sub>3</sub>, 25 °C): δ = 9.53 (m, 2H, NH), 8.73 (d, <sup>3</sup>*J*<sub>H,H</sub> = 7.9 Hz, 2H, phenanthrene), 8.71 (d, <sup>3</sup>*J*<sub>H,H</sub> = 8.7 Hz, 2H, phenanthrene), 8.68 (d, <sup>3</sup>*J*<sub>H,H</sub> = 8.4 Hz, 2H, phenanthrene), 8.37 (s, 2H, NDI), 8.09 (s, 2H, phenanthrene), 7.88 (d, <sup>3</sup>*J*<sub>H,H</sub> = 7.1 Hz, 2H, phenanthrene), 7.72 (d, <sup>3</sup>*J*<sub>H,H</sub> = 8.3 Hz, 4H, phenyl), 7.73-7.66 (m, 6H,

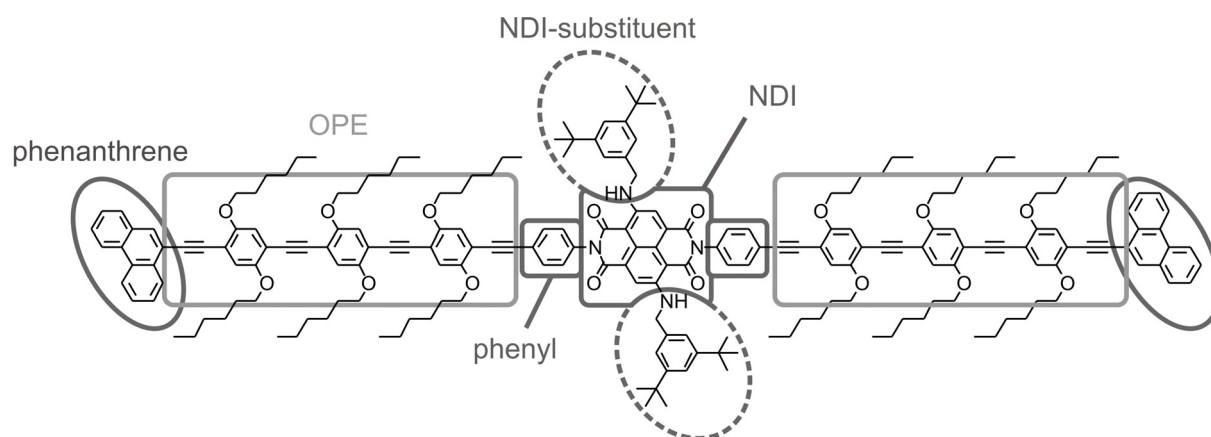
phenanthrene), 7.61 (t,  $^3J_{\text{H,H}} = 7.7$  Hz, 2H, phenanthrene), 7.36 (s, 2H, NDI substituent), 7.32 (d,  $^3J_{\text{H,H}} = 8.4$  Hz, 4H, phenyl), 7.22 (d,  $^4J_{\text{H,H}} = 1.7$  Hz, 4H, NDI-substituent), 7.15 (s, 2H, OPE), 7.08 (s, 2H, OPE), 7.044 (s, 2H, OPE), 7.039 (m, 4H, OPE), 7.035 (s, 2H, OPE), 4.64 (d,  $^3J_{\text{H,H}} = 5.1$  Hz, 4H, N-CH<sub>2</sub>), 4.11 (t,  $^3J_{\text{H,H}} = 6.6$  Hz, 8H, OCH<sub>2</sub>), 4.06 (m, 16H, OCH<sub>2</sub>), 2.00 (quin,  $^3J_{\text{H,H}} = 7.1$  Hz, 4H, CH<sub>2</sub>), 1.88 (m, 20H, CH<sub>2</sub>), 1.57 (m, 24H, CH<sub>2</sub>), 1.37 (m, 48H, CH<sub>2</sub>), 1.30 (s, 36H, <sup>t</sup>Bu), 0.91 (m, 36H, CH<sub>3</sub>) ppm.

<sup>13</sup>C NMR (151 MHz, CDCl<sub>3</sub>, 25 °C):  $\delta = 166.2$  (2C, Cq, C=O), 162.8 (2C, Cq, C=O), 153.8 (2C, Cq, C-O), 153.7 (2C, Cq, C-O), 153.4 (6C, Cq, C-O), 153.3 (2C, Cq, C-O), 151.2 (4C, Cq, NDI-substituent), 149.3 (2C, Cq, C-N), 135.7 (2C, Cq, NDI-substituent), 134.8 (2C, Cq, C(phenyl)), 132.4 (4C, Ct, CH(phenyl)), 131.3 (2C, Ct, CH(phenanthrene)), 131.1 (2C, Cq, C(phenanthrene)), 131.0 (2C, Cq, C(phenanthrene)), 130.2 (2C, Cq, C(phenanthrene)), 129.9 (2C, Cq, C(phenanthrene)), 128.6 (4C, Ct, CH(phenyl)), 128.4 (2C, Ct, CH(phenanthrene)), 127.2 (2C, Ct, CH(phenanthrene)), 127.1 (2C, Ct, CH(phenanthrene)), 126.9 (2C, Ct, CH(phenanthrene)), 126.8 (2C, Ct, CH(phenanthrene)), 126.72 (2C, Ct, CH(phenanthrene)), 126.2 (2C, Cq, NDI), 124.2 (2C, Cq, C(phenyl)), 122.5 (2C, Ct, CH(phenanthrene)), 122.4 (2C, Ct, CH(phenanthrene)), 122.1 (4C, Ct, NDI-substituent), 121.9 (2C, Ct, NDI-substituent), 121.8 (2C, Cq, NDI), 119.8 (2C, Cq, C(phenanthrene)), 119.2 (2C, Ct, CH(NDI)), 117.0 (8C, Ct, CH(OPE)), 116.8 (2C, Ct, CH(OPE)), 116.3 (2C, Ct, CH(OPE)), 114.4 (2C, Cq, C(OPE)), 114.3 (2C, Cq, C(OPE)), 114.1 (4C, Cq, C(OPE)), 113.6 (2C, Cq, C(OPE)), 113.5 (2C, Cq, C(OPE)), 102.1 (2C, Cq, NDI), 93.9 (2C, Cq, C $\equiv$ C), 93.3 (2C, Cq, C $\equiv$ C), 91.4 (2C, Cq, C $\equiv$ C), 91.3 (6C, Cq, C $\equiv$ C), 90.6 (2C, Cq, C $\equiv$ C), 86.9 (2C, Cq, C $\equiv$ C), 69.6 (2C, Cs, OCH<sub>2</sub>), 69.5 (8C, Cs, OCH<sub>2</sub>), 69.2 (2C, Cs, OCH<sub>2</sub>), 61.6 (2C, Ct, alkyl- $\beta$ -CH<sub>2</sub>), 48.1 (2C, Cs, N-CH<sub>2</sub>), 34.6 (4C, Cq, <sup>t</sup>Bu), 31.69 (2C, Ct, alkyl- $\beta$ -CH<sub>2</sub>), 31.66 (6C, Ct, alkyl- $\beta$ -CH<sub>2</sub>), 31.65 (2C, Ct, alkyl- $\beta$ -CH<sub>2</sub>), 31.3 (12C, Cp, <sup>t</sup>Bu), 29.6 (2C, Ct, alkyl- $\gamma$ -CH<sub>2</sub>), 29.37 (2C, Ct, alkyl- $\gamma$ -CH<sub>2</sub>), 29.34 (6C, Ct, alkyl- $\gamma$ -CH<sub>2</sub>), 29.31 (2C, Ct, alkyl- $\gamma$ -CH<sub>2</sub>), 25.81 (2C, Ct, alkyl- $\delta$ -CH<sub>2</sub>), 25.77 (2C, Ct, alkyl- $\delta$ -CH<sub>2</sub>), 25.72 (6C, Ct, alkyl- $\delta$ -CH<sub>2</sub>), 25.70 (2C, Ct, alkyl- $\delta$ -CH<sub>2</sub>), 22.68 (4C, Ct, alkyl- $\epsilon$ -CH<sub>2</sub>), 22.67 (4C, Ct, alkyl- $\epsilon$ -CH<sub>2</sub>), 22.66 (2C, Ct, alkyl- $\epsilon$ -CH<sub>2</sub>), 22.65 (2C, Ct, alkyl- $\epsilon$ -CH<sub>2</sub>), 14.08 (2C, Cp, alkyl-CH<sub>3</sub>), 14.072 (4C, Cp, alkyl-CH<sub>3</sub>), 14.065 (4C, Cp, alkyl-CH<sub>3</sub>), 14.03 (2C, Cp, alkyl-CH<sub>3</sub>) ppm.

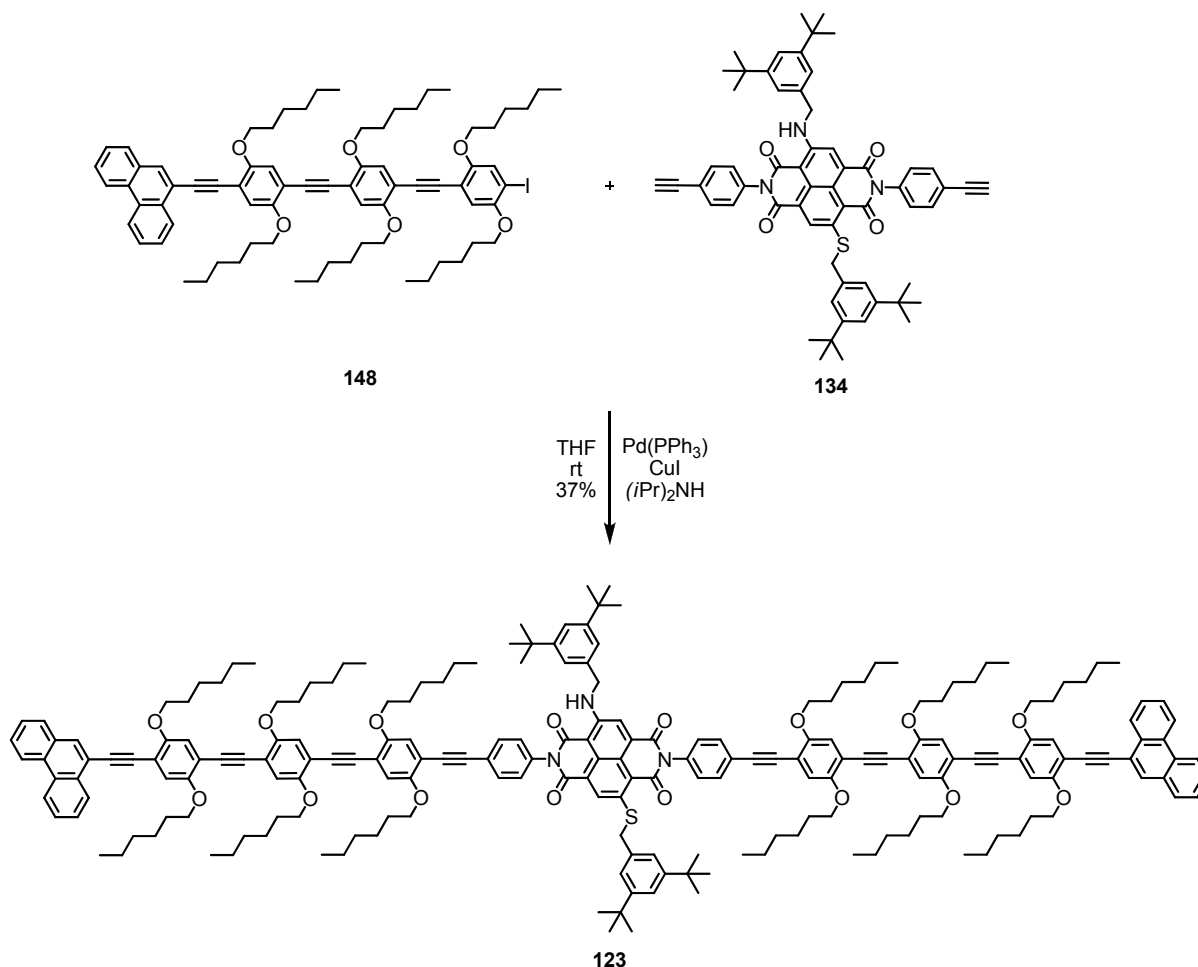
MS (MALDI-TOF): found  $m/z$  (%) = 3058.24 (24), 3057.26 (51), 3056.27 (85), 3055.27 (100), 3054.27 (87), 3053.26 (40) [ $M^+$ ]; calculated for  $C_{208}H_{244}N_4O_{16}$ : 3058.86 (22), 3057.85 (48), 3056.85 (82), 3055.85 (100), 3054.84 (90), 3053.84 (40).

UV/Vis:  $\lambda_{max}$  609, 563, 415 nm.

GPC (oligopore 6  $\mu m$ , toluene, UV/vis photodiode array detector) area 99.5% (at 12.34 min.)



***N,N'*-bis(9-((4-(4-(4-iodo-2,5-dihexyloxy-phenyl)ethynyl)-2,5-dihexyloxy-phenyl)ethynyl)-2,5-dihexyloxy-phenyl)ethynyl)phenanthrenyl)-2-((3,5-di-tert-butylphenyl)methansulfide)-6-((3,5-di-tert-butylphenyl)methanamine)-1,4,5,8-tetracarboxylic acid diimide (**123**)**



The pink acetylene **134** (25.0 mg, 0.0272 mmol, 1.0 eq.) and the yellow iodide **148** (68.0 mg, 0.0564 mmol, 2.07 eq.) were dissolved in 28 ml THF and 2.5 ml diisopropylamine in a 50-ml-2-neckflask (dry, Ar). It was degassed for 15 minutes, then Pd(PPh<sub>3</sub>)<sub>4</sub> (7 mg, 0.0061, 22 mol%) and CuI (1 mg, 20 mol%) were added. It was then stirred for 15 hours at room temperature. The reaction mixture was evaporated and chromatographed (silica gel, 2 x 12 cm, hex:CH<sub>2</sub>Cl<sub>2</sub> = 1:2 -> 1:5) to give compound **124** as a reddish solid (31 mg, 0.0101 mmol, 37 %).

TLC  $R_f$  0.70 (CH<sub>2</sub>Cl<sub>2</sub>:hex = 5:1).

<sup>1</sup>H NMR (600 MHz, CDCl<sub>3</sub>, 25 °C):  $\delta$  = 9.98 (s, 1H, NH), 8.88 (s, 1H, NDI), 8.73 (d, <sup>3</sup> $J_{\text{H,H}}$  = 7.7 Hz, 2H, phenanthrene), 8.71 (d, <sup>3</sup> $J_{\text{H,H}}$  = 8.1 Hz, 2H, phenanthrene), 8.68 (d, <sup>3</sup> $J_{\text{H,H}}$  = 8.3 Hz, 2H, phenanthrene), 8.44 (s, 1H, NDI), 8.09 (s, 2H, phenanthrene), 7.88 (d, <sup>3</sup> $J_{\text{H,H}}$  = 7.5 Hz, 2H, phenanthrene), 7.74-7.66 (m, 10H), 7.61 (t, <sup>3</sup> $J_{\text{H,H}}$  = 7.5

Hz, 2H, phenanthrene), 7.38 (s, 1H, NDI-substituent), 7.34 (d,  $^3J_{H,H} = 8.2$  Hz, 2H, phenyl), 7.33 (d,  $^4J_{H,H} = 1.3$  Hz, 1H, NDI-substituent), 7.32 (d,  $^3J_{H,H} = 8.3$  Hz, 2H, phenyl), 7.30 (d,  $^4J_{H,H} = 1.4$  Hz, 2H, NDI-substituent), 7.22 (d,  $^4J_{H,H} = 1.4$  Hz, 2H, NDI-substituent), 7.16 (s, 2H, OPE), 7.08 (s, 2H, OPE), 7.05 (m, 8H, OPE) 4.70 (d,  $^3J_{H,H} = 5.3$  Hz, 2H, N-CH<sub>2</sub>), 4.39 (s, 2H, S-CH<sub>2</sub>) 4.11 (t,  $^3J_{H,H} = 6.6$  Hz, 8H, OCH<sub>2</sub>), 4.09-4.03 (m, 16H, OCH<sub>2</sub>), 2.00 (quin,  $^3J_{H,H} = 7.1$  Hz, 4H, CH<sub>2</sub>), 1.88 (m, 20H, CH<sub>2</sub>), 1.57 (m, 24H, CH<sub>2</sub>), 1.37 (m, 48H, CH<sub>2</sub>), 1.31 (s, 18H, <sup>t</sup>Bu), 1.30 (s, 18H, <sup>t</sup>Bu), 0.911 (m, 30H, CH<sub>3</sub>), 0.908 (m, 6H, CH<sub>3</sub>) ppm.

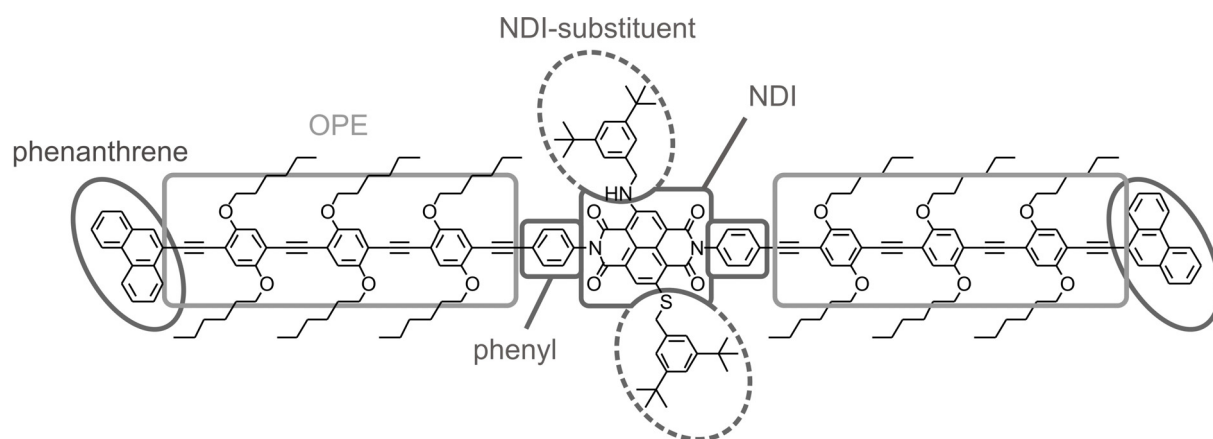
<sup>13</sup>C NMR (151 MHz, CDCl<sub>3</sub>, 25 °C):  $\delta = 166.496$  (1C, Cq, C=O), 166.301 (1C, Cq, C=O), 162.784 (1C, Cq, C=O), 162.393 (1C, Cq, C=O), 153.993 (2C, Cq, C-O), 153.602 (8C, Cq, C-O), 153.406 (2C, Cq, C-O), 151.257 (1C, Cq, N-C), 151.257 (4C, Cq, NDI-substituent), 144.42 (1C, Cq, S-C), 135.237 (1C, Cq, NDI-substituent), 134.847 (1C, Cq, phenyl), 134.456 (1C, Cq, phenyl), 133.675 (1C, Cq, NDI-substituent), 132.435 (2C, Ct, phenyl), 132.269 (2C, Ct, phenyl), 131.33 (2C, Cq, C(phenanthrene)), 131.273 (2C, Ct, CH(phenanthrene)), 131.135 (2C, Cq, C(phenanthrene)), 130.158 (2C, Cq, C(phenanthrene)), 128.45 (1C, Ct, NDI), 128.45 (4C, Ct, phenyl), 128.367 (2C, Ct, CH(phenanthrene)), 127.228 (1C, Cq, NDI), 127.205 (2C, Ct, CH(phenanthrene)), 127.205 (2C, Ct, CH(phenanthrene)), 127.032 (2C, Cq, C(phenanthrene)), 126.79 (4C, Ct, CH(phenanthrene)), 126.707 (2C, Ct, CH(phenanthrene)), 126.641 (1C, Cq, NDI), 123.906 (2C, Cq, phenyl), 123.552 (2C, Ct, NDI-substituent), 123.32 (1C, Cq, NDI), 122.473 (2C, Ct, CH(phenanthrene)), 122.39 (2C, Ct, CH(phenanthrene)), 122.141 (1C, Ct, NDI-substituent), 121.975 (2C, Ct, NDI-substituent), 121.725 (1C, Ct, NDI-substituent), 121.562 (1C, Cq, NDI), 120.314 (1C, Ct, NDI), 119.999 (2C, Cq, C(phenanthrene)), 119.804 (1C, Cq, NDI), 116.91 (8C, Ct, CH(OPE)), 116.827 (2C, Ct, CH(OPE)), 116.27 (2C, Ct, CH(OPE)), 114.333 (2C, Cq, C(OPE)), 113.943 (8C, Cq, C(OPE)), 113.747 (2C, Cq, C(OPE)), 100.853 (1C, Cq, NDI), 94.015 (2C, Cq, C $\equiv$ C), 93.429 (2C, Cq, C $\equiv$ C), 91.671 (2C, Cq, C $\equiv$ C), 91.476 (6C, Cq, C $\equiv$ C), 90.89 (2C, Cq, C $\equiv$ C), 87.178 (2C, Cq, C $\equiv$ C), 69.797 (2C, Cs, O-CH<sub>2</sub>), 69.722 (2C, Cs, O-CH<sub>2</sub>), 69.662 (4C, Cs, O-CH<sub>2</sub>), 69.56 (2C, Cs, O-CH<sub>2</sub>), 69.376 (2C, Cs, O-CH<sub>2</sub>), 48.086 (1C, Cs, N-CH<sub>2</sub>), 37.875 (1C, Cs, S-CH<sub>2</sub>), 34.82 (4C, Cq, <sup>t</sup>Bu), 31.667 (2C, Cs, CH<sub>2</sub> Alkyl  $\beta$ ), 31.635 (8C, Cs, CH<sub>2</sub> Alkyl  $\beta$ ), 31.596 (2C, Cs, CH<sub>2</sub> Alkyl  $\beta$ ), 31.394 (12C, Cp, <sup>t</sup>Bu), 29.531 (2C, Cs, CH<sub>2</sub> Alkyl  $\gamma$ ), 29.304 (8C, Cs, CH<sub>2</sub> Alkyl  $\gamma$ ), 29.277 (2C, Cs, CH<sub>2</sub> Alkyl  $\gamma$ ), 25.784 (2C, Cs, CH<sub>2</sub> Alkyl

$\delta$ ), 25.749 (2C, Cs, CH<sub>2</sub> Alkyl  $\delta$ ), 25.689 (8C, Cs, CH<sub>2</sub> Alkyl  $\delta$ ), 22.648 (12C, Cs, CH<sub>2</sub> Alkyl  $\epsilon$ ), 14.053 (10C, Cs, CH<sub>3</sub> alkyl), 14.01 (2C, Cs, CH<sub>3</sub> alkyl) ppm

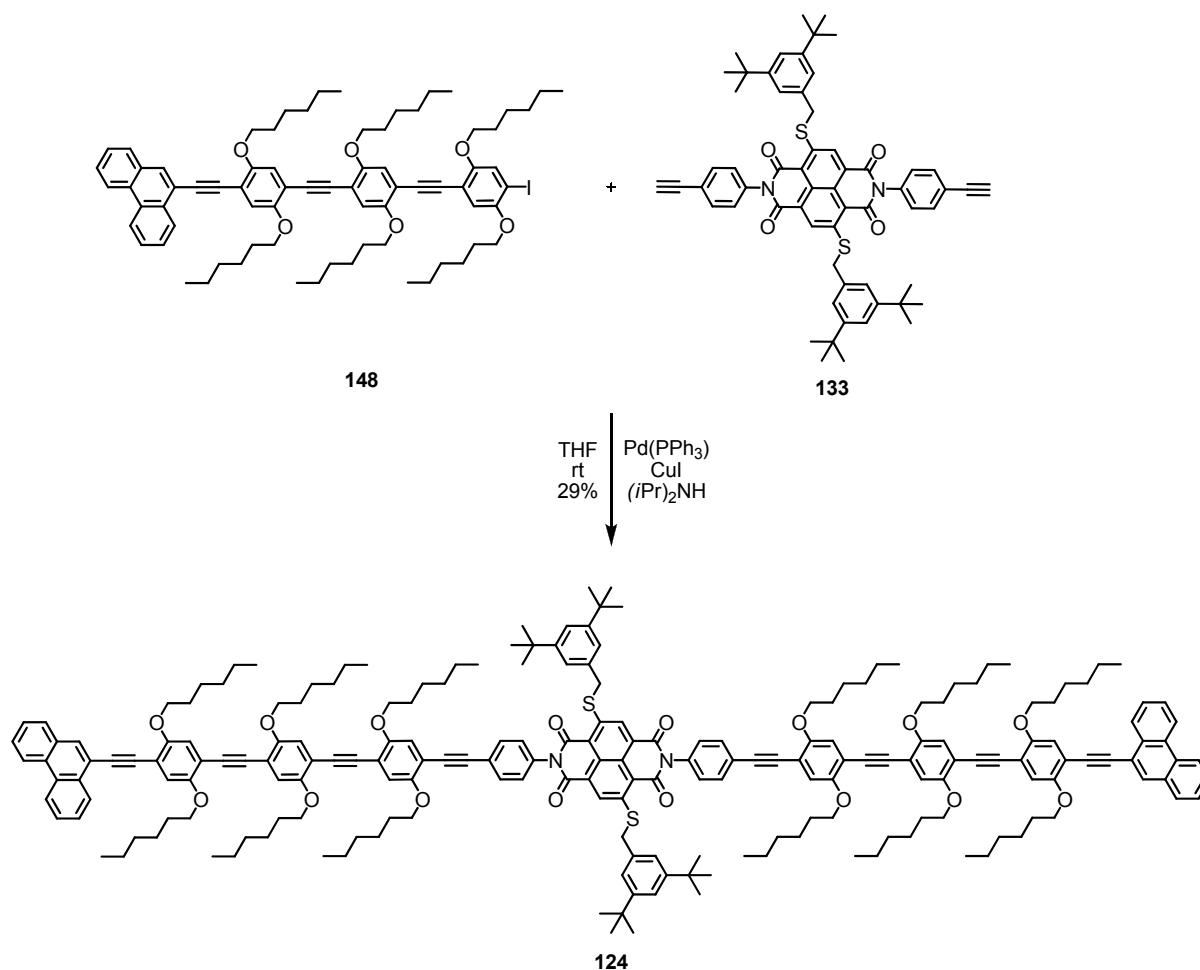
MS (MALDI-TOF): found  $m/z$  (%) = 3075.39 (21), 3074.40 (50), 3073.40 (83), 3072.39 (100), 3071.39 (86), 3070.39 (41) [ $M^+$ ]; calculated for C<sub>208</sub>H<sub>243</sub>N<sub>3</sub>O<sub>16</sub>S: 3075.81 (25), 3074.81 (51), 3073.81 (85), 3072.81 (100), 3071.81 (90), 3070.80 (40).

UV/Vis:  $\lambda_{\max}$  567, 530, 415 nm.

GPC (oligopore 6  $\mu$ m, toluene, UV/vis photodiode array detector) area 99.0% (at 12.28 min.)



***N,N'*-bis(9-((4-(4-(4-iodo-2,5-dihexyloxy-phenyl)ethynyl)-2,5-dihexyloxy-phenyl)ethynyl)-2,5-dihexyloxy-phenyl)ethynyl)phenanthrenyl)-2,6-di-((3,5-di-tert-butylphenyl)methansulfide)-1,4,5,8-tetracarboxylicacid diimide (**124**)**



The violet acetylene **133** (16.5 mg, 0.0176 mmol, 1.0 eq.) and the yellow iodide **148** (44 mg, 0.0365 mmol, 2.07 eq.) were dissolved in 25 ml THF and 2 ml diisopropylamine in a 50-ml-2-neckflask (dry, Ar). It was degassed for 15 minutes, then Pd(PPh<sub>3</sub>)<sub>4</sub> (5 mg, 0.0043mmol, 24 mol%) and CuI (0.7 mg, 20 mol%) were added. It was then stirred for 21 hours at room temperature. The reaction mixture was evaporated and chromatographed (silica gel, 1 x 12 cm, hex:CH<sub>2</sub>Cl<sub>2</sub> =1:2 -> 1:10) to give compound **124** as reddish solid (16 mg, 0.0051, 29 %).

TLC  $R_f$  0.86 (CH<sub>2</sub>Cl<sub>2</sub>).

<sup>1</sup>H NMR (600 MHz, CDCl<sub>3</sub>, 25 °C): δ = 8.95 (s, 2H, NDI), 8.73 (d, <sup>3</sup>J<sub>H,H</sub> = 7.8 Hz, 2H, phenanthrene), 8.71 (d, <sup>3</sup>J<sub>H,H</sub> = 8.7 Hz, 2H, phenanthrene), 8.67 (d, <sup>3</sup>J<sub>H,H</sub> = 8.3 Hz, 2H, phenanthrene), 8.08 (s, 2H, phenanthrene), 7.87 (d, <sup>3</sup>J<sub>H,H</sub> = 7.3 Hz, 2H, phenanthrene), 7.71 (d, <sup>3</sup>J<sub>H,H</sub> = 8.3 Hz, 4H, phenyl), 7.73-7.66 (m, 6H, phenanthrene), 7.61 (t, <sup>3</sup>J<sub>H,H</sub> = 7.6 Hz, 2H, phenanthrene), 7.34 (d, <sup>4</sup>J<sub>H,H</sub> = 1.6 Hz, 2H,

NDI substituent), 7.33 (d,  $^3J_{\text{H,H}} = 8.5$  Hz, 4H, phenyl), 7.30 (d,  $^4J_{\text{H,H}} = 1.5$  Hz, 4H, NDI-substituent), 7.16 (s, 2H, OPE), 7.08 (s, 2H, OPE), 7.05 (s, 2H, OPE), 7.042 (m, 4H, OPE), 7.038 (s, 2H, OPE), 4.43 (s, 4H, S-CH<sub>2</sub>), 4.11 (t,  $^3J_{\text{H,H}} = 6.6$  Hz, 8H, OCH<sub>2</sub>), 4.09-4.03 (m, 16H, OCH<sub>2</sub>), 2.00 (quin,  $^3J_{\text{H,H}} = 7.1$  Hz, 4H, CH<sub>2</sub>), 1.88 (m, 20H, CH<sub>2</sub>), 1.57 (m, 24H, CH<sub>2</sub>), 1.37 (m, 48H, CH<sub>2</sub>), 1.30 (s, 36H, <sup>t</sup>Bu), 0.91 (m, 30H, CH<sub>3</sub>), 0.87 (m, 6H, CH<sub>3</sub>) ppm.

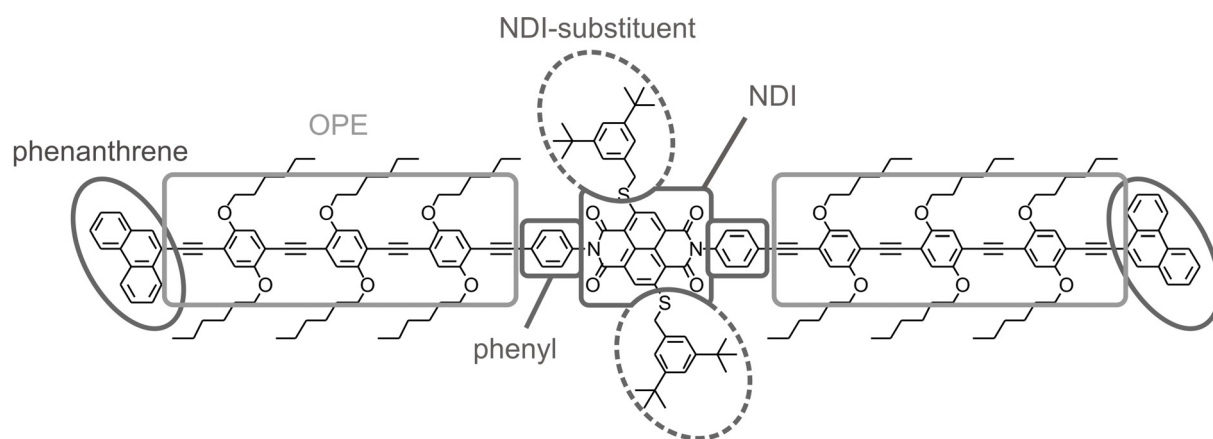
<sup>13</sup>C NMR (151 MHz, CDCl<sub>3</sub>, 25 °C):  $\delta$  = 163.4 (2C, Cq, C=O), 162.3 (2C, Cq, C=O), 153.9 (2C, Cq, C-O), 153.8 (2C, Cq, C-O), 153.5 (8C, Cq, C-O), 151.2 (4C, Cq, NDI-substituent), 149.4 (2C, Cq, C-S), 134.0 (2C, Cq, phenyl), 133.2 (2C, Cq, NDI-substituent), 132.4 (4C, Ct, phenyl), 131.3 (2C, Ct, phenanthrene), 131.1 (2C, Cq, phenanthrene), 131.0 (2C, Cq, phenanthrene), 130.1 (2C, Cq, phenanthrene), 128.8 (2C, Ct, NDI), 128.5 (4C, Ct, phenyl), 128.4 (2C, Ct, phenanthrene), 127.2 (2C, Ct, phenanthrene), 126.81 (2C, Cq, phenanthrene), 126.8 (4C, Ct, phenanthrene), 126.7 (2C, Ct, phenanthrene), 125.3 (2C, Cq, NDI), 124.4 (2C, Cq, phenyl), 123.8 (2C, Cq, NDI), 123.5 (4C, Ct, NDI-substituent), 122.5 (2C, Ct, phenanthrene), 122.4 (2C, Ct, phenanthrene), 122.2 (2C, Ct, phenanthrene), 121.9 (2C, Ct, NDI-substituent), 119.7 (2C, Cq, phenanthrene), 118.9 (2C, Cq, NDI), 117.0 (8C, Ct, CH(OPE)), 116.8 (2C, Ct, CH(OPE)), 116.3 (2C, Ct, CH(OPE)), 114.5 (2C, Cq, C(OPE)), 114.2 (2C, Cq, C(OPE)), 114.1 (4C, Cq, C(OPE)), 113.6 (2C, Cq, C(OPE)), 113.5 (2C, Cq, C(OPE)), 93.8 (2C, Cq, C $\equiv$ C), 93.2 (2C, Cq, C $\equiv$ C), 91.5 (6C, Cq, C $\equiv$ C), 91.4 (2C, Cq, C $\equiv$ C), 90.6 (2C, Cq, C $\equiv$ C), 87.9 (2C, Cq, C $\equiv$ C), 69.82 (2C, Cs, OCH<sub>2</sub>), 69.75 (2C, Cs, OCH<sub>2</sub>), 69.7 (4C, Cs, OCH<sub>2</sub>), 69.6 (2C, Cs, OCH<sub>2</sub>), 69.4 (2C, Cs, OCH<sub>2</sub>), 38.2 (2C, Cs, S-CH<sub>2</sub>), 34.8 (4C, Cq, <sup>t</sup>Bu), 31.6 (12C, Cs, Alkyl- $\beta$ -CH<sub>2</sub>), 31.4 (12C, Cp, <sup>t</sup>Bu), 29.5 (2C, Cs, Alkyl- $\gamma$ -CH<sub>2</sub>), 29.3 (10C, Cs, Alkyl- $\gamma$ -CH<sub>2</sub>), 25.79 (2C, Cs, Alkyl- $\delta$ -CH<sub>2</sub>), 25.75 (2C, Cs, Alkyl- $\delta$ -CH<sub>2</sub>), 25.70 (8C, Cs, Alkyl- $\delta$ -CH<sub>2</sub>), 22.7 (12C, Cs, Alkyl- $\epsilon$ -CH<sub>2</sub>), 14.1 (10C, Cp, Alkyl-CH<sub>3</sub>), 14.0 (10C, Cp, Alkyl-CH<sub>3</sub>) ppm.

MS (MALDI-TOF): found  $m/z$  (%) = 3093.10 (13), 3092.09 (27), 3091.08 (58), 3090.10 (94), 3089.11 (100), 3088.11 (81), 3087.10 (37)[M<sup>+</sup>]; calculated for C<sub>208</sub>H<sub>242</sub>N<sub>2</sub>O<sub>16</sub>S<sub>2</sub>: 3093.78 (12), 3092.78 (28), 3091.78 (57), 3090.77 (15), 3089.77 (100), 3088.77 (90), 3087.76 (40).

UV/Vis:  $\lambda_{\text{max}}$  530, 497, 415 nm.

GPC (oligopore 6  $\mu\text{m}$ , toluene, UV/vis photodiode array detector) area 99.0% (at 12.30 min.)







## 8 Abbreviations

A	acceptor
Ac	acetyl
AC	alternating current
Ac <sub>2</sub> O	acetic acid anhydride
AIBN	2,2'-azobis(2-methylpropionitrile)
aq.	aqueous
br	broad
BTMA ICl <sub>2</sub>	benzyltrimethylammonium dichloroiodate
CBQT <sup>4+</sup>	cyclobis(paraquat-p-phenylene)
CMOS	complementary metal-oxide-semiconductor
CNT	carbon nano tube
COSY	correlation spectroscopy
Cp	primary carbon
Cq	quarternary carbon
Cs	secondary carbon
Ct	tertiary carbon
CV	cyclovoltammetry
d	duplet
D	Donor
DC	direct current
DCM	dichloromethane
diglyme	dimethylethyl glycol
DIPA	diisopropylamine
DMF	<i>N,N</i> -dimethylformamide
DMI	<i>N,N</i> -dimethyl imidazolidinone
DMSO	dimethylsulfoxide
DNP	dioxynaphtalene
EA	elemental analysis
EDG	electron donating group
EI	electron impact
eq.	equivalent
ESI	electron spray ionization

---

Et	ethyl
ethyl-TMS	ethyl-trimethylsilane
EtOAc	ethyl acetate
EWG	electron withdrawing group
FAB	fast atom bombardment
Fc	ferrocene
FRET	Förster resonance energy transfer
GPC	gel permeation chromatography
GSCC	ground state coconformer
hex	hexane
HMBC	heteronuclear multiple bond coherence
HMQC	heteronuclear multiple quantum Coherence
HOMO	highest occupied molecular orbital
HOPG	highly-ordered-pyrolytic-graphite
HPLC	high performance liquid chromatography
HWE	Horner-Wadsworth-Emmons
h $\nu$	light
ITO	indium tin oxide
LB	Langmuir-Blodgett films
LDA	lithium diisopropylamine
LUMO	lowest unoccupied molecular orbital
m	multiplet
m/z	mass per charge
MALDI	matrix-assisted laser desorption/ionization
MCBJ	mechanical controllable break junction
Me	methyl
MIM	mechanically interlocked molecules
Mp	melting point
MS	mass spectrometry
MSCC	metastable coconformer
MSTJ	molecular switch tunnel junctions
NBS	<i>N</i> -bromosuccinimide
<i>n</i> -BuLi	<i>n</i> -butyl lithium
NDI	naphthalene diimide

---

NKR	Newman-Kwart rearrangement
NMR	nuclear magnetic resonance
NOESY	nuclear Overhauser effect spectroscopy
OP	oligophenylene
OPE	oligo(phenylene ethynylene)
OPV	oligo(phenylene vinylene)
OWL	on-wire lithography
PDMS	polydimethylsiloxane
Pg	protection group
Ph	phenyl
ppm	parts per million
q	quartet
quant.	quantitative
Rf	retention factor
RR	rectification ratio
rt	room temperature
s	singlet
SAM	self assembled monolayers
SECM	scanning electrochemical microscopy
SEM	scanning electron microscopy
SERS	surface-enhanced Raman scattering
Sia <sub>2</sub> BH	bis(3-methyl-2-butyl)borane
STM	scanning tunneling microscopy
STS	scanning tunneling spectroscopy
SWNT	single walled carbon nano tube
t	triplet
TBAF	tetra- <i>n</i> -butylammonium fluoride
TBAOH	tetrabutyl ammonium hydroxide
TBME	<i>tert</i> -butyl methyl ether
<sup>t</sup> Bu	<i>tert</i> -butyl
TCNQ	tetracyanoquinodimethane
TEM	transmission electron microscope
TFA	trifluoroacetic acid
THF	tetrahydrofuran

TIPS	tri-iso-propylsilyl
TLC	thin layer chromatography
TMEDA	<i>N,N,N',N'</i> -tetramethylenediamine
TMS	trimethylsilyl
TMS	tetramethylsilane
TOCSY	totally correlated spectroscopy
ToF	time of flight
Trt	trityl
TTF	tetra-thiafulvalene
UV/vis	ultraviolet and visible
v/v	volume per volume

## 9 Literature

- [1] N. Weibel, S. Grunder, M. Mayor, *Organic & Biomolecular Chemistry* **2007**, *5*, 2343.
- [2] R. L. Carroll, B. G. Christopher, *Angewandte Chemie International Edition* **2002**, *41*, 4378.
- [3] C. Joachim, J. K. Gimzewski, A. Aviram, *Nature (London)* **2000**, *408*, 541.
- [4] M. Mayor, H. B. Weber, *Chimia* **2003**, *56*, 494.
- [5] N. J. Tao, *Nature Nanotechnology* **2006**, *1*, 173.
- [6] R. M. Metzger, *Journal of Materials Chemistry* **2008**, *18*, 4364.
- [7] G. E. Moore, *Electronics* **1965**, *38*, 114.
- [8] R. R. Schaller, *Spectrum, IEEE* **1997**, *34*, 52.
- [9] G. E. Moore, *Digest of the 2003 Solid-State Circuits Conference, IEEE International* **2003**, *1*, 20.
- [10] B. A. Mantooh, P. S. Weiss, *Proceedings of the IEEE* **2003**, *91*, 1785.
- [11] Y. Wada, *Pure and Applied Chemistry* **1999**, *71*, 2055.
- [12] J. M. Tour, *Accounts of Chemical Research* **2000**, *33*, 791.
- [13] R. Beckman, K. Beverly, A. Boukai, Y. Bunimovich, J. W. Choi, E. Delonno, J. Green, E. Johnston-Halperin, Y. Luo, B. Sheriff, J. F. Stoddart, J. R. Heath, *Faraday Discussions* **2006**, *131*, 9.
- [14] Huang, Xu, Chen, M. D. Ventra, Tao, *Nano Letters* **2006**, *6*, 1240.
- [15] Y.-C. Chen, M. Zwolak, M. Di Ventra, *Nano Letters* **2003**, *3*, 1691.
- [16] S. Chiras, D. R. Clarke, *Journal of Applied Physics* **2000**, *88*, 6302.
- [17] Y. Luo, C. P. Collier, J. O. Jeppesen, K. A. Nielsen, E. Delonno, G. Ho, J. Perkins, H.-R. Tseng, T. Yamamoto, J. F. Stoddart, J. R. Heath, *ChemPhysChem* **2002**, *3*, 519.
- [18] E. Lörtscher, J. W. Ciszek, J. Tour, H. Riel, *Small* **2006**, *2*, 973.
- [19] H. Kuhn, *Struct. Chem. Mol. Biol.* **1968**, 566.
- [20] A. Aviram, M. A. Ratner, *Chemical Physics Letters* **1974**, *29*, 277.
- [21] R. M. Metzger, *Accounts of Chemical Research* **1999**, *32*, 950.
- [22] M.-K. Ng, L. Yu, *Angewandte Chemie, International Edition* **2002**, *41*, 3598.
- [23] J. G. Kushmerick, D. B. Holt, J. C. Yang, J. Naciri, M. H. Moore, R. Shashidhar, *Physical Review Letters* **2002**, *89*, 086802.
- [24] R. E. Holmlin, R. F. Ismagilov, R. Haag, V. Mujica, M. A. Ratner, M. A. Rampi, G. M. Whitesides, *Angewandte Chemie, International Edition* **2001**, *40*, 2316.
- [25] J. M. Mativetsky, G. Pace, M. Elbing, M. A. Rampi, M. Mayor, P. Samorí, *Journal of the American Chemical Society* **2008**, *130*, 9192.
- [26] G. Pace, V. Ferri, C. Grave, M. Elbing, C. von Hänisch, M. Zharnikov, M. Mayor, M. A. Rampi, P. Samorí, *Proceedings of the National Academy of Sciences* **2007**, *104*, 9937.
- [27] J. Chen, M. A. Reed, A. M. Rawlett, J. M. Tour, *Science (Washington, D. C.)* **1999**, *286*, 1550.
- [28] A. Wassel Ronald, B. Gorman Christopher, *Angewandte Chemie, International Edition* **2004**, *43*, 5120.
- [29] R. M. Metzger, *Chemical Reviews* **2003**, *103*, 3803.
- [30] L. H. Dubois, R. G. Nuzzo, *Annual Review of Physical Chemistry* **2003**, *43*, 437.
- [31] P. E. Laibinis, G. M. Whitesides, D. L. Allara, Y. T. Tao, A. N. Parikh, R. G. Nuzzo, *Journal of the American Chemical Society* **1991**, *113*, 7152.
- [32] K. B. Blodgett, I. Langmuir, *Physical Review* **1937**, *51*, 964.

- [33] K. B. Blodgett, *Journal of the American Chemical Society* **1935**, 57, 1007.
- [34] W. Schottky, *Zeitschrift für Physik* **1942**, 118, 539.
- [35] J. G. Kushmerick, A. S. Blum, D. P. Long, *Analytica Chimica Acta* **2006**, 568, 20.
- [36] C. P. Collier, G. Matterstei, E. W. Wong, Y. Luo, K. Beverly, J. Sampaio, F. M. Raymo, J. F. Stoddart, J. R. Heath, *Science (Washington, D. C.)* **2000**, 289, 1172.
- [37] C. P. Collier, J. O. Jeppesen, Y. Luo, J. Perkins, E. W. Wong, J. R. Heath, J. F. Stoddart, *Journal of the American Chemical Society* **2001**, 123, 12632.
- [38] J. W. Choi, A. H. Flood, D. W. Steuerman, S. Nygaard, A. B. Braunschweig, N. N. P. Moonen, B. W. Laursen, Y. Luo, E. Delonno, A. J. Peters, J. O. Jeppesen, K. Xu, J. F. Stoddart, J. R. Heath, *Chemistry--A European Journal* **2005**, 12, 261.
- [39] E. Mark, B. Alfred, Istrok, Błaszczuk, C. von Hänisch, M. Marcel, F. Violetta, G. Christian, R. Maria Anita, P. Giuseppina, S. Paolo, S. Andrei, Z. Michael, *Advanced Functional Materials* **2008**, 18, 2972.
- [40] V. Ferri, M. Elbing, G. Pace, M. D. Dickey, M. Zharnikov, P. Samori, M. Mayor, M. A. Rampi, *Angewandte Chemie International Edition* **2008**, 47, 3407.
- [41] R. E. Holmlin, R. Haag, M. L. Chabiny, R. F. Ismagilov, A. E. Cohen, A. Terfort, M. A. Rampi, G. M. Whitesides, *Journal of the American Chemical Society* **2001**, 123, 5075.
- [42] X. D. Cui, X. Zarate, J. Tomfohr, O. F. Sankey, A. Primak, A. L. Moore, T. A. Moore, D. Gust, G. Harris, S. M. Lindsay, *Nanotechnology* **2002**, 13, 5.
- [43] O. M. Magnussen, B. M. Ocko, M. Deutsch, M. J. Regan, P. S. Pershan, D. Abernathy, G. Grubel, J.-F. Legrand, *Nature* **1996**, 384, 250.
- [44] H. Park, A. K. L. Lim, A. P. Alivisatos, J. Park, P. L. McEuen, *Applied Physics Letters* **1999**, 75, 301.
- [45] H. Park, J. Park, A. K. L. Lim, E. H. Anderson, A. P. Alivisatos, P. L. McEuen, *Nature* **2000**, 407, 57.
- [46] J. Park, A. N. Pasupathy, J. I. Goldsmith, C. Chang, Y. Yaish, J. R. Petta, M. Rinkoski, J. P. Sethna, H. D. Abruna, P. L. McEuen, D. C. Ralph, *Nature* **2002**, 417, 722.
- [47] J. Park, A. N. Pasupathy, J. I. Goldsmith, C. Chang, Y. Yaish, J. R. Petta, M. Rinkoski, J. P. Sethna, H. D. Abruna, P. L. McEuen, D. C. Ralph, *Nature (London, United Kingdom)* **2002**, 417, 722.
- [48] H. Haick, D. Cahen, *Progress in Surface Science* **2008**, 83, 217.
- [49] J. Liao, L. Bernard, M. Langer, C. Schönenberger, M. Calame, *Advanced Materials* **2006**, 18, 2444.
- [50] L. Bernard, Y. Kamdzhilov, M. Calame, S. J. van der Molen, J. Liao, C. Schönenberger, *The Journal of Physical Chemistry C* **2007**, 111, 18445.
- [51] J. Liao, M. A. Mangold, S. Grunder, M. Mayor, C. Schönenberger, M. Calame, *New Journal of Physics* **2008**, 10.
- [52] V. Santhanam, R. P. Andres, *Nano Letters* **2003**, 4, 41.
- [53] V. Santhanam, J. Liu, R. Agarwal, R. P. Andres, *Langmuir* **2003**, 19, 7881.
- [54] L. A. Bumm, J. J. Arnold, M. T. Cygan, T. D. Dunbar, T. P. Burgin, L. Jones, II, D. L. Allara, J. M. Tour, P. S. Weiss, *Science (Washington, D. C.)* **1996**, 271, 1705.
- [55] X. D. Cui, A. Primak, X. Zarate, J. Tomfohr, O. F. Sankey, A. L. Moore, T. A. Moore, D. Gust, G. Harris, S. M. Lindsay, *Science (Washington, DC, United States)* **2001**, 294, 571.



- [56] M. A. Reed, C. Zhou, C. J. Muller, T. P. Burgin, J. M. Tour, *Science (Washington, D. C.)* **1997**, *278*, 252.
- [57] J. Reichert, R. Ochs, D. Beckmann, H. B. Weber, M. Mayor, H. von Lohneysen, *Physical Review Letters* **2002**, *88*, 176804/1.
- [58] R. Huber, M. T. Gonzalez, S. Wu, M. Langer, S. Grunder, V. Horhoiu, M. Mayor, M. R. Bryce, C. Wang, R. Jitchati, C. Schönenberger, M. Calame, *Journal of the American Chemical Society* **2008**, *130*, 1080.
- [59] S. Wu, M. T. Gonzalez, R. Huber, S. Grunder, M. Mayor, C. Schönenberger, M. Calame, *Nature Nanotechnology* **2008**, *3*, 569.
- [60] L. Gruter, M. T. Gonzalez, R. Huber, M. Calame, C. Schönenberger, *Small* **2005**, *1*, 1067.
- [61] Z. M. Wu, M. Steinacher, R. Huber, M. Calame, S. J. van der Molen, C. Schönenberger, *Applied Physics Letters* **2007**, *91*, 053118.
- [62] R. H. M. Smit, Y. Noat, C. Untiedt, N. D. Lang, M. C. van Hemert, J. M. van Ruitenbeek, *Nature* **2002**, *419*, 906.
- [63] M. T. Gonzalez, S. Wu, R. Huber, S. J. van der Molen, C. Schönenberger, M. Calame, *Nano Letters* **2006**, *6*, 2238.
- [64] M. T. Gonzalez, S. Wu, R. Huber, S. J. van der Molen, C. Schönenberger, M. Calame, *Nano Letters* **2006**, *6*, 2238.
- [65] B. Xu, N. J. Tao, *Science (Washington, DC, United States)* **2003**, *301*, 1221.
- [66] M. D. Newton, *Chemical Reviews* **2002**, *91*, 767.
- [67] G. C. Solomon, D. Q. Andrews, R. H. Goldsmith, T. Hansen, M. R. Wasielewski, R. P. Van Duyne, M. A. Ratner, *Journal of the American Chemical Society* **2008**, *130*, 17301.
- [68] A. Salomon, D. Cahen, S. Lindsay, J. Tomfohr, V. B. Engelkes, C. D. Frisbie, *Advanced Materials (Weinheim, Germany)* **2003**, *15*, 1881.
- [69] Y. Xue, M. A. Ratner, *Physical Review B* **2004**, *69*, 085403.
- [70] F. Chen, X. Li, J. Hihath, Z. Huang, N. Tao, *Journal of the American Chemical Society* **2006**, *128*, 15874.
- [71] J. M. Beebe, V. B. Engelkes, L. L. Miller, C. D. Frisbie, *Journal of the American Chemical Society* **2002**, *124*, 11268.
- [72] S.-H. Ke, H. U. Baranger, W. Yang, *Journal of the American Chemical Society* **2004**, *126*, 15897.
- [73] H. Basch, R. Cohen, M. A. Ratner, *Nano Letters* **2005**, *5*, 1668.
- [74] Y. Hu, Y. Zhu, H. Gao, H. Guo, *Physical Review Letters* **2005**, *95*, 156803.
- [75] K. H. Muller, *Physical Review B (Condensed Matter and Materials Physics)* **2006**, *73*, 045403.
- [76] F. Chen, X. Li, J. Hihath, Z. Huang, N. Tao, *Journal of the American Chemical Society* **2006**, *128*, 15874.
- [77] A. Ulman, *Chemical Reviews* **1996**, *96*, 1533.
- [78] B. Xu, X. Xiao, N. J. Tao, *Journal of the American Chemical Society* **2003**, *125*, 16164.
- [79] B. Kim, J. M. Beebe, Y. Jun, X. Y. Zhu, C. D. Frisbie, *Journal of the American Chemical Society* **2006**, *128*, 4970.
- [80] L. Patrone, S. Palacin, J. P. Bourgoin, *Applied Surface Science* **2003**, *212-213*, 446.
- [81] L. Patrone, S. Palacin, J. Charlier, F. Armand, J. P. Bourgoin, H. Tang, S. Gauthier, *Physical Review Letters* **2003**, *91*, 096802.

- [82] S. Yasuda, S. Yoshida, J. Sasaki, Y. Okutsu, T. Nakamura, A. Taninaka, O. Takeuchi, H. Shigekawa, *Journal of the American Chemical Society* **2006**, *128*, 7746.
- [83] L. Venkataraman, J. E. Klare, I. W. Tam, C. Nuckolls, M. S. Hybertsen, M. L. Steigerwald, *Nano Letters* **2006**, *6*, 458.
- [84] L. Venkataraman, J. E. Klare, C. Nuckolls, M. S. Hybertsen, M. L. Steigerwald, *Nature(London, United Kingdom)* **2006**, *442*, 904.
- [85] E. Lörtscher, M. Elbing, M. Tschudy, C. von Hänisch, H. B. Weber, M. Mayor, H. Riel, *ChemPhysChem* **2008**, *9*, 2252.
- [86] D. Vonlanthen, A. Mishchenko, M. Elbing, M. Neuburger, T. Wandlowski, M. Mayor, *Angewandte Chemie International Edition* **2009**, *48*, 8886.
- [87] H. B. W. J. R. M. E. C. v. H. D. B. M. F. Marcel Mayor, *Angewandte Chemie International Edition* **2003**, *42*, 5834.
- [88] W. Wang, T. Lee, M. A. Reed, *Physical Review B* **2003**, *68*, 035416.
- [89] J. He, O. Sankey, M. Lee, N. Tao, X. Li, S. Lindsay, *Faraday Discussions* **2006**, *131*, 145.
- [90] M. Mayor, C. von Hänisch, B. Weber Heiko, J. Reichert, D. Beckmann, *Angewandte Chemie International Edition* **2002**, *41*, 1183.
- [91] H. Yu, Y. Luo, K. Beverly, J. F. Stoddart, H.-R. Tseng, R. Heath James, *Angewandte Chemie International Edition* **2003**, *42*, 5706.
- [92] S. Kubatkin, A. Danilov, M. Hjort, J. Cornil, J.-L. Bredas, N. Stuhr-Hansen, P. Hedegard, T. Bjornholm, *Nature (London, United Kingdom)* **2003**, *425*, 698.
- [93] W. Liang, M. P. Shores, M. Bockrath, J. R. Long, H. Park, *Nature* **2002**, *417*, 725.
- [94] A. C. Brady, B. Hodder, A. S. Martin, J. R. Sambles, C. P. Ewels, R. Jones, P. R. Briddon, A. M. Musa, C. A. Panetta, D. L. Mattern, *J. Mater. Journal of Materials Chemistry* **1999**, *9*, 2271.
- [95] N. Okazaki, J. R. Sambles, M. J. Jory, G. J. Ashwell, *Applied Physics Letters* **2002**, *81*, 2300.
- [96] R. M. Metzger, *Chemical Physics* **2006**, *326*, 176.
- [97] C. Krzeminski, C. Delerue, G. Allan, D. Vuillaume, R. M. Metzger, *Physical Review B* **2001**, *64*, 085405.
- [98] J. E. Meinhard, *Journal of Applied Physics* **1964**, *35*, 3059.
- [99] R. M. Metzger, B. Chen, U. Hopfner, M. V. Lakshmikantham, D. Vuillaume, T. Kawai, X. Wu, H. Tachibana, T. V. Hughes, H. Sakurai, J. W. Baldwin, C. Hosch, M. P. Cava, L. Brehmer, G. J. Ashwell, *Journal of the American Chemical Society* **1997**, *119*, 10455.
- [100] X. Tao, R. P. Iyer, M. V. Lakshmikantham, M. M. Robert, *Angewandte Chemie International Edition* **2001**, *40*, 1749.
- [101] R. M. Metzger, T. Xu, I. R. Peterson, *The Journal of Physical Chemistry B* **2001**, *105*, 7280.
- [102] S. Andreas, H. Peter, M. Klaus, P. R. Jürgen, *Angewandte Chemie International Edition* **1995**, *34*, 1609.
- [103] R. M. Metzger, J. W. Baldwin, W. J. Shumate, I. R. Peterson, P. Mani, G. J. Mankey, T. Morris, G. Szulczewski, S. Bosi, M. Prato, A. Comito, Y. Rubin, *The Journal of Physical Chemistry B* **2003**, *107*, 1021.
- [104] A. Honciuc, A. Jaiswal, A. Gong, K. Ashworth, C. W. Spangler, I. R. Peterson, L. R. Dalton, R. M. Metzger, *The Journal of Physical Chemistry B* **2004**, *109*, 857.

- [105] J. W. Baldwin, R. R. Amaresh, I. R. Peterson, W. J. Shumate, M. P. Cava, M. A. Amiri, R. Hamilton, G. J. Ashwell, R. M. Metzger, *The Journal of Physical Chemistry B* **2002**, *106*, 12158.
- [106] W. J. Shumate, D. L. Mattern, A. Jaiswal, D. A. Dixon, T. R. White, J. Burgess, A. Honciuc, R. M. Metzger, *The Journal of Physical Chemistry B* **2006**, *110*, 11146.
- [107] H. Gregory, R. H. James, K. Mykola, F. P. Dmitrii, A. Karin, P. Michel, R. B. Martin, *Chemistry - A European Journal* **2005**, *11*, 2914.
- [108] J. G. Kushmerick, C. M. Whitaker, S. K. Pollack, T. L. Schull, R. Shashidhar, *Nanotechnology* **2004**, *15*, S489.
- [109] J. Reichert, R. Ochs, D. Beckmann, H. B. Weber, M. Mayor, H. v. Löhneysen, *Physical Review Letters* **2002**, *88*, 176804.
- [110] O. D. Miller, B. Muralidharan, N. Kapur, A. W. Ghosh, *Physical Review B (Condensed Matter and Materials Physics)* **2008**, *77*, 125427.
- [111] V. Mujica, M. Kemp, A. Roitberg, M. Ratner, *The Journal of Chemical Physics* **1996**, *104*, 7296.
- [112] G. D. Scott, K. S. Chichak, A. J. Peters, S. J. Cantrill, J. F. Stoddart, H. W. Jiang, *Physical Review B (Condensed Matter and Materials Physics)* **2006**, *74*, 113404.
- [113] M. Elbing, R. Ochs, M. Koentopp, M. Fischer, C. von Hanisch, F. Weigend, F. Evers, B. Weber Heiko, M. Mayor, *Proceedings of the National Academy of Sciences of the United States of America* **2005**, *102*, 8815.
- [114] N. Armstrong, R. C. Hoft, A. McDonagh, M. B. Cortie, M. J. Ford, *Nano Letters* **2007**, *7*, 3018.
- [115] D. Q. Andrews, G. C. Solomon, R. P. Van Duyne, M. A. Ratner, *Journal of the American Chemical Society* **2008**, *130*, 17309.
- [116] B. L. Feringa, Editor, *Molecular Switches*, **2001**.
- [117] N. Tamai, H. Miyasaka, *Chemical Reviews* **2000**, *100*, 1875.
- [118] P. Ahonen, T. Laaksonen, D. J. Schiffrin, K. Kontturi, *Physical Chemistry Chemical Physics* **2007**, *9*, 4898.
- [119] M. E. G. P. Michael D. D. M. Z. P. S. M. M. Maria A. R. Violetta Ferri, *Angewandte Chemie International Edition* **2008**, *47*, 3407.
- [120] M. Irie, *Chemical Reviews (Washington, D. C.)* **2000**, *100*, 1685.
- [121] D. Dulic, S. J. van der Molen, T. Kudernac, H. T. Jonkman, J. J. D. de Jong, T. N. Bowden, J. van Esch, B. L. Feringa, B. J. van Wees, *Physical Review Letters* **2003**, *91*, 207402/1.
- [122] T. Kudernac, S. J. v. d. Molen, B. J. v. Wees, B. L. Feringa, *Chemical Communications* **2006**, 3597.
- [123] M. Ikeda, N. Tanifuji, H. Yamaguchi, M. Irie, K. Matsuda, *Chemical Communications* **2007**, 1355.
- [124] K. Matsuda, H. Yamaguchi, T. Sakano, M. Ikeda, N. Tanifuji, M. Irie, *The Journal of Physical Chemistry C* **2008**, *112*, 17005.
- [125] S. J. van der Molen, J. Liao, T. Kudernac, J. S. Agustsson, L. Bernard, M. Calame, B. J. van Wees, B. L. Feringa, C. Schönenberger, *Nano Letters* **2008**, *9*, 76.
- [126] A. Peters, N. R. Branda, *Journal of the American Chemical Society* **2003**, *125*, 3404.
- [127] A. Peters, N. R. Branda, *Chemical Communications* **2003**, 954.
- [128] J. Areephong, W. R. Browne, N. Katsonis, B. L. Feringa, *Chemical Communications* **2006**, 3930.

- [129] R. Baron, A. Onopriyenko, E. Katz, O. Lioubashevski, I. Willner, S. Wang, H. Tian, *Chemical Communications* **2006**, 2147.
- [130] T. J. Wigglesworth, D. Sud, T. B. Norsten, V. S. Lekhi, N. R. Branda, *Journal of the American Chemical Society* **2005**, *127*, 7272.
- [131] D. Sud, T. B. Norsten, N. R. Branda, *Angewandte Chemie, International Edition* **2005**, *44*, 2019.
- [132] V. Lemieux, S. Gauthier, N. R. Branda, *Angewandte Chemie, International Edition* **2006**, *45*, 6820.
- [133] D. I. Gittins, D. Bethell, D. J. Schiffrin, R. J. Nichols, *Nature (London)* **2000**, *408*, 67.
- [134] W. Haiss, H. Van Zalinge, S. J. Higgins, D. Bethell, H. Hoebenreich, D. J. Schiffrin, R. J. Nichols, *Journal of the American Chemical Society* **2003**, *125*, 15294.
- [135] Z. Li, B. Han, G. Meszaros, I. Pobelov, T. Wandlowski, A. Błaszczuk, M. Mayor, *Faraday Discussions* **2006**, *131*, 121.
- [136] Z. Li, I. Pobelov, B. Han, T. Wandlowski, A. Błaszczuk, M. Mayor, *Nanotechnology* **2007**, *18*, 044018/1.
- [137] B. Han, Z. Li, T. Wandlowski, A. Błaszczuk, M. Mayor, *The Journal of Physical Chemistry C* **2007**, *111*, 13855.
- [138] F. Giacalone, M. Herranz, L. Gruter, M. T. Gonzalez, M. Calame, C. Schönenberger, C. R. Arroyo, G. Rubio-Bollinger, M. Velez, N. Agrait, N. Martin, *Chemical Communications* **2007**, 4854.
- [139] J. K. Sorensen, M. Vestergaard, A. Kadziola, K. Kils, M. B. Nielsen, *Organic Letters* **2006**, *8*, 1173.
- [140] E. H. Van Dijk, D. J. T. Myles, M. H. Van der Veen, J. C. Hummelen, *Organic Letters* **2006**, *8*, 2333.
- [141] A. R. Pease, J. O. Jeppesen, J. F. Stoddart, Y. Luo, C. P. Collier, J. R. Heath, *Accounts of Chemical Research* **2001**, *34*, 433.
- [142] P. M. Mendes, A. H. Flood, J. F. Stoddart, *Applied Physics A: Materials Science & Processing* **2005**, *80*, 1197.
- [143] R. A. Bissell, E. Cordova, A. E. Kaifer, J. F. Stoddart, *Nature (London, United Kingdom)* **1994**, *369*, 133.
- [144] M. Asakawa, P. R. Ashton, V. Balzani, A. Credi, C. Hamers, G. Mattersteig, M. Montalti, A. N. Shipway, N. Spencer, J. F. Stoddart, M. S. Tolley, M. Venturi, A. J. P. White, D. J. Williams, *Angewandte Chemie, International Edition* **1998**, *37*, 333.
- [145] J. O. Jeppesen, K. A. Nielsen, J. Perkins, S. A. Vignon, A. Di Fabio, R. Ballardini, M. T. Gandolfi, M. Venturi, V. Balzani, J. Becher, J. F. Stoddart, *Chemistry--A European Journal* **2003**, *9*, 2982.
- [146] D. W. Steuerman, H.-R. Tseng, A. J. Peters, A. H. Flood, J. O. Jeppesen, K. A. Nielsen, J. F. Stoddart, J. R. Heath, *Angewandte Chemie, International Edition* **2004**, *43*, 6486.
- [147] I. C. Lee, C. W. Frank, T. Yamamoto, H.-R. Tseng, A. H. Flood, J. F. Stoddart, J. O. Jeppesen, *Langmuir* **2004**, *20*, 5809.
- [148] H.-R. Tseng, D. Wu, N. X. Fang, X. Zhang, J. F. Stoddart, *ChemPhysChem* **2004**, *5*, 111.
- [149] J. E. Green, J. Wook Choi, A. Boukai, Y. Bunimovich, E. Johnston-Halperin, E. Delonno, Y. Luo, B. A. Sheriff, K. Xu, Y. Shik Shin, H.-R. Tseng, J. F. Stoddart, J. R. Heath, *Nature* **2007**, *445*, 414.

- [150] A. S. Blum, J. G. Kushmerick, D. P. Long, C. H. Patterson, J. C. Yang, J. C. Henderson, Y. Yao, J. M. Tour, R. Shashidhar, B. R. Ratna, *Nature Materials* **2005**, *4*, 167.
- [151] K. Sonogashira, Y. Tohda, N. Hagihara, *Tetrahedron Letters* **1975**, 4467.
- [152] H. Doucet, J.-C. Hierso, *Angewandte Chemie International Edition* **2007**, *46*, 834.
- [153] R. Chinchilla, C. Najera, *Chemical Reviews* **2007**, *107*, 874.
- [154] A. de Meijere, F. Diederich, Editors, *Metal-Catalyzed Cross-Coupling Reactions, Second Completely Revised and Enlarged Edition; Volume 2*, **2004**.
- [155] R. Singh, G. Just, *The Journal of Organic Chemistry* **1989**, *54*, 4453.
- [156] W. B. Austin, N. Bilow, W. J. Kelleghan, K. S. Y. Lau, *The Journal of Organic Chemistry* **1981**, *46*, 2280.
- [157] E. Negishi, L. Anastasia, *Chemical Reviews* **2003**, *103*, 1979.
- [158] D. T. Gryko, C. Clausen, K. M. Roth, N. Dontha, D. F. Bocian, W. G. Kuhr, J. S. Lindsey, *Journal of Organic Chemistry* **2000**, *65*, 7345.
- [159] J. M. Tour, A. M. Rawlett, M. Kozaki, Y. Yao, R. C. Jagessar, S. M. Dirk, D. W. Price, M. A. Reed, C.-W. Zhou, J. Chen, W. Wang, I. Campbell, *Chemistry--A European Journal* **2001**, *7*, 5118.
- [160] J. W. Tilley, S. Zawoiski, *Journal of Organic Chemistry* **1988**, *53*, 386.
- [161] A. Błaszczuk, M. Elbing, M. Mayor, *Organic & Biomolecular Chemistry* **2004**, *2*, 2722.
- [162] S. A. Johnson, F.-Q. Liu, M. C. Suh, S. Zuercher, M. Haufe, S. S. H. Mao, T. D. Tilley, *Journal of the American Chemical Society* **2003**, *125*, 4199.
- [163] B. R. Kaafarani, A. A. Pinkerton, D. C. Neckers, *Tetrahedron Letters* **2001**, *42*, 8137.
- [164] L. Shu, Z. Mu, H. Fuchs, L. Chi, M. Mayor, *Chemical Communications* **2006**, 1862.
- [165] E. J. Corey, P. L. Fuchs, *Tetrahedron Letters* **1972**, 3769.
- [166] A. K. Flatt, Y. Yao, F. Maya, J. M. Tour, *Journal of Organic Chemistry* **2004**, *69*, 1752.
- [167] Synthesized by Michael Langer.
- [168] Huang, F. Chen, P. A. Bennett, Tao, *Journal of the American Chemical Society* **2007**, *129*, 13225.
- [169] M. D. Watson, A. Fechtenkotter, K. Müllen, *Chemical Reviews* **2001**, *101*, 1267.
- [170] K. S. Kim, P. Tarakeshwar, J. Y. Lee, *Chemical Reviews* **2000**, *100*, 4145.
- [171] F. J. M. Hoeben, P. Jonkheijm, E. W. Meijer, A. P. H. J. Schenning, *Chemical Reviews* **2005**, *105*, 1491.
- [172] C. A. Hunter, J. K. M. Sanders, *Journal of the American Chemical Society* **1990**, *112*, 5525.
- [173] L.-L. Lin, J.-C. Leng, X.-N. Song, Z.-L. Li, Y. Luo, C.-K. Wang, *The Journal of Physical Chemistry C* **2009**, *113*, 14474.
- [174] D. Mayer, T. Dretschkow, K. Ataka, T. Wandlowski, *Journal of Electroanalytical Chemistry* **2002**, 524-525, 20.
- [175] K. W. Hipps, *Science (Washington, DC, United States)* **2001**, *294*, 536.
- [176] M. Mayor, B. Weber Heiko, J. Reichert, M. Elbing, C. Von Hanisch, D. Beckmann, M. Fischer, *Angewandte Chemie, International Edition* **2003**, *42*, 5834.

- [177] B. E. Maryanoff, A. B. Reitz, *Chemical Reviews (Washington, DC, United States)* **1989**, *89*, 863.
- [178] N. Stuhr-Hansen, *Synthetic Communications* **2003**, *33*, 641.
- [179] H. O. Wirth, F. U. Herrmann, W. Kern, *Makromolekulare Chemie* **1964**, *80*, 120.
- [180] J. N. Wilson, P. M. Windscheif, U. Evans, M. L. Myrick, U. H. F. Bunz, *Macromolecules* **2002**, *35*, 8681.
- [181] R. C. Wheland, E. L. Martin, *Journal of Organic Chemistry* **1975**, *40*, 3101.
- [182] R. Brueckner, Editor, *Reaction Mechanisms in Organic Chemistry*, **1996**.
- [183] R. Ziesel, J. Suffert, M.-T. Youinou, *Journal of Organic Chemistry* **1996**, *61*, 6535.
- [184] P. J. Stang, J. A. Whiteford, C. V. Lu, P. J. Stang, *Journal of the American Chemical Society* **1997**, *119*, 2524.
- [185] J. N. Wilson, U. H. F. Bunz, *Journal of the American Chemical Society* **2005**, *127*, 4124.
- [186] P. L. McGrier, K. M. Solntsev, J. Schoenhaber, S. M. Brombosz, L. M. Tolbert, U. H. F. Bunz, *Chemical Communications (Cambridge, United Kingdom)* **2007**, 2127.
- [187] S. Grunder, R. Huber, V. Horhoiu, M. T. Gonzalez, C. Schönenberger, M. Calame, M. Mayor, *Journal of Organic Chemistry* **2007**, *72*, 8337.
- [188] X. Li, J. He, J. Hihath, B. Xu, S. M. Lindsay, N. Tao, *Journal of the American Chemical Society* **2006**, *128*, 2135.
- [189] M. S. Wong, J. F. Nicoud, *Tetrahedron Letters* **1993**, *34*, 8237.
- [190] D. S. Seferos, D. A. Banach, N. A. Alcantar, J. N. Israelachvili, G. C. Bazan, *Journal of Organic Chemistry* **2004**, *69*, 1110.
- [191] C. J. Yu, Y. Chong, J. F. Kayyem, M. Gozin, *J. Org. Chem.* **1999**, *64*, 2070.
- [192] K. Fredenberg, D. Peters, *Berichte der Deutschen Chemischen Gesellschaft [Abteilung] B: Abhandlungen* **1919**, *52B*, 1463.
- [193] M. S. Newman, H. A. Karnes, *Journal of Organic Chemistry* **1966**, *31*, 3980.
- [194] H. Kwart, E. R. Evans, *Journal of Organic Chemistry* **1966**, *31*, 410.
- [195] G. C. Lloyd-Jones, J. D. Moseley, J. S. Renny, *Synthesis* **2008**, 661.
- [196] F. Beaulieu, V. Snieckus, *Synthesis* **1992**, 112.
- [197] H. Detert, O. Sadovski, E. Sugiono, *Journal of Physical Organic Chemistry* **2004**, *17*, 1046.
- [198] J. N. Wilson, M. Josowicz, Y. Wang, U. H. F. Bunz, *Chemical Communications (Cambridge, United Kingdom)* **2003**, 2962.
- [199] V. David, M. Artem, E. Mark, N. Markus, W. Thomas, M. Marcel, *Angewandte Chemie International Edition* **2009**, 9999, NA.
- [200] J. M. Tour, L. Jones, D. L. Pearson, J. J. S. Lamba, T. P. Burgin, G. M. Whitesides, D. L. Allara, A. N. Parikh, S. Atre, *Journal of the American Chemical Society* **1995**, *117*, 9529.
- [201] J. Reichert, R. Ochs, D. Beckmann, H. B. Weber, M. Mayor, H. v. Löhneysen, *Physical Review Letters* **2002**, *88*, 176804.
- [202] M. Elbing, R. Ochs, M. Koentopp, M. Fischer, C. von Hänisch, F. Weigend, F. Evers, H. B. Weber, M. Mayor, *Proceedings of the National Academy of Sciences of the United States of America* **2005**, *102*, 8815.
- [203] M. Ruben, A. Landa, E. Lörtscher, H. Riel, M. Mayor, H. Görls, H. B. Weber, A. Arnold, F. Evers, *Small* **2008**, *4*, 2229.
- [204] A. Shaporenko, M. Elbing, A. Błaszczuk, C. von Hänisch, M. Mayor, M. Zharnikov, *The Journal of Physical Chemistry B* **2006**, *110*, 4307.

- [205] E. Lörtscher, H. B. Weber, H. Riel, *Physical Review Letters* **2007**, *98*, 176807.
- [206] G. A. Gray, *Journal of the American Chemical Society* **1973**, *95*, 7736.
- [207] G. G. A. Balavoine, G. Doisneau, T. Fillebeen-Khan, *Journal of Organometallic Chemistry* **1991**, *412*, 381.
- [208] E. Anklam, *Synthesis FIELD Full Journal Title:Synthesis* **1987**, 841.
- [209] P. Stepnicka, I. Cisarova, *Inorganic Chemistry* **2006**, *45*, 8785.
- [210] A. Ramón Gómez, A. Javier, C. Juan Carlos, *Angewandte Chemie International Edition* **2006**, *45*, 7674.
- [211] F. Bohlmann, K. M. Kleine, *Chemische Berichte* **1963**, *96*, 1229.
- [212] H. S. Broadbent, L. H. Slauch, N. L. Jarvis, *Journal of the American Chemical Society* **1954**, *76*, 1519.
- [213] K. Tachibana, I. Imaoka, H. Yoshino, T. Emura, H. Kodama, Y. Furuta, N. Kato, M. Nakamura, M. Ohta, K. Taniguchi, N. Ishikura, M. Nagamuta, E. Onuma, H. Sato, *Bioorganic & Medicinal Chemistry* **2007**, *15*, 174.
- [214] V. Cere, F. Massaccesi, S. Pollicino, A. Ricci, *Synthetic Communications* **1996**, *26*, 899.
- [215] S. Nishimura, *Handbook of Heterogeneous Catalytic Hydrogenation for Organic Synthesis*, **2001**.
- [216] R. H. Crabtree, H. Felkin, T. Fillebeen-Khan, G. E. Morris, *Journal of Organometallic Chemistry* **1979**, *168*, 183.
- [217] R. H. Crabtree, H. Felkin, G. E. Morris, *Journal of Organometallic Chemistry* **1977**, *141*, 205.
- [218] *Provided by Markus Schrems*.
- [219] J. G. de Vries, C. J. Elsevier, Editors, *Handbook of Homogeneous Hydrogenation*, **2007**.
- [220] J. Hanus, J. Vorisek, *Collection of Czechoslovak Chemical Communications* **1929**, *1*, 223.
- [221] E. J. Corey, W. L. Mock, D. J. Pasto, *Tetrahedron Letters* **1961**, *2*, 347.
- [222] T. Kauffmann, C. Kosel, W. Schoeneck, *Chemische Berichte* **1963**, *96*, 999.
- [223] H. C. Brown, K. J. Murray, *Tetrahedron* **1986**, *42*, 5497.
- [224] S. A. Getty, C. Engtrakul, L. Wang, R. Liu, S.-H. Ke, H. U. Baranger, W. Yang, M. S. Fuhrer, L. R. Sita, *Physical Review B* **2005**, *71*, 241401.
- [225] Synthesized by P. Schmidt, in *practical course*, **2008**.
- [226] N. Stuhr-Hansen, J. B. Christensen, N. Harrit, T. Bjornholm, *Journal of Organic Chemistry* **2003**, *68*, 1275.
- [227] S. P. Dudek, H. D. Sikes, C. E. D. Chidsey, *Journal of the American Chemical Society* **2001**, *123*, 8033.
- [228] J. B. Heilmann, E. A. Hillard, M.-A. Plamont, P. Pigeon, M. Bolte, G. Jaouen, A. Vessieres, *Journal of Organometallic Chemistry* **2008**, *693*, 1716.
- [229] G. D. Sproul, G. D. Stucky, *Inorganic Chemistry* **1972**, *11*, 1647.
- [230] A. L. Roe, D. J. Schneider, R. J. Mayer, J. W. Pyrz, J. Widom, L. Que, *Journal of the American Chemical Society* **1984**, *106*, 1676.
- [231] C. Elschenbroich, *Organometallics*, third ed., Wiley, **2006**.
- [232] A. M. O. B. Christopher M. A. Brett, *Electrochemistry; Principles, Methods and Applications*, Oxford Science Publications, **1993**.
- [233] S. Wu, PhD thesis, University of Basel (Basel), **2009**.
- [234] Note:, *In the break junction experiments, a constant small bias voltage  $V_b$  (0.1V) is applied between the source and drain electrodes and the current is recorded. When the Au junction breaks open, the detected current is the sum of two contributions: (a) tunneling current through single molecule due to*

- applied bias volate  $V_b$  between source and drain electrodes, which is typically in the range of  $\sim nA$ ; and (b) the electrochemical cell current between the counter electrode and the working electrodes (source/drain in MCBJ experiment). Here the electron transfer occurs between bulk reactant and the whole surface of the electrodes with the applied potential  $V_R$ . Depending on the area of the electrodes and the reactant concentration, this current can be easily as large as  $\mu A$ .
- [235] P. J. Graham, R. V. Lindsey, G. W. Parshall, M. L. Peterson, G. M. Whitman, *Journal of the American Chemical Society* **1957**, *79*, 3416.
- [236] P. Debroy, S. Roy, *Coordination Chemistry Reviews* **2007**, *251*, 203.
- [237] R. Wang, X. Hong, Z. Shan, *Tetrahedron Letters* **2008**, *49*, 636.
- [238] F. B. Dains, T. H. Vaughan, W. M. Janney, *Journal of the American Chemical Society* **1918**, *40*, 930.
- [239] J. J. Li, M. B. Norton, E. J. Reinhard, G. D. Anderson, S. A. Gregory, P. C. Isakson, C. M. Koboldt, J. L. Masferrer, W. E. Perkins, et al., *Journal of Medicinal Chemistry* **1996**, *39*, 1846.
- [240] Y. Ju, R. S. Varma, *The Journal of Organic Chemistry* **2005**, *71*, 135.
- [241] J. H. Lee, B. S. Lee, H. Shin, D. H. Nam, D. Y. Chi, *Synlett* **2006**, 65.
- [242] S. Kajigaeshi, T. Kakinami, K. Inoue, M. Kondo, H. Nakamura, M. Fujikawa, T. Okamoto, *Bulletin of the Chemical Society of Japan* **1988**, *61*, 597.
- [243] S. Kajigaeshi, T. Kakinami, H. Yamasaki, S. Fujisaki, T. Okamoto, *Bulletin of the Chemical Society of Japan* **1988**, *61*, 600.
- [244] D. B. Kimball, T. J. R. Weakley, M. M. Haley, *Journal of Organic Chemistry* **2002**, *67*, 6395.
- [245] T. V. Glukhareva, P. E. Kropotina, M. F. Kosterina, Y. I. Nein, E. V. Deeva, Y. Y. Morzherin, *Chemistry of Heterocyclic Compounds (New York, NY, United States)* **2007**, *43*, 76.
- [246] G. V. Garner, D. B. Mobbs, H. Suschitzky, J. S. Millership, *Journal of the Chemical Society [Section] C: Organic* **1971**, 3693.
- [247] J. N. Clifford, A. Gegout, S. Zhang, R. Pereira de Freitas, M. Urbani, M. Holler, P. Ceroni, J.-F. Nierengarten, N. Armaroli, *European Journal of Organic Chemistry* **2007**, 5899.
- [248] F. de Montigny, G. Argouarch, C. Lapinte, *Synthesis* **2006**, 293.
- [249] T. L. Scott, B. C. G. Soderberg, *Tetrahedron* **2003**, *59*, 6323.
- [250] S. Höger, K. Bonrad, *The Journal of Organic Chemistry* **2000**, *65*, 2243.
- [251] A. Godt, *The Journal of Organic Chemistry* **1997**, *62*, 7471.
- [252] Y. Tobe, N. Utsumi, A. Nagano, M. Sonoda, K. Naemura, *Tetrahedron* **2001**, *57*, 8075.
- [253] E. Lörtscher, Jacob W. Ciszek, J. Tour, H. Riel, *Small* **2006**, *2*, 973.
- [254] F. A. Carey, R. J. Sundberg, *Advanced Course in Organic Chemistry, Book 2: Reactions and Syntheses*, **1981**.
- [255] J. R. Heath, M. A. Ratner, *Physics Today* **2003**, *56*, 43.
- [256] J.-H. Tian, B. Liu, Li, Z.-L. Yang, B. Ren, S.-T. Wu, Tao, Z.-Q. Tian, *Journal of the American Chemical Society* **2006**, *128*, 14748.
- [257] T. Philip, S. Markus, *Angewandte Chemie International Edition* **2005**, *44*, 2642.
- [258] E. Betzig, J. K. Trautman, *Science* **1992**, *257*, 189.
- [259] W. E. Moerner, *Science* **1994**, *265*, 46.
- [260] W. E. Moerner, M. Orrit, *Science* **1999**, *283*, 1670.
- [261] F. Kulzer, M. Orrit, *Annual Review of Physical Chemistry* **2004**, *55*, 585.



- [262] D. Woll, E. Braeken, A. Deres, F. C. D. Schryver, H. Uji-i, J. Hofkens, *Chemical Society Reviews* **2009**, *38*, 313.
- [263] P. Leclère, M. Surin, P. Jonkheijm, O. Henze, A. P. H. J. Schenning, F. Biscarini, A. C. Grimsdale, W. J. Feast, E. W. Meijer, K. Müllen, J. L. Brédas, R. Lazzaroni, *European Polymer Journal* **2004**, *40*, 885.
- [264] G. Destriau, *Journal de Chimie Physique et de Physico-Chimie Biologique* **1936**, *33*, 587.
- [265] R. H. Friend, R. W. Gymer, A. B. Holmes, J. H. Burroughes, R. N. Marks, C. Taliani, D. D. C. Bradley, D. A. D. Santos, J. L. Bredas, M. Logdlund, W. R. Salaneck, *Nature* **1999**, *397*, 121.
- [266] S. Iijima, *Nature* **1991**, *354*, 56.
- [267] J. Robertson, *Materials Today*, *10*, 36.
- [268] P. Avouris, *Accounts of Chemical Research* **2002**, *35*, 1026.
- [269] A. K. Feldman, M. L. Steigerwald, X. Guo, C. Nuckolls, *Accounts of Chemical Research* **2008**, *41*, 1731.
- [270] R. Krupke, F. Hennrich, H. v. Löhneysen, M. M. Kappes, *Science* **2003**, *301*, 344.
- [271] R. Krupke, F. Hennrich, *Advanced Engineering Materials* **2005**, *7*, 111.
- [272] K. Balasubramanian, R. Sordan, M. Burghard, K. Kern, *Nano Letters* **2004**, *4*, 827.
- [273] M. Zheng, A. Jagota, E. D. Semke, B. A. Diner, R. S. McLean, S. R. Lustig, R. E. Richardson, N. G. Tassi, *Nat Mater* **2003**, *2*, 338.
- [274] R. Krupke, F. Hennrich, H. B. Weber, D. Beckmann, O. Hampe, S. Malik, M. M. Kappes, H. v. Löhneysen, *Applied Physics A: Materials Science & Processing* **2003**, *76*, 397.
- [275] A. Vijayaraghavan, S. Blatt, D. Weissenberger, M. Oron-Carl, F. Hennrich, D. Gerthsen, H. Hahn, R. Krupke, *Nano Letters* **2007**, *7*, 1556.
- [276] C. W. Marquardt, S. Dehm, A. Vijayaraghavan, S. Blatt, F. Hennrich, R. Krupke, *Nano Letters* **2008**, *8*, 2767.
- [277] T. Brintlinger, Y.-F. Chen, T. Durkop, E. Cobas, M. S. Fuhrer, J. D. Barry, J. Melngailis, *Applied Physics Letters* **2002**, *81*, 2454.
- [278] F. Würthner, S. Ahmed, C. Thalacker, T. Debaerdemaeker, *Chemistry - A European Journal* **2002**, *8*, 4742.
- [279] S. V. Bhosale, C. H. Jani, S. J. Langford, *Chemical Society Reviews* **2008**, *37*, 331.
- [280] A. Błaszczuk, M. Fischer, C. von Hänisch, M. Mayor, *Helvetica Chimica Acta* **2006**, *89*, 1986.
- [281] F. Chaignon, M. Falkenstrom, S. Karlsson, E. Blart, F. Odobel, L. Hammarstrom, *Chemical Communications* **2007**, 64.
- [282] C. Wang, A. S. Batsanov, M. R. Bryce, *The Journal of Organic Chemistry* **2005**, *71*, 108.
- [283] L. Jones, J. S. Schumm, J. M. Tour, *The Journal of Organic Chemistry* **1997**, *62*, 1388.
- [284] Available in a reaction of 2,6-dichloro-1,4,5,8-naphthalene tetracarboxylic acid anhydride with 4-((triisopropylsilyl)-ethynyl)-aniline. Synthesized by Alfred Błaszczuk.
- [285] T. M. Swager, C. J. Gil, M. S. Wrighton, *Journal of Physical Chemistry* **1995**, *99*, 4886.

- 
- [286] M. Sarobe, L. W. Jenneskens, J. Wesseling, J. D. Snoeijer, J. W. Zwikker, U. E. Wiersum, *Liebigs Annalen/Recueil* **1997**, 1207.
- [287] J. R. Lakowicz, *Principles of Fluorescence Spectroscopy*, Third ed., Springer, **2006**.
- [288] S. Grunder, R. Huber, V. Horhoiu, M. T. Gonzalez, C. Schönenberger, M. Calame, M. Mayor, *The Journal of Organic Chemistry* **2007**, 72, 8337.
- [289] A. Brikh, C. Morin, *Journal of Organometallic Chemistry* **1999**, 581, 82.
- [290] J. Eldo, E. Arunkumar, A. Ajayaghosh, *Tetrahedron Letters* **2000**, 41, 6241.
- [291] S. Höger, K. Bonrad, *Journal of Organic Chemistry* **2000**, 65, 2243.

## 10 Appendix

### 10.1 Contributions

All molecules were synthesized and characterized by Sergio Grunder except:

**55** (Viviana Horhoiu), **95, 96, 97** (Pascal Schmidt), **101, 112** (Yann Leroux), **126, 127, 129, 130, 133, 134, 139** (David Muñoz), **125** and **128** (Alfred Błaszczuk).

The MCBJ measurements in chapter 2.3 and 3.2.2 were performed by Dr. Songmei Wu (in the group of Dr. Michel Calame and Prof. Ch. Schönenberger), the MCBJ measurements in chapter 3.1.2.3, 3.1.3 and 3.1.4.3 were performed by Dr. Roman Huber (in the group of Dr. Michel Calame and Prof. Christian Schönenberger). The Investigation on the SWNT-junctions in chapter 5.5 were performed by Christoph Marquardt (in the group of Prof. Ralph Krupke).



# Curriculum Vitae

## Sergio Grunder

---

### Personal Information

Date/place of birth 16.05.1980 in Sursee (LU), Switzerland  
Nationality Swiss

### Education

- 06/2006 – 12/2009 **PhD work** at the *University of Basel, Switzerland*.  
*Department of Chemistry*  
Supervisor: Prof. Dr. Marcel Mayor.  
“New Functional Molecules in Molecular Junctions”
- 03/2006 **Master of Science** in Chemistry, *University of Basel, Switzerland*.
- 09/2005 – 03/2006 **Master thesis** in Organic Chemistry, *University of Basel, Switzerland*.  
Supervisor: Prof. Dr. Marcel Mayor. Thesis: “Electrochemical Molecular Switching Device”.
- 10/2001 – 08/2005 **Bachelor of Science** in Chemistry, *University of Basel, Switzerland*.
- 06/2000 “Maturitäts Prüfung”, Typus C, *Kantonsschule Alpenquai, Luzern, Switzerland*.

### Publications

- *Novel Oligoaryl Cruciform Structures as Model Compounds for Coordination Induced Single Molecule Switches*, **S. Grunder**, R. Huber, S. Wu, C. Schönenberger, M. Calame, and M. Mayor, *Eur. J. Org. Chem.* **2009**, DOI: 10.1002/ejoc.200901150
- *Molecular junctions based on aromatic coupling*, S. Wu, M. T. González, R. Huber, **S. Grunder**, M. Mayor, C. Schönenberger, M. Calame, *Nature Nanotech.* **2008**, *3*, 569 – 574.
- *Interlinking Au nanoparticles in 2D arrays via conjugated dithiolated molecules*, J. Liao, M. A. Mangold, **S. Grunder**, M. Mayor, C. Schönenberger, M. Calame, *New J. Phys.* **2008**, *10*, 065019
- *Electrical Conductance of Conjugated Oligomers at the Single Molecule Level*, R. Huber, M. T. González, S. Wu, M. Langer, **S. Grunder**, V. Horhoiu, M. Mayor, M. R. Bryce, C. Wang, R. Jitchati, C. Schönenberger, M. Calame, *J. Am. Chem. Soc.* **2008**, *130*, 1080 – 1084.
- *New Cruciform Structures: Toward Coordination Induced Single Molecule Switches*. **S. Grunder**, R. Huber, V. Horhoiu, M. T. González, C. Schönenberger, M. Calame, M. Mayor, *J. Org. Chem.* **2007**, *72*, 8337 – 8344.
- *Functional Molecules in Electronic Circuits*, N. Weibel, **S. Grunder**, M. Mayor, *Org. Biomol. Chem.* **2007**, *5*, 2343 – 2353.

### Scholarships and awards

- SCS/ Mettler-Toledo Prizes for best oral presentation, SCS Fall Meeting **2009**, *EPFL, Switzerland*.
  - Merck travel grant of the SCS for the 2<sup>nd</sup> EuCheMS Chemistry Congress **2008**, *Torino, Italy*.
-